Structures Research Report

University of Florida
Civil and Coastal Engineering

UF

GATOR Engineering
University of Florida
Civil and Coastal Engineering

Deliverable 8: Final report March 2021

Evaluation of Tapered Bridge Pads

Principal investigator:
Gary R. Consolazio, Ph.D.

Co-Principal investigator:
H.R. Trey Hamilton, Ph.D., P.E.

Research assistant:
Satyajeet Patil

Department of Civil and Coastal Engineering
University of Florida
P.O. Box 116580
Gainesville, Florida 32611

Sponsor:
Florida Department of Transportation (FDOT)
Christina Freeman, P.E. – Project manager

Contract:
UF Project No. P0077250 & P0077251
FDOT Contract No. BDV31-977-95

DISCLAIMER

The opinions, findings, and conclusions expressed in this publication are those of the authors and not necessarily those of the State of Florida Department of Transportation.

SI (MODERN METRIC) CONVERSION FACTORS

*APPROXIMATE CONVERSIONS **TO** SI UNITS*

SYMBOL	WHEN YOU KNOW	MULTIPLY BY	TO FIND	SYMBOL
LENGTH				
in	inches	25.4	millimeters	mm
ft	feet	0.305	meters	m
yd	yards	0.914	meters	m
mi	miles	1.61	kilometers	km
AREA				
in^2	square inches	645.2	square millimeters	mm^2
ft^2	square feet	0.093	square meters	m^2
yd^2	square yard	0.836	square meters	m^2
ac	acres	0.405	hectares	ha
mi^2	square miles	2.59	square kilometers	km^2
VOLUME				
fl oz	fluid ounces	29.57	milliliters	mL
gal	gallons	3.785	liters	L
ft^3	cubic feet	0.028	cubic meters	m^3
yd^3	cubic yards	0.765	cubic meters	m^3
NOTE: volumes greater than 1000 L shall be shown in m^3				
MASS				
oz	ounces	28.35	grams	g
lb	pounds	0.454	kilograms	kg
T	short tons (2,000 lb)	0.907	Megagrams	Mg (or "t")
TEMPERATURE (exact degrees)				
°F	Fahrenheit	5(F-32)/9 or (F-32)/1.8	Celsius	°C
FORCE and PRESSURE or STRESS				
kip	1,000 pound force	4.45	kilonewtons	kN
lbf	pound force	4.45	newtons	N
lbf/in^2	pound force per square inch	6.89	kilopascals	kPa
ksi	kips force per square inch	6.89	Megapascals	MPa

TECHNICAL REPORT DOCUMENTATION PAGE

1. Report No.	2. Government Accession No.	3. Recipient's Catalog No.

4. Title and Subtitle	5. Report Date
Evaluation of Tapered Bridge Bearing Pads	March 2021
	6. Performing Organization Code
	8. Performing Organization Report No.
7. Author(s) Gary R. Consolazio, H. R. Hamilton, Satyajeet R. Patil	2021/77250-77251
9. Performing Organization Name and Address University of Florida Department of Civil and Coastal Engineering 365 Weil Hall, P.O. Box 116580 Gainesville, FL 32611-6580	10. Work Unit No. (TRAIS) 11. Contract or Grant No. BDV31-977-95
12. Sponsoring Agency Name and Address Florida Department of Transportation Research Management Center 605 Suwannee Street, MS 30 Tallahassee, FL 32399-0450	13. Type of Report and Period Covered Final Report 14. Sponsoring Agency Code

15. Supplementary Notes

16. Abstract

Steel-reinforced elastomeric bearing pads are widely used in bridge construction to vertically support girders on piers while also accommodating translational and rotational girder deformations caused by live loads and temperature changes. To support sloped girders, flat bearing pads of uniform thicknesses are typically used with either tapered steel shim plates or an inclined concrete bearing seat. Tapered pads have the potential to reduce both construction time and cost by eliminating the need for tapered steel plates or the need to slope concrete beam seats to match the girder slope. Limited research, however, has been performed to investigate the effects of taper on relevant design properties of bearing pads such as axial stiffness, shear stiffness, horizontal restraining force and displacement generated in tapered pads under pure compression, and shear strain at slip.

In order to evaluate these properties, tapered pad configurations with varying plan view dimensions, elastomer thicknesses, and slope angles were developed by modifying elastomer thicknesses and shim orientations of standard FDOT flat pads. An experimental test setup and testing protocol was then developed to test tapered bearing pads and flat pads (control specimens). In this report, results are presented from the experimental testing that was performed to quantify the effects of taper on the design properties of bearing pads. Results obtained from the study revealed that shear stiffness was not significantly influenced by the introduction of taper angle, or the direction of shear along the length of pads. The shear stiffness of tapered pads remained within approximately 15% of the shear stiffness of corresponding flat pads. However, axial stiffness, horizontal restraining force, and horizontal displacement in tapered pads were found to depend on the taper slope angle. Axial stiffness decreased with increase in taper slope, and horizontal restraining force and displacement increased with increase in slope.

Based on the collected experimental data, generalized equations were developed to aid in the estimation of axial stiffness, shear stiffness, horizontal restraining force, and horizontal displacement. The effect that taper slope has on shear strain at pad slip was also investigated. Tapered pads bearing against concrete surfaces were found to satisfy the AASHTO requirement of minimum 0.5 shear strain before slip. However, tapered pads bearing against steel surfaces generally did not satisfy this requirement. Future research is recommended to evaluate different options to prevent premature slip of tapered pads on steel surfaces. For the design of mechanical anti-slip devices such as keeper plates, relevant design forces may be computed using horizontal pad restraining force equations developed and presented in this study.

17. Key Words	18. Distribution Statement
Neoprene, Bearing pads, Tapered, Axial stiffness, Shear stiffness, Horizontal force, Horizontal deformation, Slip	No restrictions.

19. Security Classif. (of this report)	20. Security Classif. (of this page)	21. No. of Pages	22. Price
Unclassified	Unclassified	261	

Form DOT F 1700.7 (8-72). Reproduction of completed page authorized

ACKNOWLEDGMENTS

The authors thank the Florida Department of Transportation (FDOT) for providing the funding that made this research possible. Additionally, the authors acknowledge the significant contributions made by personnel of the FDOT Structures Research Center in providing technical insights and suggestions, fabricating and constructing testing setup, providing data acquisition, and conducting bearing pad tests.

EXECUTIVE SUMMARY

Steel-reinforced elastomeric bearing pads are widely used in bridge construction to vertically support girders on piers while also accommodating translational and rotational girder deformations caused by live loads and temperature changes. To support sloped girders, flat bearing pads of uniform thicknesses are typically used with either tapered steel shim plates or an inclined concrete bearing seat. Tapered pads have the potential to reduce both construction time and cost by eliminating the need for tapered steel plates or the need to slope concrete beam seats to match the girder slope. Limited research, however, has been performed to investigate the effects of taper on relevant design properties of bearing pads such as axial stiffness, shear stiffness, horizontal restraining force and displacement generated in tapered pads under pure compression, and shear strain at slip.

In order to evaluate these properties, tapered pad configurations with varying plan view dimensions, elastomer thicknesses, and slope angles were developed by modifying elastomer thicknesses and shim orientations of standard FDOT flat pads. An experimental test setup and testing protocol was then developed to test tapered bearing pads and flat pads (control specimens). In this report, results are presented from the experimental testing that was performed to quantify the effects of taper on the design properties of bearing pads. Results obtained from the study revealed that shear stiffness was not significantly influenced by the introduction of taper angle, or the direction of shear along the length of pads. The shear stiffness of tapered pads remained within approximately 15% of the shear stiffness of corresponding flat pads. However, axial stiffness, horizontal restraining force, and horizontal displacement in tapered pads were found to depend on the taper slope angle. Axial stiffness decreased with increase in taper slope, and horizontal restraining force and displacement increased with increase in slope.

Based on the collected experimental data, generalized equations were developed to aid in the estimation of axial stiffness, shear stiffness, horizontal restraining force, and horizontal displacement. The effect that taper slope has on shear strain at pad slip was also investigated. Tapered pads bearing against concrete surfaces were found to satisfy the AASHTO requirement of minimum 0.5 shear strain before slip. However, tapered pads bearing against steel surfaces generally did not satisfy this requirement. Future research is recommended to evaluate different options to prevent premature slip of tapered pads on steel surfaces. For the design of mechanical anti-slip devices such as keeper plates, relevant design forces may be computed using horizontal pad restraining force equations developed and presented in this study.

TABLE OF CONTENTS

LIST OF FIGURES

LIST OF TABLES

CHAPTER 1
INTRODUCTION

Bridge girders and associated supporting elements, including bearing pads and substructures, are regularly subjected to combined vertical and horizontal forces. Self-weight of bridge components (girders, road deck, barriers, etc.) and weight of vehicles (trucks and cars) are primarily responsible for the vertical forces. On the other hand, thermal expansion and contraction of bridge components as well as vehicle braking forces are responsible for horizontal forces. Environmental loads such as wind and earthquake forces also impose vertical and horizontal forces on bridge structures. Structural demands caused by combinations of vertical and horizontal forces need to be considered during design to ensure bridge safety and serviceability.

At each girder support location, one or more bearings are placed between the bridge girders and the underlying substructure elements (abutments, piers) (Figure 1-1). The bearings serve both to distribute vertical forces from the bridge superstructure to the bridge substructure and to limit the transmission of horizontal forces that are caused by thermal deflections (Figure 1-2). Consequently, bridge bearings must possess sufficient stiffness and strength to distribute large vertical loads, but have sufficient flexibility to allow the superstructure to undergo horizontal movements without diminishing the structural integrity of superstructure or substructure components.

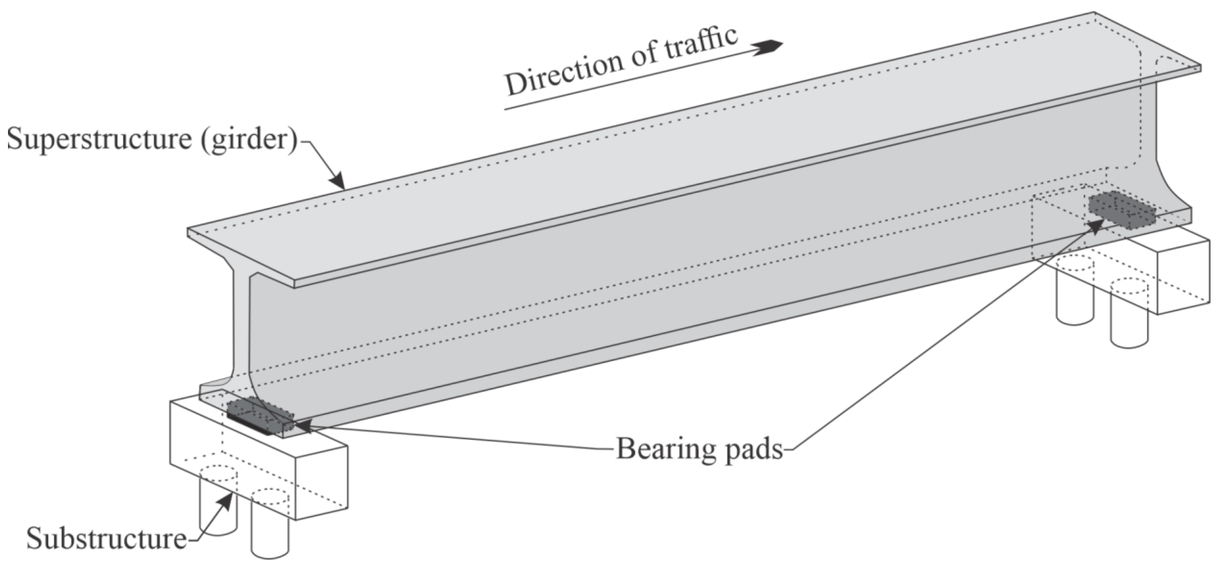

Figure 1-1 Location of bearing pads (not to scale)

Different types of bearings are available for use depending on the type of bridge and the expected deflection pattern. Elastomeric bearing pads (Figure 1-3) are one of the most commonly used bearings for bridges due to their ease of installation and maintenance (Burpulis et al., 1990; Pont, 1959). Such pads generally consist of neoprene elastomer (a synthetic rubber-like material) with embedded steel reinforcing shim plates (Figure 1-3) that vary in thickness generally from 0.1 in. to 0.15 in. Neoprene is generally used in bearing pads because it has better resistance to heat, flames, and ozone attack compared to general purpose elastomers; neoprene also has better adhesion to metals and resistance to weathering. Neoprene elastomer is flexible in shear and allows horizontal movements in bridges. However, when reinforced with steel shims, a neoprene bearing pad has high compression stiffness and can support heavy vertical forces. Compression and shear are, therefore, the important modes of deformation for bearing pads (Figure 1-4). As a result, quantifying the axial and shear stiffnesses of bearing pads is important step in bridge design.

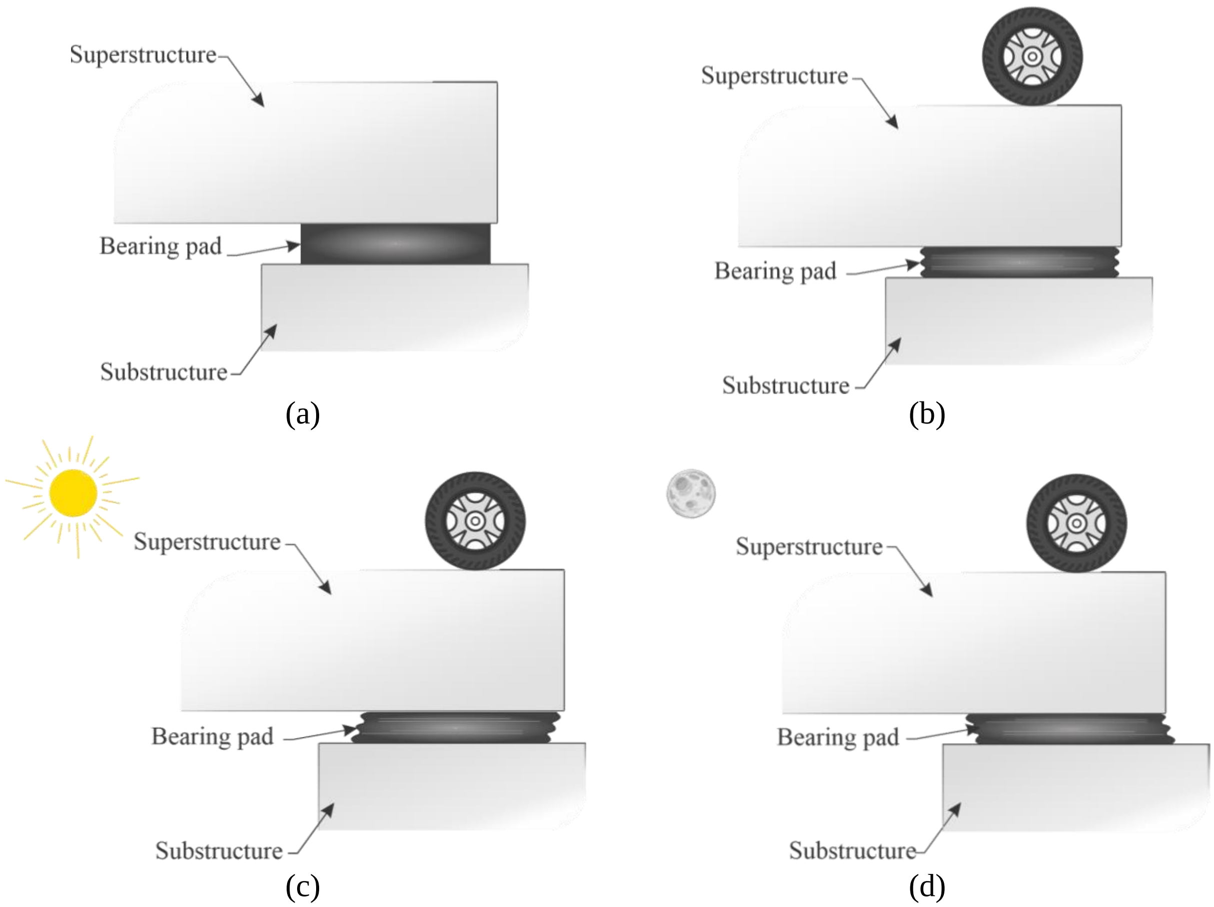

Figure 1-2 Bearing pad uses: (a) support superstructure on substructure; (b) distribute vertical load from superstructure to substructure; (c) accommodate thermal expansion of superstructure; (d) accommodate thermal contraction of superstructures

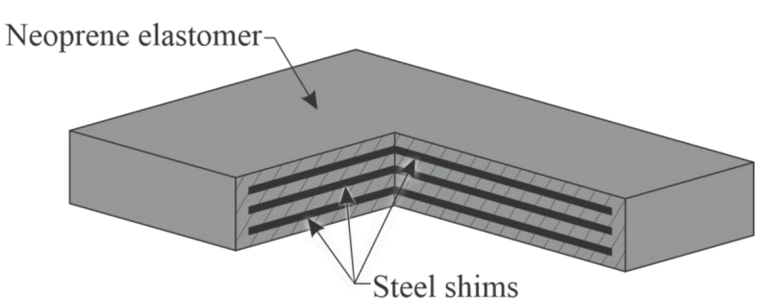

Figure 1-3 Steel-reinforced elastomeric bearing pad

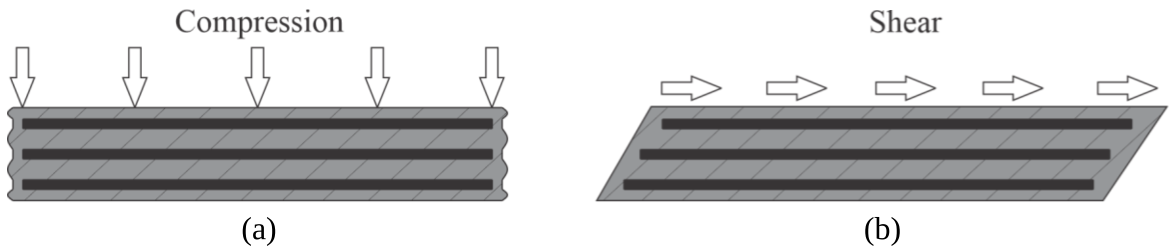

Figure 1-4 Bearing pads deformation modes: (a) Compression; (b) Shear

Elastomeric bearing pads are available in different shapes and sizes. Most commonly used elastomeric bearing pads include rectangular and circular. These pads can be directly placed on the pier top surface to support a horizontally aligned girder (Figure 1-5a). In the case of a girder at a slope, the bearing seat may be sloped, or a leveling shim may be inserted between a girder and bearing pad in order to minimize the slope mismatch between girder bottom flange and the bearing pad. The Florida Department of Transportation (FDOT) permits the use of flat pads for beams with grade less than 0.5%, but requires the use of sloped bearing seats for beam grades between 0.5% and 2% (Figure 1-5c). For beam grades greater than 2%, FDOT requires the use of leveling shims which introduce additional cost (Figure 1-5b). On the other hand, the slope mismatch can also be economically minimized by using tapered bearing pads (Figure 1-5d), which could minimize extra labor at the bridge construction site and allow quality to be be controlled during fabrication in the factory. However, after 1992, the American Association of State Highway and Transportation Officials (AASHTO, 2017) restricted the use of tapered bearing pads and therefore does not provide design guidelines for tapered pads. AASHTO states that tapered elastomer layers cause larger shear strains compared to uniform thickness elastomer layers, and that the larger strains can result in premature failure of a bearing pad (from delamination or rupture of reinforcing steel shims). However, experimental research funded by Texas Department of Transportation (Muscarella and Yura, 1995) demonstrated that tapered pads can be successfully used in bridges. As a result, the Texas Department of Transportation continued to use tapered bridge bearing pads even after the restriction imposed by AASHTO.

The goal of the present study was, therefore, to experimentally evaluate tapered bearing pad characteristics for use in Florida bridge construction. Pad characteristics that were investigated included axial stiffness, shear stiffness, horizontal deformation and restraining force in tapered pads under compression, and shear displacement at slip and coefficient of friction for tapered pads.

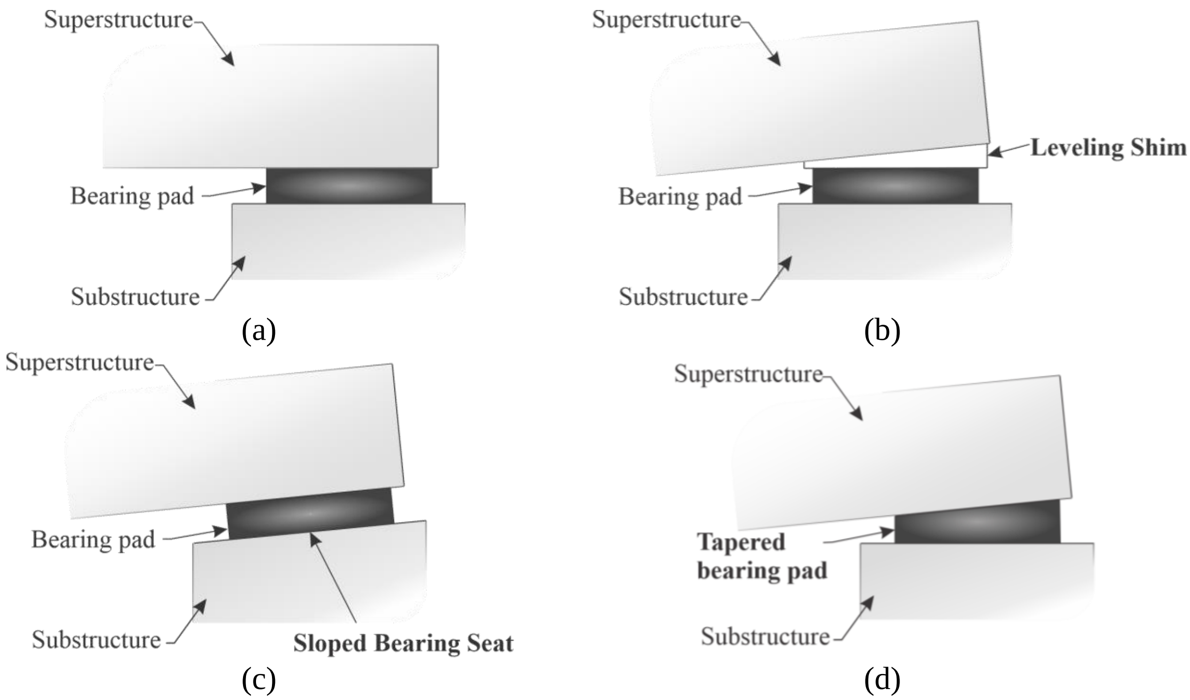

Figure 1-5 Bearing pad and bridge structure configurations using: (a) Flat bearing pad; (b) Leveling shim and flat bearing pad; (c) Bearing pad and sloped seat; (d) Tapered bearing pad

CHAPTER 2
LITERATURE REVIEW

2.1 Bridge bearing pads

The bearing pads tested in this study were rectangular neoprene elastomeric bearing pads. Such bearing pads consist of steel shims interlaced between layers of neoprene (Figure 2-1). Bearing pads have three basic modes of deformation including compression, shear and rotation (Figure 2-2). In the compression mode, the axial (compression) stiffness primarily depends on the properties and geometry of the elastomer layers. Elastomers are nearly incompressible (i.e., Poisson's ratio $\nu \cong 0.5$) and bulge when compressed. When elastomers are reinforced with steel shims, bulging (Figure 2-3) in the bearing pad is reduced as compared to plain unreinforced bearing pads. Steel shims are much stiffer than elastomer (i.e., nearly rigid in comparison) and restrain bulging of bearing pads when aligned horizontally along the plane of bulging (Hamzeh et al., 1998; Najm et al., 2002; Charles W. Roeder & Stanton, 1983; Soleimanlo & Barkhordar, 2013). As the number of shims increases, while maintaining a constant total thickness of elastomer, the axial stiffness increases due to decreases in the thicknesses of the individual elastomer layers (Muscarella & Yura, 1995). Conversely, as the thicknesses of individual elastomer layers decrease, the shear stiffnesses increase (Muscarella & Yura, 1995) and the effectiveness of a bearing pad to accommodate girder movements decreases.

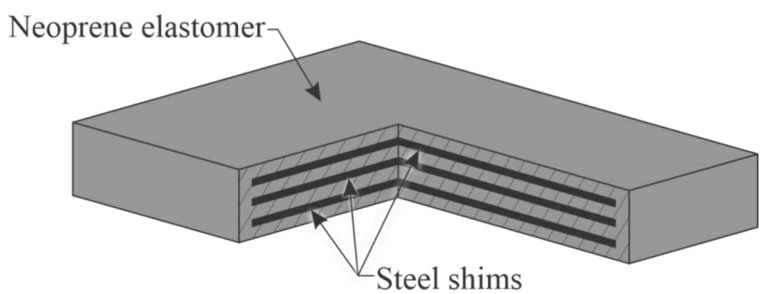

Figure 2-1 Steel reinforced neoprene elastomeric bearing pad

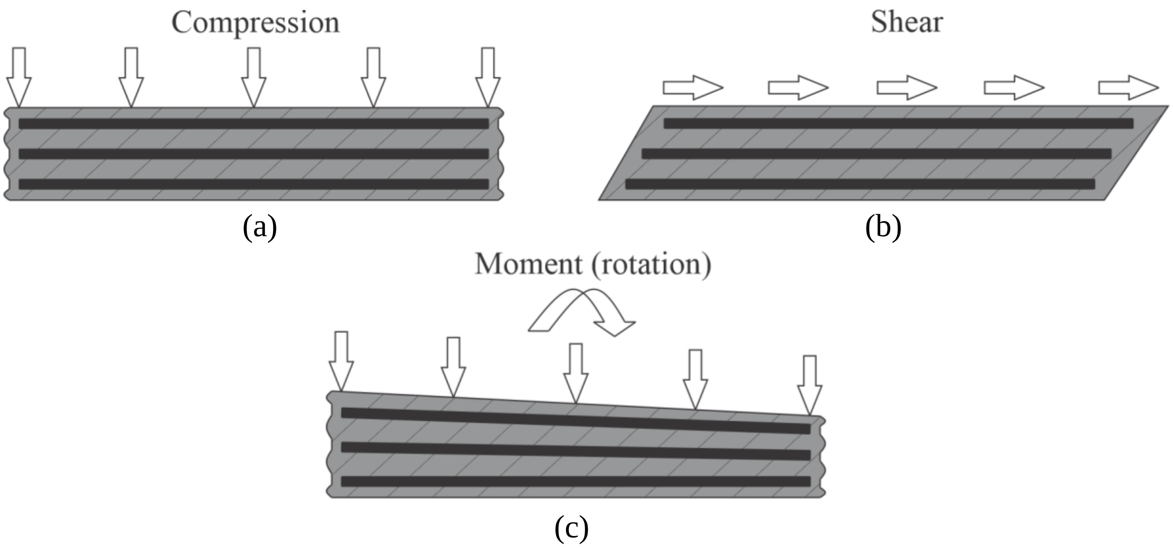

Figure 2-2 Bearing pads deformation modes: (a) Compression; (b) Shear; (c) Rotation

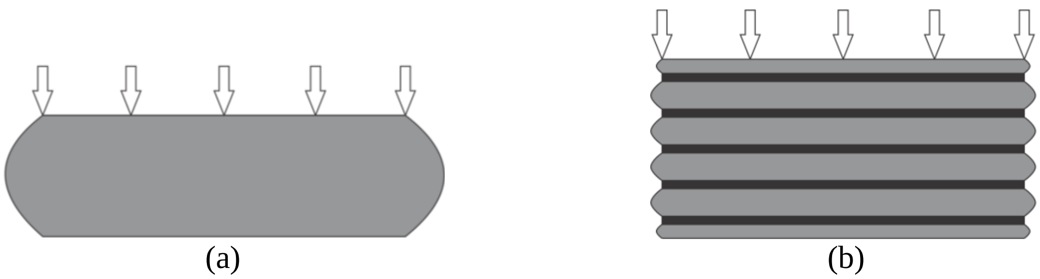

Figure 2-3 Bearing pad bulging: (a) without steel shims; (b) with steel shims

Neoprene is generally used in bridge bearing pads because it has better resistance to heat, flames, and ozone attack as compared to general purpose elastomers; neoprene also has better adhesion to metals and resistance to weathering (Gent, 2012). The molecular structure of elastomers consists of strong and weak polymer chains. Under large shear strains, the weak polymer chains tend to break, which results in reduced shear stiffness of elastomers in subsequent shear cycles at lower shear strain. This phenomenon is referred to as the Mullin's effect (Cantournet et al., 2009; Mullins, 1948). To remove the Mullin's effect, standard testing methods for determining shear stiffness and modulus of bearing pads include conditioning procedures in which large shear strain cycles are initially imposed on the test specimen before the final cycle used to determine stiffness; this process breaks the weak polymer chains that are found in newly fabricated bearing pads.

The behavior of a bearing pad can be controlled through appropriate selection of neoprene elastomer material and pad geometry. The American Association of State Highway and Transportation Officials (AASHTO, 2017) restricts the shear modulus of neoprene elastomer used in bridge bearing pads to between 80 psi and 250 psi. This restriction is imposed because neoprene elastomer materials with shear modulus over 250 psi generally fail at smaller shear strains, and have greater creep and stiffness as compared to softer neoprene. However, use of neoprene with a shear modulus of less than 80 psi may result in unfavorable driving conditions on a bridge due to excessive deformation at the girder supports.

Separate from material selection, the geometry of a bearing pad is controlled by adjusting the total elastomer thickness and the individual elastomer thicknesses. Total elastomer thickness is governed by the expected maximum horizontal deflection of the bridge superstructure, caused by thermal movement (expansion and contraction), creep, and shrinkage. AASHTO limits the shear strain in a bearing pad to 50% (i.e., $\gamma \leq 0.5$) because beyond 50% shear strain, the corners of bearing pads were found to 'roll' (Figure 2-4) and increase the risk of neoprene delamination from the steel shims (Pont 1959; Roeder et al., 1987). Consequently, total elastomer thickness should be more than twice the expected maximum horizontal deflection so as to keep the maximum shear strain under 50%. Further, individual elastomer layer thickness depends on the number of steel shims in a bearing pad. Thinner elastomer layers have higher axial stiffness than thicker elastomer layers, but can fail in shear either due to delamination from steel shims, or by rupture of the elastomer at a lower shear strain than in thicker elastomer layers. Therefore, bearing pad properties are influenced not only by elastomer shear modulus, but also by pad geometry, including total and individual elastomer layer thicknesses.

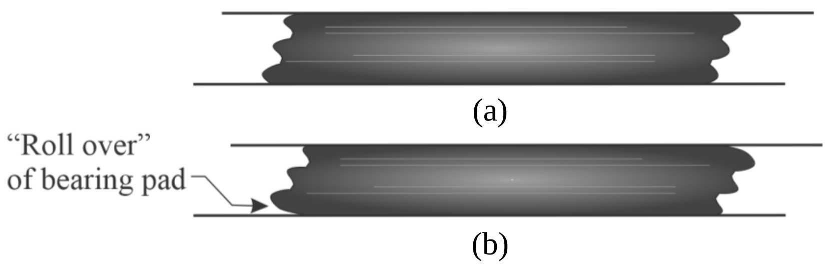

Figure 2-4 Typical shear deformation of an elastomeric bearing pad: (a) at shear strains (γ) less than 50%; (b) at shear strains greater than 50% (after Roeder et al., 1987)

Once the elastomer shear modulus and total elastomer thickness have been selected, the effect that individual elastomer layer thickness has on axial stiffness is determined by following an empirical approach. This approach was developed for flat bearing pads and utilizes the ratio of loaded area to the area free to bulge (Figure 2-5), for the thickest elastomer layer.

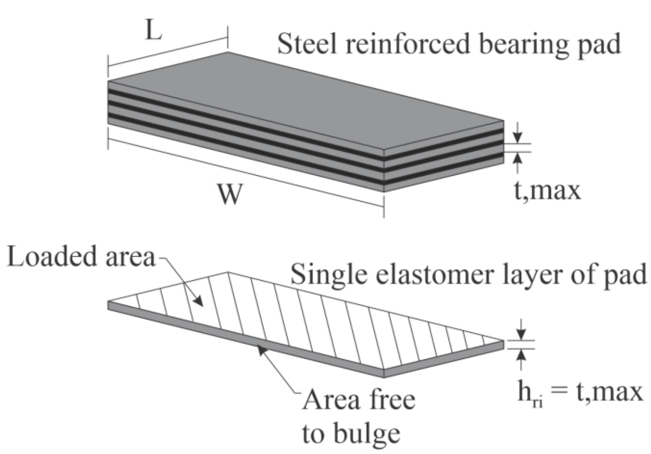

Figure 2-5 Bearing pad shape factor dimensions

The ratio is called the shape factor, S, and can be calculated as:

$$S_i = \frac{Loaded\ Area}{Perimeter\ Area\ Free\ to\ Bulge} = \frac{L \times W}{2\ h_{ri}(L+W)} \qquad (2\text{-}1)$$

for the i[th] layer of elastomer in a bearing pad. In Equation (2-1) L and W are the length and width of the pad, respectively, and h_{ri} is the thickness of i[th] layer of neoprene elastomer. For typical flat reinforced bearing pads, the shape factor is between 4 and 12 (Stanton et al., 1982). (Note that the shape factor is an empirical mechanism used for uniform thickness elastomer layers and was not developed for non-uniform thickness elastomer layers, as in the case of *tapered* bearing pads.)

Using the shape factor, the axial strain in a flat bearing pad may be computed as:

$$\varepsilon_a = \frac{\sigma_s}{3B_a G {S_i}^2} \qquad (2\text{-}2)$$

In Equation (2-2), σ_s is the sum of the static compressive stress and average cyclic compressive stress. The cyclic component is multiplied by 1.75 for applicable service load combinations. Cyclic loading shall consist of loads induced by traffic, and all other loads shall be considered to be static. The parameter G is the shear modulus of neoprene , and B_a is 1.6 for rectangular pads. However, B_a is based on work performed on flat bearing pads (Stanton et al., 2004).

AASHTO limits the combined effects of axial load, rotation, and shear (Figure 2-6) by limiting the values of shear strain that are generated by axial load, rotation, and shear forces. Shear strains due to axial load, rotation, and shear are calculated using Equations (2-3), (2-4) and (2-5) respectively and the combined effect is calculated using Equation (2-6).

$$\gamma_a = D_a \frac{\sigma_s}{GS_i} \leq 3.0 \text{ for static loading} \qquad (2\text{-}3)$$

$$\gamma_r = D_r \left(\frac{L}{h_{ri}}\right)^2 \frac{\theta_s}{n} \qquad (2\text{-}4)$$

$$\gamma_s = \frac{\Delta_s}{h_{rt}} \leq 0.5 \qquad (2\text{-}5)$$

$$(\gamma_{a,st} + \gamma_{r,st} + \gamma_{s,st}) + 1.75(\gamma_{a,cy} + \gamma_{r,cy} + \gamma_{s,cy}) \leq 5.0 \qquad (2\text{-}6)$$

In these equations, σ_s is the average compressive stress due to total static or cyclic load from applicable service load combinations, L (in.) is the plan dimension (Figure 2-7) of the bearing perpendicular to the axis of rotation under consideration (L is generally measured parallel to the direction of traffic), n is number of interior layers of elastomer (layers which are bonded on two faces), θ_s is the maximum static or cyclic service limit state design rotation angle of the elastomer, Δ_s is the maximum total static or cyclic shear deformation of the elastomer from applicable service load combinations, and D_a and D_r are constants. Similar to B_a in Equation (2-2), D_a and D_r are based on work performed for flat bearing pads (Stanton et al., 2004). Further, in Equations (2-2) to (2-5), the shape factor S and elastomer thicknesses h_{ri} and h_{rt} are defined for flat pads with uniform thickness elastomer layers. As noted previously, AASHTO restricts the use of tapered bearing pads due to larger shear strains in tapered layers and the potential for premature failure due to delamination or rupture of reinforcement. AASHTO does not therefore provide equations for the design of tapered pads. However, experimental research funded by Texas Department of Transportation (Muscarella & Yura, 1995) on tapered bearing pads did not indicate failure of tapered bearing pads during standard shear modulus testing.

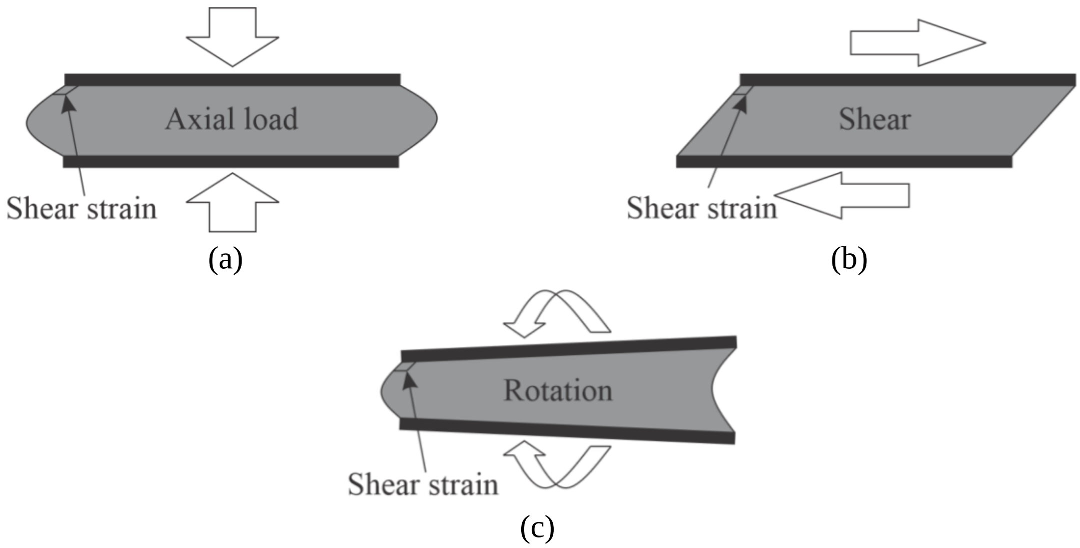

Figure 2-6 Shear strain in bearing pad due to: (a) axial load; (b) shear; (c) rotation

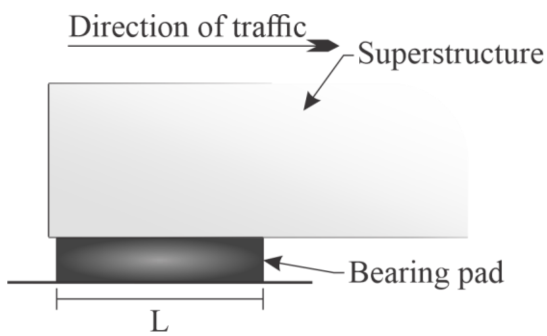

Figure 2-7 Bearing pad orientation

2.2 Past experimental studies on bearing pads

The compression behavior of flat bearing pads has been found to be dependent on the effective compression modulus. The effective compression modulus (E_c) considers additional restraint against bulging provided by steel shims in a bearing pad and can be calculated for flat bearing pads using the Equation (2-7) provided by Gent (2012):

$$E_c = \frac{G(1 + \alpha S^2)}{2(1 + \nu)} \tag{2-7}$$

In this equation, G is the elastomer shear modulus, α is an empirically determined constant, S is the shape factor of the thickest elastomer layer in the bearing pad, and ν is Poisson's ratio. Similar relationships between E_c, G and S were also provided by Podolny et al. (1982) and Stanton et al.

(2004). Therefore, the effective compression modulus increases as the shape factor of bearing pads increases (Arditzoglou et al., 1995; Gent, 2012, Pinarbasi et al., 2004; Roeder et al., 1987). The E_c for flat bearing pads also increases as shear modulus (G) increases (Arditzoglou et al., 1995; Soleimanlo & Barkhordar, 2013). However, no relationship is presented in the literature for tapered bearing pads.

Muscarella & Yura (1995) performed experimental tests on tapered bearing pads and concluded that the effect of taper on compression modulus depends on the shape factor and the elastomer hardness. Figure 2-8 compares flat and tapered bearing pads with 3 and 6 steel shims, where the total elastomer thickness was consistent regardless of number of shims. In order to maintain a consistent total thickness of elastomer, the overall thickness of the bearing pad with 6 shims was increased by 0.3 in., to account for the thickness of the additional 3 shims. It was observed that the compression modulus of a 3-steel shim tapered bearing pad decreased by only 1.5% when compared to a flat pad with the same reinforcing (steel shim) configuration. The compression modulus of a tapered bearing pad with 6-steel shims decreased by 11.3% when compared to a flat pad of the same reinforcing configuration, with the tapered pad being less stiff axially. Moreover, it was also reported that axial stiffness decreased as the bearing pad slope increased from 4% to 6%. However, Muscarella and Yura did not provide a direct relation between E_c, G and S for tapered pads.

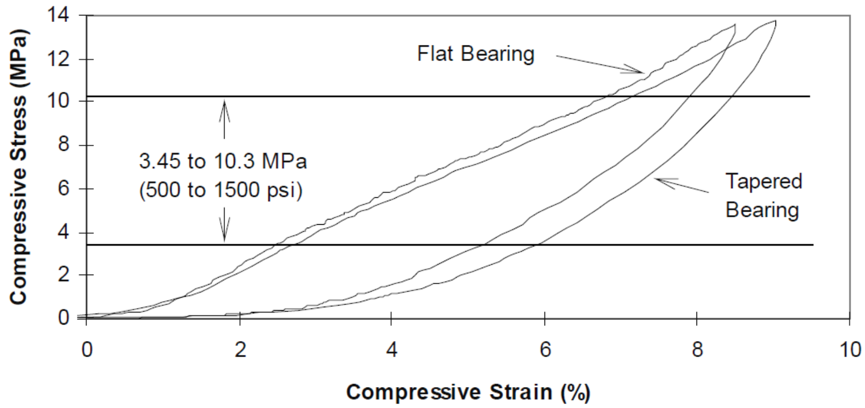

(a)

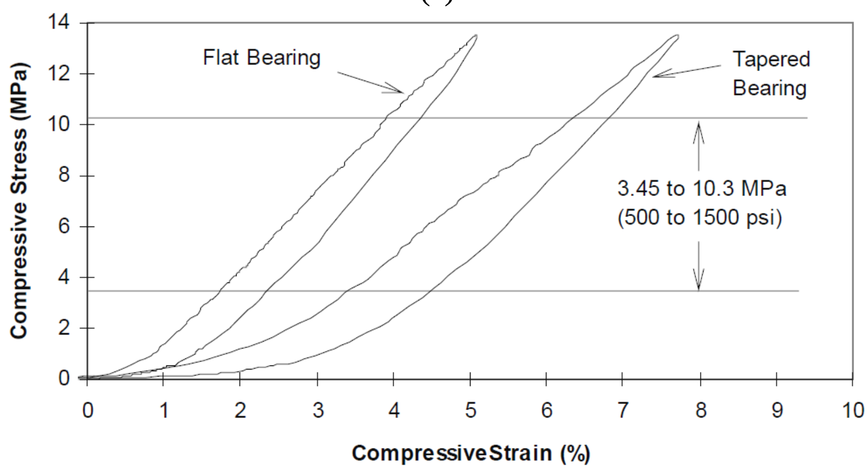

(b)

Figure 2-8 Stress-strain diagrams for flat and taper bearings (Muscarella and Yura, 1995): (a) 3-steel shims and (b) 6-steel shims

Muscarella & Yura (1995) investigated the compression behavior of tapered pads with steel shims placed in two different alignments: steel shims placed radially in the pads (Figure 2-9a); and steel shims placed horizontally (Figure 2-9b). The experimental results showed that the difference between axial deformation of bearing pads with parallel and radial alignment increased with increase in compression load, where pads with parallel alignment had marginally more axial deformation than pads with radial alignment. The percentage difference between axial deformation of pads with parallel and radial shims was reported to increase from 2.6% to 6.7% as the compression load increased from 500 psi to 1500 psi (typical load range for bearing pads).

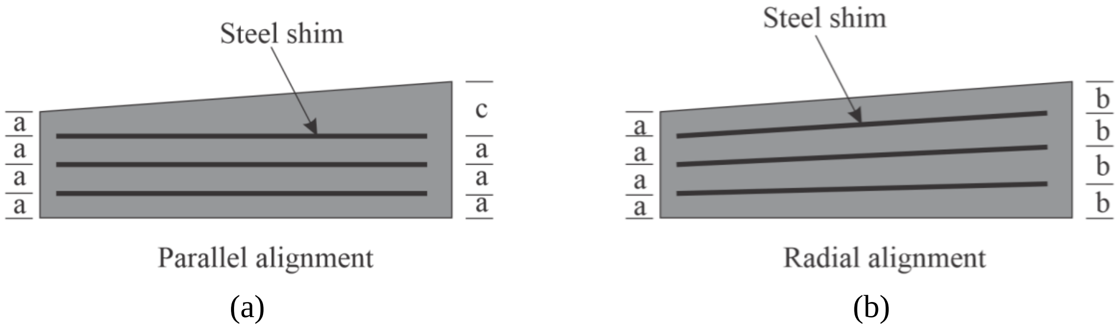

Figure 2-9 Steel shim arrangement: (a) parallel; (b) radial

Elastomeric bearing pad shear stiffness is the primary property that resists horizontal movement of girders due to thermal expansion and contraction. From a stress-strain perspective, shear stiffness is dependent on the shear modulus of the elastomer, which depends on the amount of filler that is present in the elastomeric compound during manufacturing (Arditzoglou et al., 1995). Fillers, typically carbon black, are small hard particles and are used in bearing pads to modify the hardness and stiffness of the elastomer. Shear and compressive moduli increase, and the elongation at failure decreases as the amounts of filler added to an elastomer increase. Past studies (Cook & Allen, 2009; Muscarella & Yura, 1995) have shown that shear stiffness can vary with changes of compressive stress, shear rate, and temperature. In NCHRP Report 298, Stanton and Roeder (1982) presented a relationship that expressed shear stiffness dependency on compressive strain. The relationship considered the increased shear area, caused by bulging, and the decreased height due to compression. According to this relationship, the shear force required for a particular shear displacement increased with an increase in compression strain. The compression strain in a tapered pad is not uniform due to non-uniform elastomer layer thicknesses, which could result in different apparent shear moduli depending on direction of shear movement. A relationship for shear modulus dependence on direction of shear movement in tapered pads was not found in literature. Nevertheless, Muscarella and Yura (1995) observed that alignment of shims did not influence the shear modulus of a tapered bearing pad.

Muscarella and Yura (1995) also studied the horizontal deflection and force generated in tapered pads under pure compression. Horizontal deflection (ΔH) is generated in tapered bearing pads (Figure 2-10) due to non-uniform layer thickness of the pad and P-Δ effect. Conversely, if this horizontal deflection is restrained, then horizontal force is generated. The ratio of horizontal force (H) to the compression force (P) was found to be approximately $0.392 \cdot \theta$, where θ is the slope (%) of tapered pad (Equation (2-8)).

$$\frac{H}{P} = 0.392 \cdot \theta \tag{2-8}$$

Muscarella and Yura reported that horizontal deflection was predicted using Equation (2-9).

$$\Delta_{total} = \frac{\Delta_{initial}}{1 - \frac{P}{P_{cr}}} \tag{2-9}$$

In this equation, P is the applied compression load on the bearing pad, P_{cr} is critical buckling load for a bearing pad, and $\Delta_{initial}$ is the initial horizontal deflection. Critical buckling load is the compression load at which a bearing pads fail due to instability rather than material rupture. Initial horizontal deflection was calculated using the Equation (2-10)

$$\Delta_{initial} = \frac{H \cdot h_{rt}}{G \cdot A} \tag{2-10}$$

However, the error between predicted and actual horizontal deflections increased from ±15% to ±50% as the number of shims increased from 3 to 6. Muscarella and Yura tested tapered pads with steel shims aligned either radially or horizontally (parallel). It was reported that pads with radial shim alignment produced 40% more horizontal displacement under pure compression load as compared to pads with parallel shim alignment.

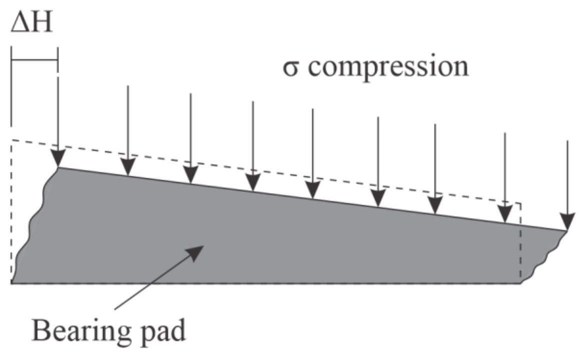

Figure 2-10 Horizontal deflection in tapered bearing pad under axial compression

In prior studies, slipping was found to be one of the failure modes for bearing pads (Chen, 1995; English et al., 1994; Fu and Angelilli, 2007). Fu and Angelilli (2007) and Muscarella and Yura (1995) conducted several field studies where bearing pads were found to ‘walk out’ primarily due to excretion of wax used in bearing pads manufactured from natural rubber. To avoid this problem, synthetic elastomers, such as neoprene, are instead predominantly used for manufacturing bridge bearing pads. Additionally, several researchers have found bearing pad slippage could be prevented if the shear stress was limited to one-fifth (0.2) of the compressive stress. That is, if the coefficient of friction between a bearing pad and the bearing surfaces was at least 0.2 (Muscarella and Yura, 1995; Pont, 1959; Stanton and Roeder, 1982), slip should not occur.

CHAPTER 3
SPECIMEN MATRIX

The configurations of the tapered pads tested in this study were developed by modifying elastomer thicknesses and shim orientations of standard flat pads. In Florida, various standard flat pad types are available for use in bridge construction (FDOT, 2016). Standard pads are labeled alphabetically (A, B, C, D, through K) and vary in terms of parameters including plan dimensions, thickness, shear modulus, number of shims and load carrying capacity. To evaluate the effect of taper on bearing pad characteristics with widely ranging parameters and to optimize this study, pad types E, F and K (Table 3-1) were selected. After selection, tapered versions of pad types E, F, and K were developed. In tests conducted by Muscarella and Yura (1995), bearing pads typically slipped at a shear strain equal to 1.5. During the test-planning phase, it was not known whether equipment at the FDOT structures research center had sufficient capacity to load standard FDOT pads to a shear strain of 1.5. Therefore, along with full-size (i.e., standard size) FDOT bridge bearing pads, half-size bearing pads of types E and F were also included in the specimen matrix to ensure that coefficient of frictions could be quantified. Each half-size bearing pad had a width equal to half that of the corresponding full-size (i.e. standard size) pad.

Table 3-1 Standard bearing pad types selected for testing (FDOT, 2016)

Bearing pad type	Plan dimensions (Length in. x width in.)	Shear modulus (ksi)	Number of shims
Full-size type E	10 x 32	110	3
Full-size type F	10 x 32	110	4
Full-size type K	12 x 32	150	6
Half-size type E	10 x 16	110	3
Half-size type F	10 x 16	110	4

Three bearing pad manufacturers were contacted regarding fabrication of tapered bearing pads. Each manufacturer responded that taper in pads can be introduced by varying pad thickness from end to end of the pad in multiples of $^1/_8$ in. or $^1/_{16}$ in.; however, a preference for increments of $^1/_8$ in was indicated. The manufacturers also noted that multiple layers of neoprene can be varied to create the desired tapered, and AASHTO M251 (2016) and FDOT (2018) fabrication tolerances would be followed in tapered pad fabrication. Based on the earlier work of Muscarella and Yura (1995), as well as discussions with current manufacturers of bearing pads, it was determined that taper would be incorporated into bearing geometry by changing the thickness of the pads in integer increments (N) of $^1/_8$ in. (Figure 3-1). Accordingly, tapered pads were produced by modifying flat pad thicknesses in multiples of $^1/_8$ in. along the length axis. The average thickness of each tapered pad was the same as the thickness of the original flat pad. Steel shims in tapered pads were aligned parallel to the bottom surface except for the top-most shim which was inclined such that the elastomer thickness above and below the shim was equal at any section transverse to the slope (Figure 3-1).

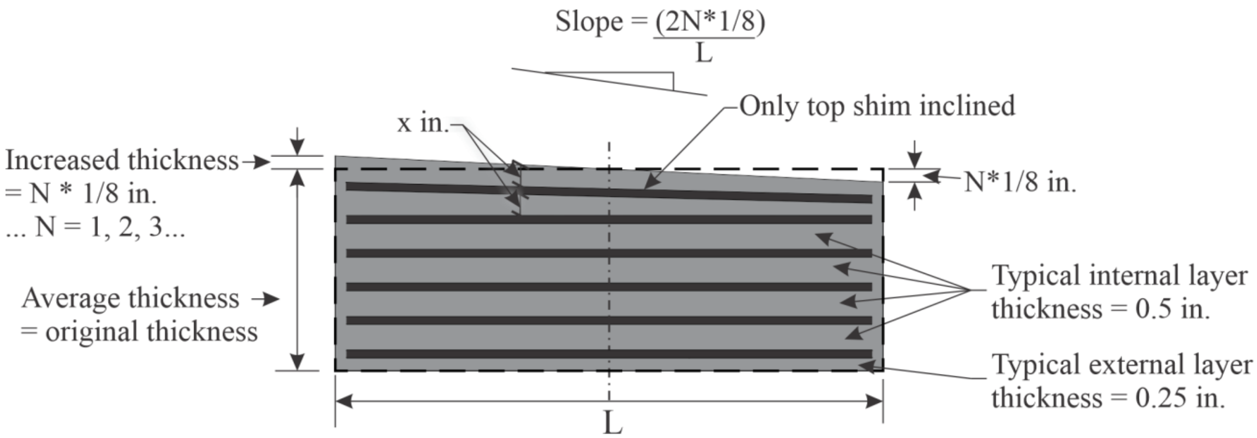

Figure 3-1 Bearing pad slope and shim configuration

Proposed Guidelines for Pedestrian Facilities in the Public Right-of-Way (United States Access Board, 2011), section R302.5, specifies a maximum slope of 5% for pedestrian access routes on highways. Further, Muscarella and Yura (1995) recommended that taper be limited to a maximum of 5%. Accordingly, for the present study, Florida Department of Transportation (FDOT) standard (flat) bearing pad types E, F and K were modified to incorporate slopes with up to two increments (N) of $^1/_8$ in. (maximum slope of 5%) as shown in Table 3-2. Appendix A provides detailed shop drawings for all bearing pad types that were tested. In the following text, each configuration of pad is assigned a name of the form “pad type-slope%”. For example, FDOT pad type E with a taper slope of 2.5% is assigned the name “E-2.5%”. As per the material certificates provided by the manufacturer, the properties of the elastomer and steel shims satisfied the material-related requirements specified by Florida test method 5-598 (FDOT, 2012) and AASHTO M251 specification (AASHTO M251-06, 2016).

Table 3-2 Slope in tapered bearing pads

Bearing pad type	L (pad dimension parallel to direction of traffic) (in.)	Slope (%)		
		N = 0	N = 1	N = 2
E	10	0	2.5	5.0
F	10	0	2.5	5.0
K	12	0	2.1	4.2

CHAPTER 4
EXPERIMENTAL TEST SETUP

An experimental test setup was designed to test a pair of matching bearing pads simultaneously and under different axial load levels. In general, the test setup consisted of a horizontally oriented hydraulic actuator (MTS, model 244.41) connected to a wide flange (W) steel section support at one end and to a middle plate assembly at other end (Figure 4-1a). The test setup further consisted of a stack of two bearing pads (of identical type), each inserted between the middle plate assembly and two steel bearing plates. To simulate typical field conditions, the bearing pads, middle plate assembly and steel plates were not mechanically connected, but instead relied solely on friction to transfer shear force between the pads and plates. A vertically oriented hydraulic actuator (Enerpac, model RR-40018) was used to load the top bearing plate to compress the pads. A horizontal actuator—connected to the middle plate assembly—was used to shear the pads at the interface between middle plate assembly and bearing pads. While shearing the pads, the axial load was maintained constant using a fine adjustment control on the vertical actuator operated by a technician. The axial load was maintained within approximately ±5 kip of the target load for each test. For tests involving tapered pads, the middle plate assembly was modified by inserting wedge plates with varying slopes (Figure 4-1b). Four square hollow structural section (HSS) steel 'arms' provided connections between the bearing plates (top and bottom) and the wide flange (W) section (Figure 4-1a). The assembly consisting of the four HSS sections and the horizontal actuator formed a self-reacting load frame within which the forces required to shear the pads remained internal to the load frame and did not generate horizontal reactions on the laboratory floor.

The vertical elevations of the top and bottom HSS arms, along with the top and bottom bearing plates, were changed between tests to accommodate pad types with different thicknesses. The top and bottom arms had multiple connection points available on the wide flange section to accommodate different pad types (Figure 4-2). The top arm was engaged in one hole at a time on the wide flange section to create a pinned connection, and the bottom arm was engaged in two holes at the same time to create a rigid connection. After connecting the arms to their respective connection points for a pad type, and applying axial load, the top arm and horizontal actuator rotated such that both the arms and the horizontal actuator were in horizontal alignment. Simultaneously, the top bearing plate and the middle plate assembly rotated to maintain both pads in horizontal alignment. The elevation of the bottom bearing plate was adjusted for different pad types by inserting steel filler plates of appropriate thicknesses underneath the plate. Details of test setup fabrication are presented in Appendix B.

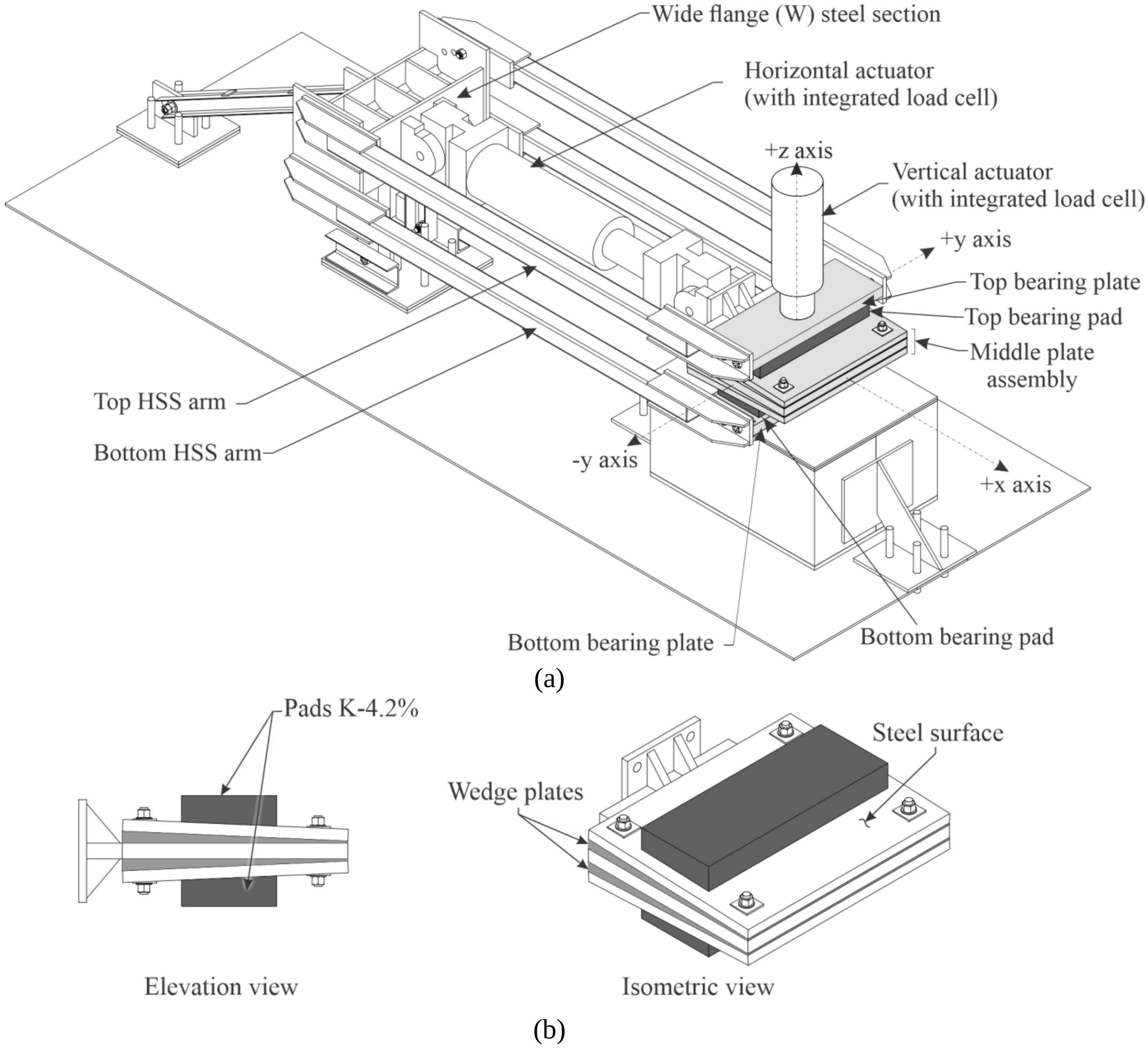

Figure 4-1 Test setup (shown configured for pad K-4.2%):
(a) Isometric view; (b) Middle plate assembly

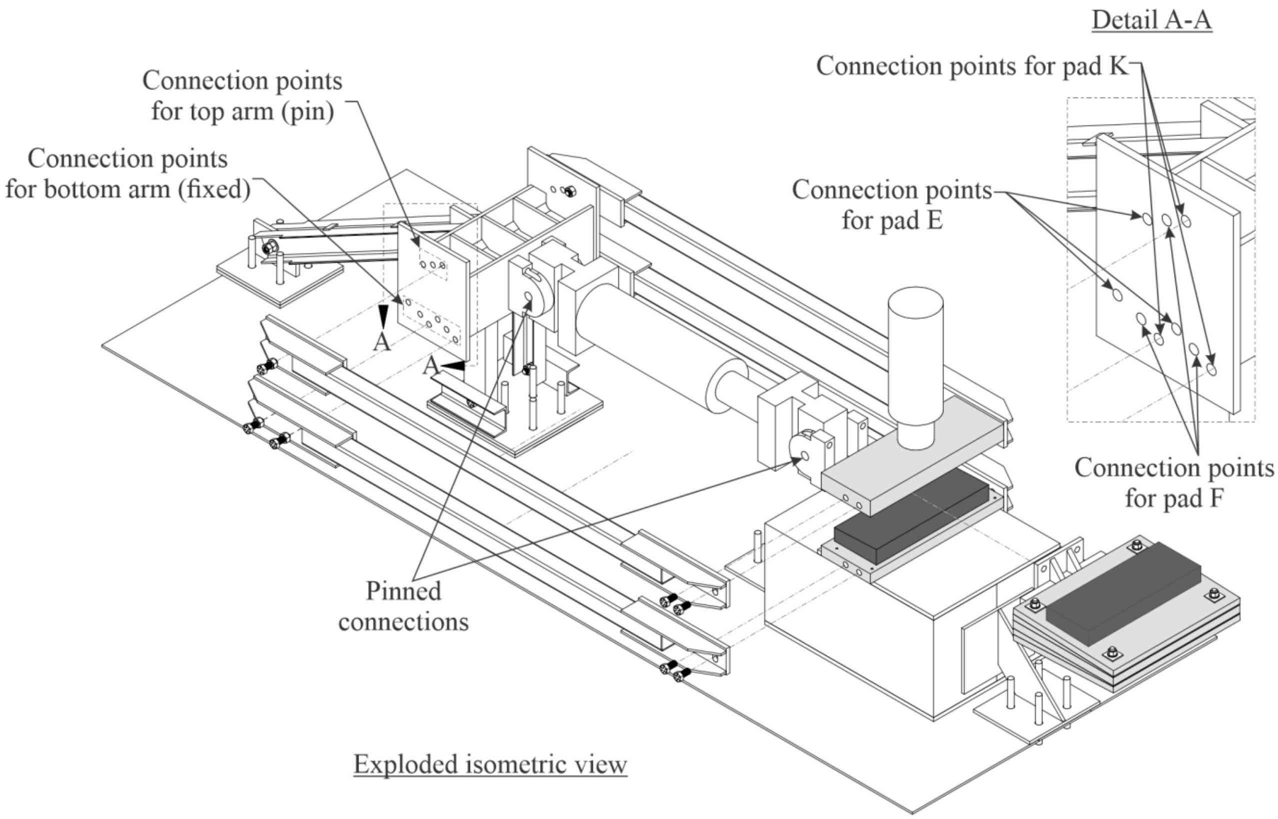

Figure 4-2 Exploded isometric view of test setup (shown configured for pad K-4.2%)

A counterweight-balance mechanism was introduced in the setup to suspend (i.e., 'float') nearly all of the weight of the horizontal hydraulic (MTS) jack so as to minimize rotation of the middle plate assembly that would have been caused by self-weight of the MTS jack. Figure 4-3 shows a schematic diagram of the counterweight-balance mechanism. Components of the mechanism included two 12 in. dia. x 48 in. long sonotubes, concrete fill, 0.5 in. dia. x 5 ft. long threaded rods, turnbuckles, 6x19 wire rope (¼ in. dia. x 100 ft. long), and suspension pulleys.

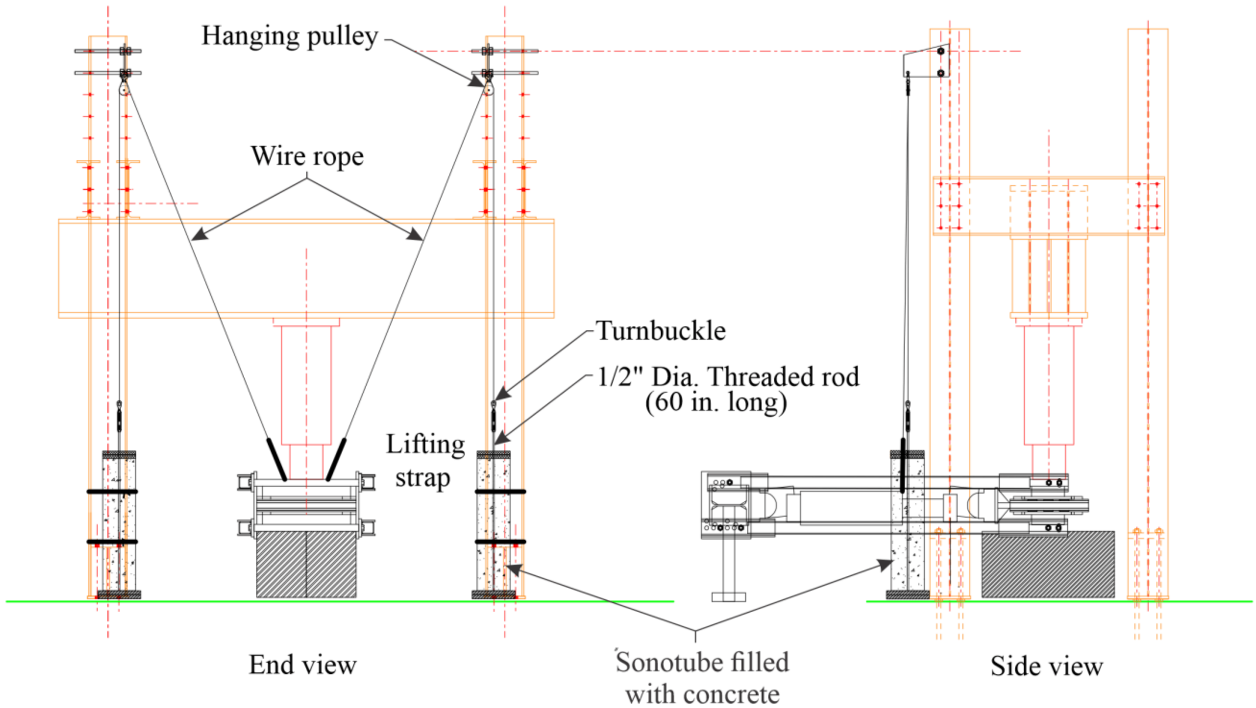

Figure 4-3 Schematic of counterweight-balance mechanism

The HSS arms and the frame support end assembly were initially designed and fabricated using standard 1/16 in. oversized holes for inserting 1.25 in. diameter bolts. During initial bearing pad shear tests, the gaps between the bolts and oversized holes were found to cause small horizontal movements in the top HSS arms and the top steel bearing plate. These movements led to undesirable horizontal forces being exerted on the vertical actuator (Enerpac) and resulted in minor hydraulic oil leakage. Further testing in this manner could have posed the risk of damaging the actuator seals. To minimize the potential for damage to the vertical actuator, the test setup was retrofitted after about one-quarter of the total number of tests were performed. Note that the test data collected were not deemed to be affected by the retrofit.

Part of the retrofit consisted of adding 4 in. x 3 in. x 1 in. thick steel plates to the ends of the upper HSS arms at the bearing pad end (Figure 4-4). Each retrofit plate included a 1.25-in. dia. (non-oversized) hole. The new plates were welded to the existing HSS end plates such that the 1.25-in. dia. holes were concentric with the existing non-slotted oversized holes. Introduction of the retrofit plates minimized the gaps between bolts and holes at the bearing pad end of the setup, and in turn, minimized the horizontal movement of the top plate with respect to the top HSS arms.

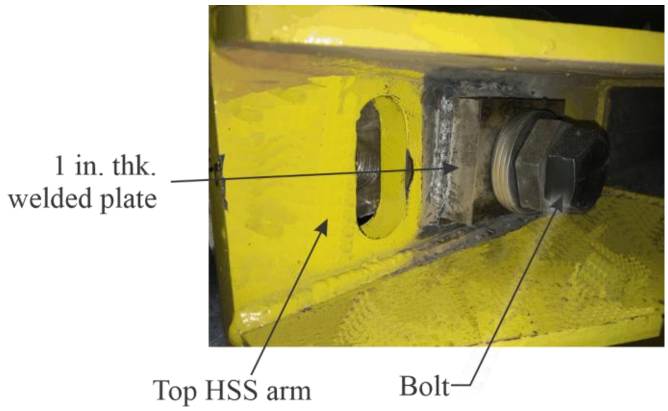

Figure 4-4 HSS arm retrofit (bearing pad end)

To reduce the movement of the top HSS arms with respect to the support end assembly, stainless steel tapered pins were fabricated to match the diameter of the existing holes (1.3125-in. diameter). The pins were held in place using clamping shaft collars (Figure 4-5).

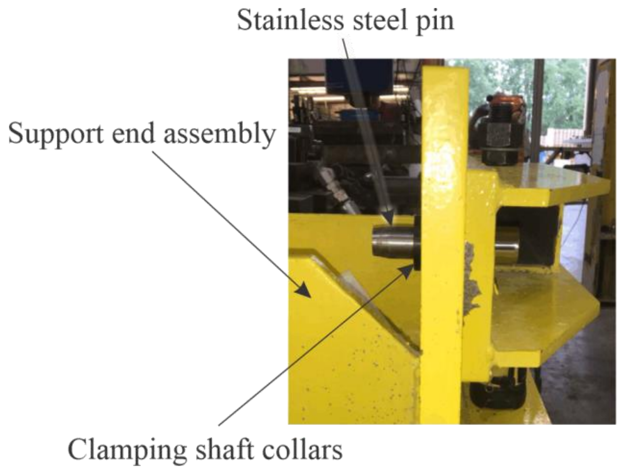

Figure 4-5 HSS arm retrofit (support end)

In order to further isolate the base of the vertical actuator from any remaining horizontal movement of the top steel bearing plate, a 10 in. x 20 in. x 2 in. thick isolation bearing pad and one or two 1.5-in. thick steel plates were placed between the top steel bearing plate and the actuator base (Figure 4-6). During testing of E and F pads, two steel plates were used, and during testing of K-pads, one steel plate was used. The isolation (non-tested) bearing pad allowed the top plate to move in the horizontal plane without generating significant horizontal force on the vertical actuator. Figure 4-7 shows a photo of the test setup after completion of fabrication. Appendix C provides detailed fabrication drawings of the test setup, including the retrofit.

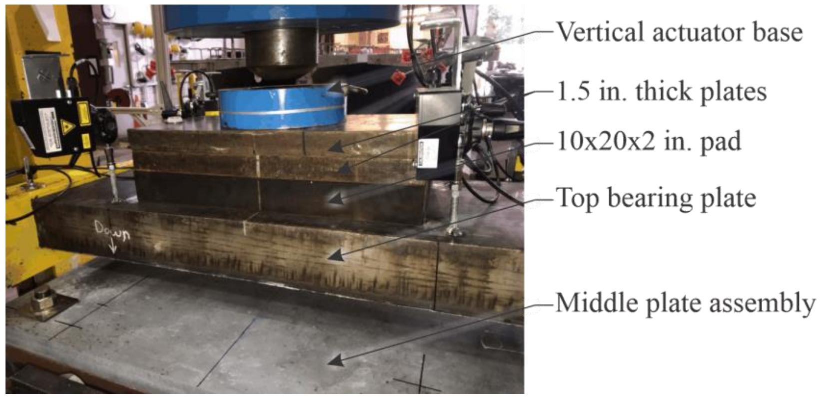

Figure 4-6 Isolate pad used in retrofit

Figure 4-7 Completed bearing pad test setup
(FDOT Structures Research Center, Tallahassee, Florida)

Test instrumentation measured forces and displacements at various locations. Load cells integrated into the vertical actuator (Enerpac) and horizontal actuator (MTS) were used to measure axial and shear loads, respectively. Six laser displacement sensors (MTI Microtrak 3 Series, model LTS 300-200, labeled as 'DX' in Figure 4-8) were used to measure shear displacements of the top and bottom bearing plates relative to the middle plate assembly, thus enabling determination of shear deformations in the bearing pads. Shear displacement of the top pad was calculated as the relative difference between the average displacement of the top plate and the average displacement of the middle plate. Similarly, shear displacement of the bottom pad was calculated as the relative difference between the average displacement of the bottom plate and average displacement of the middle plate. Eight additional laser displacement sensors (MTI Microtrak 3 Series, model LTS 300-200, labeled as 'DZ' in Figure 4-8b) were used to measure compression displacement in the top and bottom bearing pads. The top plate and the middle plate had four DZ sensors connected on each. The average measurement of the four DZ sensors on top plate provided compression displacement in top pads, and the average measurement of the four DZ sensors on the middle plate provided compression displacement in the bottom pads.

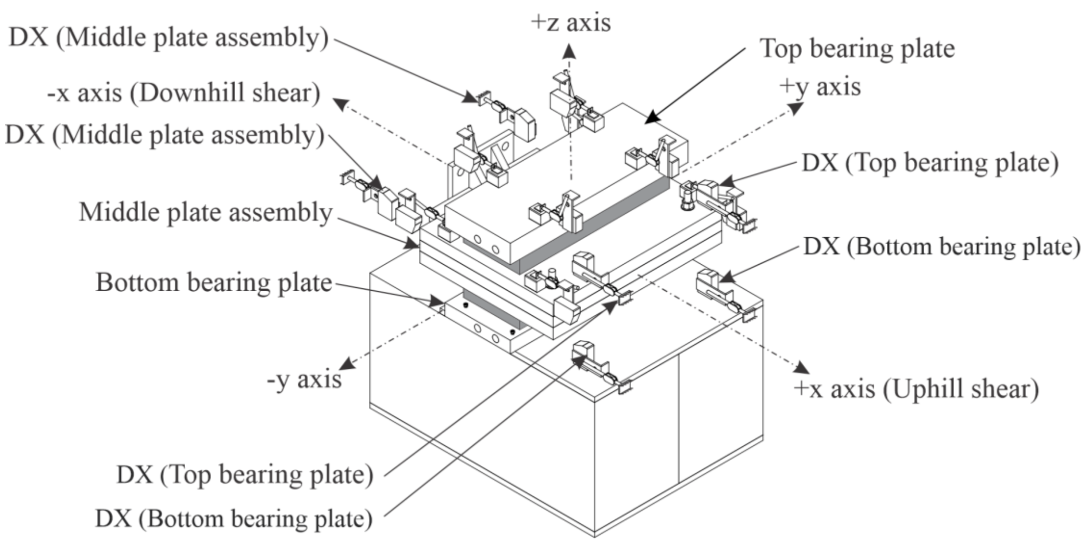

(a)

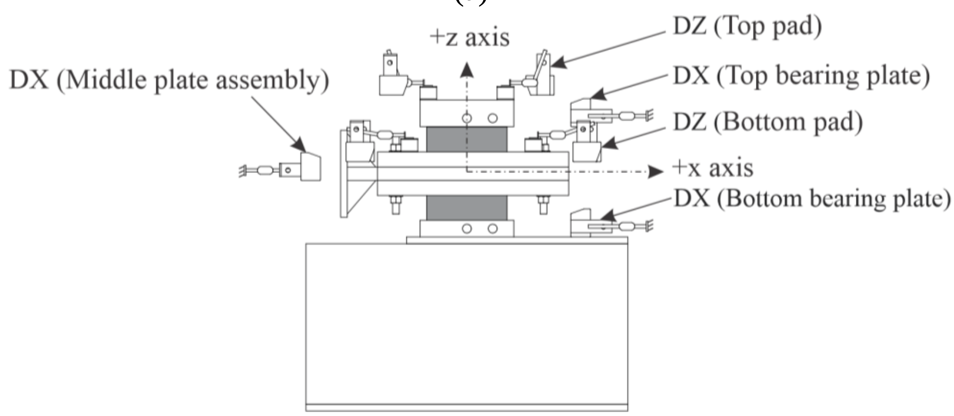

(b)

Figure 4-8 Laser sensors instrumentation plan:
(a) Isometric view; (b) Elevation view

CHAPTER 5
TEST PROCEDURES

Experimental testing objectives included quantifying: axial and shear stiffnesses; horizontal deflections and horizontal forces in tapered pads under compression load; shear displacement at slip; and bearing pad frictional coefficients for various surface conditions and axial load levels. To achieve these objectives, test procedures were performed on at least one pair of pads of each type and slope. Appendix D provides a detailed test matrix, which includes the types of pads tested and a list of test procedures performed on each pad type. Appendix E provides plots of the data collected during each test. The procedures for testing bearing pads consisted of performing four load tests, which are described in the following sections.

5.1 Axial stiffness test

For determination of axial stiffness, bearing pads were axially loaded in increments of one-fifth of the maximum design load, and at a rate specified as per the procedure for compression testing in ASTM D4014 – 03 (ASTM International, 2018) Standard Specification for Plain and Steel-Laminated Elastomeric Bearings (Figure 5-1). The maximum load, selected to be the sum of dead and live loads, was determined from the FDOT Instructions for Design Standards (IDS) Index no. 20510: Composite Elastomeric Bearing Pads - Prestressed Florida-I Beams (FDOT, 2016). Each increment of load was applied over a range of time between 1.4 to 2.6 minutes in duration, and the load was maintained constant for 30 seconds between each increment.

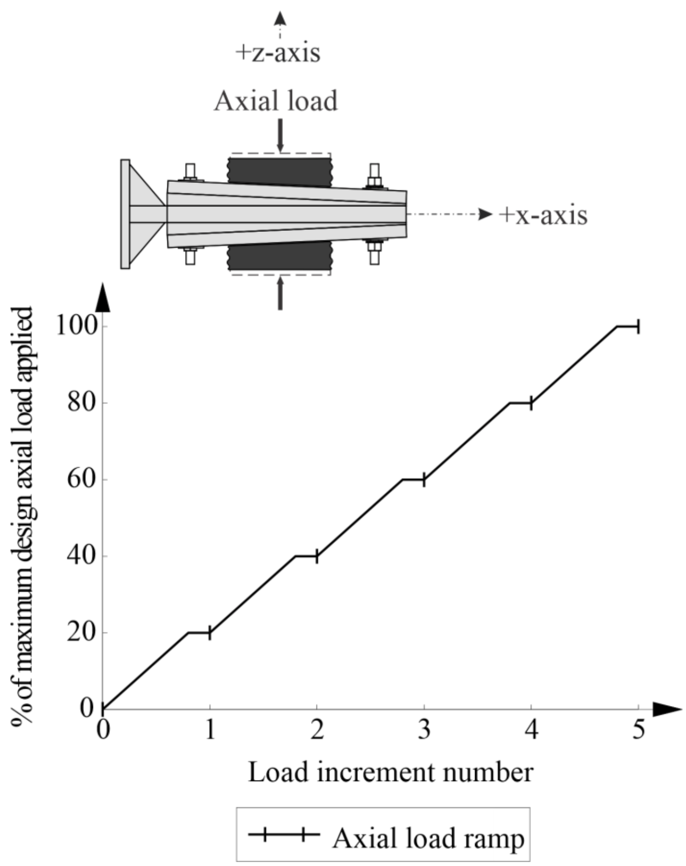

Figure 5-1 Loading for axial stiffness tests

5.2 Horizontal displacement test

Tapered bearing pads displace in the horizontal direction when axial load is applied (Figure 5-2). This horizontal displacement was quantified for tapered pads by measuring the horizontal displacement of the middle plate assembly while applying axial load during the axial stiffness test procedure described in Section 5.1. To quantify horizontal displacement, the middle plate assembly was disconnected from the horizontal (MTS) actuator and allowed to deflect freely in the horizontal direction.

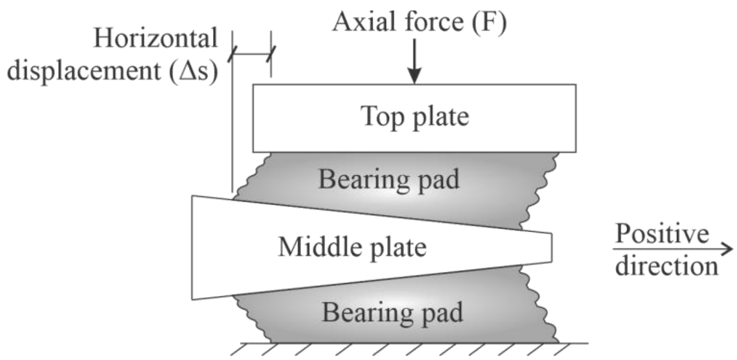

Figure 5-2 Schematic of horizontal displacement in pads during testing

5.3 Horizontal restraining force test

When the horizontal displacement of tapered pads under axial load is prevented, a horizontal restraining force is produced by the pads. This horizontal restraining force was determined by applying axial load on pads while restraining horizontal displacement of the middle plate using the horizontal actuator in the test setup (Figure 5-3). Similar to the axial stiffness test, the axial load was applied at the rate specified as per the procedure for compression testing in ASTM D4014 – 03, but without the pauses. For time efficiency, this test was combined with shear stiffness and slip tests, and was performed during the axial loading ramp stage of these tests.

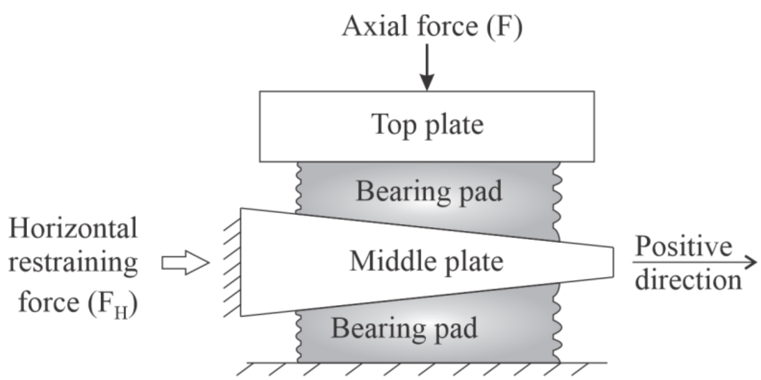

Figure 5-3 Schematic of horizontal restraining force (F_H) in pads during testing

A load cell, integrated into the horizontal actuator, was used to measure the horizontal force. Two additional tests were performed on selected pads, in which the horizontal force was measured using rod end cells (REC15K), with higher accuracy compared to the load cell in horizontal actuator. These supplementary tests confirmed that the horizontal actuator load cell was capable of measuring forces with the accuracy necessary for this study.

5.4 Shear stiffness test

The shear stiffness test included application of axial load, followed by shearing of the 'stack' that consisted of two identical pads and the middle plate assembly (Figure 5-4). During each test, pads were shear loaded and released over six cycles in the negative shear direction, where the first five cycles of $\gamma = 0.7$ shear strain were used to condition the pads, and the sixth cycle of $\gamma = 0.5$ shear strain was used to determine the shear stiffness (Figure 5-5). Note that, in this test setup, positive shear strain was defined as strain applied when the horizontal actuator piston was extended, and negative shear strain was defined as strain applied when the actuator piston was retracted. Select pairs of tapered bearing pads were also tested in the positive shear direction (Figure 5-6) to investigate whether the direction of shear loading (and deformation) would result in differences of pad shear stiffness. Both the test procedure and selection of shear strain levels were based on ASTM D4014 – 03 Standard Specification for Plain and Steel-Laminated Elastomeric Bearings for Bridges (ASTM International, 2018) and Florida method 5-598 of Test for Evaluation of Bearing Pads (FDOT, 2012). As per ASTM D4014 – 03, each cycle for testing shear stiffness was performed within a timeframe of 30 to 60 seconds. Figure 5-7 shows photos of pads K-0% and K-4.2% during shear testing.

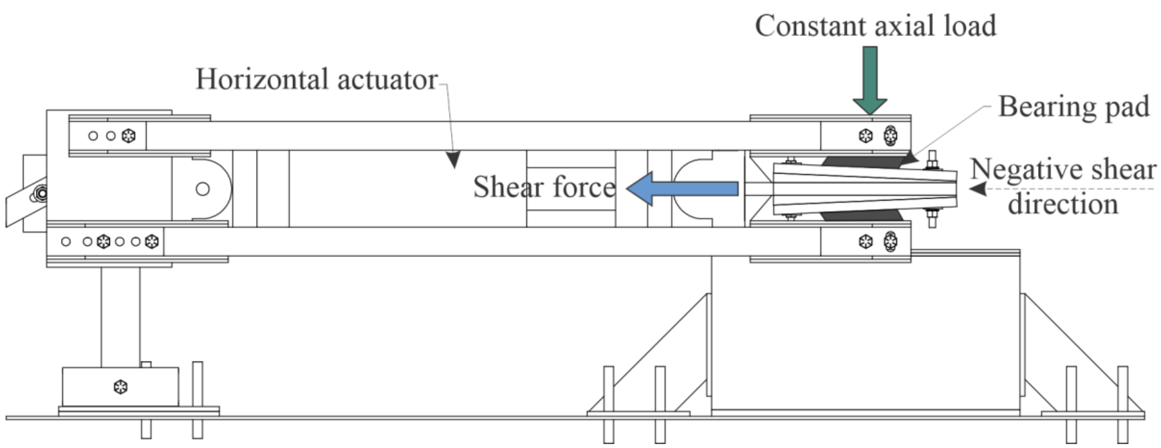

Figure 5-4 Schematic of shear stiffness test (negative shear strain shown)

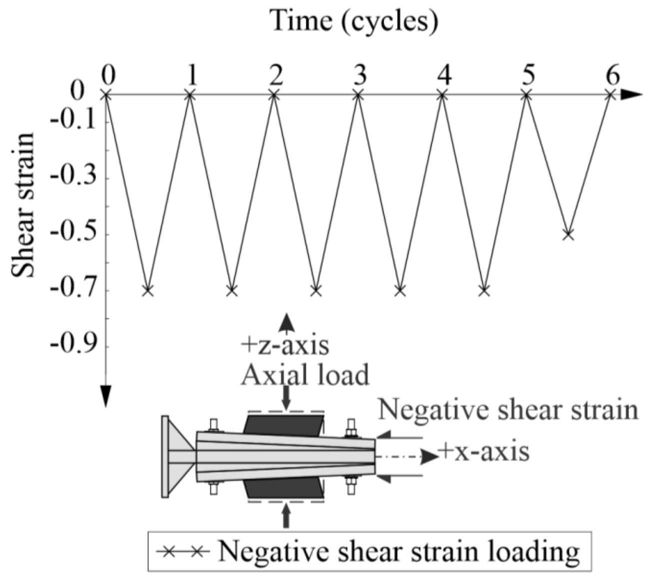

Figure 5-5 Negative shear strain loading and release cycles for shear stiffness test

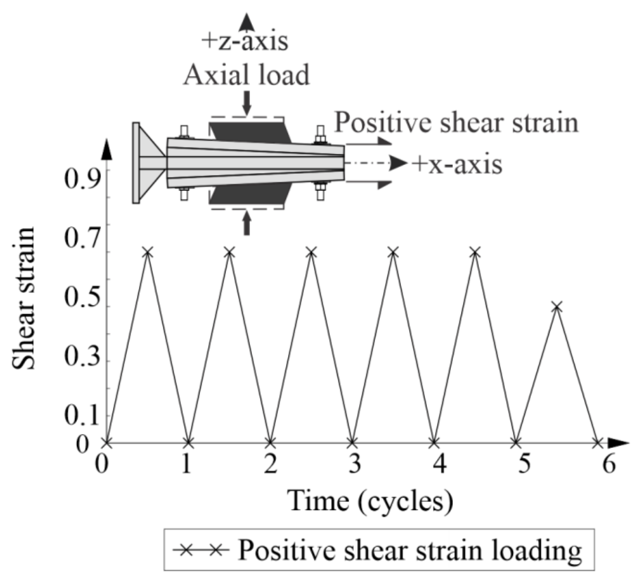

Figure 5-6 Positive shear strain loading and release cycles for shear stiffness test

(a) (b)

Figure 5-7 Pads under negative shear strain loading: (a) Pads K-0%; (b) Pads K-4.2%

During the shear tests, a constant axial load was maintained on the pads by monitoring and adjusting the vertical actuator. Minimum and maximum axial load levels were determined for each bearing pad type, where the minimum axial load represented bridge dead load acting on the pads, and the maximum load represented the sum of dead and live loads on the pads. These axial load levels (Table 5-1), were determined from the FDOT Instructions for Design Standards (IDS) Index no. 20510: Composite Elastomeric Bearing Pads - Prestressed Florida-I Beams (FDOT, 2016). Shear stiffnesses were measured at both minimum and maximum axial load levels.

Table 5-1 Minimum and maximum axial loads selected for testing

Pad type	Size	Minimum axial load (kip)	Maximum axial load (kip)
E	Full	110	380
F	Full	140	440
K	Full	390	590
E	Half	55	190
F	Half	70	220

5.5 Slip test

Slip tests were performed in two stages—shear loading stage, and axial unloading stage—to determine shear displacement (or strain) at slip, and the coefficient of friction, respectively. In the shear loading stage of each slip test, the bearing pads were sheared at a target displacement rate of 0.001 in/sec, under constant axial load, until the pads were considered to have slipped (Figure 5-8). Pads were considered to have slipped, and slip tests were terminated, when the rate of change in shear force required to shear the pad dropped to approximately 0.001 kip/sec. The axial load was kept constant by continuously monitoring and adjusting of the vertical actuator.

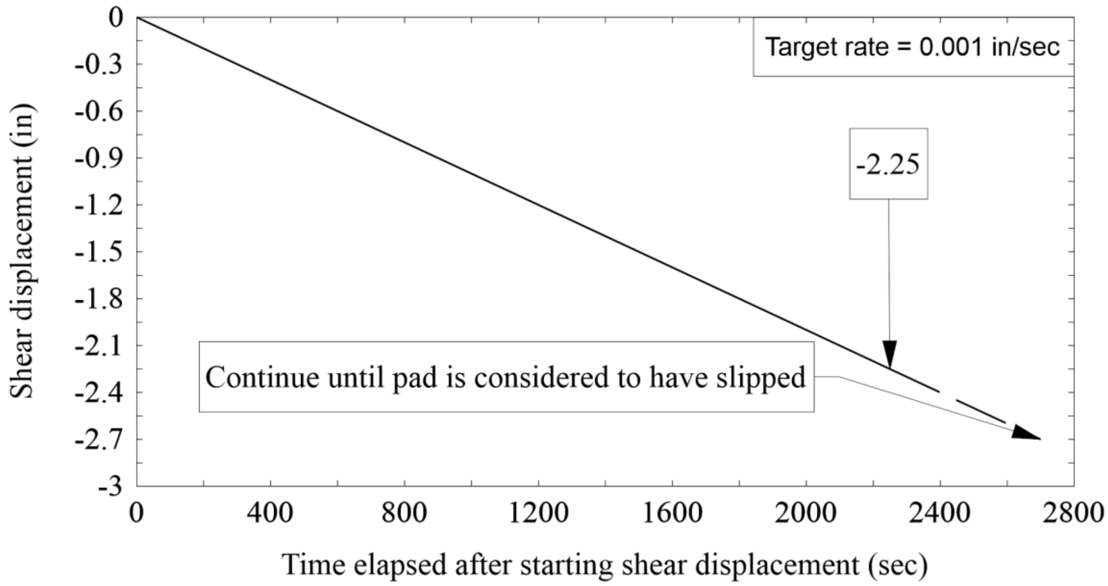

Figure 5-8 Shear displacement ramp during the shear loading stage in slip test

At the end of the shear loading stage, the middle plate assembly and horizontal actuator were fixed in the latest position, and the axial unloading stage was initiated after the force in the horizontal actuator had stabilized. (Horizontal force was assumed to have stabilized when the rate of change in force dropped below 0.015 kip/sec). During the axial unloading stage, axial load was gradually decreased in order to quantify the coefficient of friction (μ). The axial unloading load rate was the same as the axial loading rate, determined as per ASTM D4014 – 03. The shear force acting on the bearing pads (measured by the horizontal actuator load cell) was continuously recorded during release of the axial load. The coefficient of friction was determined as the ratio of shear force to axial force at the point when slip was determined to have occurred. (The procedures used to determine the occurrence of slip are detailed later in this report.)

Slip tests were performed on every type of pad (recall Table 3-1) under dry steel and dry concrete surface conditions. Slip tests were also performed on selected types of pads under wet steel and wet concrete surface conditions. To produce the wet steel surface condition, the steel surfaces on the middle plate assembly in contact with the bearing pads were saturated with water using wet paper rags (Figure 5-9a). Similarly, the bearing pad surfaces, which were in contact with the middle plate assembly, were saturated with water using wet paper rags (Figure 5-9b). The wet concrete surface condition was produced by saturating the concrete surface of the middle plate assembly under wet burlap for at least 12 hours before the testing day (Figure 5-10), followed by application of additional water using wet paper rags before each wet condition test. Slip tests were performed at both the minimum or maximum axial load levels, and were performed for all pad types in the negative shear strain direction. Select pads were also tested for slip in the positive shear direction to evaluate the effect of shear direction on slip behavior of tapered pads.

(a) (b)

Figure 5-9 Wet conditioning of: (a) steel surface; (b) pad surface

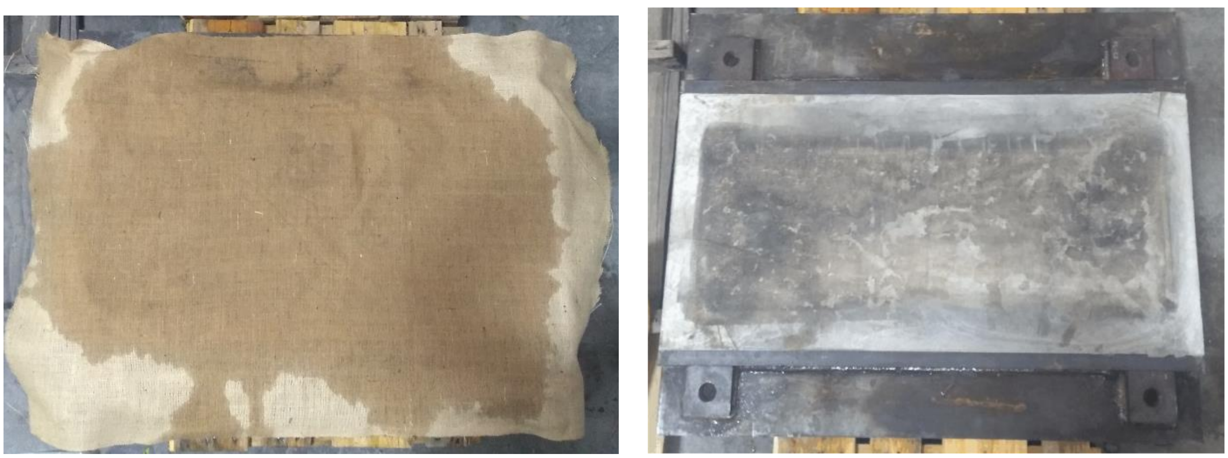

(a) (b)

Figure 5-10 Wet conditioning of concrete surface plate: (a) wet burlap placed on the concrete surface; (b) concrete surface after saturation

CHAPTER 6
TEST RESULTS

Data collected during experimental testing was analyzed to determine tapered bearing pad characteristics including axial stiffness, shear stiffness, horizontal displacement and restraining force under compression, shear displacement at slip, and coefficient of friction. The following subsections describe in detail analysis procedures used, and results obtained, for the different pad characteristics. Appendix E provides plots of data collected during each bearing pad test.

6.1 Axial stiffness test data

Axial stiffness test data consisted of axial force (F) applied on the bearing pads and the resulting compression in pads (δ) (Figure 6-1). Data corresponding to only the loading part of the test were extracted for each test. For example, Figure 6-2a shows the complete (loading and unloading) data for pad E-2.5% test 57A and Figure 6-2b shows only the loading data for test 57A. Data for top and bottom pads were averaged for each test and the average was used for further analysis.

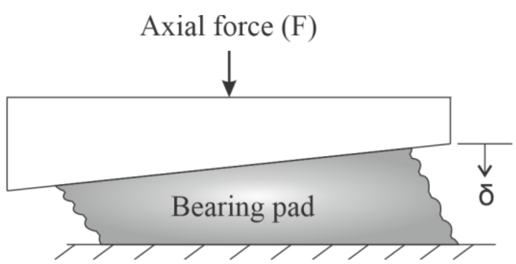

Figure 6-1 Compression of bearing pad

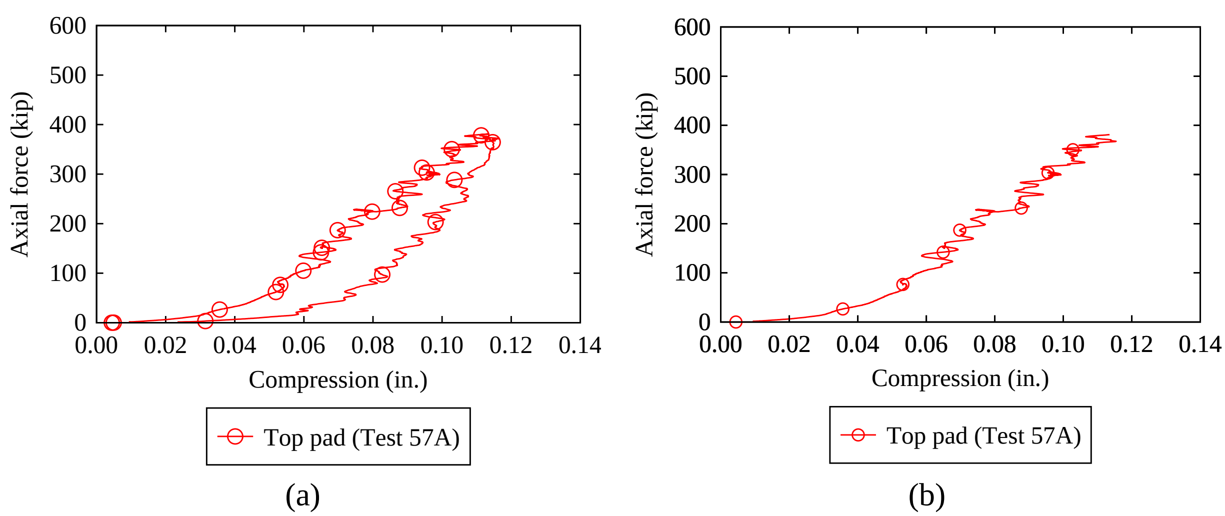

Figure 6-2 Axial stiffness test data for full-size pad E-2.5%:
(a) load and unloading parts; (b) only loading part

The initial slope of the data for each axial stiffness test was lower than the slope of the overall linear curve fit (for example see Figure 6-3a). The lower initial slope was due to experimental take up in the test setup which corresponded to closing of gaps between different parts of the setup. Data corresponding to the initial take up stage was removed prior to calculating axial pad stiffness. To remove the initial take up data, a reference slope was first calculated as the best (least square error) linear curve fit to the loading stage data ranging from one-half of maximum axial load to maximum axial load (i.e. the last half of the data set). For example, in Figure 6-3a, the reference slope based is 4143 kip/in. Next, over several iterations, successive linear curve fits were computed for the entire loading stage data set, but with incrementally larger portions of the initial data removed at each iteration. Once the slope of the fit was within 1% of the reference slope, removal of initial take up data ended. Figure 6-3 shows an example of this procedure. At each iteration, after removing initial take up data, the remaining data were shifted along x-axis such that the linear curve fit of the data would pass through the origin (Figure 6-4). This procedure was carried out repeatedly using data from every axial stiffness test.

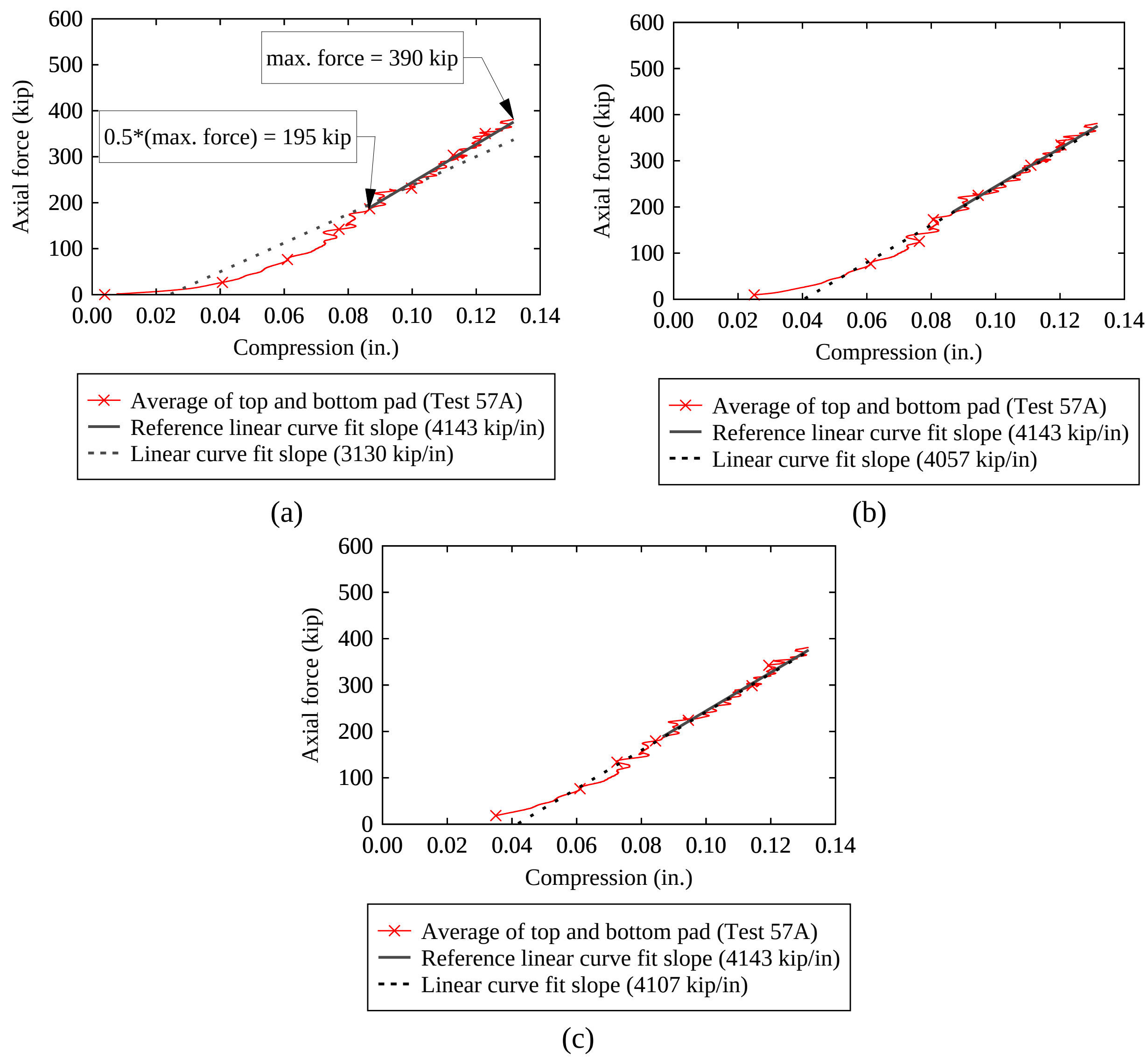

Figure 6-3 Removal of initial data for a full-size pad E-2.5% test 57A:
(a) Iteration 1; (b) Iteration 2; (c) Iteration 3

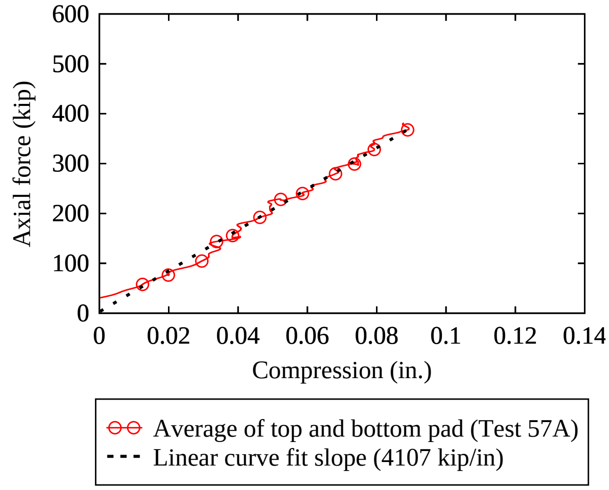

Figure 6-4 Processed axial stiffness data for full-size pad E-2.5% test 57A

The processed axial stiffness test data were then analyzed to study the effect of taper on axial stiffness of pads with different characteristics. The axial stiffness (kip/in) of elastomer layers in a bearing pad can be approximated using Eqs. 6-1, 6-2 and 6-3 (Stanton et al., 2004).

$$k_n = \frac{l \cdot w}{h_{rn}} \cdot 3 \cdot G(1 + B_a S^2) \tag{6-1}$$

$$B_a = (2.31 - 1.86 \cdot \lambda) + (-0.90 + 0.96 \cdot \lambda) \cdot \left(1 - \min\left(\frac{w}{l}, \frac{l}{w}\right)\right)^2 \tag{6-2}$$

$$\lambda = S \cdot \sqrt{\frac{3G}{K}} \tag{6-3}$$

Where, k_n, h_n, l, w and S are axial stiffness, thickness, length (excluding side cover), width (excluding side cover) and shape factor of the n^{th} elastomer layer in a pad, K and G are the shear and bulk modulus respectively of elastomer material, B_a is an empirical constant and λ is the compressibility index. A value of 200 ksi for K was used as recommended by Gent (2012) and Harper and Consolazio (2013). Eqs. 6-1 to 6-3 are applicable to flat, uniform thickness elastomer layers.

In order to include the influence of slope on axial stiffness of a tapered elastomer layer, Eqs. 6-1 and 6-2 were modified to Eqs. 6-4 and 6-5, respectively.

$$k_n = (1 - \alpha\Phi_n)\frac{l \times w}{h_{rn}} \cdot 3G(1 + B_a S^2) \tag{6-4}$$

$$B_a = \omega_1 + (\omega_2 \cdot \lambda) \cdot \left(1 - \min\left(\frac{w}{l}, \frac{l}{w}\right)\right)^2 \tag{6-5}$$

In Eq. 6-4, the term α was added to account for the influence of taper angle Φ_n (radians) in a tapered elastomer layer. Note that Φ_n is half of the total taper angle of pads (θ radians) as defined in this report. Further, Eq. 6-2 was modified into Eq. 6-5 to include empirical terms ω_1 and ω_2 which are applicable for both flat and tapered elastomer layers. Values of the empirical constants α, ω_1 and ω_2 were obtained by optimizing (minimizing) the error between Eqs. 6-4 and 6-5 and the processed data from *all* axial stiffness tests. By solving for the constants α, ω_1 and ω_2 that minimized the cumulative (or 'global') error across *all* available axial stiffness tests, a generalized fit to the data was obtained. This is in contrast to individually fitting α, ω_1 and ω_2 to each test, then attempting to compute averaged values of these constants. This latter approach would have resulted in a less accurate representation of the global set of data collected during axial stiffness testing, and would not have produced a fit that generalized well across various combinations of pad geometric parameters (dimensions, slope) or properties.

The global optimization (i.e., error minimization) process used to obtain the generalized fit for axial stiffness involved, as a starting point, the calculation of axial stiffness of each pad using Eq. 6-6 (elastomer layers in series):

$$k_{pad} = 1 \Big/ \left(\sum_{i=0}^{n} \frac{1}{k_i}\right) \tag{6-6}$$

Axial force (F) was then calculated for varying axial compression (δ) values using Eq. 6-7:

$$F = k_{pad} \times \delta \tag{6-7}$$

and compared with δ values from the processed axial stiffness data for every test. Using an iterative process, the root mean square (RMS) error between the calculated and experimentally measured values of F for all tests was determined for varying values of empirical constants α, ω_1 and ω_2. After optimization, values of the generalized empirical constants, which produced the minimum RMS error, were determined (Table 6-1). Based on the value of α, every percent increase in taper angle will reduce the axial stiffness of a tapered elastomer layer by a factor of 0.21 compared to the stiffness of a flat layer with the same average thickness and plan view dimensions. Note that, based on the value of α, Eq. 6-4 is valid for values of Φ_n between 0% and 4.76% because that is the range of slopes which were tested.

Table 6-1 Optimized values of the empirical constants

Empirical constant	Value
α	0.21
ω_1	1.62
ω_2	-3.83

The axial stiffness of each pad type was calculated using the optimized values of empirical constants and Eqs. 6-4 – 6-6. In Table 6-2, these calculated axial stiffness values were compared to the average axial stiffness values experimentally measured for each pad type. Note that the experimentally measured axial stiffness for each test was determined as the linear curve fit slope of the processed test data. The average of percentage difference between calculated and measured stiffness with respect to measured stiffness presented in Table 6-2 was approximately -2%.

Table 6-2 Comparison of calculated and measured axial stiffness

#	Pad type	Slope (%)	Size	Calculated stiffness (kip/in)	Measured stiffness (kip/in)	% difference between calculated and measured stiffness
1	E	0	Half	2245	2096	7
2		0	Full	4554	5680	-20
3		2.5	Half	2184	2014	8
4		2.5	Full	4309	4330	0
5		5	Half	1678	1384	21
6		5	Full	3289	4338	-24
7	F	0	Half	1560	1636	-5
8		0	Full	3261	4385	-26
9		2.5	Half	1531	1641	-7
10		2.5	Full	3133	3940	-20
11		5	Full	2557	3094	-17
12	K	0	Full	4195	3855	9
13		2.1	Full	4155	3275	27
14		4.2	Full	3776	3272	15

6.2 Horizontal displacement test data

Horizontal displacement data consisted of horizontal pad displacements (Δ_s) measured as axial pad force was increased (Figure 6-5). For example, Figure 6-6 shows the loading portion of horizontal displacement test data collected for full-size pad E-2.5%. Horizontal displacement was determined to be a function of three key factors: axial force (F in kip), bearing pad shear stiffness (k_s in kip/in) and bearing pad taper angle (θ in radians).

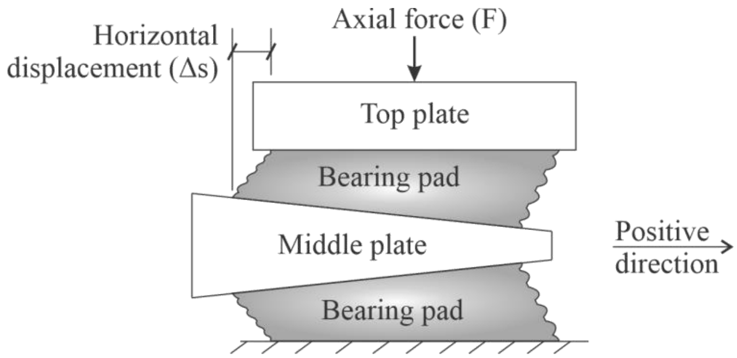

Figure 6-5 Schematic of horizontal displacement in pads during testing

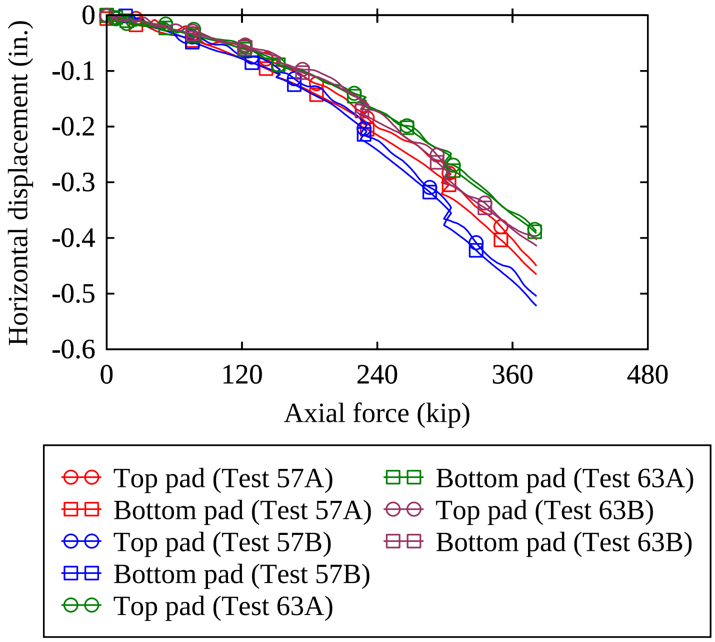

Figure 6-6 Measured horizontal displacement data for full-size pads E-2.5%

In order to quantify horizontal displacement based on these three factors, Eq. 6-8 was used:

$$\Delta s = \frac{\alpha_{hd} \cdot F \cdot \theta}{k_s} \tag{6-8}$$

where α_{hd} is a horizontal displacement fitting parameter. The shear stiffness, k_s, was calculated using Eq. 6-9, where G_{eff} is effective shear modulus. G_{eff}, calculated using Eq. 6-10, varied based on the applied axial force and buckling load for a pad (Gent, 1964; Muscarella & Yura, 1995).

$$k_s = \frac{A_s G_{eff}}{h_{rt}} \tag{6-9}$$

$$G_{eff} = G_0 \left(1 - \frac{P}{P_{cr}}\right)$$

$$G_{eff} = G_0 - P\left(\frac{\phi A_s}{2}\left\{\sqrt{1 + \frac{12 I f_r}{A_s}\left(\frac{\pi}{\phi h_{rt}}\right)^2} - 1\right\}\right)^{-1} \tag{6-10}$$

Where ϕ is the total bearing pad thickness divided by the total elastomer thickness (h_{rt}), A_s is the pad shear area, f_r is the ending stiffness coefficient (Eq. 6-11), S is shape factor, and G_0 is the shear modulus under zero axial compression.

$$f_r = 1 - 0.575\, S^2 \tag{6-11}$$

Horizontal displacement data were corrected for slip that occurred between the pad and the middle plate during testing. Total slip was determined as the residual horizontal displacement in the pad after unloading the axial force. For example, Figure 6-7 shows that for the test 57B of full-size pad E-2.5%, the total slip of the bottom pad was 0.2 in. Therefore, based on the assumption that maximum slip occurred at maximum axial load, the corrected displacement for this pad at maximum axial force of 590 kip was 0.3 in. (0.5 in. – 0.2 in.). The measured horizontal displacement at each level of axial force F, i.e. $\Delta s(at\ axial\ F)_{measured}$, was then linearly corrected using Eq. 6-12.

$$\Delta s(at\ axial\ F)_{corrected} = \Delta s(at\ axial\ F)_{measured} \cdot \left(\frac{\Delta s(at\ max.axial)_{corrected}}{\Delta s(at\ max.axial)_{measured}}\right) \quad (6\text{-}12)$$

Figure 6-8 presents corrected horizontal displacements for the full-size E-2.5% pad. Similar corrections were performed for all other horizontal displacement test data.

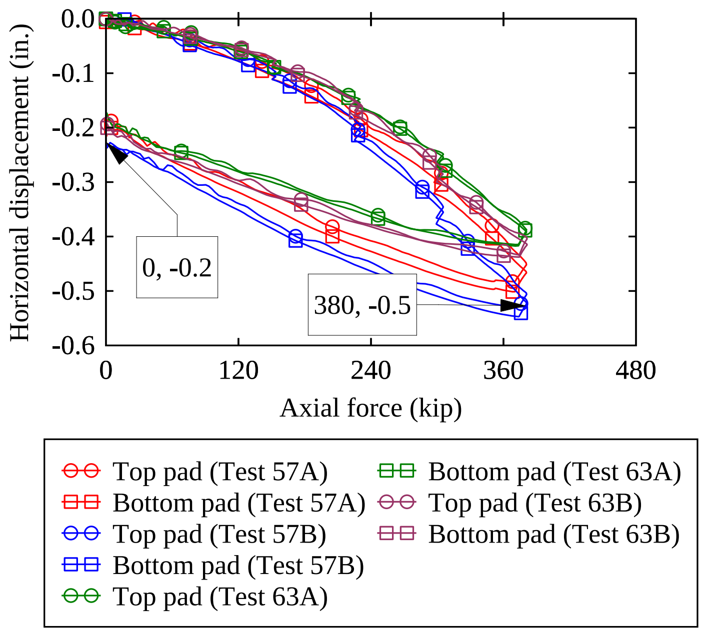

Figure 6-7 Original horizontal displacement (loading and unloading) data for full-size pads E-2.5%

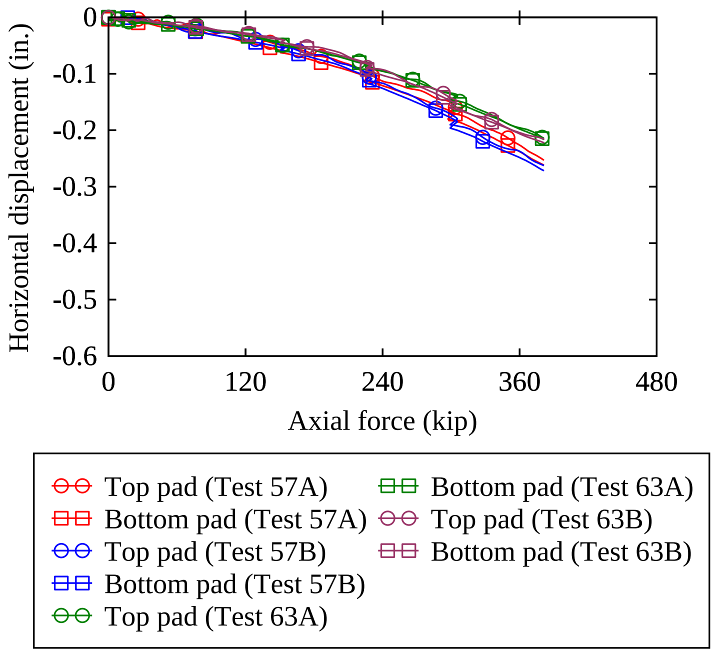

Figure 6-8 Corrected horizontal displacement data for full-size pads E-2.5%

Eq. 6-8 was globally optimized using the corrected horizontal displacement data from *all* suitable tests to compute the value of generalized fitting parameter α_{hd}. The globally optimized value of α_{hd} was determined to be 0.5. In summary, horizontal displacement was found to be directly proportional to axial force and pad taper angle, and inversely proportional to the shear stiffness of a pad. Eq. 6-13 provides the equation for determining horizontal displacement (Δs) in a pad with slope θ (radians) and under axial force (F). Figure 6-9 compares the best generalized fit curve Eq. 6-13 to the full-size pad E-2.5% horizontal displacement data.

$$\Delta s = \frac{0.5 \cdot F \cdot \theta}{k_s} \tag{6-13}$$

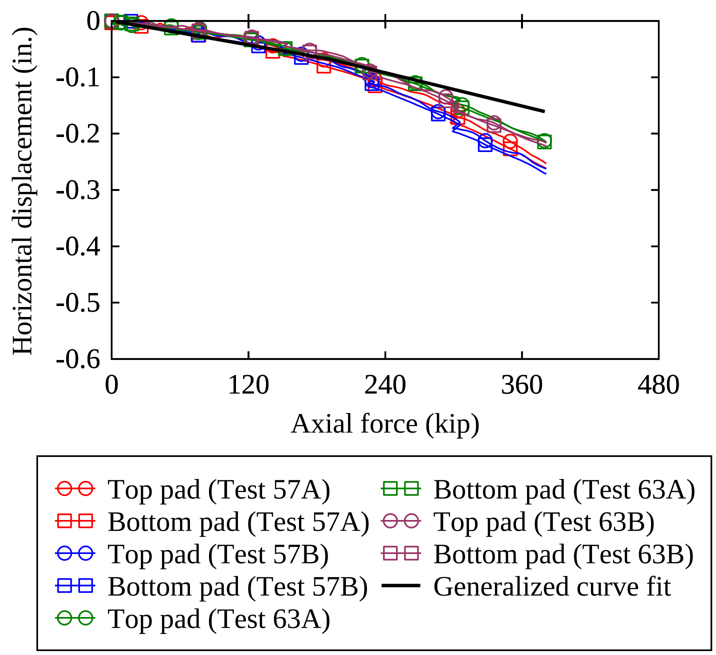

Figure 6-9 Comparison of corrected horizontal displacement data for full-size pads E-2.5% and generalized curve fit (Eq. 6-13)

6.3 Horizontal restraining force test data

Horizontal restraining force data consisted of horizontal restraining force (F_H) generated by pads under increasing axial force (F) when restrained against horizontal movement (Figure 5-3). In Figure 6-11, example horizontal restraining force test data for full-size pad E-2.5% are presented. Horizontal force (F_H) was determined to be a function of axial force (F in kip) and bearing pad taper angle (θ in radians).

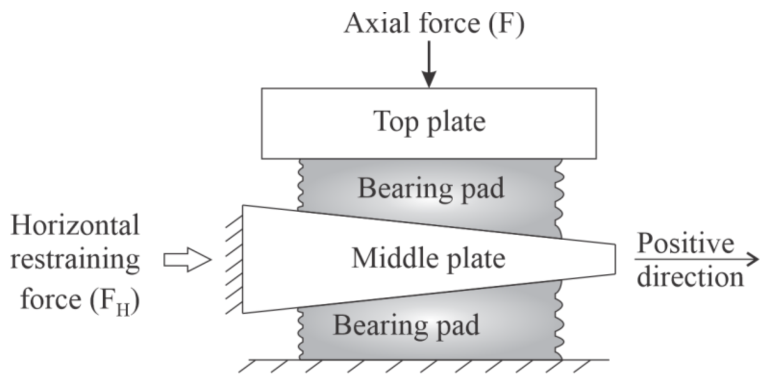

Figure 6-10 Schematic of horizontal restraining force (F_H) in pads during testing

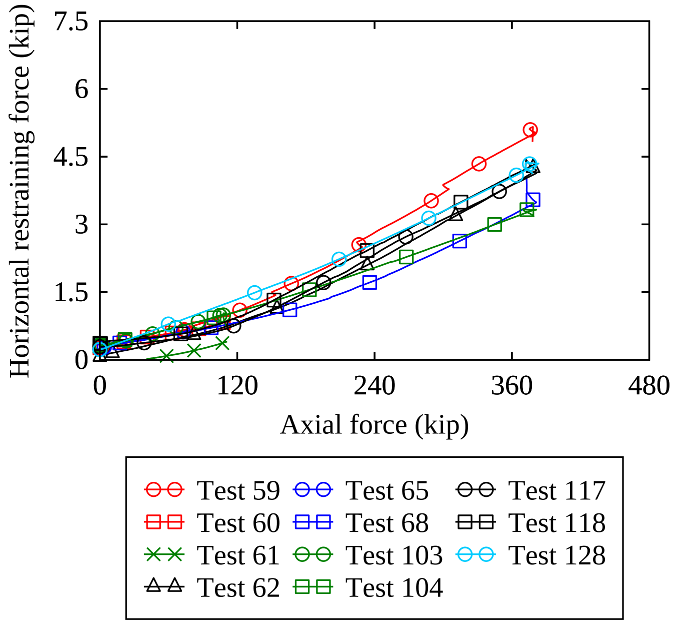

Figure 6-11 Measured horizontal restraining force data for full-size pads E-2.5%

In order to quantify horizontal restraining force based on these two factors, Eq. 6-14 was used. Constant α_{hf} was the fitting parameter was used to minimize the global error between measured data and the generalized Eq. 6-14.

$$F_H = \alpha_{hf} \cdot F \cdot \theta \tag{6-14}$$

Based on the Eq. 6-14, horizontal restraining force is assumed to be zero for flat pads where the slope angle (θ) is zero. However, due to minor misalignments and eccentricities in the test setup, some horizontal restraining force was measured even when flat pads were tested. The magnitude of horizontal restraining force that was caused by misalignments was assumed to be constant for each pad type, irrespective of taper angle. Therefore, measured horizontal restraining force for a tapered pad was corrected using the average horizontal force measured for the corresponding flat pad. For example, Figure 6-12 shows the average horizontal force for flat E pads, calculated as average of all tests. Figure 6-13 shows corrected horizontal force readings for tapered pads E-2.5% after subtracting average horizontal force obtained from flat pad E test data. Similar corrections were applied for all tapered pads.

After globally minimizing the differences between Eq. 6-14 and the corrected horizontal force data from tests of *all* pads, the generalized value of fitting parameter α_{hf} was found to be 0.5. In summary, horizontal restraining force (F_H) was found to be directly proportional to axial force (F) and pad taper angle (θ).

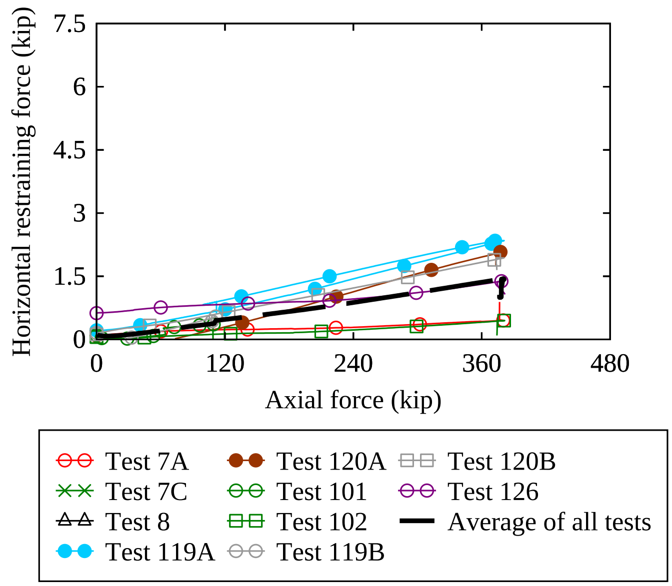

Figure 6-12 Measured horizontal force data for full-size pads E-0% and average of all tests

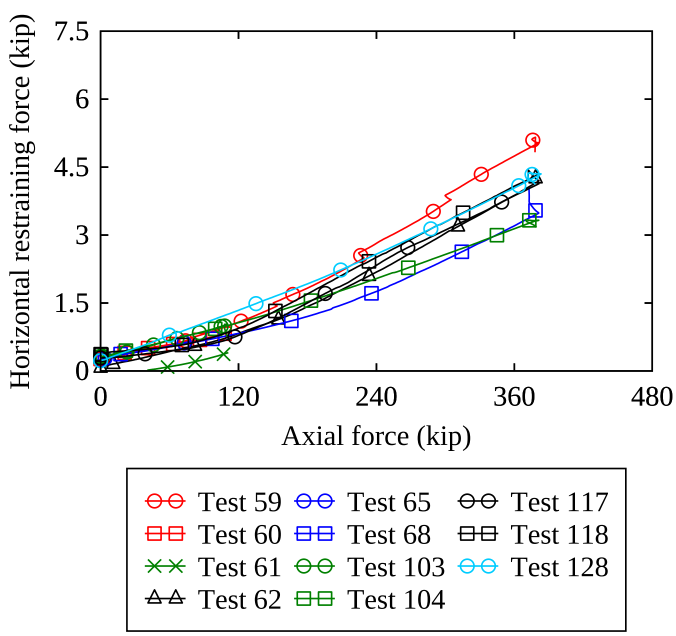

Figure 6-13 Corrected horizontal restraining force data for full-size pads E-2.5%

Eq. 6-15 provides the equation for determining horizontal restraining force (F_H) for a pad with slope θ (radians) and under axial force (F). Figure 6-14 compares the generalized curve fit plotted using Eq. 6-15 to full-size pad E-2.5% horizontal displacement test data.

$$F_H = 0.5 \cdot F \cdot \theta \tag{6-15}$$

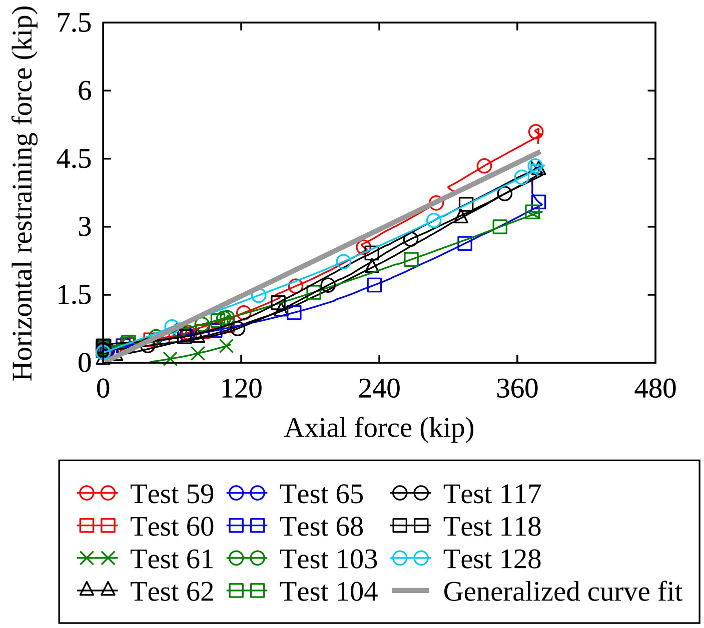

Figure 6-14 Comparison of corrected horizontal restraining force data for full-size pads E-2.5% to generalized curve fit (Eq. 6-15)

6.4 Shear stiffness test data

Shear stiffness test data consisted of shear forces (F_V) that were generated in pads when shear strains (γ) or shear displacements (Δ) were imposed (Figure 6-15). An example of such data is shown in Figure 6-16 for full-size pad E-2.5%. In the figure, the abscissa, i.e., shear displacement (Δ), is the product of shear strain (γ) and the average total elastomer thickness of each pad E-2.5%.

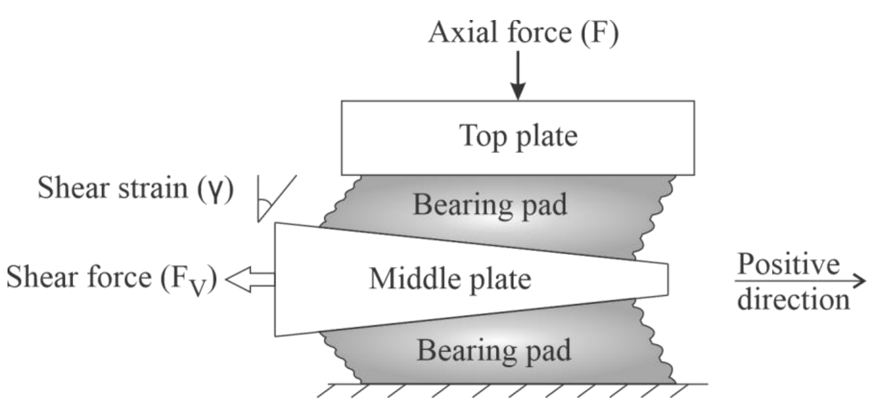

Figure 6-15 Schematic of shear displacement in pads during shear test

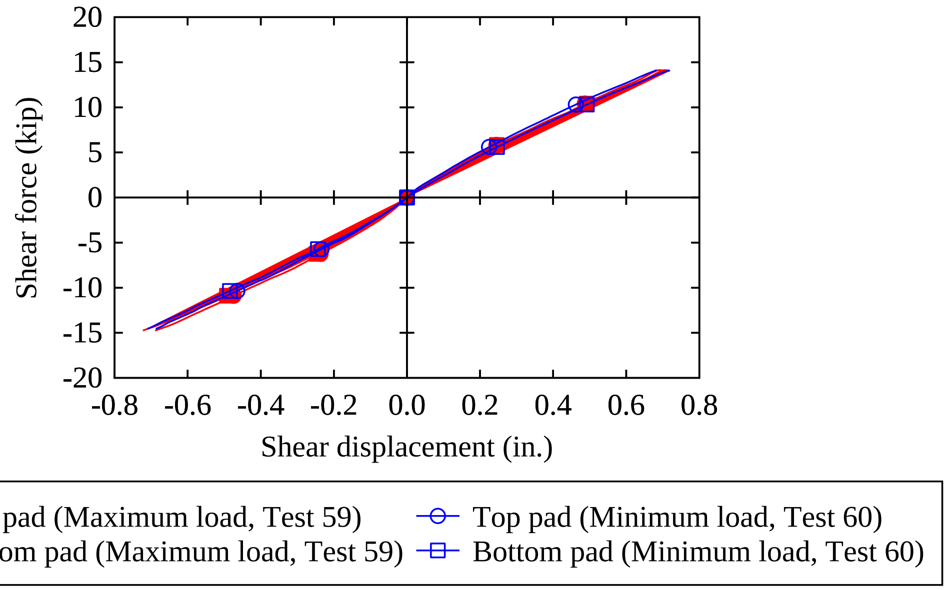

Figure 6-16 Measured shear stiffness test data for full-size pads E-2.5%

Pad shear stiffness (k_s) was determined as the linear curve fit (minimum RMS error) to the test data obtained from the *last* shear strain loading cycle (Figure 6-17), i.e. after completion of conditioning cycles to minimize the Mullins effect. Shear stiffnesses determined from negative strain cycle data were denoted the 'downhill' shear stiffnesses and stiffnesses determined using positive strain cycle data were denoted 'uphill' shear stiffnesses. These terms refer to the pad and girder combination presented in Figure 6-18 where girder motion to the left would be denoted downhill shear, and girder motion to the right would be denoted uphill shear. Shear stiffnesses were quantified for all tapered pads and corresponding flat pads. The theoretical shear stiffness (kip/in) of each pad was calculated using Eq. 6-16:

$$k_s = \frac{A_s G}{h_{rt}} \tag{6-16}$$

where A_s, G, and h_{rt} are the shear area, shear modulus, and total elastomer thickness for the pad, respectively. The average percentage differences between theoretical shear stiffness and measured shear stiffness (determined using shear stiffness test data) were 4%, 10%, and 42% for pad types E, F, and K, respectively (in each case, the measured shear stiffness was smaller than theoretical).

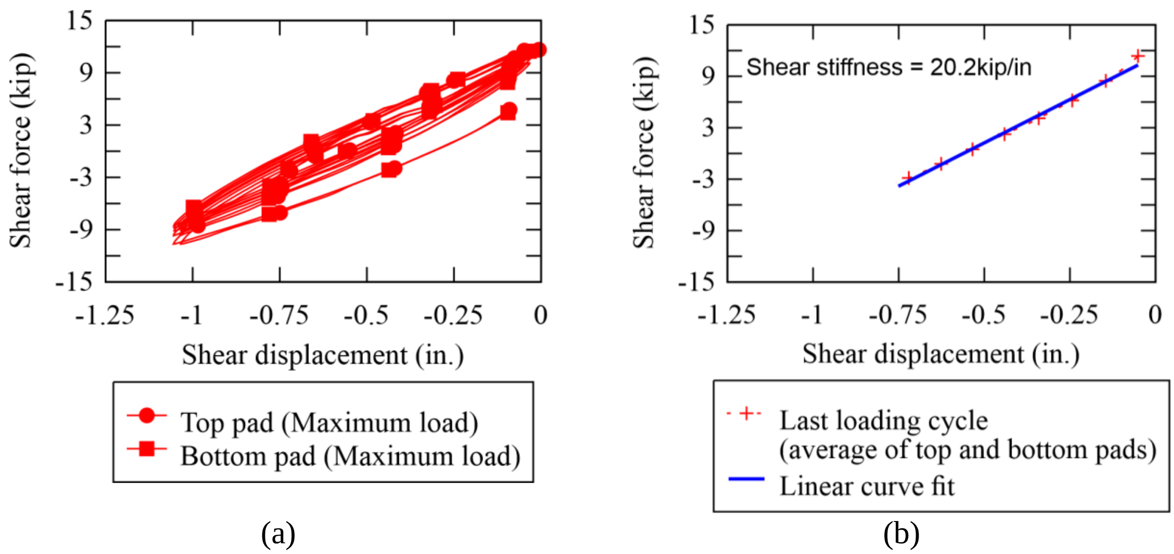

Figure 6-17 Example of processing data for downhill shear stiffness determination (pad E-2.50%) (a) Original data; (b) Data from only the last loading cycle, and linear curve fit

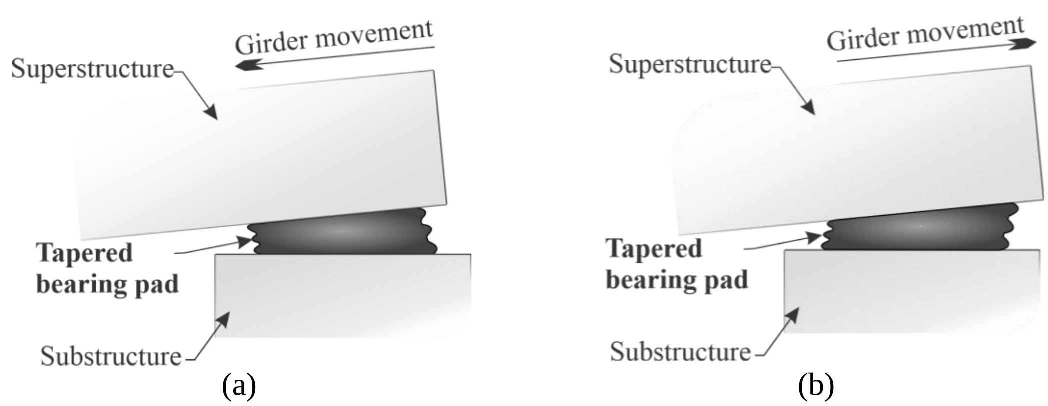

Figure 6-18 Shear direction: (a) Downhill; (b) Uphill

Differences between theoretical and measured shear stiffnesses increased as the total elastomer thickness increased. The fact that the experimentally determined shear stiffnesses were smaller than the corresponding theoretical shear stiffnesses was attributed to slip between the pads and the steel surfaces on the middle plate assembly. Slip in pads during shear stiffness testing, and the correction that was used to account for such slip, is explained using the example of K-4.2% pad data as follows. Figure 6-19 presents the six cycles of shear force and shear displacement that were applied to the K-4.2% pads. The bold dashed line indicates the shear force (horizontal force) in K-4.2% pads that was produced under pure compression (F) and at zero shear strain (γ). Since the shear stiffness (k_s) was calculated from the last cycle, the slip was also determined for the last cycle. As seen from Figures 6-20 and 6-21, at stages 1 and 3, the bearing pads had shear force corresponding to shear force under pure compression (indicated by bold dashed line in Figures 6-20). In other words, the bearing pads had zero strain at stages 1 and 3.

However, shear displacements (D1 and D2) in pads at stages 1 and 3 were different. The difference between D1 and D2 was attributed to slip that occurred in pad during the last cycle.

This slip was assumed to occur linearly from stage 1 to stage 2. Displacement data were then corrected by subtracting the linearly varying slip. Such correction was applied to all shear stiffness test data. After applying the correction, the average percentage differences between theoretical shear stiffness and measured shear stiffness were 13%, 4%, and 25% for pad types E, F, and K respectively.

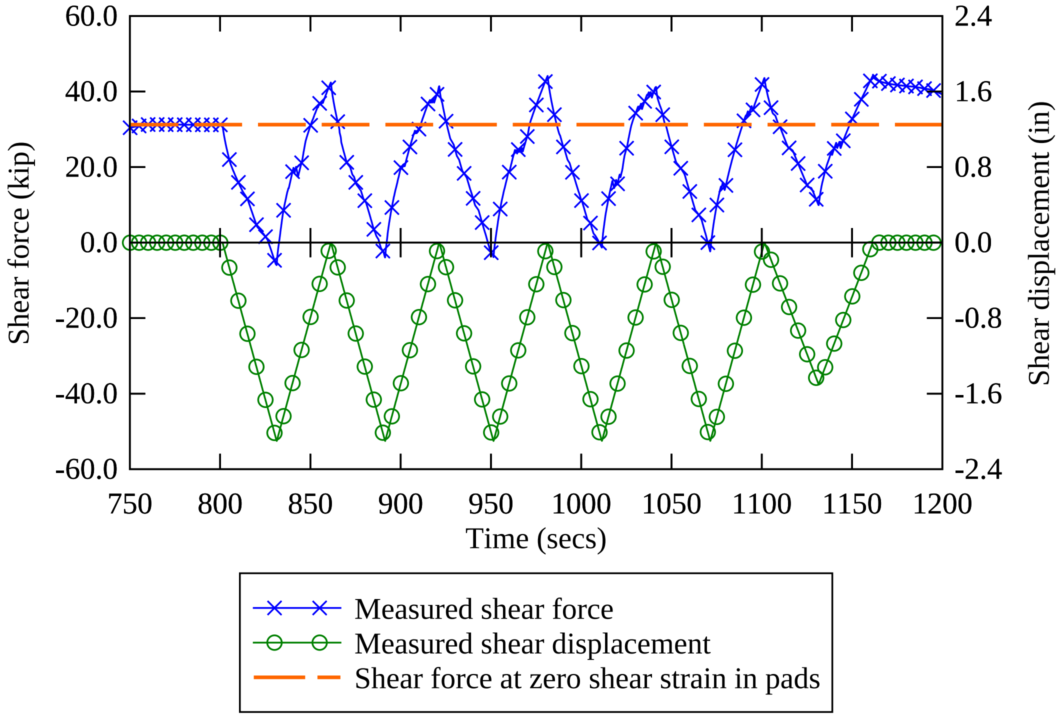

Figure 6-19 Shear stiffness test cycles for pads K-4.2%

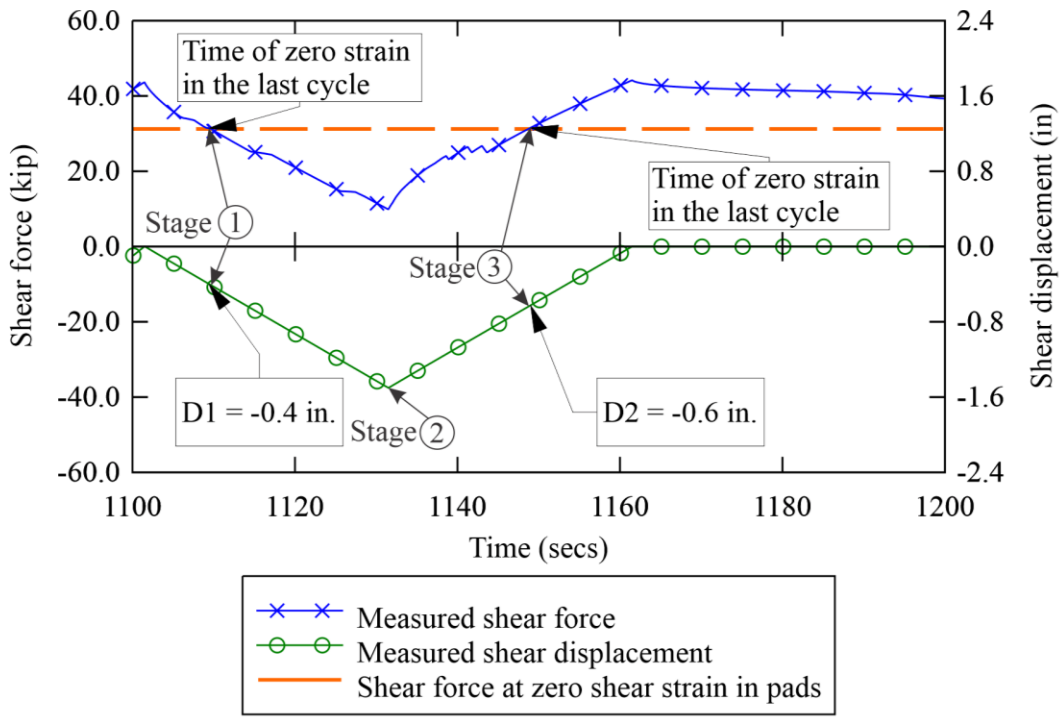

Figure 6-20 Last cycle of shear stiffness for pads K-4.2%

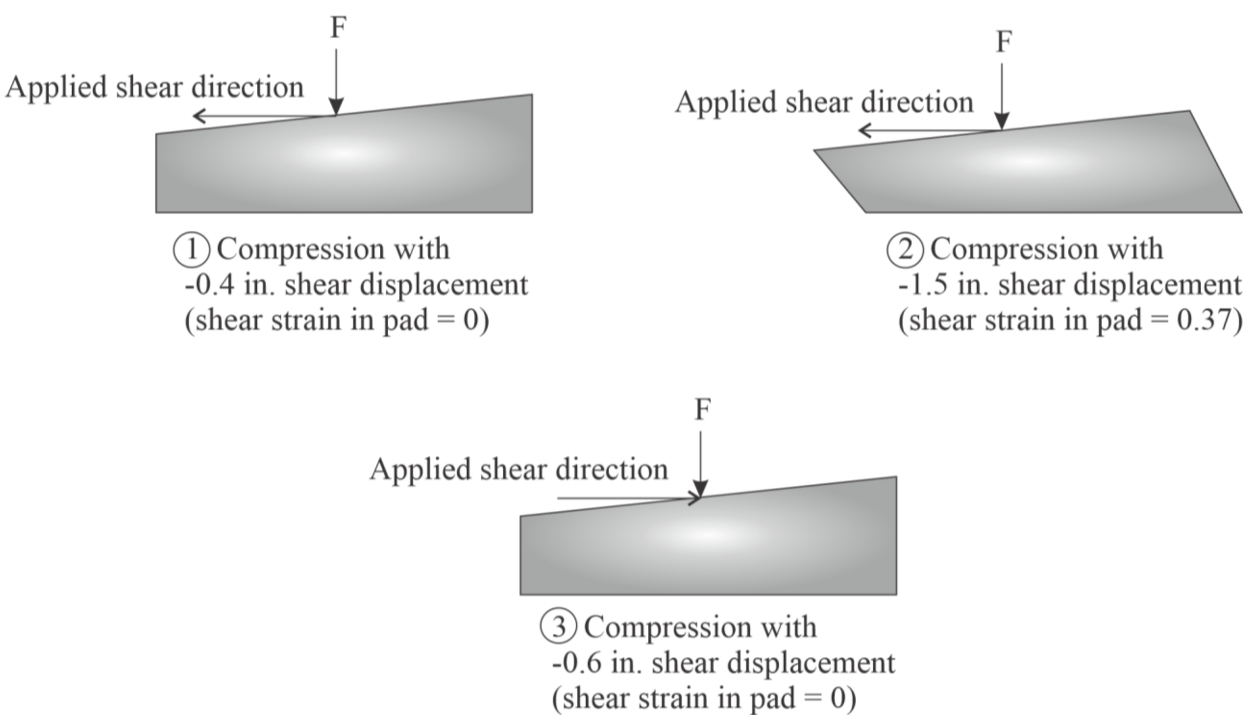

Figure 6-21 Stages in the last cycle of shear stiffness test
(Note: values shown here correspond to a test for pads K-4.2%)

After the slip correction procedure was applied to the test data, a generalized equation for pad shear stiffness was fitted as Eq. 6-17, but minimizing the RMS error across the entire global set of data collected:

$$k_s = \frac{\alpha_s A_s G_{eff}}{h_{rt}} \tag{6-17}$$

where α_s was the fitting parameter. In Eq. 6-17, effective shear modulus (G_{eff}, Eq. 6-10) was used instead of shear modulus (G) for improved accuracy. On optimizing Eq. 6-17, the value of α_s was determined to be 1.25. In Table 6-3, shear stiffness values calculated using Eq. 6-17 are divided by (i.e. normalized with respect to) the downhill shear stiffness of the corresponding flat pad at each axial load level (denoted as the 'normalizing shear stiffness').

Table 6-3 Normalized shear stiffness data

Pad type | Shear modulus (psi)	Size	Total elastomer thickness (in.) | Number of shims	Normalizing shear stiffness (kip/in) [At low axial load] | [At high axial load]	Slope (%)	Normalized shear stiffness			
					At low axial load		At high axial load	
					Uphill	Downhill	Uphill	Downhill
E | 110	Half	1.5 | 3	13.2 | 12.6	0	0.92	1.00	0.97	1.00
				2.5		1.01		1.07
				5.0				0.58
	Full		25.9 | 25.5	0	0.91	1.00	0.94	1.00
				2.5	0.84	0.90	0.90	1.02
				5.0		1.15		1.17
F | 110	Half	2 | 4	10.2 | 9.9	0	0.83	1.00	0.95	1.00
				2.5		0.87		1.01
				5.0				
	Full		20.5 | 21.5	0		1.00	0.77	1.00
				2.5	0.90	0.77	0.86	0.80
				5.0	0.77	0.84	0.85	0.81
K | 150	Full	3 | 6	12.3 | 13.6	0		1.00		1.00
				2.1		1.37		1.23
				4.2		1.08		0.93

Figure 6-22 presents the shear stiffnesses of pads with taper slopes between 0% (flat) and 5%. Table 6-4 presents the average change in shear stiffness of tapered pads compared to the corresponding flat pads, and the average change in shear stiffness due to changing from minimum to maximum axial load. Specific values of the axial load levels are reported in Table 5-1. The results presented in Table 6-4 indicate that the shear stiffness of bearing pads changed by no more than 15% from the stiffness of comparable flat pads as the result of introducing taper slope. Further, the shear stiffnesses of bearing pads at high axial load level did not differ significantly from the corresponding shear stiffnesses at low axial load level for each pad type tested. For tapered pads, the uphill shear stiffnesses were, in general, found to be smaller than the downhill shear stiffnesses, but differed by less than 10%. As expected, the shear stiffnesses of pads, both flat and tapered, were found to decrease as the average total elastomer thickness increased. For example, shear stiffness decreased by a factor of 2.0 as the total elastomer thickness increased by a factor of 2.0 from pad E-0% to pad K-0%. Also as expected, the shear stiffness of half-size pads was found to be approximately half the shear stiffness of full-size pads as shown in the Figure 6-22.

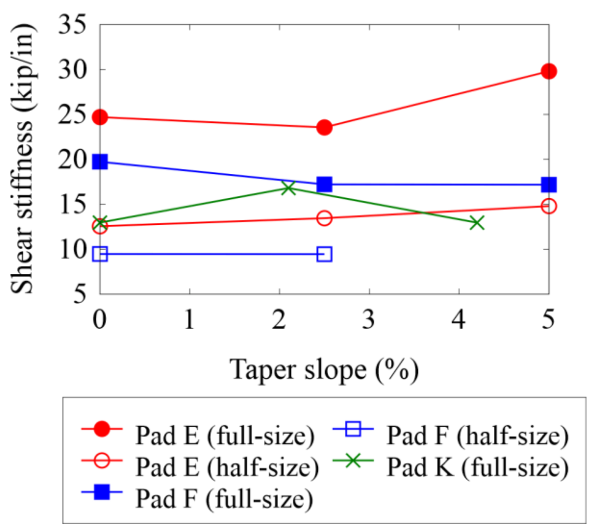

Figure 6-22 Effect of taper slope on shear stiffness

Table 6-4 Average change in shear stiffness due to introduction of taper slope and change in axial load level from minimum to maximum

Pad Type	Average change (%) in stiffness due to:	
	Taper slope	Change in axial load level from minimum to maximum
E	10.28	1.57
F	-8.65	4.66
K	14.86	1.37

6.5 Slip test data

Slip tests were performed in two stages to determine: 1) the shear displacements and shear strains at slip, and 2) to determine the coefficient of friction for tapered pads under minimum and maximum axial load levels (recall Table 5-1). Stage 1 focused on determining the shear strain (γ) at which slip occurred (for comparison to AASHTO design requirements), and involved gradually increasing shear loading on the pads. Stage 2 focused on determining the coefficient of friction (μ) between the pads and various types of surfaces (steel, concrete, dry, wet), and involved gradually decreasing the axial load on the pads. The following subsections discuss the results obtained from each stage of slip testing.

6.5.1 Stage 1: Shear strain at slip

In Stage 1 of each slip test, shear displacement and shear strain at slip were determined using the measured data. Theoretically, slip occurs when there is relative sliding motion between the surface of the pad and the surface (steel or concrete) that is being tested. In terms of experimental measurements and observations, the occurrence of slip is indicated by increasing relative displacement (between the plates positioned above and below the pad) with no further increase in measured shear force. That is, slip should result in the rate of change of measured shear force being zero, even though relative displacement continues increasing between the top and bottom surfaces of the pad. However, based on an inspection that measured data and videos recorded during various slip tests, it was determined that slip occurred when the rate of change in shear force dropped below approximately 0.005 kip/in. Two video-based methods were used to determine the time (or ‘timestamp’) at slip, and the rate of change in shear force at slip.

In the first method, the video playback speed was increased one hundred times (100x), thereby making the onset of slip visually identifiable (Figure 6-23). The time of slip was determined from each video as the instant after which shear deformation in the bearing pad remained constant even though the middle plate continued being displaced. Knowing the time at which slip occurred (determined from the video), the rate of change in shear force was then determined from the measured force data, and was found to be approximately 0.005 kip/sec.

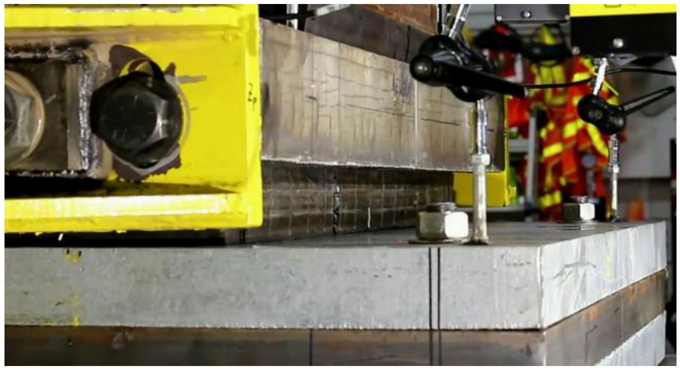

(a)

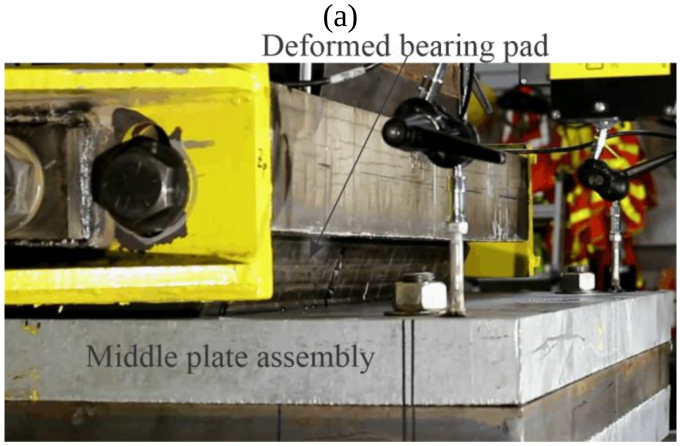

(b)

Figure 6-23 Snapshots of video for slip test of pad F-0% under wet steel surface condition: (a) at time zero; (b) at slip

In the second method, the test videos were processed using the motion analysis software ProAnalyst (Xcitex, 2017). In ProAnalyst, visually identifiable features on bearing pad and middle plate assembly were tracked to quantify the horizontal displacement of each. Figure 6-24 presents example features that were tracked, and the paths of those features as determined by ProAnalyst for pad F-0% under the wet steel surface condition. Using the tracked feature paths, the relative displacement between the middle plate and the pad F-0% was then calculated and plotted versus time (Figure 6-25). Tangents that were constructed for the initial and final parts of each displacement versus time curve (Figure 6-25) indicated different slopes, and thus different slip speeds. Note that in this context, speed = slope = (increment of displacement) / (increment of time).

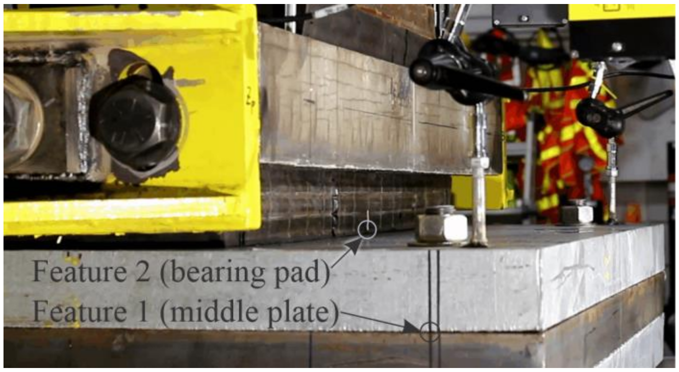

(a)

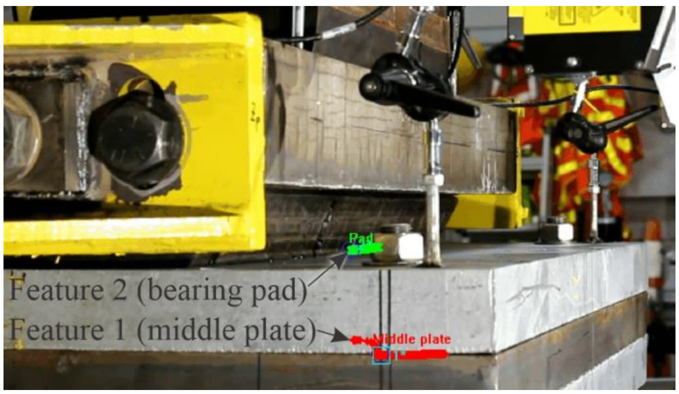

(b)

Figure 6-24 Detection of slip using the ProAnalyst software:
(a) tracked features; (b) tracked paths of features

The non-zero slope of the initial tangent, which could—incorrectly—be interpreted as apparent slip between the pad and the middle plate, was instead attributed to the influence of optical distortion (visual perspective) in processing the two-dimensional (2D) video. However, at a certain point in time during each test, a distinct change in apparent relative speed occurred, which was evidenced by a change in slope. The slope of the tangent corresponding to the final part of the displacement versus time curve was significantly greater than the initial slope. Despite the influence of perspective distortion, it was possible to identify the onset of slip based on the observed change of slope. The intersection of the tangents was used to determine the time of slip. For the pad F-0% wet steel surface slip test, this intersection point was in close agreement to the slip point determined using the first method noted above (visual inspection of video sped up by 100x). Similar slope changes were observed for two other tests (Figure 6-26 and Figure 6-27) with similar agreement between method one and method two slip determination. Based on this agreement, it was determined that, for the pads tested in this study, slip was associated with the rate of change of shear force dropping below 0.005 kip/sec.

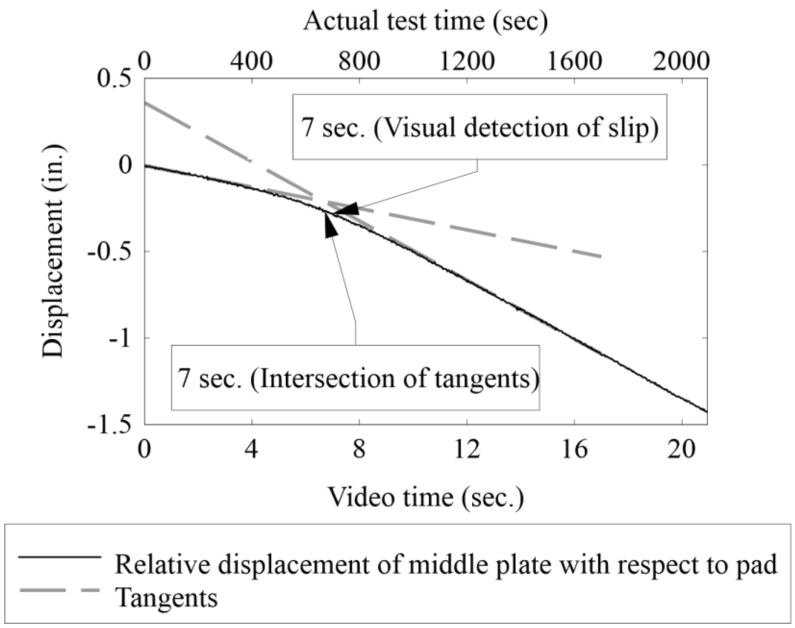

Figure 6-25 Relative displacement of middle plate with respect to pad F-0% under low axial load with wet steel surface condition, as determined using motion analysis software ProAnalyst

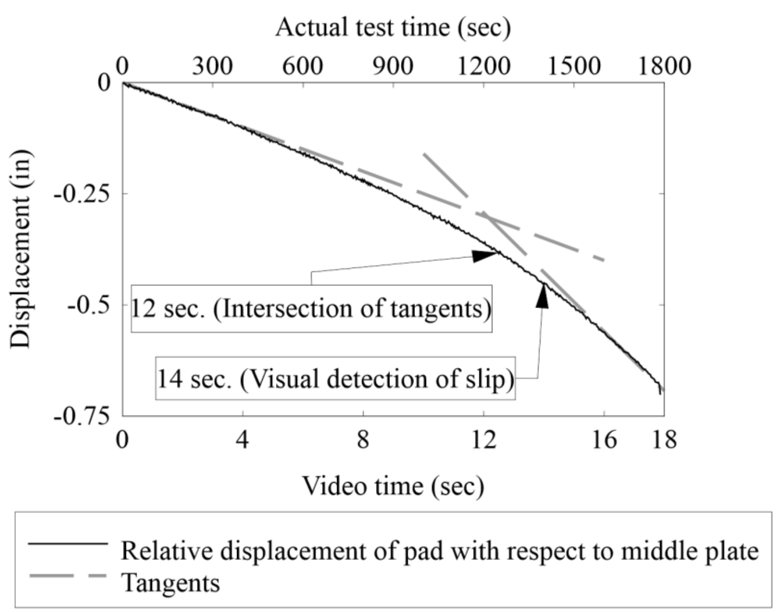

Figure 6-26 Relative displacement of middle plate with respect to pad F-0% under high axial load with wet steel surface condition, as determined using motion analysis software ProAnalyst

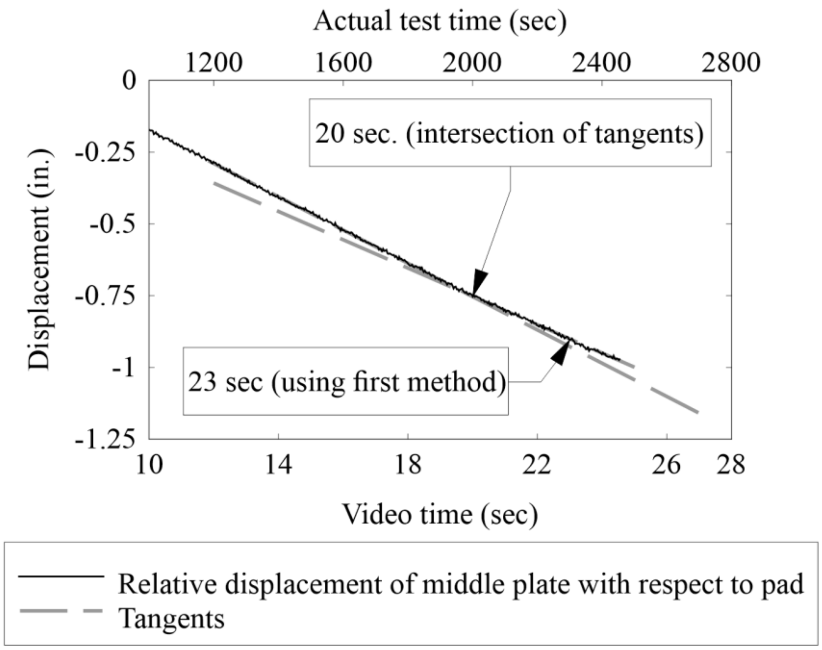

Figure 6-27 Relative displacement of middle plate with respect to pad K-4.2% under high axial load with dry concrete surface condition, as determined using motion analysis software ProAnalyst

Defining slip as the point at which the rate of change in measured shear force dropped to 0.005 kip/sec (or below), the shear displacement at slip was determined for all tested pads. Tables 6-5 – 6-9 provide shear strain ((shear displacement)/(average total elastomer thickness)) at slip for each pad type under different surface conditions and axial load levels. As per AASHTO LRFD Bridge Specifications §14.7.5.3.2 (AASHTO, 2017), bearing pads must be designed to perform without slip up to a shear strain (γ) of 0.5. Therefore, in Tables 6-5 – 6-9, shear strains less than 0.5 are shaded to indicate pads that did not satisfy the AASHTO slip criterion.

For steel surface conditions, both dry and wet, Tables 6-5 – 6-7 indicate that tapered pads did not satisfy the AASHTO slip criterion. In the cases of full-size pad types E and F, the minimum shear strain before slip on steel surface conditions (under either minimum or maximum axial load) was 0.2. However, the thicker pad type K, in some steel surface cases, slipped at zero shear strain (i.e., under pure axial compression).

In contrast, for concrete surface conditions, both dry and wet, tapered pads satisfied the AASHTO criterion by achieving a shear strain γ of 0.5 before slip. Furthermore, for some concrete surface condition cases, pads did not slip even after achieving a shear strain γ of approximately 1.0. Such tests were terminated to conserve time, and are marked with a '*' in Table 6-8 – 6-9.

Table 6-5 Shear strain (γ) at slip under dry steel surface condition (half-size pads)

Slope	Pad type E		Pad type F		Pad type K	
(for pad E and F/ K)	Min. axial load	Max. axial load	Min. axial load	Max. axial load	Min. axial load	Max. axial load
0	No test	No test	0.18	0.15	No test	No test
2.5/2.1	0.42	0.37	0.35	0.23	No test	No test
5/4.2	0.33	0.33	No test	No test	No test	No test

Shaded cells indicate cases for which the AASHTO shear strain requirement of γ > 0.5 was not satisfied.

Table 6-6 Shear strain (γ) at slip under dry steel surface condition (full-size pads)

Slope	Pad type E		Pad type F		Pad type K	
(for pad E and F/ K)	Min. axial load	Max. axial load	Min. axial load	Max. axial load	Min. axial load	Max. axial load
0	0.53	0.70	0.43	0.70	0.50	0.50
2.5/2.1	0.33	0.33	0.45	0.35	0.20	0.12
5/4.2	0.53	0.47	0.40	0.50	0.13	0.00

Shaded cells indicate cases for which the AASHTO shear strain requirement of γ > 0.5 was not satisfied.

Table 6-7 Shear strain (γ) at slip under wet steel surface condition (full-size pads)

Slope	Pad type E		Pad type F		Pad type K	
(for pad E and F/ K)	Min. axial load	Max. axial load	Min. axial load	Max. axial load	Min. axial load	Max. axial load
0	0.27	0.40	0.40	0.65	0.32	0.37
2.5/2.1	0.37	0.27	0.35	0.30	No test	0.00
5/4.2	0.20	0.20	0.45	0.20	No test	0.00

Shaded cells indicate cases for which the AASHTO shear strain requirement of γ > 0.5 was not satisfied.

Table 6-8 Shear strain (γ) at slip under dry concrete surface condition (full-size pads)

Slope	Pad type E		Pad type F		Pad type K	
(for pad E and F/ K)	Min. axial load	Max. axial load	Min. axial load	Max. axial load	Min. axial load	Max. axial load
0	1.27	1.60	1.40*	0.98*	1.03*	0.92
2.5/2.1	1.53*	1.47	1.05	1.50*	1.07*	0.73
5/4.2	1.00	1.67*	0.63	1.35*	No test	0.83

*Pad did not slip, slip test was terminated to conserve time

Table 6-9 Shear strain (γ) at slip under wet concrete surface condition (full-size pads)

Slope	Pad type E		Pad type F		Pad type K	
(for pad E and F/ K)	Min. axial load	Max. axial load	Min. axial load	Max. axial load	Min. axial load	Max. axial load
0	No test	0.93*	0.95	1.00	1.10*	0.67
2.5/2.1	No test	1.33*	No test	No test	No test	0.68
5/4.2	No test	0.80	No test	1.05	No test	0.80

*Pad did not slip, slip test was terminated to conserve time

In regard to the effect that shear direction (uphill vs. downhill; recall Figure 6-18) has on slip, Table 6-10 provides comparative results from this study. The data indicate that tapered bearing pads slipped at lower shear strains (γ) when sheared in the downhill direction as compared to the uphill direction. This outcome is attributed to the fact that, even under pure axial load, a tapered pad will shear in the downhill direction (recall Section 6.2), thus increasing the potential for slip before shear force is even applied.

Table 6-10 Effect of direction of shear on shear strain (γ) at slip under dry steel surface condition (full-size pads)

Direction of shear	Pad E-2.5%		Pad F-2.5%		Pad K-2.1%	
	Min. axial load	Max. axial load	Min. axial load	Max. axial load	Min. axial load	Max. axial load
Uphill	No test	0.67	0.60	0.75	No test	0.17
Downhill	0.33	0.33	0.45	0.35	No test	0.12

Shaded cells indicate cases for which the AASHTO shear strain requirement of $\gamma > 0.5$ was not satisfied.

6.5.2 Stage 2: Coefficient of friction at slip

Based on the Coulomb friction model, the coefficient of friction (μ) is defined as the ratio of shear force (F_v) to axial force (F) when slip occurs. Therefore, shear force and axial force data recorded during each slip test were used to determine the coefficients of friction for various surface conditions. In Stage 2 of each slip test, axial load was gradually reduced while maintaining the shear strain that had been produced during Stage 1 (details of the slip test procedure are provided in deliverable 5). As the axial force (F) acting on a pad is gradually reduced, the frictional shear force resisting pad slip ($F_v = \mu \cdot F$) is also reduced. When the frictional force drops below the threshold required to hold the pad at the initial shear strain, the pad slips to attain a lower shear strain level than the initial (Figure 6-28). Consequently, the shear force drops to correspond to the reduced shear strain. This reduction in frictional shear force further continues until the shear strain drops to zero and the pad stops slipping. To determine the coefficient of friction, the time at which slipping initiated was determined, and then the ratio of shear to axial force was computed.

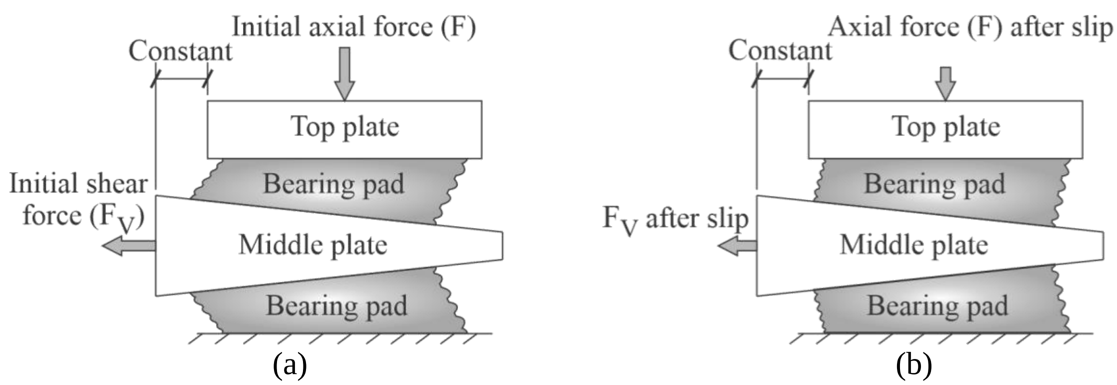

Figure 6-28 Schematic diagrams for coefficient of friction test: (a) significant shear strain (γ) before slip; (b) reduced shear strain (γ) after slip

As an illustration of this process, Figure 6-29 presents slip test data that were used to calculate the coefficient of friction for full-size tapered pads E-2.5%. In Figure 6-29a, the axial and shear forces have been normalized relative to the respective maximum magnitude force values that were achieved during slip tests. As seen from Figure 6-29a, as the axial force was reduced, the shear force value did not initially change, indicating that the shear strain in pads did not change and that the pads were not slipping; this was defined as Phase 1 of the unloading process. As axial force was further reduced, the shear force started to decrease. Initially the decrease was gradual in form, but later the decrease was rapid, indicating continuous pad slip; this latter response was defined as Phase 2. Between the well-defined phases 1 and 2 was a transition zone. Initiation of pad slip was assumed to occur in the transition zone. To establish a time at which slip initiated, the rate of change in shear force (i.e., the time derivative of shear force) was plotted (Figure 6-29b). Tangents were constructed for Phase 1 and Phase 2 of the curve. The time corresponding to the intersection of the tangents was taken to be the time at which slip initiated. The coefficient of friction was then calculated as the ratio of shear to axial force at this time.

Following this general procedure, coefficients of friction were determined for all tested pads. Tables 6-11 – 6-15 summarize coefficients of friction for different types of pad (flat, tapered), different surface conditions (dry, wet), and different axial load levels. Prior researchers have reported that bearing pad slip can be prevented if the shear stress acting on a bearing pad is limited to no more than one-fifth (0.2) of the compressive stress, i.e., if the coefficient of friction between the bearing pad and bearing surfaces is at least 0.2 (Muscarella & Yura, 1995; Pont, 1959; Stanton & Roeder, 1982). In Tables 6-11 – 6-15, all coefficients of friction smaller than 0.2 are shaded to indicate a failure to meet the no-slip criterion reported by prior researchers.

For steel surfaces (Tables 6-11 – 6-13), both dry and wet, the experimentally determined coefficients of friction for tapered pads failed to satisfy the required minimum of 0.2. Note that values in the tables are marked as '*~Zero*' when the coefficients of friction were close to zero (i.e., when pad slip occurred due solely to the application of axial load, without shear load). In contrast, for concrete surfaces (Tables 6-14 and 6-15), both dry and wet, the experimentally determined coefficients of friction for tapered pads did satisfy the required minimum of 0.2. These observations are similar to the observations found in the analysis of shear displacement at slip, as discussed previously.

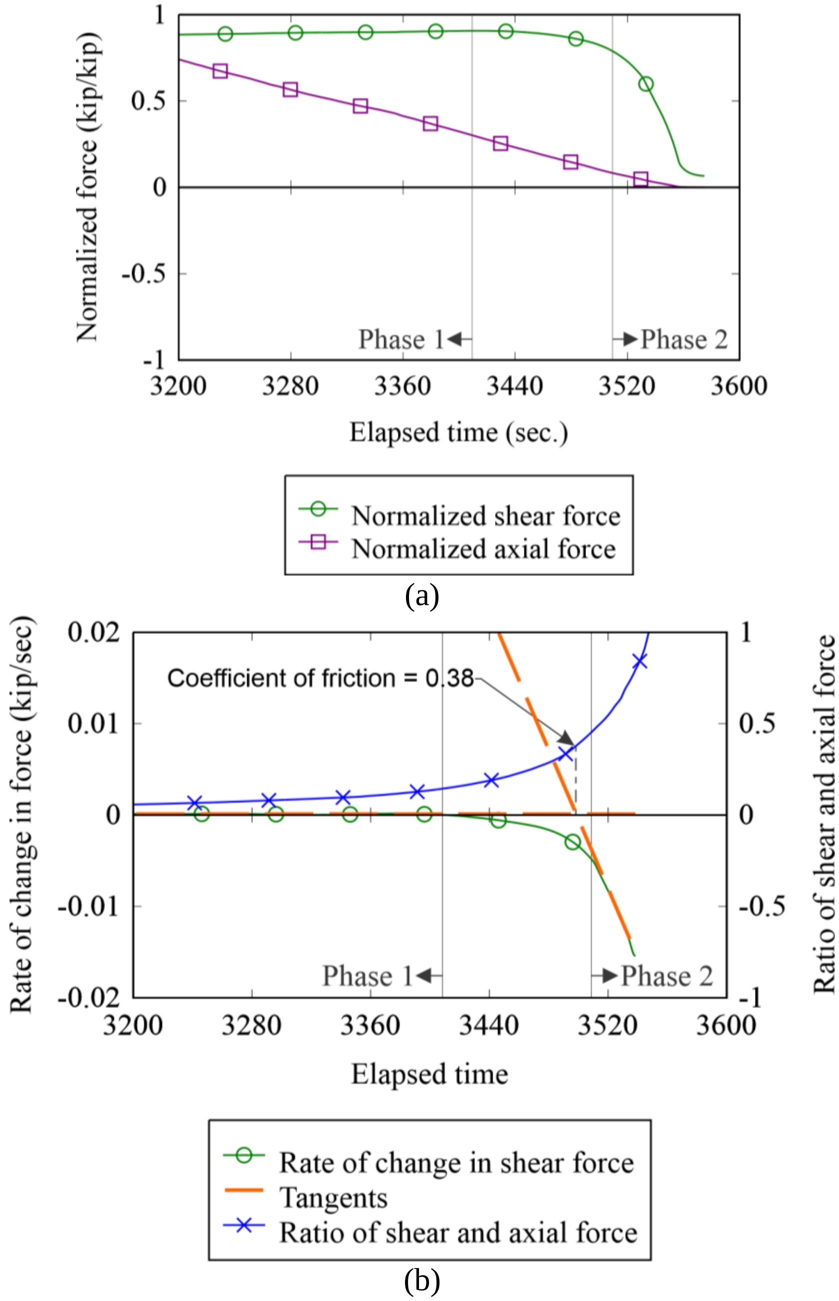

Figure 6-29 Slip test data for determining coefficient of friction for full-size pad E-2.5%: (a) change in shear force; (b) change in rate of change in shear force

Table 6-11 Coefficient of friction under dry steel surface condition (half-size pads)

Slope (%)	Pad type E		Pad type F		Pad type K	
(for pad E and F/ K)	Min. axial load	Max. axial load	Min. axial load	Max. axial load	Min. axial load	Max. axial load
0	No test	No test	No test	No test	No test	No test
2.5/2.1	0.25	0.11	0.39	0.21	No test	No test
5/4.2	0.25	~Zero†	No test	No test	No test	No test

Shaded cells indicate cases for which the coefficient of friction μ was less than 0.2
†Value of coefficient of friction close to zero indicating pad slipped under pure compression

Table 6-12 Coefficient of friction under dry steel surface condition (full-size pads)

Slope (%)	Pad type E		Pad type F		Pad type K	
(for pad E and F/ K)	Min. axial load	Max. axial load	Min. axial load	Max. axial load	Min. axial load	Max. axial load
0	0.34	0.34	0.54	0.31	0.3	0.29
2.5/2.1	0.24	~Zero †	0.39	0.22	~Zero	~Zero
5/4.2	0.26	~Zero	0.24	~Zero	~Zero	~Zero

Shaded cells indicate cases for which the coefficient of friction μ was less than 0.2
†Value of coefficient of friction close to zero indicating pad slipped under pure compression

Table 6-13 Coefficient of friction under wet steel surface condition (full-size pads)

Slope (%)	Pad type E		Pad type F		Pad type K	
(for pad E and F/ K)	Min. axial load	Max. axial load	Min. axial load	Max. axial load	Min. axial load	Max. axial load
0	0.25	0.2	0.54	0.37	0.25	0.25
2.5/2.1	0.23	~Zero †	0.35	~Zero	No test	~Zero
5/4.2	~Zero	~Zero	0.34	~Zero	No test	~Zero

Shaded cells indicate cases for which the coefficient of friction μ was less than 0.2
†Value of coefficient of friction close to zero indicating pad slipped under pure compression

Table 6-14 Coefficient of friction under dry concrete surface condition (full-size pads)

Slope (%)	Pad type E		Pad type F		Pad type K	
(for pad E and F/ K)	Min. axial load	Max. axial load	Min. axial load	Max. axial load	Min. axial load	Max. axial load
0	0.5	0.42	0.54	0.56	0.47	0.38
2.5/2.1	0.37	0.38	0.58	0.41	0.51	0.34
5/4.2	0.49	0.33	0.47	0.36	No test	0.32

Table 6-15 Coefficient of friction under wet concrete surface condition (full-size pads)

Slope (%)	Pad type E		Pad type F		Pad type K	
(for pad E and F/ K)	Min. axial load	Max. axial load	Min. axial load	Max. axial load	Min. axial load	Max. axial load
0	No test	0.52	0.67	0.46	0.46	0.36
2.5/2.1	No test	0.3	No test	No test	No test	0.35
5/4.2	No test	0.25	No test	0.33	No test	0.35

In regard to the effect that shear direction (uphill vs. downhill; recall Figure 6-18) has on coefficient of friction, Table 6-16 provides comparative results. The data indicate that the coefficient of friction (μ) was lower when tapered pads were sheared in the downhill direction as compared to the uphill direction. This outcome is attributed to the fact that, even under pure axial load, a tapered pad will shear in the downhill direction (recall Section 6.2), thus increasing the potential for slip and reducing the observed coefficient of friction.

Table 6-16 Effect of direction of shear on coefficient (μ) of friction at slip under dry steel surface condition (full-size pads)

Direction of shear	Pad E-2.5%		Pad F-2.5%		Pad type K-2.1%	
	Min. axial load	Max. axial load	Min. axial load	Max. axial load	Min. axial load	Max. axial load
Uphill	No test	0.32	0.56	0.3	No test	0.21
Downhill	0.24	~Zero †	0.39	0.22	No test	~Zero

Shaded cells indicate cases for which the coefficient of friction μ was less than 0.2

†Value of coefficient of friction close to zero indicating pad slipped under pure compression

CHAPTER 7
RECOMMENDATIONS

The following subsections provide recommendations for tapered bearing pads based on the analysis of test data and results.

7.1 Shape factor

Potential thickness parameters that can be used to compute the shape factor (S) of a tapered elastomer layer include: minimum thickness, average thickness, and maximum thickness. In this study, the thickness parameter that produced the minimum RMS error between calculated and experimentally measured axial stiffness values was selected as the recommended thickness for shape factor calculation. To determine the most appropriate thickness parameter, Eqs. 6-4 – 6-7 were optimized three separate times, each time using the entire processed axial stiffness test data and one of three different choices of characteristic thickness (minimum, average, or maximum). For each choice of characteristic thickness, optimized values of the empirical constants α, ω_1, and ω_2 were determined from RMS error minimization. Table 7-1 indicates that the values of ω_1 and ω_2 were nearly the same for all the three choices of thicknesses. In contrast, values of α decreased as the characteristic elastomer thickness increased (i.e., as the shape factor decreased).

Table 7-1 Values of empirical constants obtained for different choices of thickness (as used in shape factor calculation)

Thickness used to compute shape factor	α	ω_1	ω_2
Minimum	0.29	1.56	-3.52
Average	0.21	1.62	-3.83
Maximum	0.09	1.64	-3.95

To compare the experimentally measured axial stiffness data to axial stiffnesses computed using different choices of characteristic thickness (and thus different shape factors), Eqs. 7-1 – 7-4 were used:

$$RMS = \sqrt{\frac{\sum\left[\frac{(Calculated - measured\ )axial\ force}{Maximum\ axial\ force}\right]^2}{Number\ of\ data\ points}} \tag{7-1}$$

$$MV_1 = \frac{\sum\frac{(Calculated - measured)\ axial\ stiffness\ per\ pad\ type}{Measured\ axial\ stiffness} \times 100}{Number\ of\ pad\ types} \tag{7-2}$$

$$MV_2 = \frac{\sum\frac{absolute[(Calculated - measured)\ axial\ stiffness\ ]}{Measured\ axial\ stiffness} \times 100}{Number\ of\ pad\ types} \tag{7-3}$$

$$SD = \sqrt{\frac{\Sigma\left(\frac{(Calculated - measured)\ axial\ stiffness}{Measured\ axial\ stiffness} \times 100 - MV_1\right)^2}{Number\ of\ pad\ types}} \tag{7-4}$$

Table 7-2 compares axial stiffnesses, calculated using different thickness values for the shape factor, to the experimentally measured axial stiffness data. The shape factor calculated using the maximum thickness was found to produce the least error in axial stiffness calculation. However, errors associated with calculating the shape factor using the average thickness were only about 1% larger. Given this relatively small difference, and given that the use of average thickness in calculating shape factor is likely to be more intuitive to designers, the use of average thickness is recommended for the calculation of shape factor and axial stiffness of tapered bearing pads.

Table 7-2 Comparison of axial stiffness results for different thicknesses used for shape factor

Thickness used to compute shape factor	RMS error using normalized force values	Mean value of percentage error between calculated and measured stiffness (MV_1)	Mean value of absolute percentage error between calculated and measured stiffness (MV_2)	Standard deviation of percentage error between calculated and measured stiffness (SD)
Minimum	0.112	-2.8%	16.8%	19.6
Average	0.108	-2.3%	14.8%	16.8
Maximum	0.107	-1.6%	13.9%	16.0

7.2 Tapered bearing pad configuration

Three bearing pad manufacturers were contacted regarding fabrication of tapered bearing pads. Each manufacturer responded that taper in pads can be introduced by varying pad thickness from end to end of the pad in multiples of 1/8 in. or 1/16 in.; manufacturers indicated a preference for 1/8 in. The manufacturers also mentioned that multiple layers of neoprene can be varied to create the desired tapered. Based on the earlier work of Muscarella and Yura (1995), as well as discussions with current manufacturers of bearing pads, it was determined that taper could be incorporated into bearing geometry by changing the thickness of the pads in increments (N) of 1/8 in. Accordingly, tapered pads in this research were produced by incorporating taper in flat bearing pads along the length by changing bearing pad thickness in multiples of 1/8 in. such that the average thickness of each tapered pad was same as the thickness of the original flat pad (Figure 7-1). Steel shims were aligned parallel to the bottom pad surface except for the top shim which was inclined such that the elastomer thicknesses above and below the top shim was equal. Only the top shim was inclined because past research on tapered pads (Muscarella & Yura, 1995) found out that inclined shims were more prone to misalignment than parallel shims, and pads under compression with only inclined shims horizontally displaced 40% more compared to pads with only parallel shims.

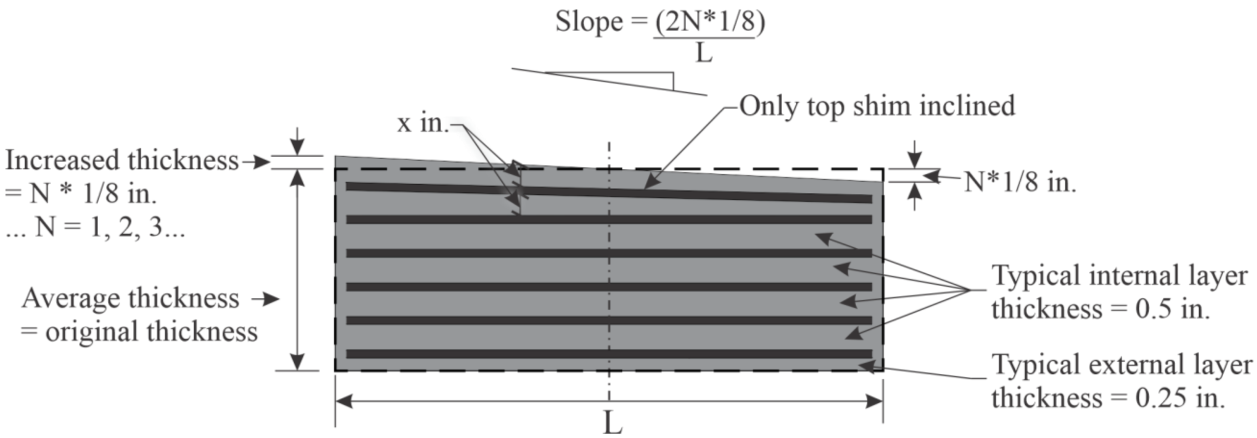

Figure 7-1 Tapered bearing pad configuration

In order to verify whether the pads tested in this study were fabricated in accordance with AASHTO M251 (2016) and FDOT (2018) tolerances, thirteen (13) full-size tapered pads were dissected. Additionally, four (4) full-size flat pads were dissected to compare fabrication errors between flat and tapered pads. Pads were dissected as shown in Figure 7-2 using a band saw. Table 7-3 provides a list of the dissected pads. All pads *except* E-0%, F-0% and K-2.1%, were selected for dissection because unexpected results were measured during experimental testing.

Thickness of each elastomer layer was measured at both ends of a pad (for example see Figure 7-3) and at each dissected cross-section. The difference between actual and target elastomer thicknesses (error) was calculated for each elastomer layer in all dissected pads and plotted on a histogram as shown in Figure 7-4. The count on the y-axis was normalized to compare results from tests on dissected tapered and flat pads. Similarly, ratio of actual and target elastomer layer thicknesses was plotted on a normalized histogram as shown in Figure 7-5. The tolerance for difference between actual and target elastomer layer thicknesses as per FDOT Standard Specifications for Road and Bridge Construction (FDOT, 2018) is ±0.125 in. Based on the measurements on dissected pads, 10.5% and 10% of total elastomer layers from tapered and flat pads respectively had thicknesses out of tolerance. Further, the mean and standard deviation of error in elastomer layer thicknesses were similar for flat and tapered pads (Figure 7-4). The coefficients of variation (COV) for the ratios of actual and target thicknesses were also similar for flat and tapered pads (approximately 23%). Therefore, the measurements on dissected pads indicated that tapered pads had similar error in elastomer layer thickness compared to flat pads. In other words, use of one inclined shim in tapered pads did not affect the fabrication tolerances for elastomer layer thickness and shim alignment in bearing pads. Figure 7-6 shows example photos of dissected pads.

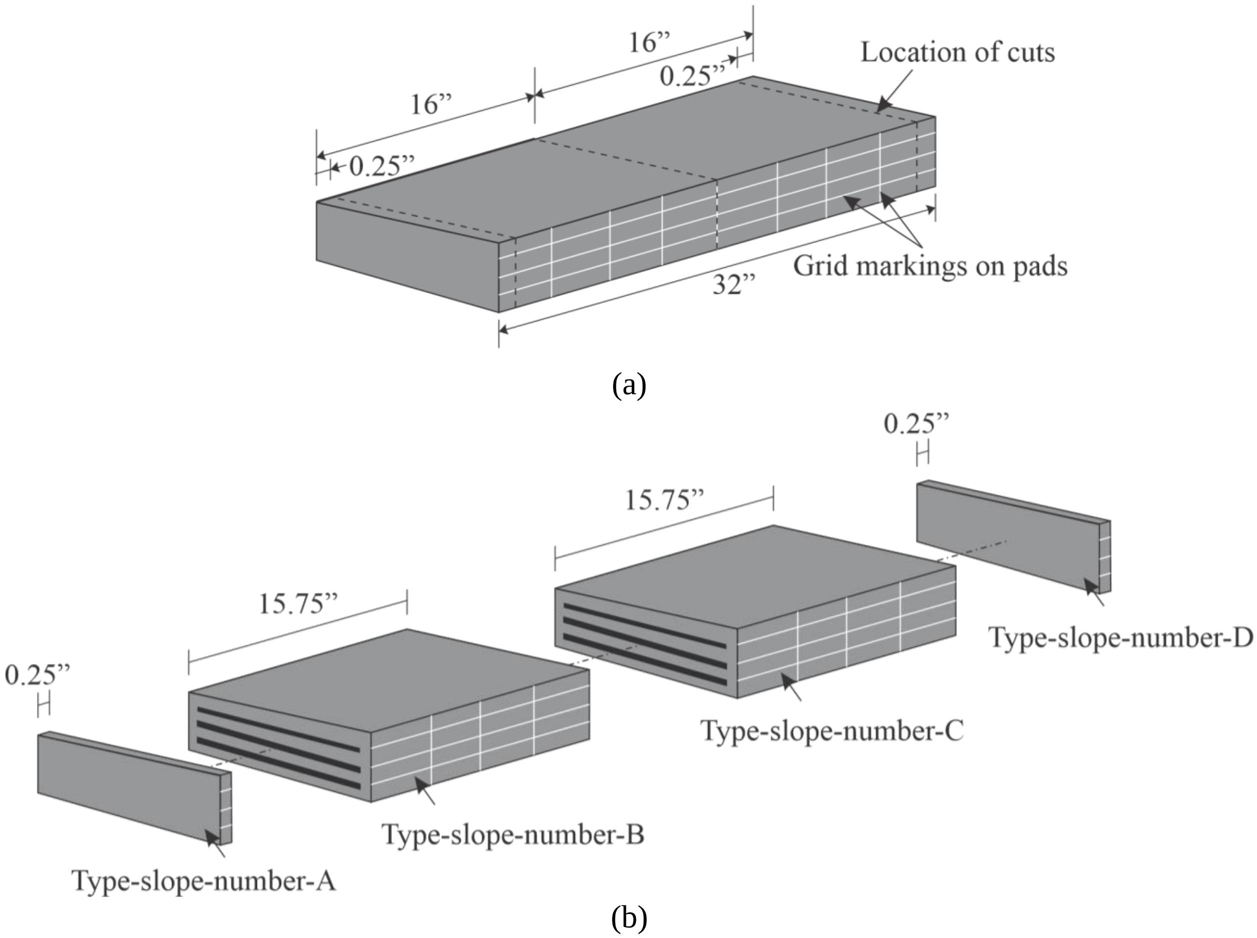

Figure 7-2 Bearing pad dissection schematic: (a) location of cuts; (b) dissected component labels

Table 7-3 List of pads dissected

#	Pad type – slope	Pad numbers	Type-slope-number label
1	E-5.0%	1, 2	E-500-1, E-500-2
2	E-2.5%	1, 2	E-250-1, E-250-2
3	E-2.5%	3, 4	E-250-3, E-250-4
4	E-0.0%	1	E-000-1
5	F-5.0%	1, 2	F-500-1, F-500-2
6	F-2.5%	1, 2	F-250-1, F-250-2
7	F-0.0%	1	F-000-1
8	K-4.2%	1, 2	K-420-1, K-420-2
9	K-2.1%	1	K-210-1
10	K-0.0%	1, 2	K-000-1, K-000-2

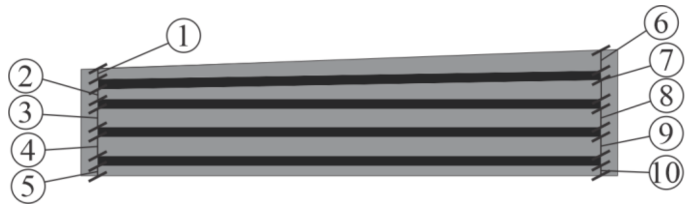

Figure 7-3 Illustration of bearing pad dissection measurement (pad type F)

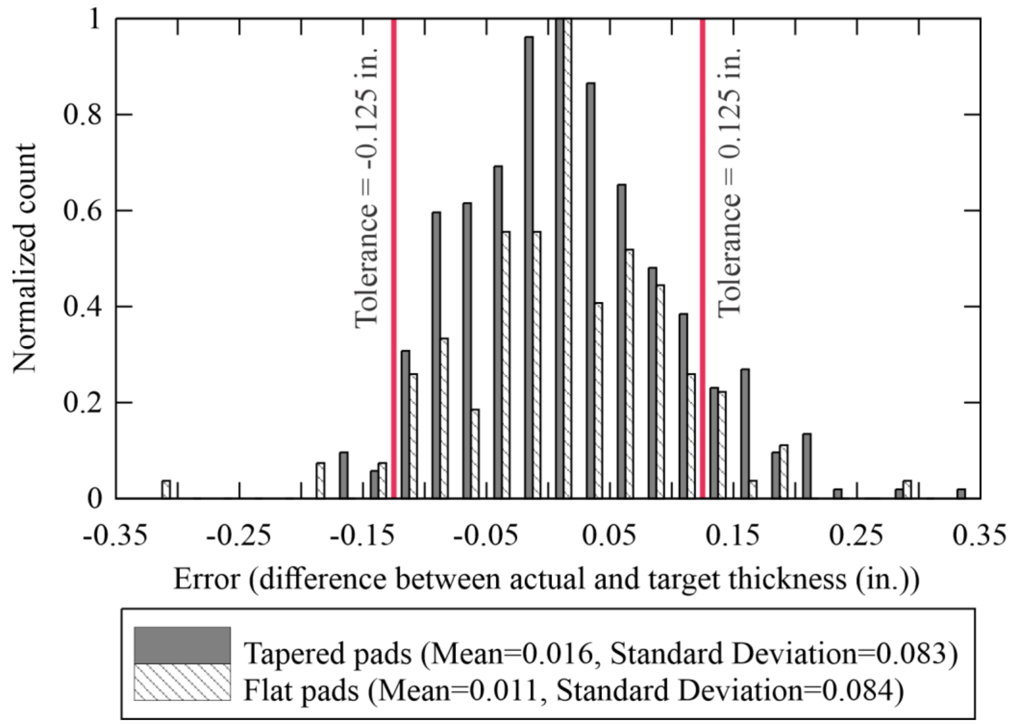

Figure 7-4 Normalized histogram for error (difference between actual and target elastomer thicknesses) in flat and tapered pads

In order to measure the errors in fabricated pad slopes, the slopes (in radians) of top surfaces with respect to bottom surfaces for *all* pads acquired for this research were calculated. Slope was calculated for each bearing pad at three locations as shown in Figure 7-7. Average of absolute differences between measured and target slope (error) at each measurement location was calculated for each bearing pad. Figure 7-8 shows normalized histogram for the average errors in slopes for all flat and tapered pads. The tolerance for bearing pad slope is ±0.005 radians (AASHTO M251-06, 2016; FDOT, 2018). Accordingly, no flat pad had slope out of tolerance. On the other hand, about 27% of tapered pads had slopes out of tolerance. This indicated that fabrication of tapered pads could not satisfy the tolerance for slope.

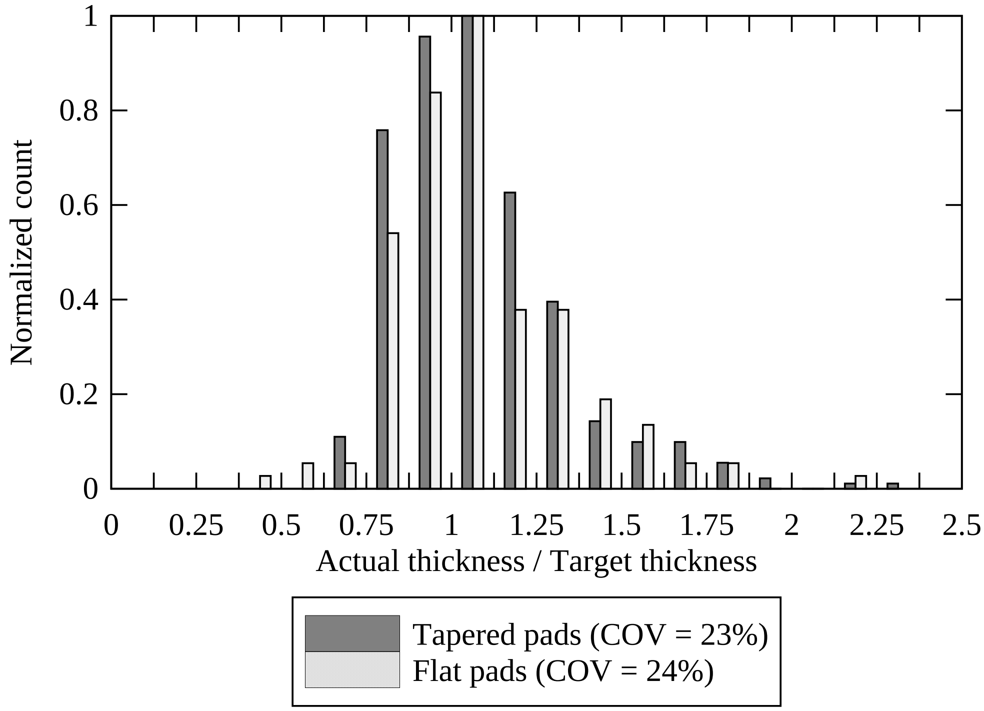

Figure 7-5 Normalized histogram for ratio between actual and target elastomer layer thicknesses in flat and tapered pads

(a) (b)

Figure 7-6 Example of dissected pads: (a) pad F-5%; (b) pad K-4.2%

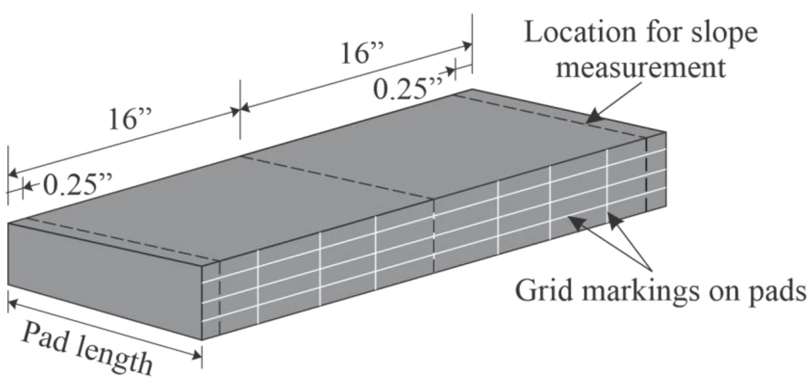

Figure 7-7 Location for bearing pad slope measurements

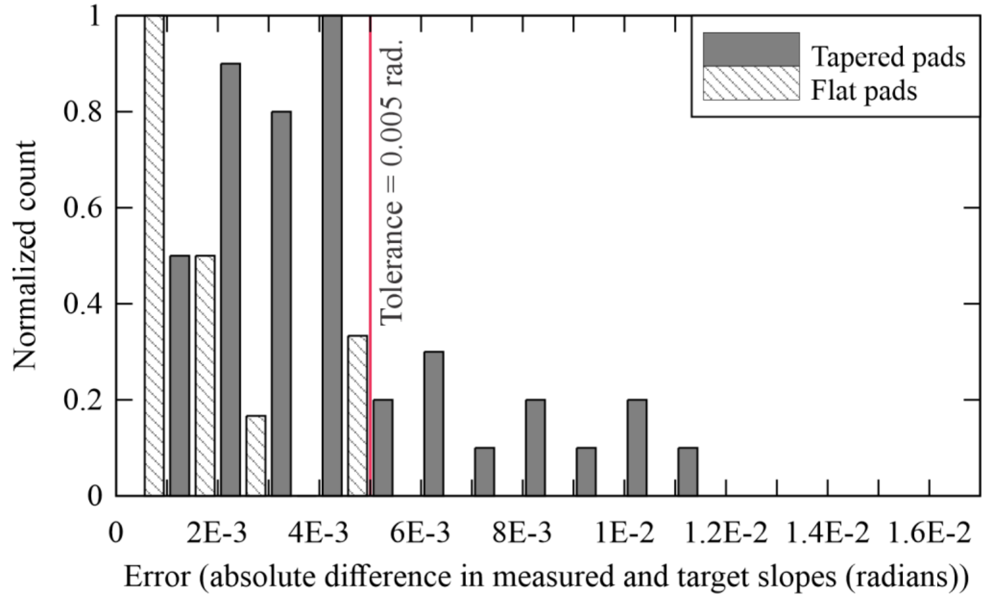

Figure 7-8 Normalized histogram for absolute difference between measured and target slopes

7.3 Structural surface conditions

Slip tests were conducted for both steel and concrete surface conditions. However, in all cases, the *extreme* top and *extreme* bottom steel plate surfaces (Figure 7-9) in contact with the bearing pads were roughened using coarse grit that was adhered to the steel plates with epoxy. The presence of the grit prevented slip from occurring at these locations and forced slip to instead occur at the intended interface between pads and the *middle* plate. Based on slip test results, tapered pads were found to slip before achieving a shear strain (γ) of 0.5, (required by AASHTO LRFD Bridge Design Specifications, 2017) on wet and dry galvanized steel surface conditions which are typical of Florida-I beams (FIBs) at the interface between FIBs and bearing pads. However, tapered pads did achieve a shear strain of 0.5 before slipping on wet and dry concrete surface conditions during experimental testing. Future research is therefore recommended to evaluate different options to prevent premature slip of tapered pads on steel surfaces. Options that should be investigated to prevent premature slip include: the use of keeper plates positioned around the perimeter of the bearing pads; or the use of roughened steel surfaces. Investigation of surface roughening via epoxied grit would further require an evaluation of the service life of such a surface treatment. If mechanical devices, such as keeper plates, were instead used to restrain tapered pad movement, then the horizontal restraining force described in Section 6.3 could be considered as the design force for developing such systems. Note that, full-size tapered pad types E and F could achieve a minimum of 0.2 shear strain before slipping under minimum axial load. Therefore, these tapered pads can be used for shear strain and axial load levels lesser than the existing design levels without modifying the currently used structural surface conditions for FIBs.

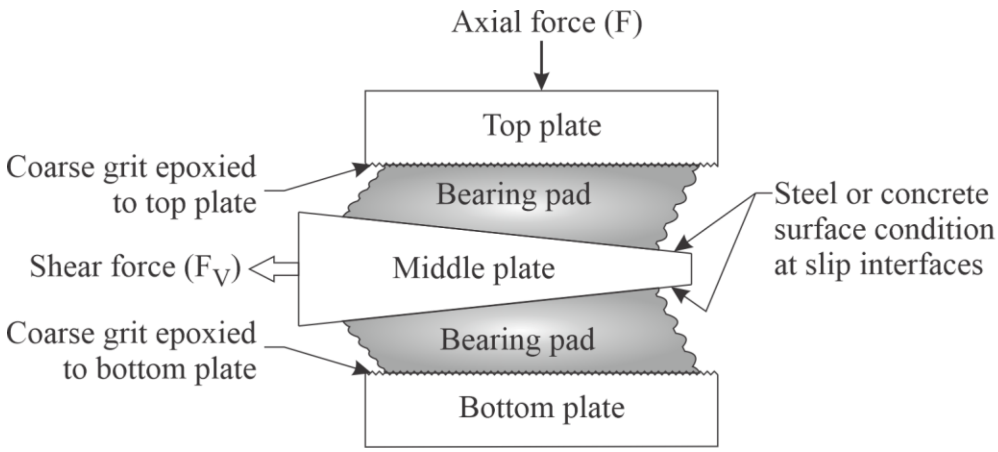

Figure 7-9 Schematic of structural surface conditions used during slip tests

CHAPTER 8
SUMMARY AND CONCLUSIONS

In the present study, "Evaluation of Tapered Bridge Bearing Pads", tapered bearing pads were configured by modifying existing standard FDOT bearing pads. These tapered pads, along with corresponding flat pads, were tested to study the effect of taper on bearing pad properties. An experimental test setup was designed and fabricated to test bearing pads. This setup was designed to apply axial and shear loads on pads in accordance with ASTM standards. The setup was fabricated at the Florida Department of Transportation (FDOT) Structures Research Lab. Using this setup, flat and tapered bearing pads were tested experimentally to determine axial and shear stiffnesses. Tests were also performed to determine horizontal displacement and restraining force in axially loaded tapered pads. Slip tests were performed on pads to determine shear displacement at slip and coefficient of friction under various surface conditions (steel, concrete, dry, wet) and under different axial load levels.

Measurements collected during experimental testing were evaluated, processed if required, and interpreted. Based on the interpretation, equations were developed to approximately calculate bearing pad parameters including axial stiffness, shear stiffness, horizontal displacement and horizontal restraining force in bearing pads. These equations were optimized using respective test data to obtain suitable fitting parameters which produced minimum error between calculated and experimentally measured bearing pad parameters. Axial stiffness of tapered elastomer layers was found to decrease by 21% for every one percent (%) increase in taper slope compared to the stiffness of a flat layer with the same average thickness and same plan dimensions.

Horizontal displacement in tapered pads under pure axial load was found to increase proportional to axial load and taper slope, and inversely proportional to shear stiffness. Further, horizontal restraining force under pure axial load was found to also increase proportional to axial load and taper slope. In contrast, shear stiffness was found to vary by no more than 15% from the stiffness of comparable flat pads as a result of the introduction of taper slope. Shear stiffness was found to be a function of effective shear modulus, pad shear area, and total elastomer thickness, but not a strong function of taper slope.

Shape factors for tapered elastomer layers, calculated using either maximum or average elastomer thickness, produced similar errors between calculated and measured axial stiffness values. Therefore, for simplicity, it is recommended that shape factors for tapered elastomer layers be calculated using average elastomer thickness.

Tapered bearing pads tested in this study were fabricated by changing bearing pad thicknesses in increments of 1/8 in. Tapered pads manufactured in this manner and standard flat pads had similar percentage (approximately 10%) of elastomer layers with out of tolerance thicknesses (>±0.125 in.). The coefficients of variation (COV) for the ratios of actual-to-target thicknesses were also similar for flat and tapered pads (approximately 20%). Measurements on dissected pads indicated that both flat and tapered pads had similar errors in fabrication of the elastomer layer thickness. As such, utilization of a single inclined steel shim plate in tapered pads did not adversely affect the fabrication tolerances for elastomer layer thickness or shim alignment. However, approximately 27% of *all* tapered pads had out-of-tolerance (±0.005 rad.) slopes as compared to 0% of the flat pads. This finding indicates that achieving acceptable slope tolerances in the fabrication of tapered pads will require process improvements on the part of pad manufacturers.

Based on slip test results, tapered pads were found to slip prior to achieving a shear strain of 0.5 (as required by AASHTO) on galvanized steel surface conditions that are typical of Florida-I beams (FIBs). However, tapered pads achieved a shear strain of 0.5 before slipping for both wet and dry concrete surface conditions. Future research is recommended to evaluate different options to prevent premature slip of tapered pads on steel surfaces (e.g. the use of roughened surface texture or mechanical restraint devices). For the design of mechanical devices such as keeper plates, the horizontal pad restraining force, presented in Section 6.3, may be taken as the design force. Note that, full-size tapered pad types E and F achieved a minimum of 0.2 shear strain before slipping under minimum axial load. Therefore, these tapered pads can be used for shear strain and axial load levels lesser than the existing design shear strain and axial load levels without modifying the currently used structural surface conditions for FIBs.

REFERENCES

AASHTO (2017), *AASHTO LRFD Bridge Design Specifications (8th ed.)*, American Association of State Highway and Transportation Officials, Washington, D.C.

AASHTO M251-06. (2016), *Standard Specification for Plain and Steel-Laminated Elastomeric Bearings*, American Association of State Highway and Transportation Officials, Washington, D.C.

Arditzoglou, Y. J., Yura, J. A., & Haines, A. H. (1995), *Test Method for Elastomeric Bearings on Bridges (Report No. FHWA-TX-96/1304-2)*, Texas Department of Transportation, Austin, TX.

ASTM International. (2018), *D4014-03 Standard Specification for Plain and Steel-Laminated Elastomeric Bearings for Bridges*, ASTM International, West Conshohocken, PA, https://doi.org/https://doi.org/10.1520/D4014-03R18.

Burpulis, J. S., Seay, J. R., & Graff, R. S. (1990), *Neoprene in bridge bearing pads - The proven performance*, ASTM Special Technical Publication (Issue 1100, pp. 32–43), American Society for Testing and Materials, Philadelphia, PA, https://doi.org/10.1520/stp14539s.

Cantournet, S., Desmorat, R., & Besson, J. (2009), *Mullins effect and cyclic stress softening of filled elastomers by internal sliding and friction thermodynamics model,* International Journal of Solids and Structures, 46(11–12), 2255–2264. https://doi.org/10.1016/j.ijsolstr.2008.12.025.

Chen, R. A. (1995), *Elastomeric Bridge Bearings: Ozone Protection, Leachate Analysis and National Survey on Movement,* MS Thesis, The University of Texas, Austin, Texas.

Cook, R. A., & Allen, D. T. (2009), *Stiffness Evaluation of Neoprene Bearing Pads Under Long-Term Loads (Report No. BD545 RPWO #39)*, Florida Department of Transportation, Tallahassee, FL.

English, B. A., Klingner, R. E., & Yura, J. A. (1994), *Elastomeric Bearings: Background Information and Field Study (Report No. FHWA/TX-95+ 1304-1),* Texas Department of Transportation, Austin, TX.

FDOT. (2012), *Florida Method of Test for Evaluation of Bearing Pads*, Florida Department of Transportation, Tallahassee, FL.

FDOT. (2016), *IDS Index 20510 Composite Elastomeric Bearing Pads - Prestressed Florida-I Beams*, Florida Department of Transportation, Tallahassee, FL.

FDOT. (2018), *Florida Department of Transportation Standard Specifications for Road and Bridge Construction,* Florida Department of Transportation, Tallahassee, FL.

Fu, C. C., & Angelilli, C. (2007), *Investigation of the Performance of Elastomeric Bearings on Maryland Concrete Bridges (Report No. MD-07-SP608B4L)*, Maryland Department of

Transportation, Baltimore, MD.

Gent, A. N. (1964). *Elastic Stability of Rubber Compression Springs*, Journal of Mechanical Engineering Science, 6(4), 318–326.

Gent, A. N. (2012), *Engineering with Rubber: How to Design Rubber Components 3rd Edition*, Hanser Gardner Publications, Inc., Cincinnati, OH.

Hamzeh, O. N., Tassoulas, J. L., & Becker, E. B. (1998), *Behavior of Elastomeric Bridge Bearings: Computational Results*, Journal of Bridge Engineering, 3(20), 140–146. ISSN 1084-0702198/0003-0140-0146.

Harper, Z. S., & Consolazio, G. R. (2013), *Calculation Method for Quantifying Axial and Roll Stiffnesses of Rectangular Steel-Reinforced Elastomeric Bridge Bearing Pads*, Transportation Research Record: Journal of the Transportation Research Board, Washington, D.C. https://doi.org/10.3141/2331-01

Mullins, L. (1948), *Effect of Stretching on the Properties of Rubber*, Rubber Chemistry and Technology, 21(2), 281–300. https://doi.org/10.5254/1.3546914

Muscarella, J. V, & Yura, J. A. (1995), *An Experimental Study of Elastomeric Bridge Bearings with Design Recommendations (Report No. FHWA/TX-98/1304-3)*, Texas Department of Transportation, Austin, TX.

Najm, H., Nassif, H., & Bezgin, N. O. (2002), *Circular Elastomeric Bearings (Report No. FHWA-NJ-2002-005)*, New Jersey Department of Transportation, Trenton, NJ.

Pinarbasi, S., & Akyuz, U. (2004), *Investigation of Compressive Stiffness of Elastomeric Bearings*, 6th International Congress on Advances in Civil Engineering, October, 6–8, Istanbul, Turkey. https://doi.org/10.1007/BF02686319

Podolny, W., & Muller, J. (1982), *Construction and Design of Prestressed Concrete Segmental Bridges*, John Wiley & Sons, New York, NY.

Pont, D. (1959), *Design of Neoprene Bearing Pads*, E.I. du Pont de Nemours and Company, Wilmington, Delaware.

Roeder, C. W., Stanton, J. F., & Taylor, A. W. (1987), *NCHRP Report 298 - Performance of Elastomeric Bearings*, Transportation Research Board, Washington, D.C.

Roeder, Charles W., & Stanton, J. F. (1983), *Elastomeric bearings: state-of-the-art*, Journal of Structural Engineering, Vol. 109, No. 12, pp. 2853–2871.

Soleimanlo, H. S., & Barkhordar, M. A. (2013), *Effect of Shape Factor and Rubber Stiffness of Fiber-reinforced Elastomeric Bearings on the Vertical Stiffness of Isolators*, Trends in Applied Sciences Research, Vol. 8, Issue 1, pp. 14–25, https://doi.org/10.3923/tasr.2013.14.25

Stanton, J. F., & Roeder, C. W. (1982), *NCHRP Report 248 - Elastomeric bearings design, construction, and materials*, Transportation Research Board, Washington, D.C.

Stanton, J. F., Roeder, C. W., Mackenzie-Helnwein, P., White, C., Kuester, C., & Craig, B. (2004), *NCHRP 12-68 Rotational Limits for Elastomeric Bearings Final Report Appendix F*, Transportation Research Record, Washington, D.C.

United States Access Board. (2011), *Proposed Guidelines for Pedestrian Facilities in the Public Right-of-Way*, United States Access Board, Washington, D.C.

Xcitex. (2017), *ProAnalyst User Guide*, Xcitex Inc., Woburn, MA

APPENDIX A
BEARING PAD SHOP DRAWINGS

On the following pages, shop drawings are provided for flat and tapered bearing pads fabricated for this study.

NO.	MK	QTY.	Thick	Dia.	Width	Length	Part	Material	Coating	Remarks	WT	Oracle Seed
1	1A	4					VERSIFLEX ELASTOMERIC BEARING				75.6	1103AT-A^
1.1	eb1	1	4.057	A	16.000	12.000	Elastomeric Bearing	150 PSI +/- 15% GR. 3 Neoprene	Plain	BEVELED	34.8	
1.2	es1	6	10 GA.		15.500	11.500	Shim (internal)	A1011 GR. 36	Plain		6.8	

ASSEMBLY SCHEDULE		
MK	LOCATION	QTY.
1A	TYPE K HALF SIZE W/ 4.17% SLOPE	4

TOLERANCE TABLE	
DESCRIPTION	TOLERANCE (INCHES U.N.O.)
ELASTOMERIC BEARING DESIGN THICKNESS ≤ 1.250"	-0, +0.125
ELASTOMERIC BEARING DESIGN THICKNESS > 1.250"	-0, +0.25
ELASTOMERIC BEARING PLAN DIMENSIONS ≤ 36"	-0, +0.25
ELASTOMERIC BEARING PLAN DIMENSIONS > 36"	-0, +0.50
THICKNESS OF INDIVIDUAL LAYERS OF ELASTOMER (LAMINATED BEARINGS ONLY) AT ANY POINT WITHIN THE BEARING	±0.125
VARIATION FROM A PLANE PARALLEL TO THE THEORETICAL SURFACE (AS DETERMINED BY MEASUREMENTS AT THE EDGE OF THE BEARINGS) (PARALLELISM):	
TOP & BOTTOM	≤ 0.005 RAD
SIDES	±0.250
POSITION OF EXPOSED CONNECTION MEMBERS	±0.125
ELASTOMERIC EDGE COVER	-0, +0.125
ELASTOMERIC BEARING HOLE OR SLOT SIZE	±0.125
ELASTOMERIC BEARING HOLE OR SLOT LOCATION	±0.125

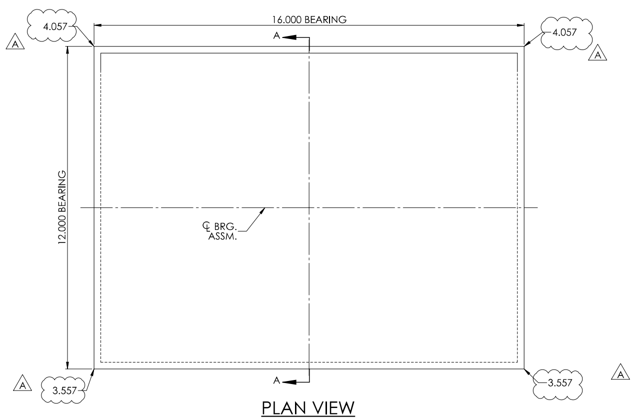

PLAN VIEW
(SEE ASSEMBLY SCHEDULE)

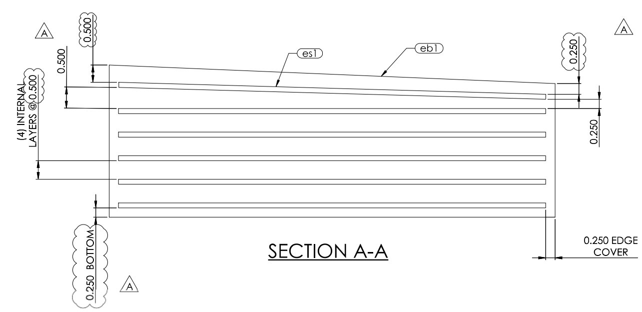

SECTION A-A

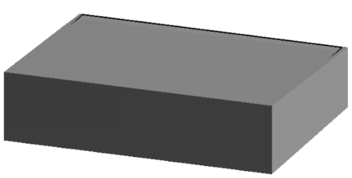

GENERAL NOTES:

1. ALL MATERIALS SHALL CONFORM TO THE 2018 FLORIDA DEPARTMENT OF TRANSPORTATION STANDARD SPECIFICATIONS FOR ROAD AND BRIDGE CONSTRUCTION.
2. THIS SHOP DRAWING WAS PREPARED IN ACCORDANCE WITH THE CONTRACT PLANS AND SPECIFICATIONS. THE D.S. BROWN COMPANY DOES NOT ACCEPT LIABILITY FOR THE DESIGN OF THE PRODUCTS DETAILED IN THIS SHOP DRAWING.
3. THE D.S. BROWN COMPANY TO SUPPLY ONLY THE PARTS SHOWN ON THIS DRAWING.
4. EXPOSED LAMINATES ON THE OUTSIDE SURFACES OF THE PAD, APPARENT AS A RESULT OF MANUFACTURING TECHNIQUES, SHALL BE SEALED FLUSH ON THE FINISHED BEARING PAD WITH A BONDED VULCANIZED PATCH CONSISTING OF MATERIAL EQUIVALENT TO THAT USED IN THE MANUFACTURING OF THE PAD.
5. INTERNAL ALIGNMENT PINS: AFTER FABRICATION, HOLES TO BE FILLED WITH ELASTOMER MATERIAL EQUIVALENT TO THAT USED IN THE MANUFACTURING OF THE PAD.
6. WELDING PROCEDURES, IF APPLICABLE, SHALL BE ESTABLISHED BY THE CONTRACTOR TO RESTRICT THE MAXIMUM TEMPERATURE REACHED BY SURFACES IN CONTACT WITH THE ELASTOMER TO 200°F (93°C). TEMPERATURES SHALL BE DETERMINED BY TEMPERATURE INDICATING WAX PENCILS OR OTHER SUITABLE MEANS.

REV.	DESCRIPTION	DATE	DET.	CKD.
A	REVISED AS NOTED	4/17/19	RTP	EMF

D.S. BROWN
A GIBRALTAR INDUSTRIES COMPANY

THE D.S. BROWN COMPANY
300 E. CHERRY STREET
NORTH BALTIMORE, OHIO 45872
419.257.3561
FAX: 419.257.0332
WWW.DSBROWN.COM

CUSTOMER — UNIVERSITY OF FLORIDA

DESCRIPTION	SCALE	DRAWN BY	CHECKED BY	DATE	
VERSIFLEX ELASTOMERIC BEARING ALACHUA COUNTY, FLORIDA	N.T.S.	RTP	EMF	3/19	-
	PROJECT NUMBER	PRODUCT CODE	UNITS	SHEET	
	4001021	1103	INCHES	01	

FILE SAVED: 4/18/19 9:46:41 AM

NO.	MK	QTY.	Thick	Dia.	Width	Length	Part	Material	Coating	Remarks	WT	Oracle Seed
1	2A	4	A				VERSIFLEX ELASTOMERIC BEARING				75.6	1103AT-8^
1.1	eb2	1	3.932		16.000	12.000	Elastomeric Bearing	150 PSI +/- 15% GR. 3 Neoprene	Plain	BEVELED	34.8	
1.2	es2	6	10 GA.		15.500	11.500	Shim (internal)	A1011 GR. 36	Plain		6.8	

ASSEMBLY SCHEDULE		
MK	LOCATION	QTY.
2A	TYPE K HALF SIZE W/ 2.09% SLOPE	4

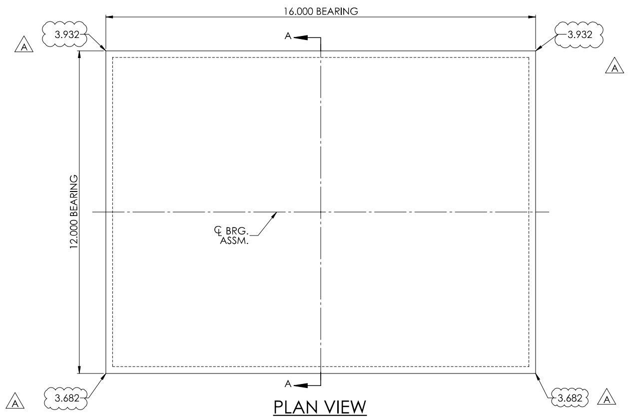

PLAN VIEW

(SEE ASSEMBLY SCHEDULE)

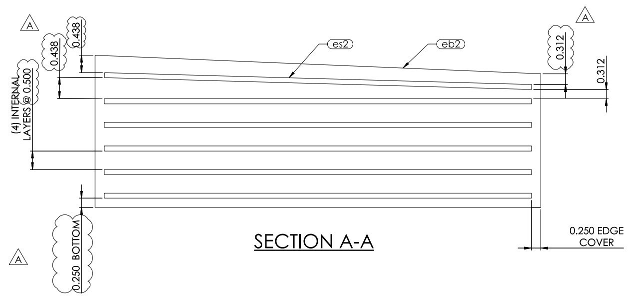

SECTION A-A

TOLERANCE TABLE	
DESCRIPTION	TOLERANCE (INCHES U.N.O.)
ELASTOMERIC BEARING DESIGN THICKNESS ≤ 1.250"	-0, +0.125
ELASTOMERIC BEARING DESIGN THICKNESS > 1.250"	-0, +0.25
ELASTOMERIC BEARING PLAN DIMENSIONS ≤ 36"	-0, +0.25
ELASTOMERIC BEARING PLAN DIMENSIONS > 36"	-0, +0.50
THICKNESS OF INDIVIDUAL LAYERS OF ELASTOMER (LAMINATED BEARINGS ONLY) AT ANY POINT WITHIN THE BEARING	±0.125
VARIATION FROM A PLANE PARALLEL TO THE THEORETICAL SURFACE (AS DETERMINED BY MEASUREMENTS AT THE EDGE OF THE BEARINGS) (PARALLELISM):	
TOP & BOTTOM	≤ 0.005 RAD
SIDES	±0.250
POSITION OF EXPOSED CONNECTION MEMBERS	±0.125
ELASTOMERIC EDGE COVER	-0, +0.125
ELASTOMERIC BEARING HOLE OR SLOT SIZE	±0.125
ELASTOMERIC BEARING HOLE OR SLOT LOCATION	±0.125

GENERAL NOTES:

1. ALL MATERIALS SHALL CONFORM TO THE 2018 FLORIDA DEPARTMENT OF TRANSPORTATION STANDARD SPECIFICATIONS FOR ROAD AND BRIDGE CONSTRUCTION.
2. THIS SHOP DRAWING WAS PREPARED IN ACCORDANCE WITH THE CONTRACT PLANS AND SPECIFICATIONS. THE D.S. BROWN COMPANY DOES NOT ACCEPT LIABILITY FOR THE DESIGN OF THE PRODUCTS DETAILED IN THIS SHOP DRAWING.
3. THE D.S. BROWN COMPANY TO SUPPLY ONLY THE PARTS SHOWN ON THIS DRAWING.
4. EXPOSED LAMINATES ON THE OUTSIDE SURFACES OF THE PAD, APPARENT AS A RESULT OF MANUFACTURING TECHNIQUES, SHALL BE SEALED FLUSH ON THE FINISHED BEARING PAD WITH A BONDED VULCANIZED PATCH CONSISTING OF MATERIAL EQUIVALENT TO THAT USED IN THE MANUFACTURING OF THE PAD.
5. INTERNAL ALIGNMENT PINS: AFTER FABRICATION, HOLES TO BE FILLED WITH ELASTOMER MATERIAL EQUIVALENT TO THAT USED IN THE MANUFACTURING OF THE PAD.
6. WELDING PROCEDURES, IF APPLICABLE, SHALL BE ESTABLISHED BY THE CONTRACTOR TO RESTRICT THE MAXIMUM TEMPERATURE REACHED BY SURFACES IN CONTACT WITH THE ELASTOMER TO 200°F (93°C). TEMPERATURES SHALL BE DETERMINED BY TEMPERATURE INDICATING WAX PENCILS OR OTHER SUITABLE MEANS.

REV.	DESCRIPTION	DATE	DET.	CKD.
A	REVISED AS NOTED	4/17/19	RTP	EMF

D.S. BROWN
A GIBRALTAR INDUSTRIES COMPANY

THE D.S. BROWN COMPANY
300 E. CHERRY STREET
NORTH BALTIMORE, OHIO 45872
419.257.3561
FAX: 419.257.0332
WWW.DSBROWN.COM

CUSTOMER — UNIVERSITY OF FLORIDA

DESCRIPTION	SCALE	DRAWN BY	CHECKED BY	DATE	
VERSIFLEX ELASTOMERIC BEARING ALACHUA COUNTY, FLORIDA	N.T.S.	RTP	EMF	3/19	-
	PROJECT NUMBER	PRODUCT CODE	UNITS	SHEET	
	4001021	1103	INCHES	02	

FILE SAVED: 4/18/19 9:46:41 AM

NO.	MK	QTY.	Thick	Dia.	Width	Length	Part	Material	Coating	Remarks	WT	Oracle Seed
1	3A	2	A				VERSIFLEX ELASTOMERIC BEARING				75.6	1103AT-C^
1.1	eb3	1	3.807		16.000	12.000	Elastomeric Bearing	150 PSI +/- 15% GR. 3 Neoprene	Plain		34.8	
1.2	es3	6	10 GA.		15.500	11.500	Shim (internal)	A1011 GR. 36	Plain		6.8	

ASSEMBLY SCHEDULE		
MK	LOCATION	QTY.
3A	TYPE K HALF SIZE - FLAT	2

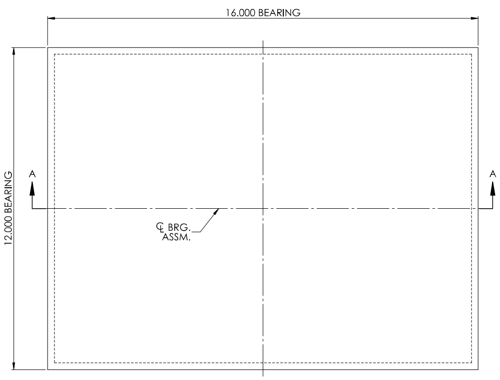

PLAN VIEW
(SEE ASSEMBLY SCHEDULE)

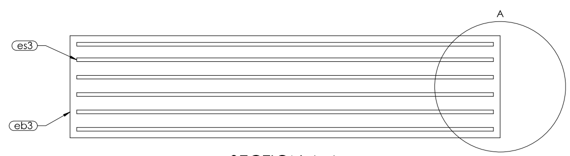

SECTION A-A

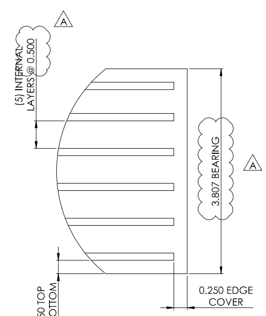

DETAIL A

TOLERANCE TABLE	
DESCRIPTION	TOLERANCE (INCHES U.N.O.)
ELASTOMERIC BEARING DESIGN THICKNESS ≤ 1.250"	-0, +0.125
ELASTOMERIC BEARING DESIGN THICKNESS > 1.250"	-0, +0.25
ELASTOMERIC BEARING PLAN DIMENSIONS ≤ 36"	-0, +0.25
ELASTOMERIC BEARING PLAN DIMENSIONS > 36"	-0, +0.50
THICKNESS OF INDIVIDUAL LAYERS OF ELASTOMER (LAMINATED BEARINGS ONLY) AT ANY POINT WITHIN THE BEARING	±0.125
VARIATION FROM A PLANE PARALLEL TO THE THEORETICAL SURFACE (AS DETERMINED BY MEASUREMENTS AT THE EDGE OF THE BEARINGS) (PARALLELISM):	
TOP & BOTTOM	< 0.005 RAD
SIDES	±0.250
POSITION OF EXPOSED CONNECTION MEMBERS	±0.125
ELASTOMERIC EDGE COVER	-0, +0.125
ELASTOMERIC BEARING HOLE OR SLOT SIZE	±0.125
ELASTOMERIC BEARING HOLE OR SLOT LOCATION	±0.125

GENERAL NOTES:

1. ALL MATERIALS SHALL CONFORM TO THE 2018 FLORIDA DEPARTMENT OF TRANSPORTATION STANDARD SPECIFICATIONS FOR ROAD AND BRIDGE CONSTRUCTION.
2. THIS SHOP DRAWING WAS PREPARED IN ACCORDANCE WITH THE CONTRACT PLANS AND SPECIFICATIONS. THE D.S. BROWN COMPANY DOES NOT ACCEPT LIABILITY FOR THE DESIGN OF THE PRODUCTS DETAILED IN THIS SHOP DRAWING.
3. THE D.S. BROWN COMPANY TO SUPPLY ONLY THE PARTS SHOWN ON THIS DRAWING.
4. EXPOSED LAMINATES ON THE OUTSIDE SURFACES OF THE PAD, APPARENT AS A RESULT OF MANUFACTURING TECHNIQUES, SHALL BE SEALED FLUSH ON THE FINISHED BEARING PAD WITH A BONDED VULCANIZED PATCH CONSISTING OF MATERIAL EQUIVALENT TO THAT USED IN THE MANUFACTURING OF THE PAD.
5. INTERNAL ALIGNMENT PINS: AFTER FABRICATION, HOLES TO BE FILLED WITH ELASTOMER MATERIAL EQUIVALENT TO THAT USED IN THE MANUFACTURING OF THE PAD.
6. WELDING PROCEDURES, IF APPLICABLE, SHALL BE ESTABLISHED BY THE CONTRACTOR TO RESTRICT THE MAXIMUM TEMPERATURE REACHED BY SURFACES IN CONTACT WITH THE ELASTOMER TO 200°F (93°C). TEMPERATURES SHALL BE DETERMINED BY TEMPERATURE INDICATING WAX PENCILS OR OTHER SUITABLE MEANS.

REV.	DESCRIPTION	DATE	DET.	CKD.
A	REVISED AS NOTED	4/17/19	RTP	EMF

D.S. BROWN
A GIBRALTAR INDUSTRIES COMPANY

THE D.S. BROWN COMPANY
300 E. CHERRY STREET
NORTH BALTIMORE, OHIO 45872
419.257.3561
FAX: 419.257.0332
WWW.DSBROWN.COM

CUSTOMER — UNIVERSITY OF FLORIDA

DESCRIPTION	SCALE	DRAWN BY	CHECKED BY	DATE	
VERSIFLEX ELASTOMERIC BEARING	N.T.S.	RTP	EMF	3/19	-
ALACHUA COUNTY, FLORIDA	PROJECT NUMBER 4001021	PRODUCT CODE 1103	UNITS INCHES	SHEET 03	

FILE SAVED: 4/18/19 9:46:42 AM

NO.	MK	QTY.	Thick	Dia.	Width	Length	Part	Material	Coating	Remarks	WT	Oracle Seed
1	4A	4					VERSIFLEX ELASTOMERIC BEARING				31.4	1103AT-D^
1.1	eb4	1	2.154 A		16.000	10.000	Elastomeric Bearing	110 PSI +/- 15% GR. 3 Neoprene	Plain	BEVELED	14.6	
1.2	es4	3	10 GA.		15.500	9.500	Shim (internal)	A1011 GR. 36	Plain		5.6	

ASSEMBLY SCHEDULE		
MK	LOCATION	QTY.
4A	TYPE E HALF SIZE W/ 5% SLOPE	4

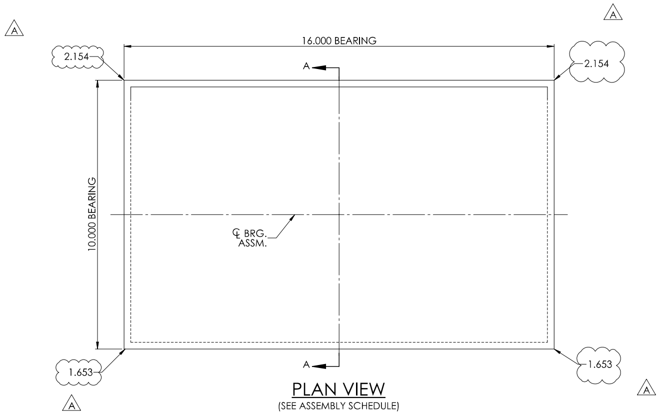

PLAN VIEW
(SEE ASSEMBLY SCHEDULE)

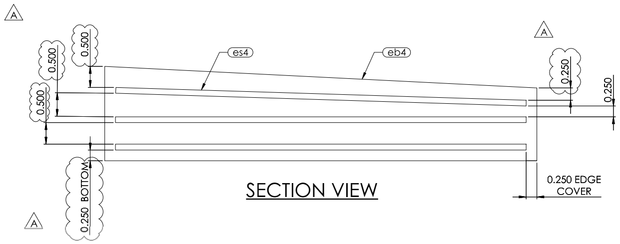

SECTION VIEW

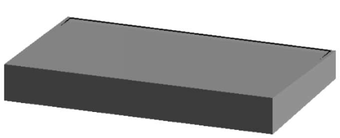

TOLERANCE TABLE	
DESCRIPTION	TOLERANCE (INCHES U.N.O.)
ELASTOMERIC BEARING DESIGN THICKNESS ≤ 1.250"	-0, +0.125
ELASTOMERIC BEARING DESIGN THICKNESS > 1.250"	-0, +0.25
ELASTOMERIC BEARING PLAN DIMENSIONS ≤ 36"	-0, +0.25
ELASTOMERIC BEARING PLAN DIMENSIONS > 36"	-0, +0.50
THICKNESS OF INDIVIDUAL LAYERS OF ELASTOMER (LAMINATED BEARINGS ONLY) AT ANY POINT WITHIN THE BEARING	±0.125
VARIATION FROM A PLANE PARALLEL TO THE THEORETICAL SURFACE (AS DETERMINED BY MEASUREMENTS AT THE EDGE OF THE BEARINGS) (PARALLELISM):	
TOP & BOTTOM	< 0.005 RAD
SIDES	±0.250
POSITION OF EXPOSED CONNECTION MEMBERS	±0.125
ELASTOMERIC EDGE COVER	-0, +0.125
ELASTOMERIC BEARING HOLE OR SLOT SIZE	±0.125
ELASTOMERIC BEARING HOLE OR SLOT LOCATION	±0.125

GENERAL NOTES:

1. ALL MATERIALS SHALL CONFORM TO THE 2018 FLORIDA DEPARTMENT OF TRANSPORTATION STANDARD SPECIFICATIONS FOR ROAD AND BRIDGE CONSTRUCTION.
2. THIS SHOP DRAWING WAS PREPARED IN ACCORDANCE WITH THE CONTRACT PLANS AND SPECIFICATIONS. THE D.S. BROWN COMPANY DOES NOT ACCEPT LIABILITY FOR THE DESIGN OF THE PRODUCTS DETAILED IN THIS SHOP DRAWING.
3. THE D.S. BROWN COMPANY TO SUPPLY ONLY THE PARTS SHOWN ON THIS DRAWING.
4. EXPOSED LAMINATES ON THE OUTSIDE SURFACES OF THE PAD, APPARENT AS A RESULT OF MANUFACTURING TECHNIQUES, SHALL BE SEALED FLUSH ON THE FINISHED BEARING PAD WITH A BONDED VULCANIZED PATCH CONSISTING OF MATERIAL EQUIVALENT TO THAT USED IN THE MANUFACTURING OF THE PAD.
5. INTERNAL ALIGNMENT PINS: AFTER FABRICATION, HOLES TO BE FILLED WITH ELASTOMER MATERIAL EQUIVALENT TO THAT USED IN THE MANUFACTURING OF THE PAD.
6. WELDING PROCEDURES, IF APPLICABLE, SHALL BE ESTABLISHED BY THE CONTRACTOR TO RESTRICT THE MAXIMUM TEMPERATURE REACHED BY SURFACES IN CONTACT WITH THE ELASTOMER TO 200°F (93°C). TEMPERATURES SHALL BE DETERMINED BY TEMPERATURE INDICATING WAX PENCILS OR OTHER SUITABLE MEANS.

REV.	DESCRIPTION	DATE	DET.	CKD.
A	REVISED AS NOTED	4/17/19	RTP	EMF

D.S. BROWN
A GIBRALTAR INDUSTRIES COMPANY

THE D.S. BROWN COMPANY
300 E. CHERRY STREET
NORTH BALTIMORE, OHIO 45872
419.257.3561
FAX: 419.257.0332
WWW.DSBROWN.COM

CUSTOMER — UNIVERSITY OF FLORIDA

DESCRIPTION: VERSIFLEX ELASTOMERIC BEARING
ALACHUA COUNTY, FLORIDA

SCALE	DRAWN BY	CHECKED BY	DATE	
N.T.S.	RTP	EMF	3/19	-
PROJECT NUMBER	PRODUCT CODE	UNITS	SHEET	
4001021	1103	INCHES	04	

FILE SAVED: 4/18/19 9:46:43 AM

NO.	MK	QTY.	Thick	Dia.	Width	Length	Part	Material	Coating	Remarks	WT	Oracle Seed
1	5A	4					VERSIFLEX ELASTOMERIC BEARING				31.4	1103AT-E^
1.1	eb5	1	2.029	A	16.000	10.000	Elastomeric Bearing	110 PSI +/- 15% GR. 3 Neoprene	Plain	BEVELED	14.6	
1.2	es5	3	10 GA.		15.500	9.500	Shim (internal)	A1011 GR. 36	Plain		5.6	

ASSEMBLY SCHEDULE		
MK	LOCATION	QTY.
5A	TYPE E HALF SIZE W/ 2.51% SLOPE	4

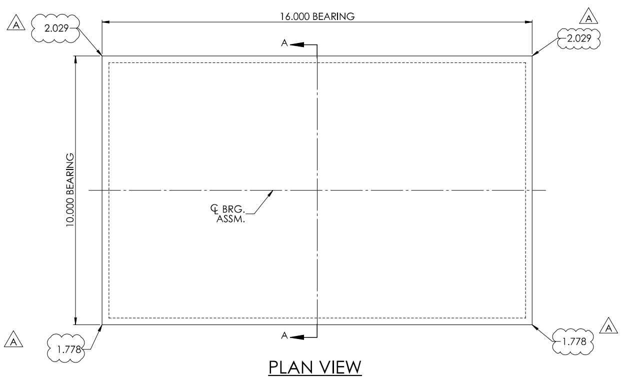

PLAN VIEW
(SEE ASSEMBLY SCHEDULE)

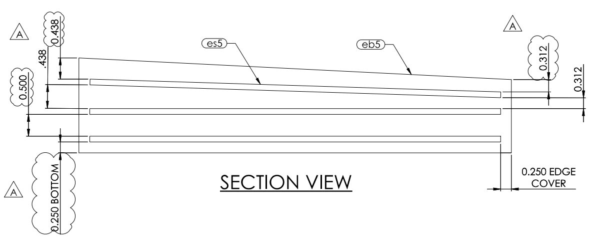

SECTION VIEW

TOLERANCE TABLE	
DESCRIPTION	TOLERANCE (INCHES U.N.O.)
ELASTOMERIC BEARING DESIGN THICKNESS ≤ 1.250"	-0, +0.125
ELASTOMERIC BEARING DESIGN THICKNESS > 1.250"	-0, +0.25
ELASTOMERIC BEARING PLAN DIMENSIONS ≤ 36"	-0, +0.25
ELASTOMERIC BEARING PLAN DIMENSIONS > 36"	-0, +0.50
THICKNESS OF INDIVIDUAL LAYERS OF ELASTOMER (LAMINATED BEARINGS ONLY) AT ANY POINT WITHIN THE BEARING	±0.125
VARIATION FROM A PLANE PARALLEL TO THE THEORETICAL SURFACE (AS DETERMINED BY MEASUREMENTS AT THE EDGE OF THE BEARINGS) (PARALLELISM):	
TOP & BOTTOM	≤ 0.005 RAD
SIDES	±0.250
POSITION OF EXPOSED CONNECTION MEMBERS	±0.125
ELASTOMERIC EDGE COVER	-0, +0.125
ELASTOMERIC BEARING HOLE OR SLOT SIZE	±0.125
ELASTOMERIC BEARING HOLE OR SLOT LOCATION	±0.125

GENERAL NOTES:

1. ALL MATERIALS SHALL CONFORM TO THE 2018 FLORIDA DEPARTMENT OF TRANSPORTATION STANDARD SPECIFICATIONS FOR ROAD AND BRIDGE CONSTRUCTION.

2. THIS SHOP DRAWING WAS PREPARED IN ACCORDANCE WITH THE CONTRACT PLANS AND SPECIFICATIONS. THE D.S. BROWN COMPANY DOES NOT ACCEPT LIABILITY FOR THE DESIGN OF THE PRODUCTS DETAILED IN THIS SHOP DRAWING.

3. THE D.S. BROWN COMPANY TO SUPPLY ONLY THE PARTS SHOWN ON THIS DRAWING.

4. EXPOSED LAMINATES ON THE OUTSIDE SURFACES OF THE PAD, APPARENT AS A RESULT OF MANUFACTURING TECHNIQUES, SHALL BE SEALED FLUSH ON THE FINISHED BEARING PAD WITH A BONDED VULCANIZED PATCH CONSISTING OF MATERIAL EQUIVALENT TO THAT USED IN THE MANUFACTURING OF THE PAD.

5. INTERNAL ALIGNMENT PINS: AFTER FABRICATION, HOLES TO BE FILLED WITH ELASTOMER MATERIAL EQUIVALENT TO THAT USED IN THE MANUFACTURING OF THE PAD.

6. WELDING PROCEDURES, IF APPLICABLE, SHALL BE ESTABLISHED BY THE CONTRACTOR TO RESTRICT THE MAXIMUM TEMPERATURE REACHED BY SURFACES IN CONTACT WITH THE ELASTOMER TO 200°F (93°C). TEMPERATURES SHALL BE DETERMINED BY TEMPERATURE INDICATING WAX PENCILS OR OTHER SUITABLE MEANS.

REV.	DESCRIPTION	DATE	DET.	CKD.
A	REVISED AS NOTED	4/17/19	RTP	EMF

D.S. BROWN
A GIBRALTAR INDUSTRIES COMPANY

THE D.S. BROWN COMPANY
300 E. CHERRY STREET
NORTH BALTIMORE, OHIO 45872
419.257.3561
FAX: 419.257.0332
WWW.DSBROWN.COM

CUSTOMER — UNIVERSITY OF FLORIDA

DESCRIPTION	SCALE	DRAWN BY	CHECKED BY	DATE	
VERSIFLEX ELASTOMERIC BEARING ALACHUA COUNTY, FLORIDA	N.T.S.	RTP	EMF	3/19	-
	PROJECT NUMBER	PRODUCT CODE	UNITS	SHEET	
	4001021	1103	INCHES	05	

FILE SAVED: 4/18/19 9:46:43 AM

NO.	MK	QTY.	Thick	Dia.	Width	Length	Part	Material	Coating	Remarks	WT	Oracle Seed
1	6A	2		A			VERSIFLEX ELASTOMERIC BEARING				31.4	1103AT-F^
1.1	eb6	1	1.904		16.000	10.000	Elastomeric Bearing	110 PSI +/- 15% GR. 3 Neoprene	Plain		14.6	
1.2	es6	3	10 GA.		15.500	9.500	Shim (internal)	A1011 GR. 36	Plain		5.6	

ASSEMBLY SCHEDULE		
MK	LOCATION	QTY.
6A	TYPE E HALF SIZE - FLAT	2

TOLERANCE TABLE	
DESCRIPTION	TOLERANCE (INCHES U.N.O.)
ELASTOMERIC BEARING DESIGN THICKNESS ≤ 1.250"	-0, +0.125
ELASTOMERIC BEARING DESIGN THICKNESS > 1.250"	-0, +0.25
ELASTOMERIC BEARING PLAN DIMENSIONS ≤ 36"	-0, +0.25
ELASTOMERIC BEARING PLAN DIMENSIONS > 36"	-0, +0.50
THICKNESS OF INDIVIDUAL LAYERS OF ELASTOMER (LAMINATED BEARINGS ONLY) AT ANY POINT WITHIN THE BEARING	±0.125
VARIATION FROM A PLANE PARALLEL TO THE THEORETICAL SURFACE (AS DETERMINED BY MEASUREMENTS AT THE EDGE OF THE BEARINGS) (PARALLELISM):	
TOP & BOTTOM	≤ 0.005 RAD
SIDES	±0.250
POSITION OF EXPOSED CONNECTION MEMBERS	±0.125
ELASTOMERIC EDGE COVER	-0, +0.125
ELASTOMERIC BEARING HOLE OR SLOT SIZE	±0.125
ELASTOMERIC BEARING HOLE OR SLOT LOCATION	±0.125

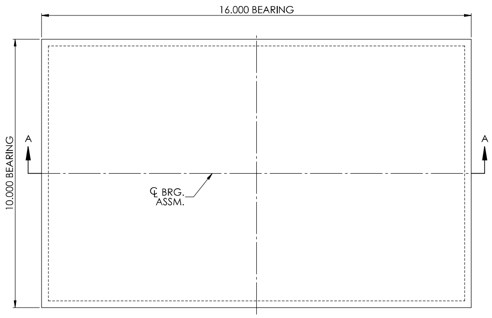

PLAN VIEW
(SEE ASSEMBLY SCHEDULE)

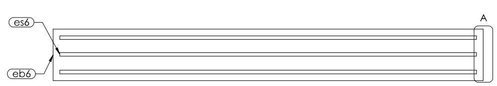

SECTION A-A

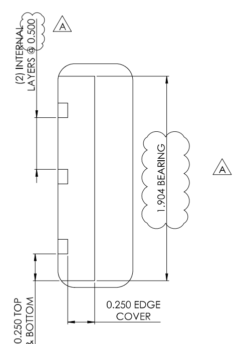

DETAIL A

GENERAL NOTES:

1. ALL MATERIALS SHALL CONFORM TO THE 2018 FLORIDA DEPARTMENT OF TRANSPORTATION STANDARD SPECIFICATIONS FOR ROAD AND BRIDGE CONSTRUCTION.
2. THIS SHOP DRAWING WAS PREPARED IN ACCORDANCE WITH THE CONTRACT PLANS AND SPECIFICATIONS. THE D.S. BROWN COMPANY DOES NOT ACCEPT LIABILITY FOR THE DESIGN OF THE PRODUCTS DETAILED IN THIS SHOP DRAWING.
3. THE D.S. BROWN COMPANY TO SUPPLY ONLY THE PARTS SHOWN ON THIS DRAWING.
4. EXPOSED LAMINATES ON THE OUTSIDE SURFACES OF THE PAD, APPARENT AS A RESULT OF MANUFACTURING TECHNIQUES, SHALL BE SEALED FLUSH ON THE FINISHED BEARING PAD WITH A BONDED VULCANIZED PATCH CONSISTING OF MATERIAL EQUIVALENT TO THAT USED IN THE MANUFACTURING OF THE PAD.
5. INTERNAL ALIGNMENT PINS: AFTER FABRICATION, HOLES TO BE FILLED WITH ELASTOMER MATERIAL EQUIVALENT TO THAT USED IN THE MANUFACTURING OF THE PAD.
6. WELDING PROCEDURES, IF APPLICABLE, SHALL BE ESTABLISHED BY THE CONTRACTOR TO RESTRICT THE MAXIMUM TEMPERATURE REACHED BY SURFACES IN CONTACT WITH THE ELASTOMER TO 200°F (93°C). TEMPERATURES SHALL BE DETERMINED BY TEMPERATURE INDICATING WAX PENCILS OR OTHER SUITABLE MEANS.

REV.	DESCRIPTION	DATE	DET.	CKD.
A	REVISED AS NOTED	4/17/19	RTP	EMF

D.S. BROWN
A GIBRALTAR INDUSTRIES COMPANY

THE D.S. BROWN COMPANY
300 E. CHERRY STREET
NORTH BALTIMORE, OHIO 45872
419.257.3561
FAX: 419.257.0332
WWW.DSBROWN.COM

CUSTOMER — UNIVERSITY OF FLORIDA

DESCRIPTION	SCALE	DRAWN BY	CHECKED BY	DATE	
VERSIFLEX ELASTOMERIC BEARING ALACHUA COUNTY, FLORIDA	N.T.S.	RTP	EMF	3/19	-
	PROJECT NUMBER	PRODUCT CODE	UNITS	SHEET	
	4001021	1103	INCHES	06	

FILE SAVED: 4/18/19 9:46:44 AM

NO.	MK	QTY.	Thick	Dia.	Width	Length	Part	Material	Coating	Remarks	WT	Oracle Seed
1	7A	4					VERSIFLEX ELASTOMERIC BEARING				41.9	1103AT-G^
1.1	eb7	1	2.788		16.000	10.000	Elastomeric Bearing	110 PSI +/- 15% GR. 3 Neoprene	Plain	BEVELED	19.4	
1.2	es7	4	10 GA.		15.500	9.500	Shim (internal)	A1011 GR. 36	Plain		5.6	

ASSEMBLY SCHEDULE		
MK	LOCATION	QTY.
7A	TYPE F HALF SIZE W/ 5% SLOPE	4

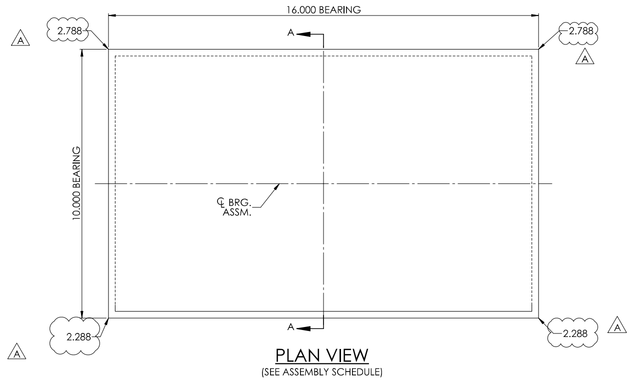

PLAN VIEW
(SEE ASSEMBLY SCHEDULE)

TOLERANCE TABLE	
DESCRIPTION	TOLERANCE (INCHES U.N.O.)
ELASTOMERIC BEARING DESIGN THICKNESS < 1.250"	-0, +0.125
ELASTOMERIC BEARING DESIGN THICKNESS > 1.250"	-0, +0.25
ELASTOMERIC BEARING PLAN DIMENSIONS < 36"	-0, +0.25
ELASTOMERIC BEARING PLAN DIMENSIONS > 36"	-0, +0.50
THICKNESS OF INDIVIDUAL LAYERS OF ELASTOMER (LAMINATED BEARINGS ONLY) AT ANY POINT WITHIN THE BEARING	±0.125
VARIATION FROM A PLANE PARALLEL TO THE THEORETICAL SURFACE (AS DETERMINED BY MEASUREMENTS AT THE EDGE OF THE BEARINGS) (PARALLELISM):	
TOP & BOTTOM	< 0.005 RAD
SIDES	±0.250
POSITION OF EXPOSED CONNECTION MEMBERS	±0.125
ELASTOMERIC EDGE COVER	-0, +0.125
ELASTOMERIC BEARING HOLE OR SLOT SIZE	±0.125
ELASTOMERIC BEARING HOLE OR SLOT LOCATION	±0.125

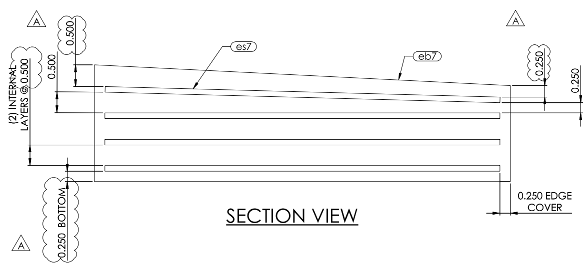

SECTION VIEW

GENERAL NOTES:

1. ALL MATERIALS SHALL CONFORM TO THE 2018 FLORIDA DEPARTMENT OF TRANSPORTATION STANDARD SPECIFICATIONS FOR ROAD AND BRIDGE CONSTRUCTION.
2. THIS SHOP DRAWING WAS PREPARED IN ACCORDANCE WITH THE CONTRACT PLANS AND SPECIFICATIONS. THE D.S. BROWN COMPANY DOES NOT ACCEPT LIABILITY FOR THE DESIGN OF THE PRODUCTS DETAILED IN THIS SHOP DRAWING.
3. THE D.S. BROWN COMPANY TO SUPPLY ONLY THE PARTS SHOWN ON THIS DRAWING.
4. EXPOSED LAMINATES ON THE OUTSIDE SURFACES OF THE PAD, APPARENT AS A RESULT OF MANUFACTURING TECHNIQUES, SHALL BE SEALED FLUSH ON THE FINISHED BEARING PAD WITH A BONDED VULCANIZED PATCH CONSISTING OF MATERIAL EQUIVALENT TO THAT USED IN THE MANUFACTURING OF THE PAD.
5. INTERNAL ALIGNMENT PINS: AFTER FABRICATION, HOLES TO BE FILLED WITH ELASTOMER MATERIAL EQUIVALENT TO THAT USED IN THE MANUFACTURING OF THE PAD.
6. WELDING PROCEDURES, IF APPLICABLE, SHALL BE ESTABLISHED BY THE CONTRACTOR TO RESTRICT THE MAXIMUM TEMPERATURE REACHED BY SURFACES IN CONTACT WITH THE ELASTOMER TO 200°F (93°C). TEMPERATURES SHALL BE DETERMINED BY TEMPERATURE INDICATING WAX PENCILS OR OTHER SUITABLE MEANS.

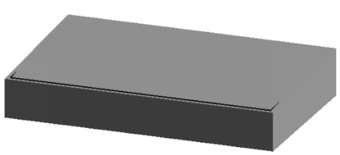

REV.	DESCRIPTION	DATE	DET.	CKD.
A	REVISED AS NOTED	4/17/19	RTP	EMF

D.S. BROWN
A GIBRALTAR INDUSTRIES COMPANY

THE D.S. BROWN COMPANY
300 E. CHERRY STREET
NORTH BALTIMORE, OHIO 45872
419.257.3561
FAX: 419.257.0332
WWW.DSBROWN.COM

CUSTOMER — UNIVERSITY OF FLORIDA

DESCRIPTION: VERSIFLEX ELASTOMERIC BEARING
ALACHUA COUNTY, FLORIDA

SCALE	DRAWN BY	CHECKED BY	DATE	
N.T.S.	RTP	EMF	3/19	-
PROJECT NUMBER	PRODUCT CODE	UNITS	SHEET	
4001021	1103	INCHES	07	

FILE SAVED: 4/18/19 9:46:45 AM

NO.	MK	QTY.	Thick	Dia.	Width	Length	Part	Material	Coating	Remarks	WT	Oracle Seed
1	8A	4	A				VERSIFLEX ELASTOMERIC BEARING				41.9	1103AT-H^
1.1	eb8	1	2.664		16.000	10.000	Elastomeric Bearing	110 PSI +/- 15% GR. 3 Neoprene	Plain	BEVELED	19.4	
1.2	es8	4	10 GA.		15.500	9.500	Shim (internal)	A1011 GR. 36	Plain		5.6	

ASSEMBLY SCHEDULE		
MK	LOCATION	QTY.
8A	TYPE F HALF SIZE W/ 2.51% SLOPE	4

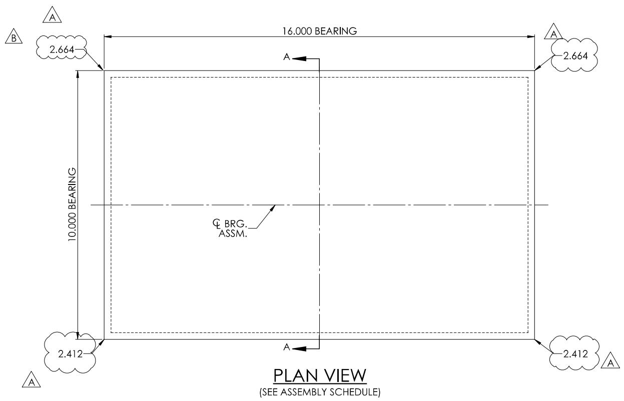

PLAN VIEW
(SEE ASSEMBLY SCHEDULE)

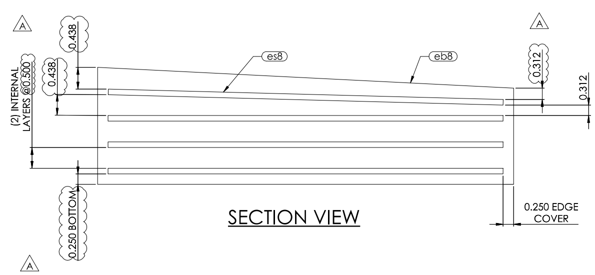

SECTION VIEW

TOLERANCE TABLE	
DESCRIPTION	TOLERANCE (INCHES U.N.O.)
ELASTOMERIC BEARING DESIGN THICKNESS ≤ 1.250"	-0, +0.125
ELASTOMERIC BEARING DESIGN THICKNESS > 1.250"	-0, +0.25
ELASTOMERIC BEARING PLAN DIMENSIONS ≤ 36"	-0, +0.25
ELASTOMERIC BEARING PLAN DIMENSIONS > 36"	-0, +0.50
THICKNESS OF INDIVIDUAL LAYERS OF ELASTOMER (LAMINATED BEARINGS ONLY) AT ANY POINT WITHIN THE BEARING	±0.125
VARIATION FROM A PLANE PARALLEL TO THE THEORETICAL SURFACE (AS DETERMINED BY MEASUREMENTS AT THE EDGE OF THE BEARINGS) (PARALLELISM):	
TOP & BOTTOM	≤ 0.005 RAD
SIDES	±0.250
POSITION OF EXPOSED CONNECTION MEMBERS	±0.125
ELASTOMERIC EDGE COVER	-0, +0.125
ELASTOMERIC BEARING HOLE OR SLOT SIZE	±0.125
ELASTOMERIC BEARING HOLE OR SLOT LOCATION	±0.125

GENERAL NOTES:

1. ALL MATERIALS SHALL CONFORM TO THE 2018 FLORIDA DEPARTMENT OF TRANSPORTATION STANDARD SPECIFICATIONS FOR ROAD AND BRIDGE CONSTRUCTION.

2. THIS SHOP DRAWING WAS PREPARED IN ACCORDANCE WITH THE CONTRACT PLANS AND SPECIFICATIONS. THE D.S. BROWN COMPANY DOES NOT ACCEPT LIABILITY FOR THE DESIGN OF THE PRODUCTS DETAILED IN THIS SHOP DRAWING.

3. THE D.S. BROWN COMPANY TO SUPPLY ONLY THE PARTS SHOWN ON THIS DRAWING.

4. EXPOSED LAMINATES ON THE OUTSIDE SURFACES OF THE PAD, APPARENT AS A RESULT OF MANUFACTURING TECHNIQUES, SHALL BE SEALED FLUSH ON THE FINISHED BEARING PAD WITH A BONDED VULCANIZED PATCH CONSISTING OF MATERIAL EQUIVALENT TO THAT USED IN THE MANUFACTURING OF THE PAD.

5. INTERNAL ALIGNMENT PINS; AFTER FABRICATION, HOLES TO BE FILLED WITH ELASTOMER MATERIAL EQUIVALENT TO THAT USED IN THE MANUFACTURING OF THE PAD.

6. WELDING PROCEDURES, IF APPLICABLE, SHALL BE ESTABLISHED BY THE CONTRACTOR TO RESTRICT THE MAXIMUM TEMPERATURE REACHED BY SURFACES IN CONTACT WITH THE ELASTOMER TO 200°F (93°C). TEMPERATURES SHALL BE DETERMINED BY TEMPERATURE INDICATING WAX PENCILS OR OTHER SUITABLE MEANS.

REV.	DESCRIPTION	DATE	DET.	CKD.
B	REVISED BEVEL THICKNESS PER REVIEW	4/24/19	RTP	EMF
A	REVISED AS NOTED	4/17/19	RTP	EMF

D.S. BROWN
A GIBRALTAR INDUSTRIES COMPANY

THE D.S. BROWN COMPANY
300 E. CHERRY STREET
NORTH BALTIMORE, OHIO 45872
419.257.3561
FAX: 419.257.0332
WWW.DSBROWN.COM

CUSTOMER — UNIVERSITY OF FLORIDA

DESCRIPTION	SCALE	DRAWN BY	CHECKED BY	DATE	
VERSIFLEX ELASTOMERIC BEARING ALACHUA COUNTY, FLORIDA	N.T.S.	RTP	EMF	3/19	-
	PROJECT NUMBER: 4001021	PRODUCT CODE: 1103		UNITS: INCHES	SHEET: 08

FILE SAVED: 4/24/19 8:45:57 AM

NO.	MK	QTY.	Thick	Dia.	Width	Length	Part	Material	Coating	Remarks	WT	Oracle Seed
1	9A	2	A				VERSIFLEX ELASTOMERIC BEARING				41.9	1103AT-J^
1.1	eb9	1	2.538		16.000	10.000	Elastomeric Bearing	110 PSI +/- 15% GR. 3 Neoprene	Plain		19.4	
1.2	es9	4	10 GA.		15.500	9.500	Shim (internal)	A1011 GR. 36	Plain		5.6	

ASSEMBLY SCHEDULE		
MK	LOCATION	QTY.
9A	TYPE F HALF SIZE - FLAT	2

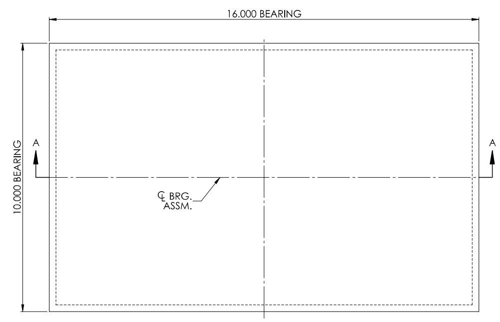

PLAN VIEW
(SEE ASSEMBLY SCHEDULE)

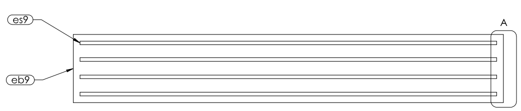

SECTION A-A

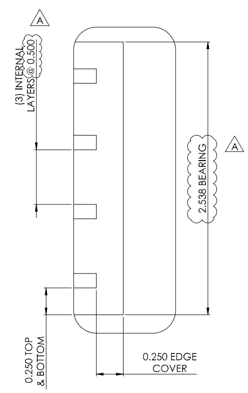

DETAIL A

TOLERANCE TABLE	
DESCRIPTION	TOLERANCE (INCHES U.N.O.)
ELASTOMERIC BEARING DESIGN THICKNESS ≤ 1.250"	-0, +0.125
ELASTOMERIC BEARING DESIGN THICKNESS > 1.250"	-0, +0.25
ELASTOMERIC BEARING PLAN DIMENSIONS ≤ 36"	-0, +0.25
ELASTOMERIC BEARING PLAN DIMENSIONS > 36"	-0, +0.50
THICKNESS OF INDIVIDUAL LAYERS OF ELASTOMER (LAMINATED BEARINGS ONLY) AT ANY POINT WITHIN THE BEARING	±0.125
VARIATION FROM A PLANE PARALLEL TO THE THEORETICAL SURFACE (AS DETERMINED BY MEASUREMENTS AT THE EDGE OF THE BEARINGS) (PARALLELISM):	
TOP & BOTTOM	≤ 0.005 RAD
SIDES	±0.250
POSITION OF EXPOSED CONNECTION MEMBERS	±0.125
ELASTOMERIC EDGE COVER	-0, +0.125
ELASTOMERIC BEARING HOLE OR SLOT SIZE	±0.125
ELASTOMERIC BEARING HOLE OR SLOT LOCATION	±0.125

GENERAL NOTES:

1. ALL MATERIALS SHALL CONFORM TO THE 2018 FLORIDA DEPARTMENT OF TRANSPORTATION STANDARD SPECIFICATIONS FOR ROAD AND BRIDGE CONSTRUCTION.
2. THIS SHOP DRAWING WAS PREPARED IN ACCORDANCE WITH THE CONTRACT PLANS AND SPECIFICATIONS. THE D.S. BROWN COMPANY DOES NOT ACCEPT LIABILITY FOR THE DESIGN OF THE PRODUCTS DETAILED IN THIS SHOP DRAWING.
3. THE D.S. BROWN COMPANY TO SUPPLY ONLY THE PARTS SHOWN ON THIS DRAWING.
4. EXPOSED LAMINATES ON THE OUTSIDE SURFACES OF THE PAD, APPARENT AS A RESULT OF MANUFACTURING TECHNIQUES, SHALL BE SEALED FLUSH ON THE FINISHED BEARING PAD WITH A BONDED VULCANIZED PATCH CONSISTING OF MATERIAL EQUIVALENT TO THAT USED IN THE MANUFACTURING OF THE PAD.
5. INTERNAL ALIGNMENT PINS: AFTER FABRICATION, HOLES TO BE FILLED WITH ELASTOMER MATERIAL EQUIVALENT TO THAT USED IN THE MANUFACTURING OF THE PAD.
6. WELDING PROCEDURES, IF APPLICABLE, SHALL BE ESTABLISHED BY THE CONTRACTOR TO RESTRICT THE MAXIMUM TEMPERATURE REACHED BY SURFACES IN CONTACT WITH THE ELASTOMER TO 200°F (93°C). TEMPERATURES SHALL BE DETERMINED BY TEMPERATURE INDICATING WAX PENCILS OR OTHER SUITABLE MEANS.

REV.	DESCRIPTION	DATE	DET.	CKD.
A	REVISED AS NOTED	4/17/19	RTP	EMF

D.S. BROWN
A GIBRALTAR INDUSTRIES COMPANY

THE D.S. BROWN COMPANY
300 E. CHERRY STREET
NORTH BALTIMORE, OHIO 45872
419.257.3561
FAX: 419.257.0332
WWW.DSBROWN.COM

CUSTOMER — UNIVERSITY OF FLORIDA

DESCRIPTION: VERSIFLEX ELASTOMERIC BEARING
ALACHUA COUNTY, FLORIDA

SCALE	DRAWN BY	CHECKED BY	DATE	
N.T.S.	RTP	EMF	3/19	-
PROJECT NUMBER	PRODUCT CODE	UNITS	SHEET	
4001021	1103	INCHES	09	

FILE SAVED: 4/18/19 9:46:46 AM

NO.	MK	QTY.	Thick	Dia.	Width	Length	Part	Material	Coating	Remarks	WT	Oracle Seed
1	10A	2					VERSIFLEX ELASTOMERIC BEARING				152.5	1103AT-K^
1.1	eb10	1	4.057		32.000	12.000	Elastomeric Bearing	150 PSI +/- 15% GR. 3 Neoprene	Plain	BEVELED	69.5	
1.2	es10	6	10 GA.		31.500	11.500	Shim (internal)	A1011 GR. 36	Plain		13.8	

ASSEMBLY SCHEDULE		
MK	LOCATION	QTY.
10A	TYPE K FULL SIZE W/ 4.17% SLOPE	2

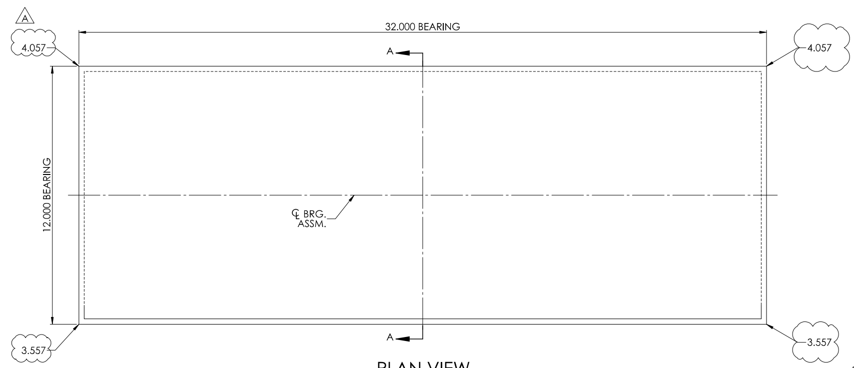

PLAN VIEW
(SEE ASSEMBLY SCHEDULE)

TOLERANCE TABLE	
DESCRIPTION	TOLERANCE (INCHES U.N.O.)
ELASTOMERIC BEARING DESIGN THICKNESS ≤ 1.250"	-0, +0.125
ELASTOMERIC BEARING DESIGN THICKNESS > 1.250"	-0, +0.25
ELASTOMERIC BEARING PLAN DIMENSIONS ≤ 36"	-0, +0.25
ELASTOMERIC BEARING PLAN DIMENSIONS > 36"	-0, +0.50
THICKNESS OF INDIVIDUAL LAYERS OF ELASTOMER (LAMINATED BEARINGS ONLY) AT ANY POINT WITHIN THE BEARING	±0.125
VARIATION FROM A PLANE PARALLEL TO THE THEORETICAL SURFACE (AS DETERMINED BY MEASUREMENTS AT THE EDGE OF THE BEARINGS) (PARALLELISM):	
TOP & BOTTOM	≤ 0.005 RAD
SIDES	±0.250
POSITION OF EXPOSED CONNECTION MEMBERS	±0.125
ELASTOMERIC EDGE COVER	-0, +0.125
ELASTOMERIC BEARING HOLE OR SLOT SIZE	±0.125
ELASTOMERIC BEARING HOLE OR SLOT LOCATION	±0.125

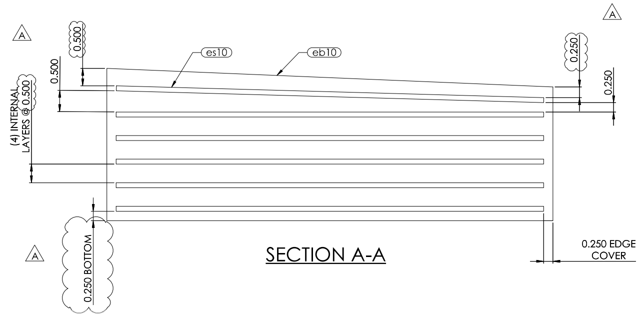

SECTION A-A

GENERAL NOTES:

1. ALL MATERIALS SHALL CONFORM TO THE 2018 FLORIDA DEPARTMENT OF TRANSPORTATION STANDARD SPECIFICATIONS FOR ROAD AND BRIDGE CONSTRUCTION.
2. THIS SHOP DRAWING WAS PREPARED IN ACCORDANCE WITH THE CONTRACT PLANS AND SPECIFICATIONS. THE D.S. BROWN COMPANY DOES NOT ACCEPT LIABILITY FOR THE DESIGN OF THE PRODUCTS DETAILED IN THIS SHOP DRAWING.
3. THE D.S. BROWN COMPANY TO SUPPLY ONLY THE PARTS SHOWN ON THIS DRAWING.
4. EXPOSED LAMINATES ON THE OUTSIDE SURFACES OF THE PAD, APPARENT AS A RESULT OF MANUFACTURING TECHNIQUES, SHALL BE SEALED FLUSH ON THE FINISHED BEARING PAD WITH A BONDED VULCANIZED PATCH CONSISTING OF MATERIAL EQUIVALENT TO THAT USED IN THE MANUFACTURING OF THE PAD.
5. INTERNAL ALIGNMENT PINS: AFTER FABRICATION, HOLES TO BE FILLED WITH ELASTOMER MATERIAL EQUIVALENT TO THAT USED IN THE MANUFACTURING OF THE PAD.
6. WELDING PROCEDURES, IF APPLICABLE, SHALL BE ESTABLISHED BY THE CONTRACTOR TO RESTRICT THE MAXIMUM TEMPERATURE REACHED BY SURFACES IN CONTACT WITH THE ELASTOMER TO 200°F (93°C). TEMPERATURES SHALL BE DETERMINED BY TEMPERATURE INDICATING WAX PENCILS OR OTHER SUITABLE MEANS.

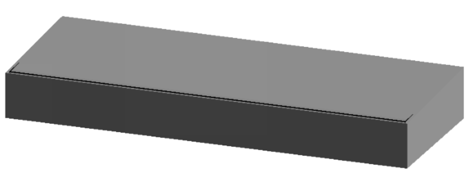

REV.	DESCRIPTION	DATE	DET.	CKD.
A	REVISED AS NOTED	4/17/19	RTP	EMF

D.S. BROWN
A GIBRALTAR INDUSTRIES COMPANY
THE D.S. BROWN COMPANY
300 E. CHERRY STREET
NORTH BALTIMORE, OHIO 45872
419.257.3561
FAX: 419.257.0332
WWW.DSBROWN.COM

CUSTOMER — UNIVERSITY OF FLORIDA

DESCRIPTION: VERSIFLEX ELASTOMERIC BEARING
ALACHUA COUNTY, FLORIDA

SCALE	DRAWN BY	CHECKED BY	DATE	
N.T.S.	RTP	EMF	3/19	-
PROJECT NUMBER	PRODUCT CODE	UNITS	SHEET	
4001021	1103	INCHES	10	

FILE SAVED: 4/18/19 9:46:47 AM

NO.	MK	QTY.	Thick	Dia.	Width	Length	Part	Material	Coating	Remarks	WT	Oracle Seed
1	11A	2		A			VERSIFLEX ELASTOMERIC BEARING				152.5	1103AT-L^
1.1	eb11	1	3.932		32.000	12.000	Elastomeric Bearing	150 PSI +/- 15% GR. 3 Neoprene	Plain	BEVELED	69.5	
1.2	es11	6	10 GA.		31.500	11.500	Shim (internal)	A1011 GR. 36	Plain		13.8	

ASSEMBLY SCHEDULE		
MK	LOCATION	QTY.
11A	TYPE K FULL SIZE W/ 2.09% SLOPE	2

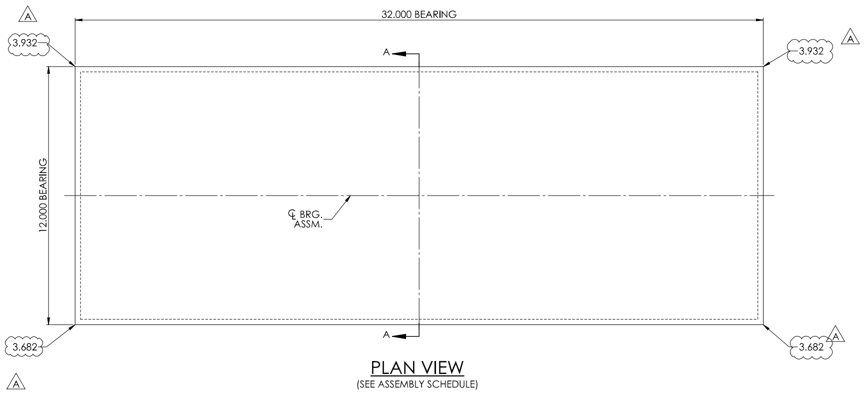

PLAN VIEW
(SEE ASSEMBLY SCHEDULE)

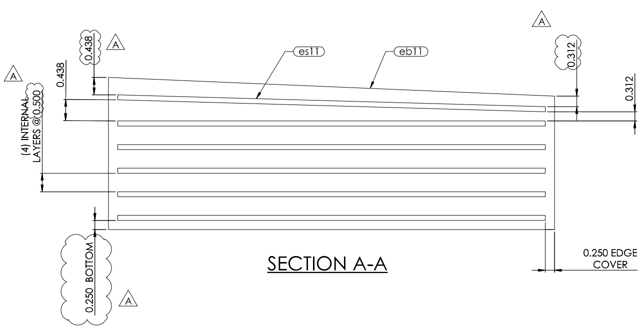

SECTION A-A

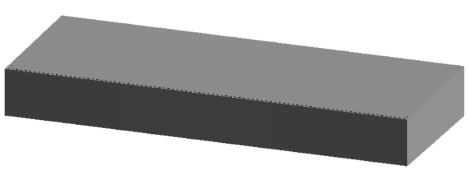

TOLERANCE TABLE	
DESCRIPTION	TOLERANCE (INCHES U.N.O.)
ELASTOMERIC BEARING DESIGN THICKNESS ≤ 1.250"	-0, +0.125
ELASTOMERIC BEARING DESIGN THICKNESS > 1.250"	-0, +0.25
ELASTOMERIC BEARING PLAN DIMENSIONS ≤ 36"	-0, +0.25
ELASTOMERIC BEARING PLAN DIMENSIONS > 36"	-0, +0.50
THICKNESS OF INDIVIDUAL LAYERS OF ELASTOMER (LAMINATED BEARINGS ONLY) AT ANY POINT WITHIN THE BEARING	±0.125
VARIATION FROM A PLANE PARALLEL TO THE THEORETICAL SURFACE (AS DETERMINED BY MEASUREMENTS AT THE EDGE OF THE BEARINGS) (PARALLELISM):	
TOP & BOTTOM	≤ 0.005 RAD
SIDES	±0.250
POSITION OF EXPOSED CONNECTION MEMBERS	±0.125
ELASTOMERIC EDGE COVER	-0, +0.125
ELASTOMERIC BEARING HOLE OR SLOT SIZE	±0.125
ELASTOMERIC BEARING HOLE OR SLOT LOCATION	±0.125

GENERAL NOTES:

1. ALL MATERIALS SHALL CONFORM TO THE 2018 FLORIDA DEPARTMENT OF TRANSPORTATION STANDARD SPECIFICATIONS FOR ROAD AND BRIDGE CONSTRUCTION.

2. THIS SHOP DRAWING WAS PREPARED IN ACCORDANCE WITH THE CONTRACT PLANS AND SPECIFICATIONS. THE D.S. BROWN COMPANY DOES NOT ACCEPT LIABILITY FOR THE DESIGN OF THE PRODUCTS DETAILED IN THIS SHOP DRAWING.

3. THE D.S. BROWN COMPANY TO SUPPLY ONLY THE PARTS SHOWN ON THIS DRAWING.

4. EXPOSED LAMINATES ON THE OUTSIDE SURFACES OF THE PAD, APPARENT AS A RESULT OF MANUFACTURING TECHNIQUES, SHALL BE SEALED FLUSH ON THE FINISHED BEARING PAD WITH A BONDED VULCANIZED PATCH CONSISTING OF MATERIAL EQUIVALENT TO THAT USED IN THE MANUFACTURING OF THE PAD.

5. INTERNAL ALIGNMENT PINS: AFTER FABRICATION, HOLES TO BE FILLED WITH ELASTOMER MATERIAL EQUIVALENT TO THAT USED IN THE MANUFACTURING OF THE PAD.

6. WELDING PROCEDURES, IF APPLICABLE, SHALL BE ESTABLISHED BY THE CONTRACTOR TO RESTRICT THE MAXIMUM TEMPERATURE REACHED BY SURFACES IN CONTACT WITH THE ELASTOMER TO 200°F (93°C). TEMPERATURES SHALL BE DETERMINED BY TEMPERATURE INDICATING WAX PENCILS OR OTHER SUITABLE MEANS.

REV.	DESCRIPTION	DATE	DET.	CKD.
A	REVISED AS NOTED	4/17/19	RTP	EMF

D.S. BROWN
A GIBRALTAR INDUSTRIES COMPANY
THE D.S. BROWN COMPANY
300 E. CHERRY STREET
NORTH BALTIMORE, OHIO 45872
419.257.3561
FAX: 419.257.0332
WWW.DSBROWN.COM

CUSTOMER — UNIVERSITY OF FLORIDA

DESCRIPTION: VERSIFLEX ELASTOMERIC BEARING
ALACHUA COUNTY, FLORIDA

SCALE	DRAWN BY	CHECKED BY	DATE	
N.T.S.	RTP	EMF	3/19	-
PROJECT NUMBER	PRODUCT CODE	UNITS	SHEET	
4001021	1103	INCHES	11	

FILE SAVED: 4/18/19 9:45:17 AM

NO.	MK	QTY.	Thick	Dia.	Width	Length	Part	Material	Coating	Remarks	WT	Oracle Seed
1	12A	2	A				VERSIFLEX ELASTOMERIC BEARING				152.5	1103AT-M^
1.1	eb12	1	3.807		32.000	12.000	Elastomeric Bearing	150 PSI +/- 15% GR. 3 Neoprene	Plain		69.5	
1.2	es12	6	10 GA.		31.500	11.500	Shim (internal)	A1011 GR. 36	Plain		13.8	

ASSEMBLY SCHEDULE		
MK	LOCATION	QTY.
12A	TYPE K FULL SIZE - FLAT	2

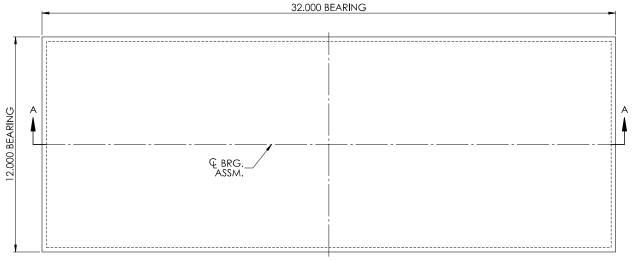

PLAN VIEW
(SEE ASSEMBLY SCHEDULE)

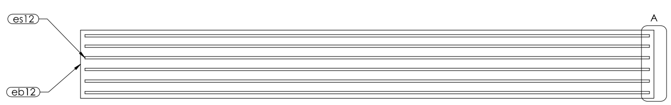

SECTION A-A

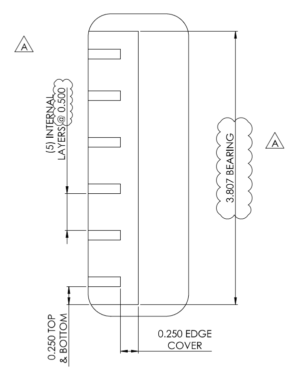

DETAIL A

TOLERANCE TABLE	
DESCRIPTION	TOLERANCE (INCHES U.N.O.)
ELASTOMERIC BEARING DESIGN THICKNESS ≤ 1.250"	-0, +0.125
ELASTOMERIC BEARING DESIGN THICKNESS > 1.250"	-0, +0.25
ELASTOMERIC BEARING PLAN DIMENSIONS ≤ 36"	-0, +0.25
ELASTOMERIC BEARING PLAN DIMENSIONS > 36"	-0, +0.50
THICKNESS OF INDIVIDUAL LAYERS OF ELASTOMER (LAMINATED BEARINGS ONLY) AT ANY POINT WITHIN THE BEARING	±0.125
VARIATION FROM A PLANE PARALLEL TO THE THEORETICAL SURFACE (AS DETERMINED BY MEASUREMENTS AT THE EDGE OF THE BEARINGS) (PARALLELISM):	
TOP & BOTTOM	< 0.005 RAD
SIDES	±0.250
POSITION OF EXPOSED CONNECTION MEMBERS	±0.125
ELASTOMERIC EDGE COVER	-0, +0.125
ELASTOMERIC BEARING HOLE OR SLOT SIZE	±0.125
ELASTOMERIC BEARING HOLE OR SLOT LOCATION	±0.125

GENERAL NOTES:

1. ALL MATERIALS SHALL CONFORM TO THE 2018 FLORIDA DEPARTMENT OF TRANSPORTATION STANDARD SPECIFICATIONS FOR ROAD AND BRIDGE CONSTRUCTION.
2. THIS SHOP DRAWING WAS PREPARED IN ACCORDANCE WITH THE CONTRACT PLANS AND SPECIFICATIONS. THE D.S. BROWN COMPANY DOES NOT ACCEPT LIABILITY FOR THE DESIGN OF THE PRODUCTS DETAILED IN THIS SHOP DRAWING.
3. THE D.S. BROWN COMPANY TO SUPPLY ONLY THE PARTS SHOWN ON THIS DRAWING.
4. EXPOSED LAMINATES ON THE OUTSIDE SURFACES OF THE PAD, APPARENT AS A RESULT OF MANUFACTURING TECHNIQUES, SHALL BE SEALED FLUSH ON THE FINISHED BEARING PAD WITH A BONDED VULCANIZED PATCH CONSISTING OF MATERIAL EQUIVALENT TO THAT USED IN THE MANUFACTURING OF THE PAD.
5. INTERNAL ALIGNMENT PINS: AFTER FABRICATION, HOLES TO BE FILLED WITH ELASTOMER MATERIAL EQUIVALENT TO THAT USED IN THE MANUFACTURING OF THE PAD.
6. WELDING PROCEDURES, IF APPLICABLE, SHALL BE ESTABLISHED BY THE CONTRACTOR TO RESTRICT THE MAXIMUM TEMPERATURE REACHED BY SURFACES IN CONTACT WITH THE ELASTOMER TO 200°F (93°C). TEMPERATURES SHALL BE DETERMINED BY TEMPERATURE INDICATING WAX PENCILS OR OTHER SUITABLE MEANS.

REV.	DESCRIPTION	DATE	DET.	CKD.
A	REVISED AS NOTED	4/18/19	RTP	EMF

D.S. BROWN
A GIBRALTAR INDUSTRIES COMPANY

THE D.S. BROWN COMPANY
300 E. CHERRY STREET
NORTH BALTIMORE, OHIO 45872
419.257.3561
FAX: 419.257.0332
WWW.DSBROWN.COM

CUSTOMER — UNIVERSITY OF FLORIDA

DESCRIPTION: VERSIFLEX ELASTOMERIC BEARING
ALACHUA COUNTY, FLORIDA

SCALE	DRAWN BY	CHECKED BY	DATE	
N.T.S.	RTP	EMF	3/19	-
PROJECT NUMBER	PRODUCT CODE	UNITS	SHEET	
4001021	1103	INCHES	12	

FILE SAVED: 4/18/19 9:46:48 AM

NO.	MK	QTY.	Thick	Dia.	Width	Length	Part	Material	Coating	Remarks	WT	Oracle Seed
1	13A	4					VERSIFLEX ELASTOMERIC BEARING				63.4	1103AT-N^
1.1	eb13	1	2.154		32.000	10.000	Elastomeric Bearing	110 PSI +/- 15% GR. 3 Neoprene	Plain	BEVELED	29.1	
1.2	es13	3	10 GA.		31.500	9.500	Shim (internal)	A1011 GR. 36	Plain		11.4	

ASSEMBLY SCHEDULE		
MK	LOCATION	QTY.
13A	TYPE E FULL SIZE W/ 5% SLOPE	4

TOLERANCE TABLE	
DESCRIPTION	TOLERANCE (INCHES U.N.O.)
ELASTOMERIC BEARING DESIGN THICKNESS ≤ 1.250"	-0, +0.125
ELASTOMERIC BEARING DESIGN THICKNESS > 1.250"	-0, +0.25
ELASTOMERIC BEARING PLAN DIMENSIONS ≤ 36"	-0, +0.25
ELASTOMERIC BEARING PLAN DIMENSIONS > 36"	-0, +0.50
THICKNESS OF INDIVIDUAL LAYERS OF ELASTOMER (LAMINATED BEARINGS ONLY) AT ANY POINT WITHIN THE BEARING	±0.125
VARIATION FROM A PLANE PARALLEL TO THE THEORETICAL SURFACE (AS DETERMINED BY MEASUREMENTS AT THE EDGE OF THE BEARINGS) (PARALLELISM):	
TOP & BOTTOM	< 0.005 RAD
SIDES	±0.250
POSITION OF EXPOSED CONNECTION MEMBERS	±0.125
ELASTOMERIC EDGE COVER	-0, +0.125
ELASTOMERIC BEARING HOLE OR SLOT SIZE	±0.125
ELASTOMERIC BEARING HOLE OR SLOT LOCATION	±0.125

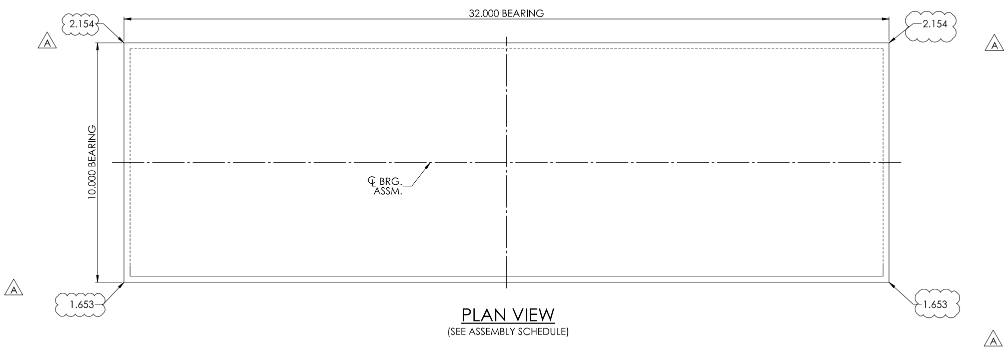

PLAN VIEW
(SEE ASSEMBLY SCHEDULE)

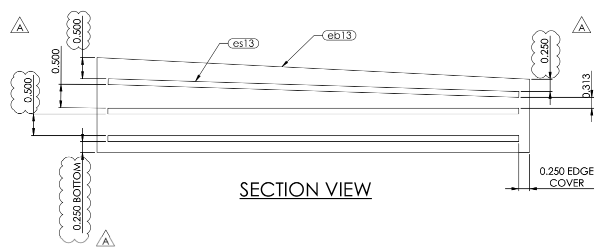

SECTION VIEW

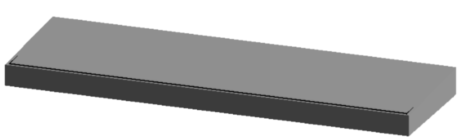

GENERAL NOTES:

1. ALL MATERIALS SHALL CONFORM TO THE 2018 FLORIDA DEPARTMENT OF TRANSPORTATION STANDARD SPECIFICATIONS FOR ROAD AND BRIDGE CONSTRUCTION.
2. THIS SHOP DRAWING WAS PREPARED IN ACCORDANCE WITH THE CONTRACT PLANS AND SPECIFICATIONS. THE D.S. BROWN COMPANY DOES NOT ACCEPT LIABILITY FOR THE DESIGN OF THE PRODUCTS DETAILED IN THIS SHOP DRAWING.
3. THE D.S. BROWN COMPANY TO SUPPLY ONLY THE PARTS SHOWN ON THIS DRAWING.
4. EXPOSED LAMINATES ON THE OUTSIDE SURFACES OF THE PAD, APPARENT AS A RESULT OF MANUFACTURING TECHNIQUES, SHALL BE SEALED FLUSH ON THE FINISHED BEARING PAD WITH A BONDED VULCANIZED PATCH CONSISTING OF MATERIAL EQUIVALENT TO THAT USED IN THE MANUFACTURING OF THE PAD.
5. INTERNAL ALIGNMENT PINS: AFTER FABRICATION, HOLES TO BE FILLED WITH ELASTOMER MATERIAL EQUIVALENT TO THAT USED IN THE MANUFACTURING OF THE PAD.
6. WELDING PROCEDURES, IF APPLICABLE, SHALL BE ESTABLISHED BY THE CONTRACTOR TO RESTRICT THE MAXIMUM TEMPERATURE REACHED BY SURFACES IN CONTACT WITH THE ELASTOMER TO 200°F (93°C). TEMPERATURES SHALL BE DETERMINED BY TEMPERATURE INDICATING WAX PENCILS OR OTHER SUITABLE MEANS.

REV.	DESCRIPTION	DATE	DET.	CKD.
A	REVISED AS NOTED	4/17/19	RTP	EMF

D.S. BROWN
A GIBRALTAR INDUSTRIES COMPANY
THE D.S. BROWN COMPANY
300 E. CHERRY STREET
NORTH BALTIMORE, OHIO 45872
419.257.3561
FAX: 419.257.0332
WWW.DSBROWN.COM

CUSTOMER — UNIVERSITY OF FLORIDA

DESCRIPTION: VERSIFLEX ELASTOMERIC BEARING
ALACHUA COUNTY, FLORIDA

SCALE	DRAWN BY	CHECKED BY	DATE	
N.T.S.	RTP	EMF	3/19	-
PROJECT NUMBER	PRODUCT CODE	UNITS	SHEET	
4001021	1103	INCHES	13	

FILE SAVED: 4/18/19 9:46:49 AM

NO.	MK	QTY.	Thick	Dia.	Width	Length	Part	Material	Coating	Remarks	WT	Oracle Seed
1	14A	4	A				VERSIFLEX ELASTOMERIC BEARING				63.4	1103AT-P^
1.1	eb14	1	2.029		32.000	10.000	Elastomeric Bearing	110 PSI +/- 15% GR. 3 Neoprene	Plain	BEVELED	29.1	
1.2	es14	3	10 GA.		31.500	9.500	Shim (internal)	A1011 GR. 36	Plain		11.4	

ASSEMBLY SCHEDULE		
MK	LOCATION	QTY.
14A	TYPE E FULL SIZE W/ 2.51% SLOPE	4

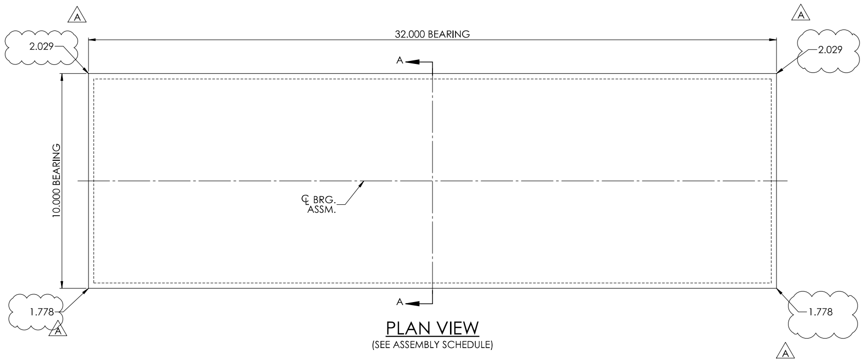

PLAN VIEW
(SEE ASSEMBLY SCHEDULE)

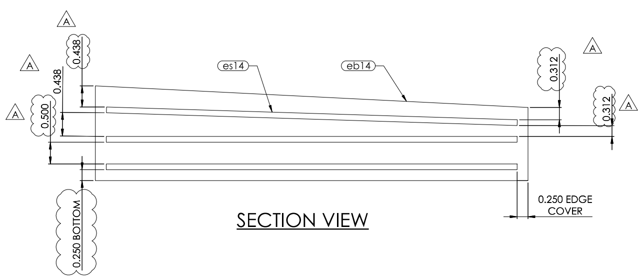

SECTION VIEW

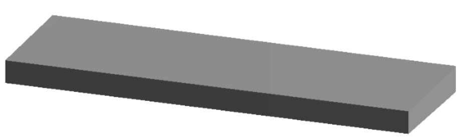

TOLERANCE TABLE	
DESCRIPTION	TOLERANCE (INCHES U.N.O.)
ELASTOMERIC BEARING DESIGN THICKNESS < 1.250"	-0, +0.125
ELASTOMERIC BEARING DESIGN THICKNESS > 1.250"	-0, +0.25
ELASTOMERIC BEARING PLAN DIMENSIONS < 36"	-0, +0.25
ELASTOMERIC BEARING PLAN DIMENSIONS > 36"	-0, +0.50
THICKNESS OF INDIVIDUAL LAYERS OF ELASTOMER (LAMINATED BEARINGS ONLY) AT ANY POINT WITHIN THE BEARING	±0.125
VARIATION FROM A PLANE PARALLEL TO THE THEORETICAL SURFACE (AS DETERMINED BY MEASUREMENTS AT THE EDGE OF THE BEARINGS) (PARALLELISM):	
TOP & BOTTOM	< 0.005 RAD
SIDES	±0.250
POSITION OF EXPOSED CONNECTION MEMBERS	±0.125
ELASTOMERIC EDGE COVER	-0, +0.125
ELASTOMERIC BEARING HOLE OR SLOT SIZE	±0.125
ELASTOMERIC BEARING HOLE OR SLOT LOCATION	±0.125

GENERAL NOTES:

1. ALL MATERIALS SHALL CONFORM TO THE 2018 FLORIDA DEPARTMENT OF TRANSPORTATION STANDARD SPECIFICATIONS FOR ROAD AND BRIDGE CONSTRUCTION.
2. THIS SHOP DRAWING WAS PREPARED IN ACCORDANCE WITH THE CONTRACT PLANS AND SPECIFICATIONS. THE D.S. BROWN COMPANY DOES NOT ACCEPT LIABILITY FOR THE DESIGN OF THE PRODUCTS DETAILED IN THIS SHOP DRAWING.
3. THE D.S. BROWN COMPANY TO SUPPLY ONLY THE PARTS SHOWN ON THIS DRAWING.
4. EXPOSED LAMINATES ON THE OUTSIDE SURFACES OF THE PAD, APPARENT AS A RESULT OF MANUFACTURING TECHNIQUES, SHALL BE SEALED FLUSH ON THE FINISHED BEARING PAD WITH A BONDED VULCANIZED PATCH CONSISTING OF MATERIAL EQUIVALENT TO THAT USED IN THE MANUFACTURING OF THE PAD.
5. INTERNAL ALIGNMENT PINS: AFTER FABRICATION, HOLES TO BE FILLED WITH ELASTOMER MATERIAL EQUIVALENT TO THAT USED IN THE MANUFACTURING OF THE PAD.
6. WELDING PROCEDURES, IF APPLICABLE, SHALL BE ESTABLISHED BY THE CONTRACTOR TO RESTRICT THE MAXIMUM TEMPERATURE REACHED BY SURFACES IN CONTACT WITH THE ELASTOMER TO 200°F (93°C). TEMPERATURES SHALL BE DETERMINED BY TEMPERATURE INDICATING WAX PENCILS OR OTHER SUITABLE MEANS.

REV.	DESCRIPTION	DATE	DET.	CKD.
A	REVISED AS NOTED	4/17/19	RTP	EMF

D.S. BROWN
A GIBRALTAR INDUSTRIES COMPANY

THE D.S. BROWN COMPANY
300 E. CHERRY STREET
NORTH BALTIMORE, OHIO 45872
419.257.3561
FAX: 419.257.0332
WWW.DSBROWN.COM

CUSTOMER — UNIVERSITY OF FLORIDA

DESCRIPTION: VERSIFLEX ELASTOMERIC BEARING
ALACHUA COUNTY, FLORIDA

SCALE	DRAWN BY	CHECKED BY	DATE	
N.T.S.	RTP	EMF	3/19	-
PROJECT NUMBER	PRODUCT CODE	UNITS	SHEET	
4001021	1103	INCHES	14	

FILE SAVED: 4/18/19 9:46:50 AM

NO.	MK	QTY.	Thick	Dia.	Width	Length	Part	Material	Coating	Remarks	WT	Oracle Seed
1	15A	2	A				VERSIFLEX ELASTOMERIC BEARING				63.4	1103AT-R^
1.1	eb15	1	1.904		32.000	10.000	Elastomeric Bearing	110 PSI +/- 15% GR. 3 Neoprene	Plain		29.1	
1.2	es15	3	10 GA.		31.500	9.500	Shim (internal)	A1011 GR. 36	Plain		11.4	

TOLERANCE TABLE	
DESCRIPTION	TOLERANCE (INCHES U.N.O.)
ELASTOMERIC BEARING DESIGN THICKNESS < 1.250"	-0, +0.125
ELASTOMERIC BEARING DESIGN THICKNESS > 1.250"	-0, +0.25
ELASTOMERIC BEARING PLAN DIMENSIONS < 36"	-0, +0.25
ELASTOMERIC BEARING PLAN DIMENSIONS > 36"	-0, +0.50
THICKNESS OF INDIVIDUAL LAYERS OF ELASTOMER (LAMINATED BEARINGS ONLY) AT ANY POINT WITHIN THE BEARING	±0.125
VARIATION FROM A PLANE PARALLEL TO THE THEORETICAL SURFACE (AS DETERMINED BY MEASUREMENTS AT THE EDGE OF THE BEARINGS) (PARALLELISM):	
TOP & BOTTOM	< 0.005 RAD
SIDES	±0.250
POSITION OF EXPOSED CONNECTION MEMBERS	±0.125
ELASTOMERIC EDGE COVER	-0, +0.125
ELASTOMERIC BEARING HOLE OR SLOT SIZE	±0.125
ELASTOMERIC BEARING HOLE OR SLOT LOCATION	±0.125

ASSEMBLY SCHEDULE		
MK	LOCATION	QTY.
15A	TYPE E FULL SIZE - FLAT	2

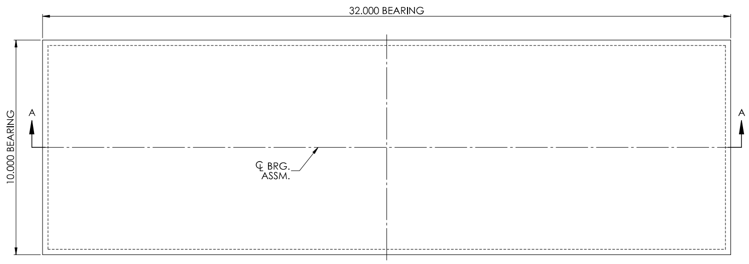

PLAN VIEW
(SEE ASSEMBLY SCHEDULE)

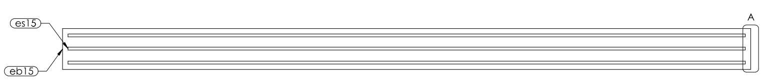

SECTION A-A

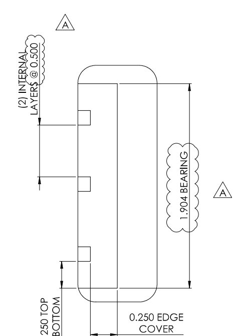

DETAIL A

GENERAL NOTES:

1. ALL MATERIALS SHALL CONFORM TO THE 2018 FLORIDA DEPARTMENT OF TRANSPORTATION STANDARD SPECIFICATIONS FOR ROAD AND BRIDGE CONSTRUCTION.
2. THIS SHOP DRAWING WAS PREPARED IN ACCORDANCE WITH THE CONTRACT PLANS AND SPECIFICATIONS. THE D.S. BROWN COMPANY DOES NOT ACCEPT LIABILITY FOR THE DESIGN OF THE PRODUCTS DETAILED IN THIS SHOP DRAWING.
3. THE D.S. BROWN COMPANY TO SUPPLY ONLY THE PARTS SHOWN ON THIS DRAWING.
4. EXPOSED LAMINATES ON THE OUTSIDE SURFACES OF THE PAD, APPARENT AS A RESULT OF MANUFACTURING TECHNIQUES, SHALL BE SEALED FLUSH ON THE FINISHED BEARING PAD WITH A BONDED VULCANIZED PATCH CONSISTING OF MATERIAL EQUIVALENT TO THAT USED IN THE MANUFACTURING OF THE PAD.
5. INTERNAL ALIGNMENT PINS: AFTER FABRICATION, HOLES TO BE FILLED WITH ELASTOMER MATERIAL EQUIVALENT TO THAT USED IN THE MANUFACTURING OF THE PAD.
6. WELDING PROCEDURES, IF APPLICABLE, SHALL BE ESTABLISHED BY THE CONTRACTOR TO RESTRICT THE MAXIMUM TEMPERATURE REACHED BY SURFACES IN CONTACT WITH THE ELASTOMER TO 200°F (93°C). TEMPERATURES SHALL BE DETERMINED BY TEMPERATURE INDICATING WAX PENCILS OR OTHER SUITABLE MEANS.

REV.	DESCRIPTION	DATE	DET.	CKD.
A	REVISED AS NOTED	4/18/19	RTP	EMF

D.S. BROWN
A GIBRALTAR INDUSTRIES COMPANY
THE D.S. BROWN COMPANY
300 E. CHERRY STREET
NORTH BALTIMORE, OHIO 45872
419.257.3561
FAX: 419.257.0332
WWW.DSBROWN.COM

CUSTOMER — UNIVERSITY OF FLORIDA

DESCRIPTION	SCALE	DRAWN BY	CHECKED BY	DATE	
VERSIFLEX ELASTOMERIC BEARING ALACHUA COUNTY, FLORIDA	N.T.S.	RTP	EMF	3/19	-
	PROJECT NUMBER	PRODUCT CODE	UNITS	SHEET	
	4001021	1103	INCHES	15	

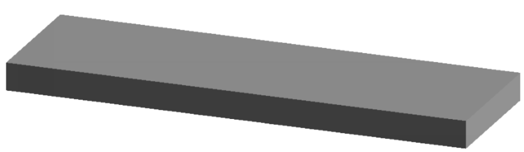

FILE SAVED: 4/18/19 9:46:50 AM

NO.	MK	QTY.	Thick	Dia.	Width	Length	Part	Material	Coating	Remarks	WT	Oracle Seed
1	16A	4	A				VERSIFLEX ELASTOMERIC BEARING				88.4	1103AT-S^
1.1	eb16	1	2.788		32.000	10.000	Elastomeric Bearing	110 PSI +/- 15% GR. 3 Neoprene	Plain	BEVELED	42.6	
1.2	es16	4	10 GA.		31.500	9.500	Shim (internal)	A1011 GR. 36	Plain		11.4	

ASSEMBLY SCHEDULE		
MK	LOCATION	QTY.
16A	TYPE F FULL SIZE W/ 5% SLOPE	4

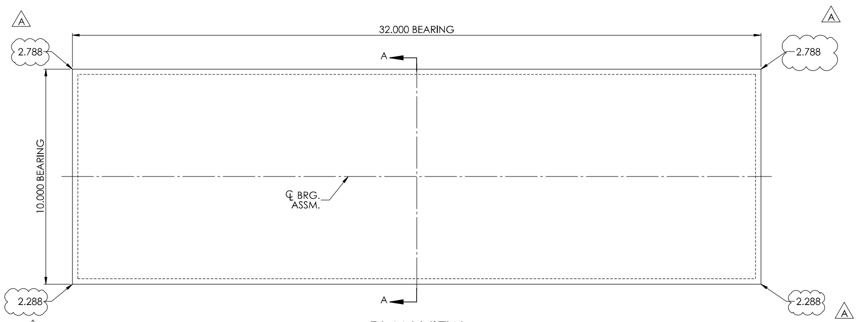

PLAN VIEW
(SEE ASSEMBLY SCHEDULE)

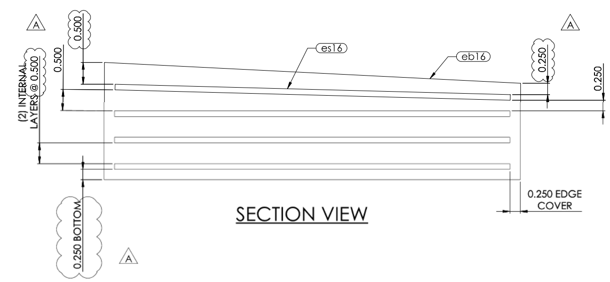

SECTION VIEW

TOLERANCE TABLE	
DESCRIPTION	TOLERANCE (INCHES U.N.O.)
ELASTOMERIC BEARING DESIGN THICKNESS ≤ 1.250"	-0, +0.125
ELASTOMERIC BEARING DESIGN THICKNESS > 1.250"	-0, +0.25
ELASTOMERIC BEARING PLAN DIMENSIONS ≤ 36"	-0, +0.25
ELASTOMERIC BEARING PLAN DIMENSIONS > 36"	-0, +0.50
THICKNESS OF INDIVIDUAL LAYERS OF ELASTOMER (LAMINATED BEARINGS ONLY) AT ANY POINT WITHIN THE BEARING	±0.125
VARIATION FROM A PLANE PARALLEL TO THE THEORETICAL SURFACE (AS DETERMINED BY MEASUREMENTS AT THE EDGE OF THE BEARINGS) (PARALLELISM):	
TOP & BOTTOM	< 0.005 RAD
SIDES	±0.250
POSITION OF EXPOSED CONNECTION MEMBERS	±0.125
ELASTOMERIC EDGE COVER	-0, +0.125
ELASTOMERIC BEARING HOLE OR SLOT SIZE	±0.125
ELASTOMERIC BEARING HOLE OR SLOT LOCATION	±0.125

GENERAL NOTES:

1. ALL MATERIALS SHALL CONFORM TO THE 2018 FLORIDA DEPARTMENT OF TRANSPORTATION STANDARD SPECIFICATIONS FOR ROAD AND BRIDGE CONSTRUCTION.
2. THIS SHOP DRAWING WAS PREPARED IN ACCORDANCE WITH THE CONTRACT PLANS AND SPECIFICATIONS. THE D.S. BROWN COMPANY DOES NOT ACCEPT LIABILITY FOR THE DESIGN OF THE PRODUCTS DETAILED IN THIS SHOP DRAWING.
3. THE D.S. BROWN COMPANY TO SUPPLY ONLY THE PARTS SHOWN ON THIS DRAWING.
4. EXPOSED LAMINATES ON THE OUTSIDE SURFACES OF THE PAD, APPARENT AS A RESULT OF MANUFACTURING TECHNIQUES, SHALL BE SEALED FLUSH ON THE FINISHED BEARING PAD WITH A BONDED VULCANIZED PATCH CONSISTING OF MATERIAL EQUIVALENT TO THAT USED IN THE MANUFACTURING OF THE PAD.
5. INTERNAL ALIGNMENT PINS: AFTER FABRICATION, HOLES TO BE FILLED WITH ELASTOMER MATERIAL EQUIVALENT TO THAT USED IN THE MANUFACTURING OF THE PAD.
6. WELDING PROCEDURES, IF APPLICABLE, SHALL BE ESTABLISHED BY THE CONTRACTOR TO RESTRICT THE MAXIMUM TEMPERATURE REACHED BY SURFACES IN CONTACT WITH THE ELASTOMER TO 200°F (93°C). TEMPERATURES SHALL BE DETERMINED BY TEMPERATURE INDICATING WAX PENCILS OR OTHER SUITABLE MEANS.

REV.	DESCRIPTION	DATE	DET.	CKD.
A	REVISED AS NOTED	4/18/19	RTP	EMF

D.S. BROWN
A GIBRALTAR INDUSTRIES COMPANY

THE D.S. BROWN COMPANY
300 E. CHERRY STREET
NORTH BALTIMORE, OHIO 45872
419.257.3561
FAX: 419.257.0332
WWW.DSBROWN.COM

CUSTOMER — UNIVERSITY OF FLORIDA

DESCRIPTION	SCALE	DRAWN BY	CHECKED BY	DATE	
VERSIFLEX ELASTOMERIC BEARING ALACHUA COUNTY, FLORIDA	N.T.S.	RTP	EMF	3/19	-
	PROJECT NUMBER	PRODUCT CODE	UNITS	SHEET	
	4001021	1103	INCHES	16	

FILE SAVED: 4/18/19 9:46:12 AM

NO.	MK	QTY.	Thick	Dia.	Width	Length	Part	Material	Coating	Remarks	WT	Oracle Seed
1	17A	4	A				VERSIFLEX ELASTOMERIC BEARING				86.5	1103AT-T^
1.1	eb17	1	2.664		32.000	10.000	Elastomeric Bearing	110 PSI +/- 15% GR. 3 Neoprene	Plain	BEVELED	40.7	
1.2	es17	4	10 GA.		31.500	9.500	Shim (internal)	A1011 GR. 36	Plain		11.4	

ASSEMBLY SCHEDULE		
MK	LOCATION	QTY.
17A	TYPE F FULL SIZE W/ 2.51% SLOPE	4

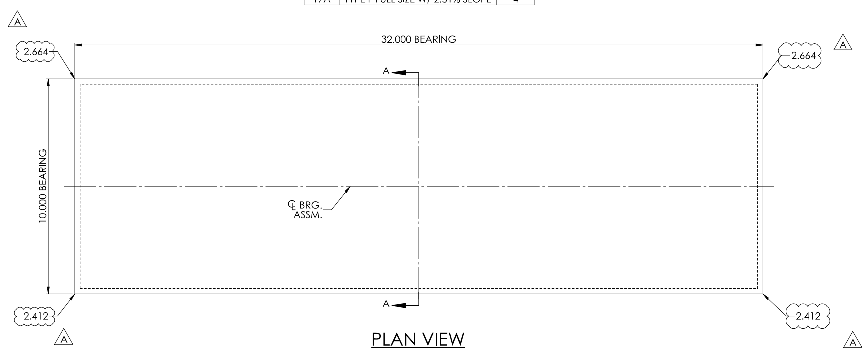

PLAN VIEW
(SEE ASSEMBLY SCHEDULE)

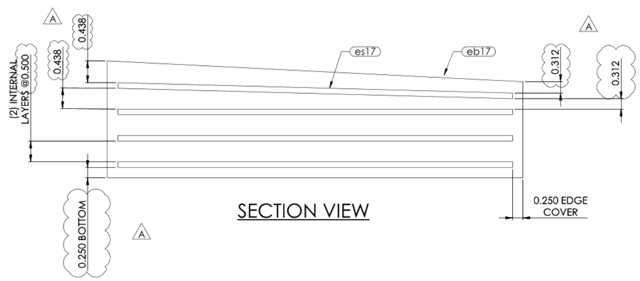

SECTION VIEW

TOLERANCE TABLE	
DESCRIPTION	TOLERANCE (INCHES U.N.O.)
ELASTOMERIC BEARING DESIGN THICKNESS ≤ 1.250"	-0, +0.125
ELASTOMERIC BEARING DESIGN THICKNESS > 1.250"	-0, +0.25
ELASTOMERIC BEARING PLAN DIMENSIONS ≤ 36"	-0, +0.25
ELASTOMERIC BEARING PLAN DIMENSIONS > 36"	-0, +0.50
THICKNESS OF INDIVIDUAL LAYERS OF ELASTOMER (LAMINATED BEARINGS ONLY) AT ANY POINT WITHIN THE BEARING	±0.125
VARIATION FROM A PLANE PARALLEL TO THE THEORETICAL SURFACE (AS DETERMINED BY MEASUREMENTS AT THE EDGE OF THE BEARINGS) (PARALLELISM):	
TOP & BOTTOM	< 0.005 RAD
SIDES	±0.250
POSITION OF EXPOSED CONNECTION MEMBERS	±0.125
ELASTOMERIC EDGE COVER	-0, +0.125
ELASTOMERIC BEARING HOLE OR SLOT SIZE	±0.125
ELASTOMERIC BEARING HOLE OR SLOT LOCATION	±0.125

GENERAL NOTES:

1. ALL MATERIALS SHALL CONFORM TO THE 2018 FLORIDA DEPARTMENT OF TRANSPORTATION STANDARD SPECIFICATIONS FOR ROAD AND BRIDGE CONSTRUCTION.
2. THIS SHOP DRAWING WAS PREPARED IN ACCORDANCE WITH THE CONTRACT PLANS AND SPECIFICATIONS. THE D.S. BROWN COMPANY DOES NOT ACCEPT LIABILITY FOR THE DESIGN OF THE PRODUCTS DETAILED IN THIS SHOP DRAWING.
3. THE D.S. BROWN COMPANY TO SUPPLY ONLY THE PARTS SHOWN ON THIS DRAWING.
4. EXPOSED LAMINATES ON THE OUTSIDE SURFACES OF THE PAD, APPARENT AS A RESULT OF MANUFACTURING TECHNIQUES, SHALL BE SEALED FLUSH ON THE FINISHED BEARING PAD WITH A BONDED VULCANIZED PATCH CONSISTING OF MATERIAL EQUIVALENT TO THAT USED IN THE MANUFACTURING OF THE PAD.
5. INTERNAL ALIGNMENT PINS: AFTER FABRICATION, HOLES TO BE FILLED WITH ELASTOMER MATERIAL EQUIVALENT TO THAT USED IN THE MANUFACTURING OF THE PAD.
6. WELDING PROCEDURES, IF APPLICABLE, SHALL BE ESTABLISHED BY THE CONTRACTOR TO RESTRICT THE MAXIMUM TEMPERATURE REACHED BY SURFACES IN CONTACT WITH THE ELASTOMER TO 200°F (93°C). TEMPERATURES SHALL BE DETERMINED BY TEMPERATURE INDICATING WAX PENCILS OR OTHER SUITABLE MEANS.

REV.	DESCRIPTION	DATE	DET.	CKD.
A	REVISED AS NOTED	4/18/19	RTP	EMF

D.S. BROWN
A GIBRALTAR INDUSTRIES COMPANY

THE D.S. BROWN COMPANY
300 E. CHERRY STREET
NORTH BALTIMORE, OHIO 45872
419.257.3561
FAX: 419.257.0332
WWW.DSBROWN.COM

—
—
—
—
—
—

CUSTOMER — UNIVERSITY OF FLORIDA

DESCRIPTION
VERSIFLEX ELASTOMERIC BEARING
ALACHUA COUNTY, FLORIDA

SCALE	DRAWN BY	CHECKED BY	DATE	
N.T.S.	RTP	EMF	3/19	-
PROJECT NUMBER	PRODUCT CODE	UNITS	SHEET	
4001021	1103	INCHES	17	

FILE SAVED: 4/18/19 9:46:51 AM

NO.	MK	QTY.	Thick	Dia.	Width	Length	Part	Material	Coating	Remarks	WT	Oracle Seed
1	18A	2	A				VERSIFLEX ELASTOMERIC BEARING				84.5	1103AT-U^
1.1	eb18	1	2.538		32.000	10.000	Elastomeric Bearing	110 PSI +/- 15% GR. 3 Neoprene	Plain		38.8	
1.2	es18	4	10 GA.		31.500	9.500	Shim (internal)	A1011 GR. 36	Plain		11.4	

ASSEMBLY SCHEDULE

MK	LOCATION	QTY.
18A	TYPE F FULL SIZE - FLAT	2

TOLERANCE TABLE

DESCRIPTION	TOLERANCE (INCHES U.N.O.)
ELASTOMERIC BEARING DESIGN THICKNESS ≤ 1.250"	-0, +0.125
ELASTOMERIC BEARING DESIGN THICKNESS > 1.250"	-0, +0.25
ELASTOMERIC BEARING PLAN DIMENSIONS < 36"	-0, +0.25
ELASTOMERIC BEARING PLAN DIMENSIONS > 36"	-0, +0.50
THICKNESS OF INDIVIDUAL LAYERS OF ELASTOMER (LAMINATED BEARINGS ONLY) AT ANY POINT WITHIN THE BEARING	±0.125
VARIATION FROM A PLANE PARALLEL TO THE THEORETICAL SURFACE (AS DETERMINED BY MEASUREMENTS AT THE EDGE OF THE BEARINGS) (PARALLELISM):	
TOP & BOTTOM	< 0.005 RAD
SIDES	±0.250
POSITION OF EXPOSED CONNECTION MEMBERS	±0.125
ELASTOMERIC EDGE COVER	-0, +0.125
ELASTOMERIC BEARING HOLE OR SLOT SIZE	±0.125
ELASTOMERIC BEARING HOLE OR SLOT LOCATION	±0.125

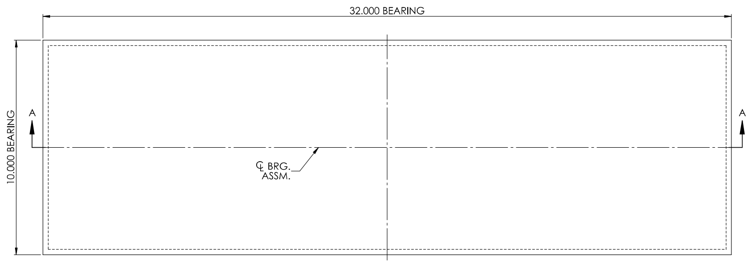

PLAN VIEW
(SEE ASSEMBLY SCHEDULE)

SECTION A-A

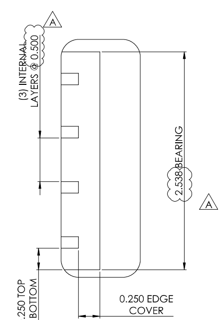

DETAIL A

GENERAL NOTES:

1. ALL MATERIALS SHALL CONFORM TO THE 2018 FLORIDA DEPARTMENT OF TRANSPORTATION STANDARD SPECIFICATIONS FOR ROAD AND BRIDGE CONSTRUCTION.
2. THIS SHOP DRAWING WAS PREPARED IN ACCORDANCE WITH THE CONTRACT PLANS AND SPECIFICATIONS. THE D.S. BROWN COMPANY DOES NOT ACCEPT LIABILITY FOR THE DESIGN OF THE PRODUCTS DETAILED IN THIS SHOP DRAWING.
3. THE D.S. BROWN COMPANY TO SUPPLY ONLY THE PARTS SHOWN ON THIS DRAWING.
4. EXPOSED LAMINATES ON THE OUTSIDE SURFACES OF THE PAD, APPARENT AS A RESULT OF MANUFACTURING TECHNIQUES, SHALL BE SEALED FLUSH ON THE FINISHED BEARING PAD WITH A BONDED VULCANIZED PATCH CONSISTING OF MATERIAL EQUIVALENT TO THAT USED IN THE MANUFACTURING OF THE PAD.
5. INTERNAL ALIGNMENT PINS: AFTER FABRICATION, HOLES TO BE FILLED WITH ELASTOMER MATERIAL EQUIVALENT TO THAT USED IN THE MANUFACTURING OF THE PAD.
6. WELDING PROCEDURES, IF APPLICABLE, SHALL BE ESTABLISHED BY THE CONTRACTOR TO RESTRICT THE MAXIMUM TEMPERATURE REACHED BY SURFACES IN CONTACT WITH THE ELASTOMER TO 200°F (93°C). TEMPERATURES SHALL BE DETERMINED BY TEMPERATURE INDICATING WAX PENCILS OR OTHER SUITABLE MEANS.

REV.	DESCRIPTION	DATE	DET.	CKD.
A	REVISED AS NOTED	4/18/19	RTP	EMF

D.S. BROWN
A GIBRALTAR INDUSTRIES COMPANY

THE D.S. BROWN COMPANY
300 E. CHERRY STREET
NORTH BALTIMORE, OHIO 45872
419.257.3561
FAX: 419.257.0332
WWW.DSBROWN.COM

—
—
—
—
—
—

CUSTOMER — UNIVERSITY OF FLORIDA

DESCRIPTION: VERSIFLEX ELASTOMERIC BEARING
ALACHUA COUNTY, FLORIDA

SCALE	DRAWN BY	CHECKED BY	DATE	
N.T.S.	RTP	EMF	3/19	-
PROJECT NUMBER	PRODUCT CODE	UNITS	SHEET	
4001021	1103	INCHES	18	

FILE SAVED: 4/18/19 9:30:01 AM

APPENDIX B
TEST SETUP FABRICATION

Figure B-1 shows an overview of the test setup. Structural steel components for fabricating the test setup were ordered from several steel suppliers. These components were either partially or completely prefabricated by the supplier, or fabricated at the FDOT Structures Research Center or the University of Florida Structures Laboratory. The steel components included steel plates of various shapes and sizes, a wide flange beam, hollow square sections, angles, channels and fasteners. Table B-1 shows list of steel plates (PL) and hot rolled steel sections with descriptions as purchased from suppliers. The fabrication of partially prefabricated components was completed at the FDOT Structures Research Center, such as drilling holes per fabrication drawings.

Two scissor jacks, each with a lifting capacity of 5000 lbf, were purchased to facilitate separating the top and bottom HSS arms as shown in Figure B-2. Grit 16 aluminum oxide and Sikadur-31 epoxy were purchased to increase the friction at the interface between the bearing pads and the top and bottom steel bearing plates.

A rod end compression (REC) load-cell of 15 kip capacity was purchased to be used along with another identical load-cell available at the FDOT Structures Research Lab. These load-cells were used to measure horizontal force/thrust generated by tapered bearing pads under pure axial load. Figure B-3a shows the location of the REC load-cells in the test setup. To facilitate ease of installation and removal of the REC load-cells, a rod end cell assembly was developed which included the PL-REC plate, REC cells and bolts that screw into the load-cells. The PL-REC plate was purchased prefabricated with holes from a local steel fabricator.

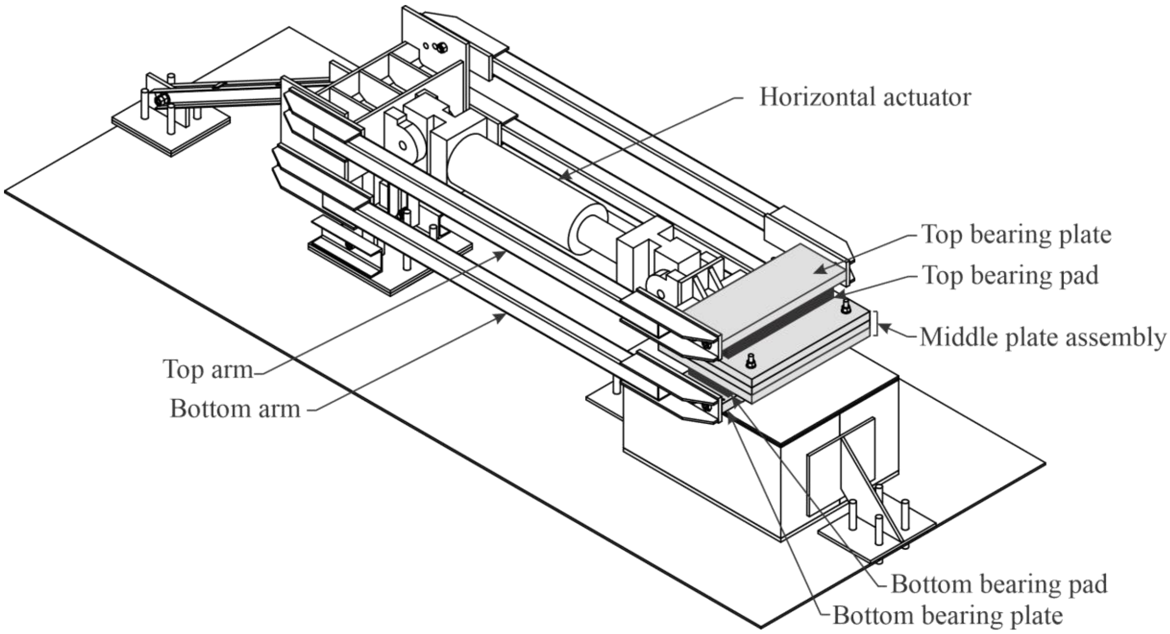

(a)

(b)

Figure B-1 Overview of bearing pad test setup: (a) schematic; (b) after fabrication

Table B-1 List of plates and hot rolled sections as purchased

Item	Quantity	Description
PL-M	1	PL – 2”x33”x36” w/(4) 1-1/16”Φ holes
PL-C	1	PL – 1”x13”x13” w/(4) 1-5/16” Φ holes
PL-F0	2	PL – 0.75”x28.5”x36” w/(4) 1-3/16” Φ holes
PL-F1	2	PL – Bev 1.125” to 0.5”x28.5”x36” w/(4) 1-3/16” Φ holes
PL-F2	2	PL – Bev 1.125” to 0.25”x28.5”x36” w/(4) 1-3/16” Φ holes
PL-F3	2	PL – 2.25”x28.5”x36” w/(4) 1-3/16” Φ holes
PL-F4	2	PL – 1.5”x28.5”x36” w/(4) 1-3/16” Φ holes
PL-F5	2	PL – 0.5”x36”x48”
PL-F6	2	PL – 1.25”x33”x36”
PL-B	1	PL – 2.5”x14”x38” w/(4) Φ1.25-7 x 1-1/2”D holes
PL-B	1	PL – 4”x14”x38” w/(4) Φ1.25-7 x 1-1/2”D holes
PL-V	2	PL – 1”x19.5”x24.5”
PL-S1	4	PL – 0.75”x7.0625”12.5625” w/(2) chamfer corners
PL-S1-h	2	PL – 0.75”x7.0625”12.5625” w/(1) 1-5/16” Φ hole w/(2) chamfer corners
PL-S3	2	PL – 1”x8”x12” w/(1) 1-5/16” Φ holes
PL-T1	2	PL – 1”x6.5”x22”
PL-T2	4	PL – 1”x5”x22”
PL-1	4	PL – 1”x6.5”x25”
PL-2	8	PL – 1”x6.5”x25” w/ chamfer corners
PL-B1	2	PL – 1”x6.5”28.25”
PL-B2	4	PL – 1”x5”x28.25”
PL-S2	4	PL – 1.25”x4.25”x5”
PL-C1	2	PL – 0.5”x28.5”x36” w/(4)1-3/16”Φ, (9)3”Φ, (9)3.5”Φx1/4”D
PL-C2	8	PL – 1”x3”x3” w/(1) 1-3/16” Φ holes
PL-C3	4	PL – 1”x1”x36” w/(1)
LW-1	8	PL – Bev 0.25” to 3/16”x3”x3” w/(1) 1-3/16”Φ hole
LW-2	8	PL – Bev 0.25” to 0.125”x3”x3” w/(1) 1-3/16”Φ hole
PL-F8	1	PL – 0.75”x25”x25”
PL-F9	1	PL – 0.25”x18”x18”
PL-CR1	2	PL – 0.75”x16”x20”
PL-CR2	2	PL – 0.75”x18-3/8”x18-3/8”
PL-CR3	2	PL – 0.75”x16”x20”
W	1	W.F. beam (14”x109)x3’ long (ASTM A572/A992 Gr 50)
HT	2	HSS (4.5”x0.25”)x8’-9” long (ASTM A500 Gr B)
HB	2	HSS (4.5”x0.25”)x8’-6.25” long (ASTM A500 Gr B)
CH-1	2	Ship channel (6”x15.3”)x2’-6.75” long (Dual ASTM A36/ Gr 50)
CH-2	2	Ship channel (6”x15.3”)x1’-6” long (Dual ASTM A36/ Gr 50)
CH-3	2	Ship channel (6”x15.3”)x5’-6” long (Dual ASTM A36/ Gr 50)
A-1	4	Angle (2.5”x1.5”x1.25”)x38” long

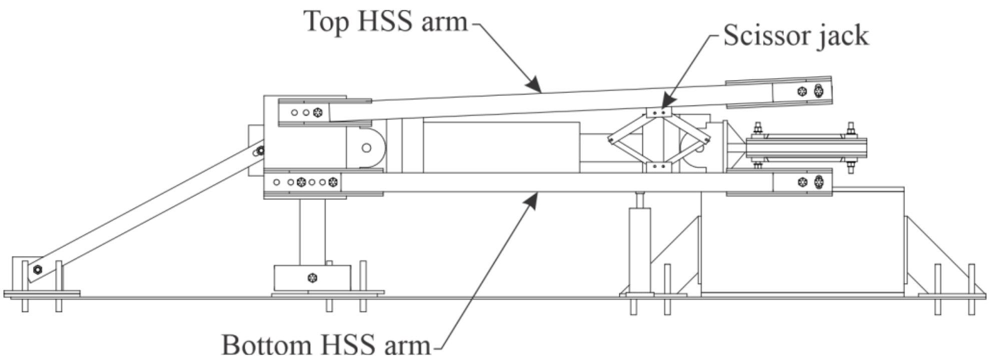

Figure B-2 Illustration of use of scissor jacks to separate top and bottom HSS arms

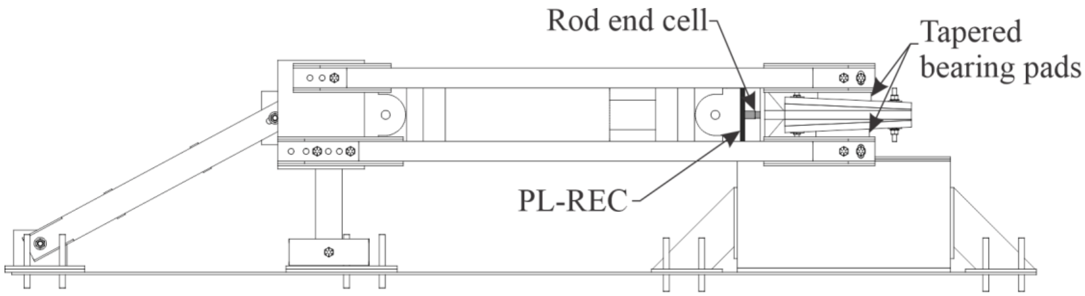

(a)

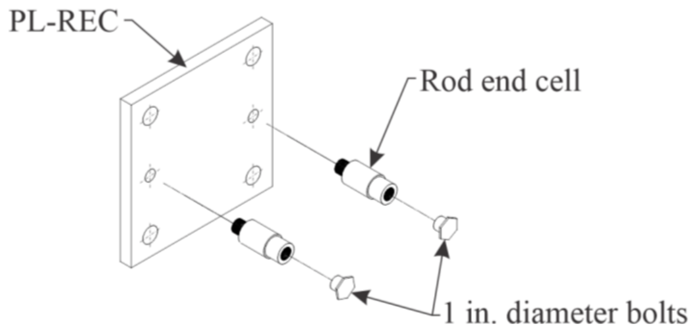

(b)

Figure B-3 Rod end cell assembly: (a) Location of rod end cell in the test setup; (b) Exploded view of rod end cell assembly

The fabrication of the test setup began after all materials were acquired. Before starting fabrication, the steel components delivered were inspected for size. All the components were found to have dimensions within standard tolerances, except for plate PL-F5. The plate PL-F5 was found to be warped and out of tolerance, and was not able to be flattened due to the small thickness compared to plan dimensions (Figure B-4). PL-F5 was, therefore, excluded from the test setup. PL-F5 was replaced by layer of hydrostone.

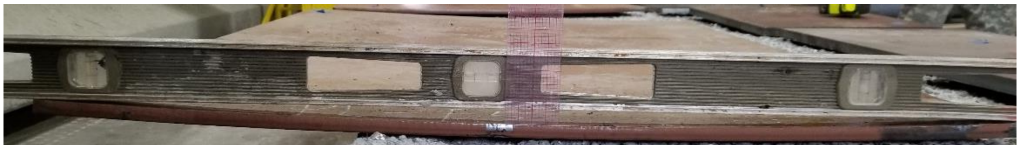

Figure B-4 Warping in plate PL-F5

Holes were drilled into components which were not ordered with prefabricated holes. Then test setup was first built into smaller assemblies. On completion, each assembly was coated with primer and paint to protect against corrosion. The HSS arms assemblies were first fabricated by welding plates to the HSS tubes per the fabrication drawings and then coated with primer (Figure B-5). Similarly, other assemblies were fabricated, and coated with primer and paint as shown in Figure B-6.

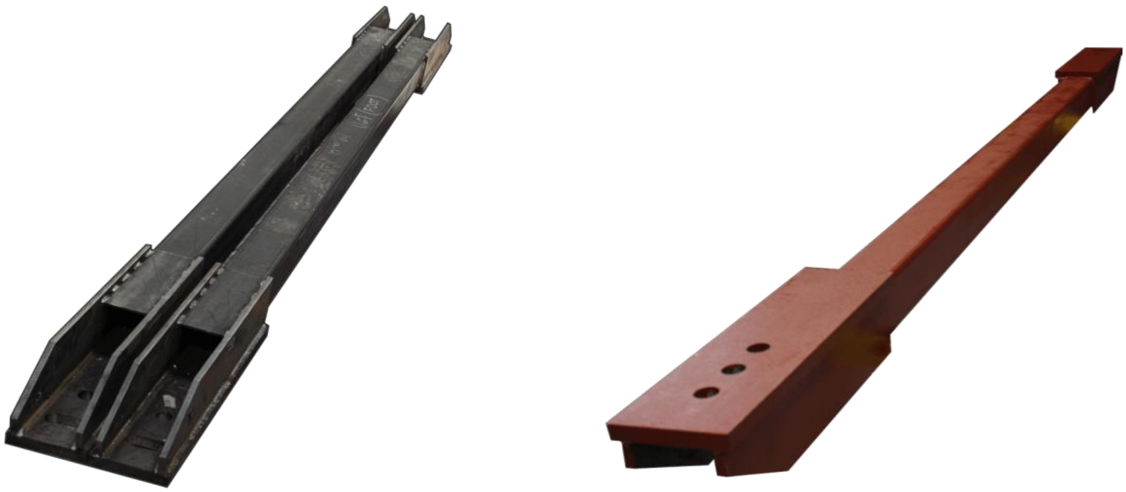

(a) (b)

Figure B-5 HSS arms: (a) Before primer coating; (b) After primer coating

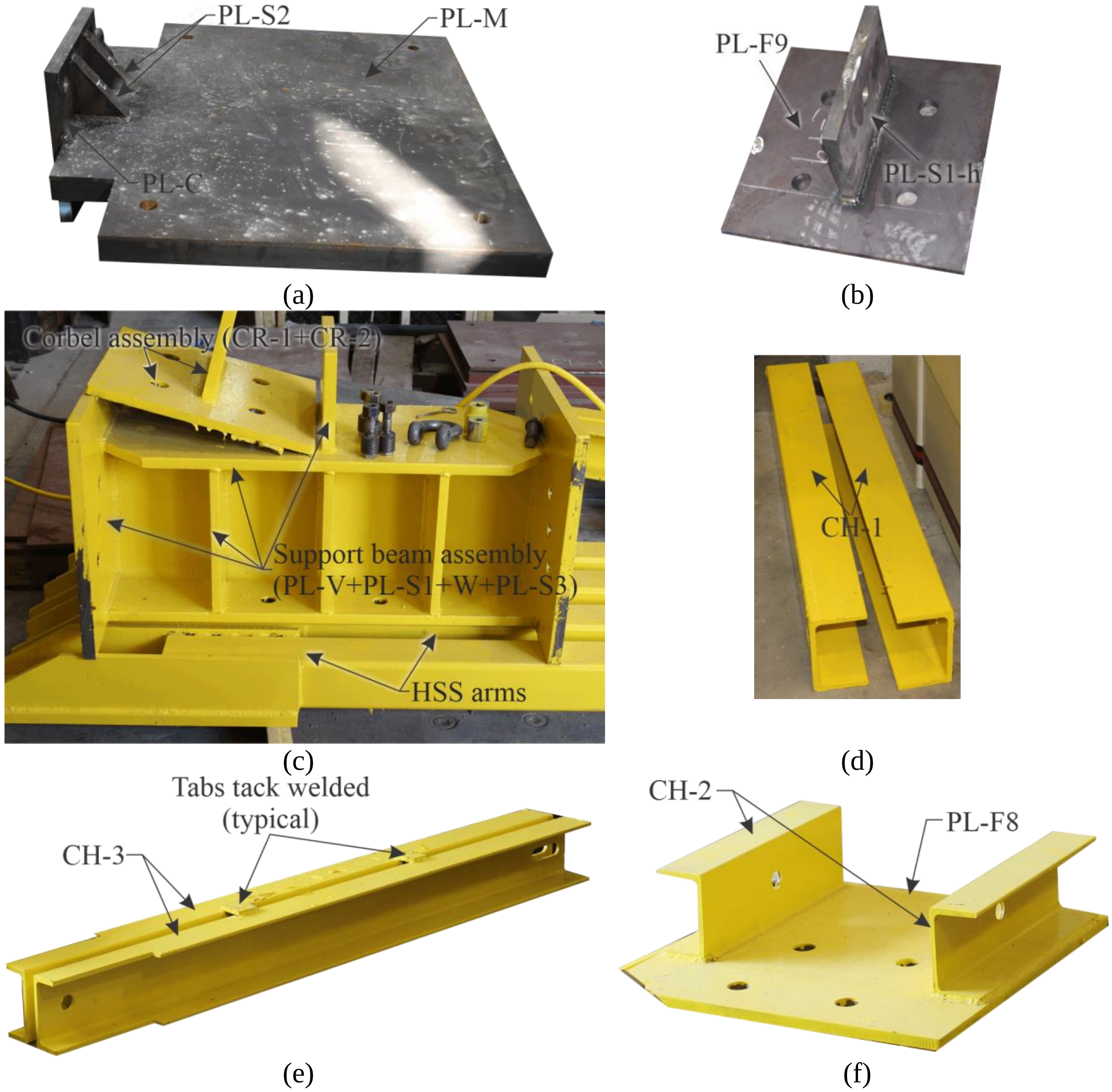

Figure B-6 Test setup assemblies: (a) Parent middle plate assembly; (b) PL-F9 and PL-S1-h assembly; (c) HSS arms, support beam, and corbel assemblies; (d) CH-1 coated with paint; (e) CH-3 assembly; (f) CH-2 and PL-F8 assembly

After fabricating individual assemblies, the test setup supports were fabricated as shown in Figures B-7 through B-9. Grout pads were placed under the supports to provide a level surface for the setup. The supports were anchored to the strong floor using 1.5” threaded anchor rods.

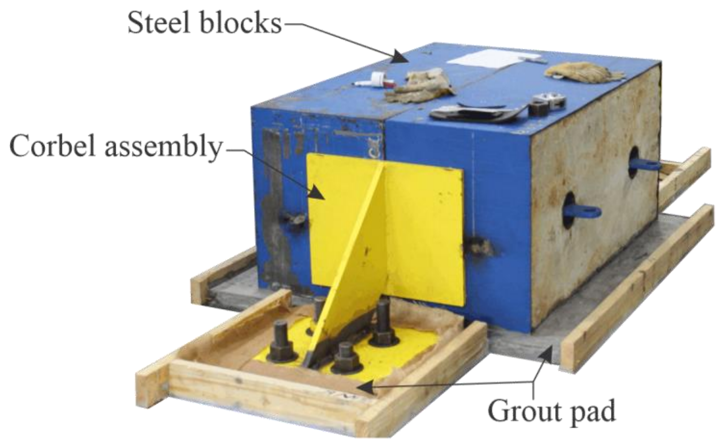

Figure B-7 Corbel assembly and steel blocks

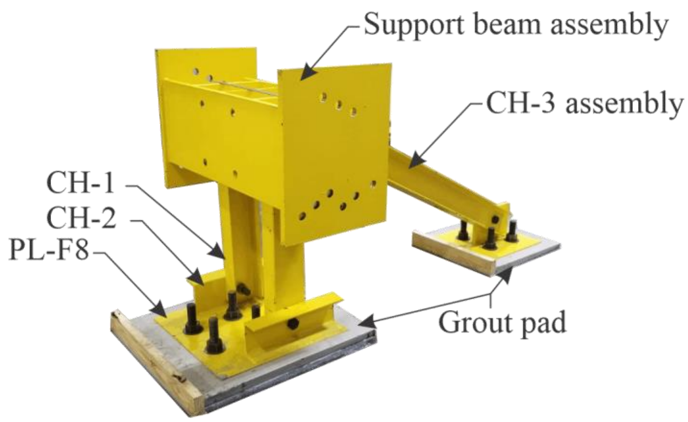

Figure B-8 Frame support end assembly

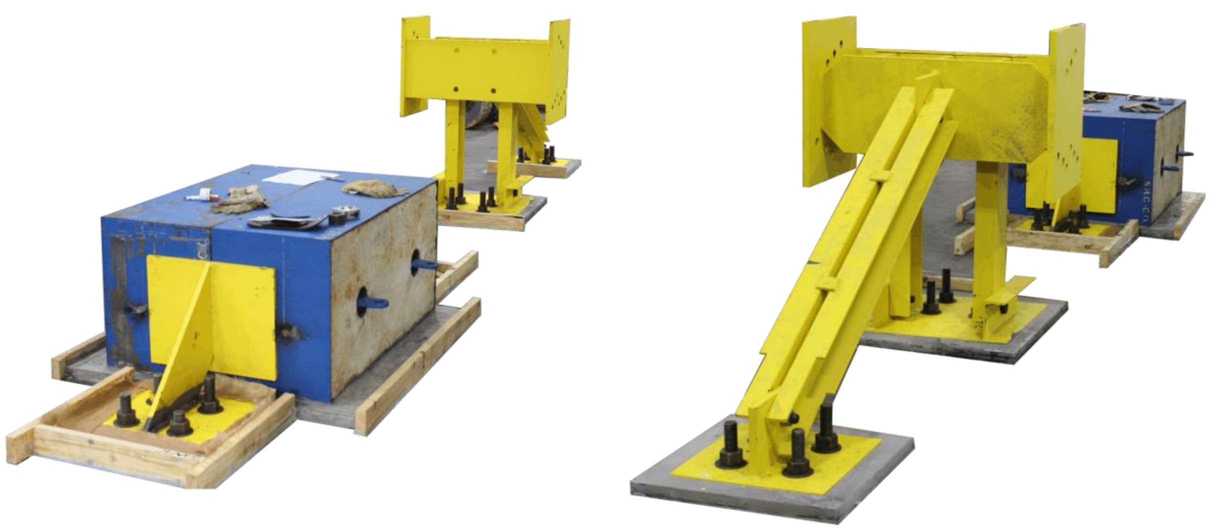

(a) (b)

Figure B-9 Test setup supports in place: (a) Front view; (b) Back view

After the grout pads were cured, horizontal actuator (model: MTS) and HSS arm assemblies were installed in the setup (Figures B-10 and B-11). Simultaneously, top and bottom bearing plates, and middle plate assembly were installed (Figure B-12). Before installing the top and bottom bearing plates, an approximately 1/32-in. thick layer of epoxy and aluminum oxide grit was adhered to the surfaces which will be in contact with bearing pads (Figure B-13).

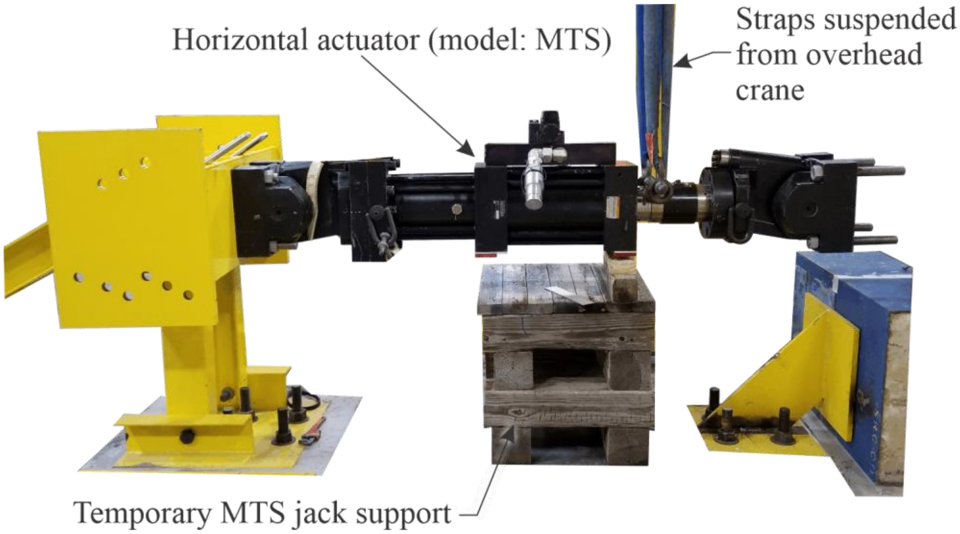

Figure B-10 Horizontal actuator (model: MTS) installed in the test setup

Figure B-11 HSS arms installed in the setup

(a)

(b)

Figure B-12 Bearing pad end assembly: (a) Front view; (b) Side view

(a)

(b)

Figure B-13 Aluminum oxide grit pasted on bearing plates (PL-B and PL-B-top): (a) Top view; (b) Close-up view

As shown in Figure B-3b, each rod end compression (REC) cell had a 1 in. bolt, which will be used as a bearing surface to bear against the middle plate assembly in order to measure lateral force generated by axially loading tapered bearing pads (Figure B-14). To reduce the transverse (vertical) force acting on the REC cells, due to vertical movement of middle plate, Teflon sheets taped into position between the REC cell bolts and middle plate assembly as shown in Figure B-14b. The hex-heads of the bolts were milled down to a thickness of 1/8 in. so that the REC cell assembly would fit between the horizontal actuator (MTS) and the middle plate assembly

(Figure B-15). The bolts were also cut to a length equal to 1 in., so that they could be screwed completely into the REC cells.

(a) (b)

Figure B-14 REC cells in place: (a) Side view; (b) Top view

(a) (b)

Figure B-15 Rod end compression cell assembly: (a) 1 in. diameter 1 in. length bolt with reduce head thickness; (b) REC cell with bolt

Two scissor jack assemblies were fabricated in order to facilitate separating the top and bottom HSS arms as shown in Figure B-16. Two 23 in. long angles (L 2.5”x1.5”x0.25”) were welded on top and bottom faces of both scissor jacks to fabricate a built-up channel section wide enough to fit the HSS arms between the angles. This ensured that the scissor jacks will not slip out of plane while lifting. Figure B-16 shows schematic and fabricated scissor jack assembly.

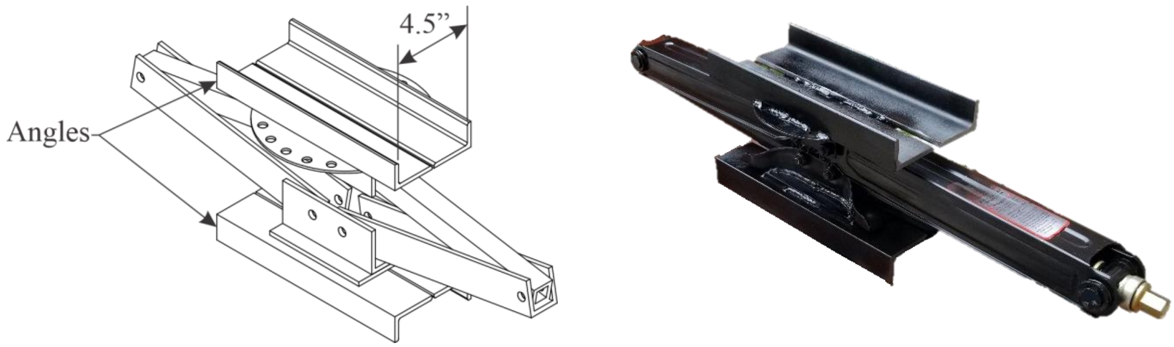

(a) (b)

Figure B-16 Scissor jack assembly: (a) Schematic drawing; (b) Fabricated assembly

Displacement gauges were installed in the test setup as per the instrumentation drawings (Figures B-17). Support frames for the DX laser gauges were fabricated at the FDOT Structures Research Center lab using slotted framing components (Figure B-18) that were readily available (from McMaster Carr). DZ gauges were mounted using metal studs that were welded to the top and bottom steel bearing plates (Figure B-19).

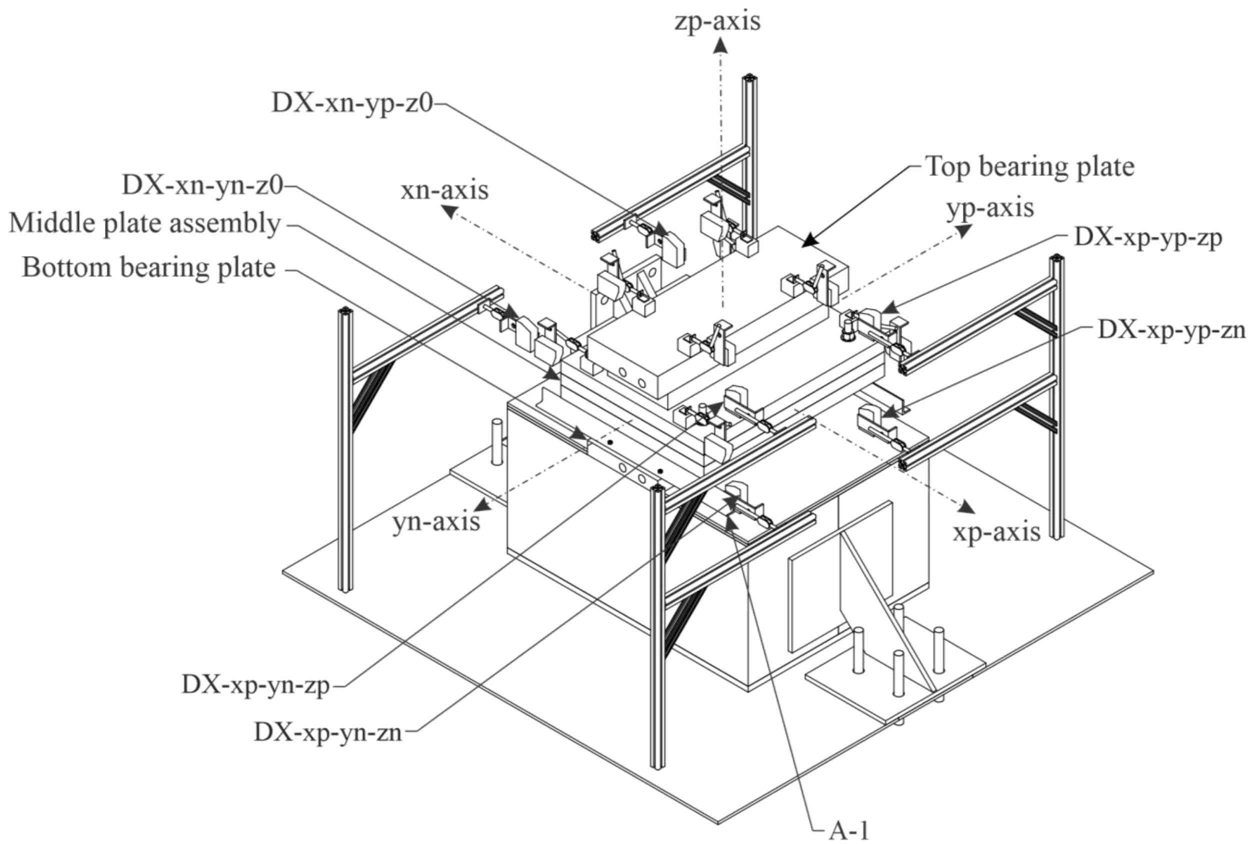

Figure B-17 Laser sensors instrumentation plan (isometric View)

Figure B-18 Supporting frames for DX laser gauges

Figure B-19 Typical metal stud used for mounting DZ laser gauges

APPENDIX C
TEST SETUP FABRICATION DRAWINGS

On the following pages, fabrication drawings for the bearing pad test setup are provided. The drawings include details of *all* parts in the test setup, and proposed test setup operating procedures.

SHEET LIST		SHEET LIST	
SHEET NO.	SHEET NAME	SHEET NO.	SHEET NAME
1	Table of content - page 1	27	Concrete plate assembly detail
2	Table of content - page 2	28	Concrete plate assembly ~ PL-C1
3	Test Setup Overview	29	Concrete plate assembly ~ PL-C2 and C3
4	Support beam assembly	30	Concrete plate assembly steps
5	Support beam assembly parts (PL-V W)	31	Concrete plate formwork assembly
6	Support beam assembly parts (PL-S1 PL-S1-h PL-S3)	32	Concrete plate construction ~ FW-1 FW-2 and FW-3
7	Support beam assembly - Step 1	33	Concrete plate construction
8	Support beam assembly - Step 2	34	Bearing plates ~ Schedule of plates
9	Top HSS assembly	35	Bearing plates ~ PL-F0 to F4
10	Top HSS assembly ~ PL-T1 PL- Attachment 1	36	Bearing plates ~ PL-B
11	Top HSS assembly ~ PL-T2	37	Bearing plates ~PL-B-top
12	Top HSS assembly ~ PL-1	38	Middle plate ~ Fasteners-1 TR-1 W-1 N-1 LW-1 and LW-2
13	Top HSS assembly ~ PL-2		
14	Top HSS Assembly - Step 1	39	Middle-plate-flat-concrete-config
15	Top HSS Assembly - Step 2	40	Middle-plate-flat-steel-config
16	Bottom HSS Assembly	41	Middle-plate-2slope-concrete-config
17	Bottom HSS Assembly ~ PL-B1	42	Middle-plate-2slope-steel-config
18	Bottom HSS Assembly ~ PL-B2	43	Middle-plate-4slope-concrete-config
19	Bottom HSS Assembly ~ PL-1	44	Middle-plate-4slope-steel-config
20	Bottom HSS Assembly ~ PL-2	45	Frame-support ~ CH-1 CH-2 CH-3 PL-F8 and PL-F9
21	Bottom HSS Assembly - Step 1	46	Frame-support ~ Fastners-2 B-1 B-2 N-2 and W-2
22	Bottom HSS Assembly - Step 2	47	Frame-support ~ Fastners-3 R-1 CS-1 B-3 and W-3
23	Parent middle plate assembly details	48	Frame-support-to-floor-assembly
24	Parent middle plate assembly ~ PL-M PL-C and PL-S2	49	Frame-support-to-floor-assembly-2
25	Parent middle plate - Step 1	50	Frame-support-to-floor-assembly
26	Parent middle plate assembly- Step 2	51	Corbel-assembly-parts ~ PL-CR1 PL-CR2 AND PL-CR3
		52	Corbel-assembly-steps

Table of content				Scale
	11/12/2019	University of Florida	SHEET 1 OF 93	Revision:

SHEET LIST	
SHEET NO.	SHEET NAME
53	Bearing-end-support-assembly-1
54	Bearing-end-support-assembly-1
55	Summary-of-configs-Bearing-end-plates
56	Summary-of-configs-Bearing-end-plates-table
57	Summary-of-configs-PL-V-hole-attachements
58	Flat-K-steel-config-assembly
59	Flat-K-steel-config-assembly-exploded
60	Flat-K-steel-config-assembly-views
61	Flat-K-concrete-config-assembly-exploded
62	2slope-K-steel-config-assembly-exploded
63	4slope-K-steel-config-assembly-exploded
64	Flat-F-steel-config-assembly-exploded
65	Flat-E-steel-config-assembly-exploded
66	Instrumentation Assembly ~ A-1 T-1 T-2 and B-3
67	Instrumentation Assembly ~ PL-REC REC-15K
68	Instrumentation Assembly at bearing-end-support
69	Instrumentation Assembly ~ DX and DZ
70	Instrumentation Assembly ~ DX only
71	Instrumentation Assembly ~ DZ only
72	Instrumentation Assembly for Flat K-type pad-detailed views
73	Instrumentation Assembly for Flat K-type pad
74	Instrumentation Assembly for tapered K-type pad
75	Instructions set 1 From type flat pad K to tapered pad K
76	Instructions set 1 From type flat pad K to tapered pad K
77	Instructions set 1 From type flat pad K to tapered pad K
78	Instructions set 1 From type flat pad K to tapered pad K

SHEET LIST	
SHEET NO.	SHEET NAME
79	Instructions set 1 From type flat pad K to tapered pad K
80	Instructions set 1 From type flat pad K to tapered pad K
81	Instructions set 2 From type flat pad F to flat pad K
82	Instructions set 2 From type flat pad F to flat pad K
83	Instructions set 2 From type flat pad F to flat pad K
84	Instructions set 2 From type flat pad F to flat pad K
85	Instructions set 2 From type flat pad F to flat pad K
86	Instructions set 2 From type flat pad F to flat pad K
87	Instructions set 3 Retract MTS
88	Installing REC-15K instrumentation
89	Installing REC-15K instrumentation
90	Scissor-jack-parts
91	Scissor-jack-assembly
92	Weight balance mechanism
93	Pulley drawing

Table of content				*Scale*
	11/12/2019	*University of Florida*	*SHEET 2 OF 93*	*Revision:*

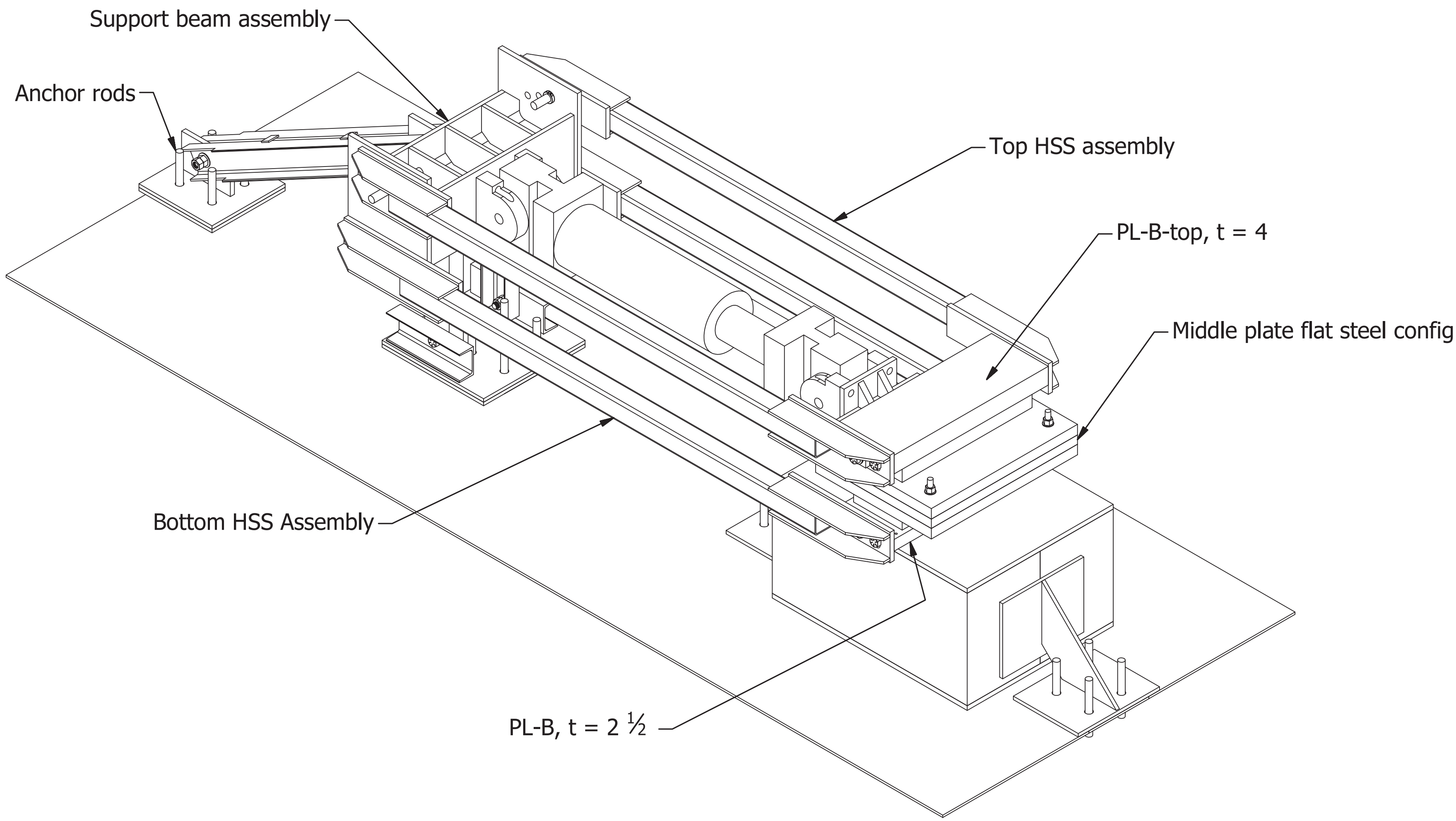

Bearing Pad Test Setup - Overview				Scale	0 2′ 4′
Test assembly	11/12/2019	University of Florida	SHEET 3 OF 93	Revision:	

PARTS LIST - 1					
ITEM	PART NAME	CROSS-SECTION	LENGTH	QTY	MATERIAL
1	W	14 X 109	36	1	STEEL, ASTM-A572 Gr-50
2	PL-V	24 1/2 x 1	19 1/2	2	STEEL, ASTM-A572 Gr-50
3	PL-S1/S1-h	7 1/32 x 3/4	12 9/16	6	STEEL, ASTM-A572 Gr-50
4	PL-S3	8 x 1	12	2	STEEL GR-36

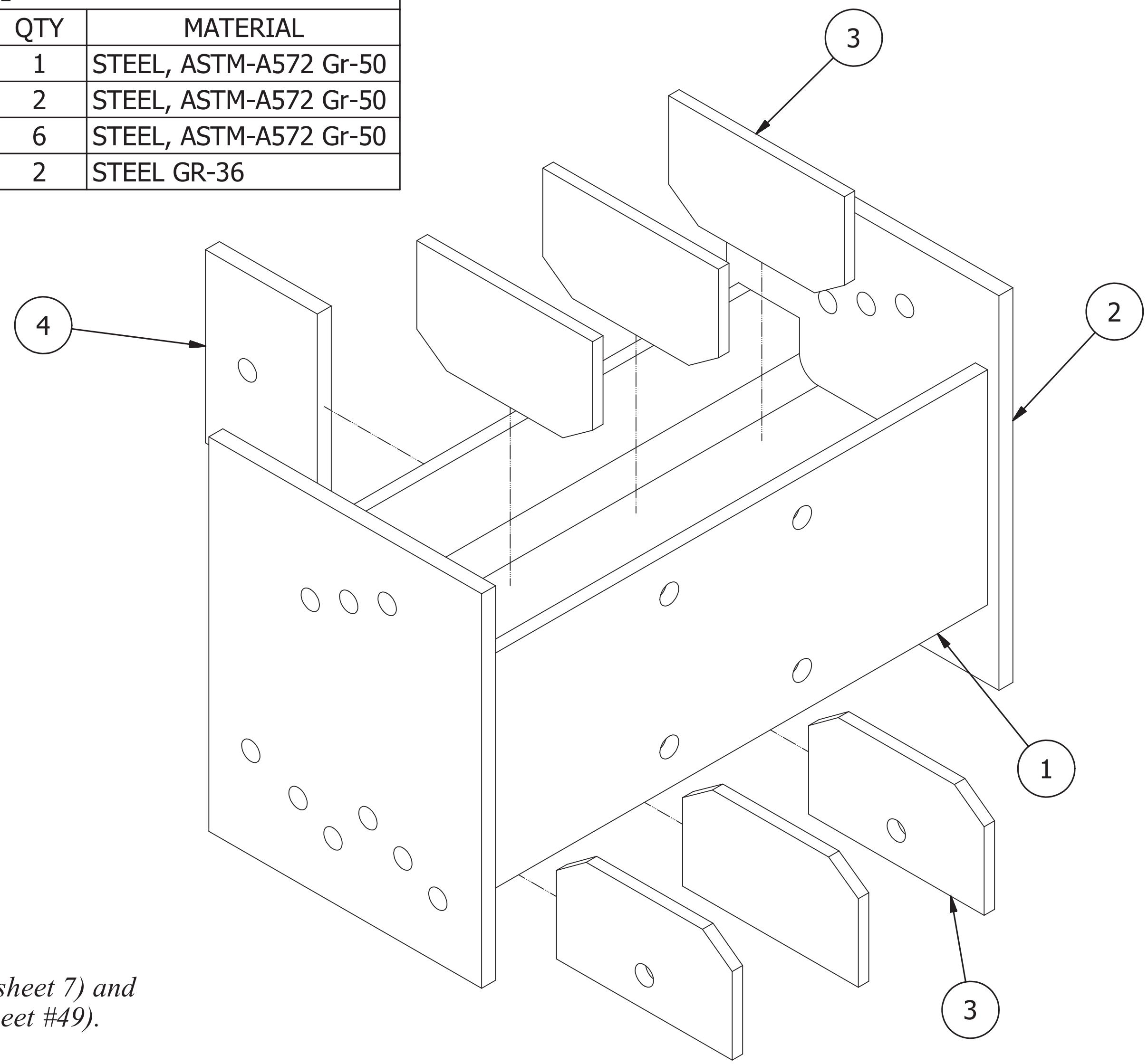

Note: One PL-S3 is connected to part W (see sheet 7) and the other PL-S3 is connected to PL-F9 (see sheet #49).

3D exploded view				*Scale*	
Support beam assembly	*11/12/2019*	*University of Florida*	*SHEET 4 OF 93*	*Revision:*	

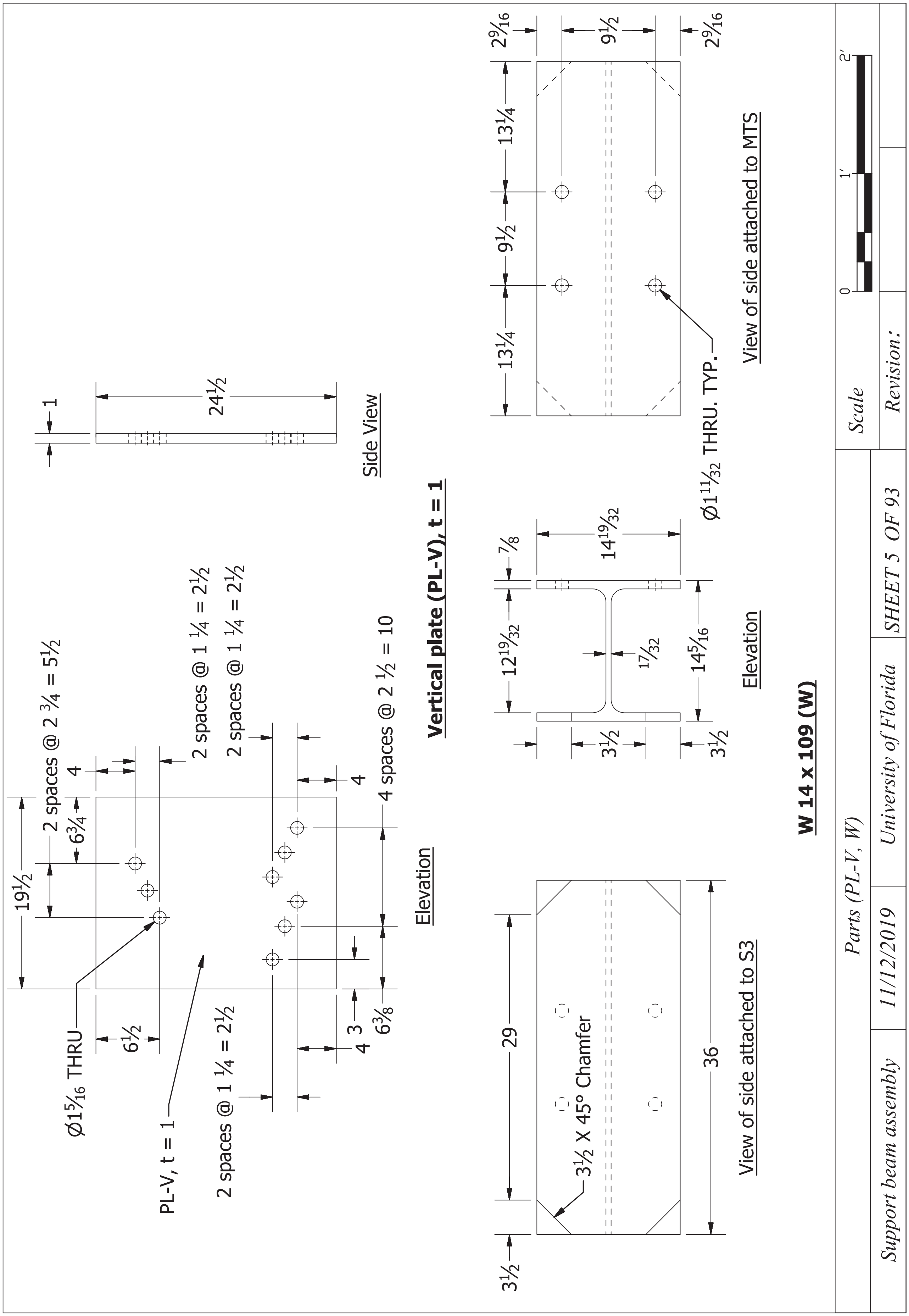

Vertical plate (PL-V), t = 1
Elevation
Side View
PL-V, t = 1
Ø1 5/16 THRU
2 spaces @ 2 3/4 = 5 1/2
2 spaces @ 1 1/4 = 2 1/2
4 spaces @ 2 1/2 = 10
W 14 x 109 (W)
View of side attached to S3
View of side attached to MTS
3 1/2 X 45° Chamfer
Ø1 11/32 THRU. TYP.
Support beam assembly
11/12/2019
University of Florida
SHEET 5 OF 93
Parts (PL-V, W)
Scale
Revision:

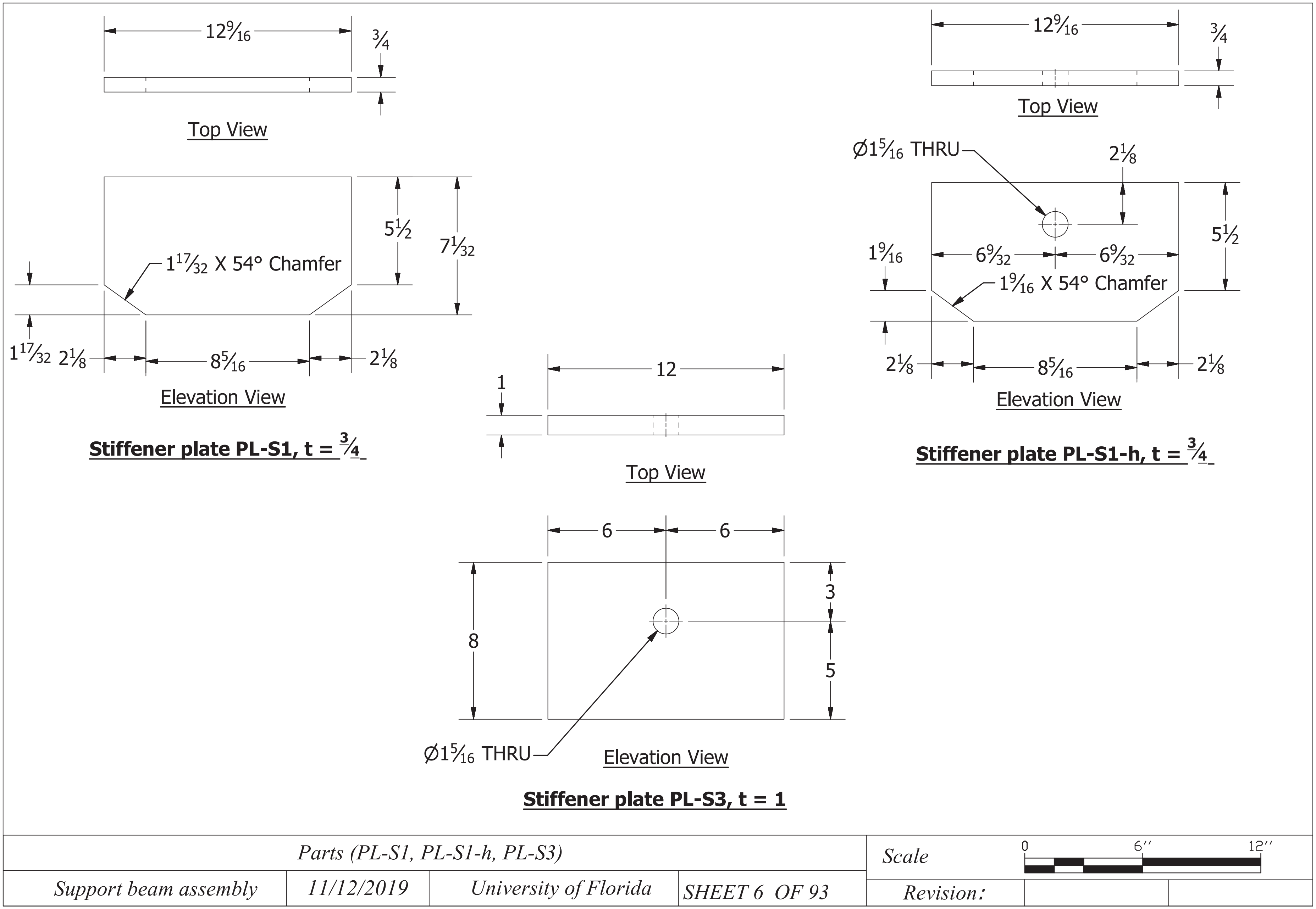
12 9/16
3/4
Top View
1 17/32 X 54° Chamfer
5 1/2
7 1/32
1 17/32 2 1/8
8 5/16
2 1/8
Elevation View
Stiffener plate PL-S1, t = 3/4
12
1
Top View
6
6
8
3
5
Ø1 5/16 THRU
Elevation View
Stiffener plate PL-S3, t = 1
12 9/16
3/4
Top View
Ø1 5/16 THRU
2 1/8
5 1/2
1 9/16
6 9/32
6 9/32
1 9/16 X 54° Chamfer
2 1/8
8 5/16
2 1/8
Elevation View
Stiffener plate PL-S1-h, t = 3/4
Parts (PL-S1, PL-S1-h, PL-S3)
Scale
0
6''
12''
Support beam assembly
11/12/2019
University of Florida
SHEET 6 OF 93
Revision:

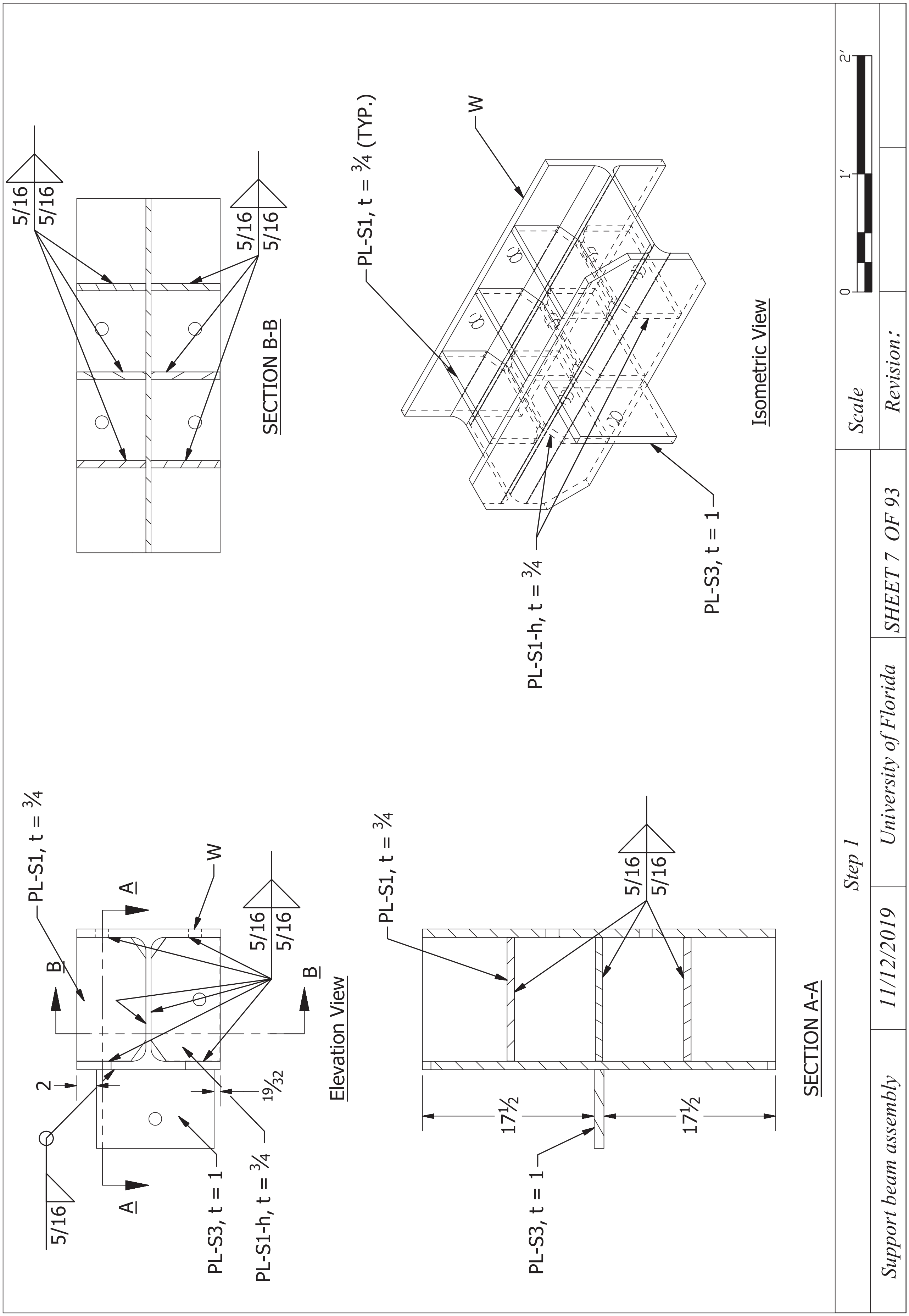

Elevation View
SECTION A-A
SECTION B-B
Isometric View
PL-S1, t = ¾
PL-S1, t = ¾ (TYP.)
PL-S1-h, t = ¾
PL-S3, t = 1
W
5/16
2
19/32
17½
A
B
Support beam assembly
11/12/2019
Step 1
University of Florida
SHEET 7 OF 93
Scale
Revision:
0
1′
2′

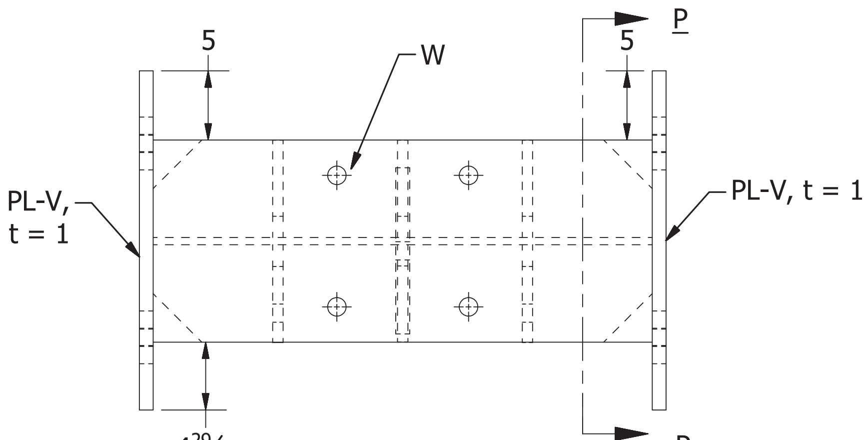

Elevation View

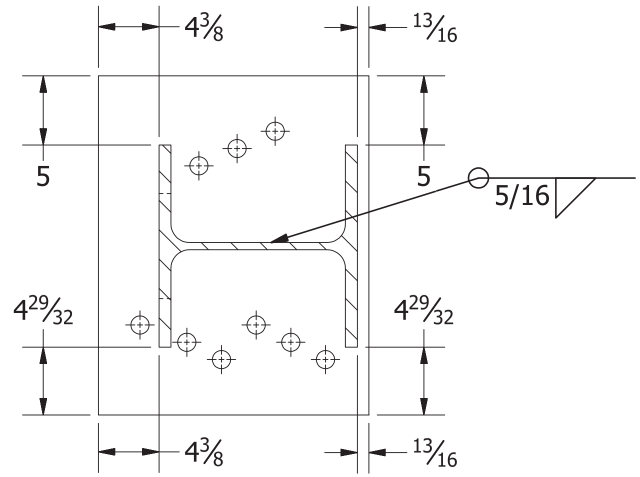

SECTION P-P

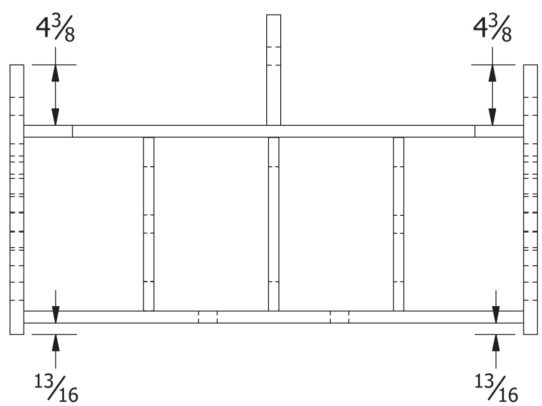

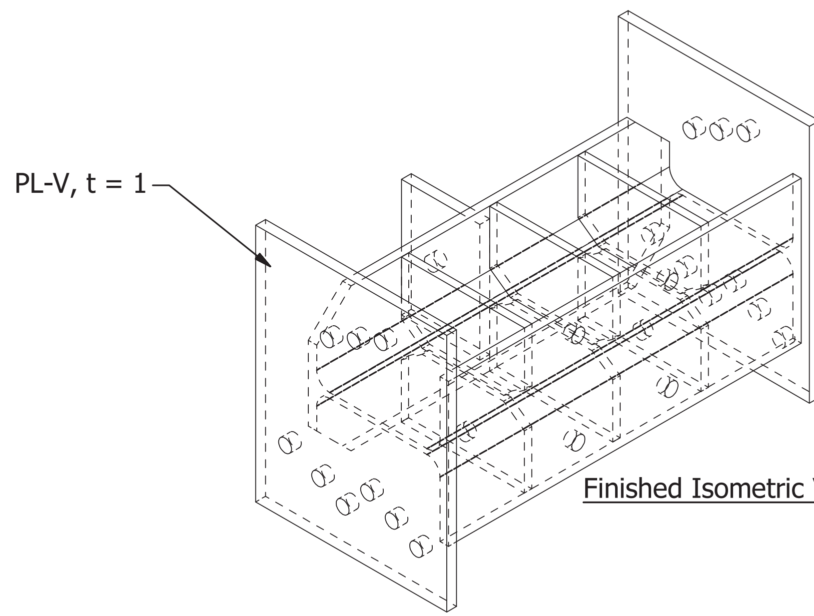

Finished Isometric View

Step 2				Scale	0 1′ 2′
Support beam assembly	11/12/2019	University of Florida	SHEET 8 OF 93	Revision:	

PARTS LIST - 2					
ITEM	PART NAME	CROSS-SECTION	LENGTH	QTY	MATERIAL
1	HT	4.5 x 0.25	105	2	STEEL, Gr-46
2	PL-T1	6 1/2 x 1	22	2	STEEL, ASTM-A572 Gr-50
3	PL-T2	5 x 1/2	22	4	STEEL, ASTM-A572 Gr-50
4	PL-1	6 1/2 x 1	25	2	STEEL, ASTM-A572 Gr-50
5	PL-2	5 x 1/2	25	4	STEEL, ASTM-A572 Gr-50
7	PL-Attachement 1	3 x 1	4	2	STEEL, ASTM-A572 Gr-50

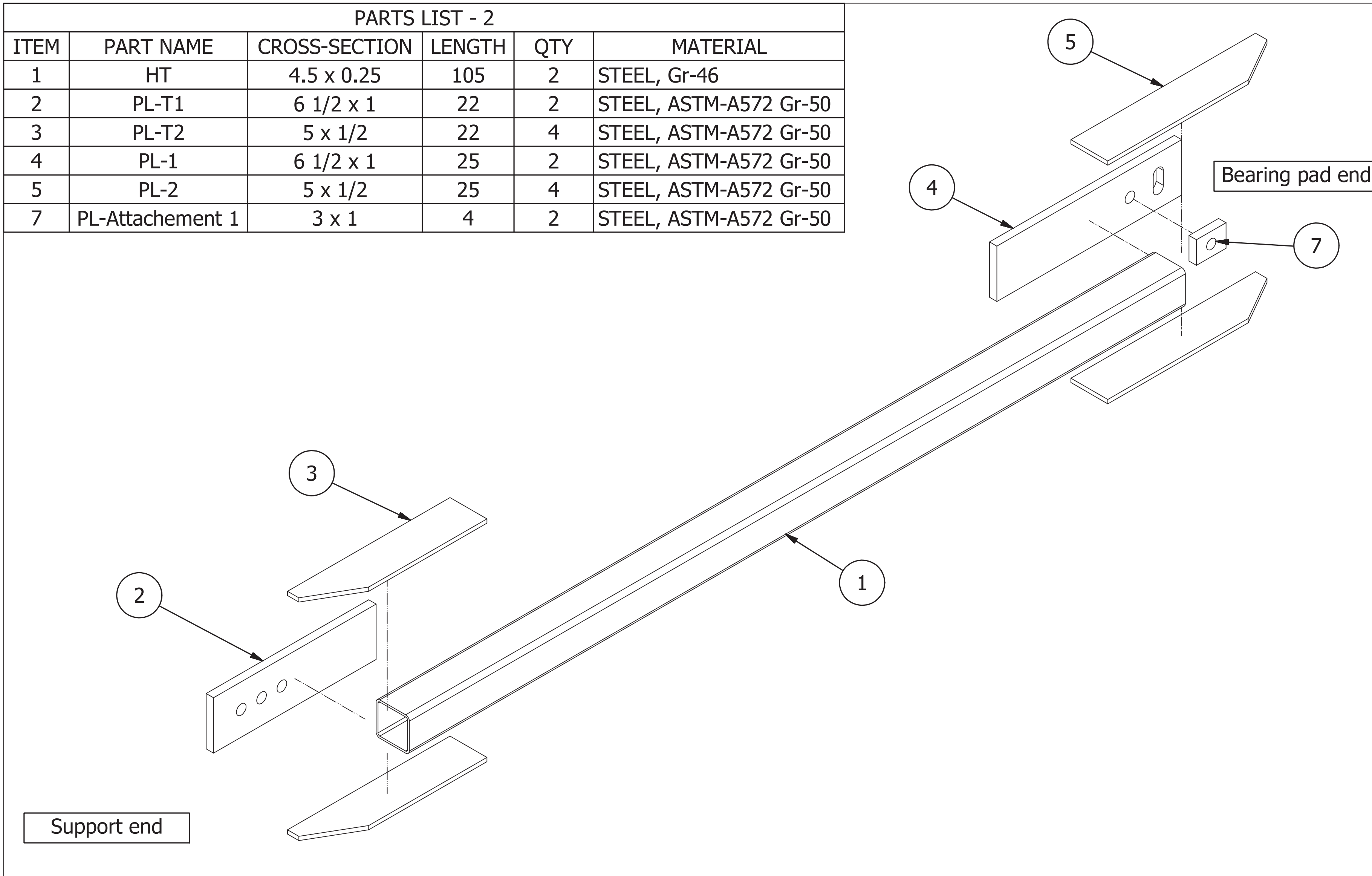

3D exploded view				Scale
Top HSS arm	11/12/2019	University of Florida	SHEET 9 OF 93	Revision:

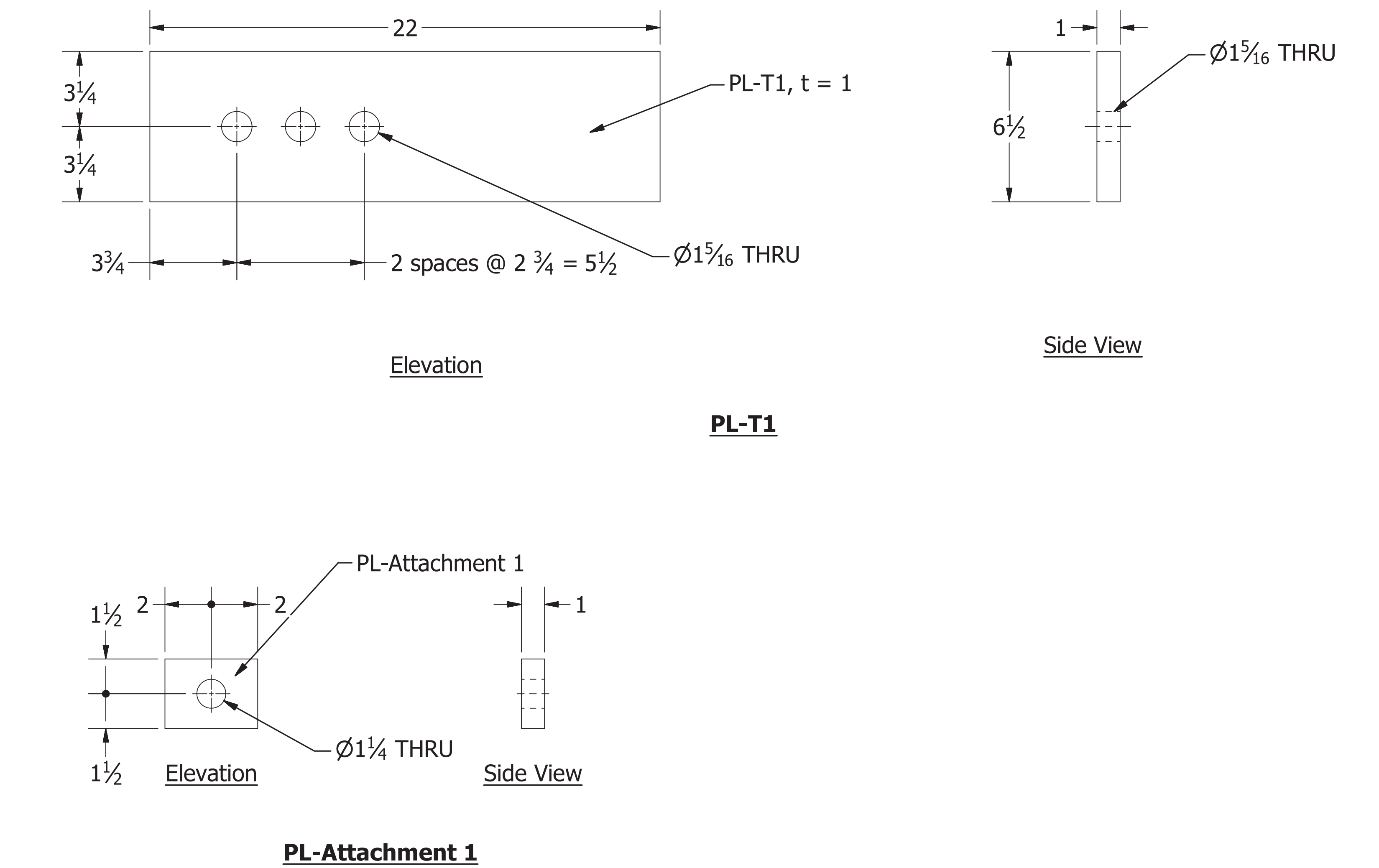

PL-T1, PL- Attachment 1				*Scale*	0 6″ 12″	
Top HSS arm	*11/12/2019*	*University of Florida*	*SHEET 10 OF 93*	*Revision:*		

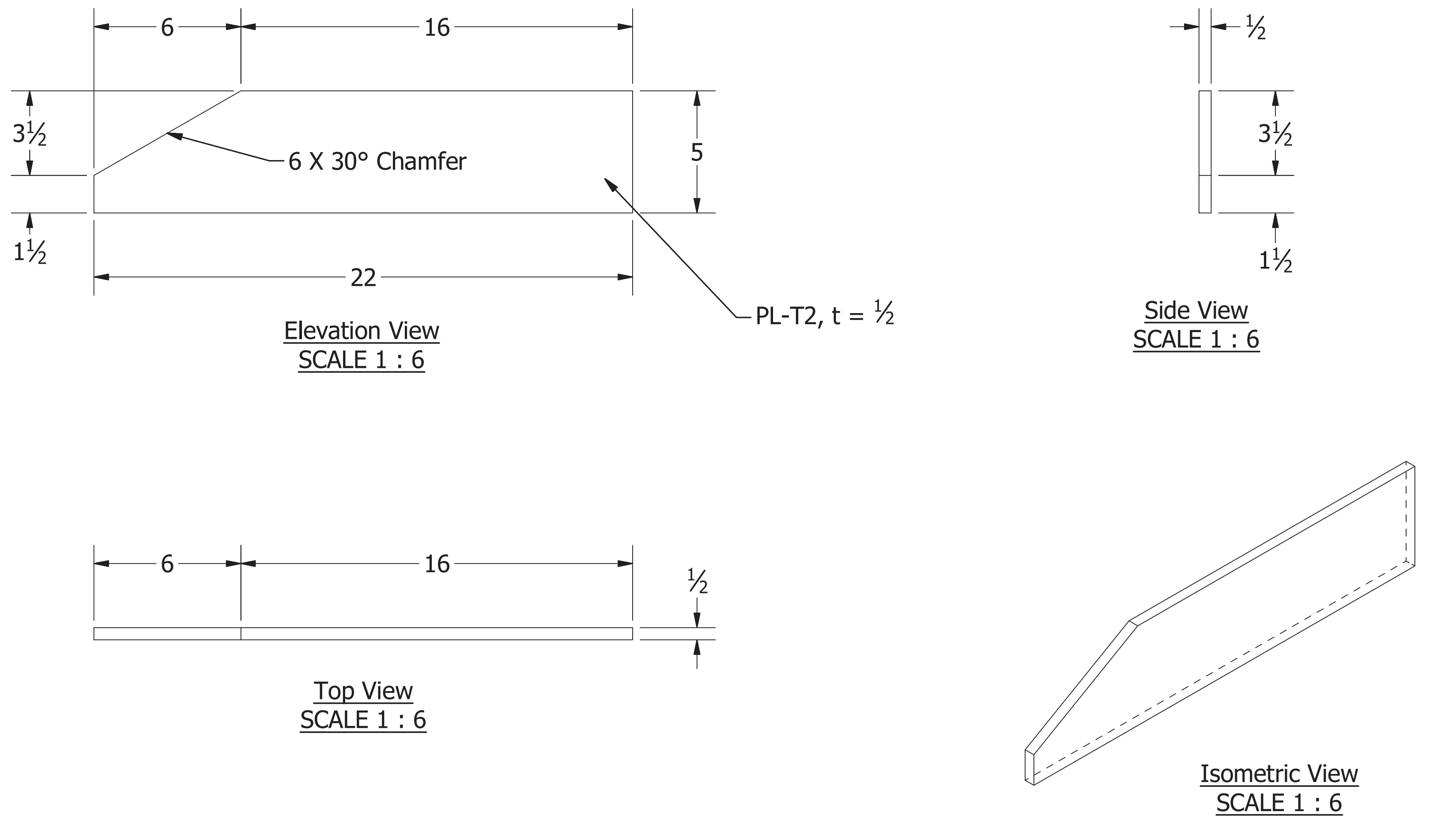

PL-T2				*Scale*	0 6'' 12''
Top HSS arm	*11/12/2019*	*University of Florida*	*SHEET 11 OF 93*	*Revision:*	

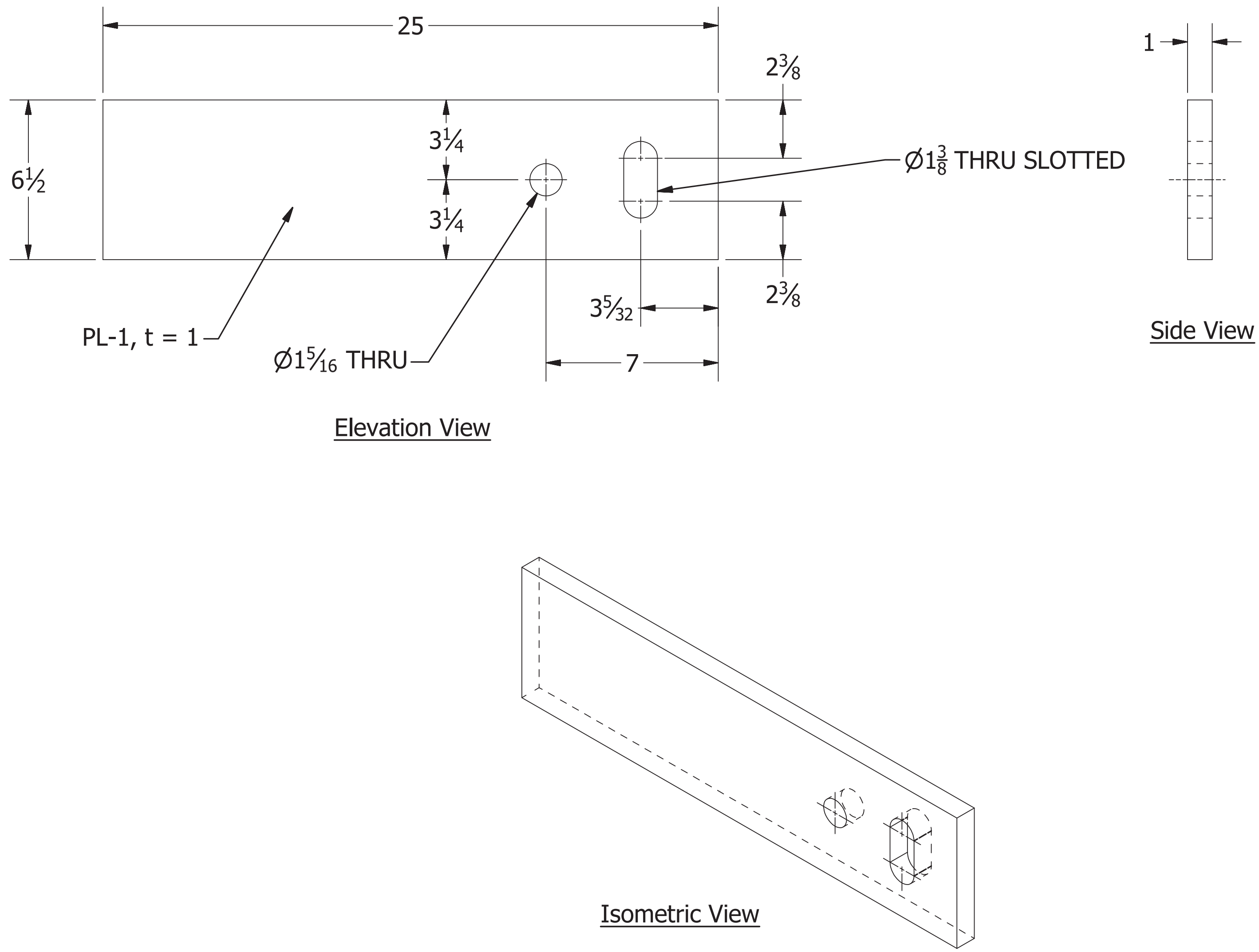

PL-1				Scale	0 6'' 12''
Bottom HSS arm	11/12/2019	University of Florida	SHEET 12 OF 93	Revision:	

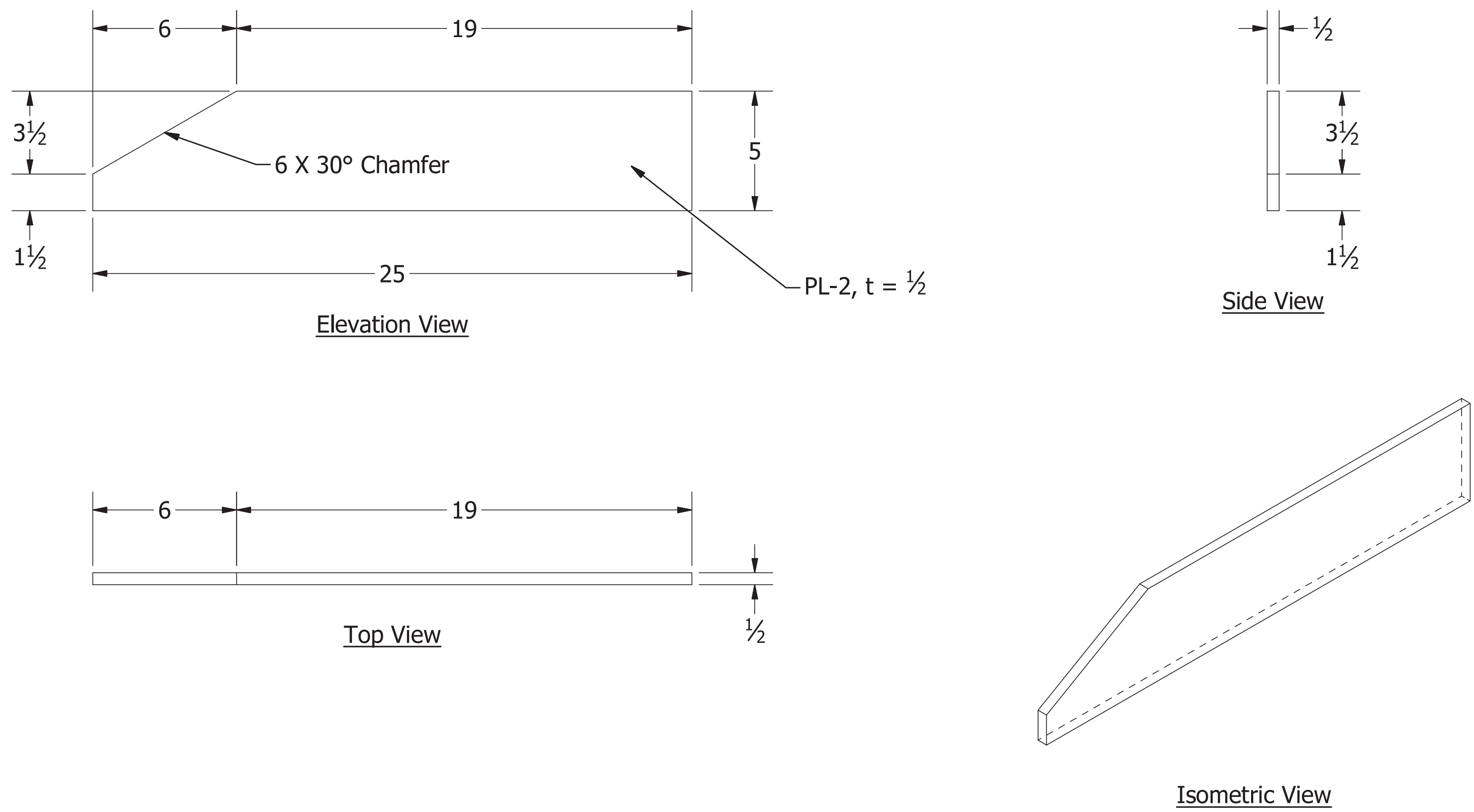

PL-2			
Bottom HSS arm	*11/12/2019*	*University of Florida*	*SHEET 13 OF 93*

Scale 0 6'' 12''

Revision:

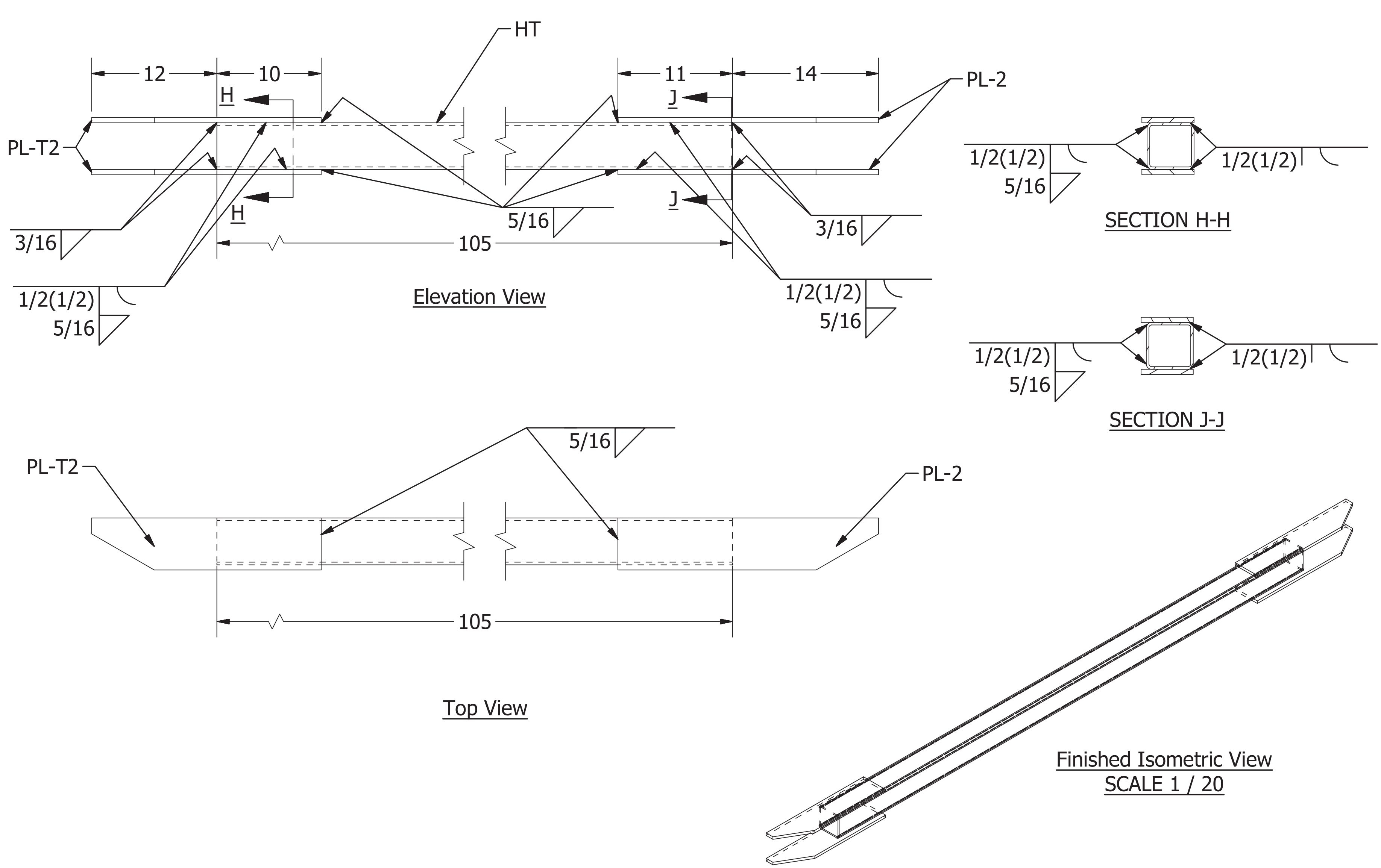

Step 1				*Scale* 0 1′ 2′
Top HSS arm	*11/12/2019*	*University of Florida*	*SHEET 14 OF 93*	*Revision:*

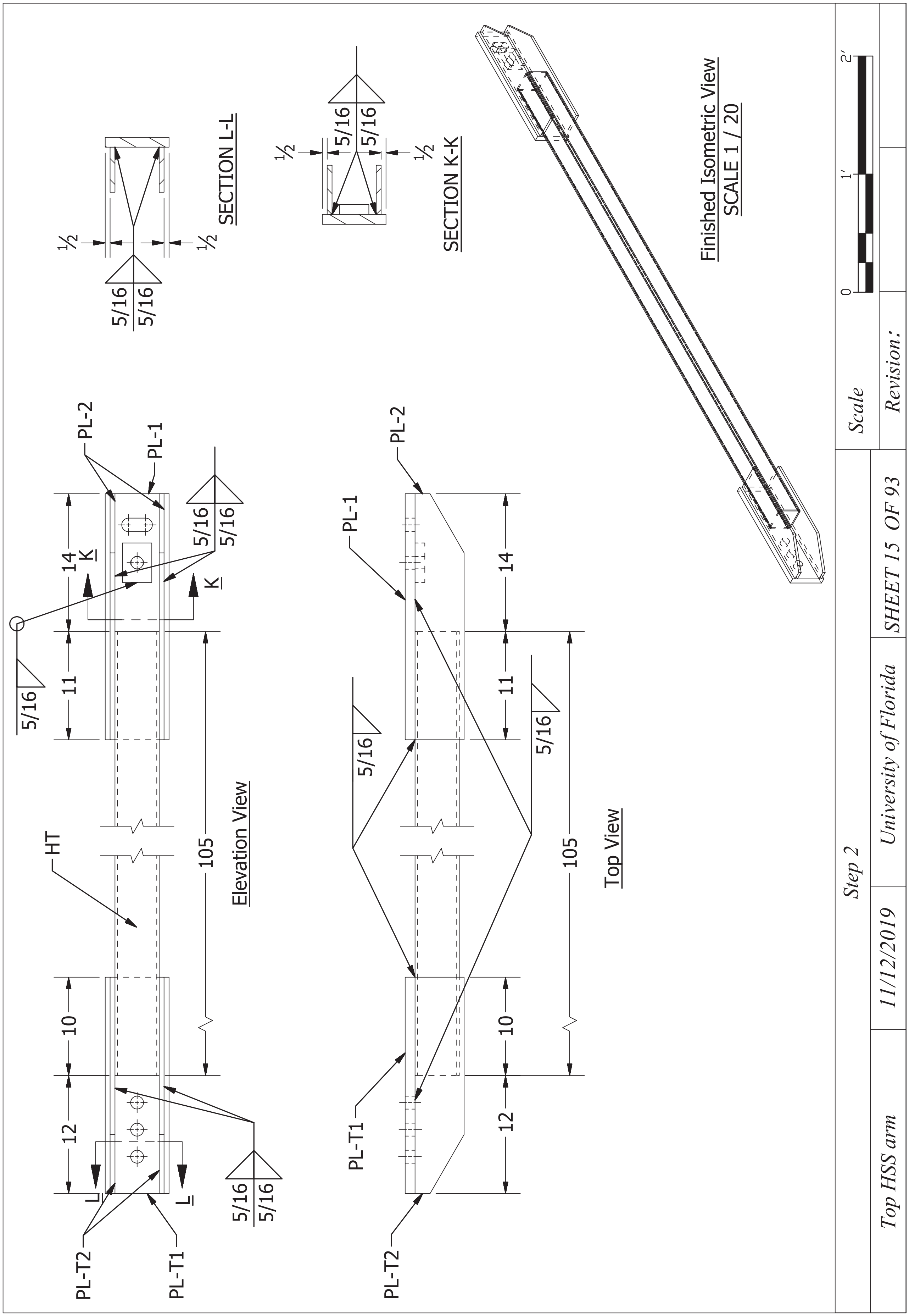

Elevation View
Top View
SECTION L-L
SECTION K-K
Finished Isometric View
SCALE 1 / 20
PL-1
PL-2
PL-T1
PL-T2
HT
5/16
½
14
11
105
10
12
K
L
0
1'
2'
Top HSS arm
11/12/2019
Step 2
University of Florida
SHEET 15 OF 93
Scale
Revision:

PARTS LIST - 3					
ITEM	PART NAME	CROSS SECTION	LENGTH	QTY	MATERIAL
1	HB	4.5 X 0.25	102 1/4	2	STEEL, Gr-46
2	PL-B1	6 1/2 x 1	28 1/4	2	STEEL, ASTM-A572 Gr-50
3	PL-B2	5 x 1/2	28 1/4	4	STEEL, ASTM-A572 Gr-50
4	PL-1	6 1/2 x 1	25	2	STEEL, ASTM-A572 Gr-50
5	PL-2	5 x 1/2	25	4	STEEL, ASTM-A572 Gr-50

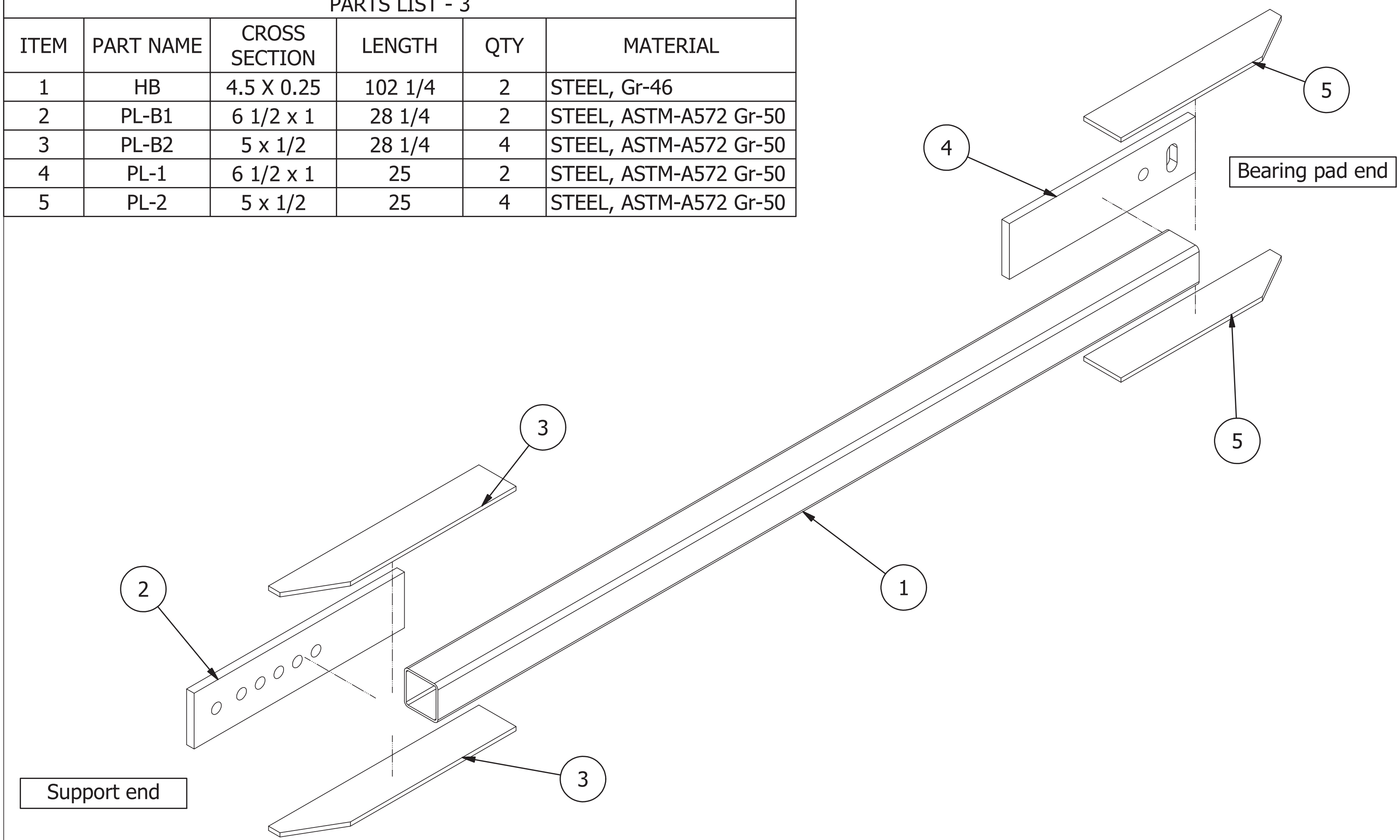

3D exploded view

Bottom HSS arm	*11/12/2019*	*University of Florida*	*SHEET 16 OF 93*	*Scale* / *Revision:*

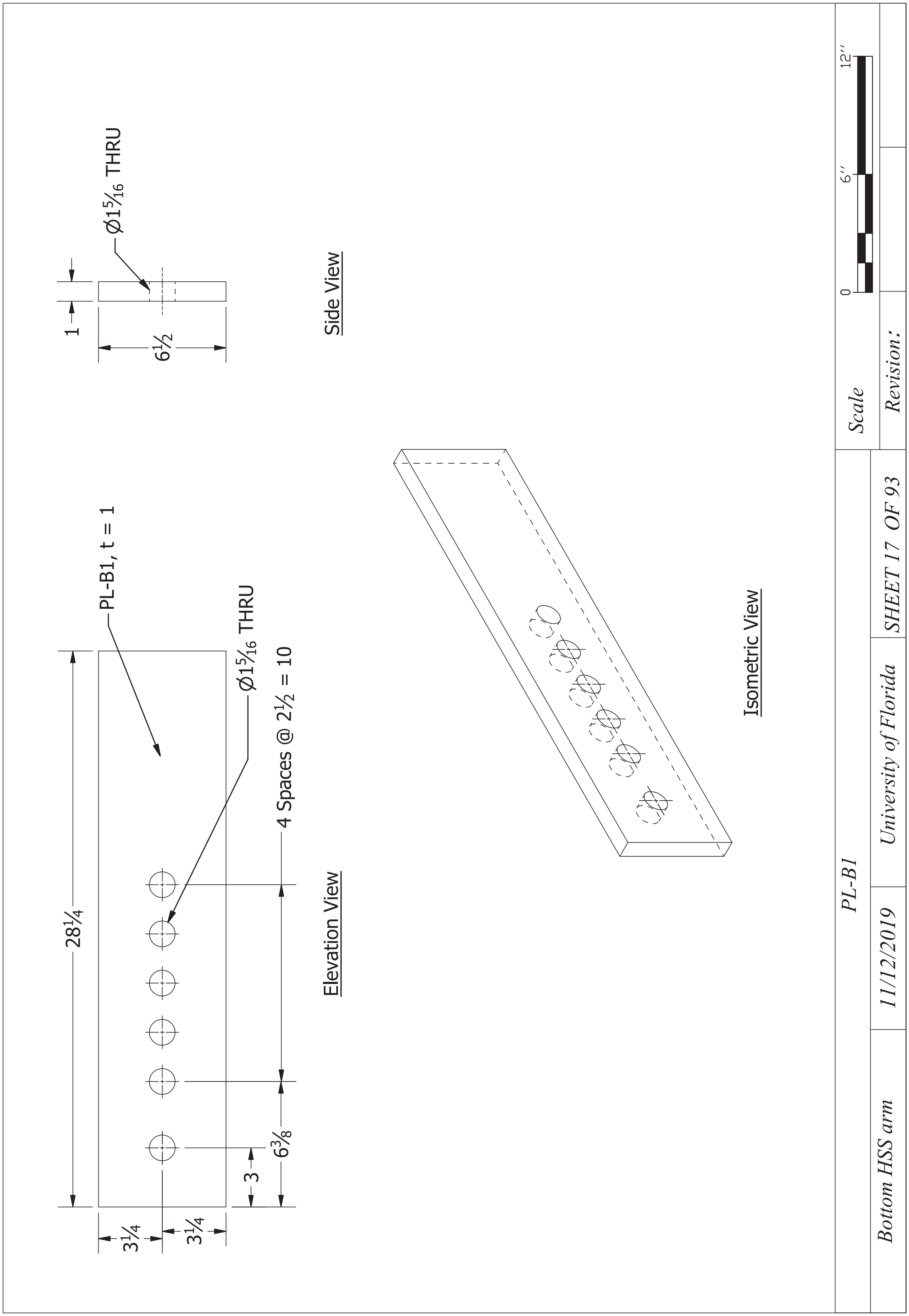
PL-B1, t = 1
Ø1⁵⁄₁₆ THRU
4 Spaces @ 2½ = 10
28¼
6⅜
3
3¼
3¼
Elevation View
Ø1⁵⁄₁₆ THRU
1
6½
Side View
Isometric View
Bottom HSS arm
11/12/2019
PL-B1
University of Florida
SHEET 17 OF 93
Scale
Revision:
0
6''
12''

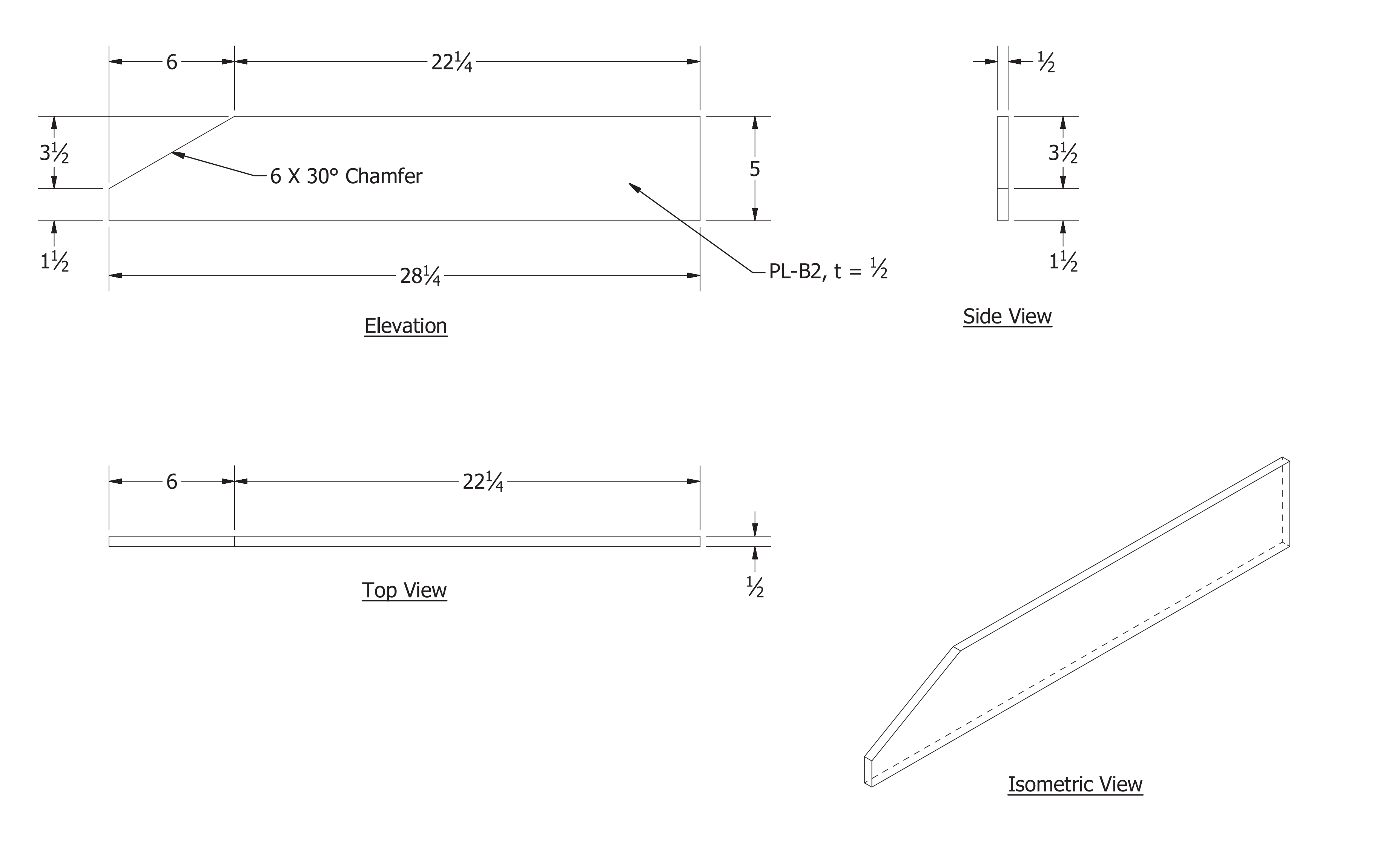

PL-B2				Scale	0 6'' 12''
Bottom HSS arm	11/12/2019	University of Florida	SHEET 18 OF 93	Revision:	

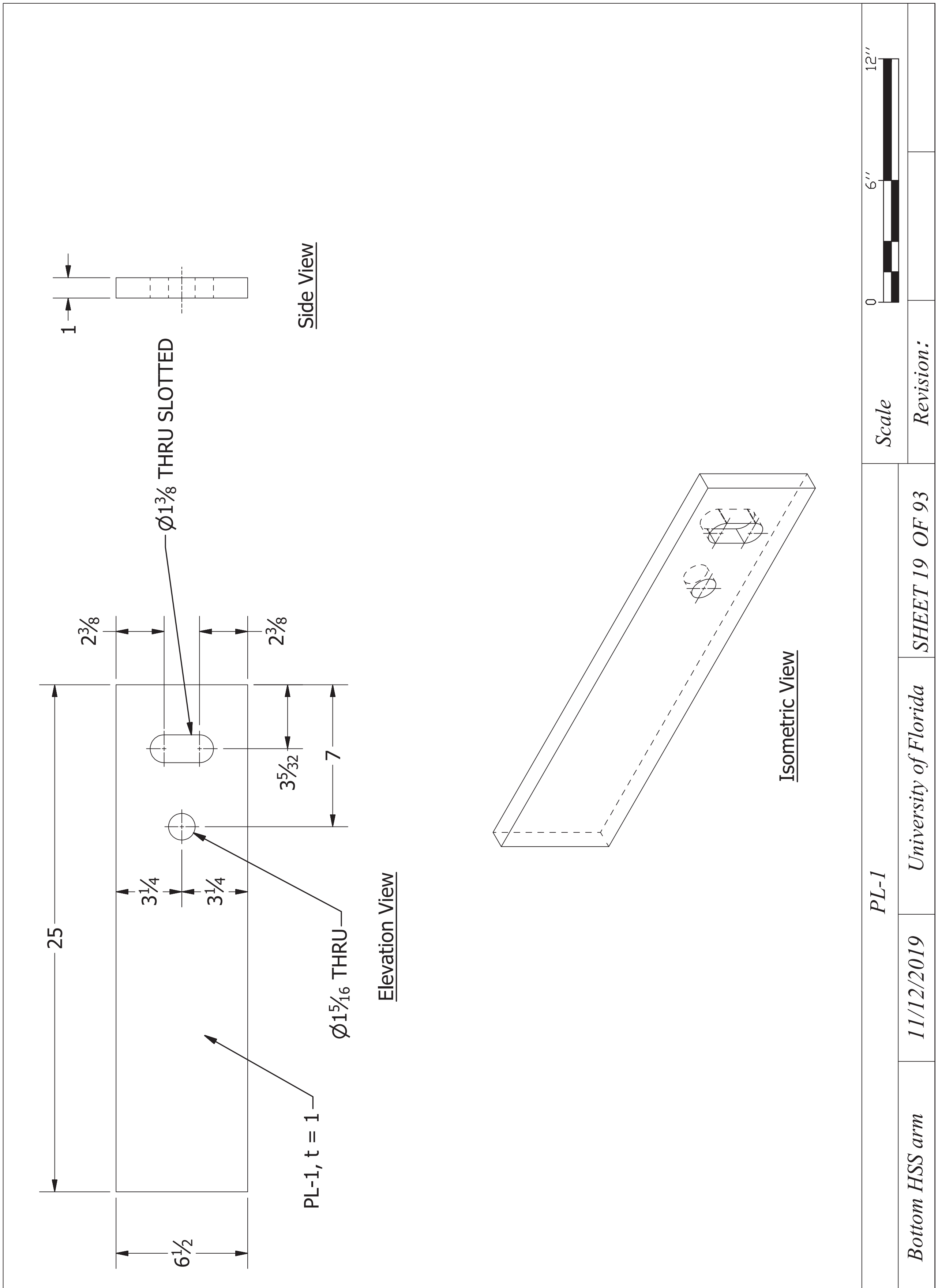
Ø1⅜ THRU SLOTTED
2⅜
2⅜
1
Side View
25
3 5/32
7
3¼
3¼
Ø1 5/16 THRU
Elevation View
PL-1, t = 1
6½
Isometric View
Bottom HSS arm
11/12/2019
PL-1
University of Florida
SHEET 19 OF 93
Scale
Revision:
0
6''
12''

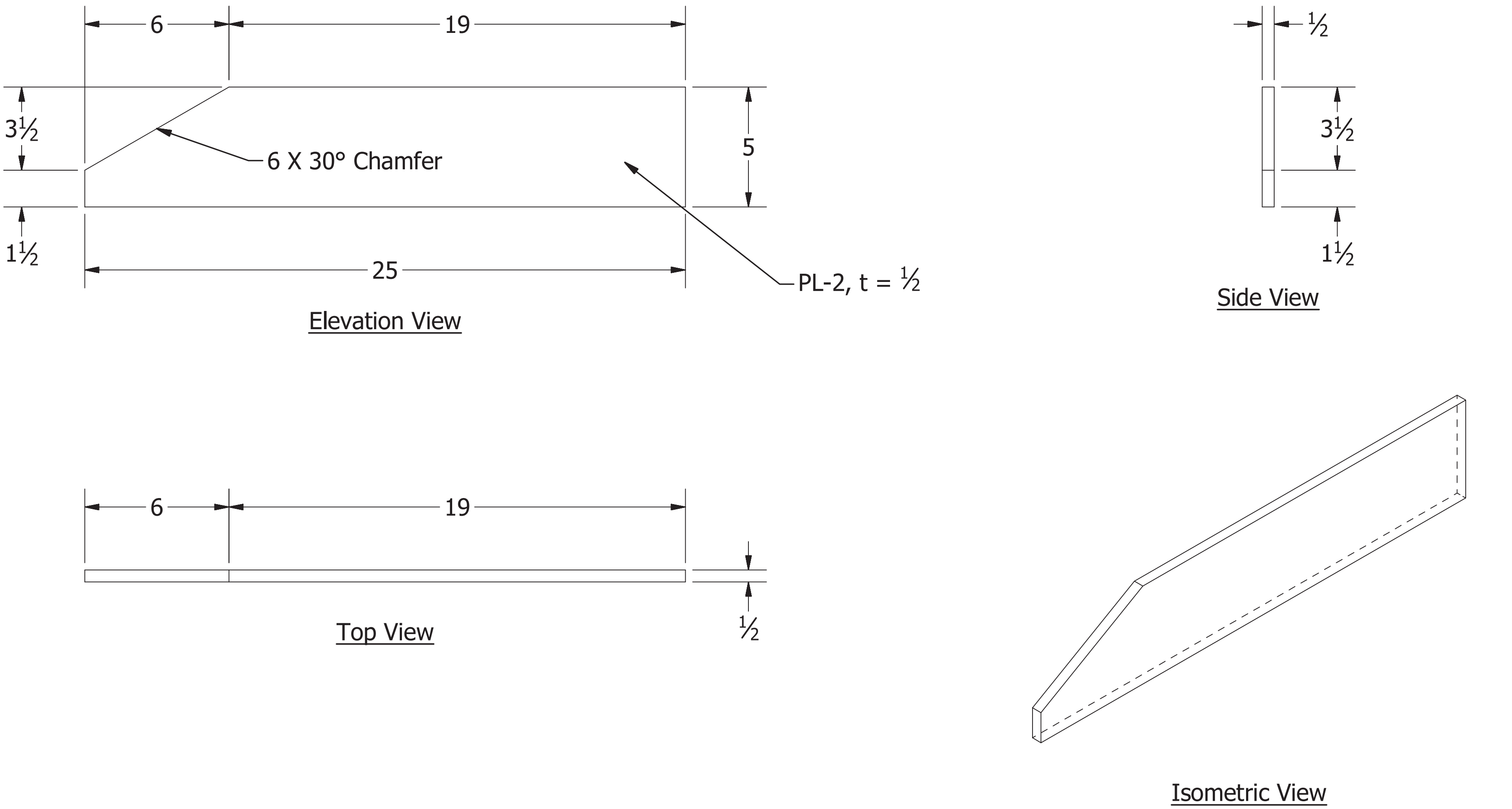

PL-2				Scale 0 6'' 12''
Bottom HSS arm	11/12/2019	University of Florida	SHEET 20 OF 93	Revision:

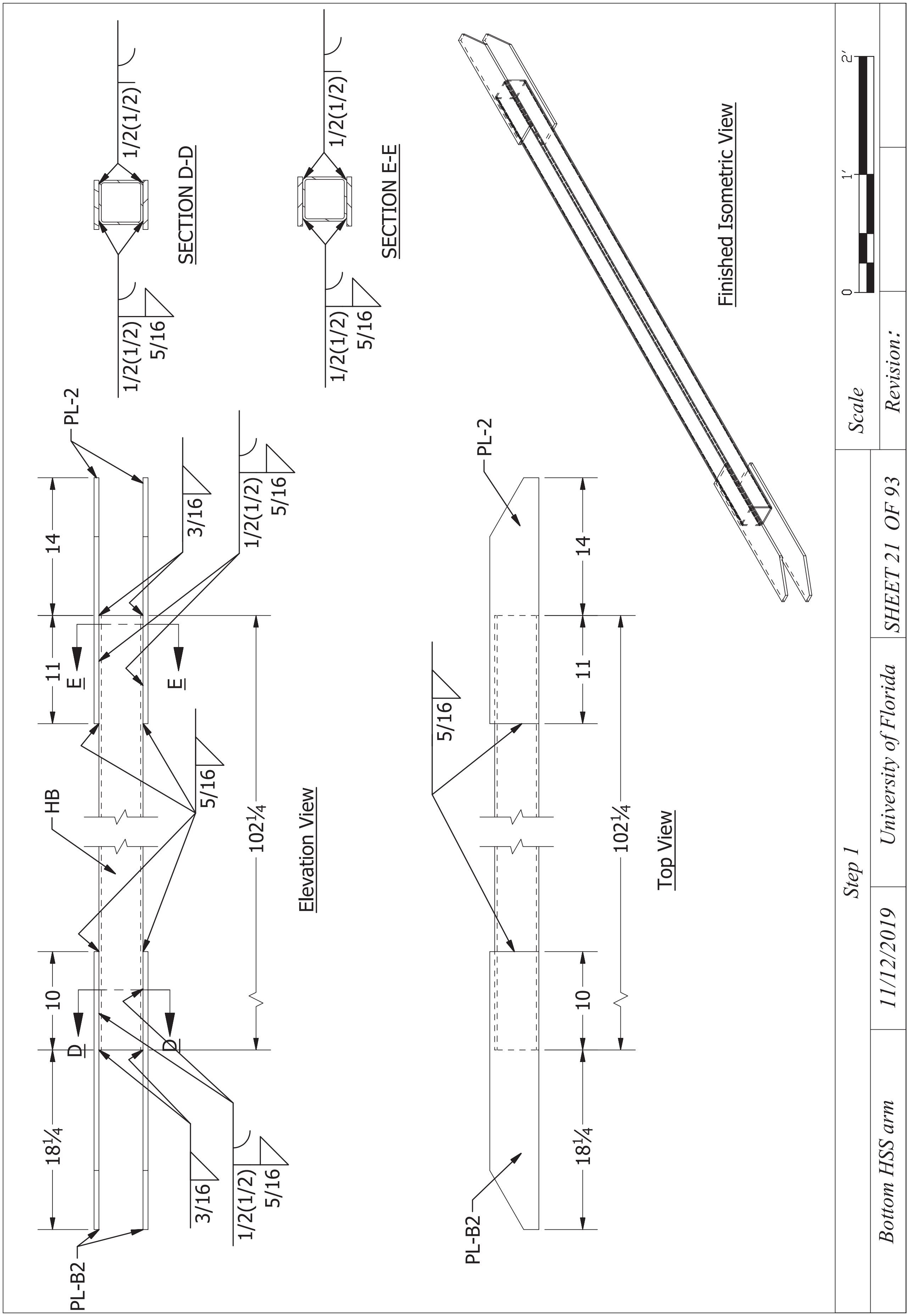

PL-B2
PL-2
HB
D
E
18¼
10
11
14
102¼
3/16
5/16
1/2(1/2)
Elevation View
Top View
SECTION D-D
SECTION E-E
Finished Isometric View
Bottom HSS arm
11/12/2019
Step 1
University of Florida
SHEET 21 OF 93
Scale
Revision:
0
1'
2'

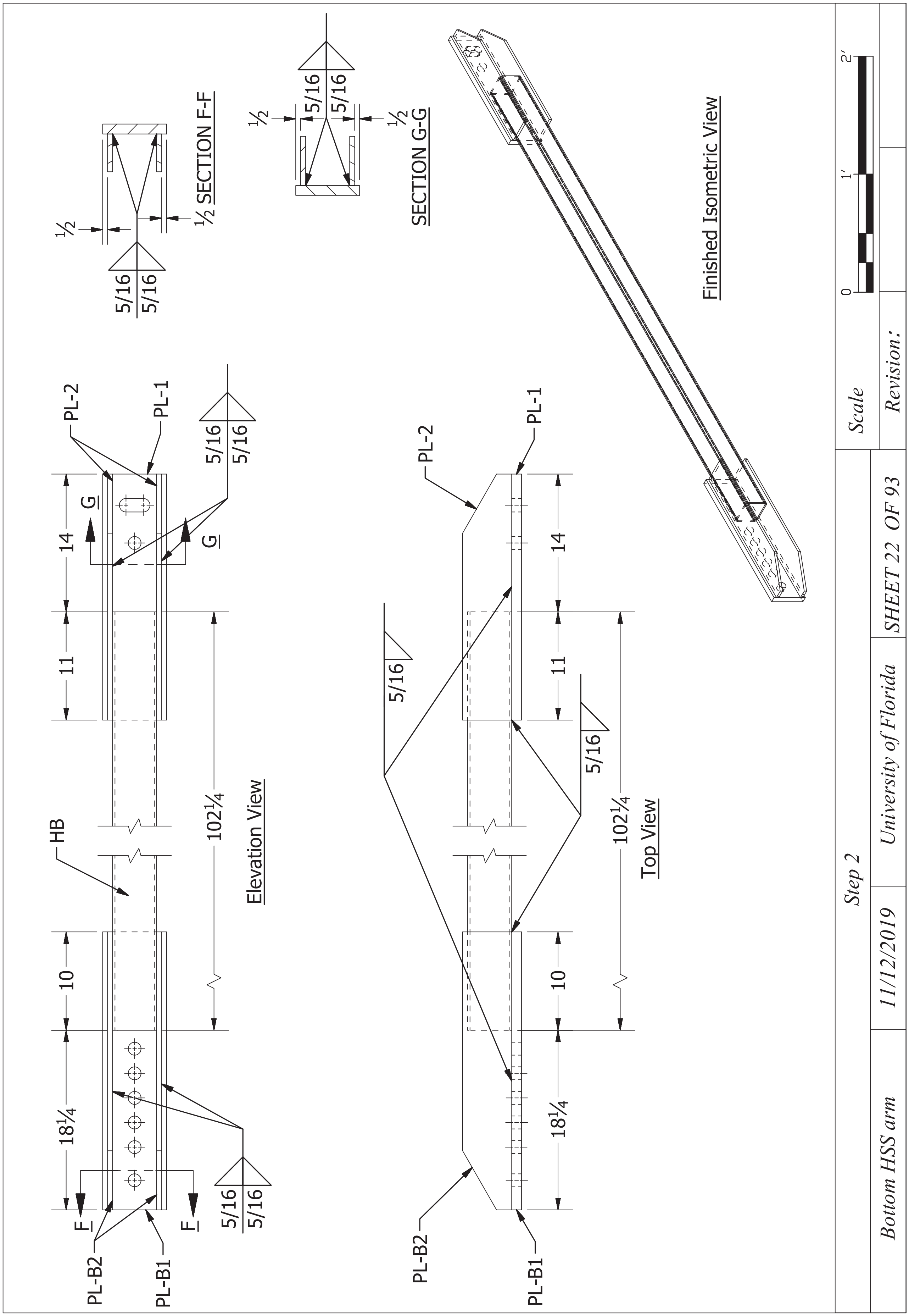

Elevation View
Top View
SECTION F-F
SECTION G-G
Finished Isometric View
PL-1
PL-2
PL-B1
PL-B2
HB
14
11
10
18¼
102¼
5/16
½
F
G
0
1′
2′
Bottom HSS arm
11/12/2019
Step 2
University of Florida
SHEET 22 OF 93
Scale
Revision:

PARTS LIST - 4

ITEM	PART NAME	CROSS-SECTION	LENGTH	QTY	MATERIAL
1	PL-M	33 X 2	36	1	STEEL, ASTM-A572 Gr-50
2	PL-C	13 X 1	13	1	STEEL, ASTM-A572 Gr-50
3	PL-S2	5 X 1-1/4	4 1/4	4	STEEL, ASTM-A572 Gr-50

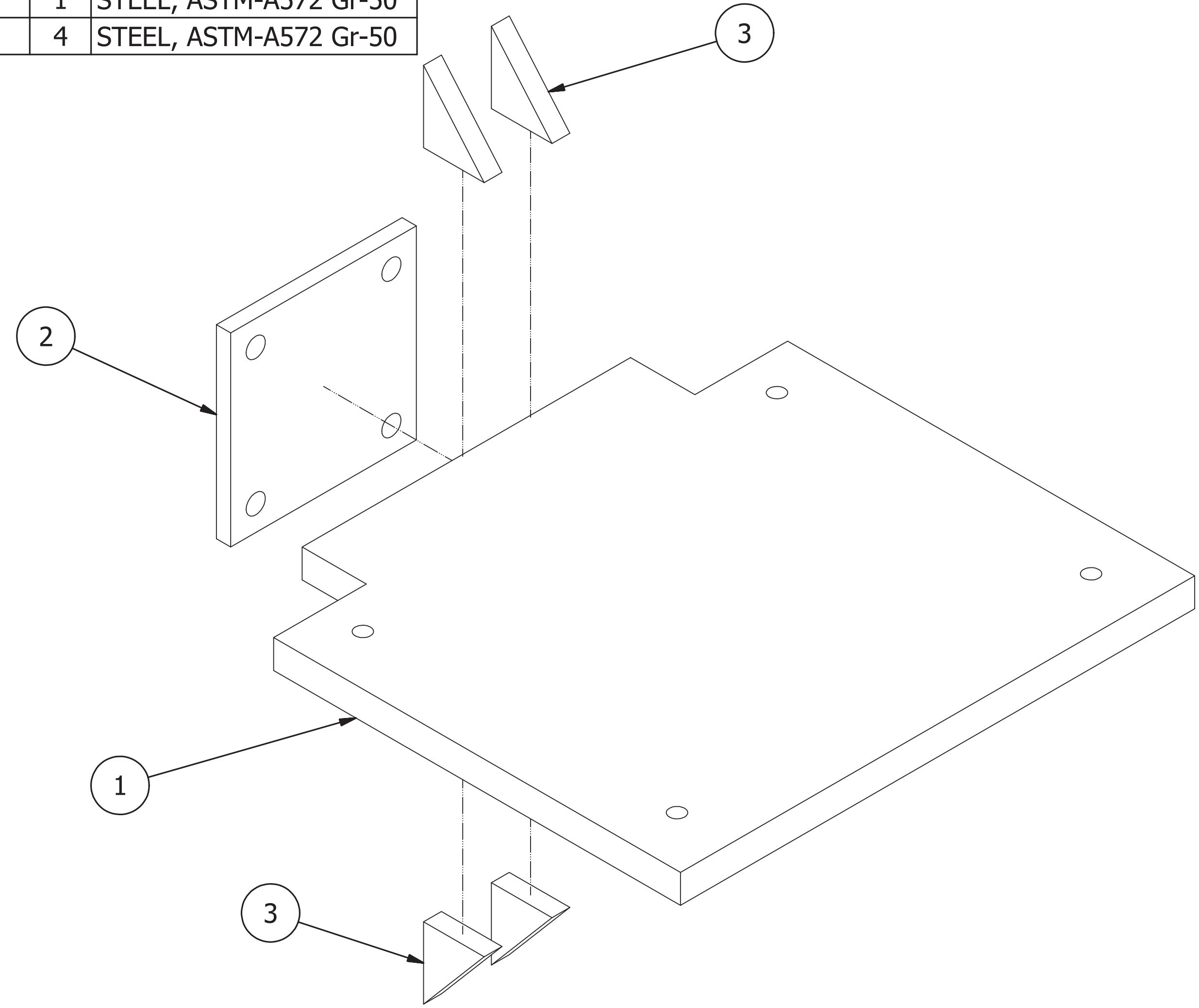

3D exploded view				Scale
Parent middle plate assembly	11/12/2019	University of Florida	SHEET 23 OF 93	Revision:

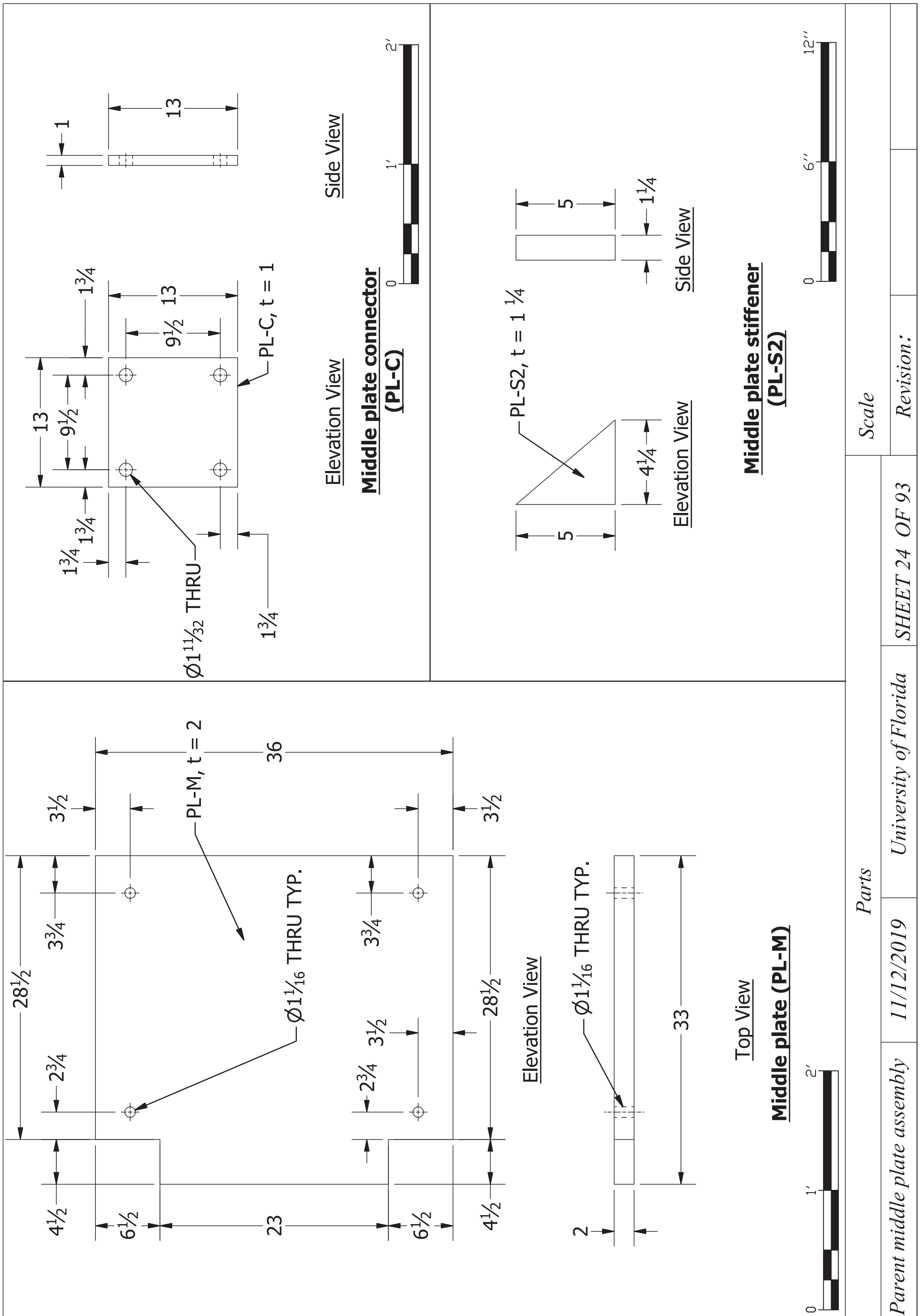
Side View
Elevation View
Middle plate connector (PL-C)
PL-C, t = 1
Ø1 11/32 THRU
Middle plate stiffener (PL-S2)
PL-S2, t = 1 1/4
Middle plate (PL-M)
PL-M, t = 2
Ø1 1/16 THRU TYP.
Top View
Parts
Scale
Revision:
Parent middle plate assembly
11/12/2019
University of Florida
SHEET 24 OF 93

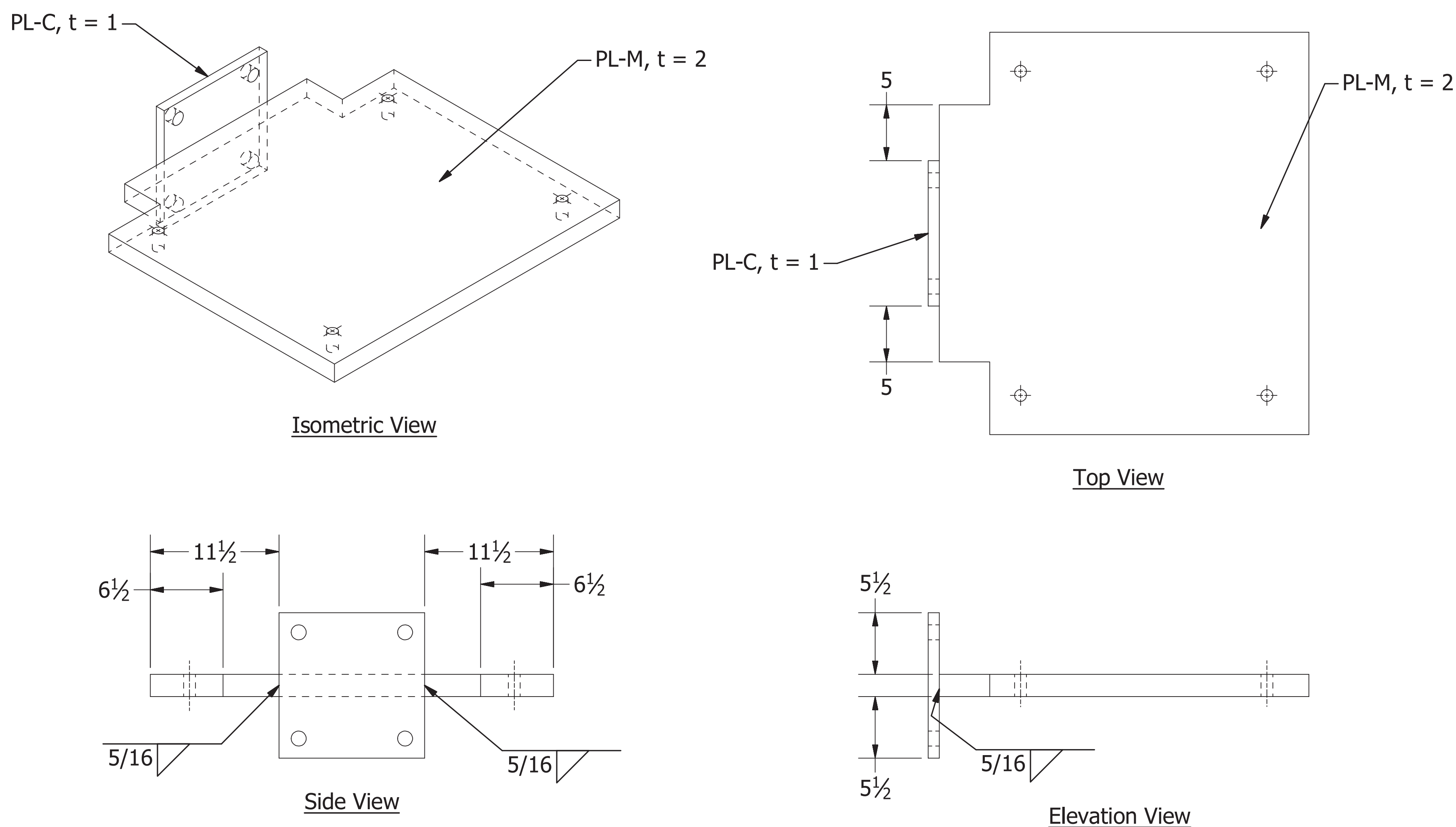

Step 1				Scale 0 1′ 2′
Parent middle plate assembly	11/12/2019	University of Florida	SHEET 25 OF 93	Revision:

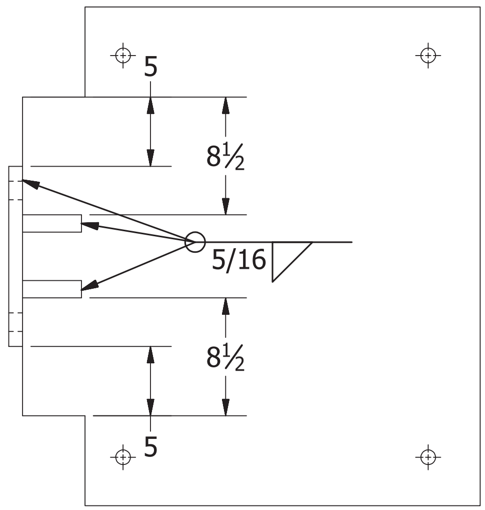

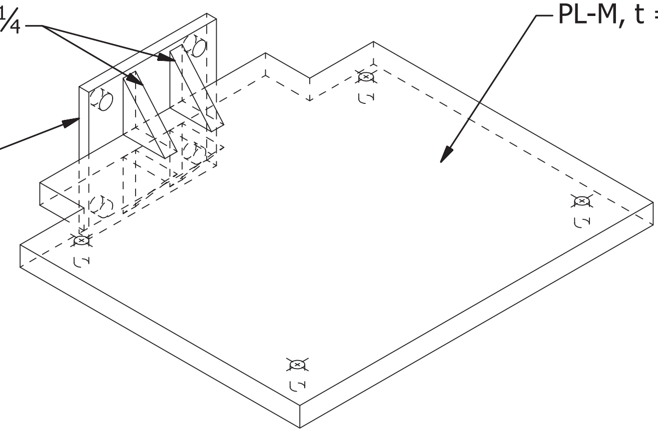

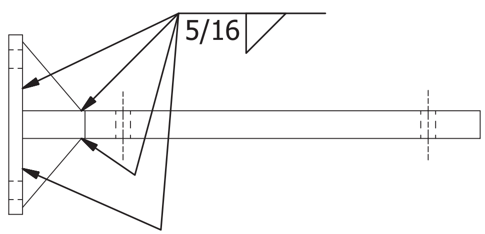

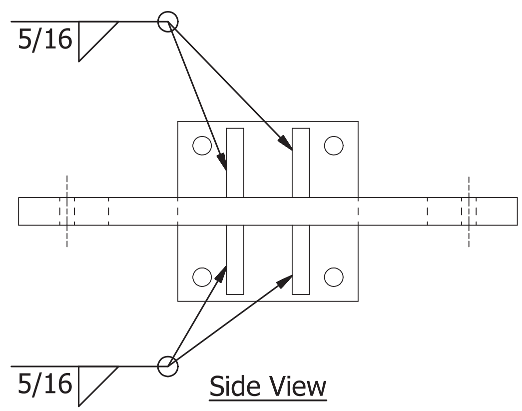

Step 2			
Parent middle plate assembly	*11/12/2019*	*University of Florida*	*SHEET 26 OF 93*

Scale 0 1′ 2′

Revision:

PARTS LIST - 5					
ITEM	PART NAME	CROSS-SECTION	LENGTH	QTY	MATERIAL
1	PL-C1	36 x 1/2	28-1/2	2	STEEL, ASTM-A572 Gr-50
2	PL-C2	3 x 1	3	8	STEEL, ASTM-A572 Gr-50
3	PL-C3	1 x 1	36	4	STEEL, ASTM-A572 Gr-50

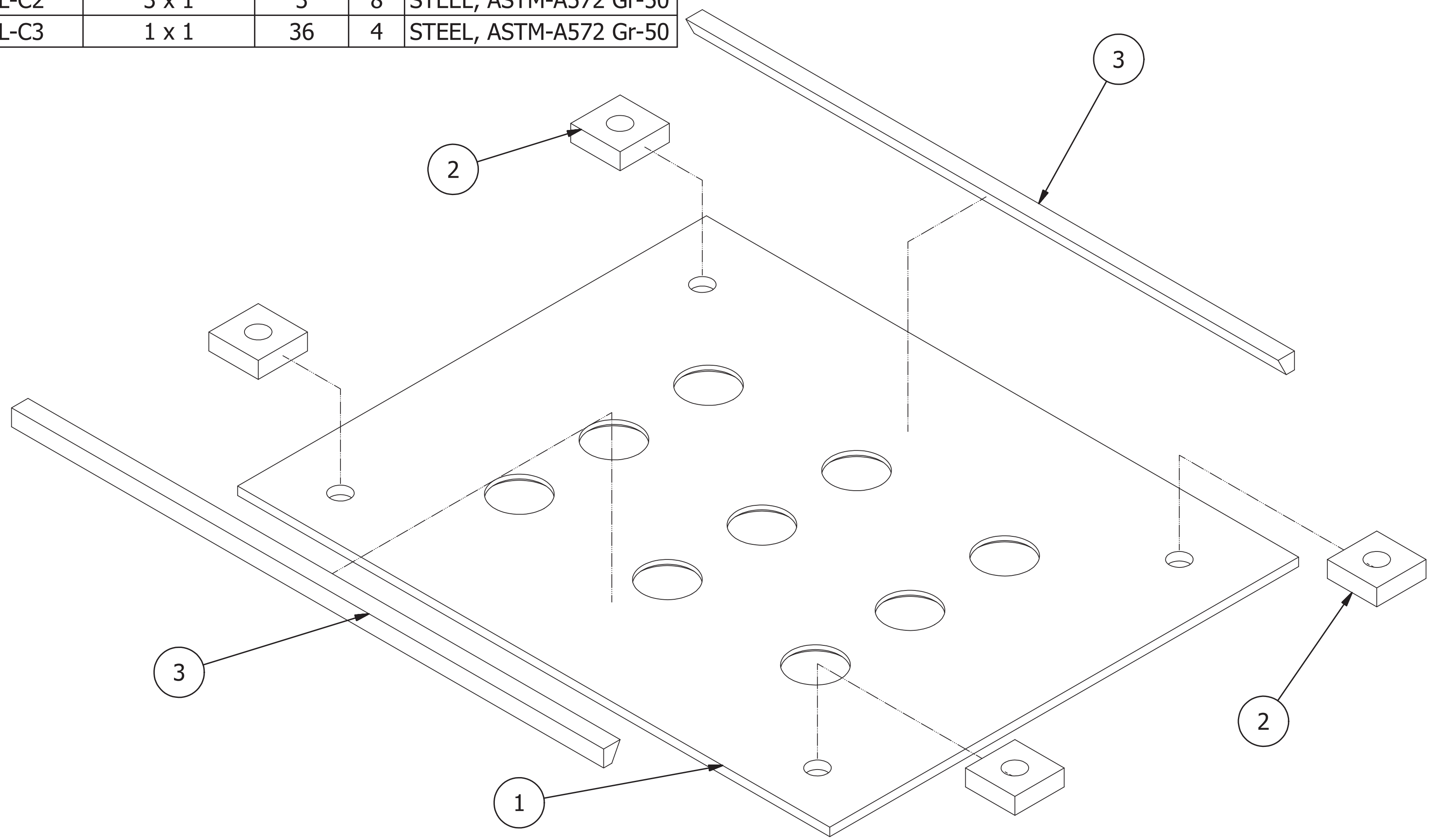

3D exploded view				Scale		
Concrete plate assembly	*11/12/2019*	*University of Florida*	*SHEET 27 OF 93*	*Revision:*		

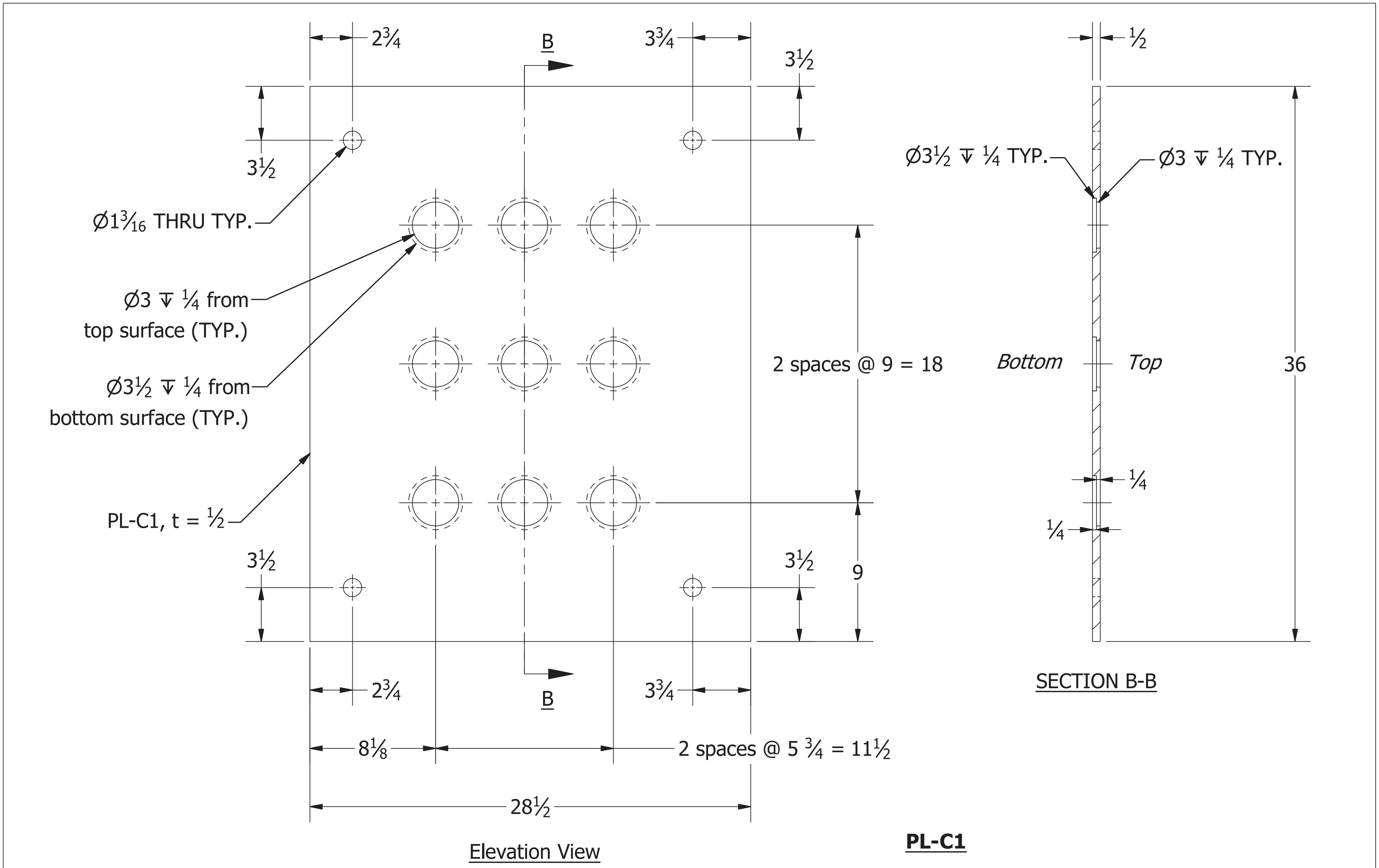

PL-C1				Scale 0 8′ 16′
Concrete plate assembly	11/12/2019	University of Florida	SHEET 28 OF 93	Revision:

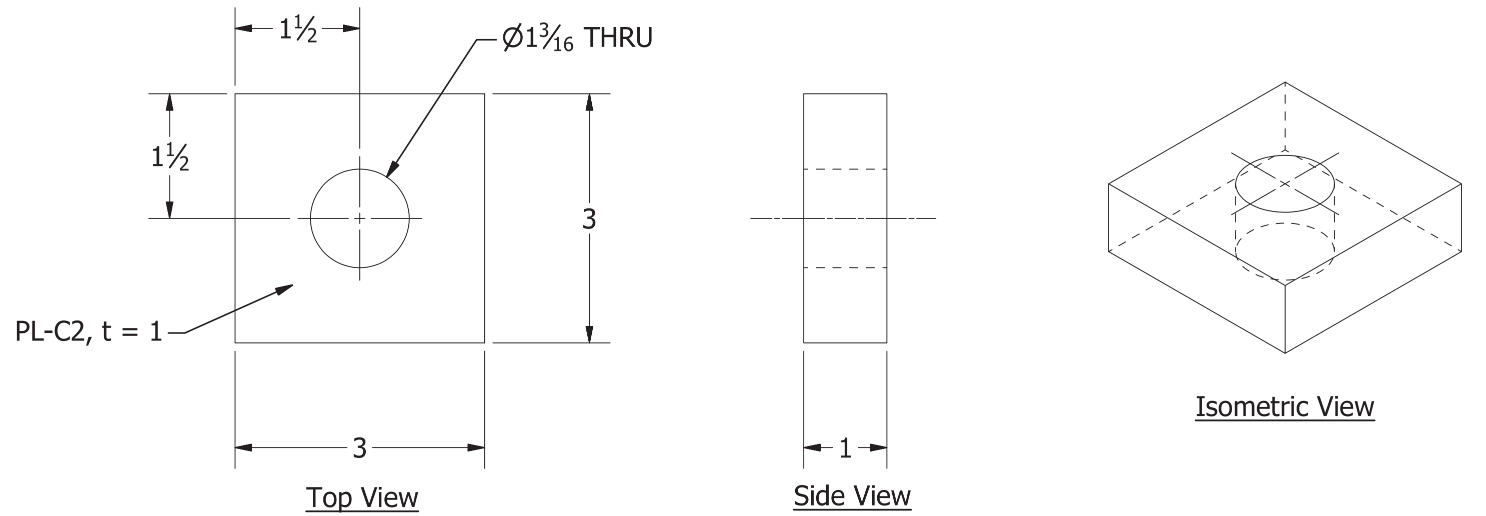

PL-C2

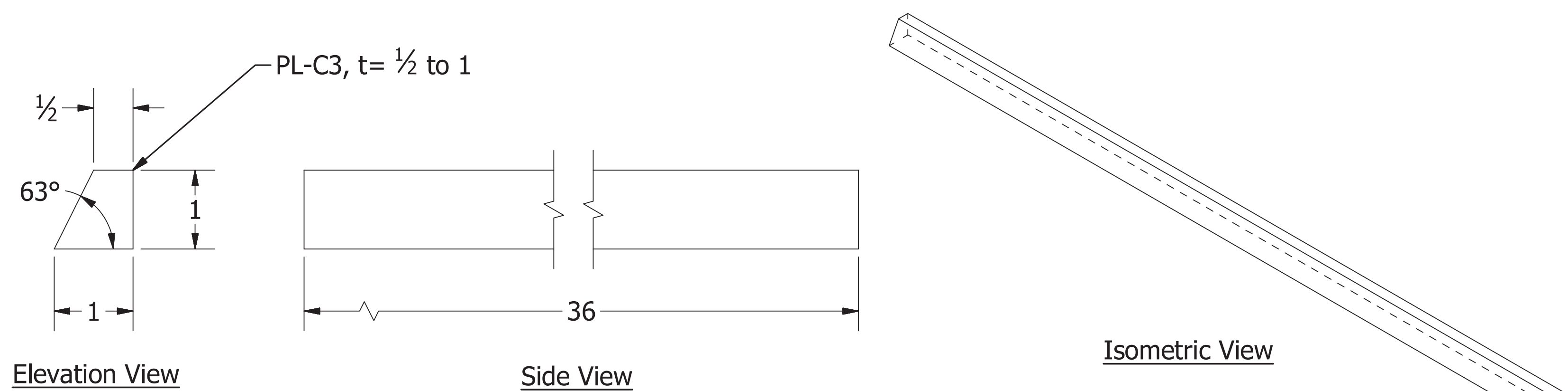

PL-C3

PL-C2 and PL-C3				*Scale* 0 2″ 4″
Concrete plate assembly	*11/12/2019*	*University of Florida*	*SHEET 29 OF 93*	*Revision:*

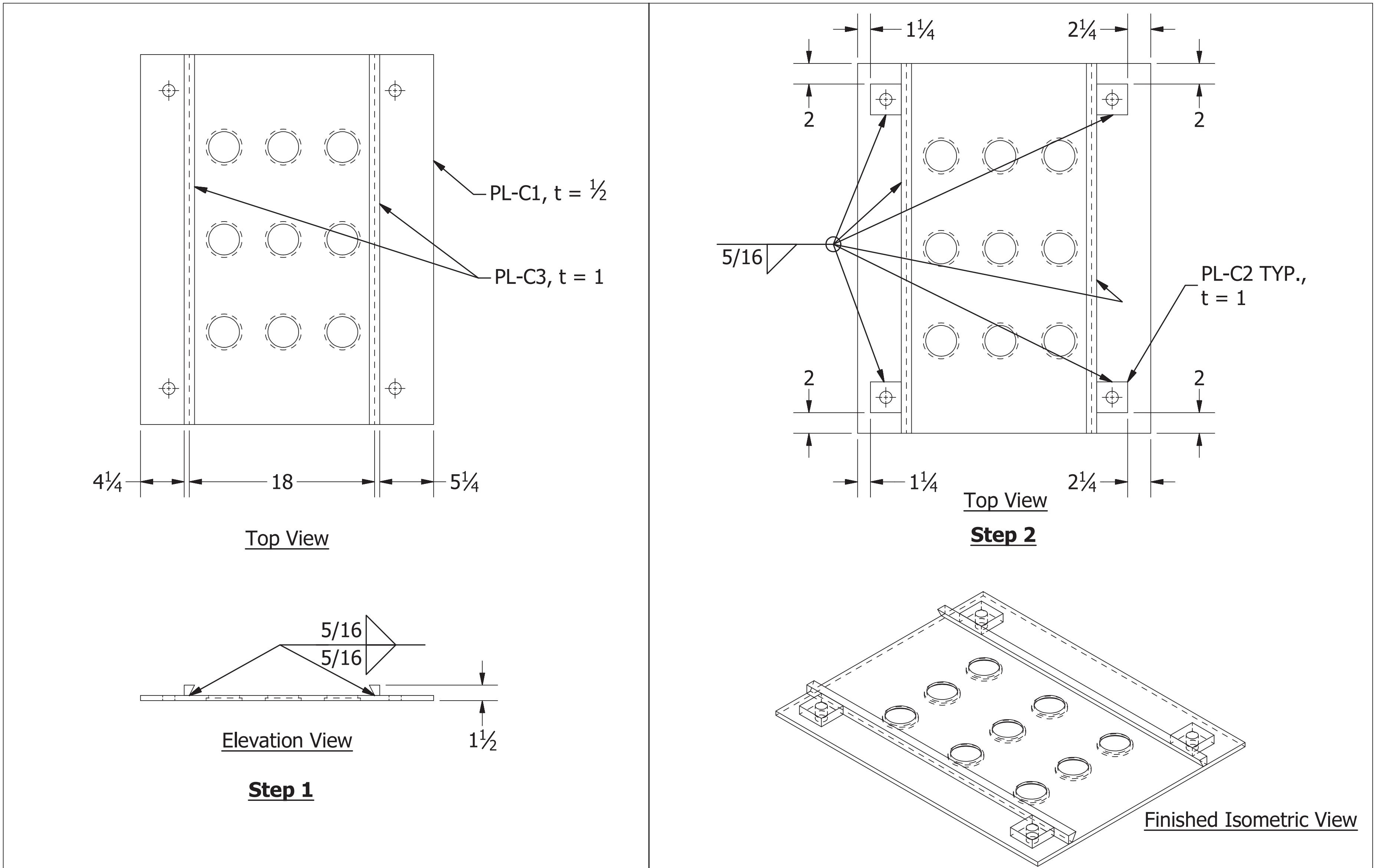

Steps				Scale	0 1′ 2′
Concrete plate assembly	11/12/2019	University of Florida	SHEET 30 OF 93	Revision:	

PARTS LIST - 6					
ITEM	PART NAME	CROSS-SECTION	LENGTH	QTY	MATERIAL
1	FW-1	4x2	32-1/2	4	WOOD
2	FW-2	4x2	36	4	WOOD
3	FW-3	32-1/2x1/2	39	2	WOOD

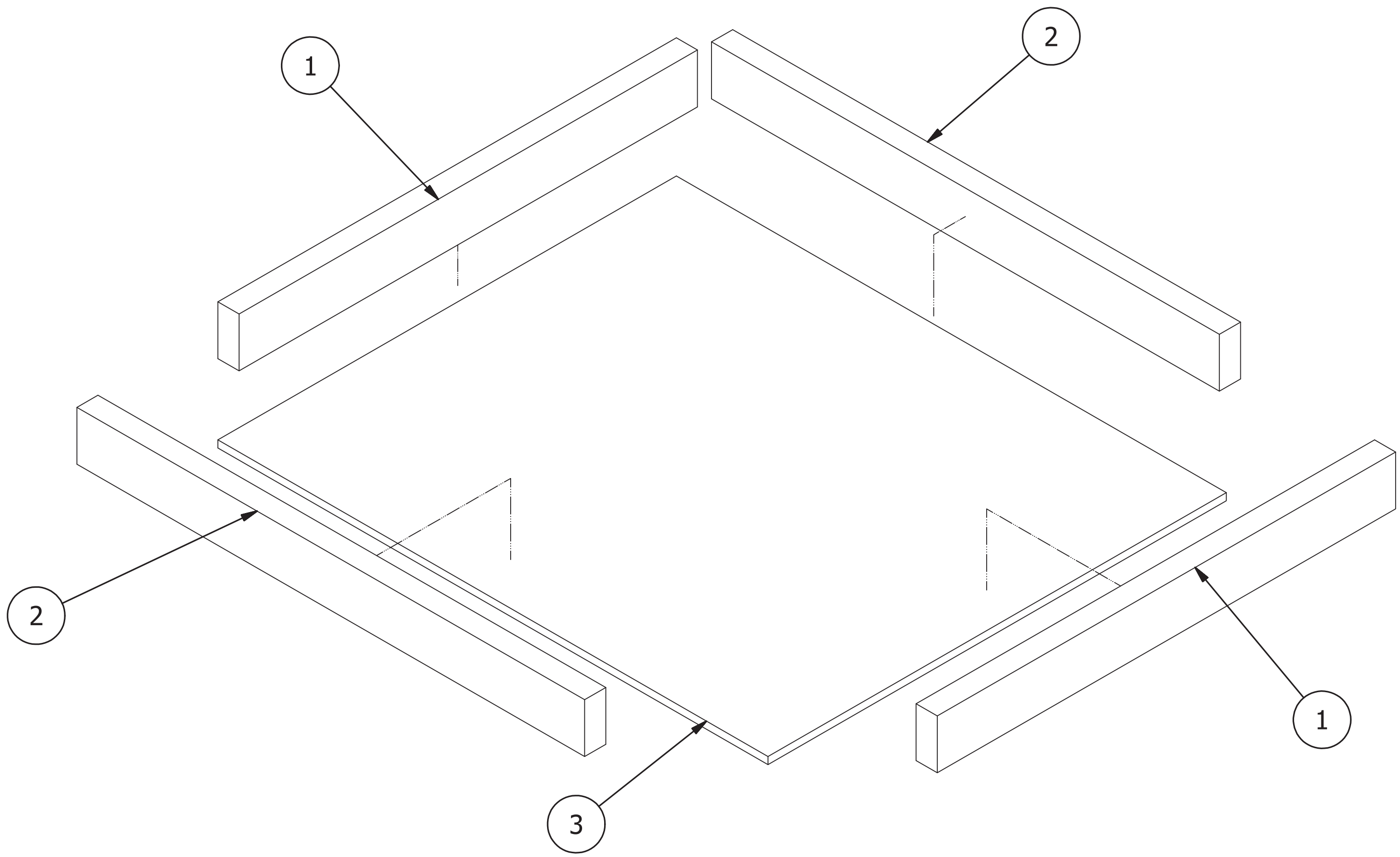

3D exploded view				Scale
Concrete plate formwork	11/12/2019	University of Florida	SHEET 31 OF 93	Revision:

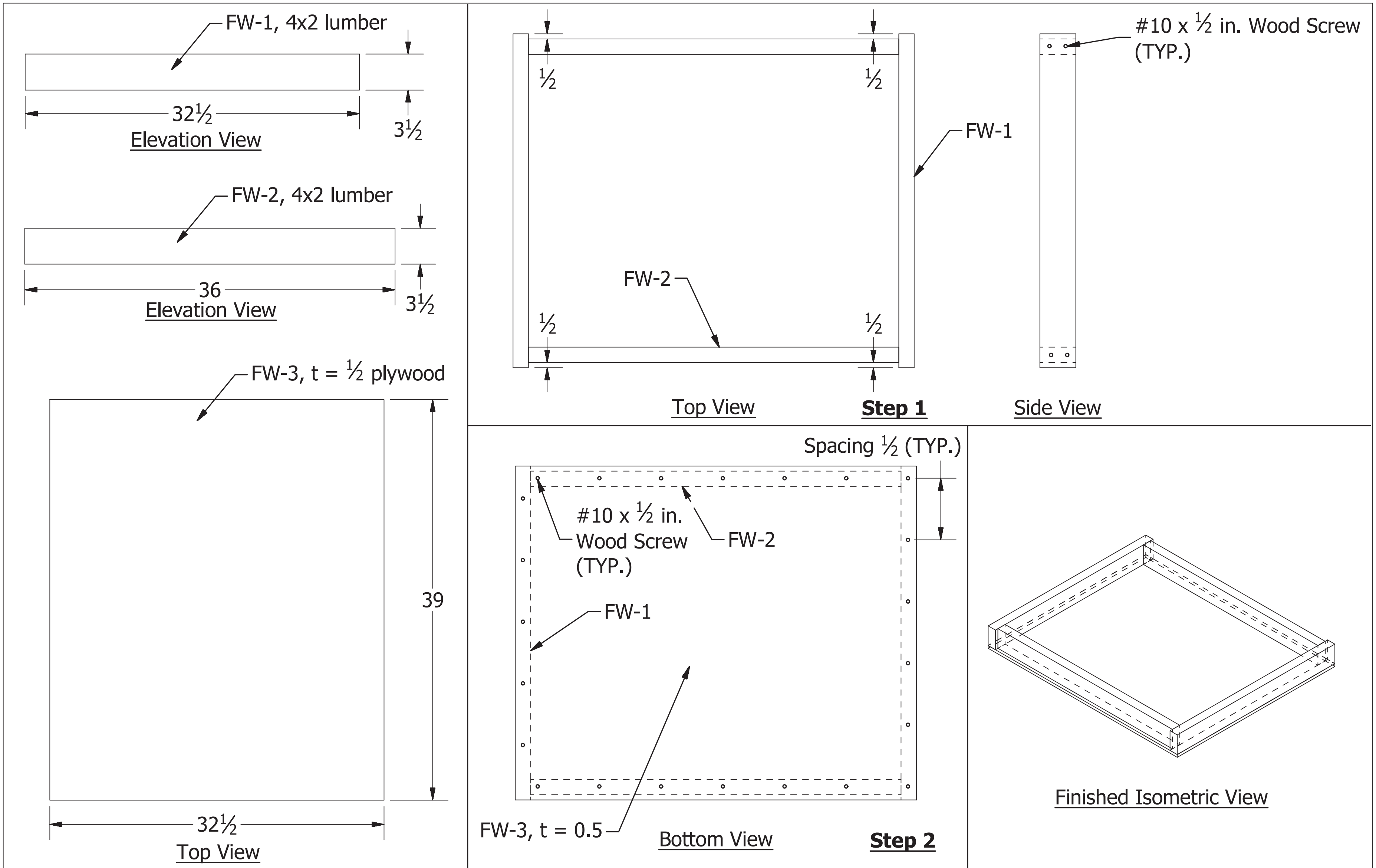

Parts and steps				*Scale*	0 1′ 2′
Concrete plate formwork	*11/12/2019*	*University of Florida*	*SHEET 32 OF 93*	*Revision:*	

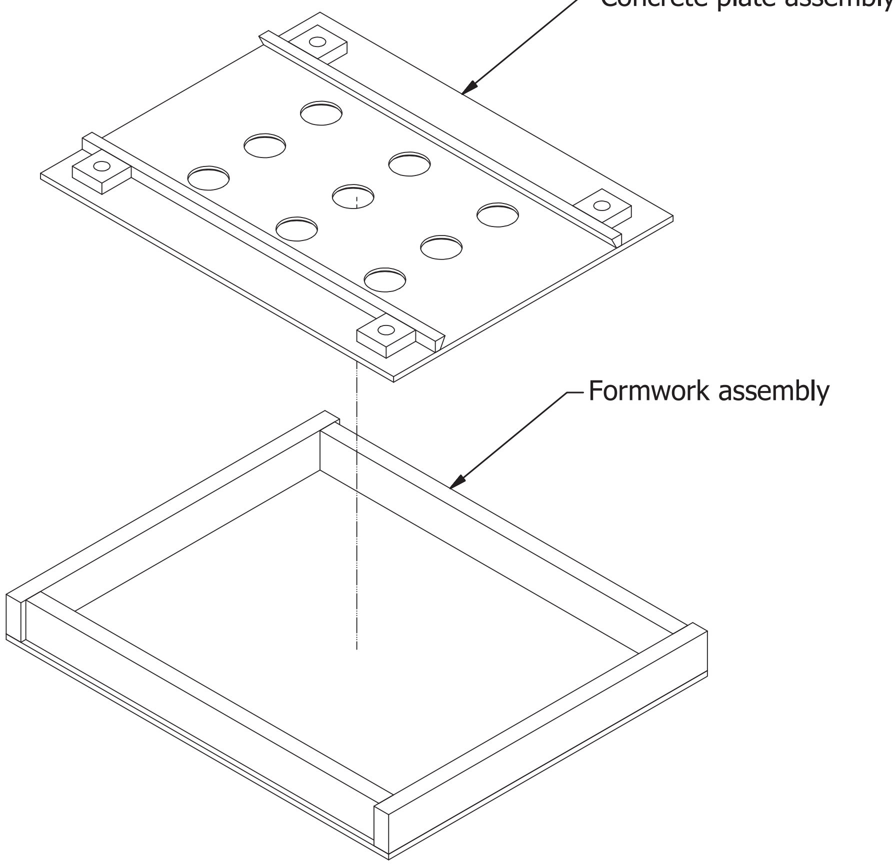

Step 1
Place the concrete plate assembly in the formwork assembly

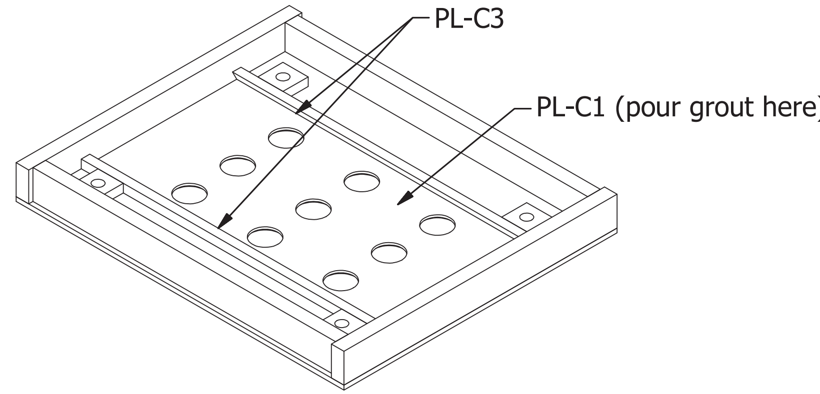

Step 2
Pour grout on plate PL-C1 in the between PL-C3 plates

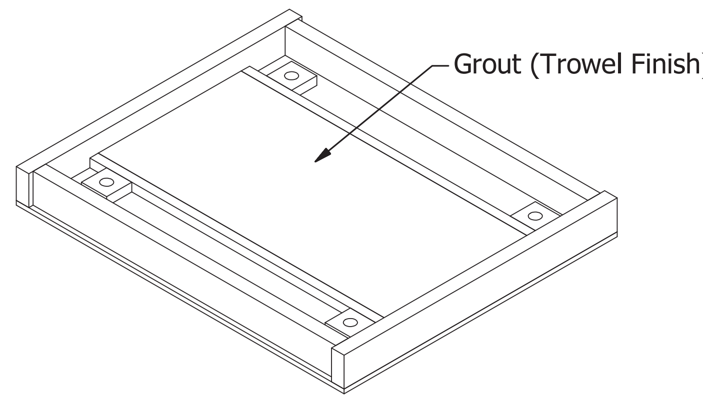

Step 3
Trowel finish the grout surface

Steps				*Scale*		
Concrete plate construction	*11/12/2019*	*University of Florida*	*SHEET 33 OF 93*	*Revision:*		

PARTS LIST - 7					
ITEM	PART NAME	CROSS-SECTION	LENGTH	QTY	MATERIAL
1	PL-F0	$28\frac{1}{2}$ X $\frac{3}{4}$	36	2	STEEL, ASTM-A572 Gr-50
2	PL-F1	$28\frac{1}{2}$ X BEV. FROM $1\frac{1}{8}$ TO $\frac{1}{2}$	36	2	STEEL, ASTM-A572 Gr-50
3	PL-F2	$28\frac{1}{2}$ X BEV. FROM $1\frac{1}{2}$ TO $\frac{1}{4}$	36	2	STEEL, ASTM-A572 Gr-50
4	PL-F3	$28\frac{1}{2}$ X $2\frac{1}{4}$	36	2	STEEL, ASTM-A572 Gr-50
5	PL-F4	$28\frac{1}{2}$ X $1\frac{1}{2}$	36	2	STEEL, ASTM-A572 Gr-50
6	PL-F6	33 X $1\frac{1}{4}$	36	2	STEEL, ASTM-A572 Gr-50
7	PL-B	14 X $2\frac{1}{2}$	38	1	STEEL, ASTM-A514 GRADE B Gr-100
8	PL-B-top	14 X 4	38	1	STEEL, ASTM-A514 GRADE B Gr-100

Schedule of plates				*Scale*
Bearing plates	*11/12/2019*	*University of Florida*	*SHEET 34 OF 93*	*Revision:*

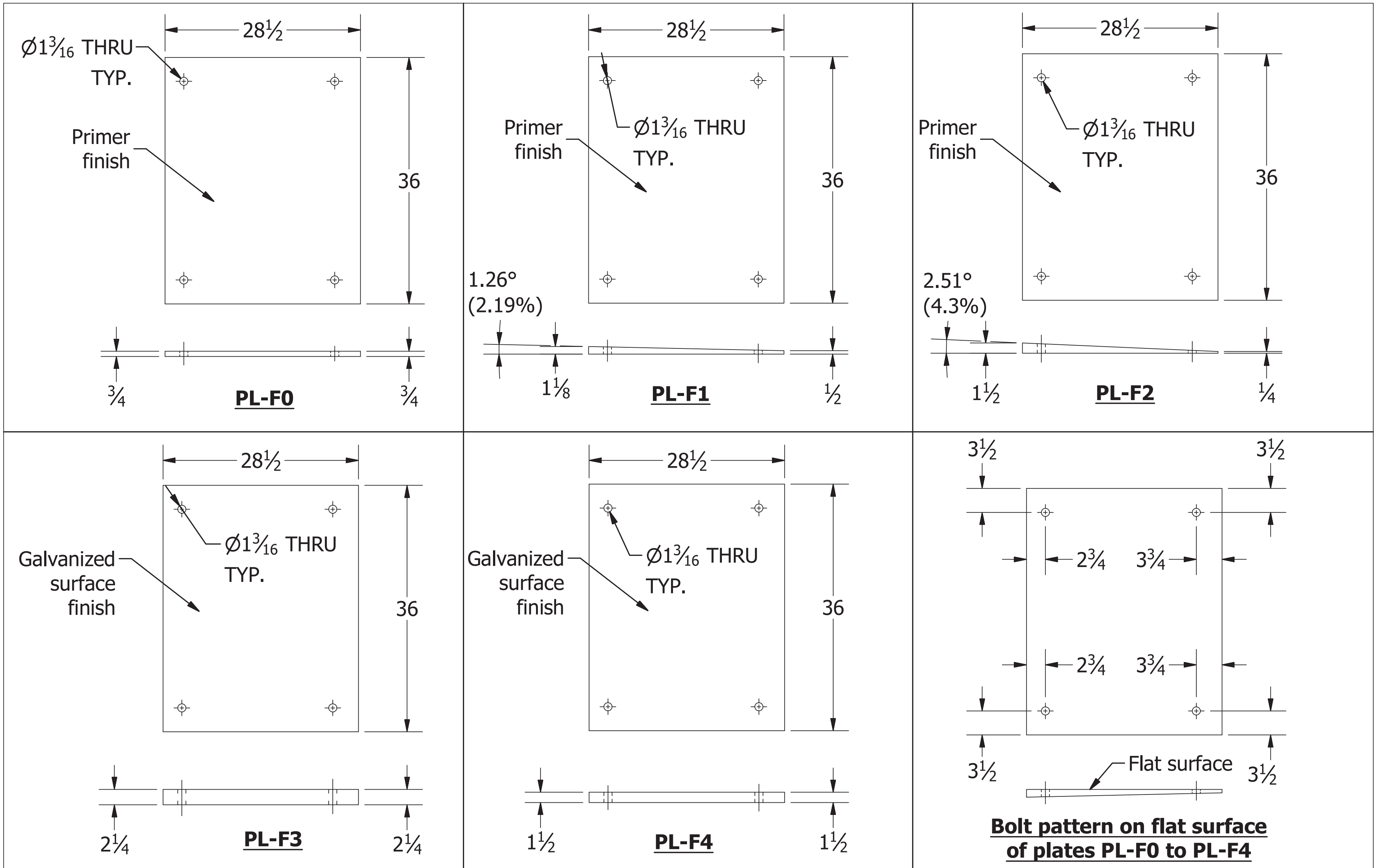

Plates - PL- F0 to PL - F5				Scale 0 18″ 36″
Bearing plates	11/12/2019	University of Florida	SHEET 35 OF 93	Revision:

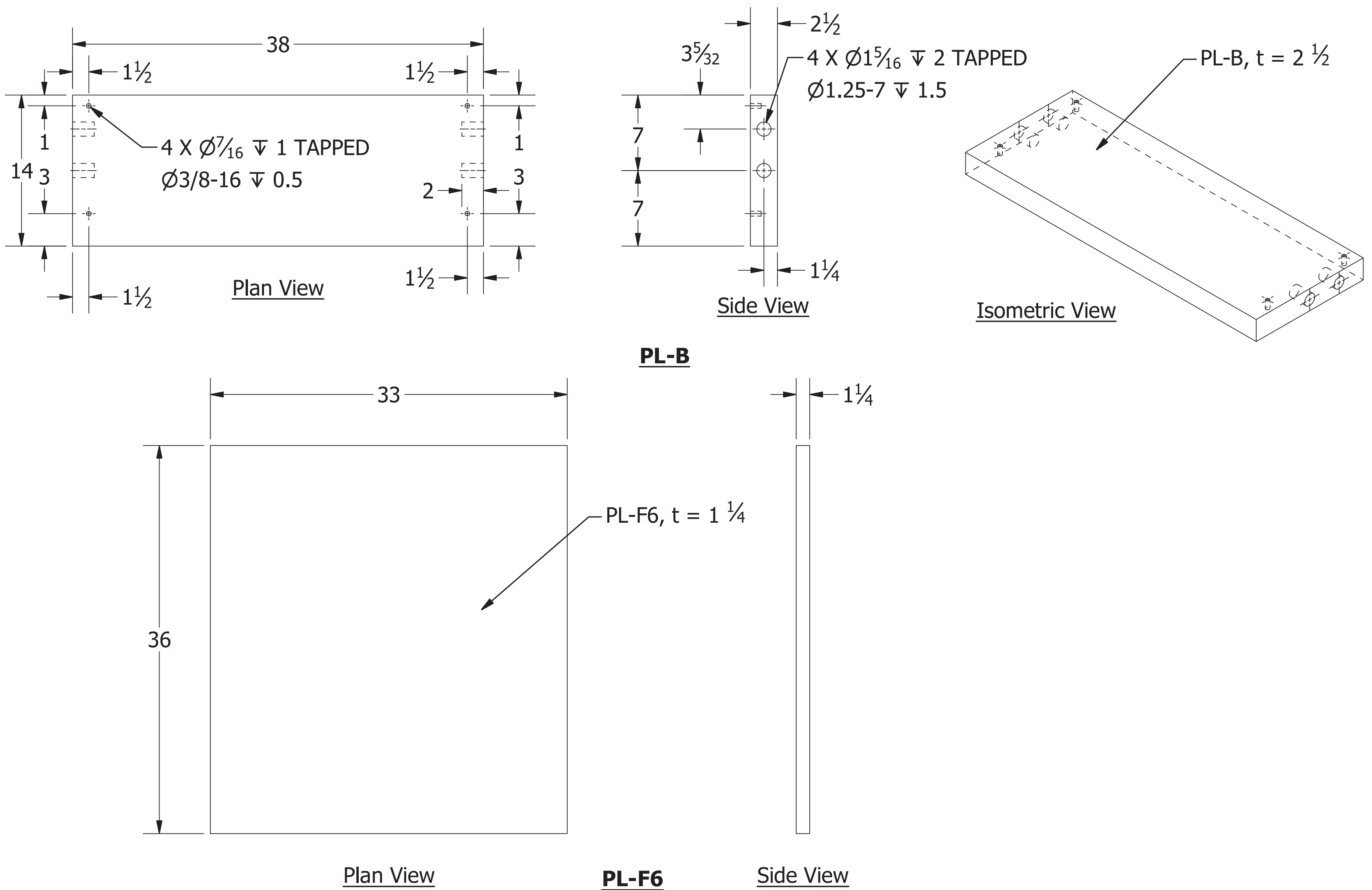

Plates - PL-B, PL-F6				Scale 0 1′ 2′
Bearing plates	11/12/2019	University of Florida	SHEET 36 OF 93	Revision:

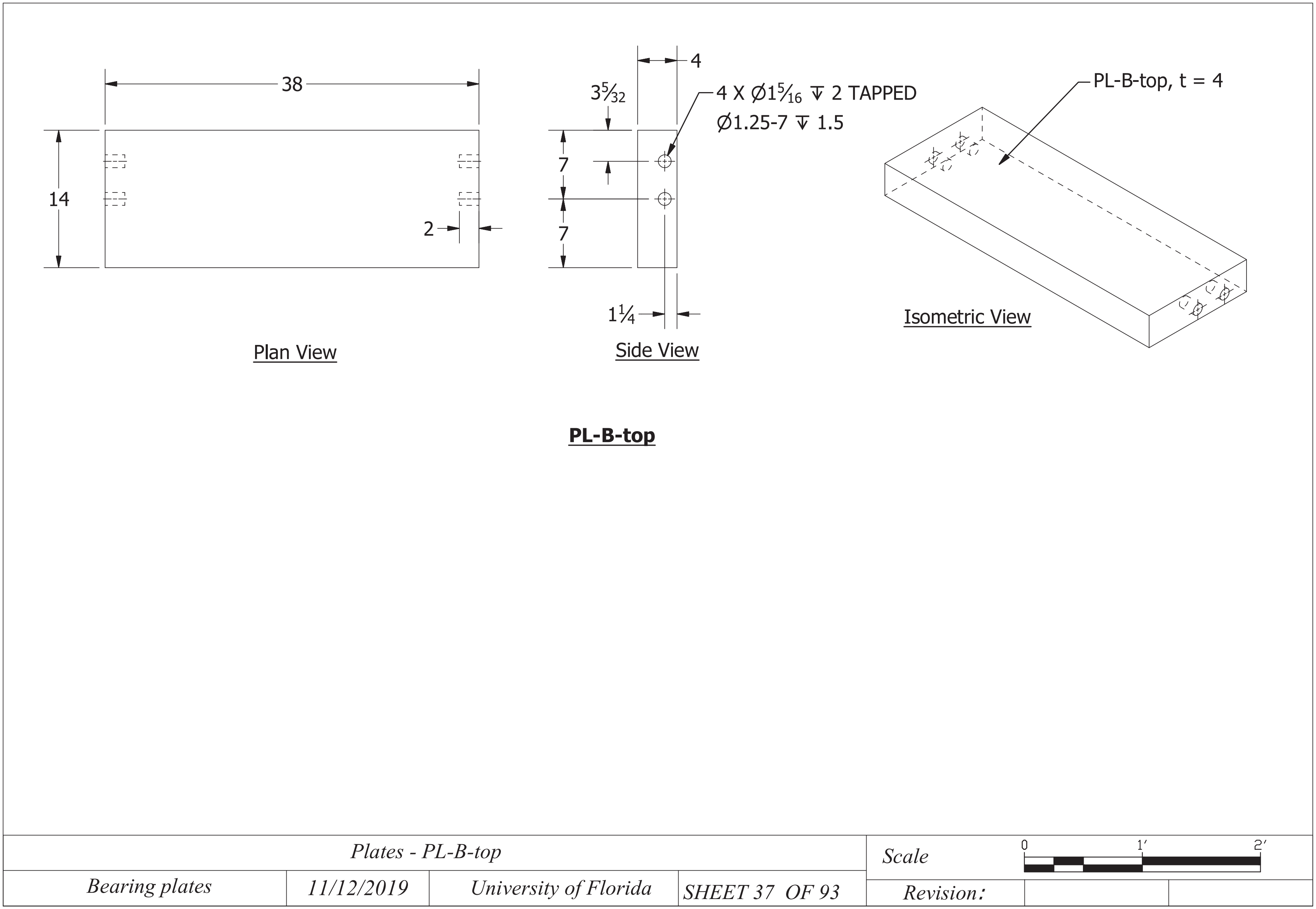
38
14
2
Plan View
4
3 5/32
7
7
1 1/4
4 X Ø1 5/16 ↧ 2 TAPPED
Ø1.25-7 ↧ 1.5
Side View
PL-B-top, t = 4
Isometric View
PL-B-top
Plates - PL-B-top
Bearing plates
11/12/2019
University of Florida
SHEET 37 OF 93
Scale
0
1′
2′
Revision:

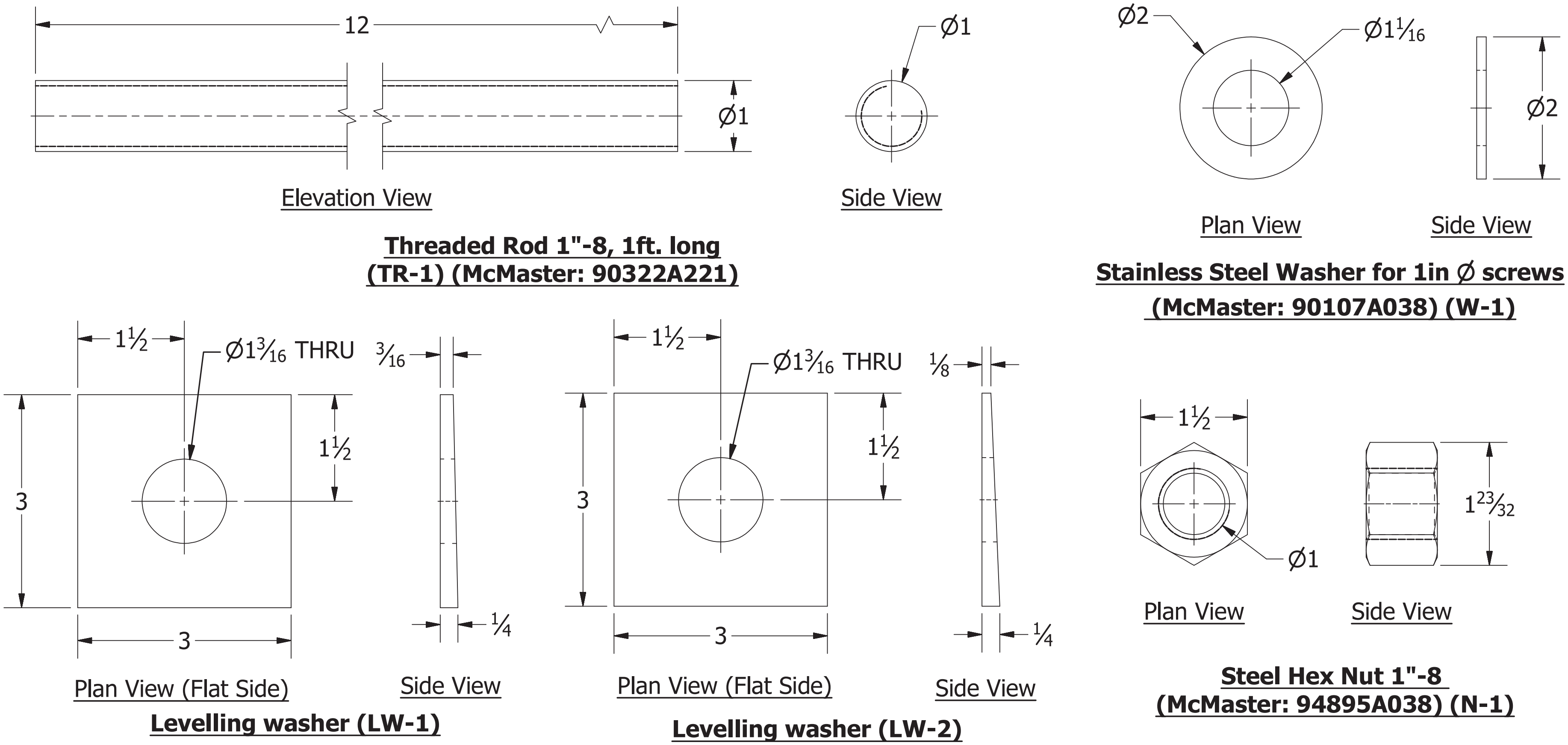

PARTS LIST - 8					
ITEM	PART NAME	CROSS-SECTION	LENGTH	QTY	MATERIAL
1	TR-1	DIA-1	12	4	STEEL, Gr-150
2	W-1	DIA-1 $\frac{1}{16}$	-	8	STAINLESS STEEL
3	N-1	DIA-1	-	8	STEEL, Grade-8
4	LW-1	3 X BEV FROM $\frac{1}{4}$ TO $\frac{3}{16}$	3	8	STEEL, ASTM-A572 Gr-50
5	LW-2	3 X BEV FROM $\frac{1}{4}$ TO $\frac{1}{8}$	3	8	STEEL, ASTM-A572 Gr-50

Fasteners-1 TR-1, W-1, N-1, LW-1 and LW-2				*Scale* 0 2'' 4''
Middle plate assembly	*11/12/2019*	*University of Florida*	*SHEET 38 OF 93*	*Revision:*

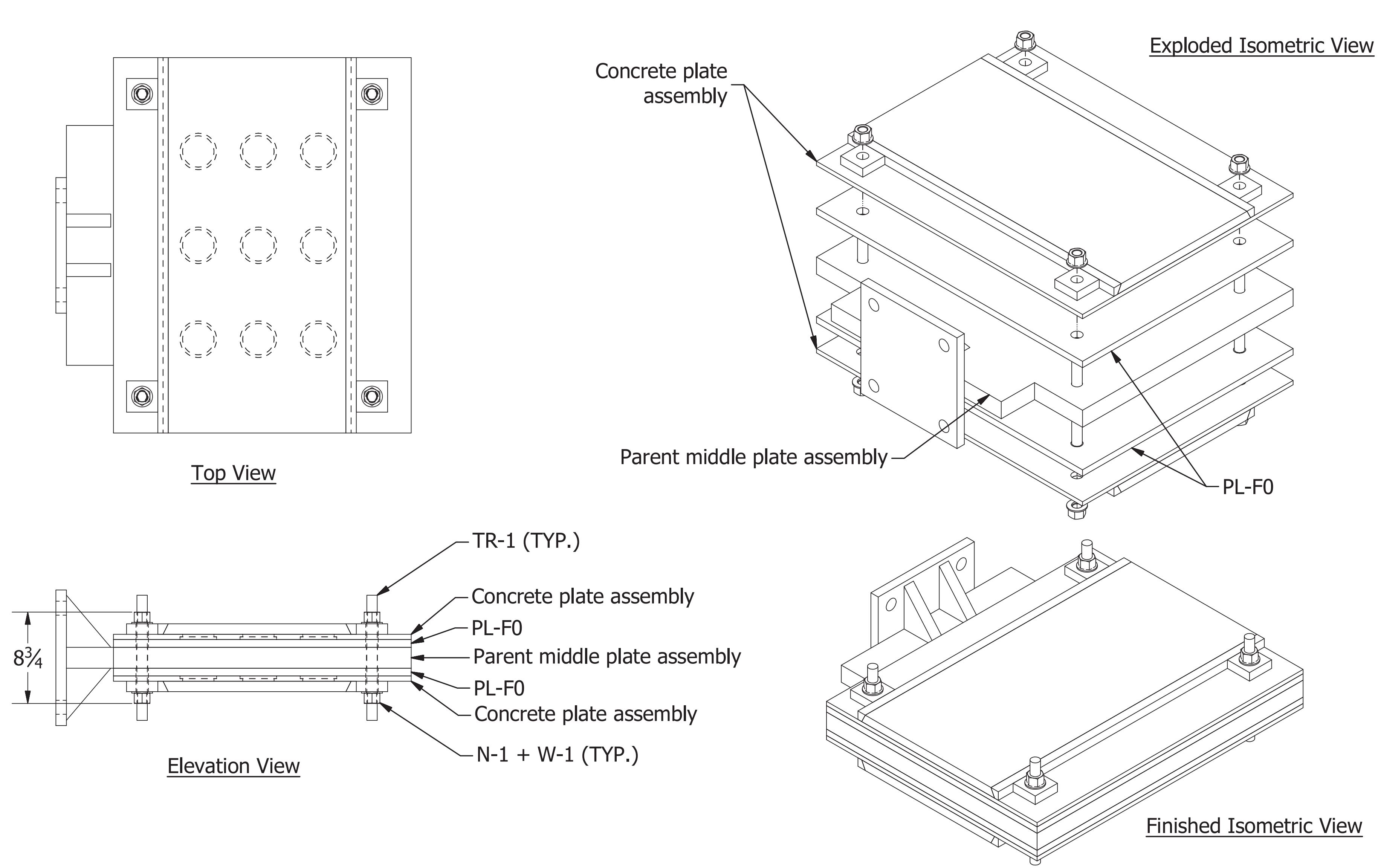

Flat pad, concrete surface assembly				*Scale* 0 1′ 2′
Middle plate assembly	*11/12/2019*	*University of Florida*	*SHEET 39 OF 93*	*Revision:*

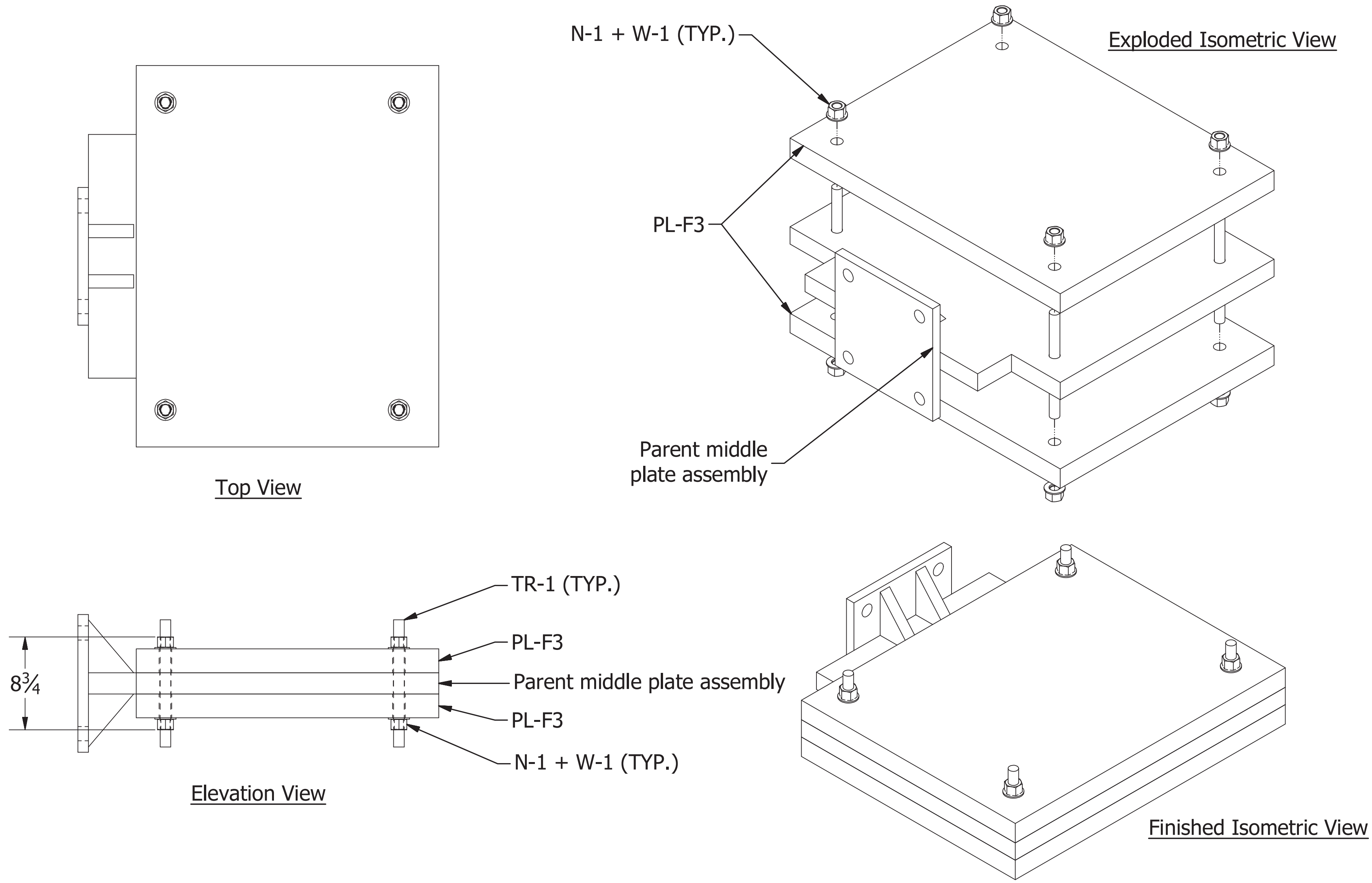

Flat pad, steel surface assembly				Scale 0 1′ 2′
Middle plate assembly	11/12/2019	University of Florida	SHEET 40 OF 93	Revision:

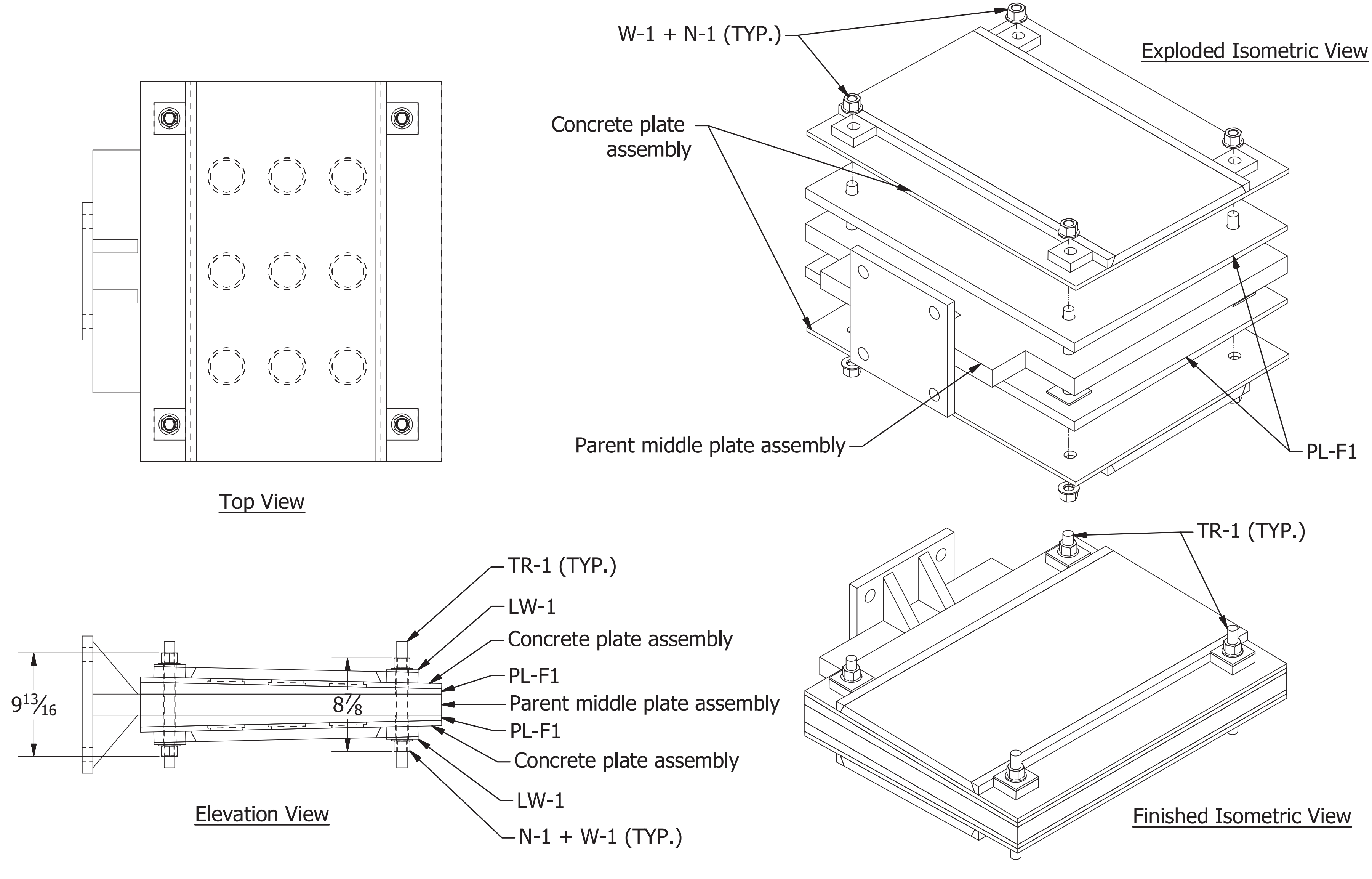

2.19% slope pad, concrete surface assembly				*Scale*	0 1′ 2′
Middle plate assembly	*11/12/2019*	*University of Florida*	*SHEET 41 OF 93*	*Revision:*	

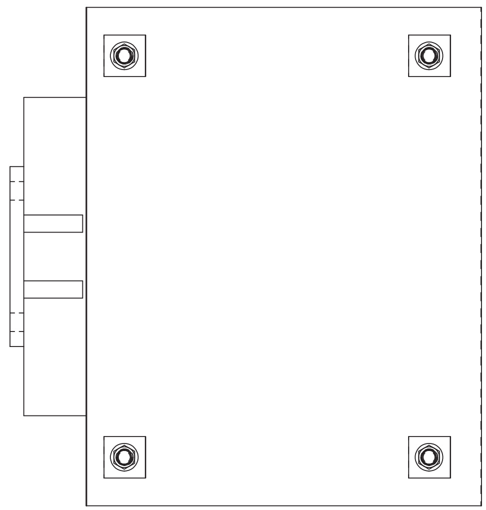

Top View

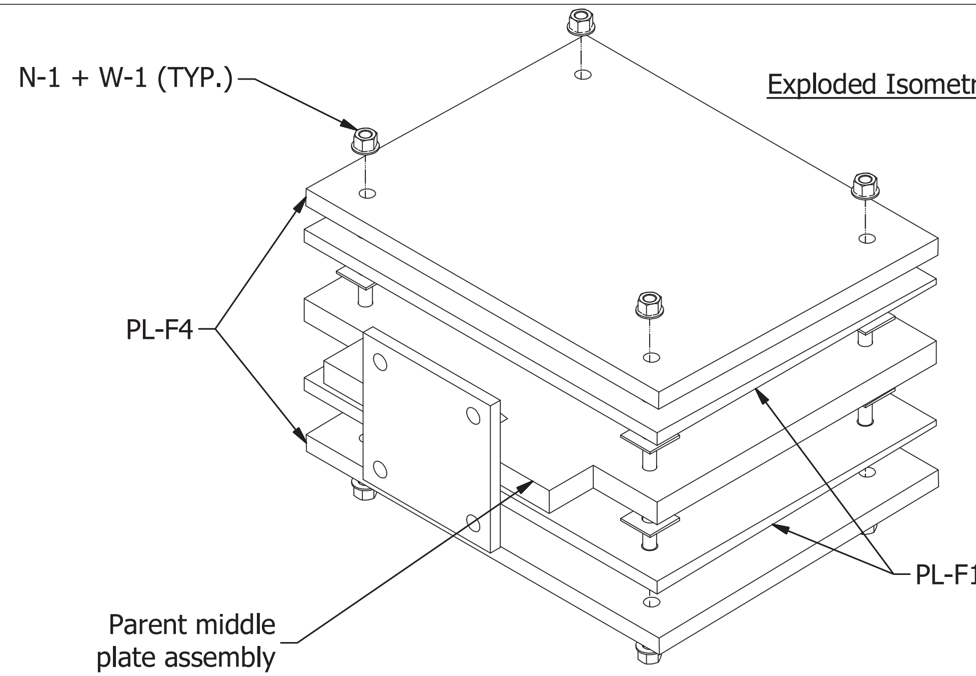

Exploded Isometric View

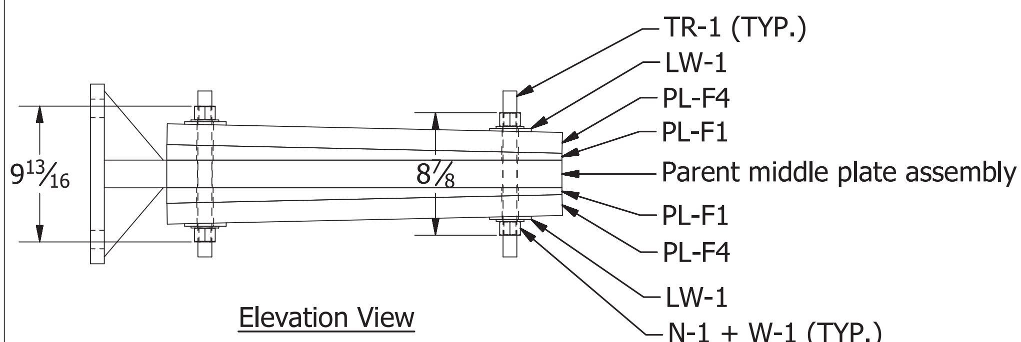

Elevation View

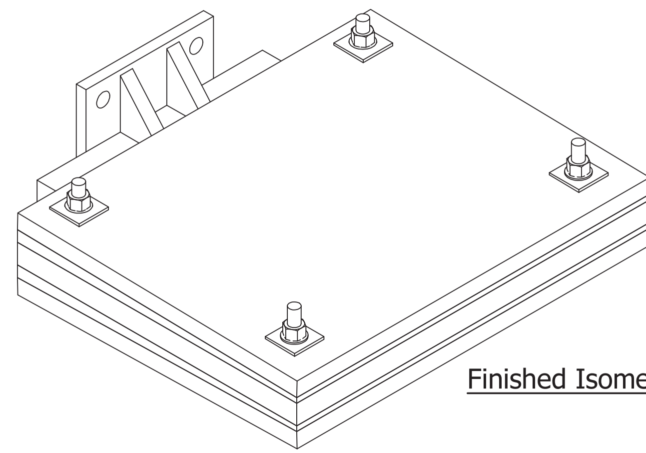

Finished Isometric View

2.19% slope pad, steel surface assembly				*Scale*	0 1′ 2′
Middle plate assembly	*11/12/2019*	*University of Florida*	*SHEET 42 OF 93*	*Revision:*	

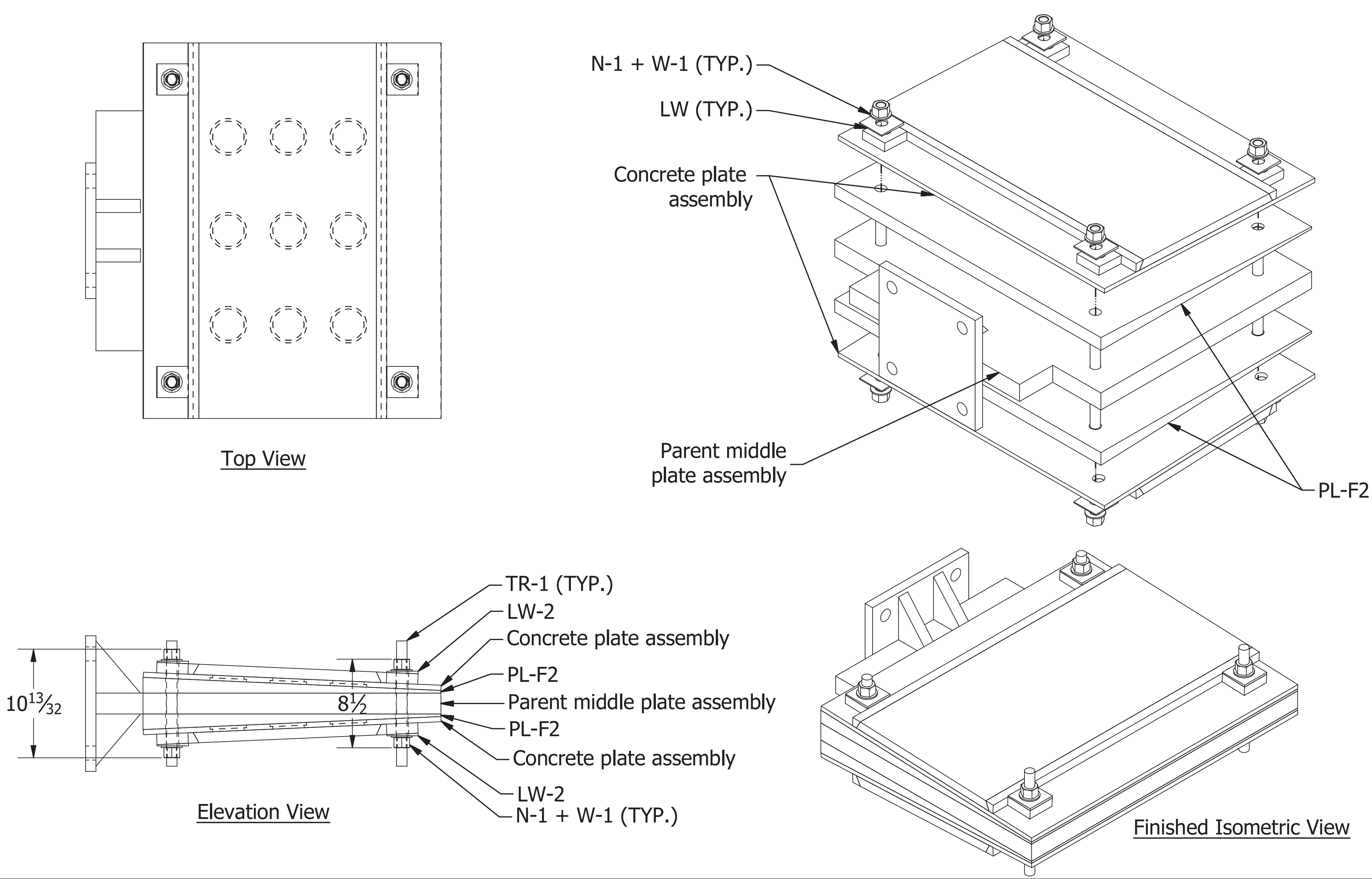

4.3% slope pad, concrete surface assembly				*Scale* 0 1′ 2′
Middle plate assembly	*11/12/2019*	*University of Florida*	*SHEET 43 OF 93*	*Revision:*

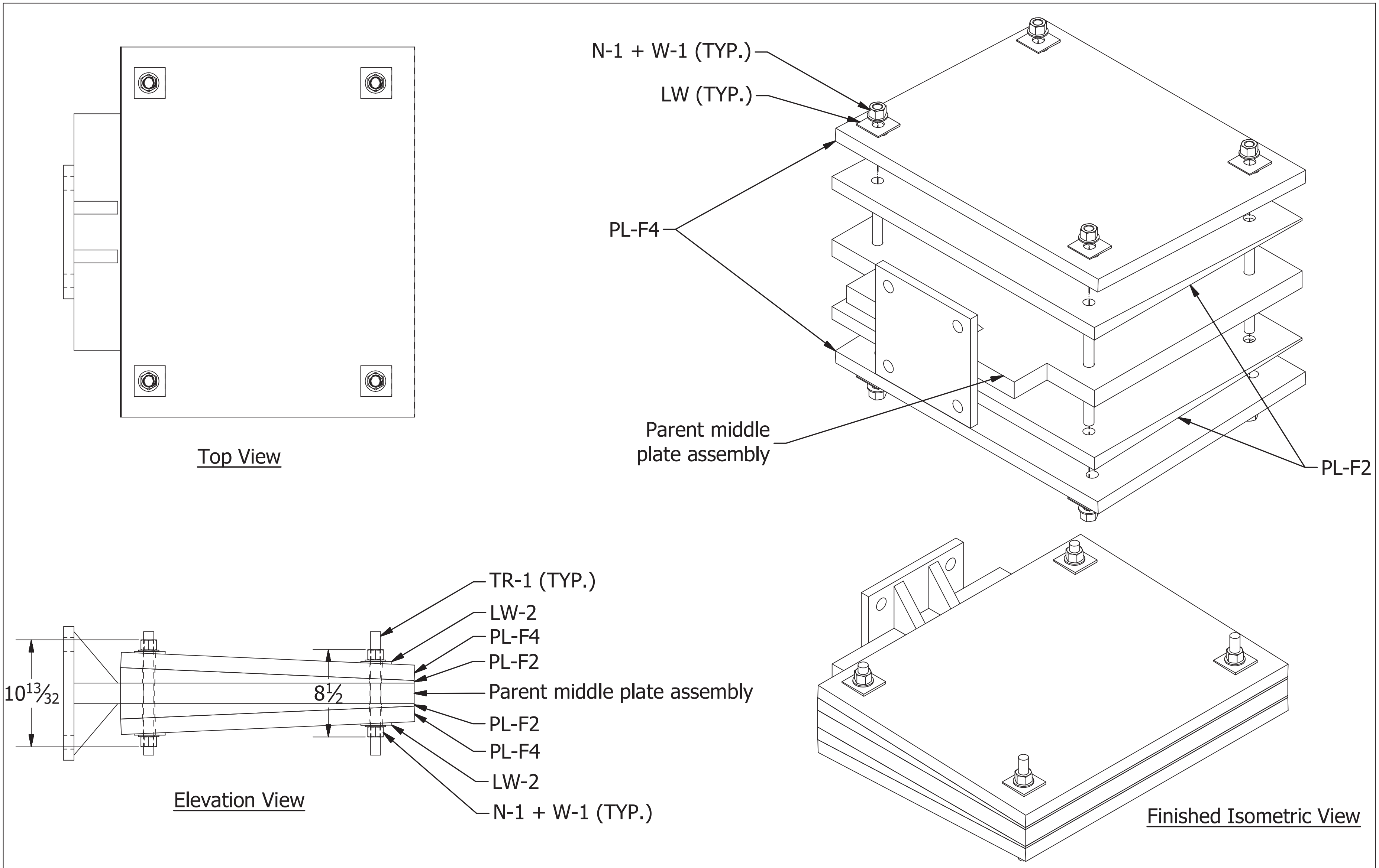

4.3% slope pad, steel surface assembly				*Scale*	0 1′ 2′
Middle plate assembly	*11/12/2019*	*University of Florida*	*SHEET 44 OF 93*	*Revision:*	

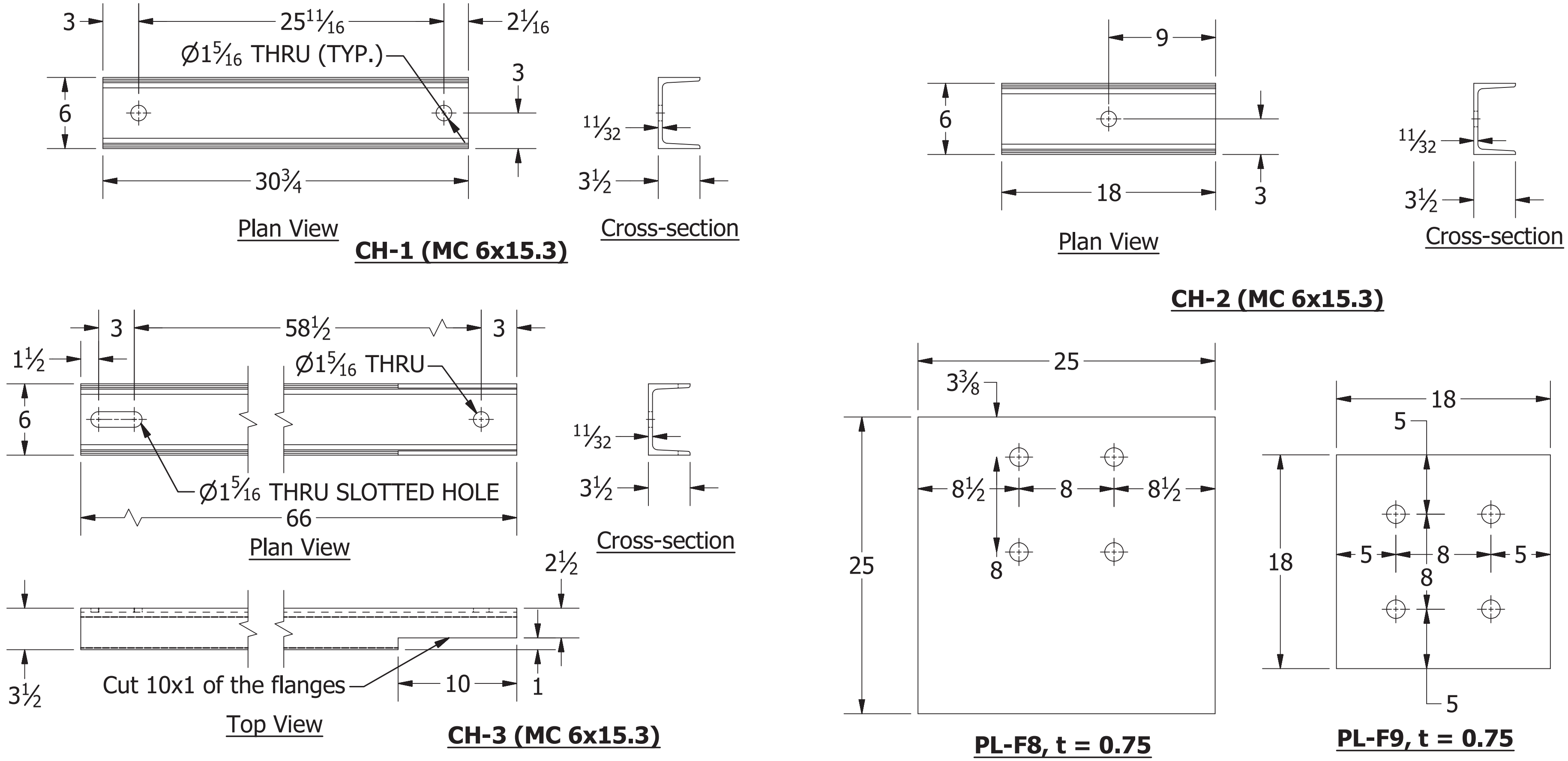

PARTS LIST - 9					
ITEM	PART NAME	CROSS-SECTION	LENGTH	QTY	MATERIAL
1	CH-1	MC 6X15.3	30 3/4	2	STEEL, Gr-50
2	CH-2	MC 6X15.3	18	2	STEEL, Gr-50
3	CH-3	MC 6X15.3	66	2	STEEL, Gr-50
4	PL-F8	25 X 0.75	25	1	STEEL, Gr-36
5	PL-F9	18 X 0.75	18	1	STEEL, Gr-36

CH-1, CH-2, A, PL-F8 and PL-F9				*Scale* 0 1′ 2′
Frame support	*11/12/2019*	*University of Florida*	*SHEET 45 OF 93*	*Revision:*

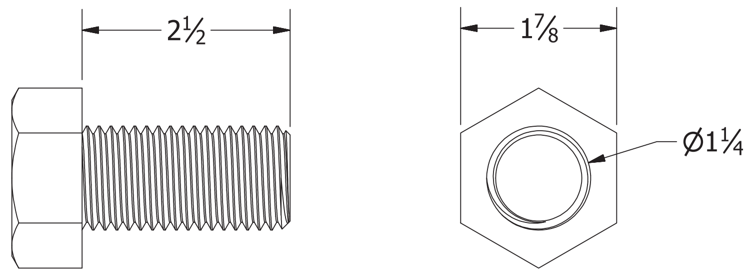

Steel Hex Head Screw 1.25"-7
(McMaster: 91268A213) (B-1)

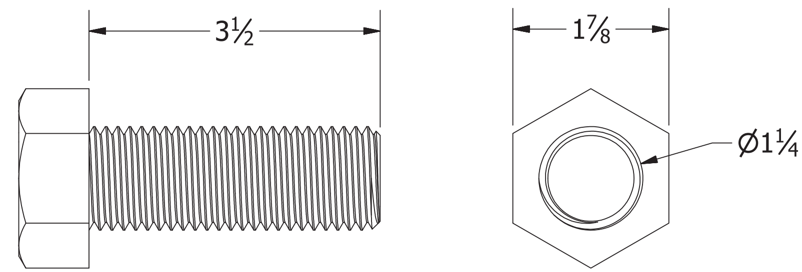

Steel Hex Head Screw 1.25"-7
(McMaster: 91268A217) (B-2)

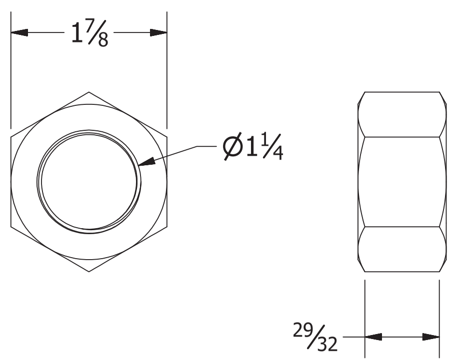

Steel Hex Nut 1.25"-7
(McMaster: 93827A287) (N-2)

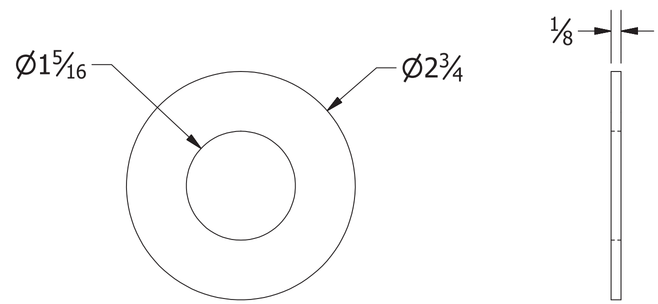

Stainless Steel Washer for 1.25in Ø screws
(McMaster: 90107A040) (W-2)

PARTS LIST - 10

ITEM	PART NAME	CROSS-SECTION	LENGTH	QTY	MATERIAL
1	B-1	DIA-1 $\frac{1}{4}$	2 1/2	8	STEEL, Gr-150
2	B-2	DIA-1 $\frac{1}{4}$	3 1/2	12	STEEL, Gr-150
3	N-2	DIA-1 $\frac{1}{4}$	-	18	STEEL, Gr-150
4	W-2	DIA-1 $\frac{5}{16}$	-	2	-

Fasteners-2 B1, B2, N2 and W2				*Scale*	0 2″ 4″
Frame support	*11/12/2019*	*University of Florida*	*SHEET 46 OF 93*	*Revision:*	

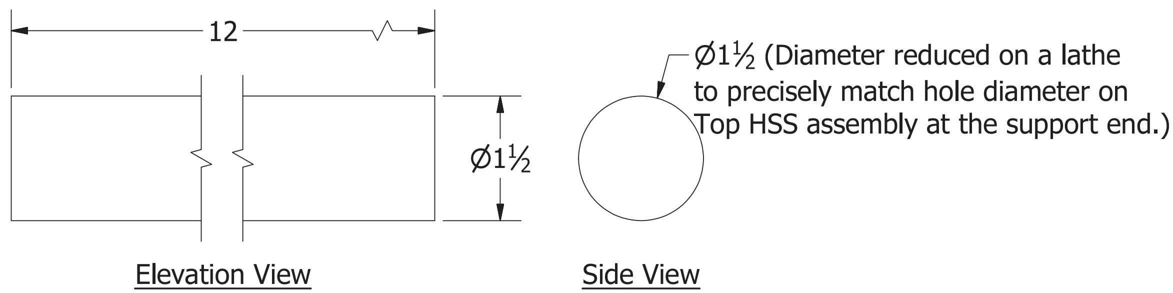

Stainless Steel Rod, 1-1/2" Diameter, 1 Foot Long
(McMaster: 9094K25) (R-1)

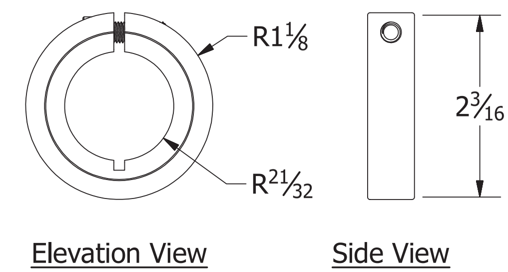

Clamping Shaft Collar for 1-5/16" Diameter,
(McMaster: 6435K56) (CS-1)

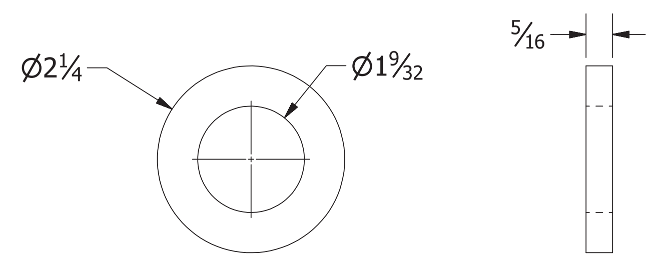

Stainless Steel Oversized Washer for 1.25in Ø screws
(McMaster: 91201A040) (W-3)

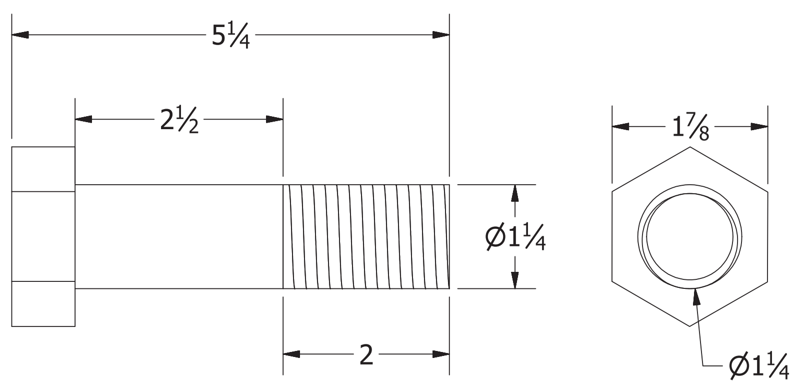

Steel Hex Head Screw 1-1/4"-7
(McMaster: 91268A223) (B-3)

PARTS LIST - 11

ITEM	PART NAME	CROSS-SECTION	LENGTH	QTY	MATERIAL
1	R-1	DIA-1 $\frac{1}{2}$	12	2	Tight-Tolerance Bearing-Quality 440C Stainless
2	CS-1	DIA-1 $\frac{5}{16}$	-	4	Steel
3	B-3	DIA-1 $\frac{1}{4}$	-	2	STEEL, Gr-150
4	W-3	DIA-1 $\frac{9}{32}$	-	4	-

Fasteners-3 R1, CS1, B3 and W3

Scale 0 2″ 4″

Frame support | *11/12/2019* | *University of Florida* | *SHEET 47 OF 93* | *Revision:*

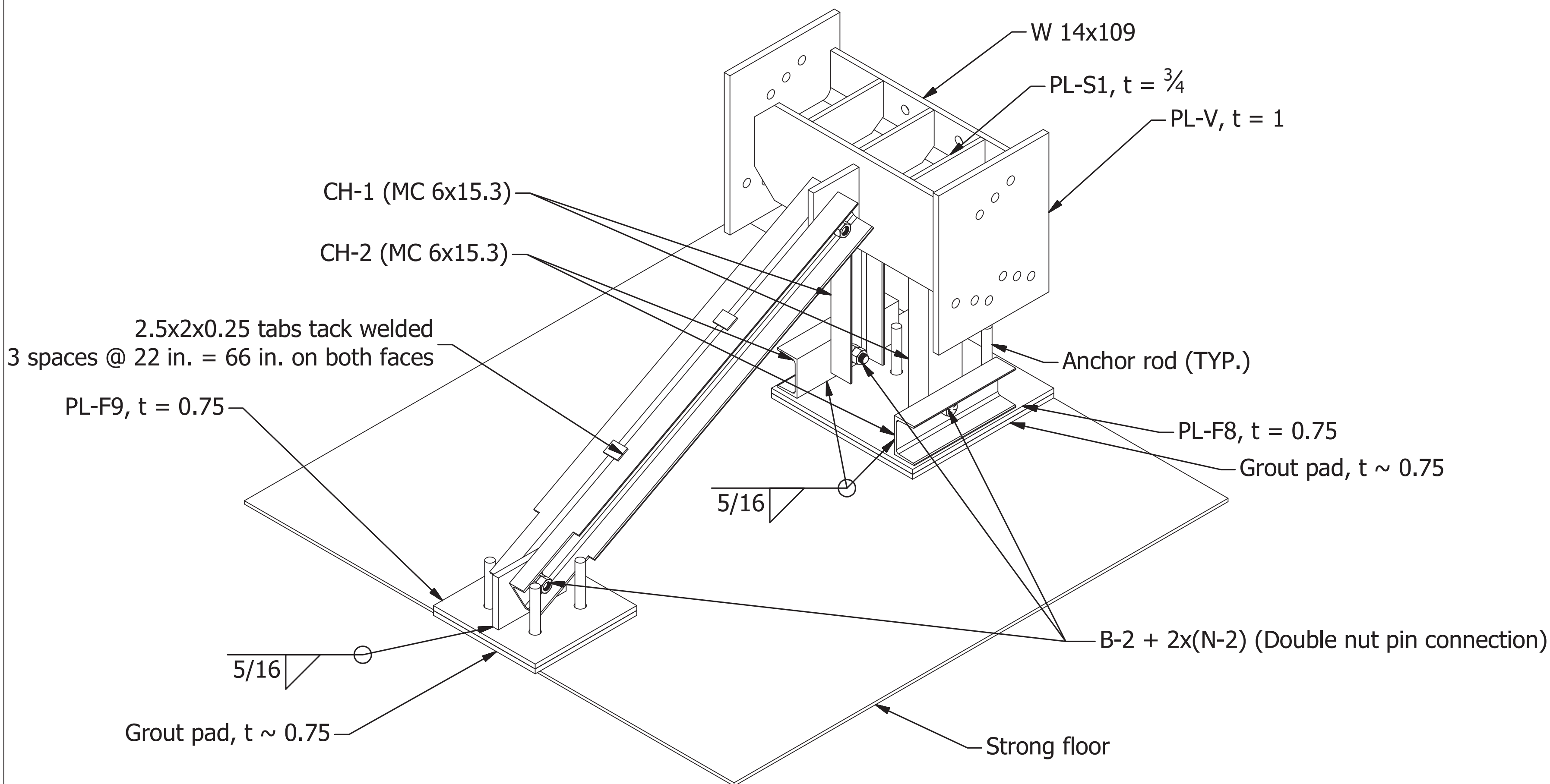

Assembly - Details 1 (Isometric View)				*Scale*	0 18'' 36''
Frame support	*11/12/2019*	*University of Florida*	*SHEET 48 OF 93*	*Revision:*	

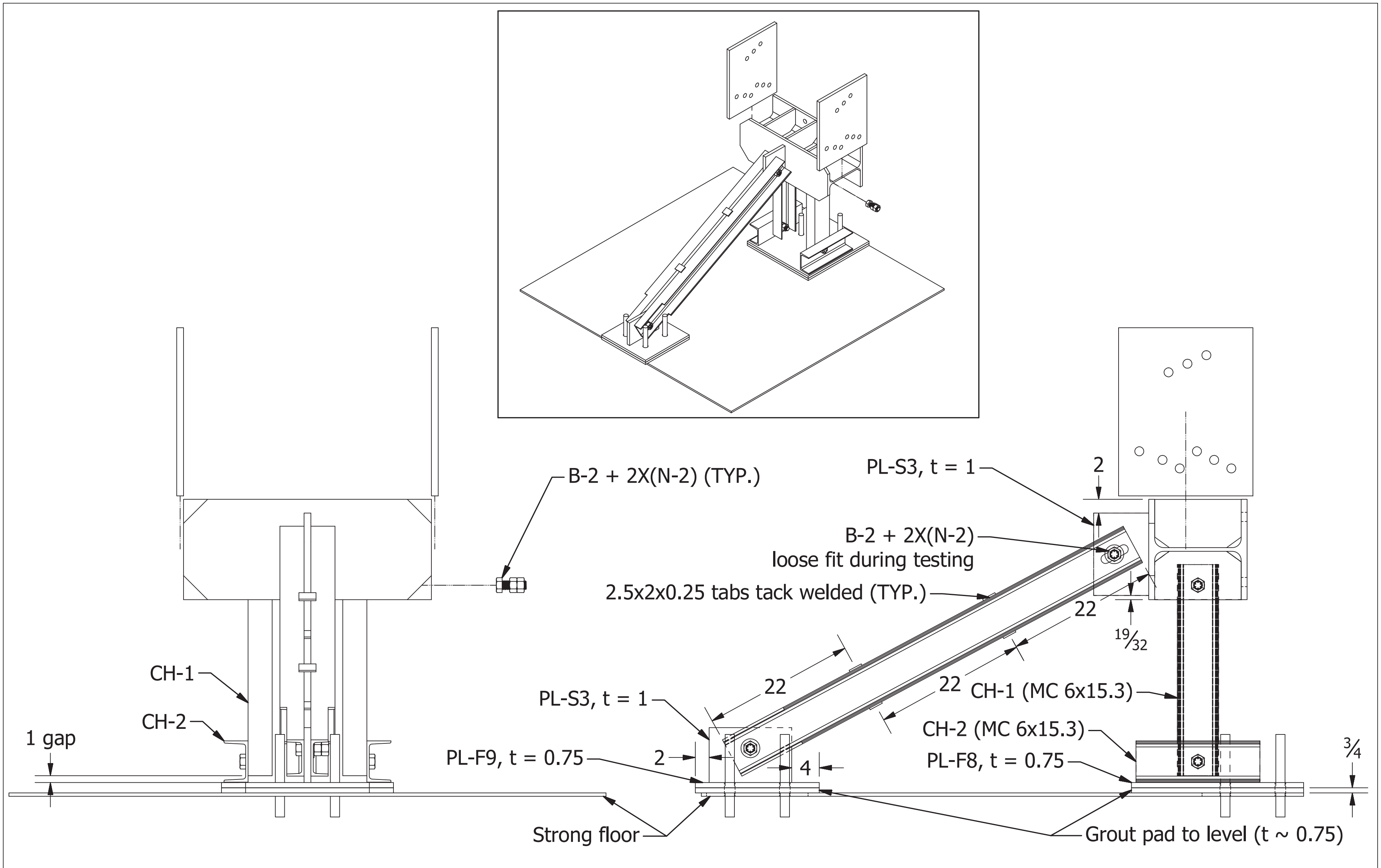

Assembly - Details 2 (Exploded View)				*Scale* 0 18″ 36″
Frame support	*11/12/2019*	*University of Florida*	*SHEET 49 OF 93*	*Revision:*

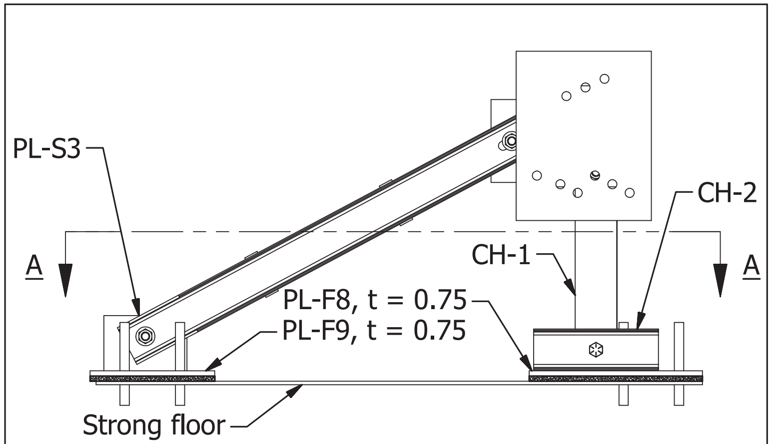

Elevation View

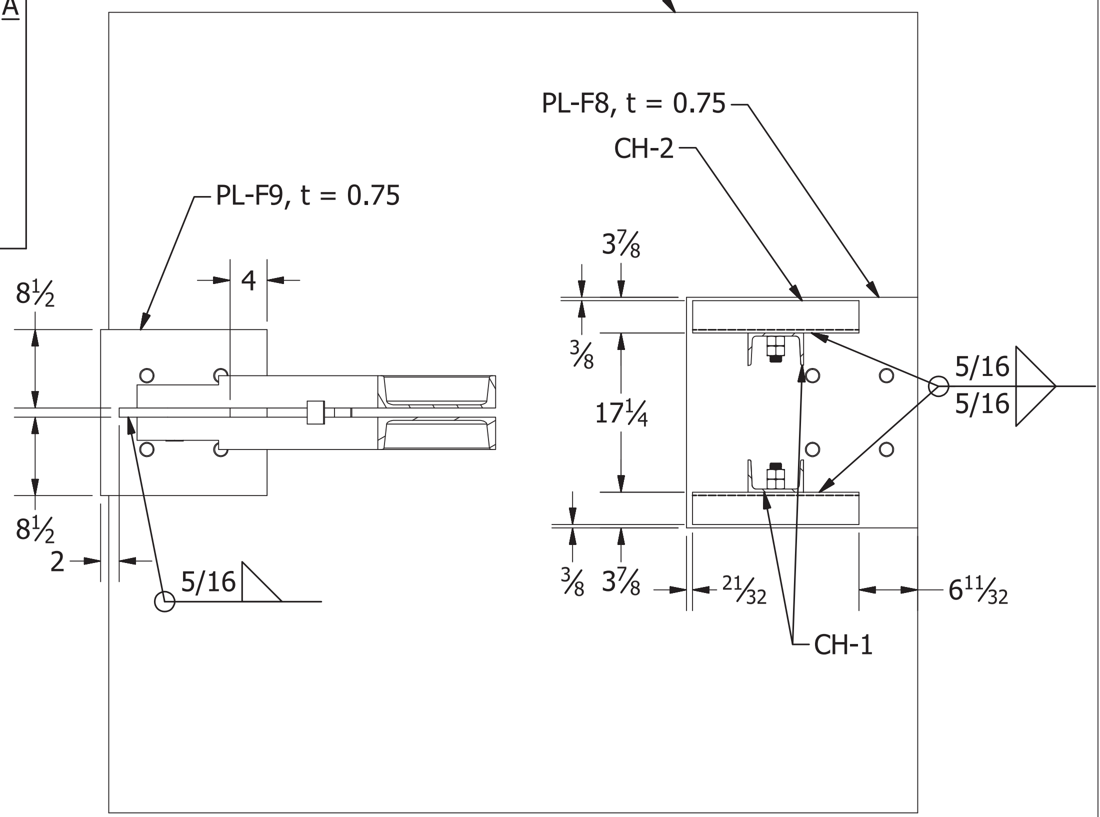

SECTION A-A

Assembly - Detail of channel placement				*Scale* 0 18'' 36''
Frame support	*11/12/2019*	*University of Florida*	*SHEET 50 OF 93*	*Revision:*

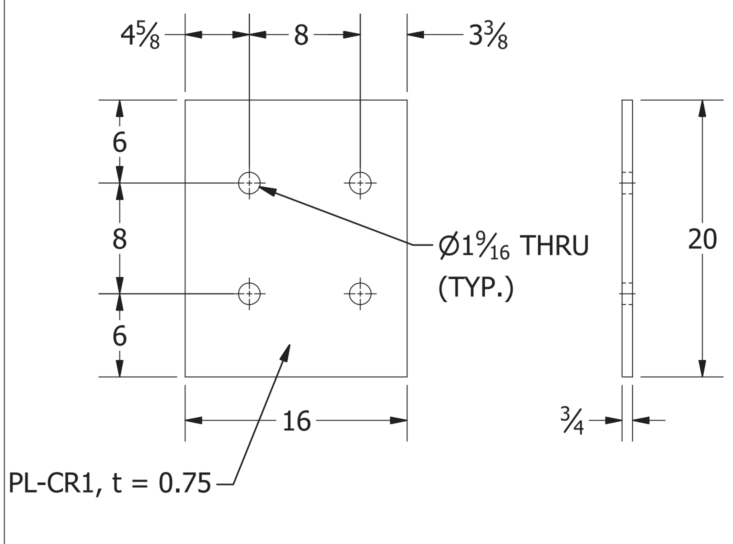

PL-CR1

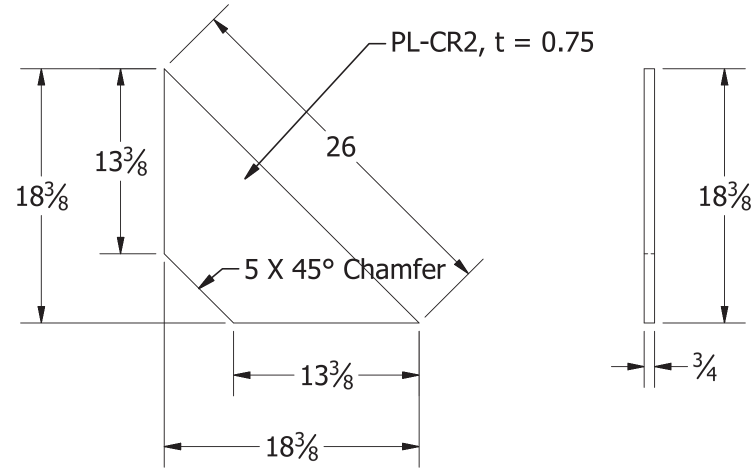

PL-CR2

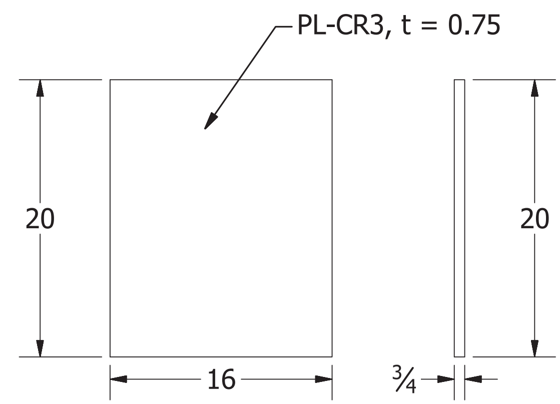

PL-CR3

PARTS LIST - 12					
ITEM	PART NAME	SIZE	THICKNESS	QTY	MATERIAL
1	PL-CR1	20 X 16	0.75	2	STEEL, Gr-50
2	PL-CR2	TRI 18.375 x 18.375	0.75	2	STEEL, Gr-50
3	PL-CR3	20 x 16	0.75	2	STEEL, Gr-50

Parts - PL-CR1, PL-CR2 and PL-CR3				*Scale*	0 8′ 16′
Corbel assembly	*11/12/2019*	*University of Florida*	*SHEET 51 OF 93*	*Revision:*	

Step 1: Weld PL-CR2 to PL-CR3

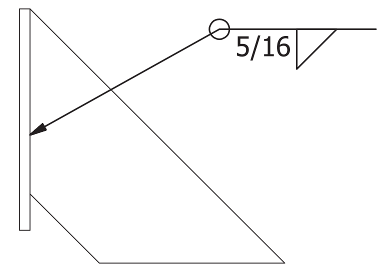

Side View

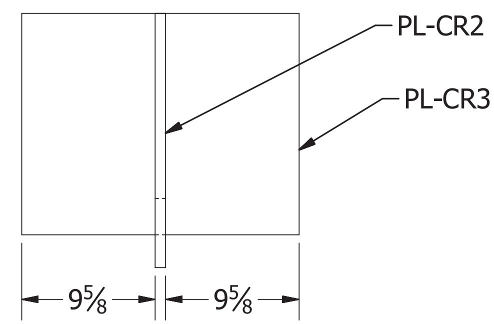

Front View

Step 2: Connect PL-CR1 to anchor plate using anchor bolts

Step 3: Weld PL-CR2 and PL-CR3 assembly to PL-CR1 such that PL-CR3 mates with the steel load block

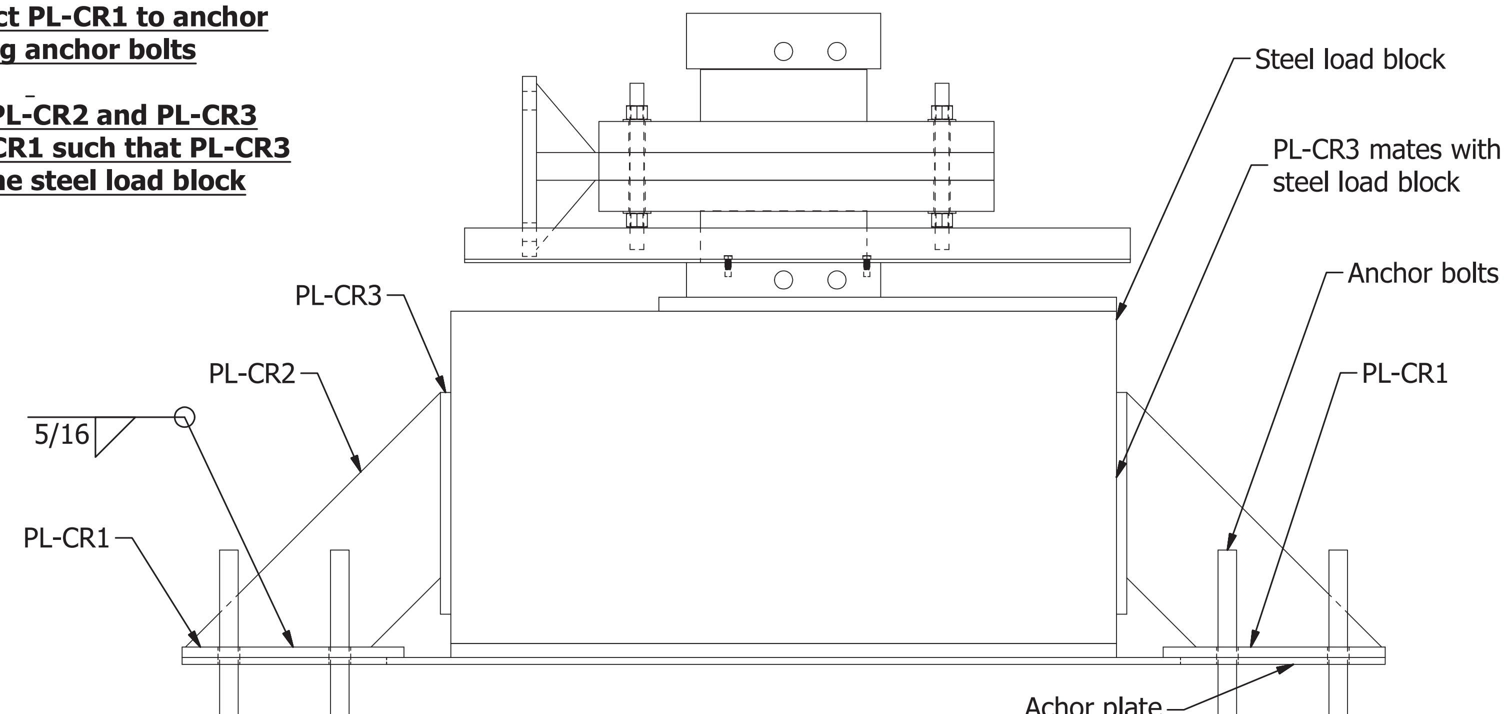

Steps				*Scale*	0 1′ 2′
Corbel assembly	*11/12/2019*	*University of Florida*	*SHEET 52 OF 93*	*Revision:*	

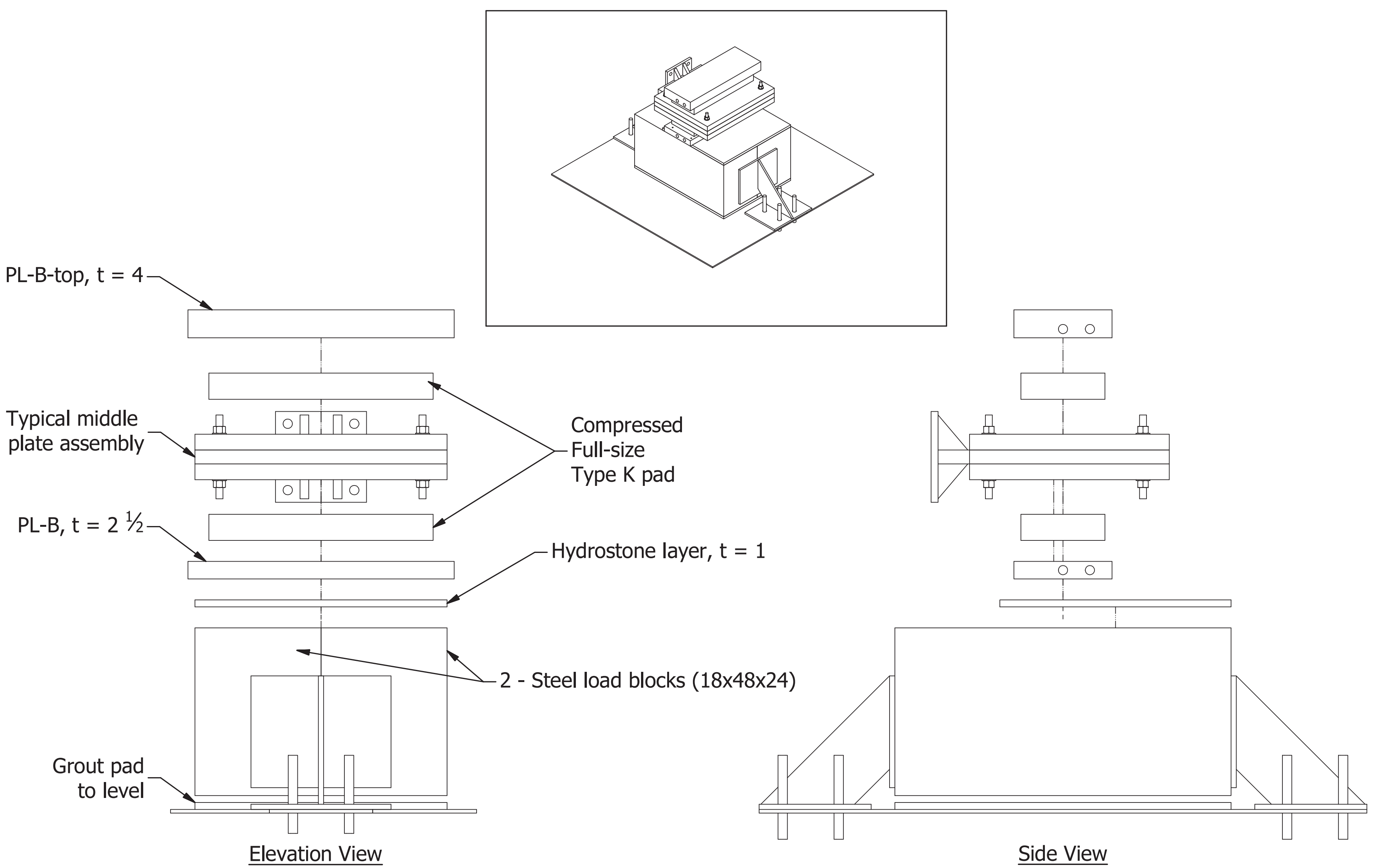

Assembly - Detail 1 (Exploded View)				*Scale* 0 18″ 36″
Bearing end support	*11/12/2019*	*University of Florida*	*SHEET 53 OF 93*	*Revision:*

Note: For all types of bearing pads, hydrostone layer has same plan dimensions (36 in. x 33 in. x 1 in.). However, hydrostone layer needs to be reconstructed for pad K after testing pad E and F.

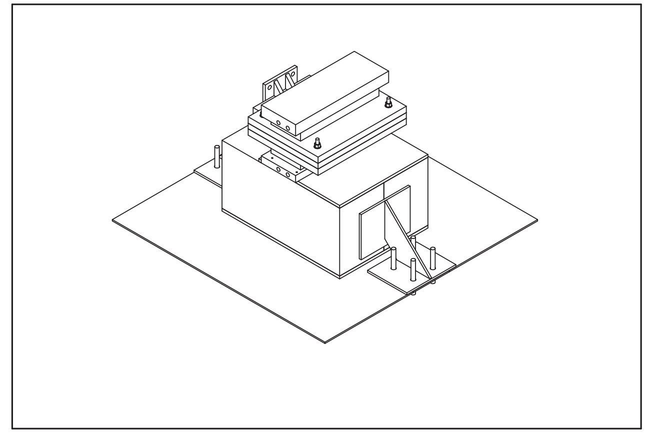

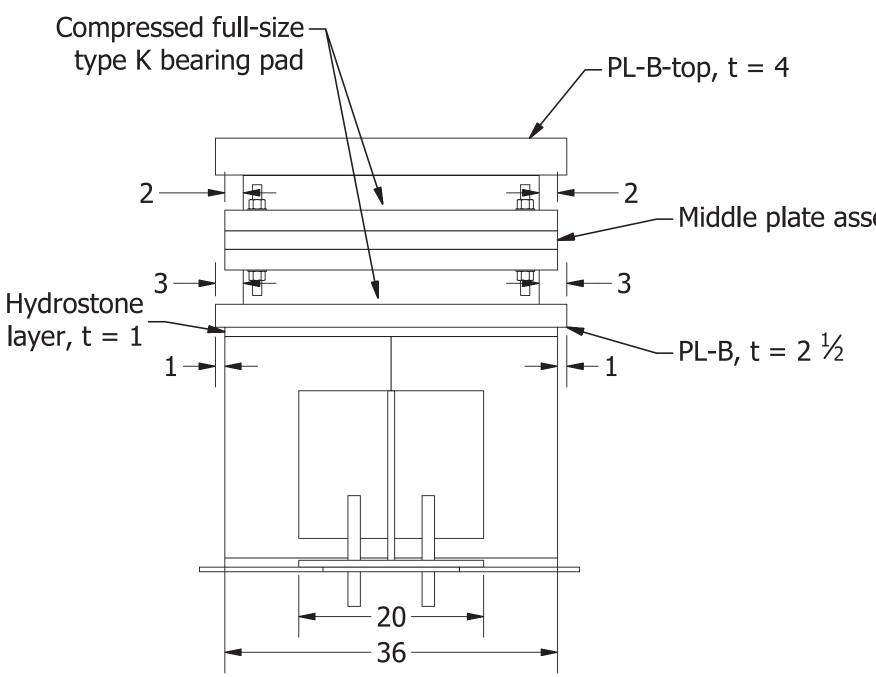

Front View

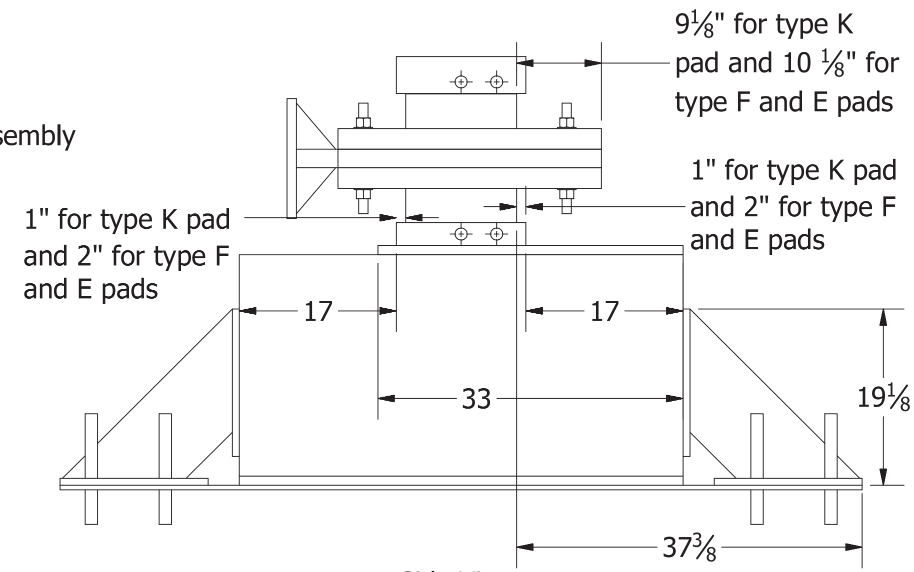

Side View

Assembly - Detail 2 (Full size bearing pad positioning)				*Scale* 0 18″ 36″
Bearing end support	*11/12/2019*	*University of Florida*	*SHEET 54 OF 93*	*Revision:*

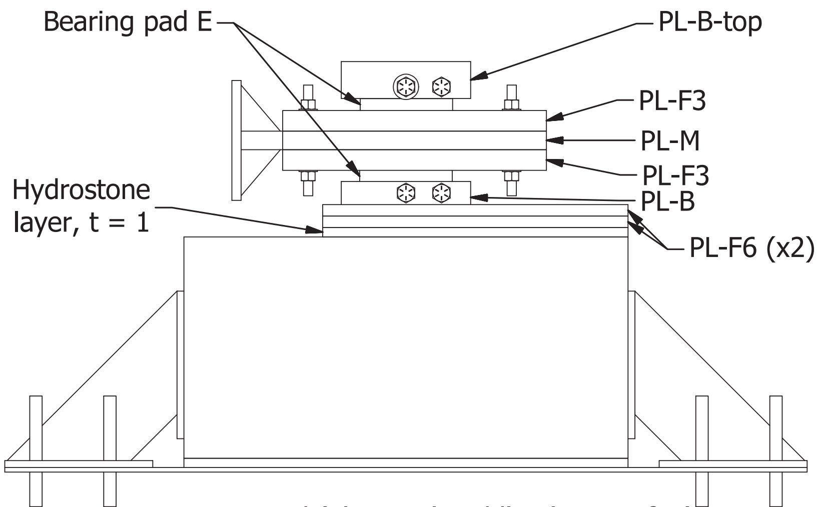

Type E pad (Flat steel middle plate config.)

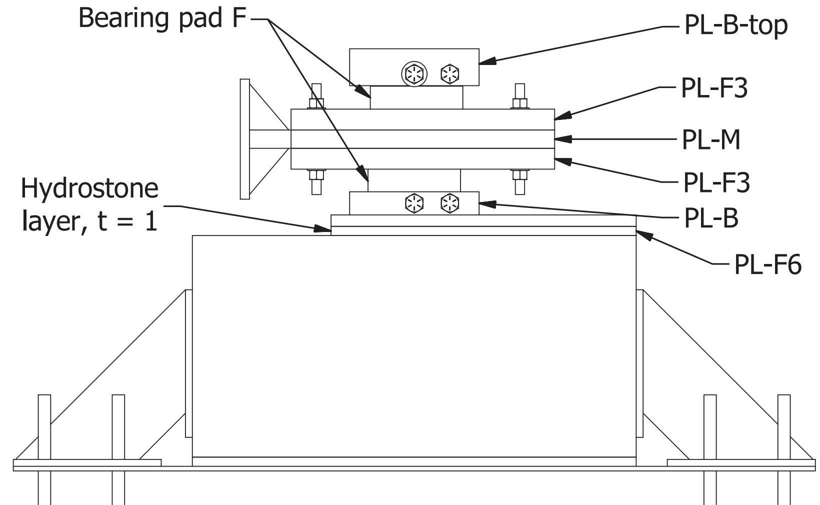

Type F pad (Flat steel middle plate config.)

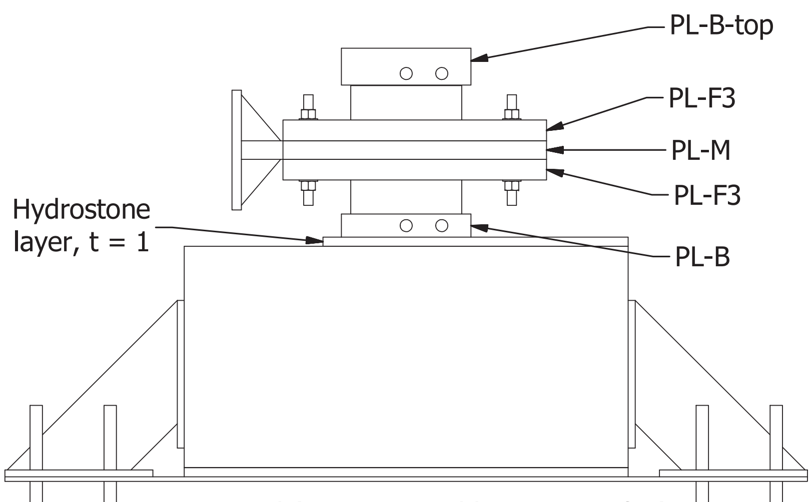

Type K pad (Flat steel middle plate config.)

Notes:
1. See sheet number 39 to 44 for more middle plate configurations.

Bearing pad end plates				*Scale*	0 18'' 36''
Summary of configurations	*11/12/2019*	*University of Florida*	*SHEET 55 OF 93*	*Revision:*	

Summary of plates used for different types of bearing pads

Bearing pad E											
Slope	Surface	PL-B/PL-B-top	PL-M	PL-F0	PL-F1	PL-F2	PL-F3	PL-F4	PL-F6	Concrete plate	Hydrostone layer
0	Concrete	x (2)	x (1)	x (2)					x (2)	x (2)	1 in.
0	Steel	x (2)	x (1)				x (2)		x (2)		1 in.
2.19	Concrete	x (2)	x (1)		x (2)				x (2)	x (2)	1 in.
2.19	Steel	x (2)	x (1)		x (2)			x (2)	x (2)		1 in.
4.3	Concrete	x (2)	x (1)			x (2)			x (2)	x (2)	1 in.
4.3	Steel	x (2)	x (1)			x (2)		x (2)	x (2)		1 in.

Bearing pad F											
Slope	Surface	PL-B/PL-B-top	PL-M	PL-F0	PL-F1	PL-F2	PL-F3	PL-F4	PL-F6	Concrete plate	Hydrostone layer
0	Concrete	x (2)	x (1)	x (2)					x (1)	x (2)	1 in.
0	Steel	x (2)	x (1)				x (2)		x (1)		1 in.
2.19	Concrete	x (2)	x (1)		x (2)				x (1)	x (2)	1 in.
2.19	Steel	x (2)	x (1)		x (2)			x (2)	x (1)		1 in.
4.3	Concrete	x (2)	x (1)			x (2)			x (1)	x (2)	1 in.
4.3	Steel	x (2)	x (1)			x (2)		x (2)	x (1)		1 in.

Bearing pad K											
Slope	Surface	PL-B/PL-B-top	PL-M	PL-F0	PL-F1	PL-F2	PL-F3	PL-F4	PL-F6	Concrete plate	Hydrostone layer
0	Concrete	x (2)	x (1)	x (2)					-	x (2)	1 in.
0	Steel	x (2)	x (1)				x (2)		-		1 in.
2.19	Concrete	x (2)	x (1)		x (2)				-	x (2)	1 in.
2.19	Steel	x (2)	x (1)		x (2)			x (2)	-		1 in.
4.3	Concrete	x (2)	x (1)			x (2)			-	x (2)	1 in.
4.3	Steel	x (2)	x (1)			x (2)		x (2)	-		1 in.

Bearing pad end plates table				*Scale*
Summary of configurations	*11/12/2019*	*University of Florida*	*SHEET 56 OF 93*	*Revision:*

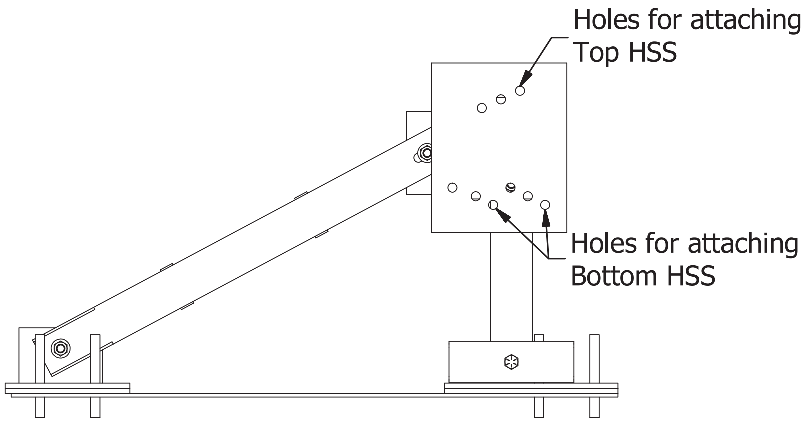

Bearing pad K configuration

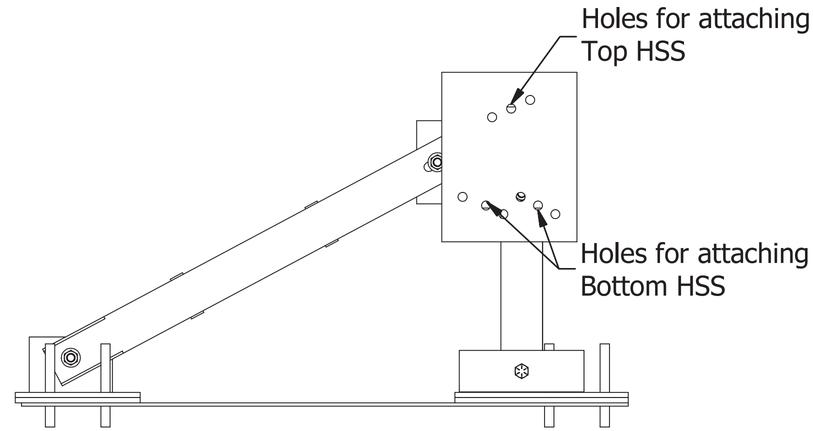

Bearing pad F configuration

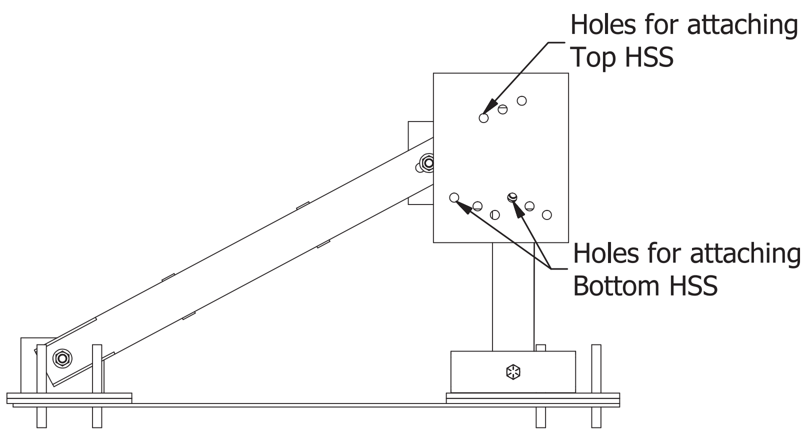

Bearing pad E configuration

PL-V hole attachments				*Scale*	0 24'' 48''
Summary of configurations	*11/12/2019*	*University of Florida*	*SHEET 57 OF 93*	*Revision:*	

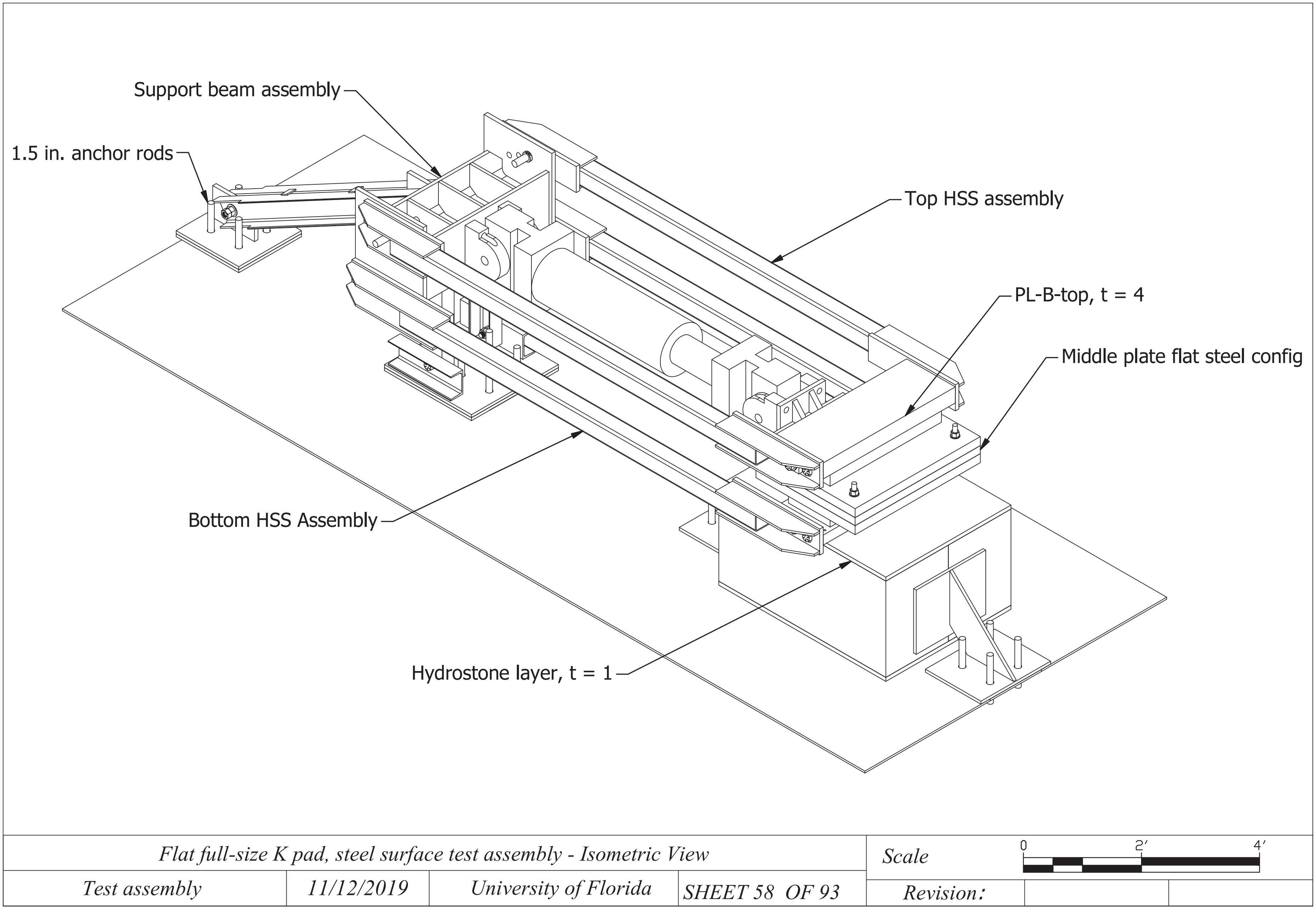

Support beam assembly
1.5 in. anchor rods
Top HSS assembly
PL-B-top, t = 4
Middle plate flat steel config
Bottom HSS Assembly
Hydrostone layer, t = 1
Flat full-size K pad, steel surface test assembly - Isometric View
Scale
0
2′
4′
Test assembly
11/12/2019
University of Florida
SHEET 58 OF 93
Revision:

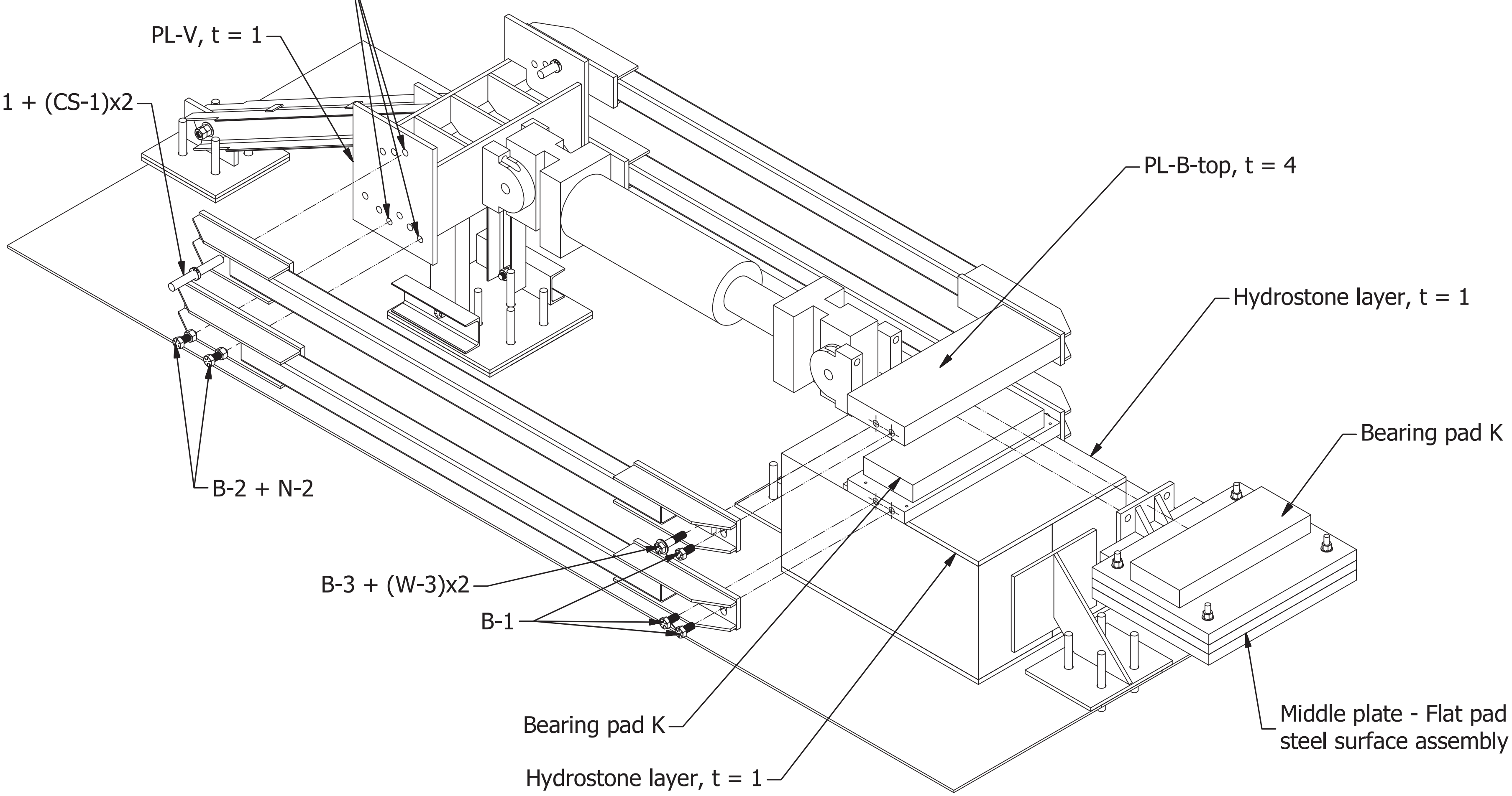

Flat full-size K pad, steel surface test assembly - Exploded Isometric View				*Scale* 0 2′ 4′
Test assembly	*11/12/2019*	*University of Florida*	*SHEET 59 OF 93*	*Revision:*

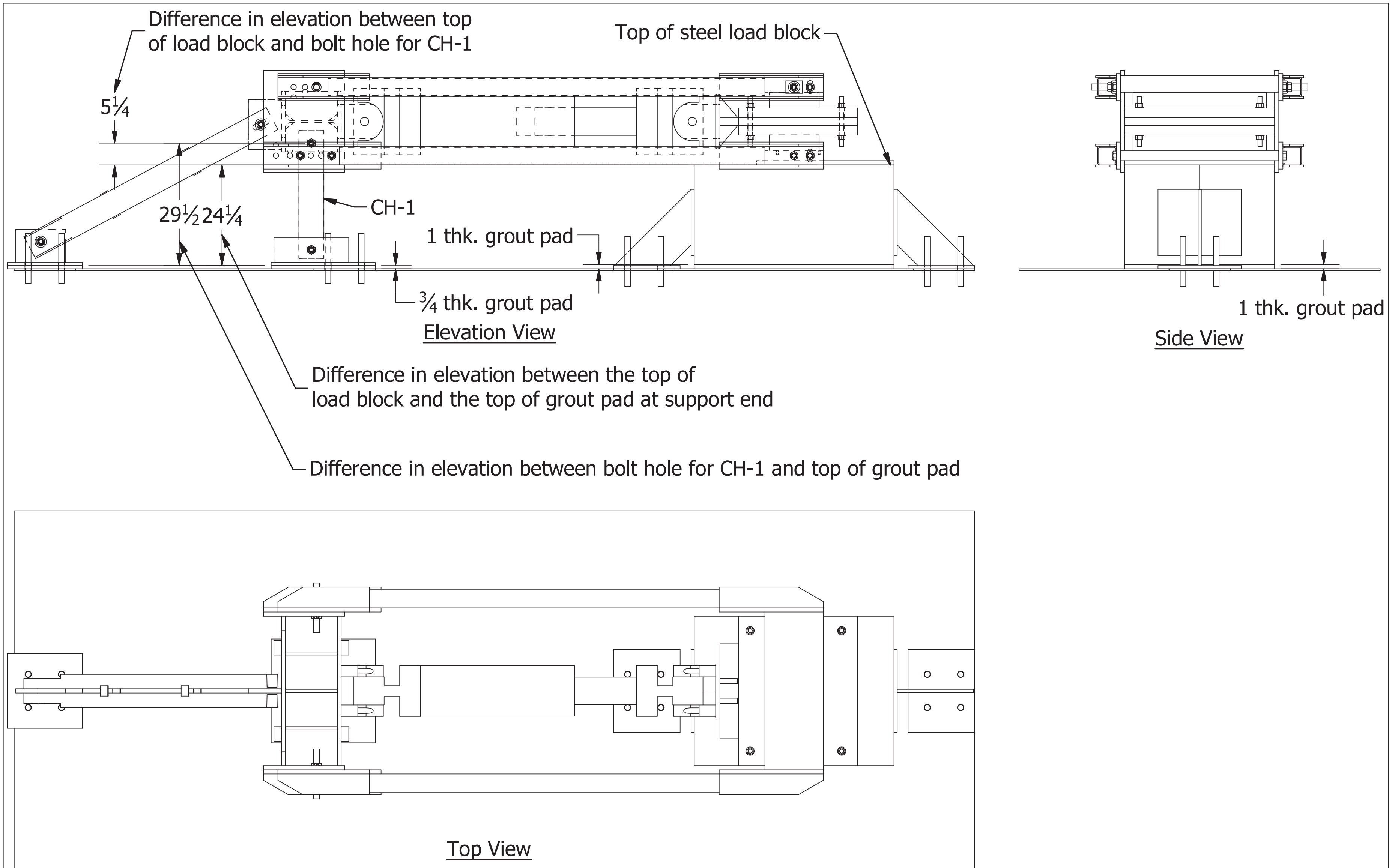

Flat full-size K pad, steel surface test assembly - Typical views				*Scale*	0 2.5′ 4.5′
Test assembly	*11/12/2019*	*University of Florida*	*SHEET 60 OF 93*	*Revision:*	

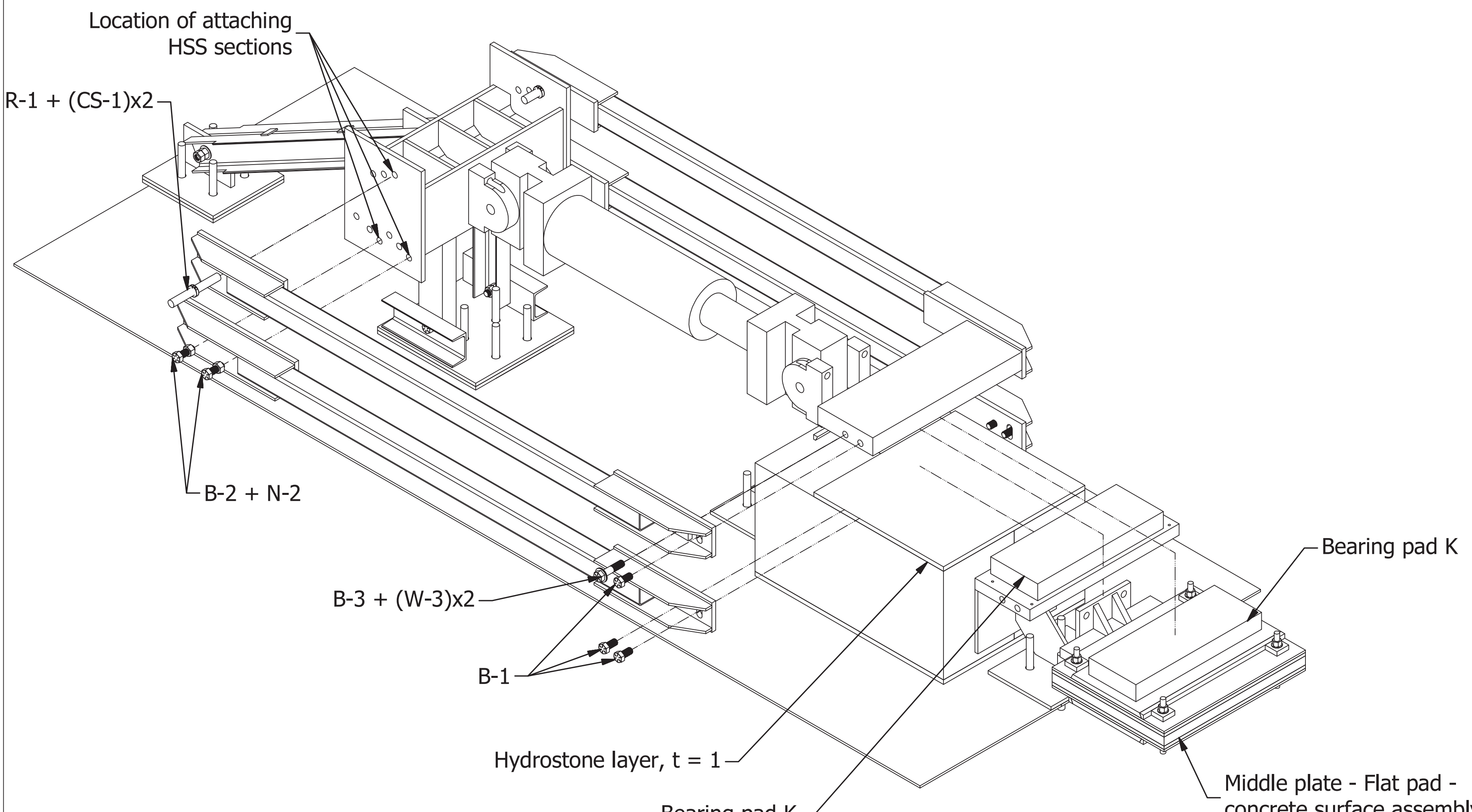

Flat full-size K pad, concrete surface test assembly - Exploded Isometric View				*Scale*	0 2′ 4′
Test assembly	*11/12/2019*	*University of Florida*	*SHEET 61 OF 93*	*Revision:*	

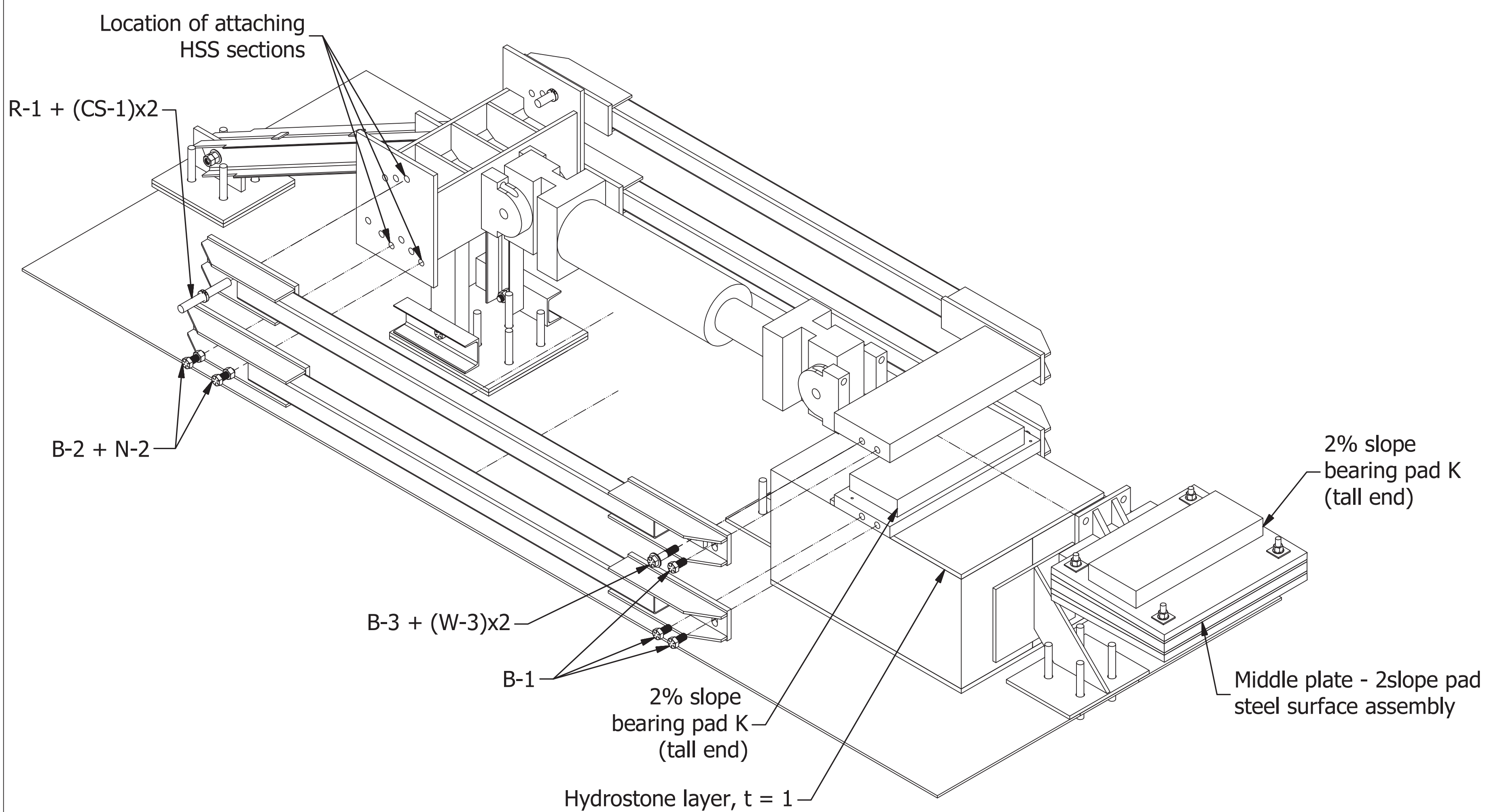

2% Tapered full-size K pad, steel surface test assembly - Exploded Isometric View				*Scale*	0 2′ 4′
Test assembly	*11/12/2019*	*University of Florida*	*SHEET 62 OF 93*	*Revision:*	

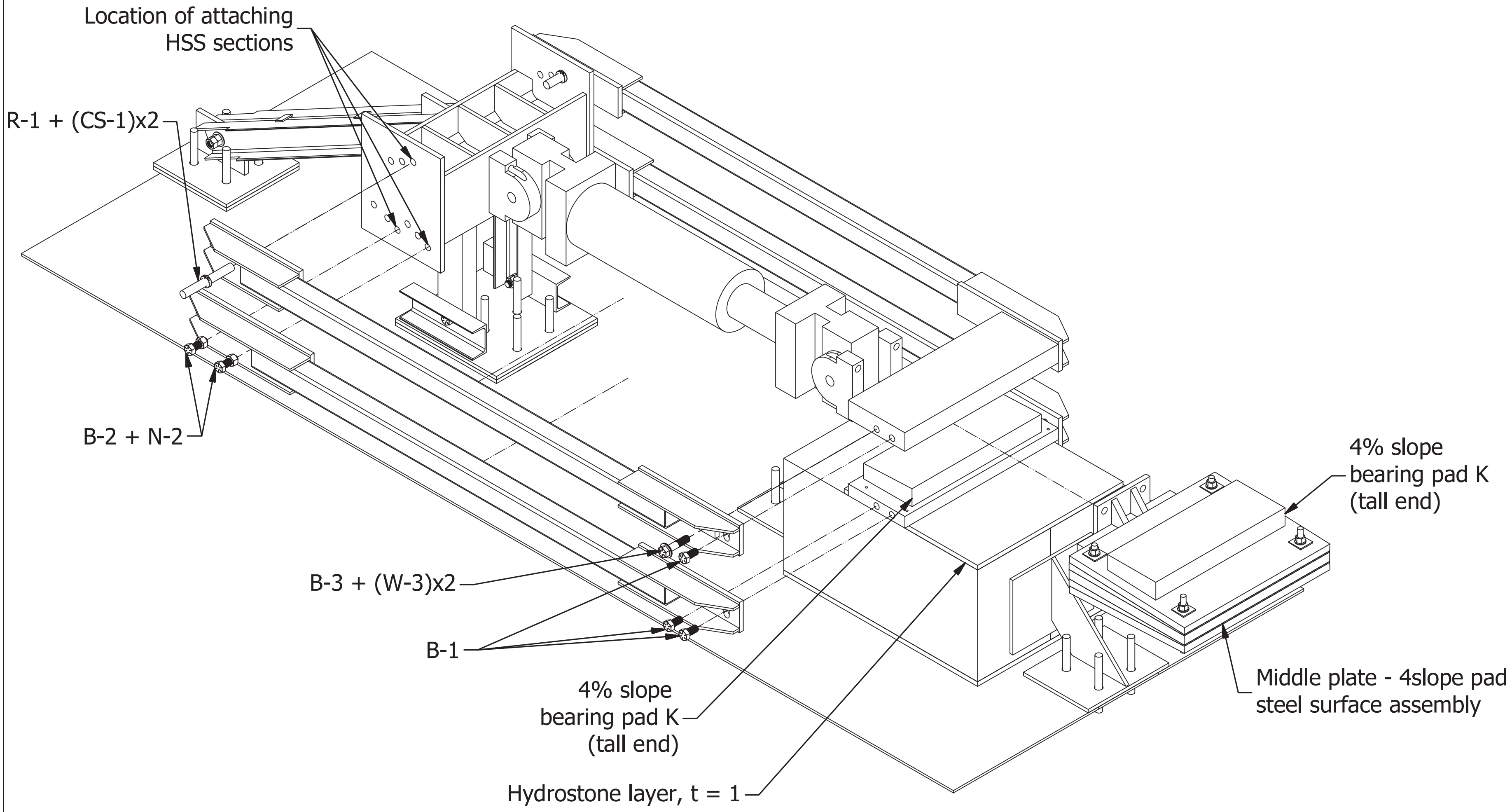

4% Tapered full-size K pad, steel surface test assembly - Exploded Isometric View				*Scale*	0 2′ 4′
Test assembly	*11/12/2019*	*University of Florida*	*SHEET 63 OF 93*	*Revision:*	

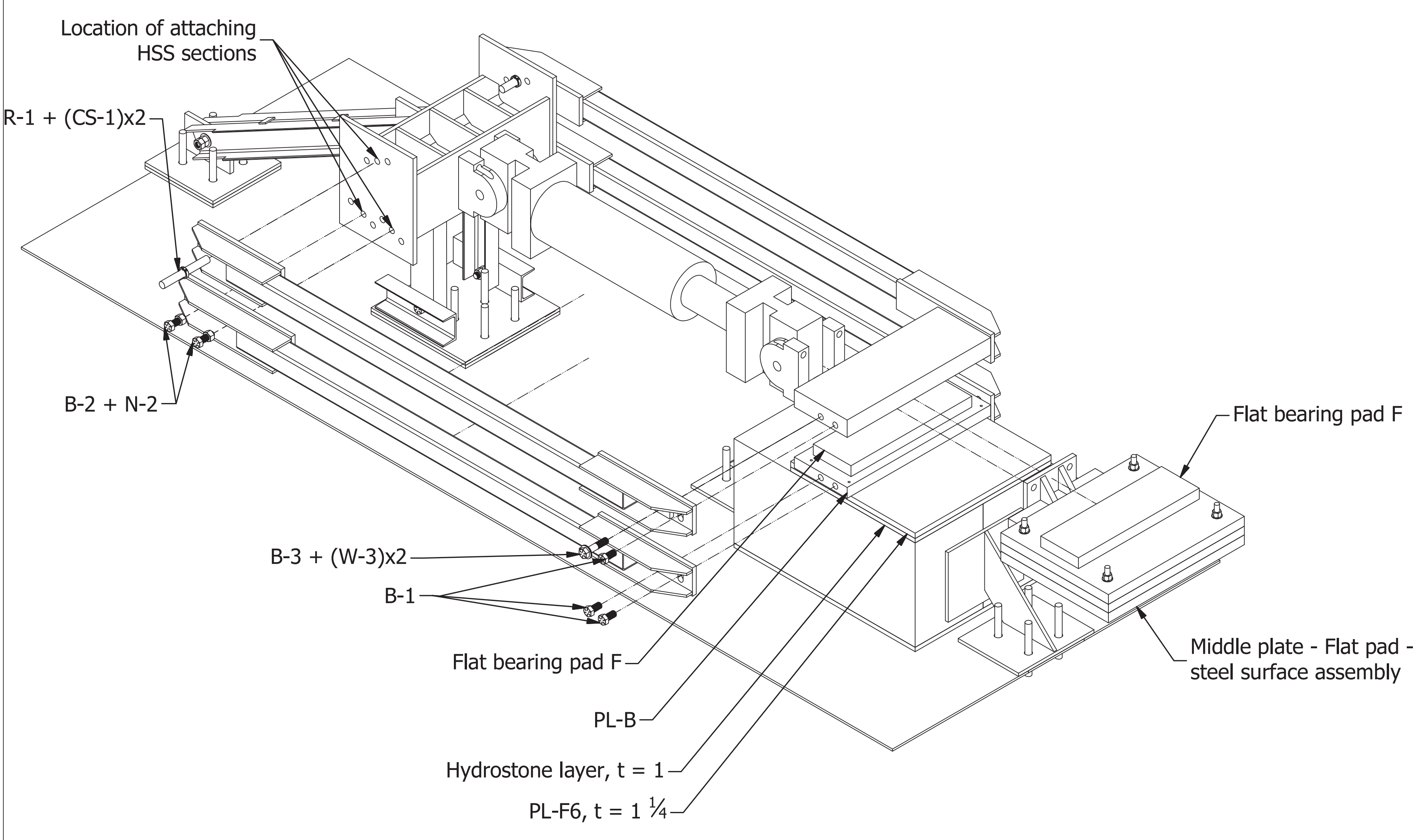

Flat full-size F pad, concrete surface test assembly - Exploded Isometric View				*Scale* 0 2′ 4′
Test assembly	*11/12/2019*	*University of Florida*	*SHEET 64 OF 93*	*Revision:*

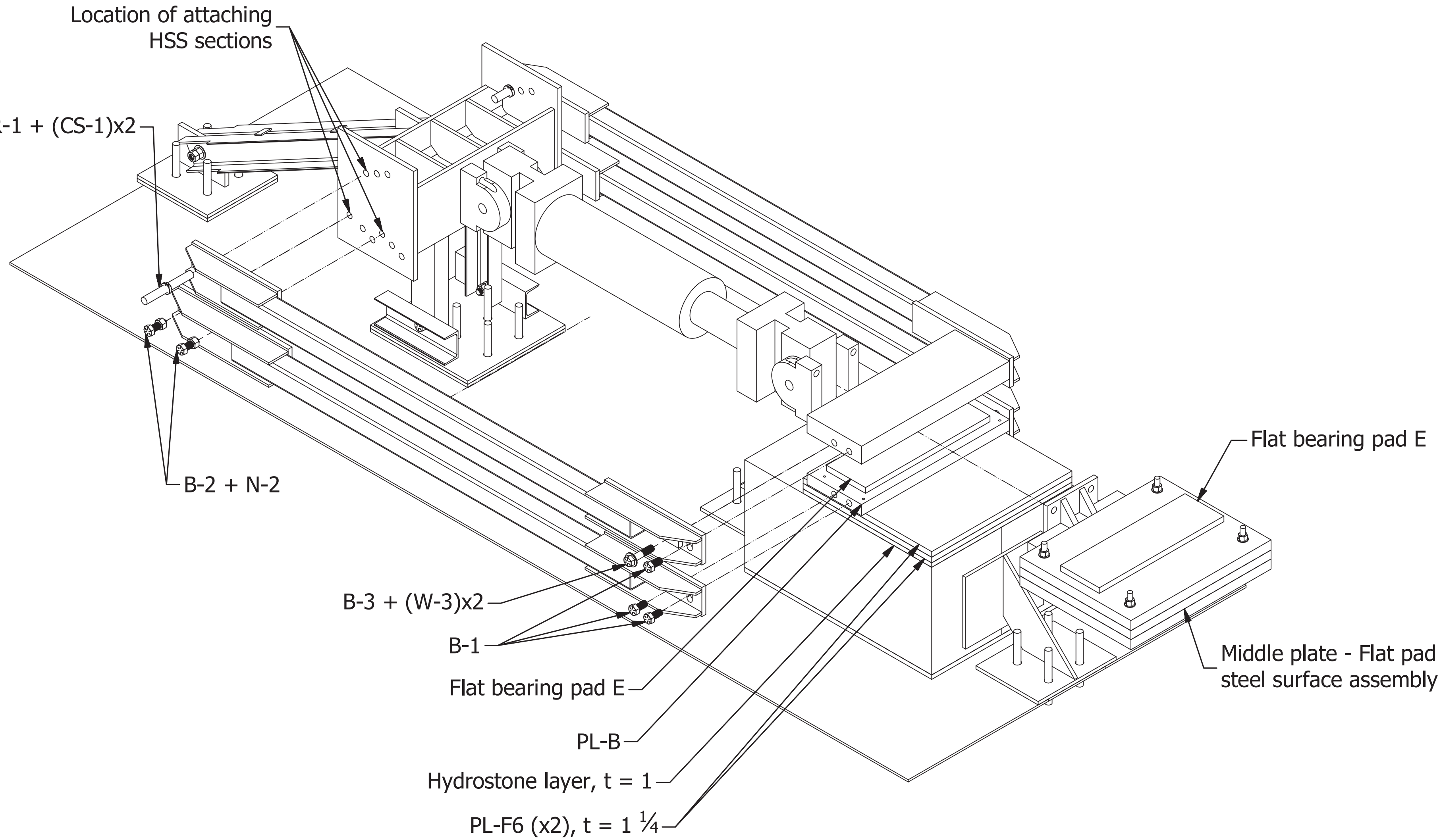

Flat full-size E pad, concrete surface test assembly - Exploded Isometric View				*Scale*	0 2′ 4′
Test assembly	*11/12/2019*	*University of Florida*	*SHEET 65 OF 93*	*Revision:*	

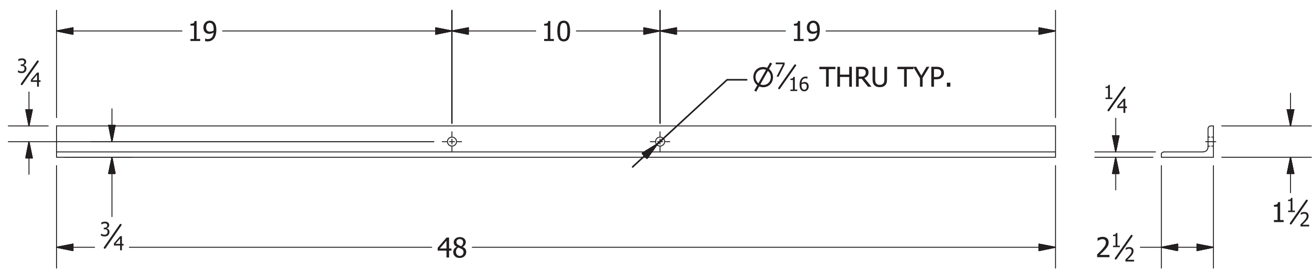

Elevation View

Cross-section

A-1 (L 2.5x1.5x0.250)

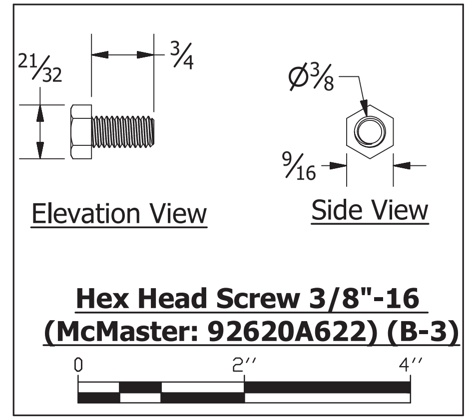

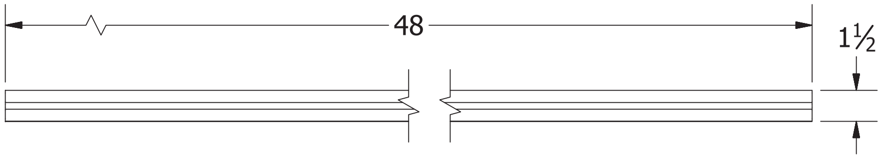

Elevation View

Cross-section

T-1 (Slotted framing)
(McMaster: 47065T507)

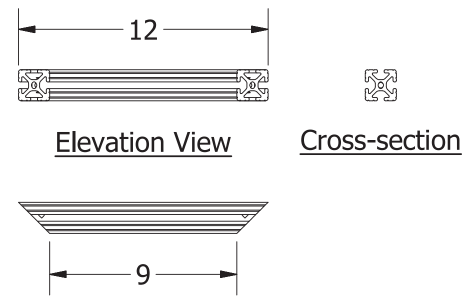

Elevation View

Cross-section

Top View

T-3 (Slotted framing)
(McMaster: 47065T270)

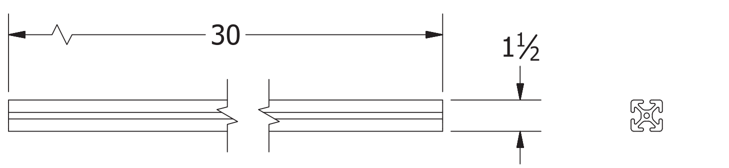

Elevation View

Cross-section

T-2 (Slotted framing)
(McMaster: 47065T507)

PARTS LIST - 13					
ITEM	PART NAME	CROSS-SECTION	LENGTH	QTY	MATERIAL
1	A-1	L 2.5X1.5X0.250	38	2	STEEL, Gr-50
2	T-1	1.5x1.5	48	4	Aluminum
3	T-2	1.5x1.5	30	6	Aluminum
4	T-3	1.5x1.5	9	6	Aluminum
5	B-3	DIA-$\frac{3}{8}$	3/4	4	STEEL, Gr-8

Instrumentation: A-1, T-1, T-2 and B-3

Scale

11/12/2019 | *University of Florida* | *SHEET 66 OF 93*

Revision:

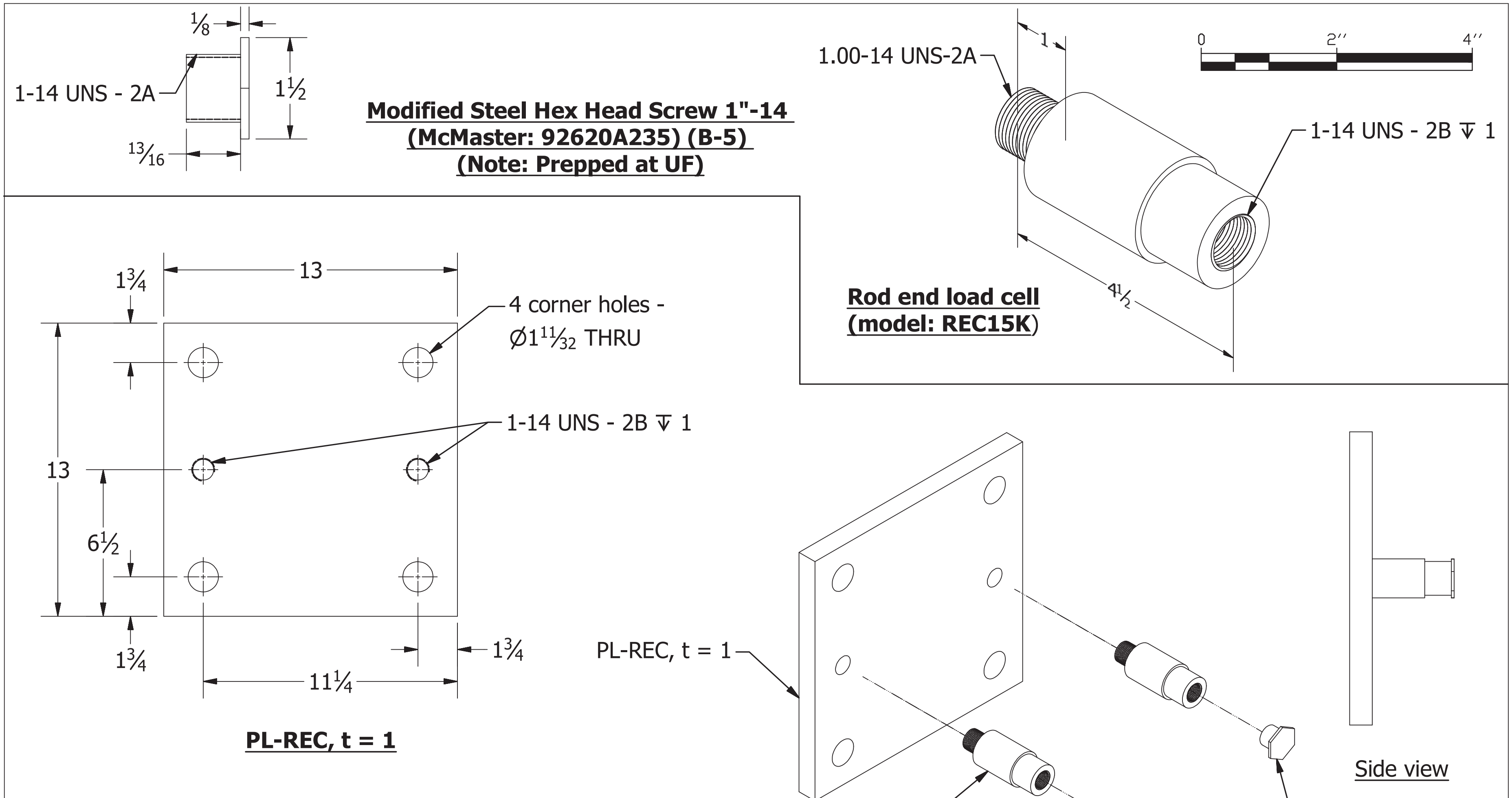

PARTS LIST - 14					
ITEM	PART NAME	CROSS-SECTION	LENGTH	QTY	MATERIAL
1	PL-REC	13x1	13	1	STEEL, Gr-36
2	REC-15K	DIA	4.5	2	-
3	B-5	DIA-1	0.8	2	STEEL, Gr-150

Instrumentation: PL-REC, REC-15 and chair glide

Scale 0 6'' 12''

Test assembly	*11/12/2019*	*University of Florida*	*SHEET 67 OF 93*	*Revision:*		

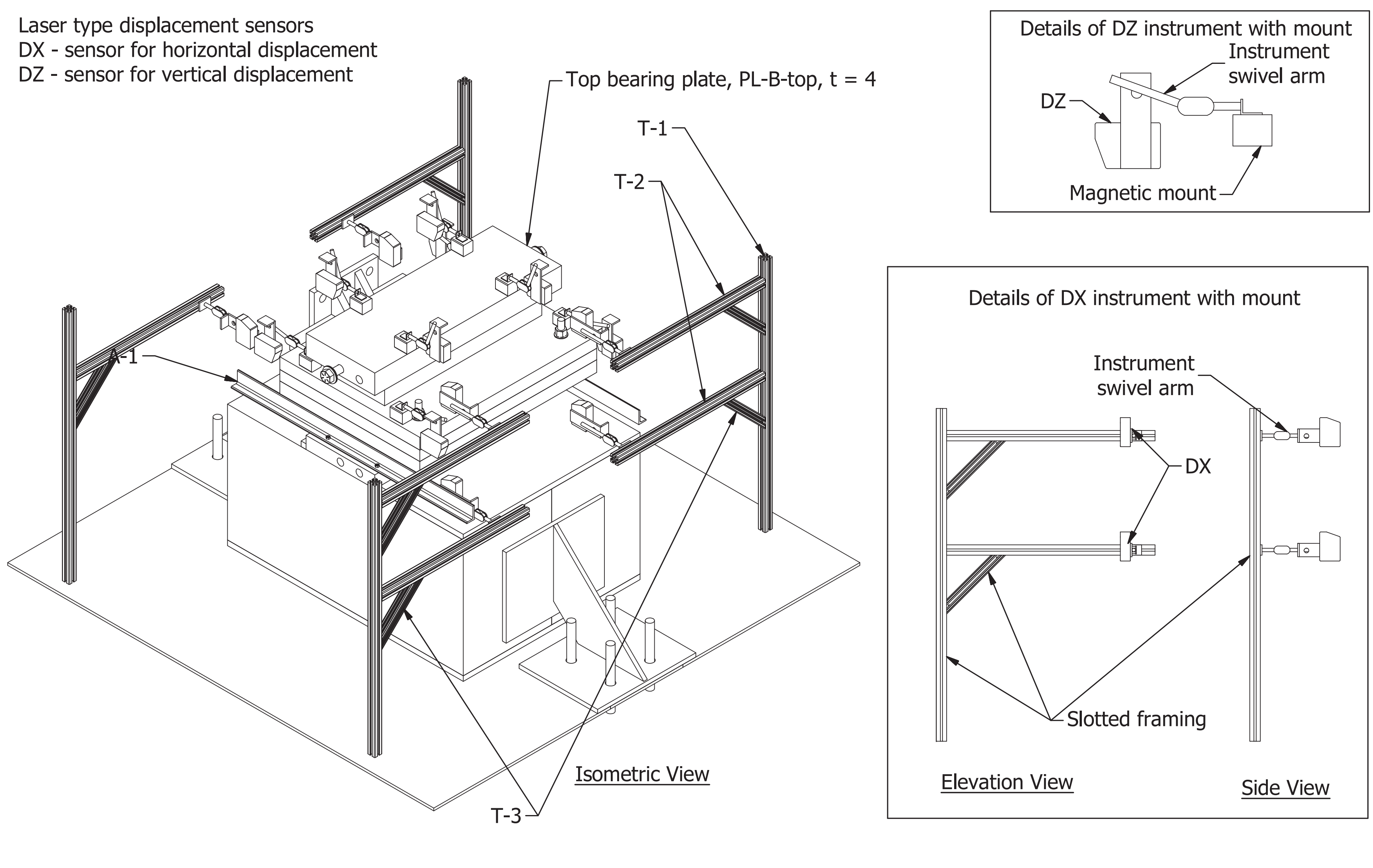

Instrumentation Assembly at Bearing Pad End			*Scale*	0 18'' 36''
	11/12/2019	*University of Florida*	*SHEET 68 OF 93*	*Revision:*

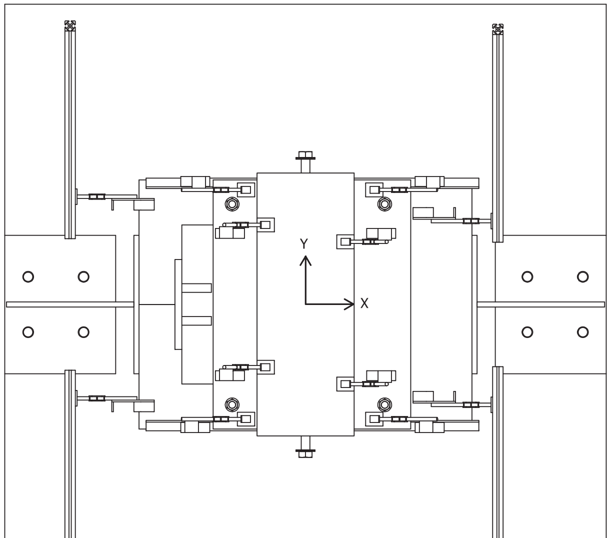

Top View

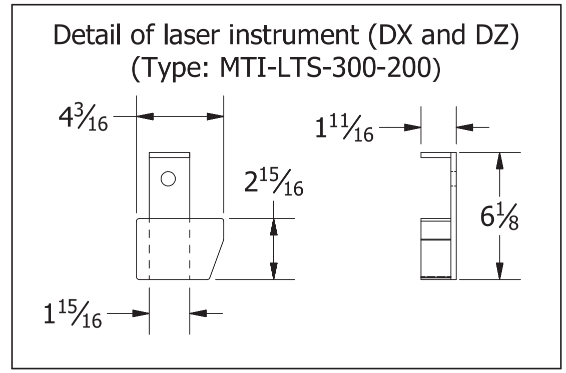

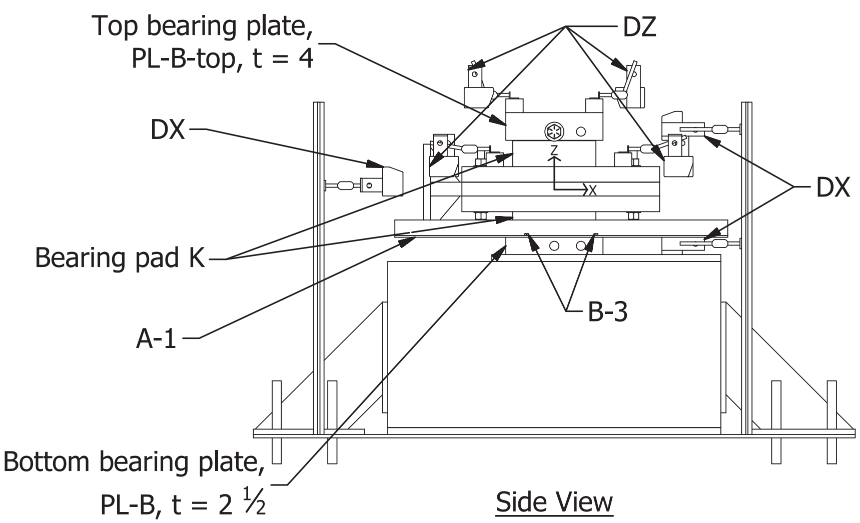

Side View

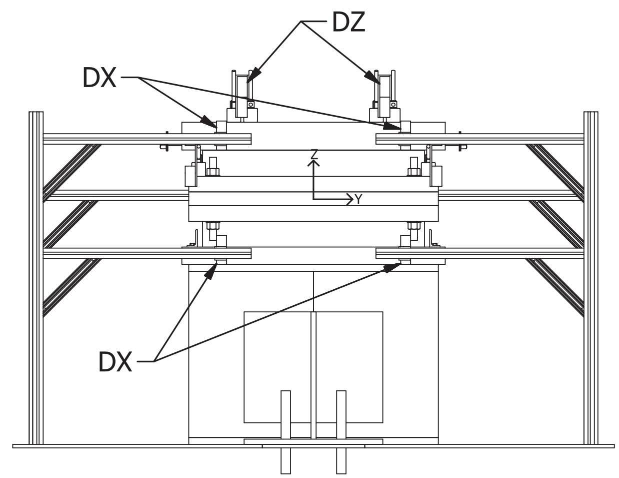

Front View

Instrumentation Assembly - Placement of both DX and DZ				Scale 0 2′ 4′
Test assembly	11/12/2019	University of Florida	SHEET 69 OF 93	Revision:

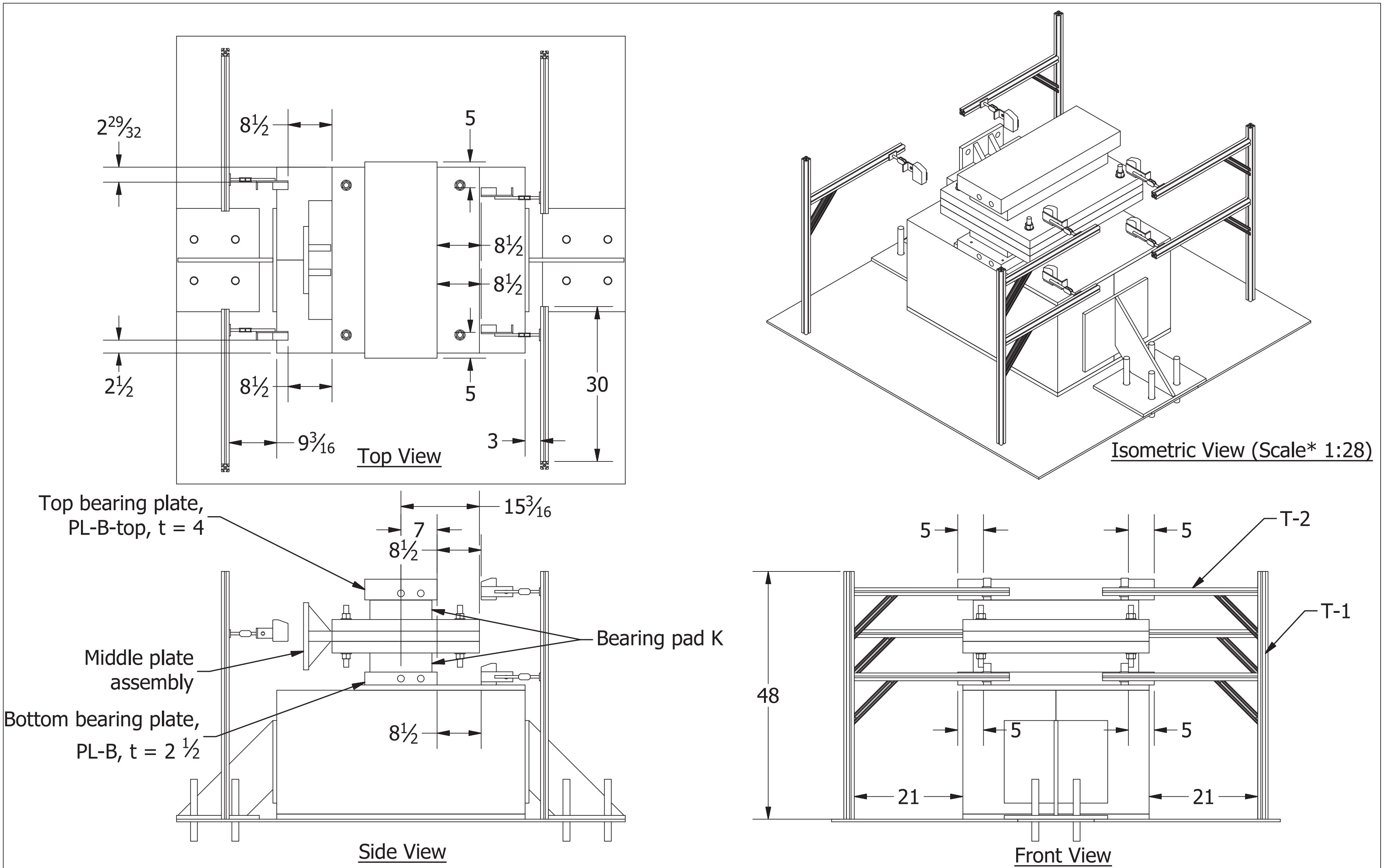

Instrumentation Assembly - Placement Detail Views for DX			*Scale* 0 2′ 4′
Test assembly	*11/12/2019*	*University of Florida*	*SHEET 70 OF 93*
Revision:			

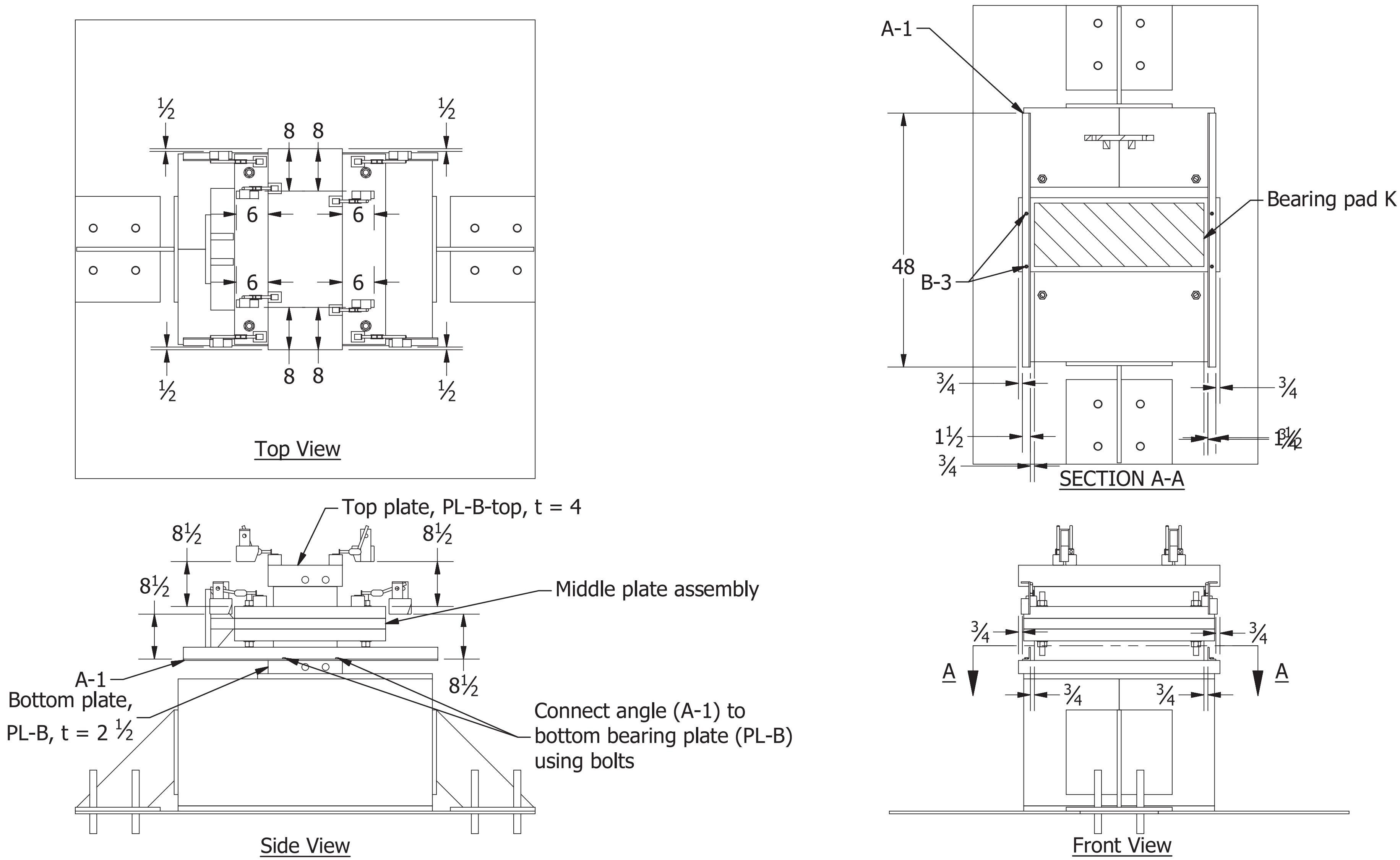

Instrumentation Assembly - Placement Detail Views for DZ			
Test assembly	*11/12/2019*	*University of Florida*	*SHEET 71 OF 93*
Scale 0 2′ 4′			
Revision:			

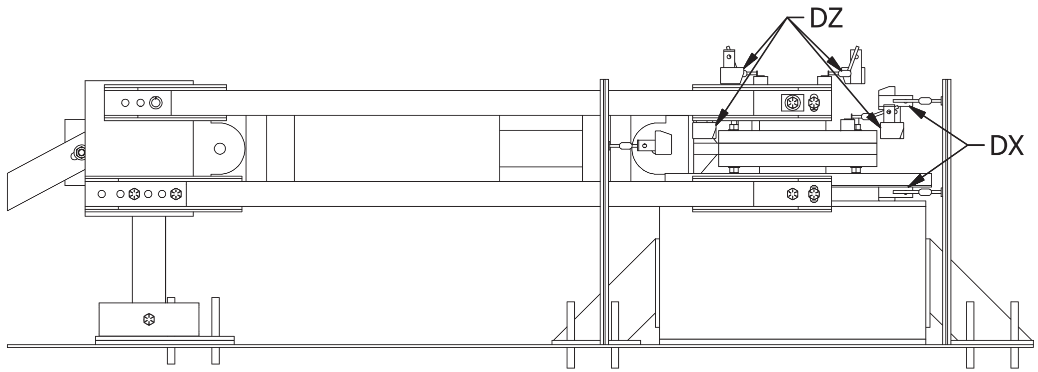

Elevation View

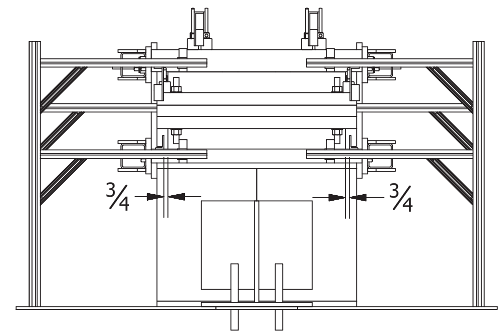

Front View

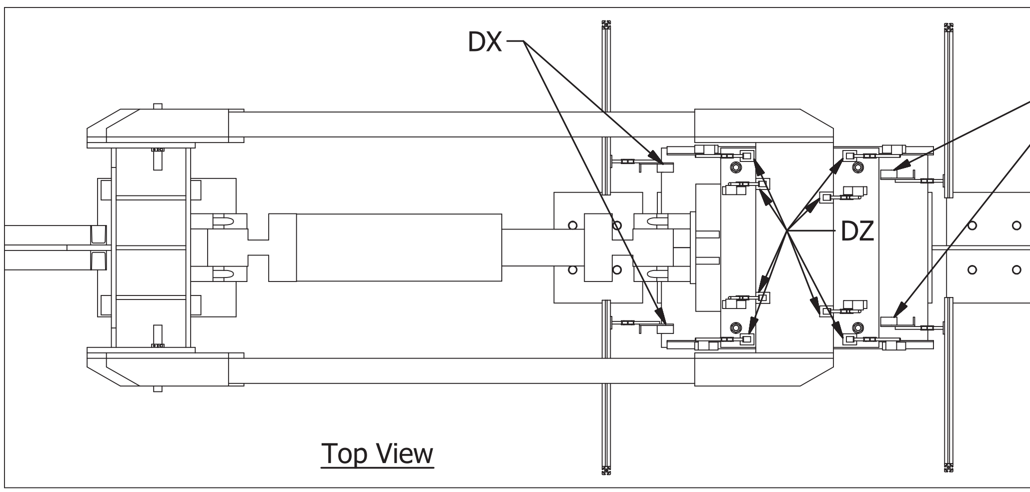

Top View

Instrumentation Assembly for Flat K-type pad - Detailed Views				*Scale*		
Test assembly	*11/12/2019*	*University of Florida*	*SHEET 72 OF 93*	*Revision:*		

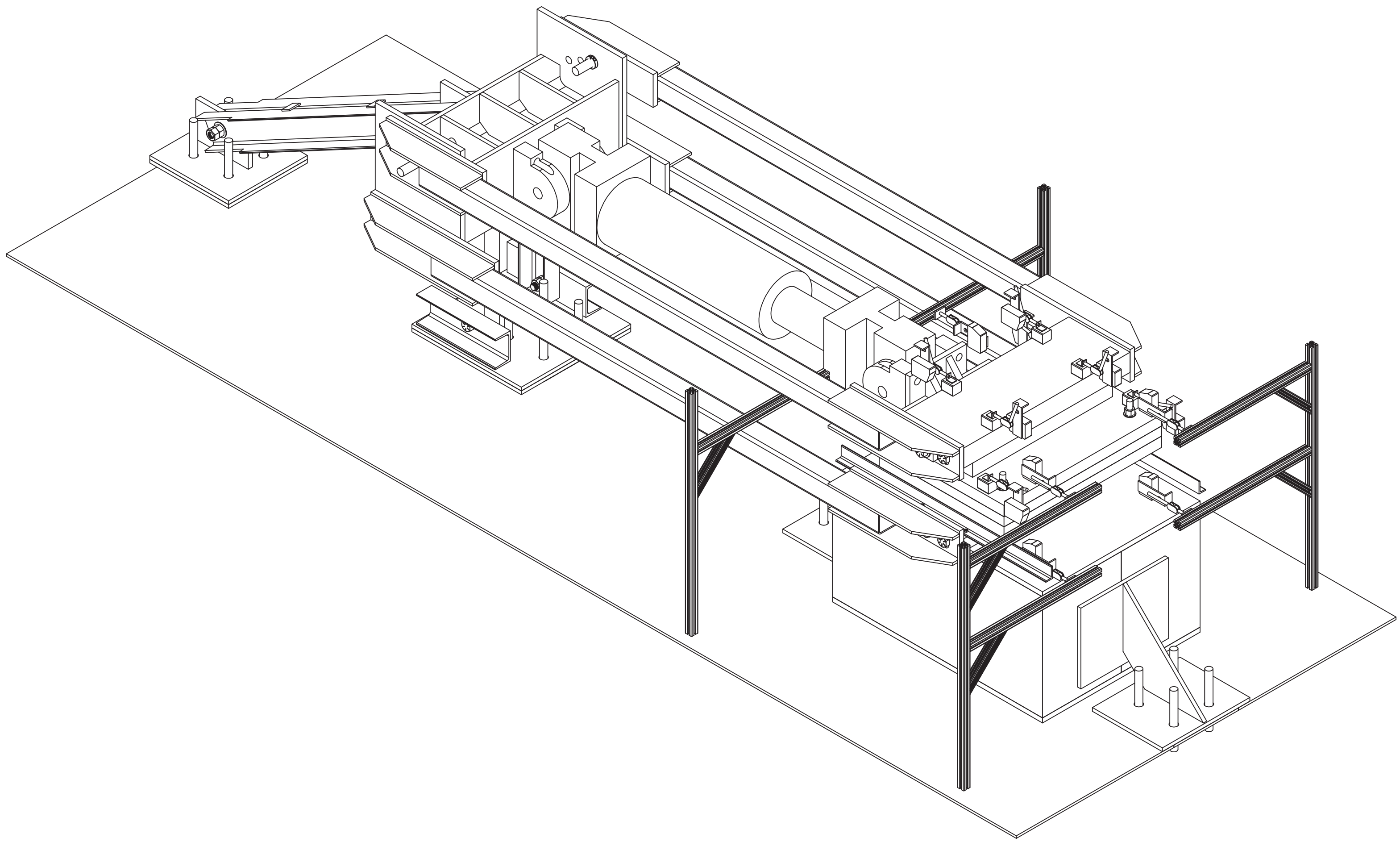

Instrumentation Assembly for Flat K-type pad				Scale 0 2′ 4′
Test assembly	11/12/2019	University of Florida	SHEET 73 OF 93	Revision:

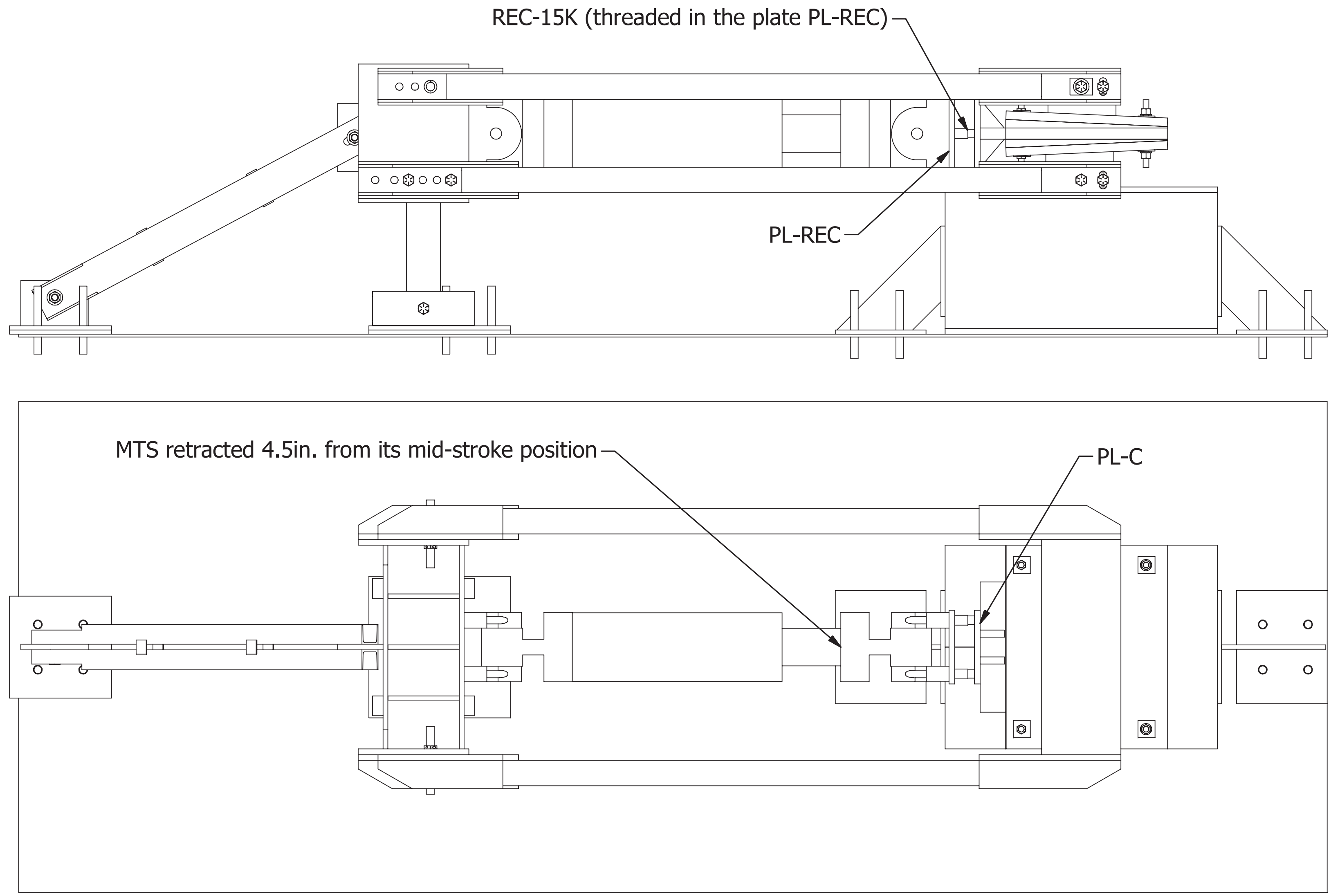

Additional REC-15K Instrumentation Assembly for Tapered pads (here: K-type pad)				*Scale*	0 24'' 48''
Test assembly	*11/12/2019*	*University of Florida*	*SHEET 74 OF 93*	*Revision:*	

Step 1: The test setup is at rest and MTS is at midstroke. Enerpac is extracted by 9 in. Place scissors jack between top and bottom HSS (HT and HB).

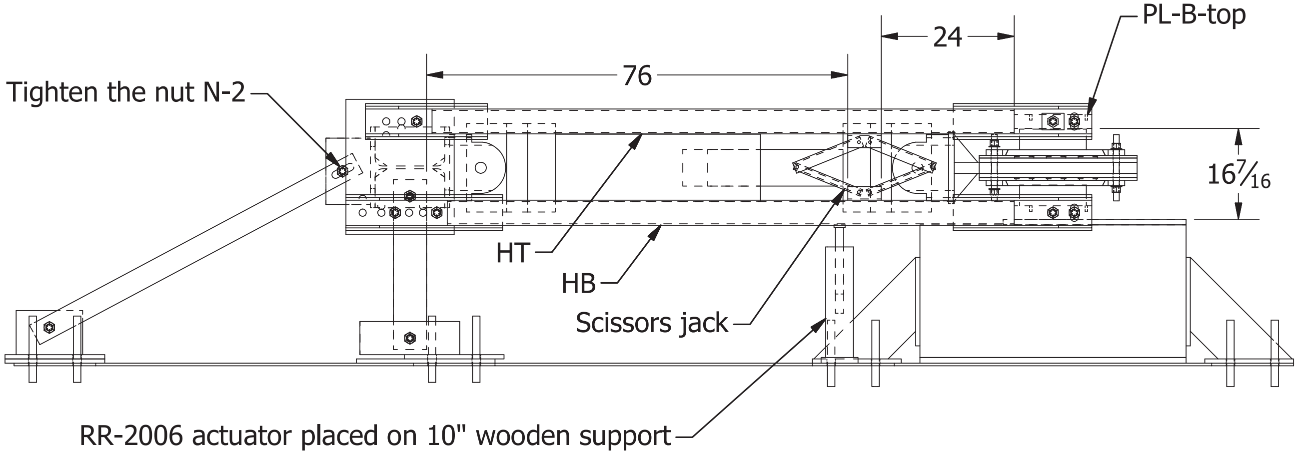

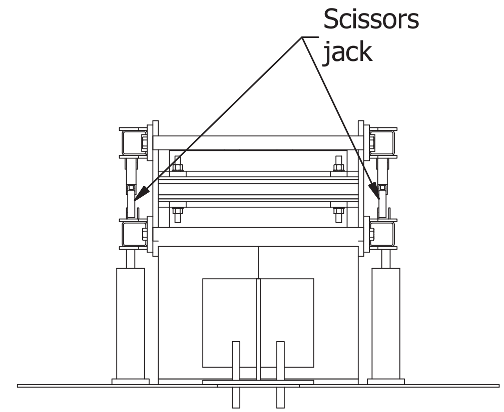

Step 2: Use scissors jack to lift the top HSS (HT) and top bearing plate (PL-B-top) to create a clearance of ~5" between top bearing pad and bearing plate.

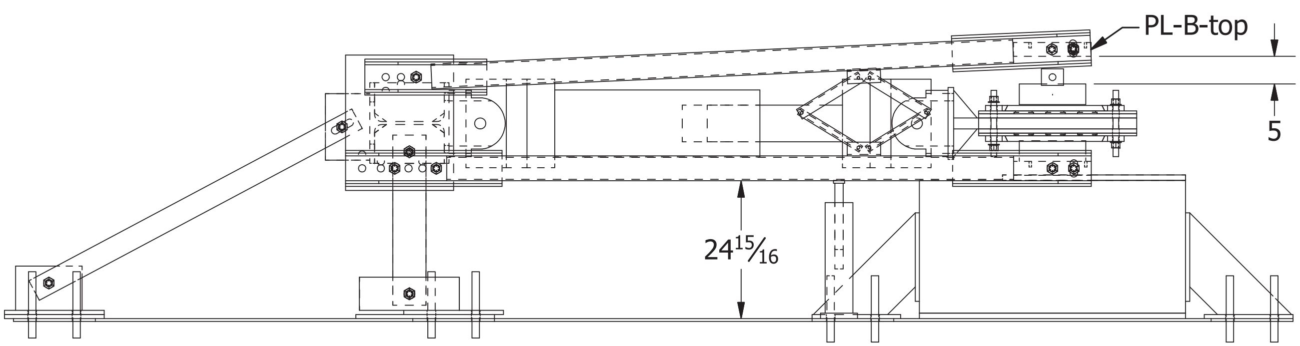

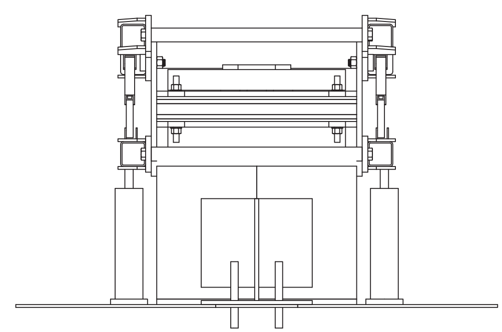

Instructions set 1: From type flat pad K to tapered pad K				Scale 0 2.5′ 4.5′
Bearing pad replacing sequence	11/12/2019	University of Florida	SHEET 75 OF 93	Revision:

Step 3: Lift the top bearing pad by about 4 in. using forklift. A clearance of approximately 1 in. between the bearing pad and top bearing plate (PL-B-top) is available for removing the bearing pad.

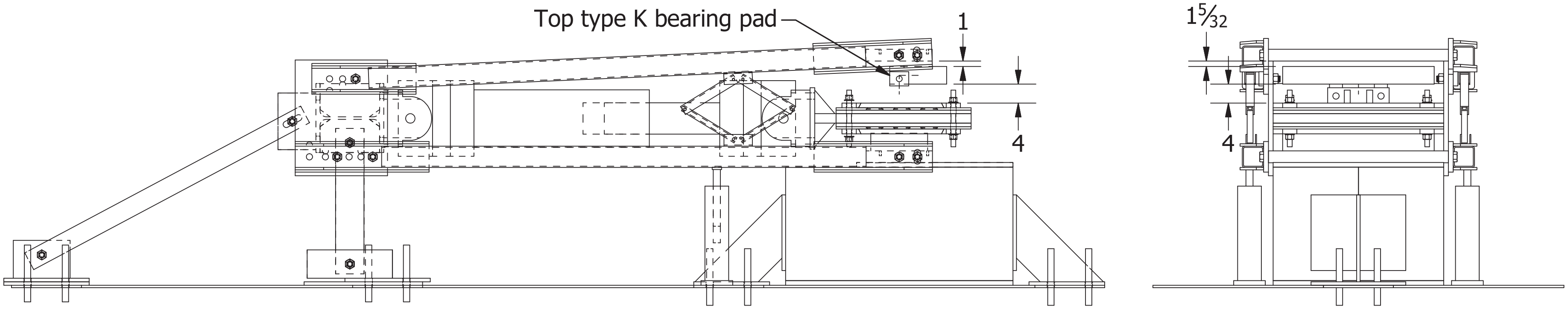

Step 4: Remove the top bearing pad using a forklift.

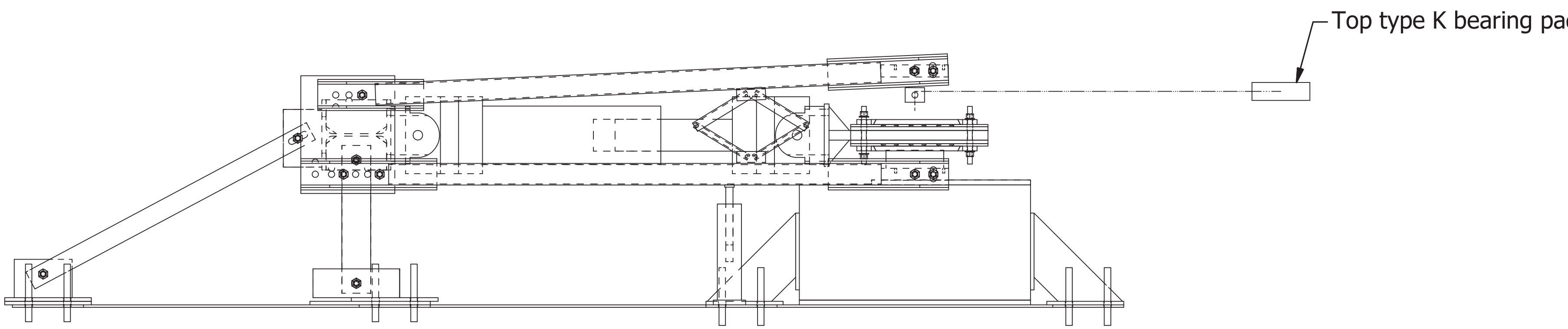

Instructions set 1: From type flat pad K to tapered pad K				Scale	0 2.5′ 4.5′
Bearing pad replacing sequence	11/12/2019	University of Florida	SHEET 76 OF 93	Revision:	

Step 5: Lift the middle plate using overhead crane connected to MTS to get a clearance of about 6 in. between the middle plate and bottom bearing pad.

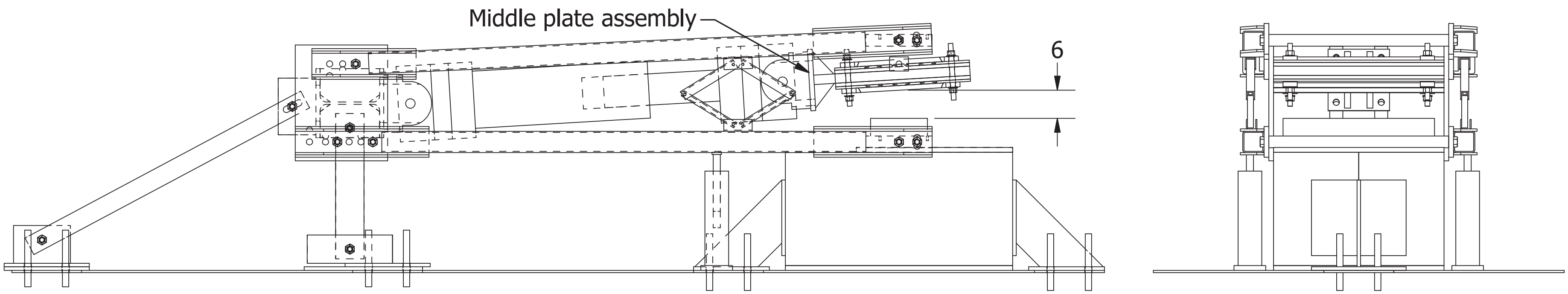

Step 6: Lift bottom bearing pad by 3 inches and remove using a forklift.

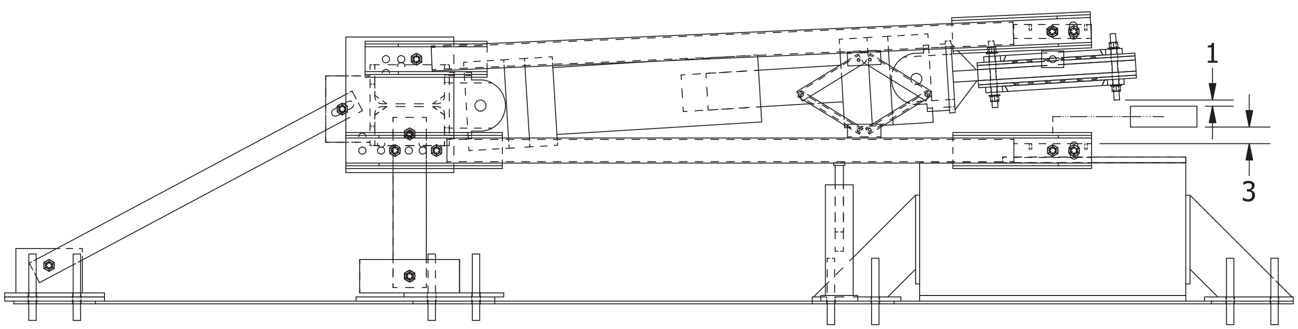

Instructions set 1: From type flat pad K to tapered pad K				*Scale*	0 2.5′ 4.5′
Bearing pad replacing sequence	*11/12/2019*	*University of Florida*	*SHEET 77 OF 93*	*Revision:*	

Step 7: Bring the middle plate back to its original position

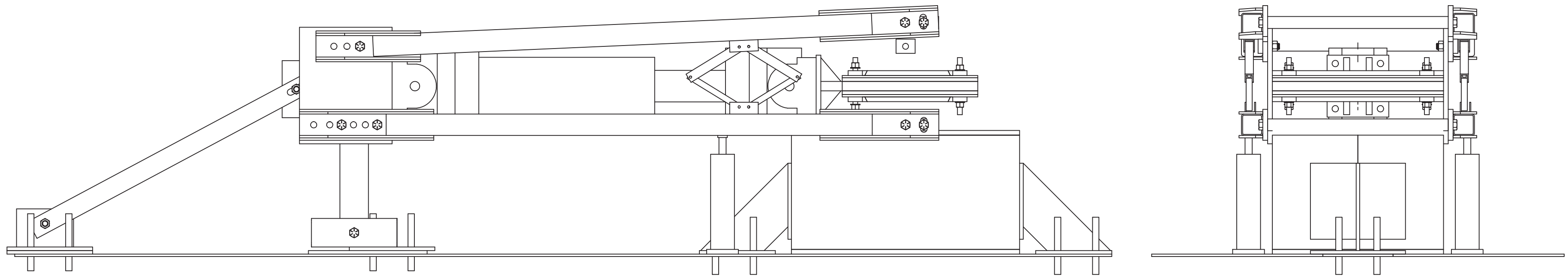

Step 8: Remove the middle plate assembly using a forklift

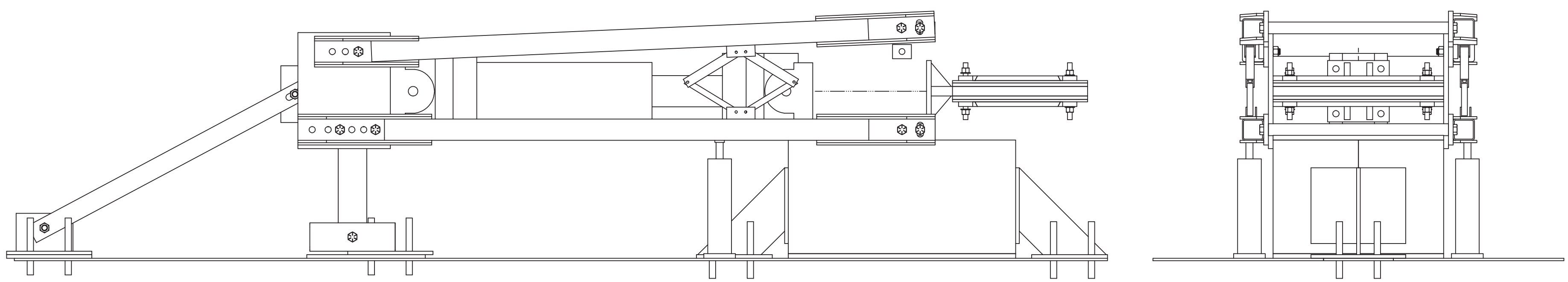

Instructions set 1: From type flat pad K to tapered pad K			Scale: 0, 2.5′, 4.5′
Bearing pad replacing sequence	11/12/2019	University of Florida	SHEET 78 OF 93
			Revision:

Step 9: Place the bottom tapered K bearing pad using a forklift.

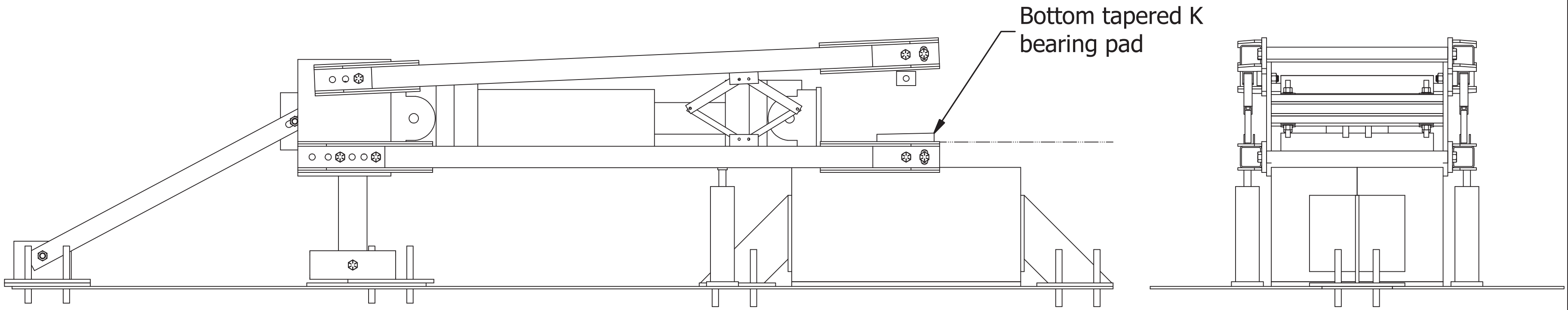

Step 10: Connect the middle plate configured for the corresponding tapered bearing pad.

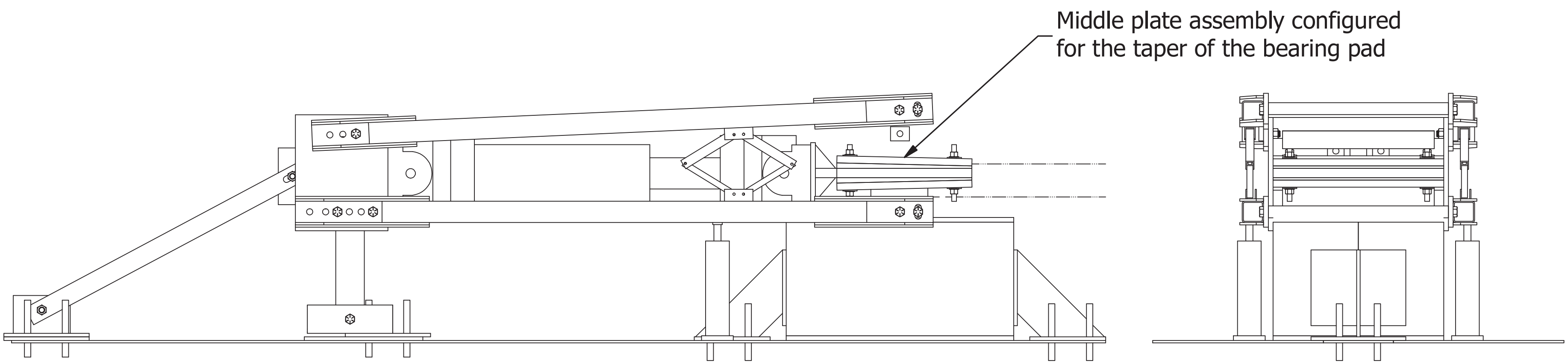

Instructions set 1: From type flat pad K to tapered pad K				*Scale* 0 2.5′ 4.5′
Bearing pad replacing sequence	*11/12/2019*	*University of Florida*	*SHEET 79 OF 93*	*Revision:*

Step 11: Place the top tapered K bearing pad using a forklift.

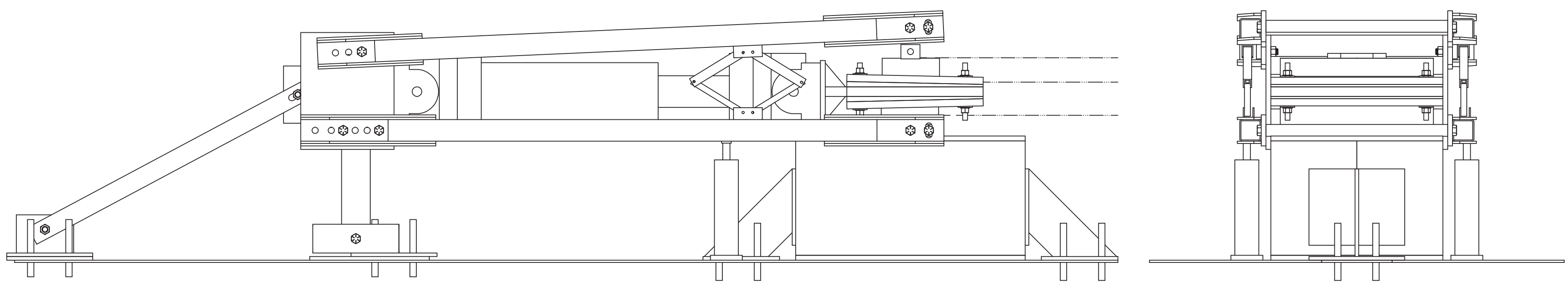

Step 12: Lower the top bearing pad using the scissor jacks.

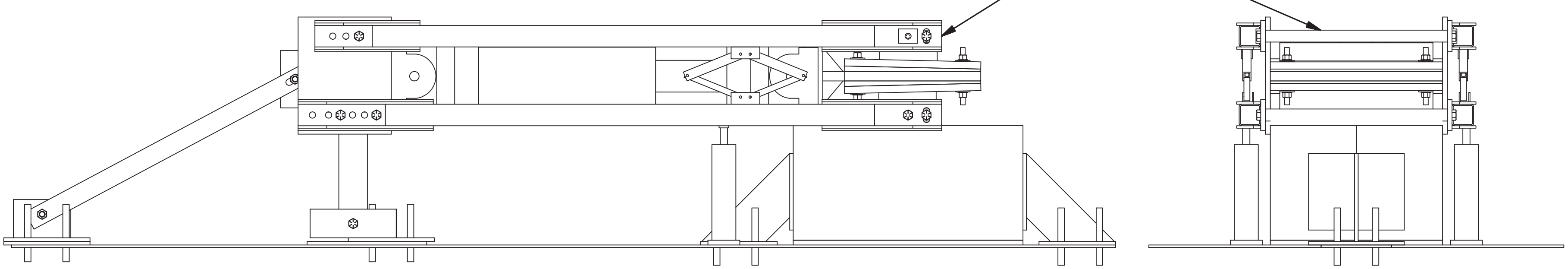

Instructions set 1: From type flat pad K to tapered pad K				*Scale*	0 2.5′ 4.5′	
Bearing pad replacing sequence	*11/12/2019*	*University of Florida*	*SHEET 80 OF 93*	*Revision:*		

Step 1: Follow steps 1 to 8 from Instructions set 1 to remove the middle plate assembly and bearing pads from the setup.

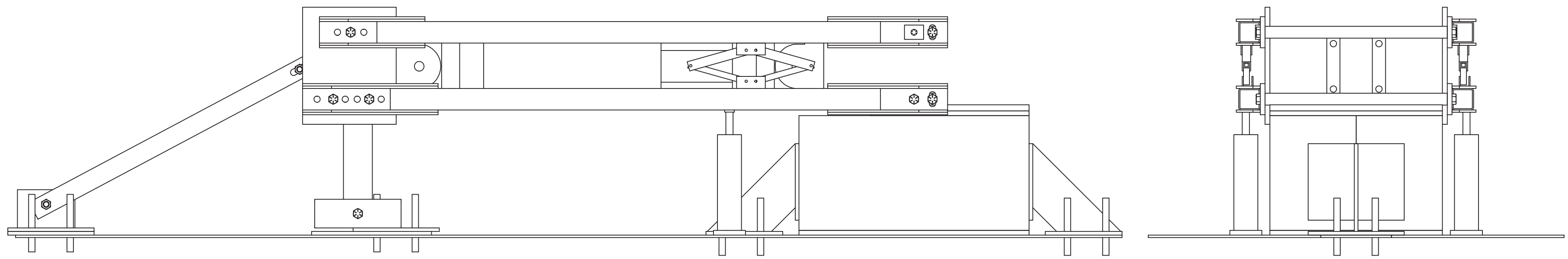

Step 2: Place dunnage between top and bottom bearing plates and remove the scissors jacks.

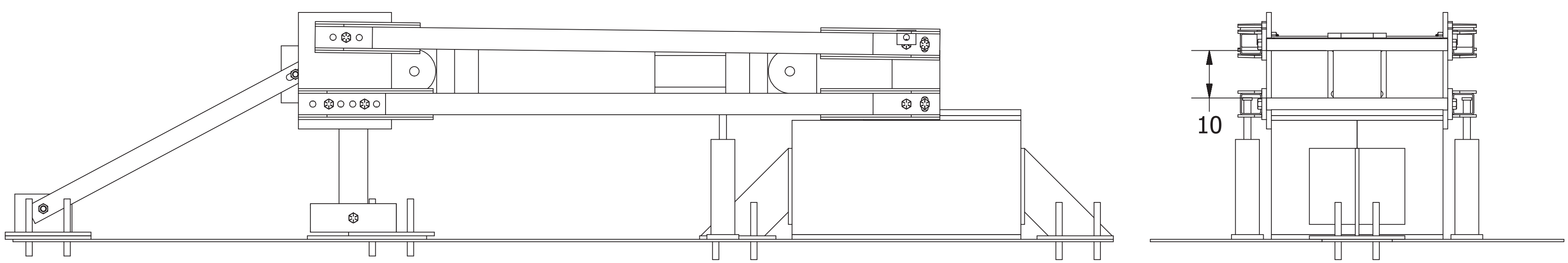

Instructions set 2: From type flat pad F to flat pad K				Scale 0 2.5′ 4.5′
Bearing pad replacing sequence	11/12/2019	University of Florida	SHEET 81 OF 93	Revision:

Step 3: Disengage one of the bottom HSS (HB) bolts and raise the bearing plates and remove PL-F6 and hydrostone layer

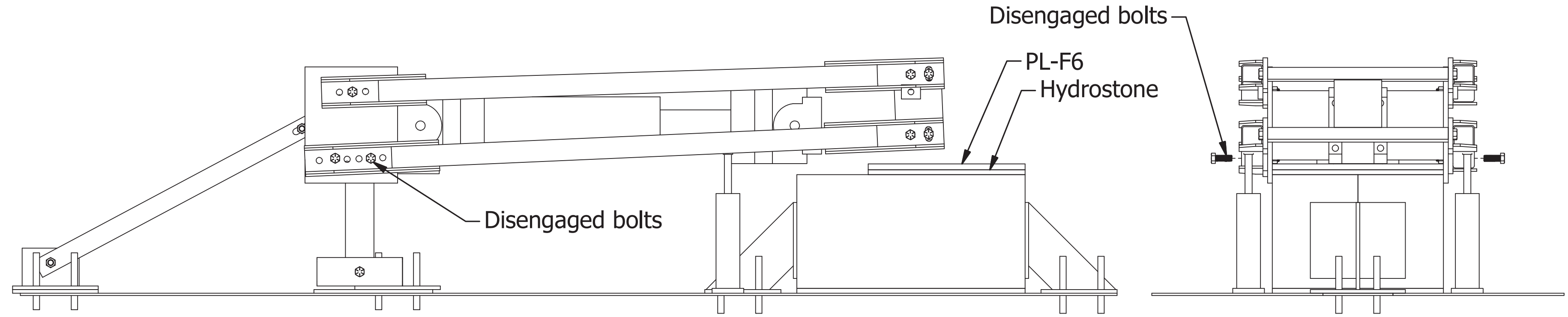

Step 4: Lower and rest PL-B on four 1 in. thick spacers. Construct a new layer of hydrostone (t = 1) between PL-B and steel blocks.

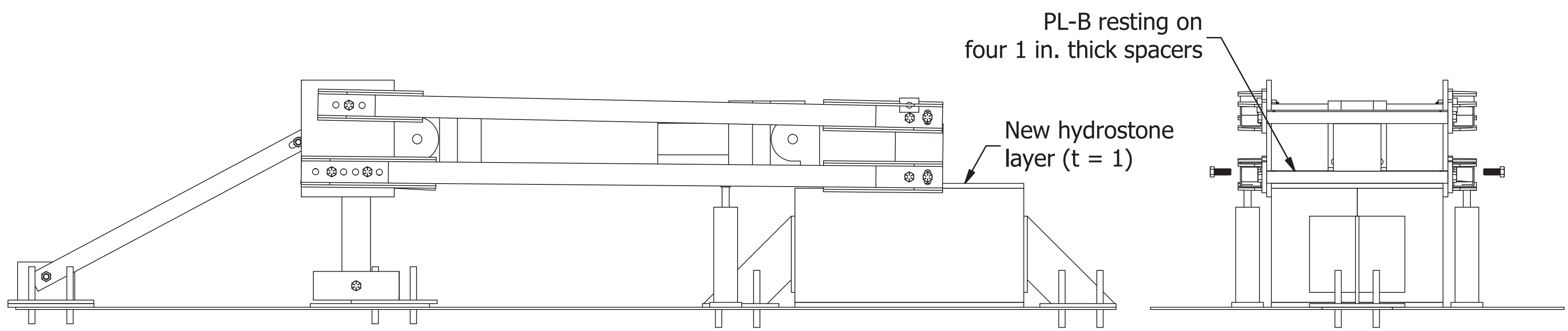

Instructions set 2: From type flat pad F to flat pad K				*Scale*	0 2.5′ 4.5′
Bearing pad replacing sequence	*11/12/2019*	*University of Florida*	*SHEET 82 OF 93*	*Revision:*	

Step 5: Disengage bolt and nut and lower the bottom HSS (HB) arms to match the hole levels for pad K (see sheet 56 of 90).

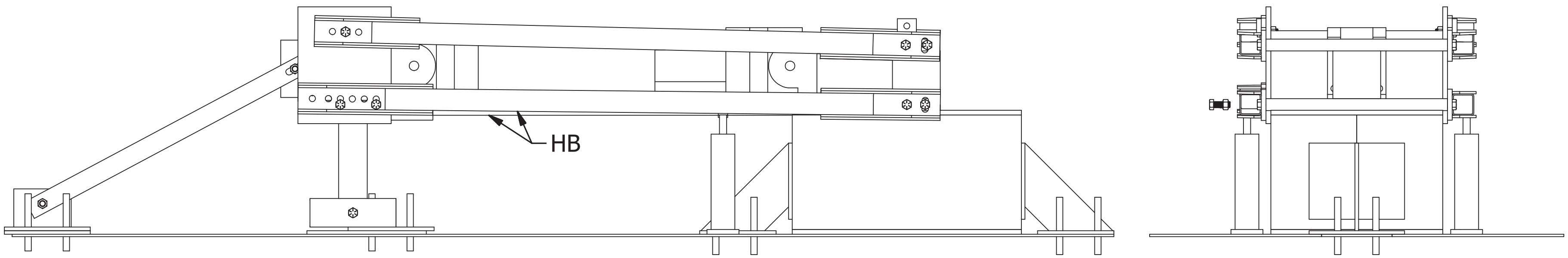

Step 6: Disengage bolt and nut and raise the top HSS (HT) arms to match the hole levels for pad K (see sheet 56 of 90).

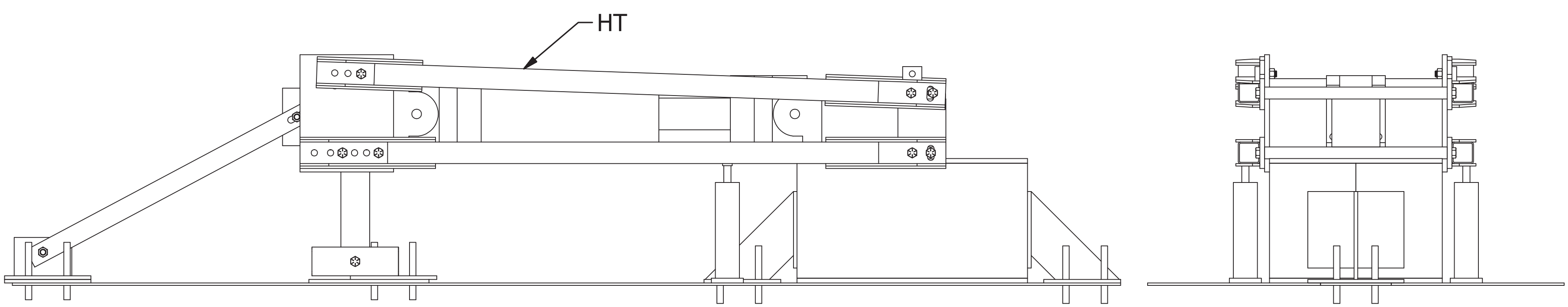

Instructions set 2: From type flat pad F to flat pad K			Scale 0 2.5′ 4.5′
Bearing pad replacing sequence	11/12/2019	University of Florida	SHEET 83 OF 93	Revision:

Step 7: Replace the dunnage with scissor jack and raise the top bearing plate.

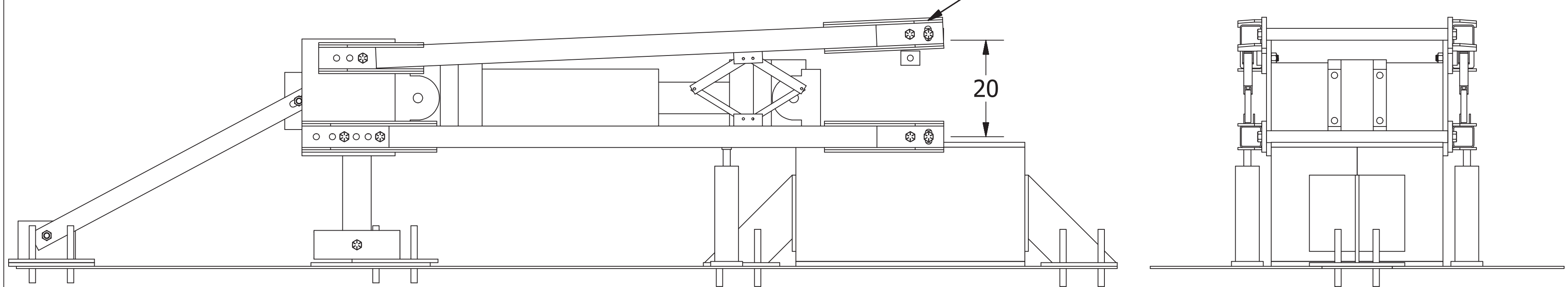

Step 8: Connect the middle plate assembly to the MTS.

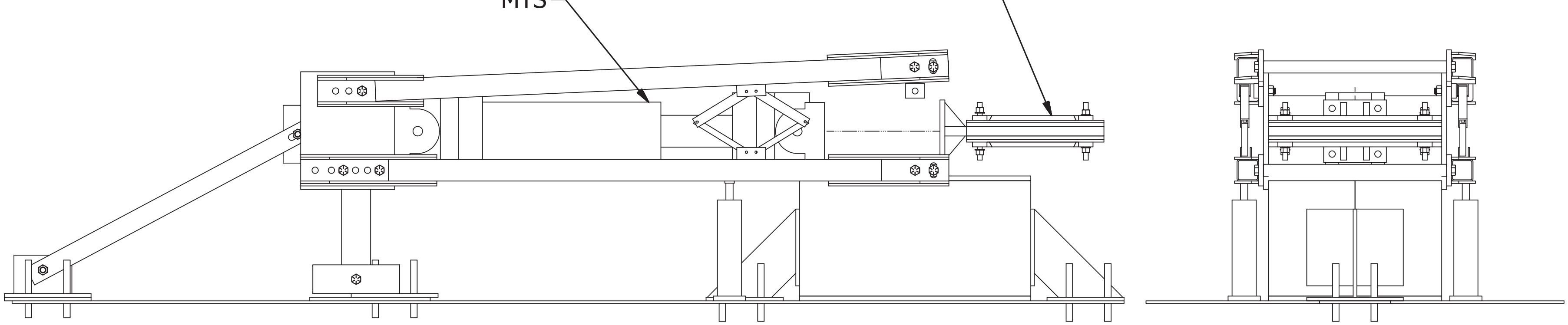

Instructions set 2: From type flat pad F to flat pad K				*Scale*	0 2.5′ 4.5′
Bearing pad replacing sequence	*11/12/2019*	*University of Florida*	*SHEET 84 OF 93*	*Revision:*	

Step 9: Adjust/check the MTS jack to the mid-stroke position.

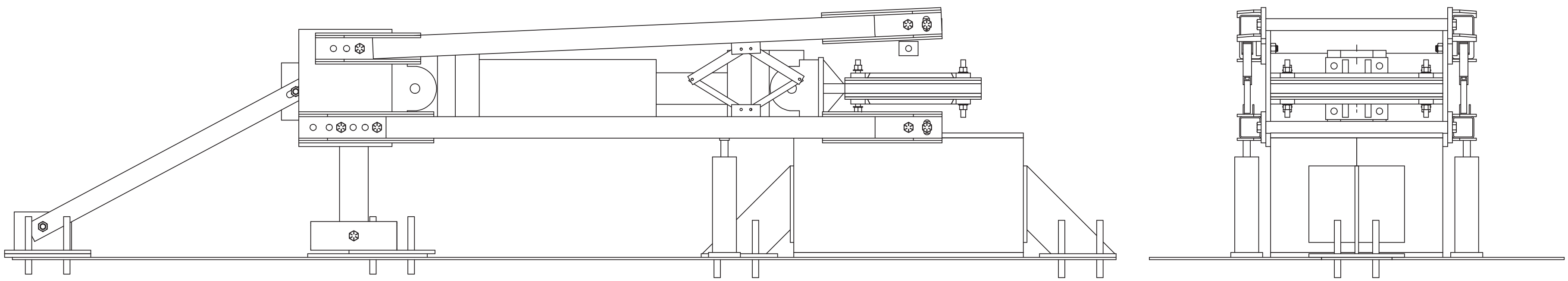

Step 10: Raise the middle plate assembly using overhead crane, and place the bottom bearing pad K in positions.

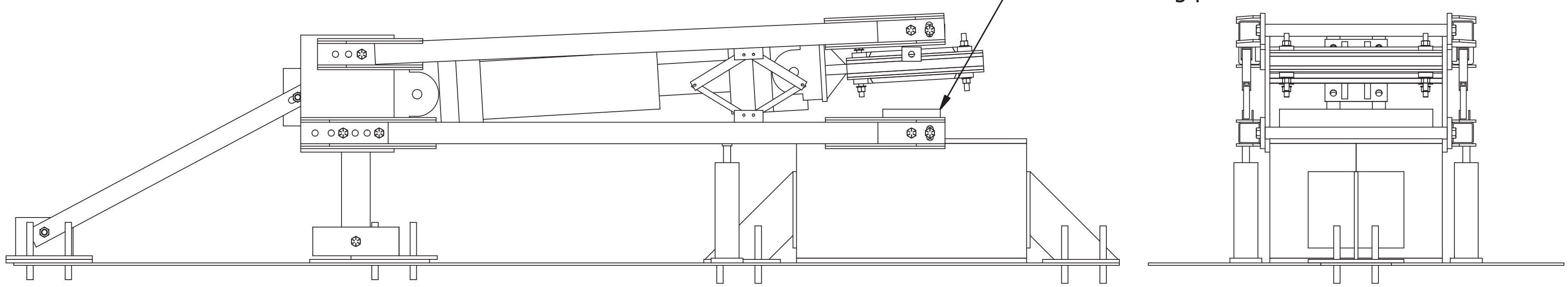

Instructions set 2: From type flat pad F to flat pad K				Scale	0 2.5′ 4.5′
Bearing pad replacing sequence	11/12/2019	University of Florida	SHEET 85 OF 93	Revision:	

Step 11: Lower the middle plate assembly and place the top bearing pad in place.

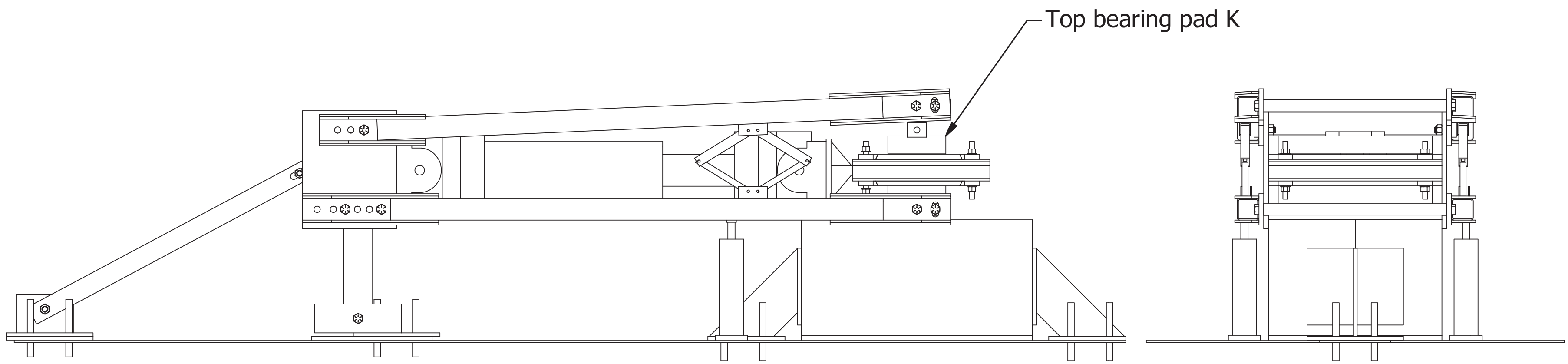

Step 12: Lower the top bearing plate.

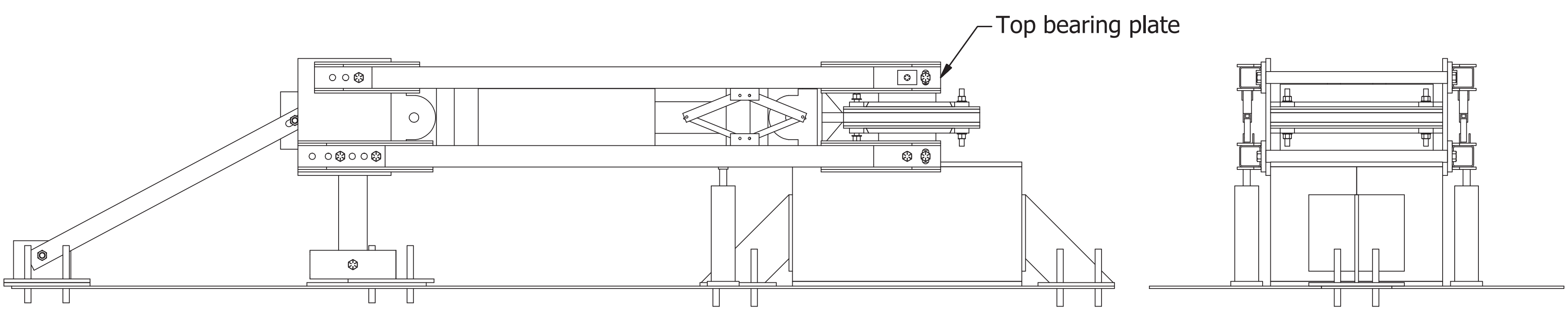

Instructions set 2: From type flat pad F to flat pad K				*Scale*		
Bearing pad replacing sequence	*11/12/2019*	*University of Florida*	*SHEET 86 OF 93*	*Revision:*		

Step 1: Place the pads in position

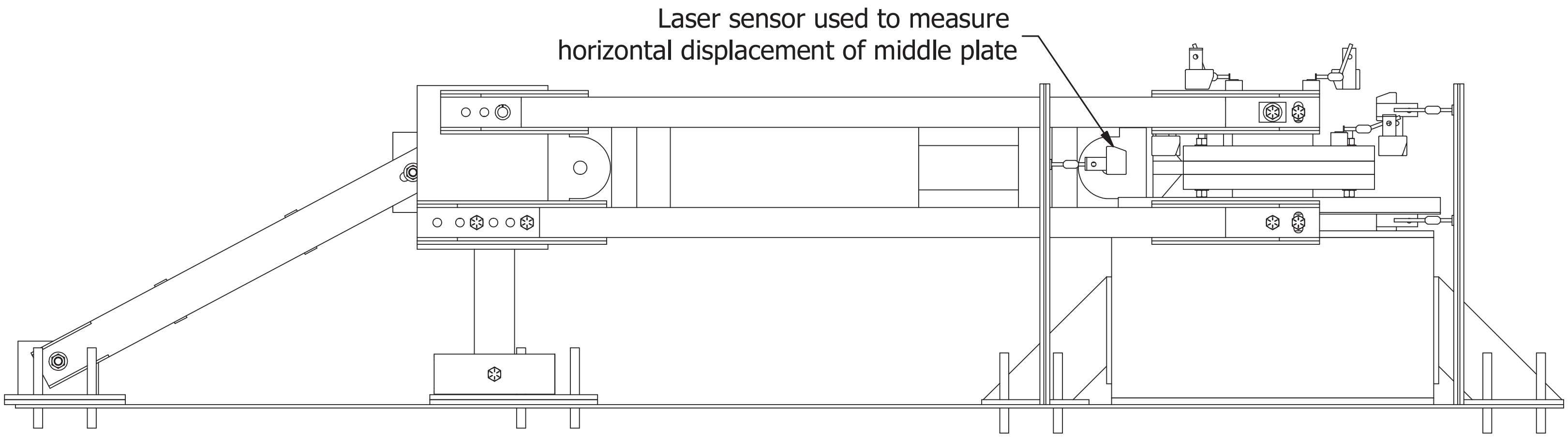

Step 2: Before compressing retract and rotate MTS to allow free movement of the middle plate

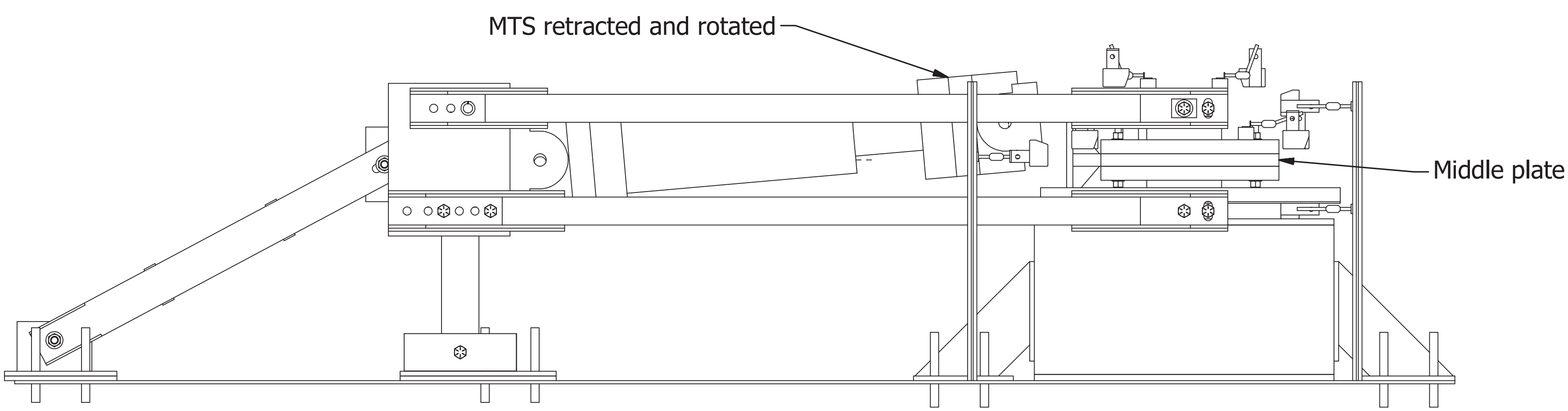

Instructions set 3: Retracting MTS jack for measurement of horizontal displacement in tapered pads				*Scale* 0 24′′ 48′′
	11/12/2019	*University of Florida*	*SHEET 87 OF 93*	*Revision:*

Steps for inserting REC-15K load cell

Step 1: Place bearing pad in position with MTS connected to the setup in midstroke position.

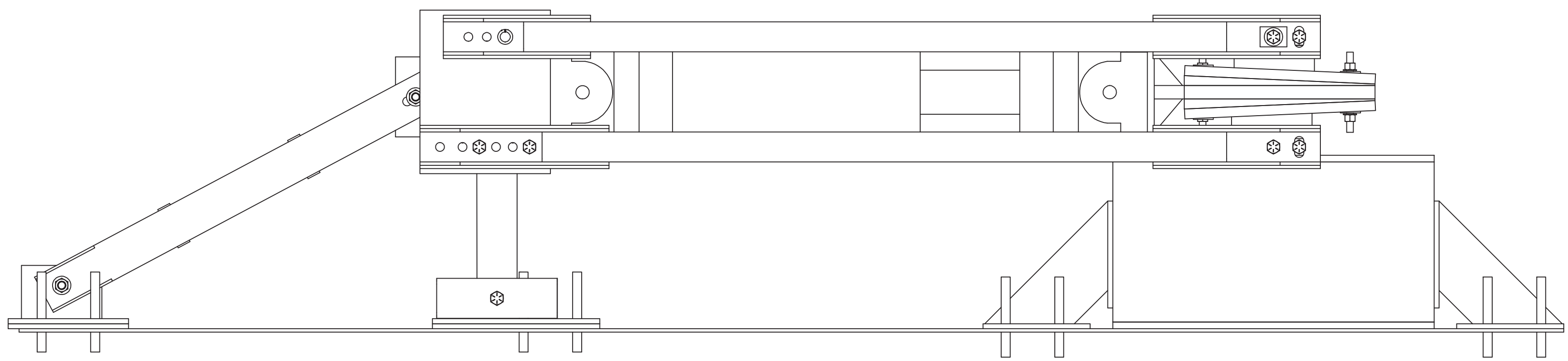

Step 2: Retract the MTS 5in from the mid-stroke position.

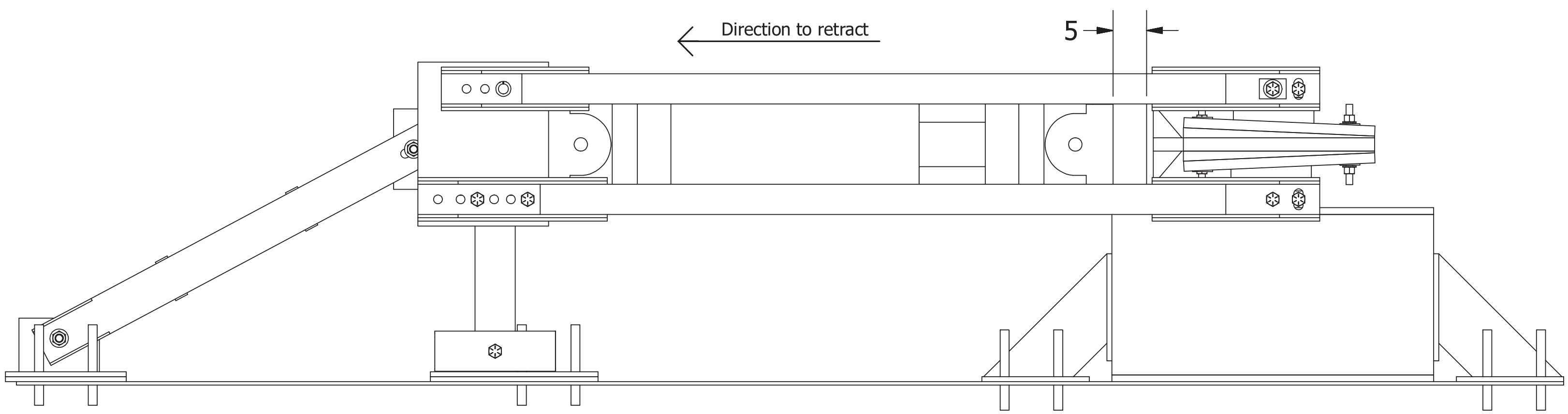

Installing REC-15K instrumentation				Scale 0 24'' 48''
Instrumentation installation sequence	11/12/2019	University of Florida	SHEET 88 OF 93	Revision:

Step 3: Fix the REC-15K load cell and PL-REC assembly into the MTS foot using at least two threaded rods. Lock the right end swivel on MTS

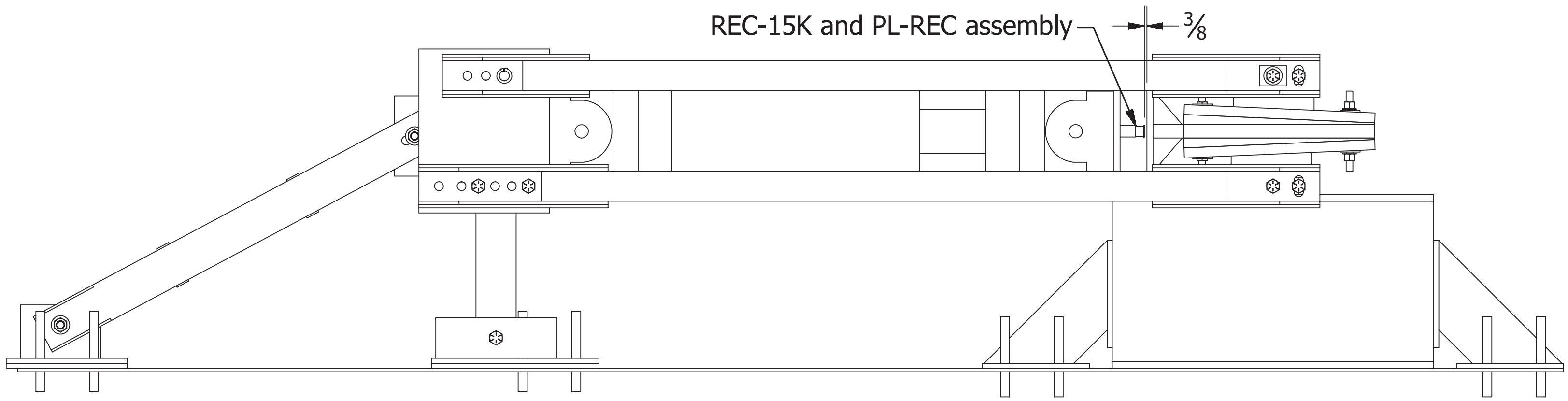

Step 4: Extract the MTS over a distance of 0.5in (4.5in away from mid stroke position)

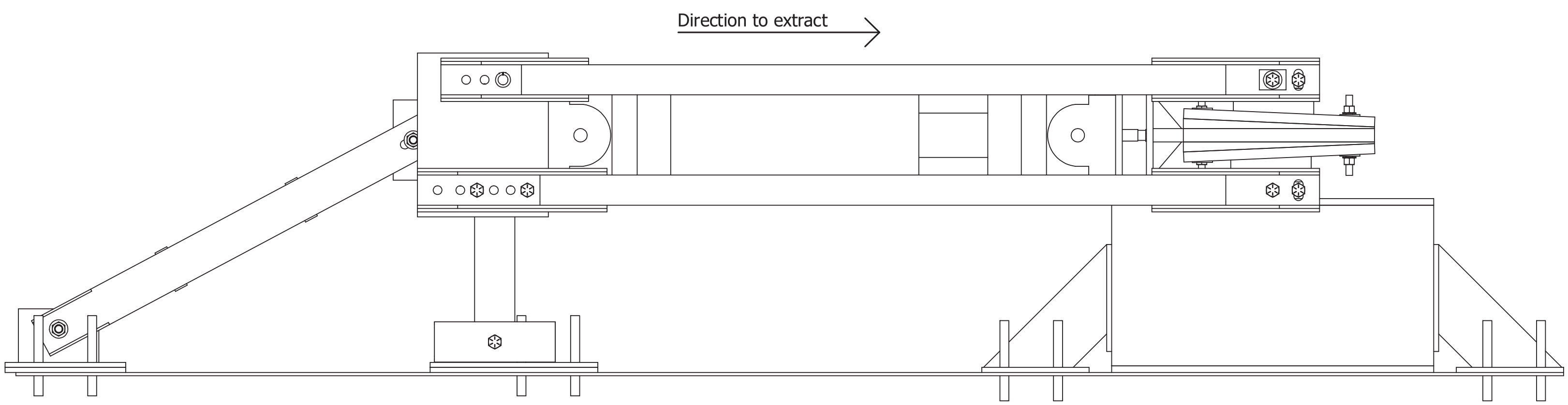

Installing REC-15K instrumentation				Scale 0 24'' 48''
Instrumentation installation sequence	11/12/2019	University of Florida	SHEET 89 OF 93	Revision:

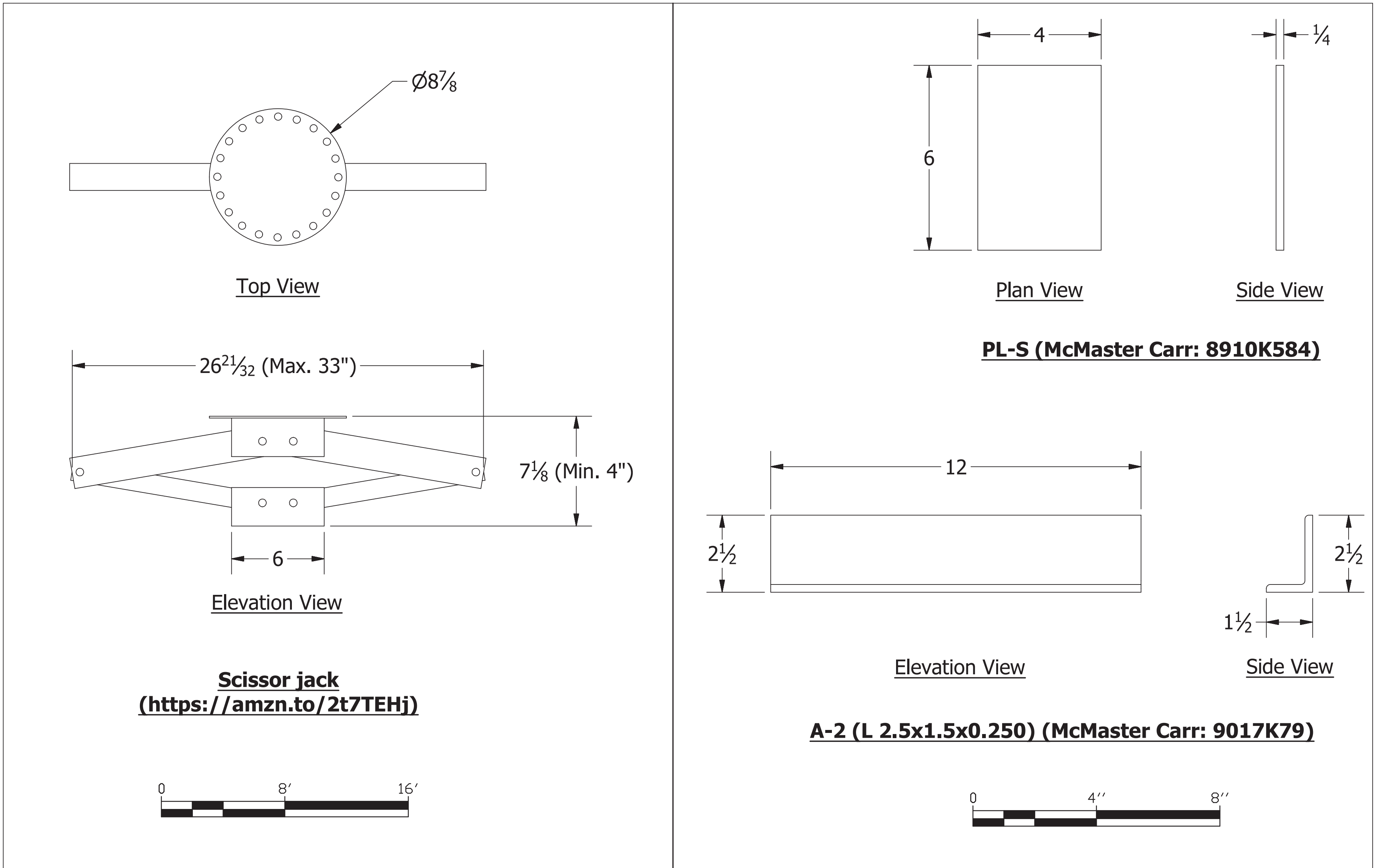

Scissor jack parts				*Scale*
Scissor jack assembly	*11/12/2019*	*University of Florida*	*SHEET 90 OF 93*	*Revision:*

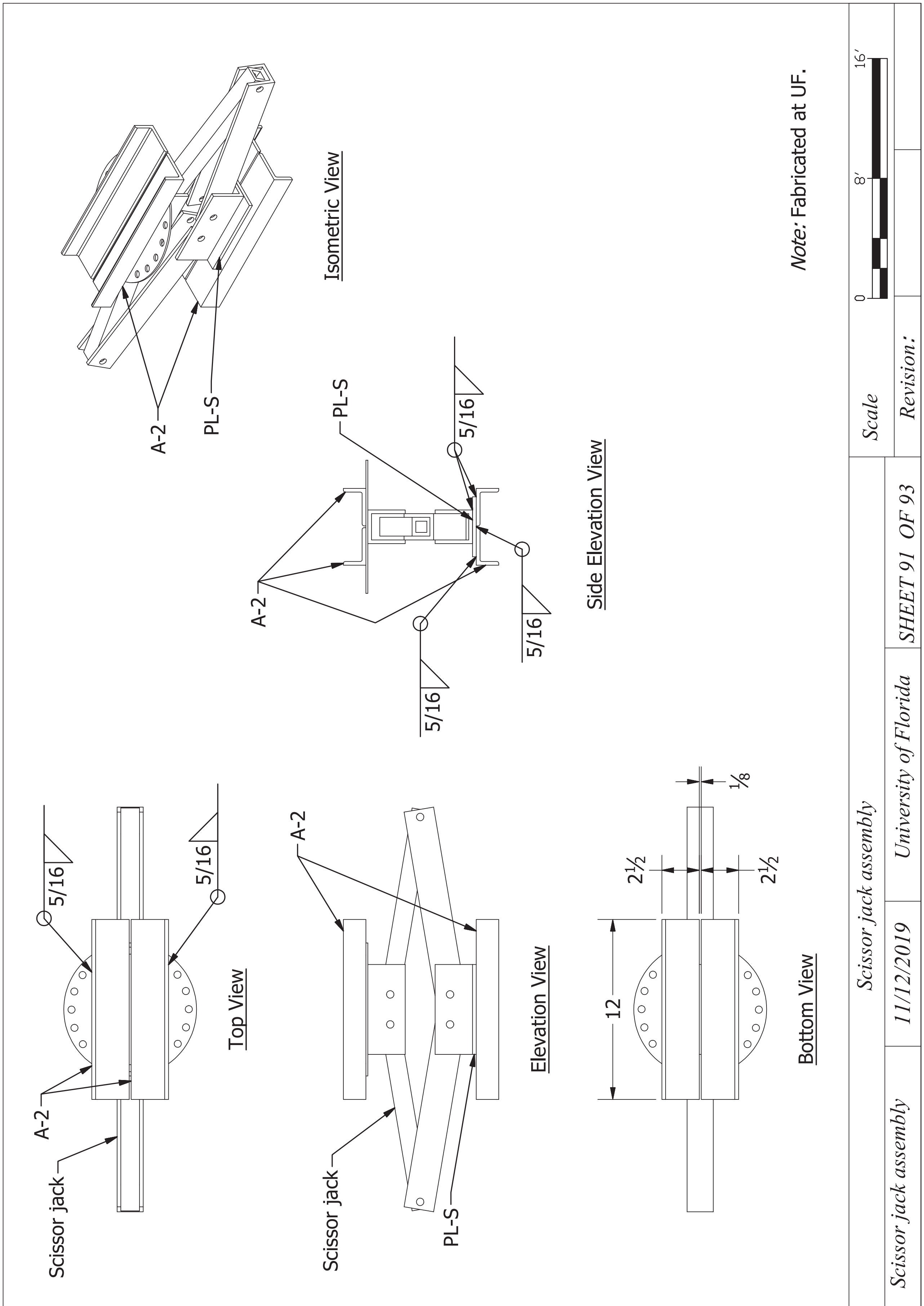
Isometric View
A-2
PL-S
Side Elevation View
A-2
PL-S
5/16
5/16
5/16
Top View
Scissor jack
A-2
5/16
5/16
Elevation View
Scissor jack
PL-S
A-2
Bottom View
12
2½
2½
⅛
Note: Fabricated at UF.
0
8′
16′
Scale
Revision:
Scissor jack assembly
Scissor jack assembly
11/12/2019
University of Florida
SHEET 91 OF 93

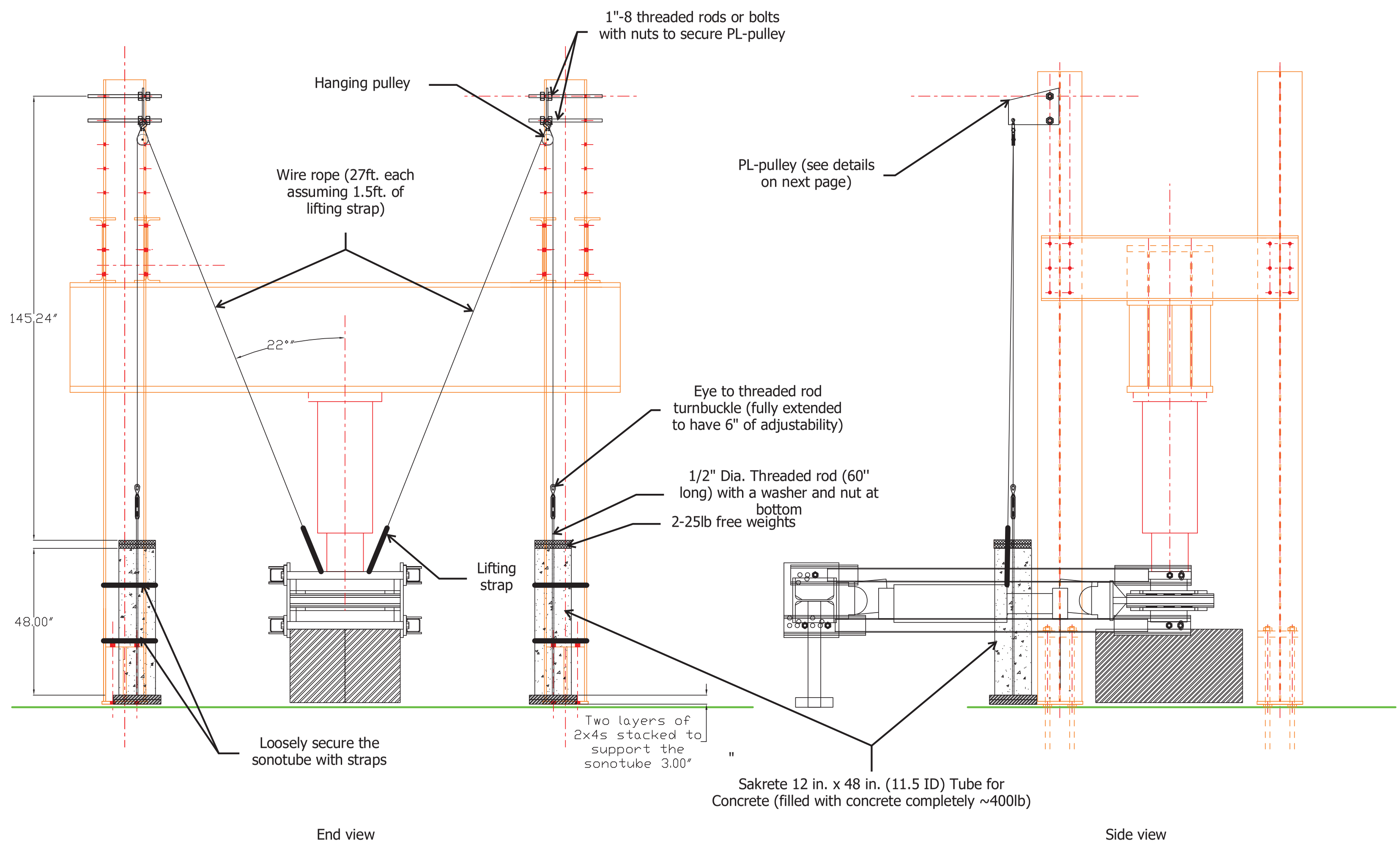

Weight balance mechanism to suspend horizontal hydraulic jack MTS				*Scale* 0 4′ 8′
	11/12/2019	*University of Florida*	*SHEET 92 OF 93*	*Revision:*

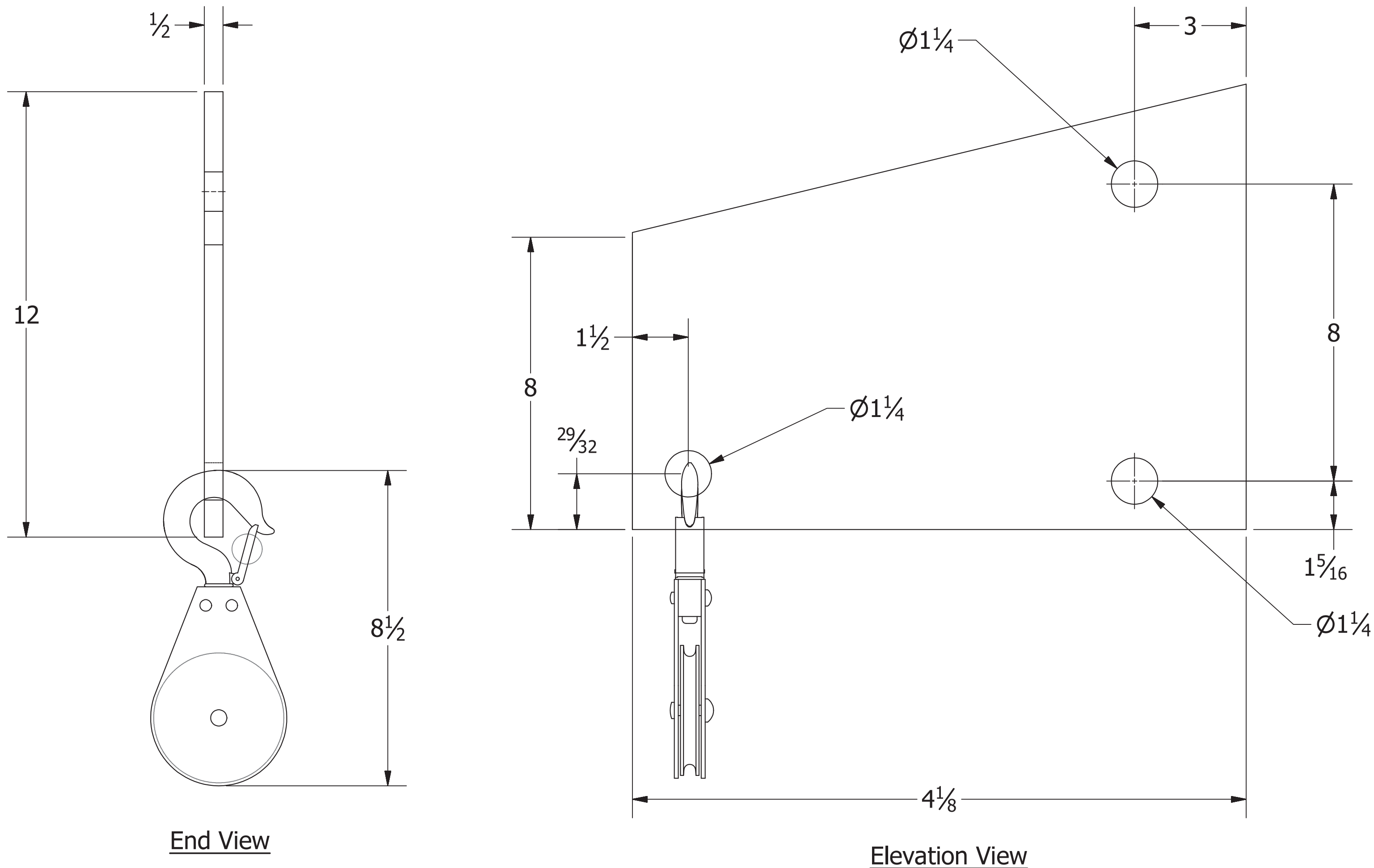

Notes:
1. Made using the PL-F5 plates which are not used in the test setup anymore.
2. Two of these plates required

Weight balance mechanism - Pulley drawing			*Scale* 0 4'' 8''
11/12/2019	*University of Florida*	*SHEET 93 OF 93*	*Revision:*

APPENDIX D
TEST MATRIX

Table D-1 provides the test matrix which includes the types of pads tested and the list of test procedures performed on each pad type. In this table, the notations k_a, k_s, Δs, and H_F mean axial stiffness, shear stiffness, horizontal displacement and horizontal restraining force respectively.

Table D-1 Bearing pad test matrix

Item #	Test #	Bearing pad type	Size	Pair #	Surface type	Surface condition	Test for	Axial load level	Direction of shear		Number of repetitions
									Neg. (-)	Pos. (+)	
1	1	E-0%	Half	1	Steel	Dry	k_a	Max			5
2	2						k_s	Min	x	x	3
3	3						k_s	Max	x	x	3
4	4						Slip	Min	x	x	1
5	5						Slip	Max	x	x	1
6	6	E-0%	Full	1	Steel	Dry	k_a	Max			3
7	7						k_s	Max	x	x	3
8	8						k_s	Min	x	x	1
9	119A						Slip	Min	x		1
10	120A						Slip	Max	x		1
11	101				Concrete		Slip	Min	x		1
12	102						Slip	Max	x		1
13	119B				Steel	Wet	Slip	Min	x		1
14	120B						Slip	Max	x		1
15	126				Concrete		Slip	Max	x		1
16	11	F-0%	Half	1	Steel	Dry	k_a	Max			4
17	12						k_s	Max	x	x	3
18	13						k_s	Min	x	x	1
19	14						Slip	Min	x		1
20	15						Slip	Max	x		1
21	16	F-0%	Full	1	Steel	Dry	ka	Max			4
22	17						ks	Max	x	x	1
23	18						ks	Min	x	x	1
24	19A						Slip	Min	x		1
25	20						Slip	Max	x		1
26	99				Concrete		Slip	Min	x		1
27	100						Slip	Max	x		1

Table D-1 Bearing pad test matrix, continued

Item #	Test #	Bearing pad type	Size	Pair #	Surface type	Surface condition	Test	Axial load level	Direction of shear		Number of repetitions
									Neg. (-)	Pos. (+)	
28	121	F-0%	Full	1	Steel	Wet	Slip	Min	x		1
29	122						Slip	Max	x		1
30	123				Concrete		Slip	Min	x		1
31	124						Slip	Max	x		1
32	45	E-2.5%	Half	1	Steel	Dry	k_a Δs	Max			2
33	47						k_s	Max	x		1
34	48						k_s	Min	x		1
35	49						Slip	Min	x		1
36	50						Slip	Max	x		1
37	51			2	Steel	Dry	k_a Δs	Max			2
38	53						k_s	Max	x		1
39	54						k_s	Min	x		1
40	55						Slip	Min	x		1
41	56						Slip	Max	x		1
42	57	E-2.5%	Full	1	Steel	Dry	k_a Δs	Max			2
43	59						k_s	Max	x	x	1
44	60						k_s	Min	x	x	1
45	61						Slip	Min	x		1
46	62						Slip	Max	x		1
47	63			2			k_a Δs	Max			2
48	65						k_s	Max	x	x	1
49	68						Slip	Max		x	1
50	103			1	Concrete		Slip	Min	x		1
51	104						Slip	Max	x		1
52	117			2	Steel	Wet	Slip	Min	x		1
53	118						Slip	Max	x		1
54	128			2	Concrete		Slip	Max	x		1

Table D-1 Bearing pad test matrix, continued

Item #	Test #	Bearing pad type	Size	Pair #	Surface type	Surface condition	Test	Axial load level	Direction of shear		Number of repetitions
									Neg. (-)	Pos. (+)	
55	21	F-2.5%	Half	1	Steel	Dry	k_a Δs	Max			3
56	22						F_H	Max			1
57	23						k_s	Max	x	x	2
58	24						k_s	Min	x		1
59	25						Slip	Min	x		1
60	26						Slip	Max	x		1
61	27			2			k_a Δs	Max			2
62	28						F_H	Max			1
63	29						k_s	Max	x		1
64	30						k_s	Min	x		1
65	31						Slip	Min	x		1
66	32						Slip	Max	x		1
67	33	F-2.5%	Full	1	Steel	Dry	F_H	Max			2
68	34						k_a Δs	Max			2
69	35						k_s	Max	x	x	1
70	36						k_s	Min	x	x	1
71	37						Slip	Min	x		1
72	38						Slip	Max	x		1
73	39	F-2.5%	Full	2	Steel	Dry	k_a Δs	Max			2
74	40						F_H	Max			1
75	41						k_s	Max	x	x	1
76	42						k_s	Min	x	x	1
77	43						Slip	Min		x	1
78	44						Slip	Max		x	1
79	105	F-2.5%	Full	1	Concrete	Dry	Slip	Min	x		1
80	106						Slip	Max	x		1
81	115			2	Steel	Wet	Slip	Min	x		1
82	116						Slip	Max	x		1

Table D-1 Bearing pad test matrix, continued

Item #	Test #	Bearing pad type	Size	Pair #	Surface type	Surface condition	Test	Axial load level	Direction of shear		Number of repetitions
									Neg. (-)	Pos. (+)	
83	69	E-5%	Half	1	Steel	Dry	k_a Δs	Max			1
84	73						Slip	Min	x		1
85	74						Slip	Max	x		1
86	76			2			k_s	Max	x		1
87	80						Slip	Max	x		1
88	81	E-5%	Full	1	Steel	Dry	k_a Δs	Max			2
89	83						k_s	Max	x		1
90	85						Slip	Min	x		1
91	87			2			k_a Δs	Max			2
92	90						k_s	Min	x		1
93	92						Slip	Max	x		1
94	109			1	Concrete	Dry	Slip	Min	x		1
95	110						Slip	Max	x		1
96	111			2	Steel	Wet	Slip	Min	x		1
97	112						Slip	Max	x		1
98	134			2	Concrete	Wet	Slip	Max	x		1
99	93	F-5%	Full	1	Steel	Dry	k_a Δs	Max			1
100	94						k_s	Max	x	x	1
101	95						Slip	Min	x		1
102	96			2			k_a Δs	Max			1
103	97						k_s	Min	x	x	1
104	98						Slip	Max	x		1

Table D-1 Bearing pad test matrix, continued

Item #	Test #	Bearing pad type	Size	Pair #	Surface type	Surface condition	Test	Axial load level	Direction of shear		Number of repetitions
									Neg. (-)	Pos. (+)	
105	107	F-5%	Full	1	Concrete	Dry	Slip	Min	x		1
106	108						Slip	Max	x		1
107	113			2	Steel	Wet	Slip	Min	x		1
108	114						Slip	Max	x		1
109	132			2	Concrete		Slip	Max	x		1
110	135	K-0%	Full	1	Steel	Dry	ka	Max			2
111	136						ks	Max	x		1
112	137						ks	Min	x		1
113	138						Slip	Min	x		1
114	139						Slip	Max	x		1
115	150				Concrete		Slip	Min	x		1
116	151						Slip	Max	x		1
117	160				Steel	Wet	Slip	Min	x		1
118	161						Slip	Max	x		1
119	162				Concrete		Slip	Min	x		1
120	163						Slip	Max	x		1
121	140	K-2.1%	Full	1	Steel	Dry	ka Δs	Max			3
122	141						ks	Max	x	x	1
123	142						ks	Min	x	x	1
124	143 A						Slip	Min	x		1
125	144						Slip	Max	x	x	2
126	152				Concrete		Slip	Min	x		1
127	153						Slip	Max	x		1
128	159				Steel	Wet	Slip	Max	x		1
129	165				Concrete		Slip	Max	x		1

Table D-1 Bearing pad test matrix, continued

<table>
<tr><th rowspan="2">Item #</th><th rowspan="2">Test #</th><th rowspan="2">Bearing pad type</th><th rowspan="2">Size</th><th rowspan="2">Pair #</th><th rowspan="2">Surface type</th><th rowspan="2">Surface condition</th><th rowspan="2">Test</th><th rowspan="2">Axial load level</th><th colspan="2">Direction of shear</th><th rowspan="2">Number of repetitions</th></tr>
<tr><th>Neg. (-)</th><th>Pos. (+)</th></tr>
<tr><td>130</td><td>145</td><td rowspan="8">K-4.2%</td><td rowspan="8">Full</td><td rowspan="8">1</td><td rowspan="3">Steel</td><td rowspan="6">Dry</td><td>k_a
Δs</td><td>Max</td><td></td><td></td><td>2</td></tr>
<tr><td>131</td><td>148</td><td>Slip</td><td>Min</td><td>x</td><td></td><td>1</td></tr>
<tr><td>132</td><td>149</td><td>Slip</td><td>Max</td><td>x</td><td></td><td>1</td></tr>
<tr><td>133</td><td>146B</td><td rowspan="3">Concrete</td><td>k_s</td><td>Max</td><td>x</td><td></td><td>1</td></tr>
<tr><td>134</td><td>147</td><td>k_s</td><td>Min</td><td>x</td><td></td><td>1</td></tr>
<tr><td>135</td><td>155</td><td>Slip</td><td>Max</td><td>x</td><td></td><td>1</td></tr>
<tr><td>136</td><td>157</td><td>Steel</td><td>Wet</td><td>Slip</td><td>Max</td><td>x</td><td></td><td>1</td></tr>
<tr><td>137</td><td>167</td><td>Concrete</td><td>Wet</td><td>Slip</td><td>Max</td><td>x</td><td></td><td>1</td></tr>
</table>

APPENDIX E
TEST RESULT PLOTS

E.1 Axial stiffness test plots

This section consists of plots for axial load versus axial displacement measured during the axial stiffness tests. The plots only include the axial loading part of each test. Spikes in the data, caused by the laser gauges missing the target plates, were removed. The laser gauges occasionally missed the target plates due to either interference by tools while tightening bolts on the middle plate, or due to excessive rotation of the top and middle plates.

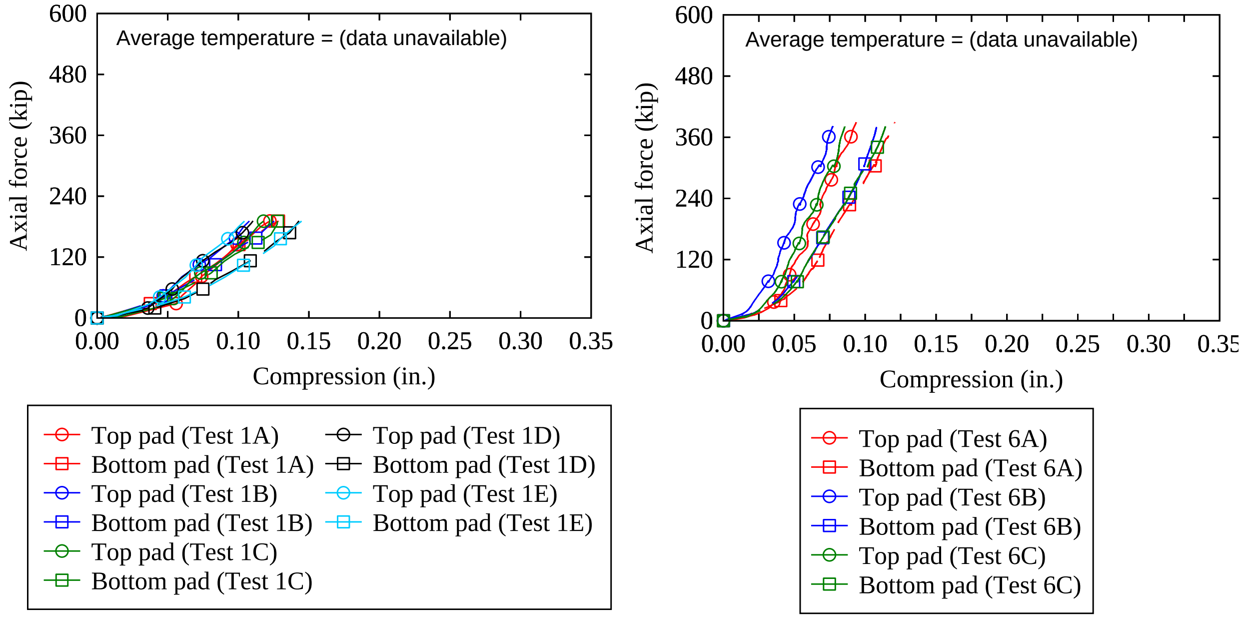

(a) (b)

Figure E-1 Axial load vs. displacement: (a) half-size E-0% pads; (b) full-size E-0% pads

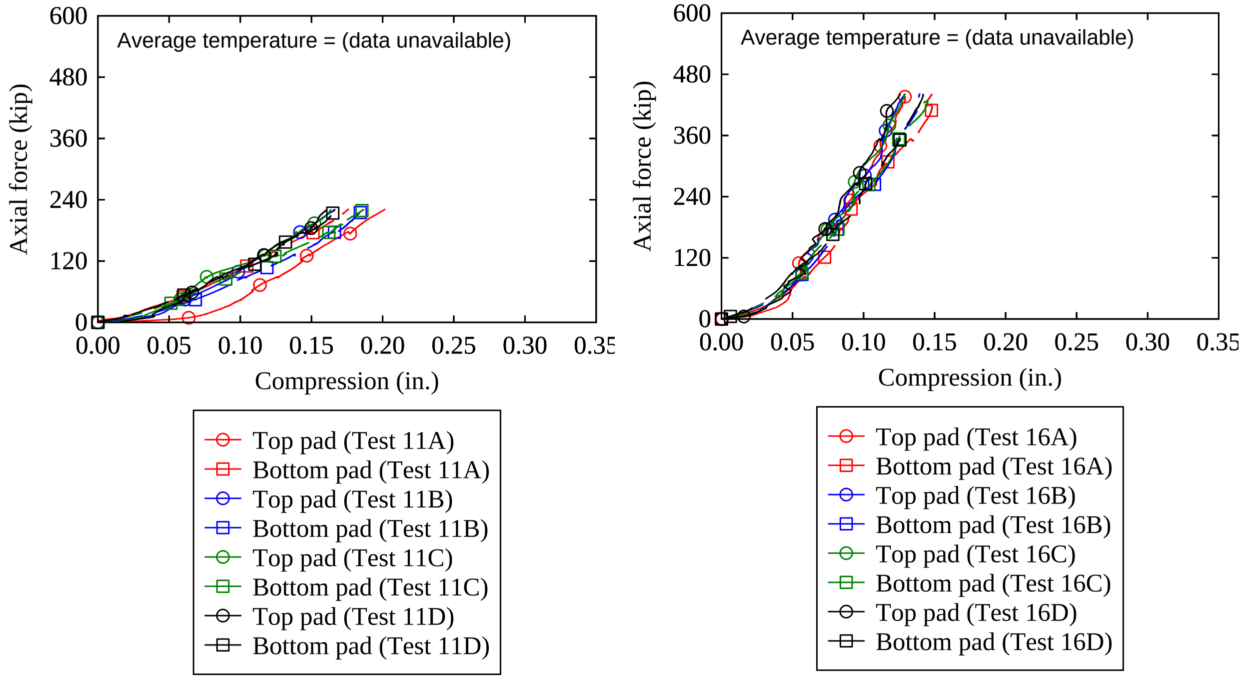

(a) (b)

Figure E-2 Axial load vs. displacement: (a) half-size F-0% pads; (b) full-size F-0% pads

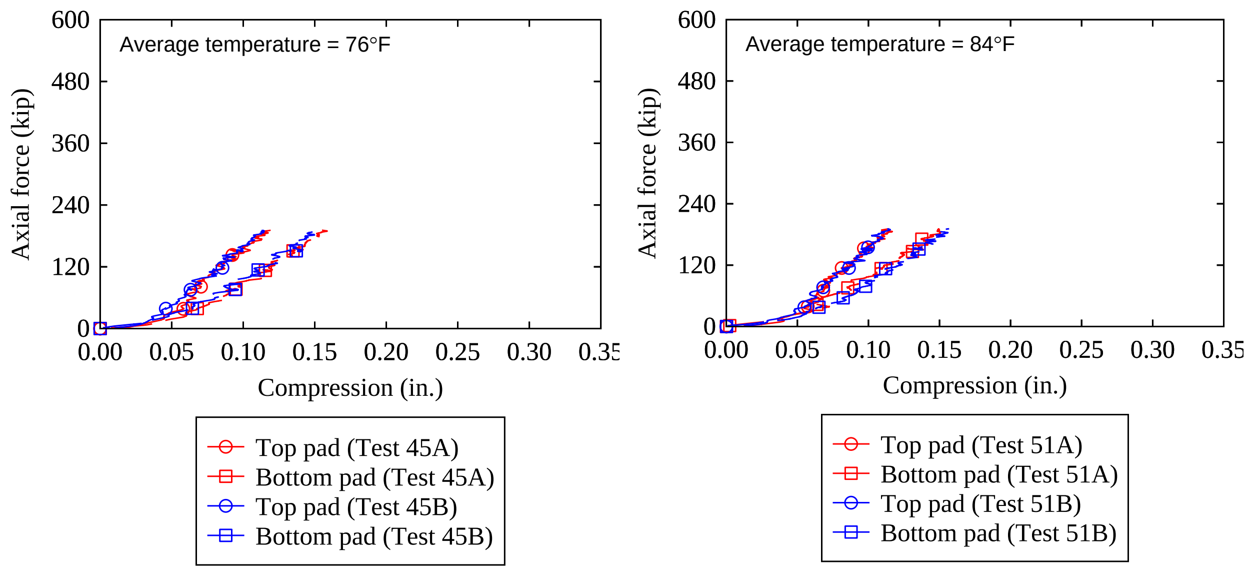

(a) (b)

Figure E-3 Axial load vs. displacement of half-size E-2.5% pads: (a) pair 1; (b) pair 2

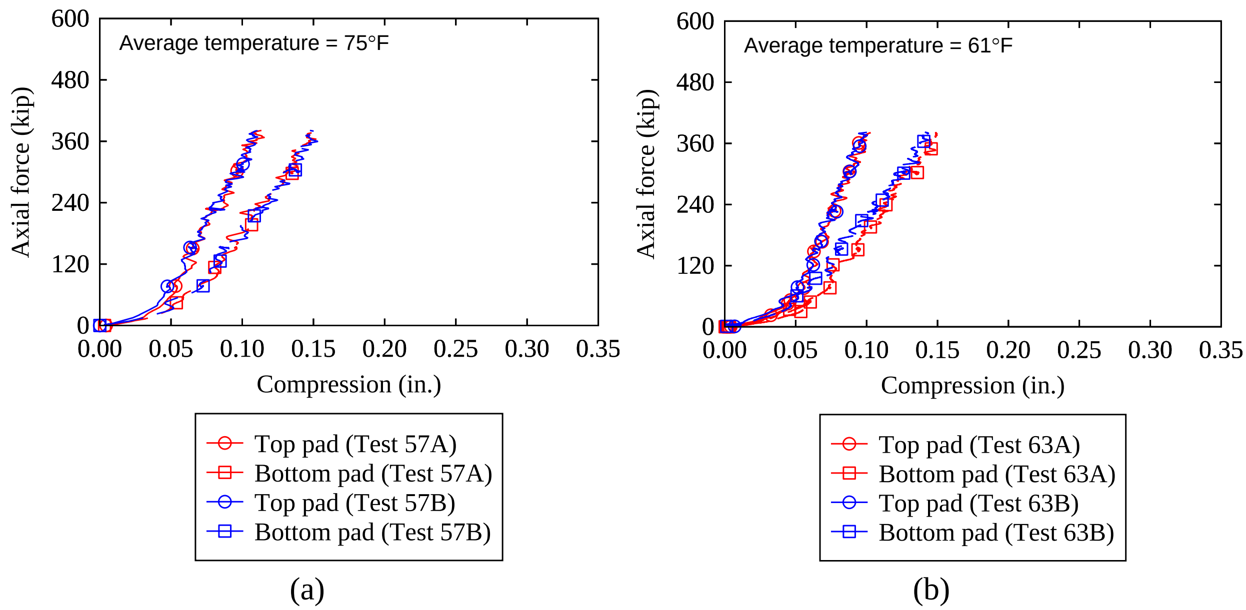

Figure E-4 Axial load vs. displacement of full-size E-2.5% pads: (a) pair 1; (b) pair 2

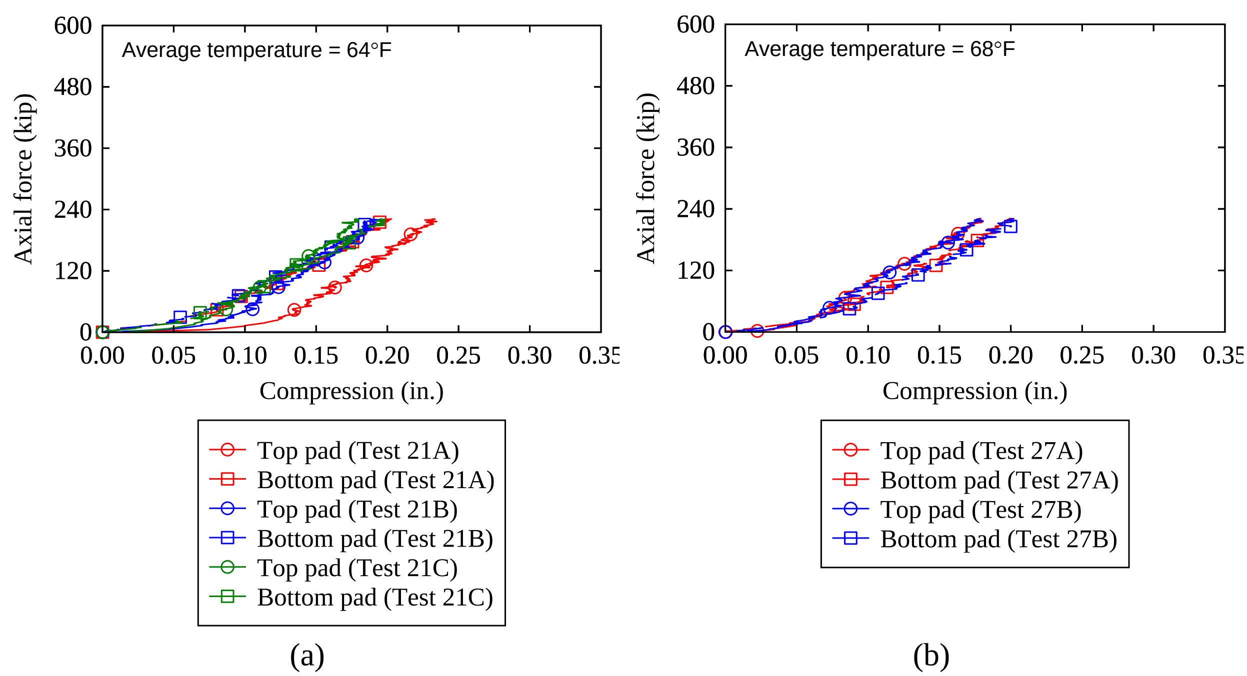

Figure E-5 Axial load vs. displacement of half-size F-2.5% pads: (a) pair 1; (b) pair 2

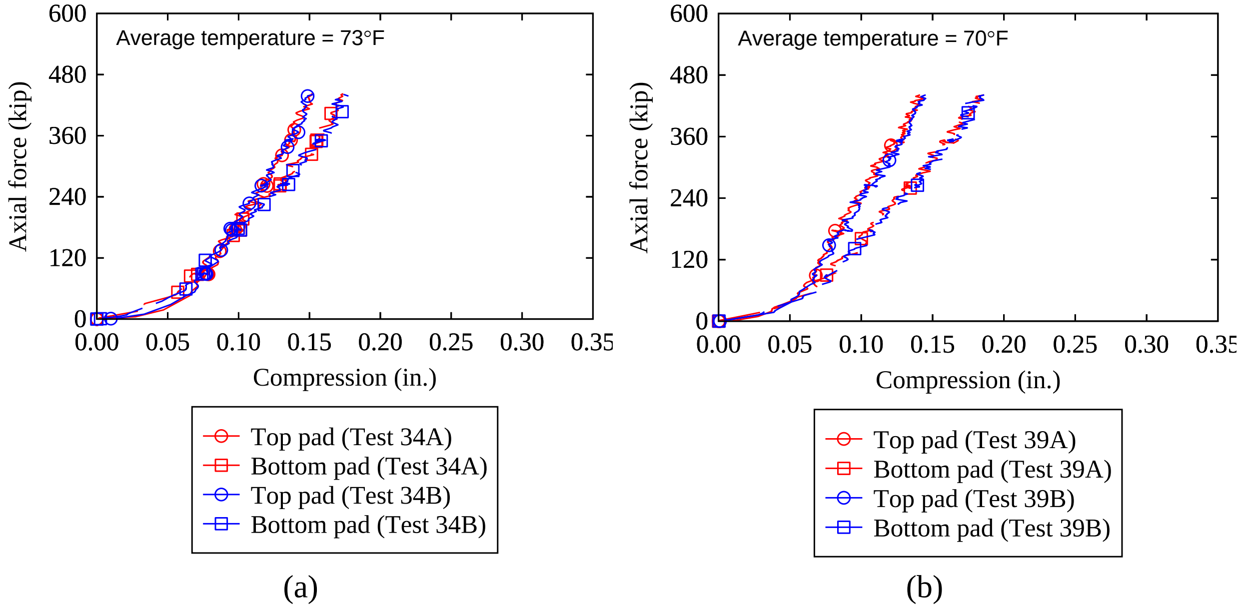

Figure E-6 Axial load vs. displacement of full-size F-2.5% pads: (a) pair 1; (b) pair 2

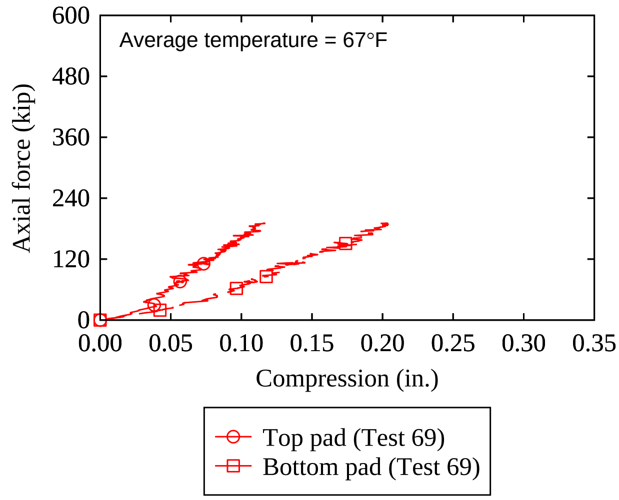

Figure E-7 Axial load vs. displacement of half-size E-5% pads (pair 1)

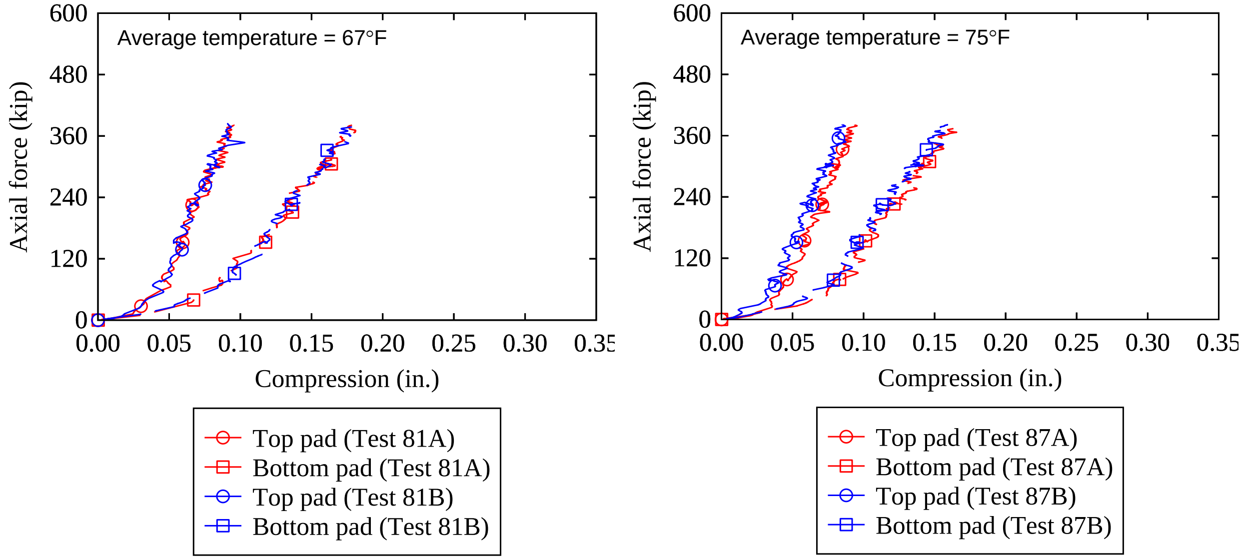

(a) (b)

Figure E-8 Axial load vs. displacement of full-size E-5% pads: (a) pair 1; (b) pair 2

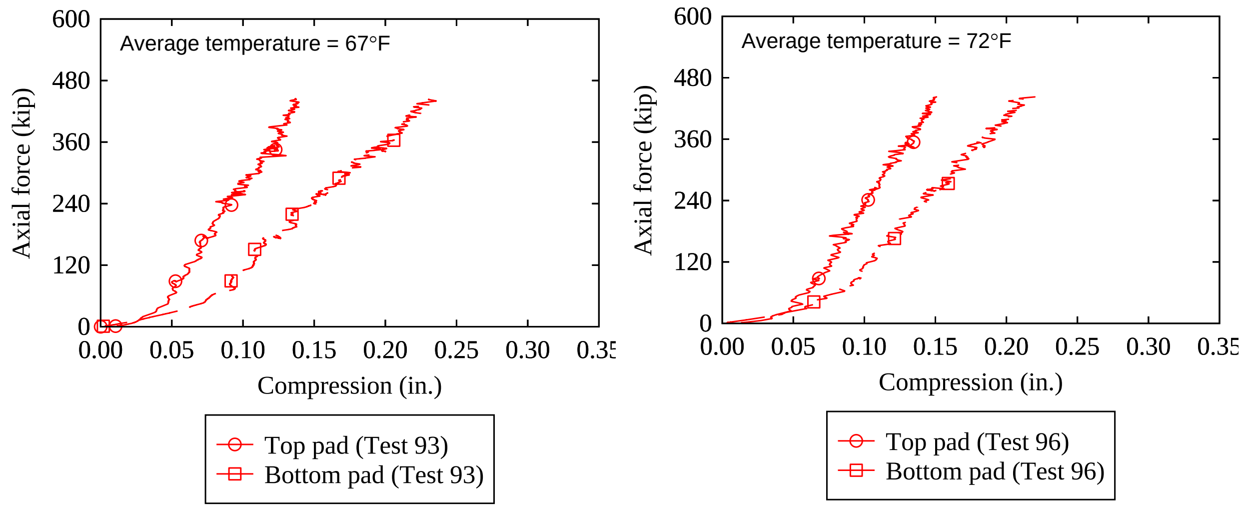

(a) (b)

Figure E-9 Axial load vs. displacement of full-size F-5% pads: (a) pair 1; (b) pair 2

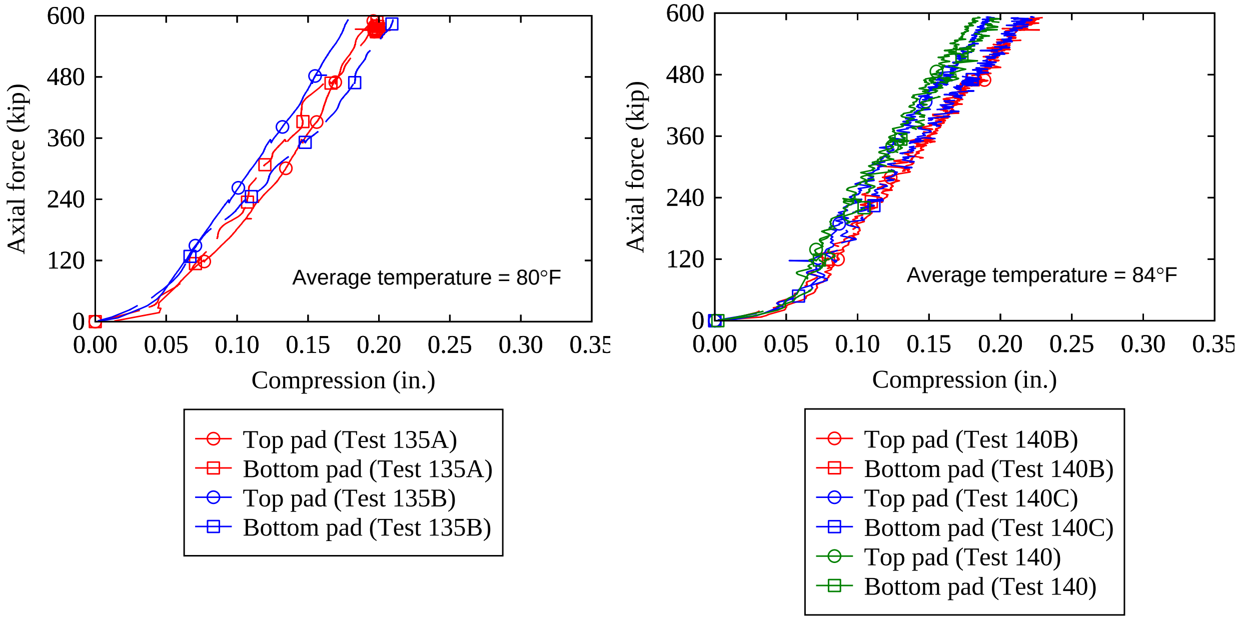

(a) (b)

Figure E-10 Axial load vs. displacement: (a) full-size K-0% pads; (b) full-size K-2.1% pads

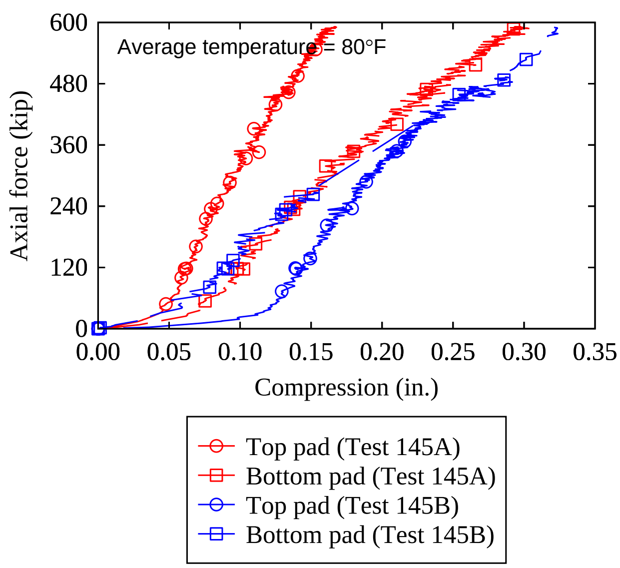

Figure E-11 Axial load vs. displacement of full-size K-4.2% pads

E.2 Horizontal displacement test plots

This section consists of plots for horizontal displacement in tapered pads under axial load measured during the loading ramp stage of axial stiffness tests. The horizontal displacement of the top pad was computed as the difference between the horizontal displacement of the middle plate assembly and top plate. Similarly, the horizontal displacement of the bottom pad was computed as difference between the horizontal displacement of the middle plate assembly and bottom plate.

Negative displacement readings indicated tapered pad displacement in the negative x direction under compression load. Erroneous data due to laser gauges missing the target plates were removed.

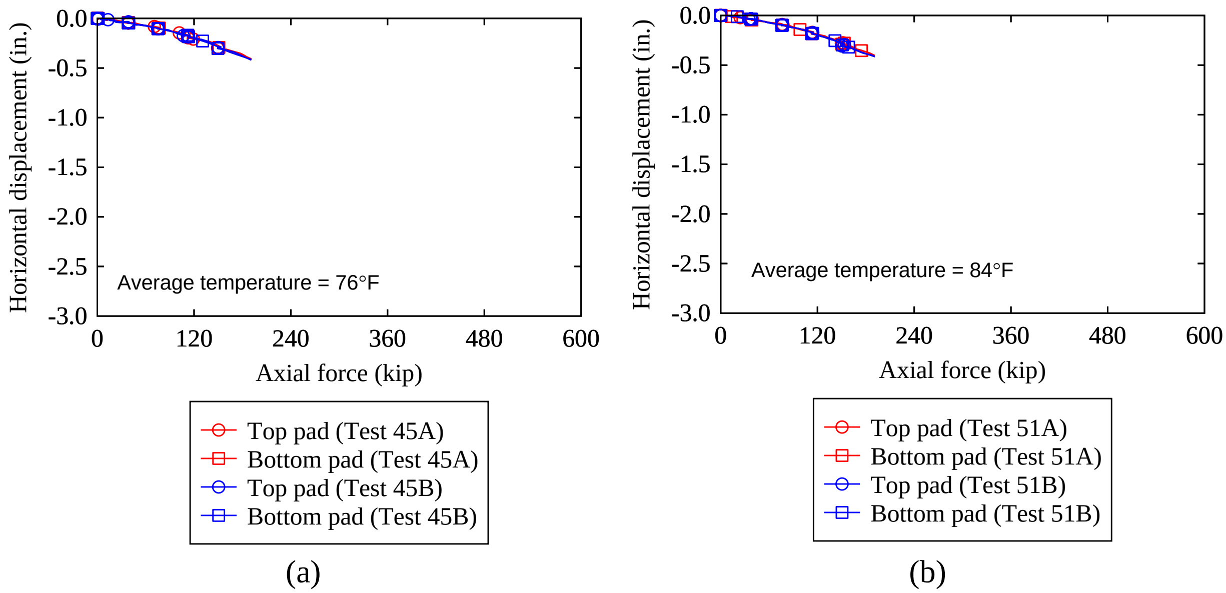

Figure E-12 Horizontal displacement vs. axial force of half-size E-2.5% pads: (a) pair 1; (b) pair 2

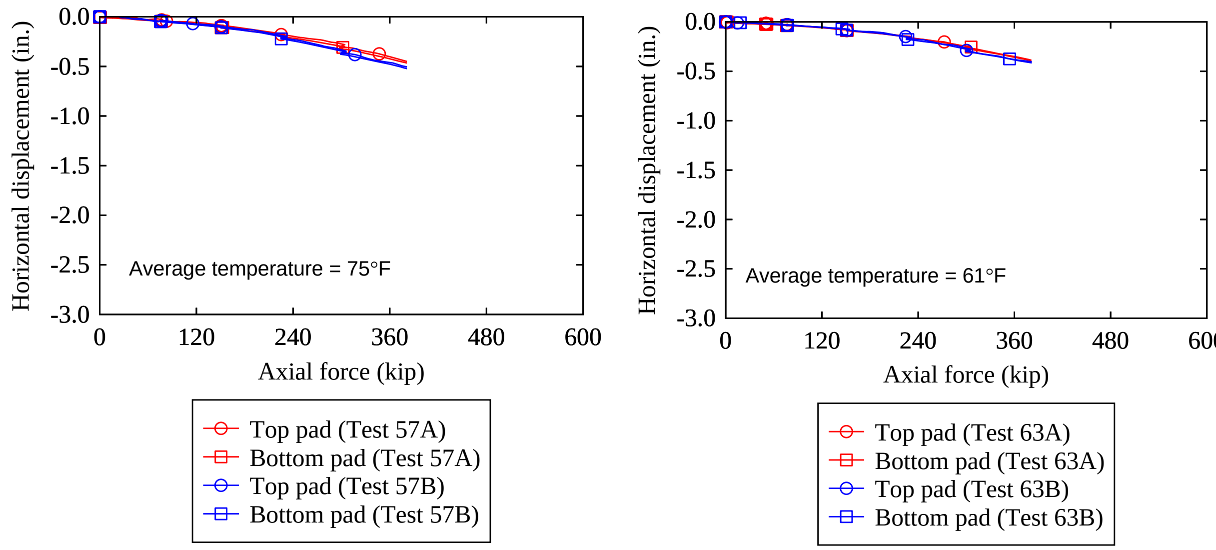

(a) (b)

Figure E-13 Horizontal displacement vs. axial force of full-size E-2.5% pads: (a) pair 1; (b) pair 2

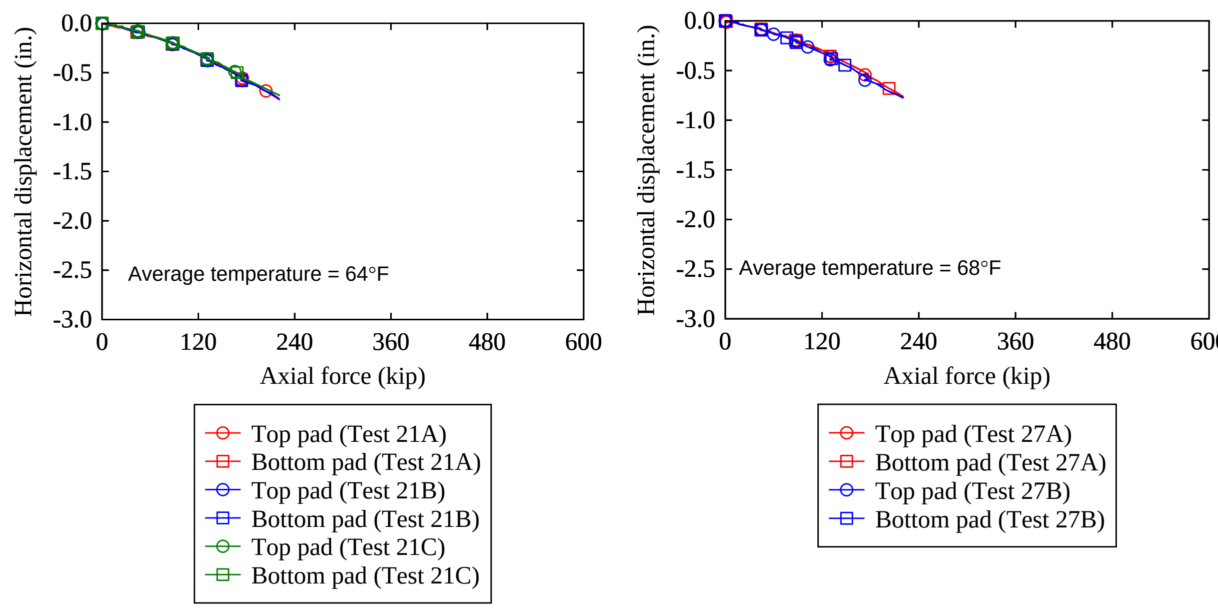

(a) (b)

Figure E-14 Horizontal displacement vs. axial force of half-size F-2.5% pads: (a) pair 1; (b) pair 2

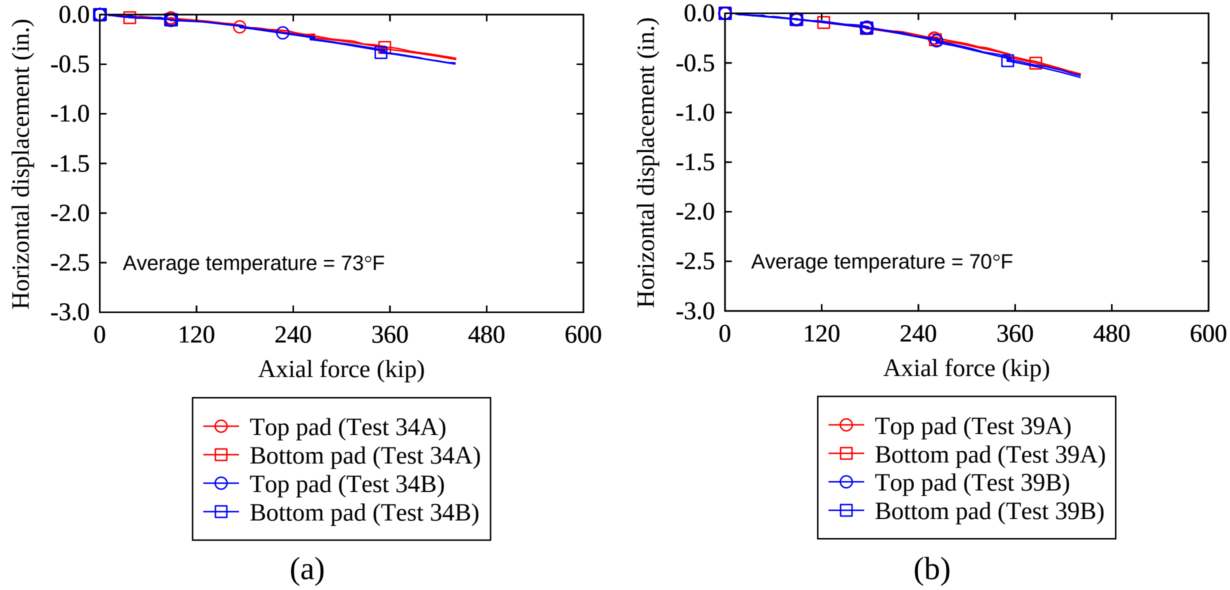

Figure E-15 Horizontal displacement vs. axial force of full-size F-2.5% pads: (a) pair 1; (b) pair 2

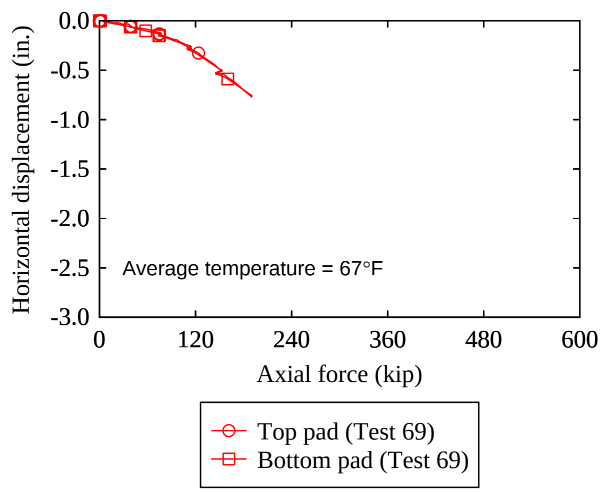

Figure E-16 Horizontal displacement vs. axial force of half-size E-5% pads (pair 1)

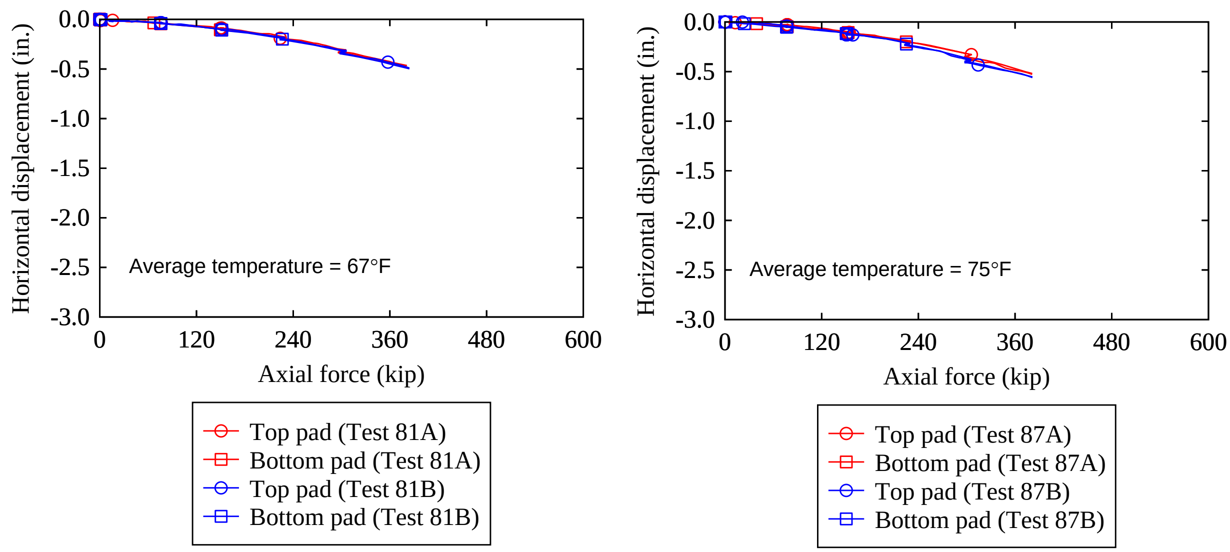

(a) (b)

Figure E-17 Horizontal displacement vs. axial force of full-size E-5% pads: (a) pair 1; (b) pair 2

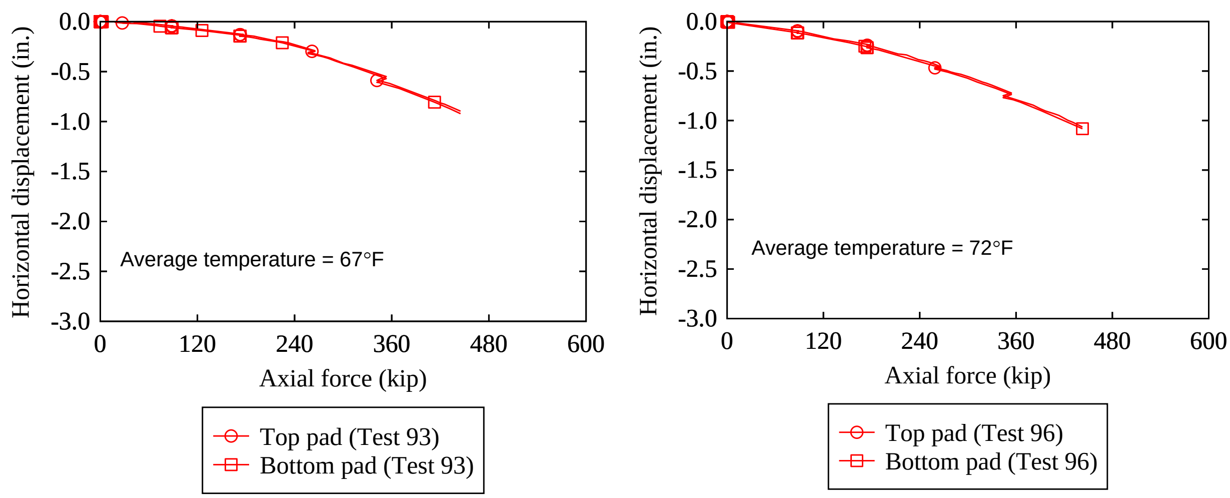

(a) (b)

Figure E-18 Horizontal displacement vs. axial force of full-size F-5% pads: (a) pair 1; (b) pair 2

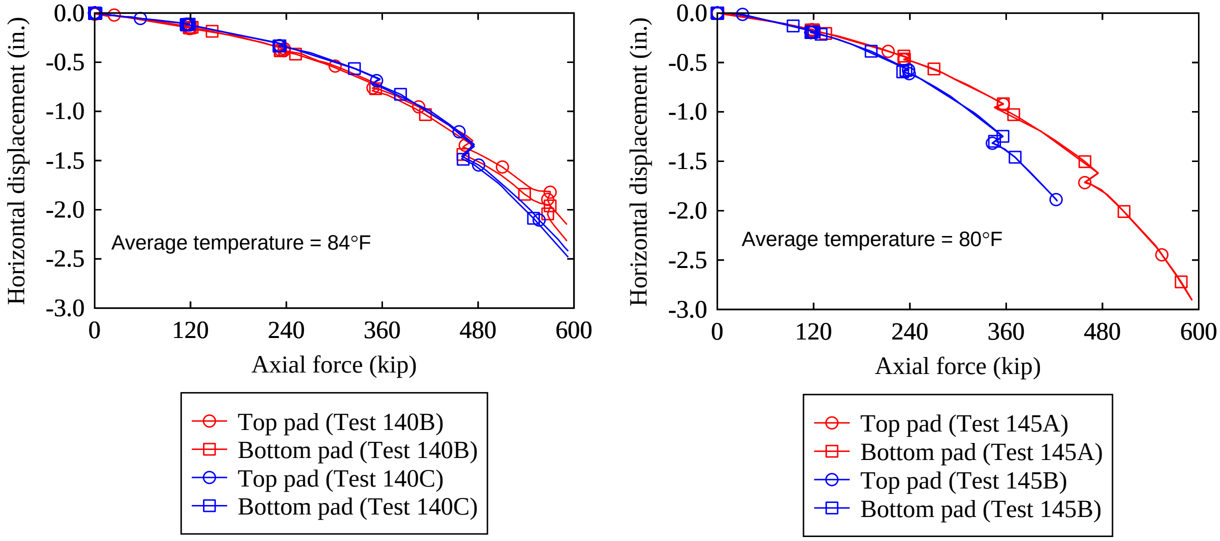

(a) (b)

Figure E-19 Horizontal displacement vs. axial force: (a) full-size K-2.1% pads; (b) full-size K-4.2% pads

E.3 Horizontal force test plots

This section includes plots of horizontal restraining force versus axial force measured for pads during the axial load ramp stage of: horizontal force tests; shear stiffness tests; and slip tests performed with dry steel surface condition.

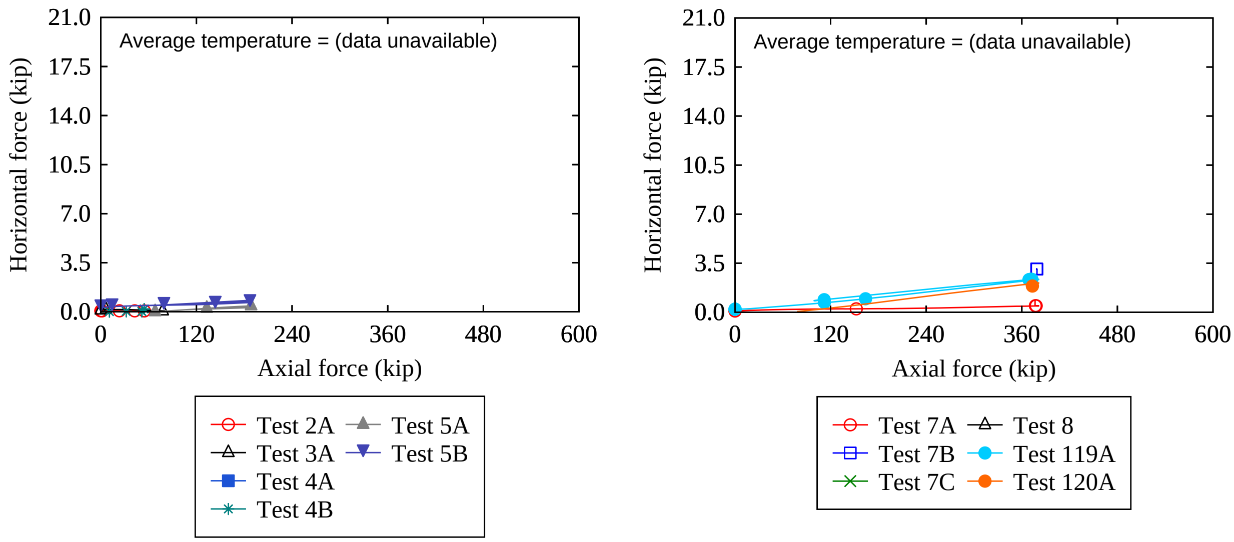

(a) (b)

Figure E-20 Horizontal force vs. axial force: (a) half-size E-0% pads; (b) full-size E-0% pads

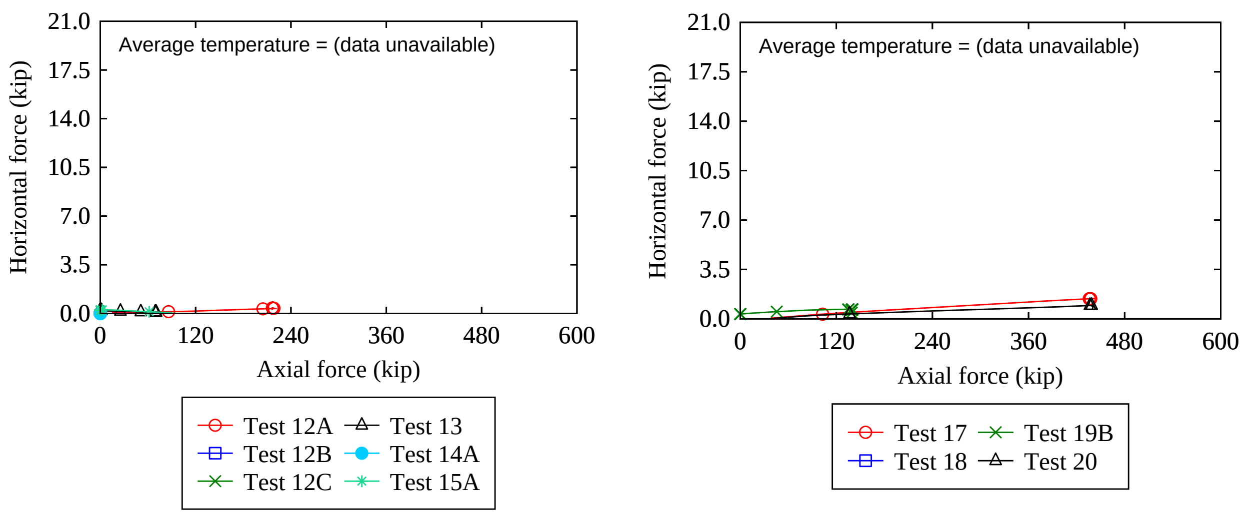

(a) (b)

Figure E-21 Horizontal force vs. axial force: (a) half-size F-0% pads; (b) full-size F-0% pads

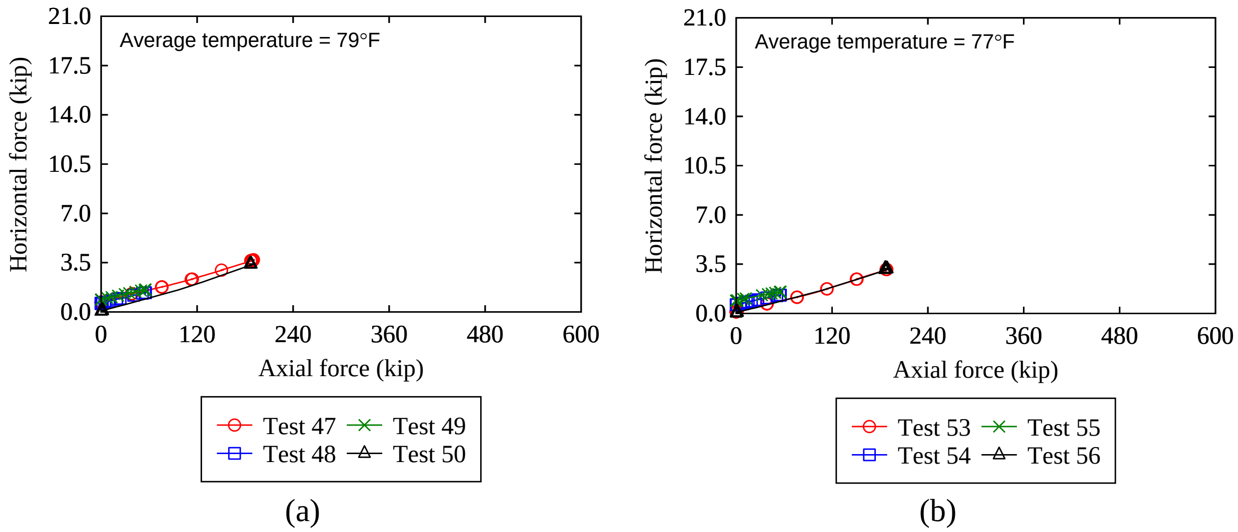

Figure E-22 Horizontal force vs. axial force of half-size E-2.5% pads: (a) pair 1; (b) pair 2

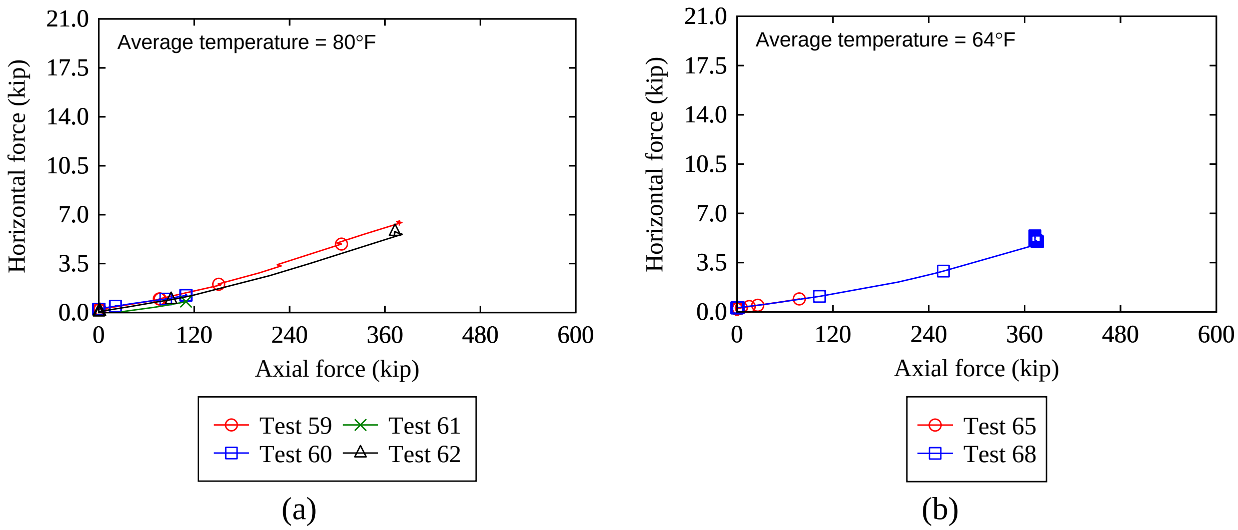

Figure E-23 Horizontal force vs. axial force of full-size E-2.5% pads: (a) pair 1; (b) pair 2

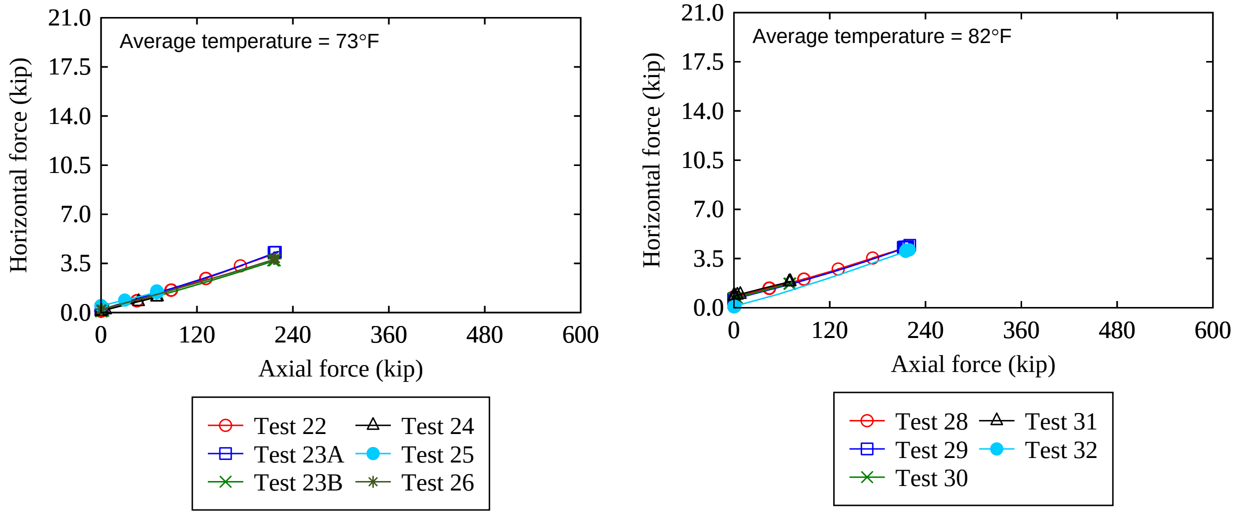

(a) (b)

Figure E-24 Horizontal force vs. axial force of half-size F-2.5% pads: (a) pair 1; (b) pair 2

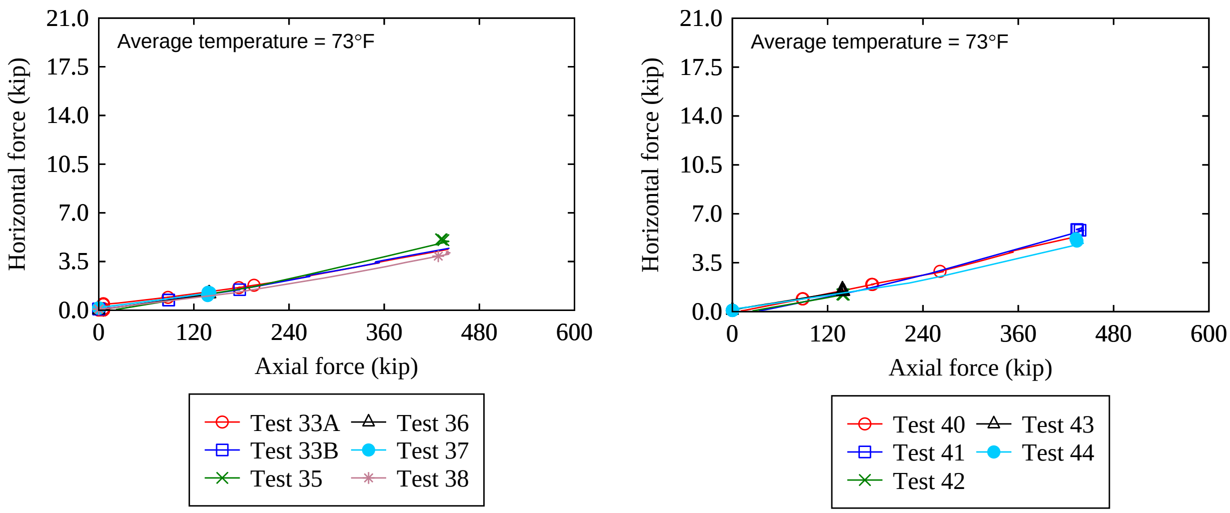

(a) (b)

Figure E-25 Horizontal force vs. axial force of full-size F-2.5% pads: (a) pair 1; (b) pair 2

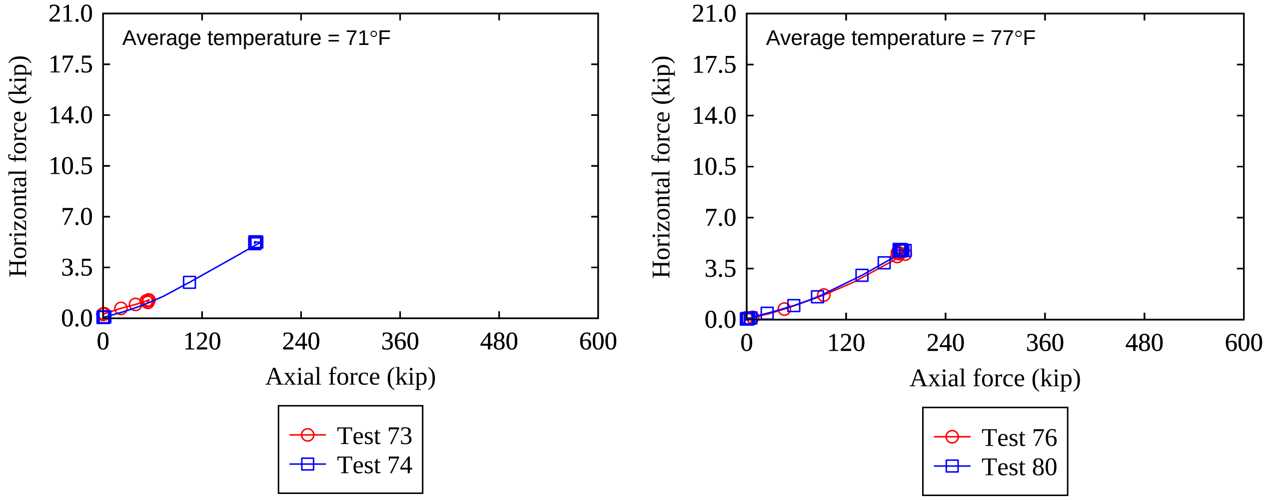

(a) (b)

Figure E-26 Horizontal force vs. axial force of half-size E-5% pads: (a) pair 1; (b) pair 2

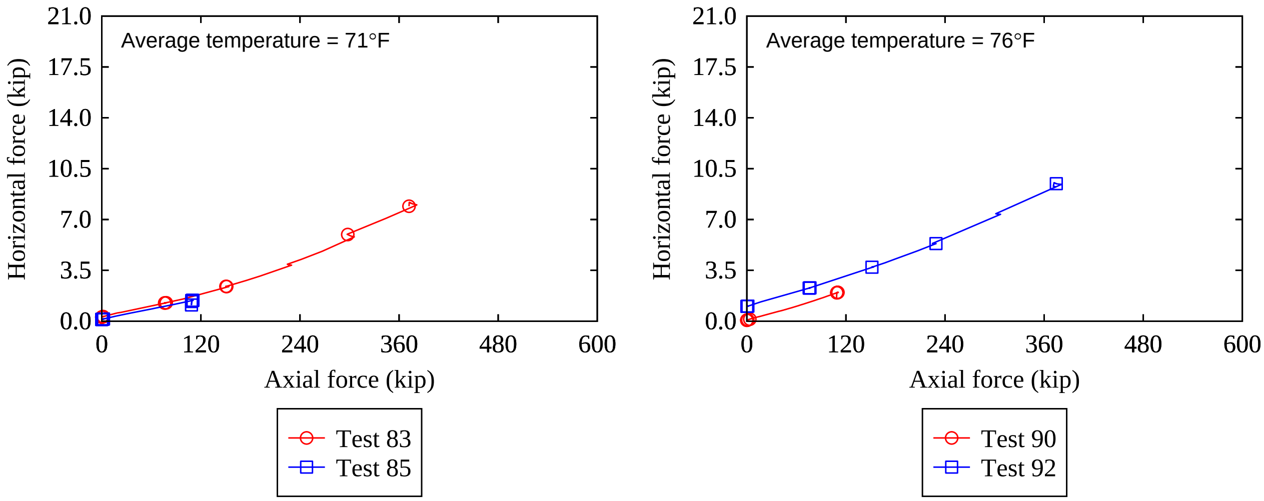

(a) (b)

Figure E-27 Horizontal force vs. axial force of full-size E-5% pads: (a) pair 1; (b) pair 2

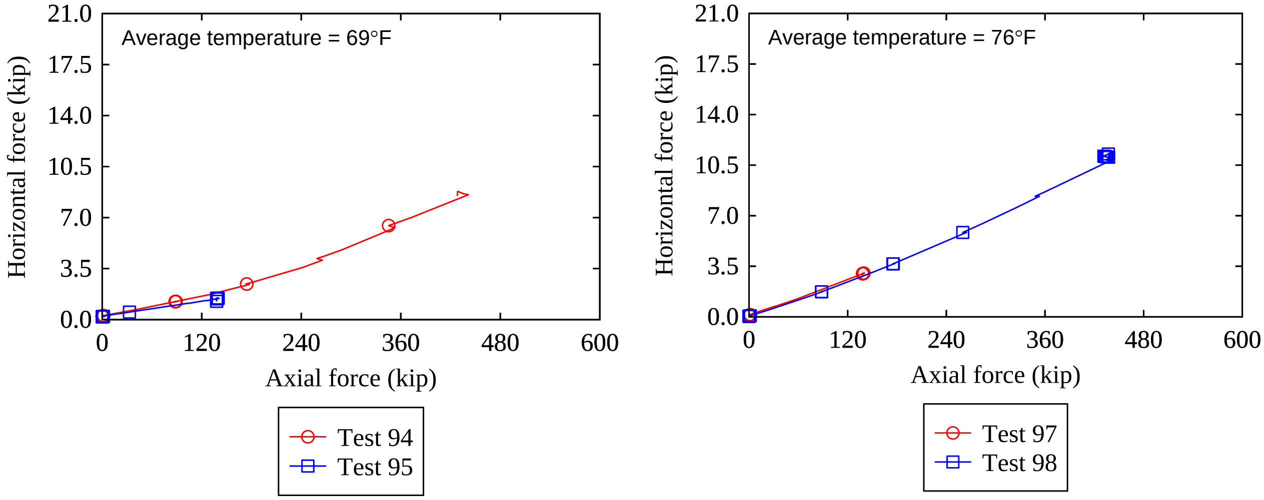

(a) (b)

Figure E-28 Horizontal force vs. axial force of full-size F-5% pads: (a) pair 1; (b) pair 2

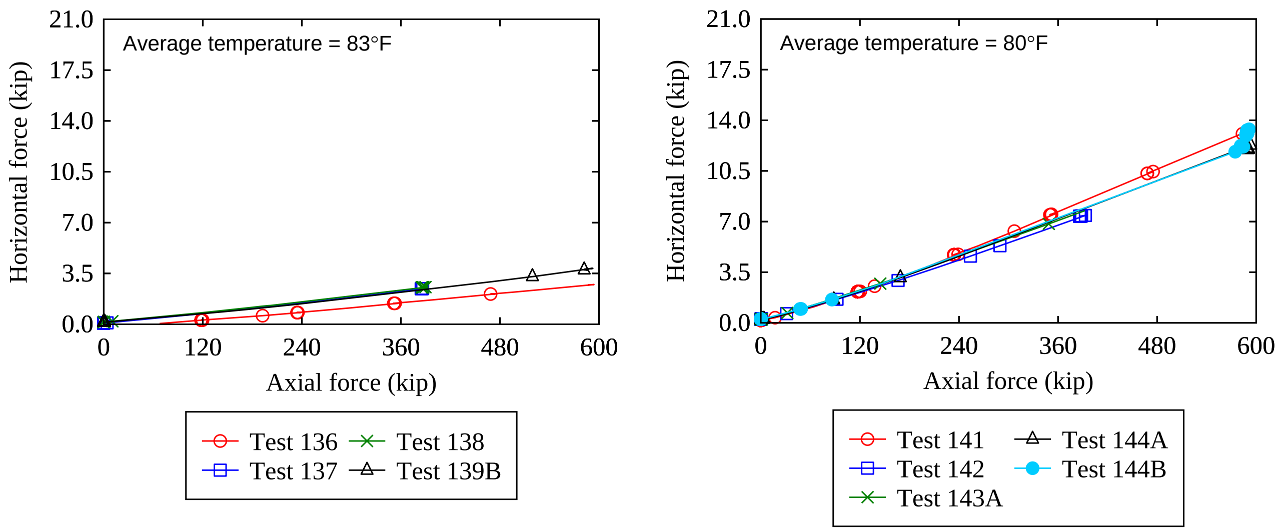

(a) (b)

Figure E-29 Horizontal force vs. axial force: (a) full-size K-0% pads; (b) full-size K-2.1% pads

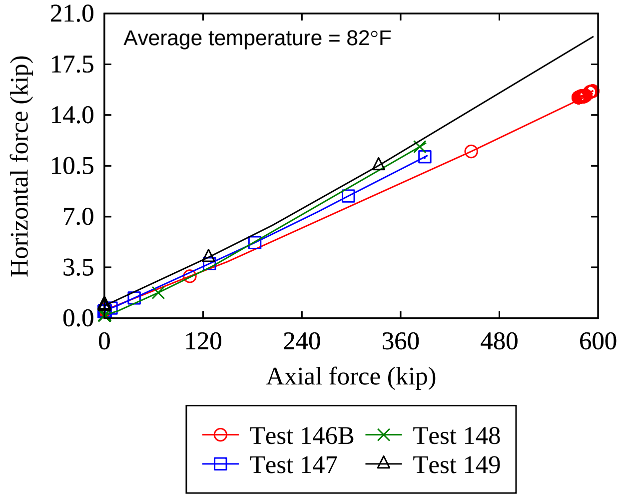

Figure E-30 Horizontal force vs. axial force of full-size K-4.2% pads

E.4 Shear stiffness test plots

This section includes plots for shear stiffness tests. These plots include data only corresponding to the last shear loading cycle, which will be used to determine pad shear stiffness. Data corresponding to negative and positive shear strain cycles are plotted in separate plots.

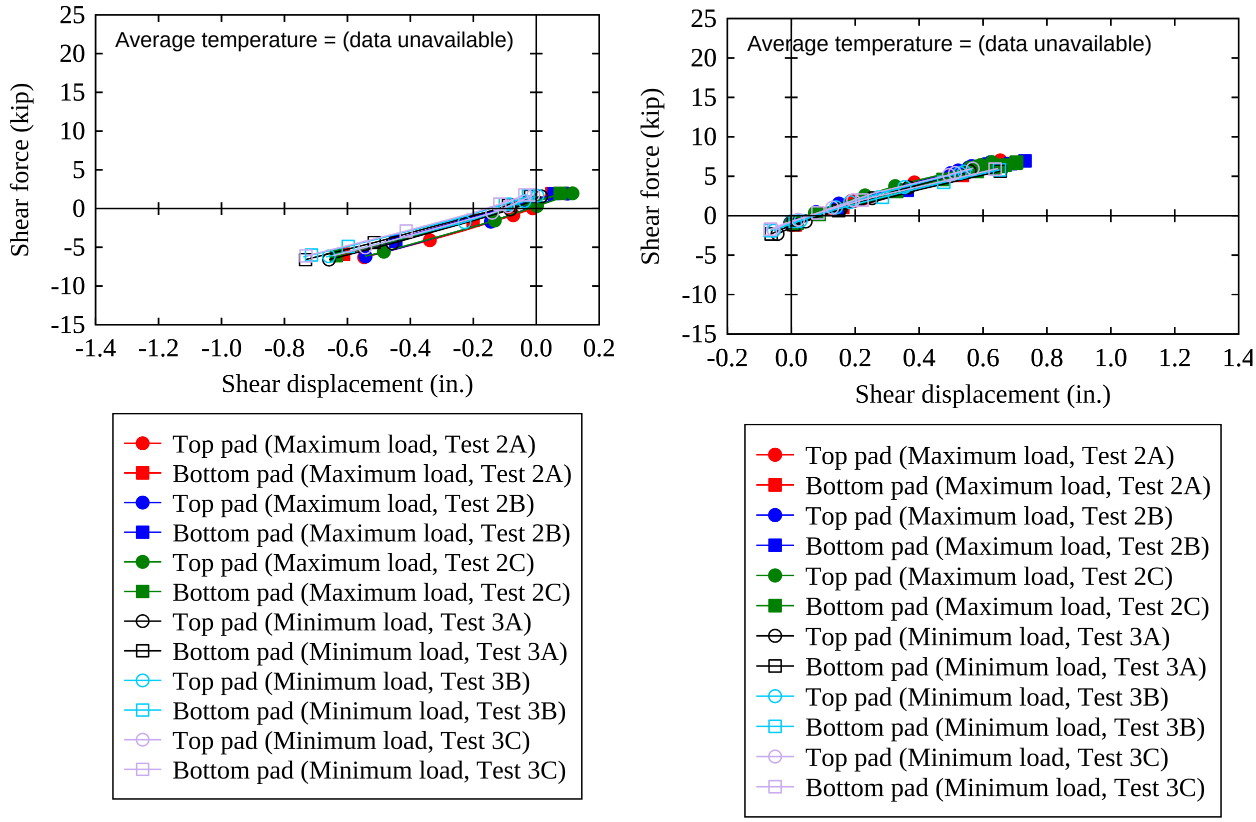

(a) (b)

Figure E-31 Shear load vs. displacement of half-size E-0% pads: (a) negative cycles (b) positive cycles

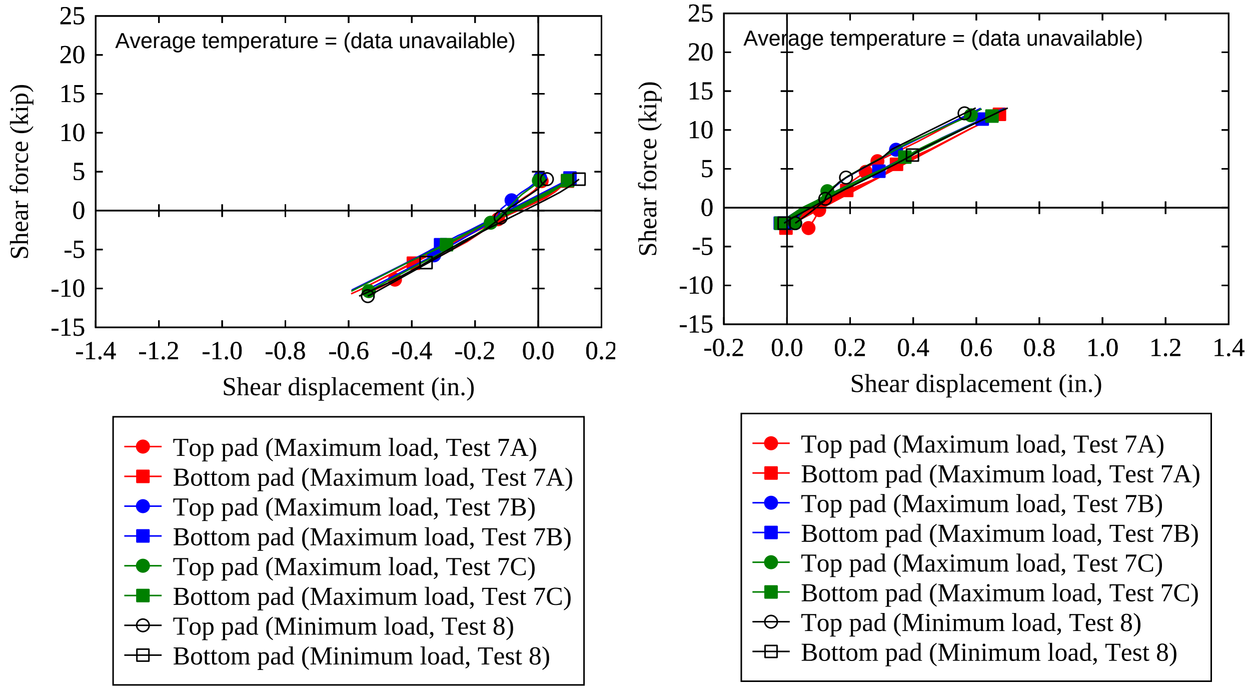

(a) (b)

Figure E-32 Shear load vs. displacement of full-size E-0% pads: (a) negative cycles (b) positive cycles

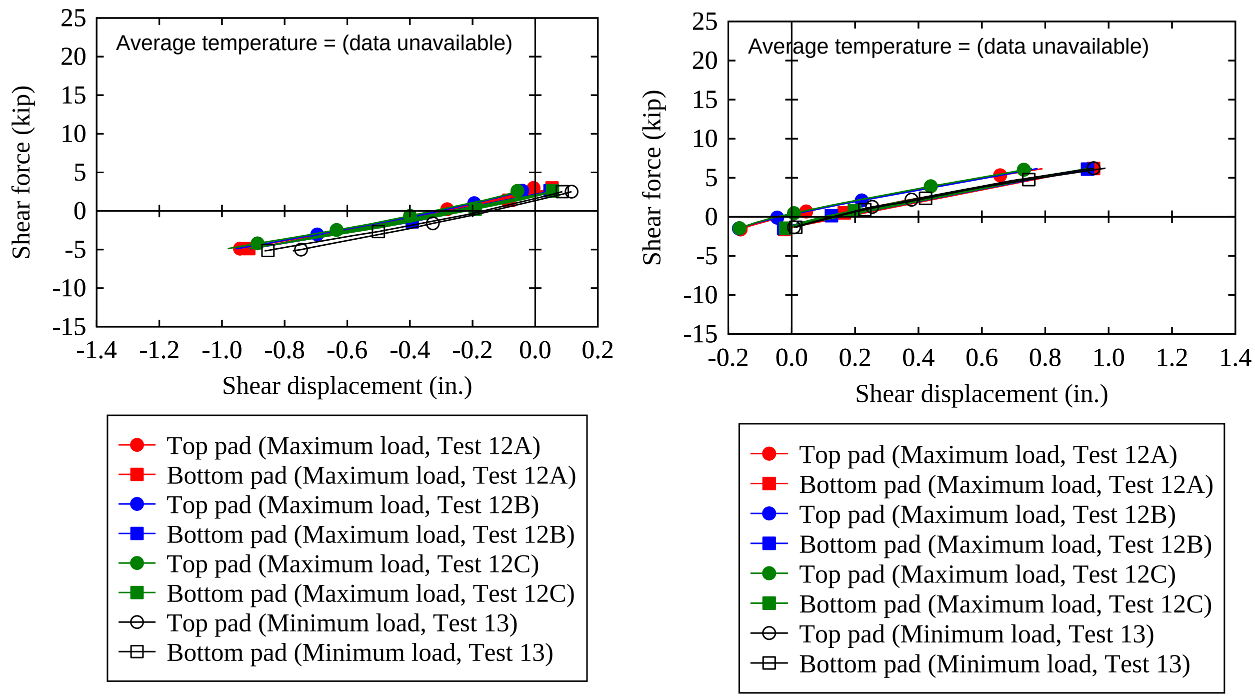

(a) (b)

Figure E-33 Shear load vs. displacement of half-size F-0% pads: (a) negative cycles (b) positive cycles

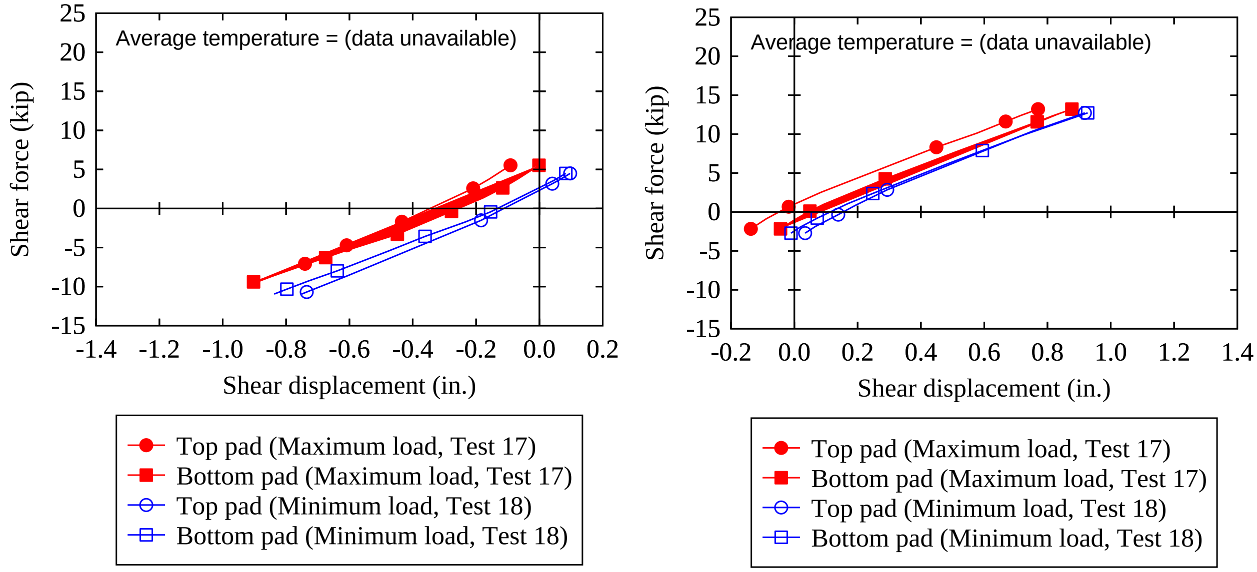

(a) (b)

Figure E-34 Shear load vs. displacement of full-size F-0% pads: (a) negative cycles (b) positive cycles

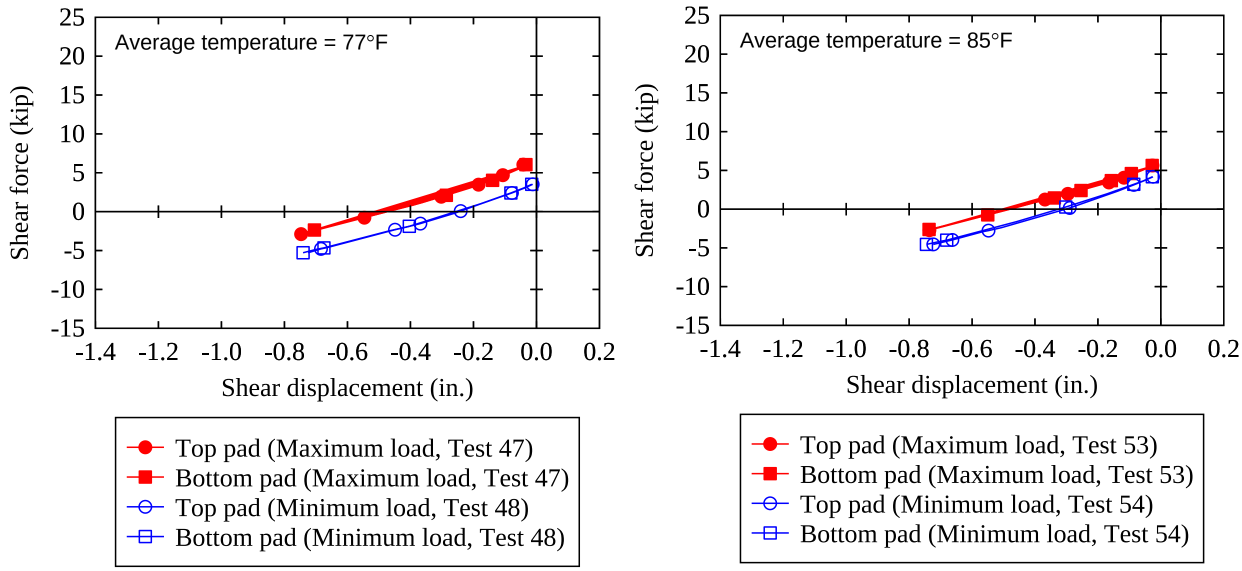

(a) (b)

Figure E-35 Shear load vs. displacement of half-size E-2.5% pads: (a) pair 1 (b) pair 2

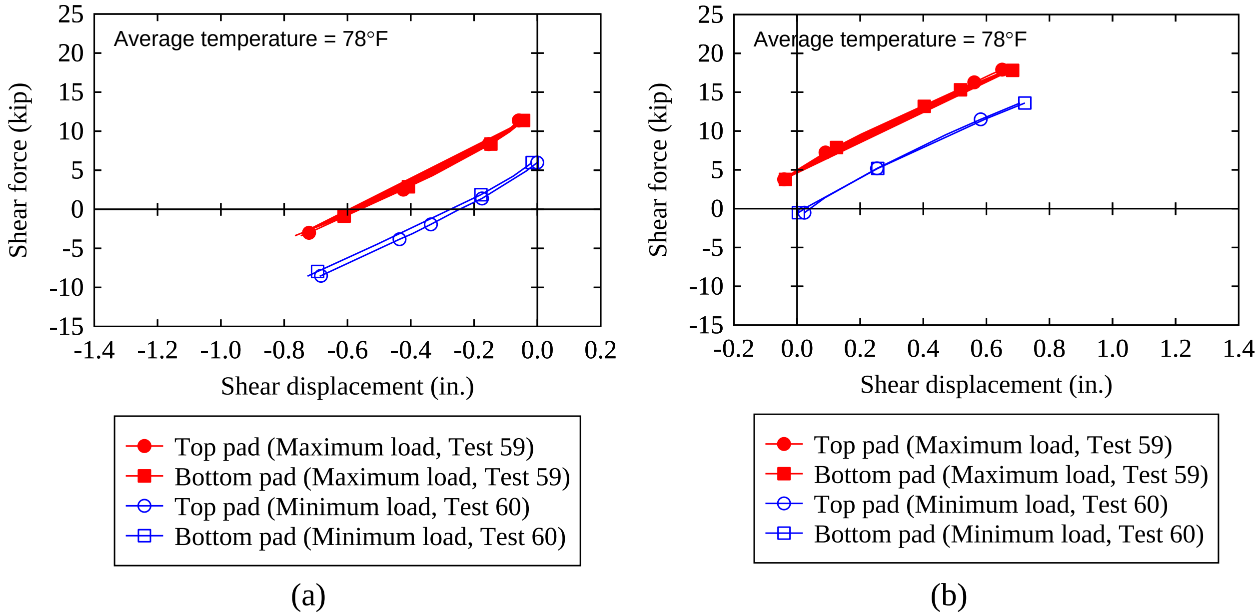

Figure E-36 Shear load vs. displacement of full-size E-2.5% pads (pair 1): (a) negative cycles (b) positive cycles

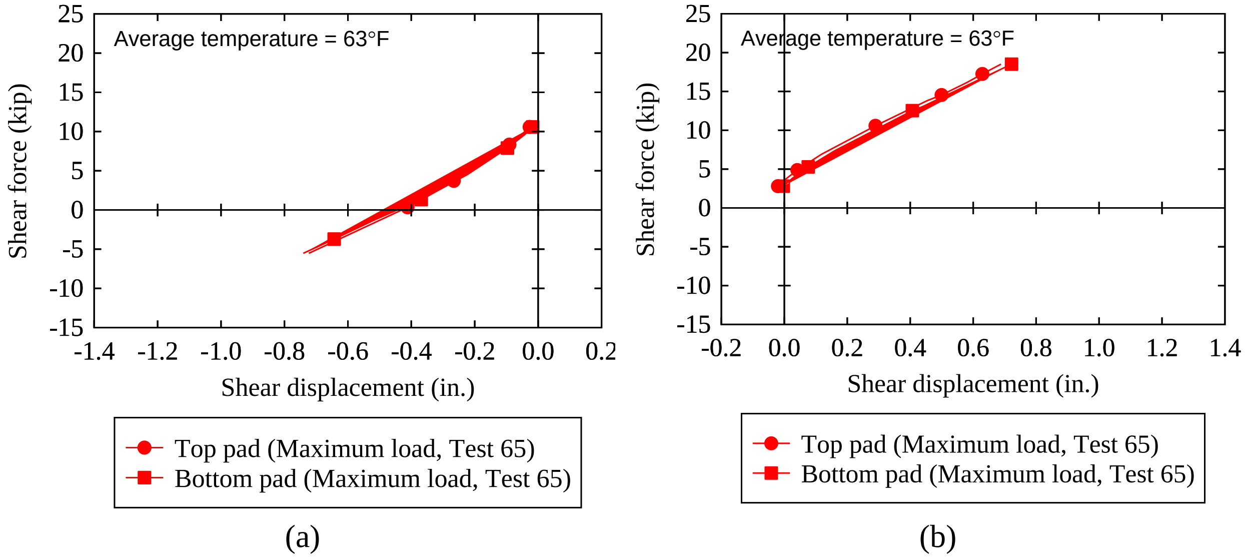

Figure E-37 Shear load vs. displacement of full-size E-2.5% pads (pair 2): (a) negative cycles (b) positive cycles

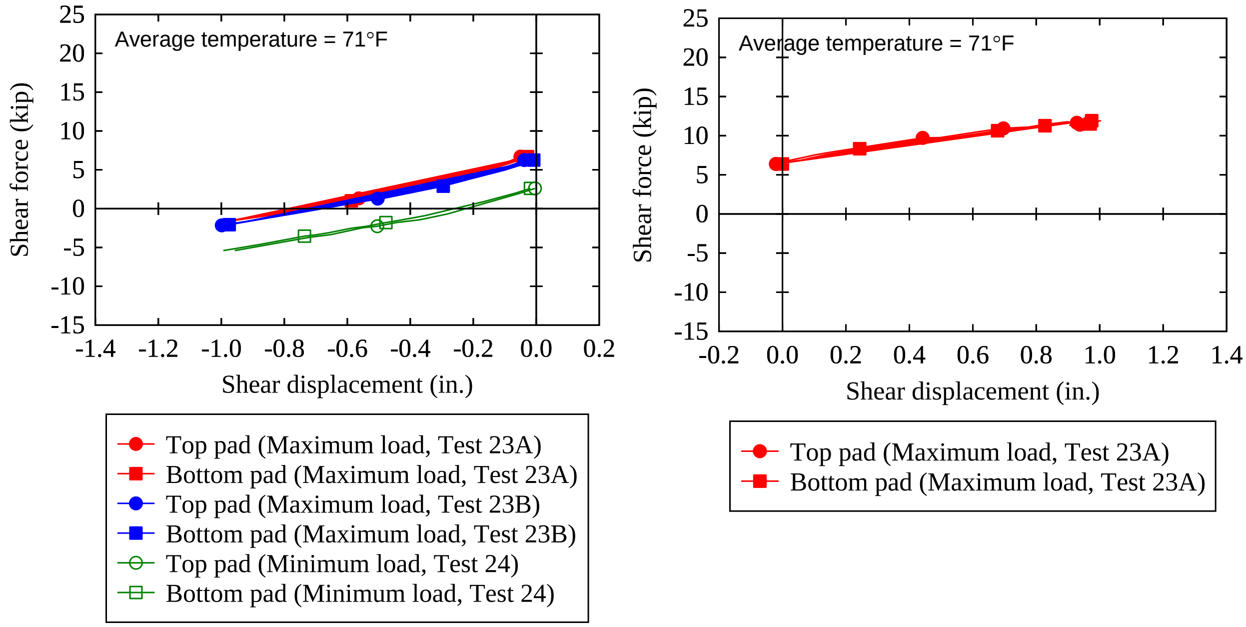

(a) (b)

Figure E-38 Shear load vs. displacement of half-size F-2.5% pads (pair 1): (a) negative cycles (b) positive cycles

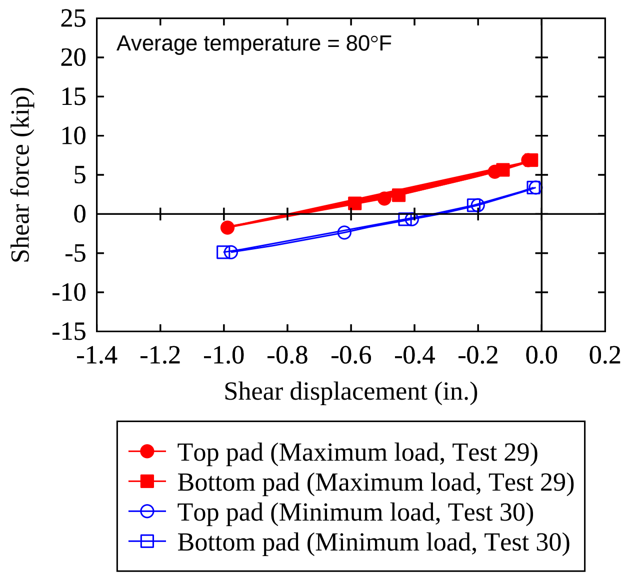

Figure E-39 Shear load vs. displacement of half-size F-2.5% pads (pair 2)

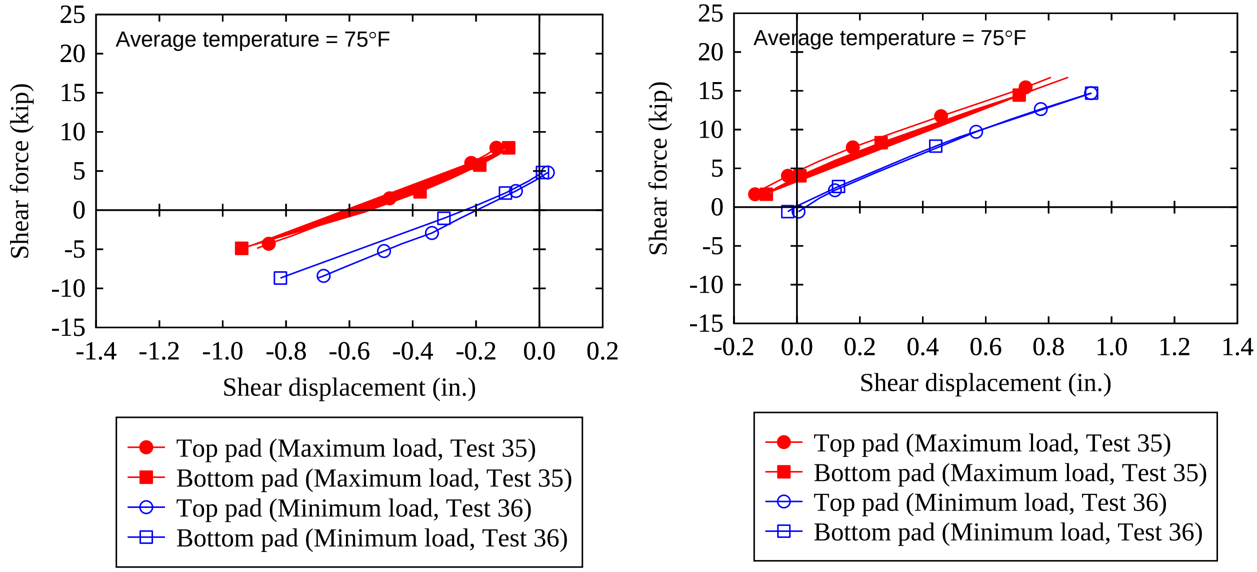

(a) (b)

Figure E-40 Shear load vs. displacement of full-size F-2.5% pads (pair 1): (a) negative cycles (b) positive cycles

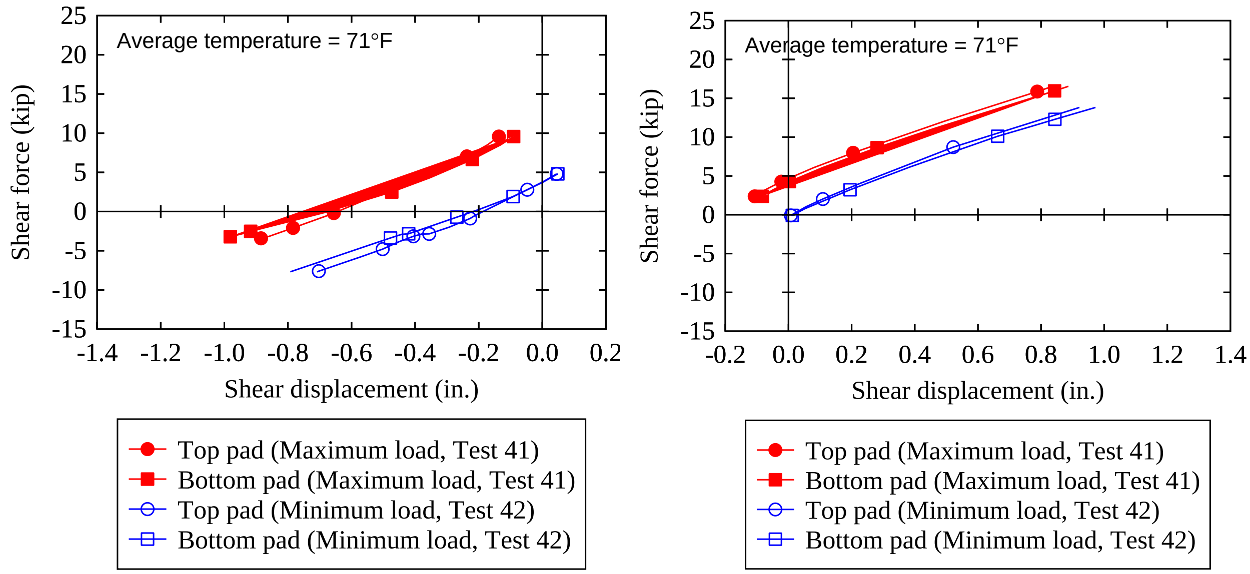

(a) (b)

Figure E-41 Shear load vs. displacement of full-size F-2.5% pads (pair 2): (a) negative cycles (b) positive cycles

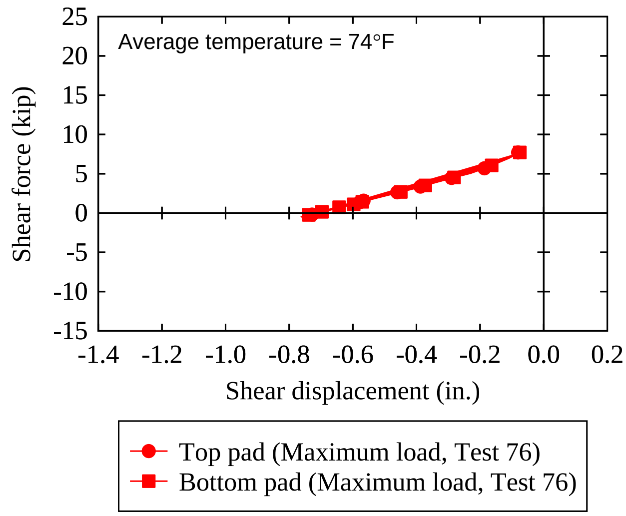

Figure E-42 Shear load vs. displacement of half-size E-5% pads (pair 2)

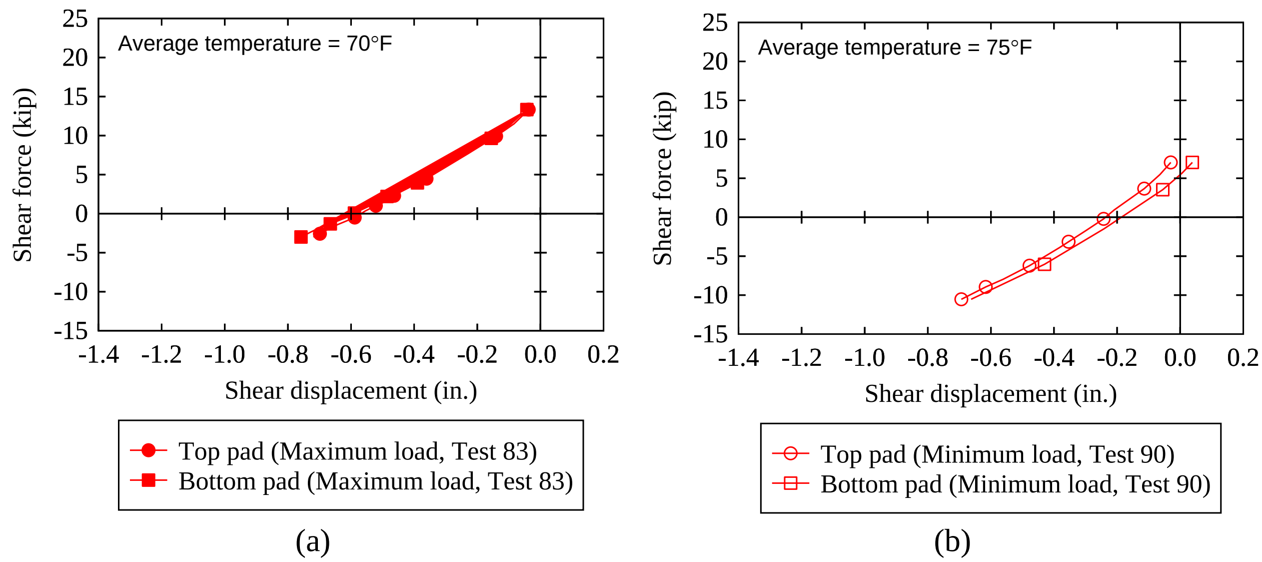

Figure E-43 Shear load vs. displacement of full-size E-5% pads: (a) pair 1 (b) pair 2

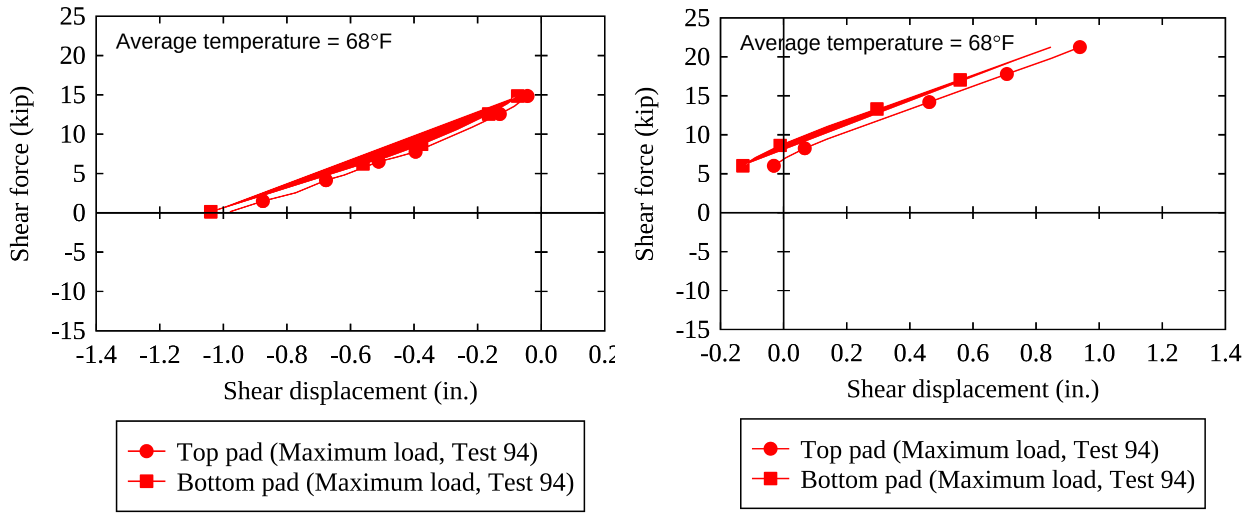

(a) (b)

Figure E-44 Shear load vs. displacement of full-size F-5% pads (pair 1): (a) negative cycles (b) positive cycles

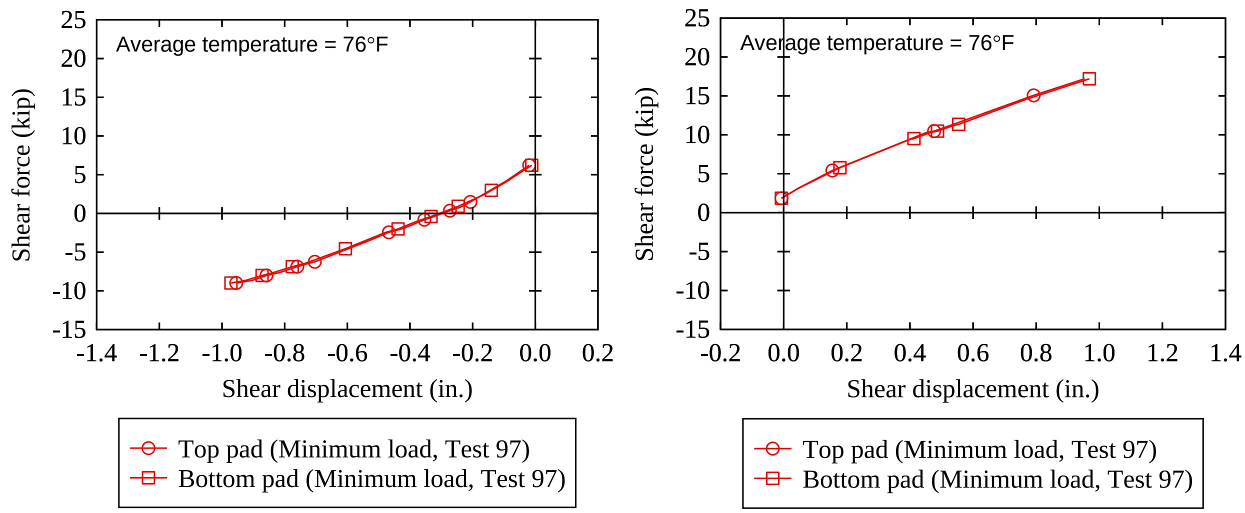

(a) (b)

Figure E-45 Shear load vs. displacement of full-size F-5% pads (pair 2): (a) negative cycles (b) positive cycles

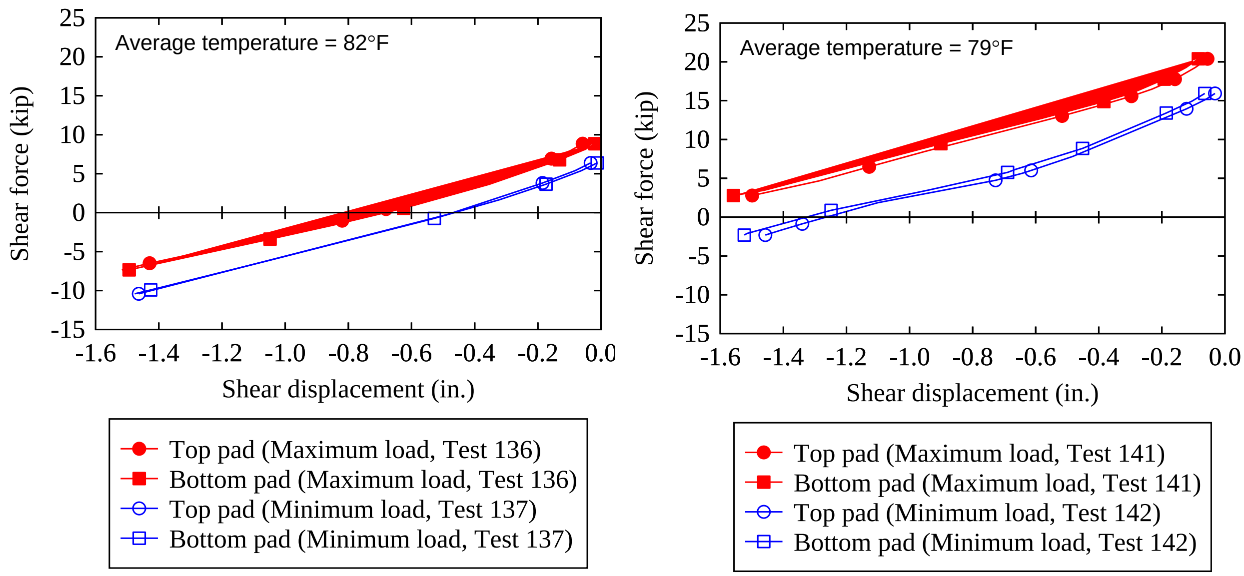

(a) (b)

Figure E-46 Shear load vs. displacement: (a) full-size K-0% pads; (b) full-size K-2.1% pads

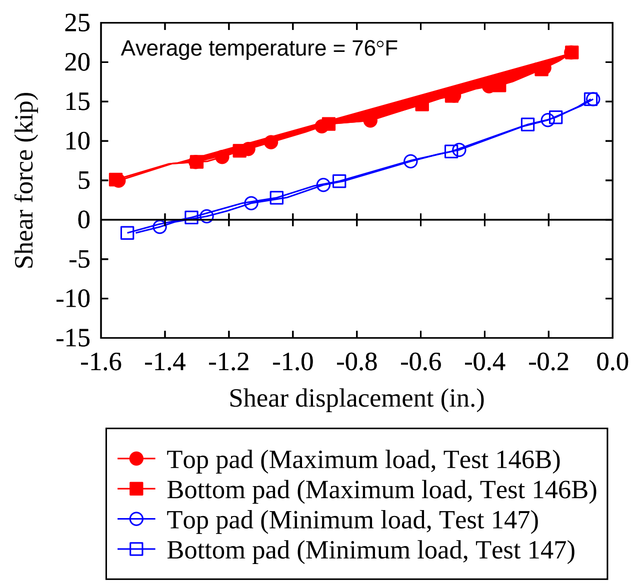

Figure E-47 Shear load vs. displacement of full-size K-4.2% pads

E.5 Slip test plots

This section includes plots for shear force versus shear displacement data measured during slip tests. Shear displacements of the top and bottom pads were computed as the difference between the displacement of the middle plate assembly and the bearing plates in contact with respective pads. Shear force was measured using the horizontal (MTS) actuator. Data from slip tests performed in the negative and positive shear strain directions on the same pair of pads are plotted in separate plots.

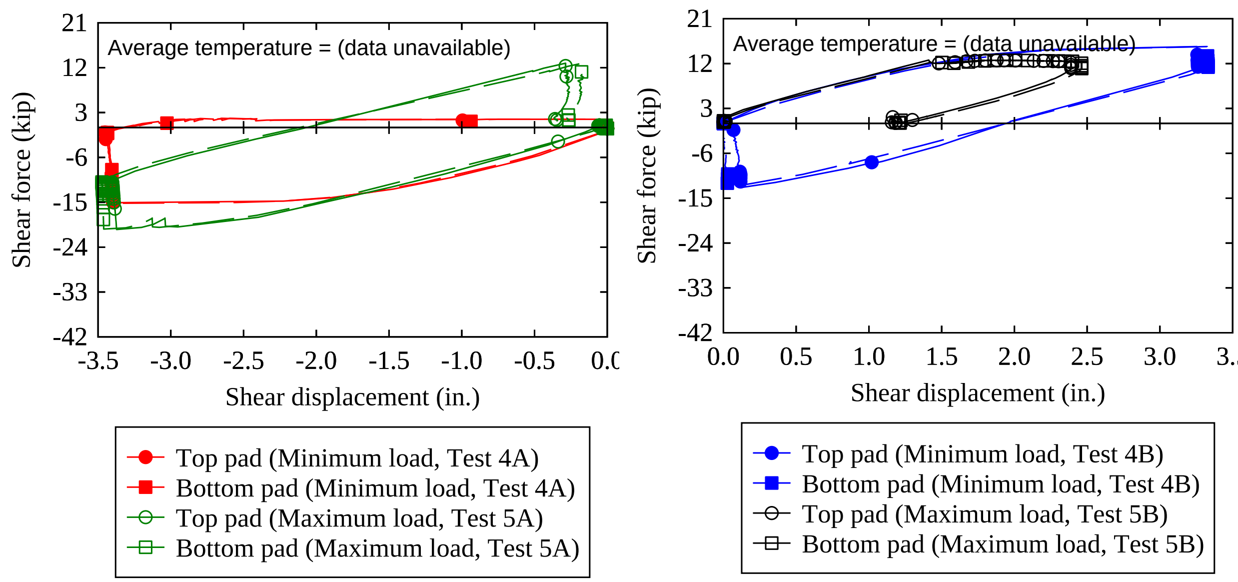

(a) (b)

Figure E-48 Dry steel surface slip test data of half-size E-0% pads: (a) negative strain (b) positive strain

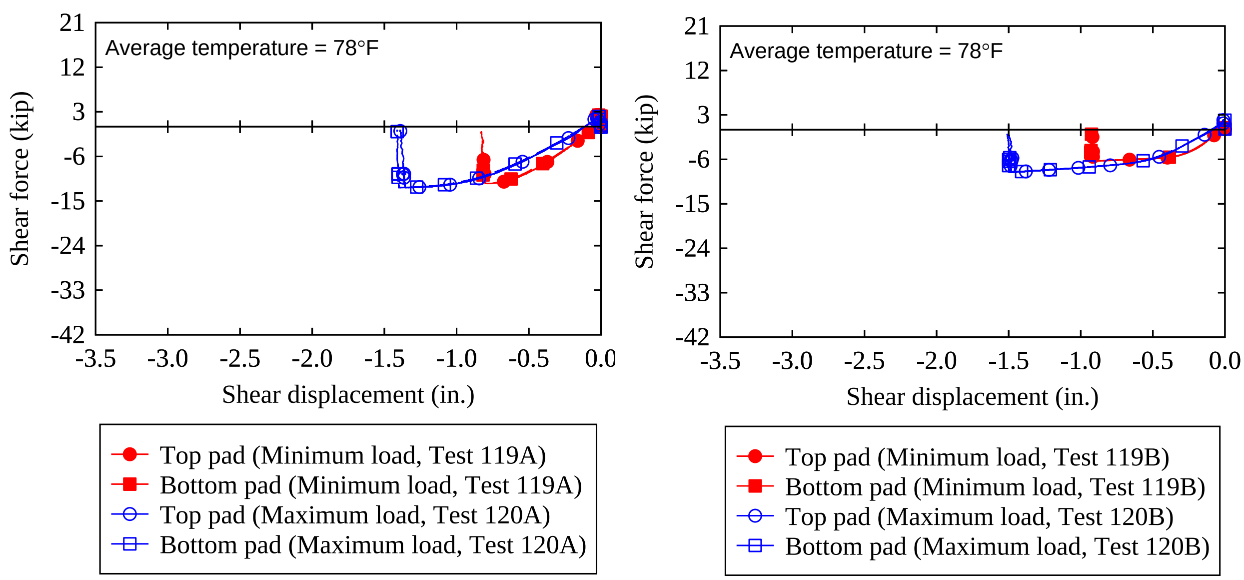

(a) (b)

Figure E-49 Slip test data of full-size E-0% pads: (a) Dry steel surface; (b) Wet steel surface

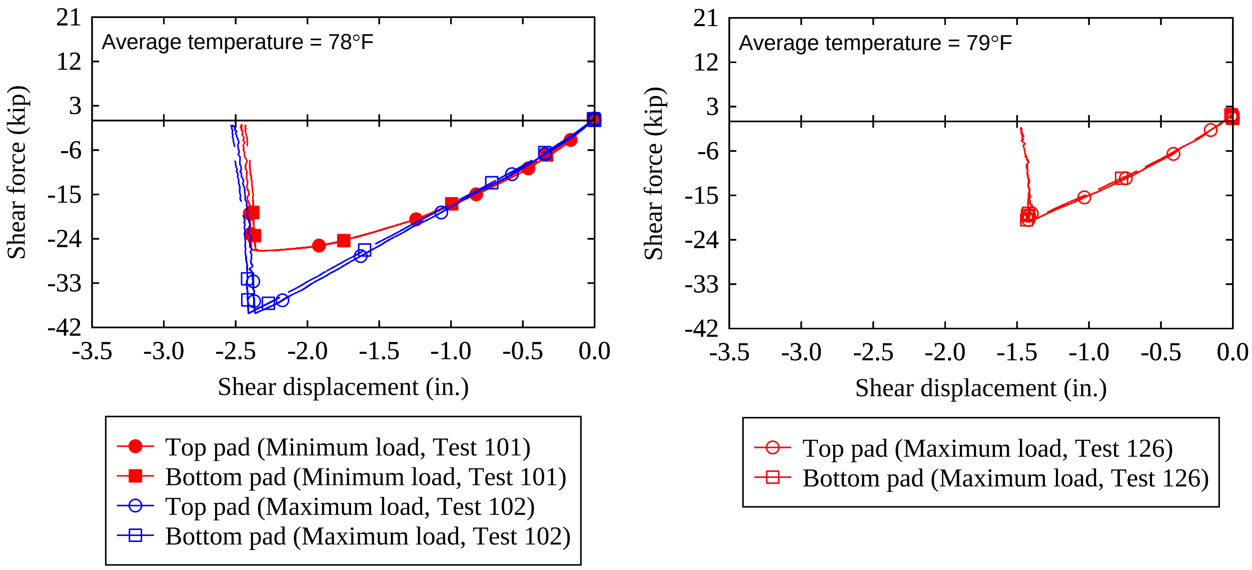

(a) (b)

Figure E-50 Slip test data of full-size E-0% pads: (a) Dry concrete surface; (b) Wet concrete surface

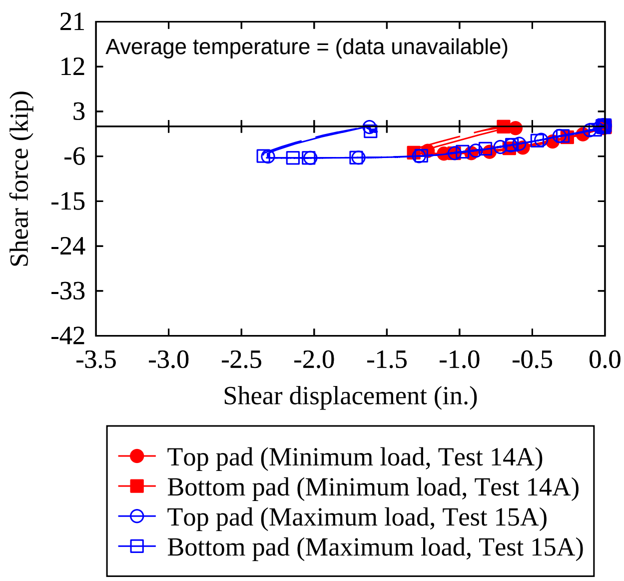

Figure E-51 Dry steel surface slip test data of half-size F-0% pads

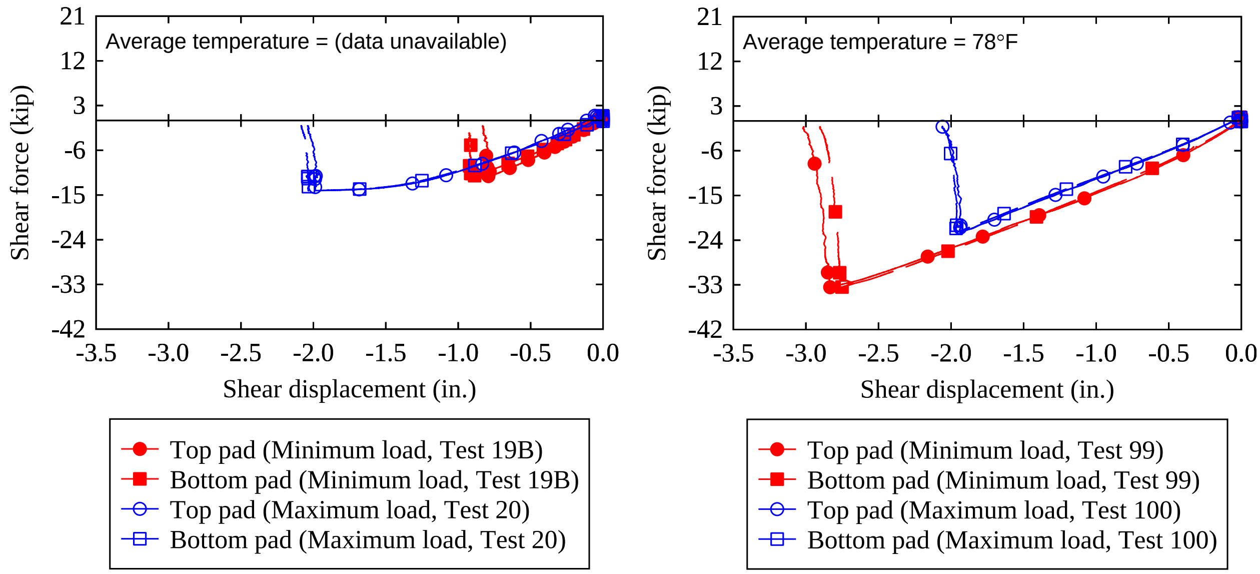

(a) (b)

Figure E-52 Slip test data of full-size F-0% pads: (a) Dry steel surface; (b) Dry concrete surface

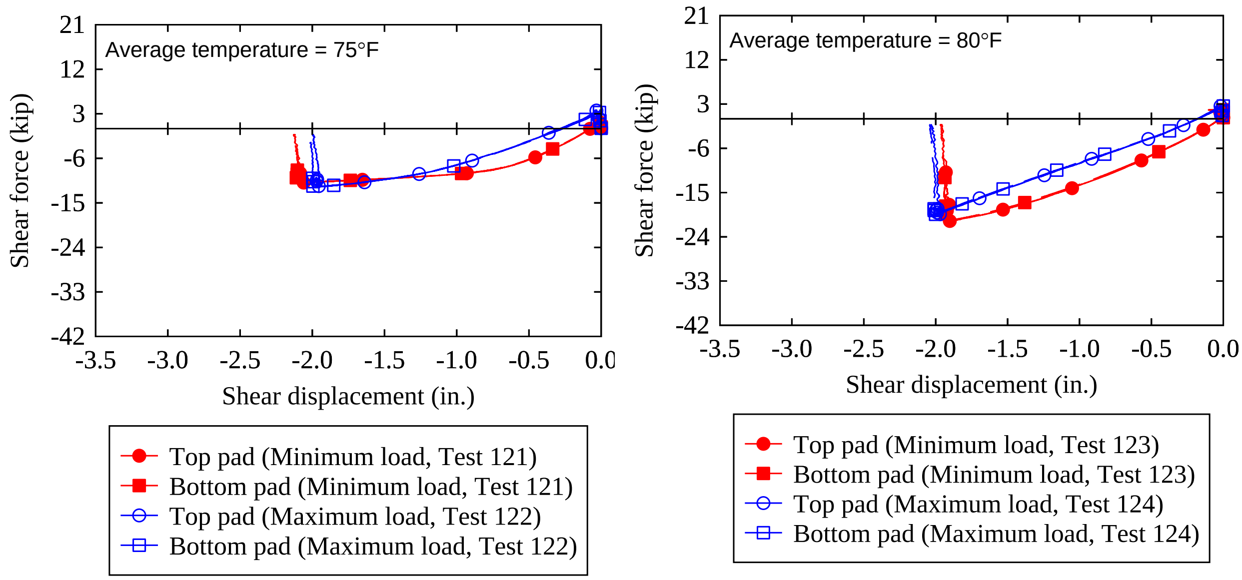

(a) (b)

Figure E-53 Slip test data of full-size F-0% pads: (a) Wet steel surface; (b) Wet concrete surface

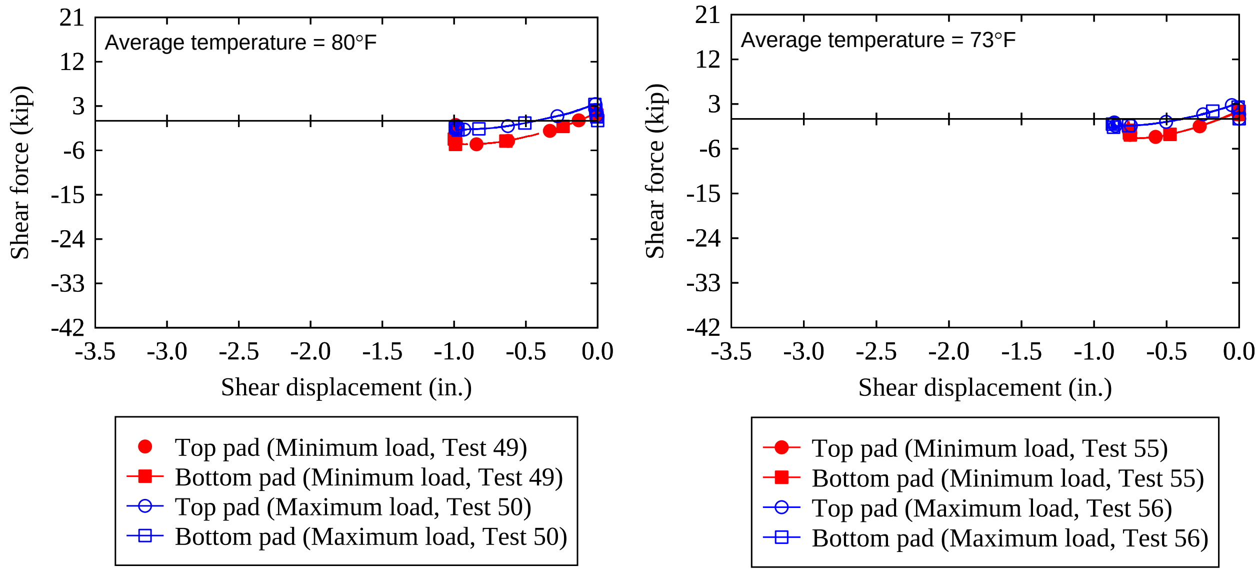

(a) (b)

Figure E-54 Dry steel surface slip test data of half-size E-2.5% pads: (a) pair 1; (b) pair 2

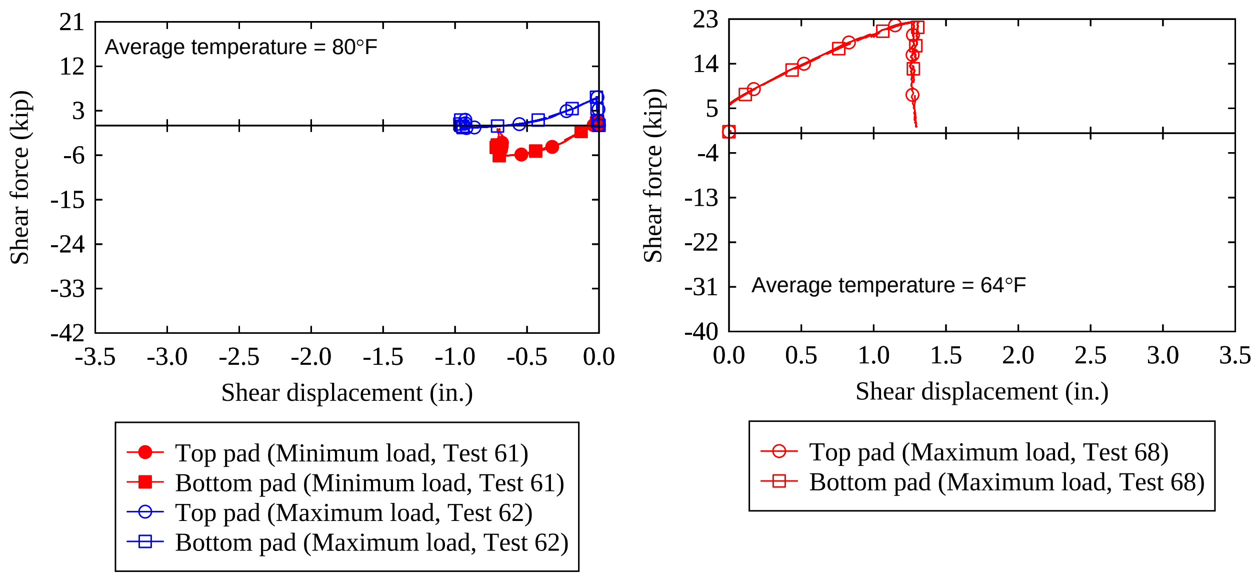

(a) (b)

Figure E-55 Dry steel surface slip test data of full-size E-2.5% pads: (a) pair 1; (b) pair 2

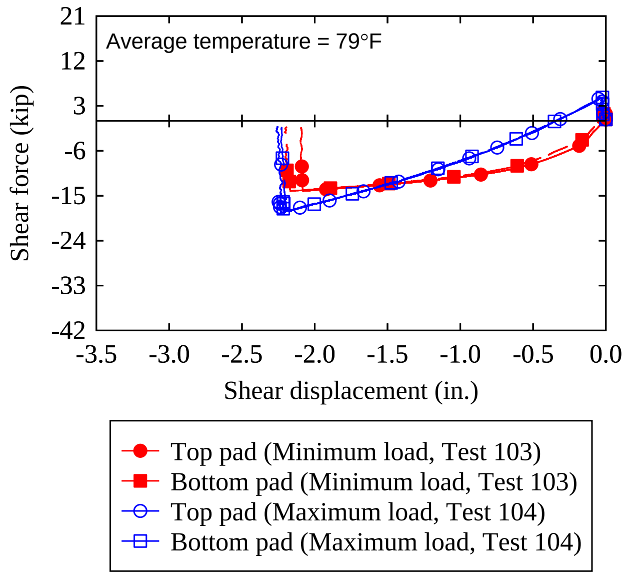

Figure E-56 Dry concrete surface slip test data of full-size E-2.5% pads (pair 1)

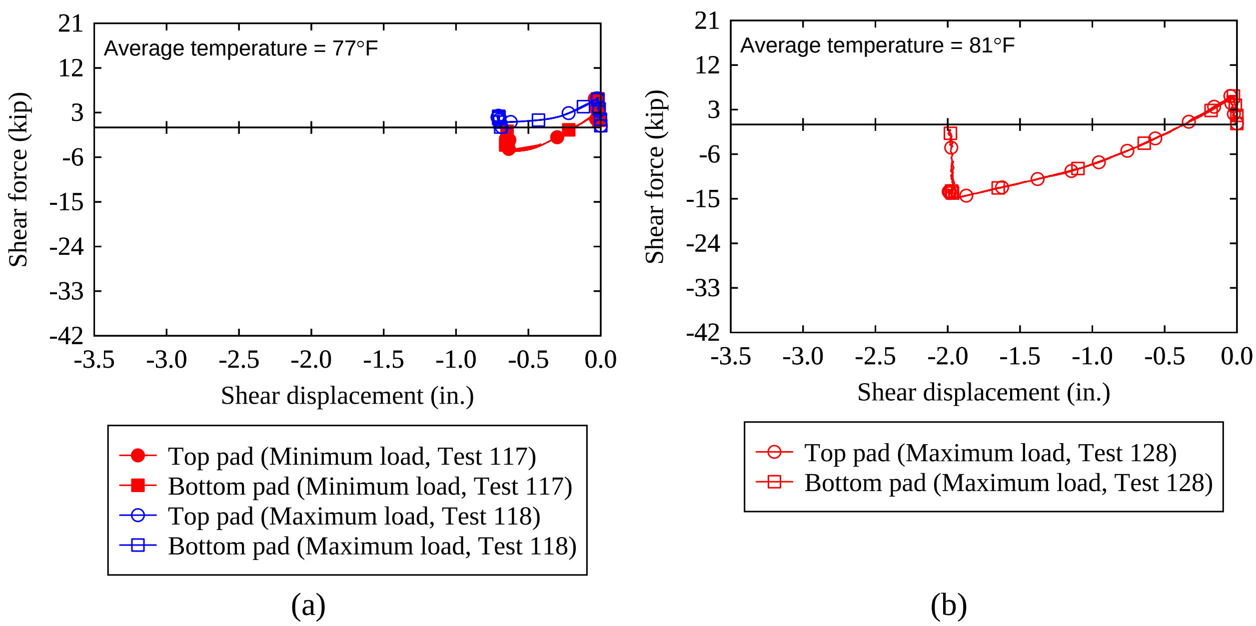

Figure E-57 Slip test data of full-size E-2.5% pads (pair 2): (a) With wet steel surface; (b) Wet concrete surface

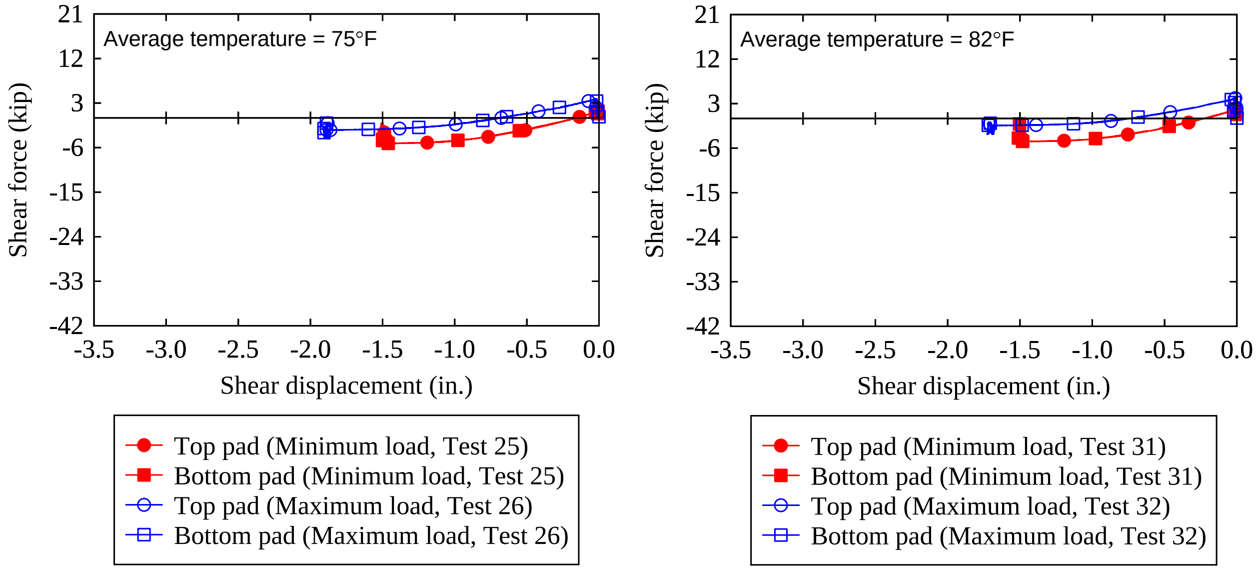

(a) (b)

Figure E-58 Dry steel surface slip test data of half-size F-2.5% pads: (a) pair 1; (b) pair 2

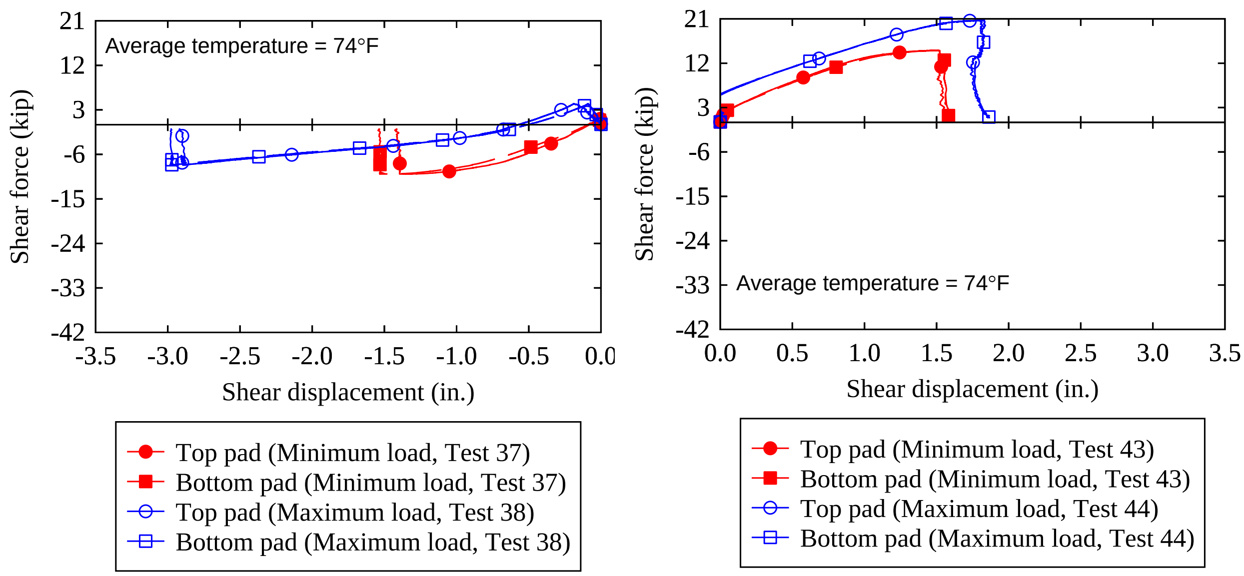

(a) (b)

Figure E-59 Dry steel surface slip test data of full-size F-2.5% pads: (a) pair 1; (b) pair 2

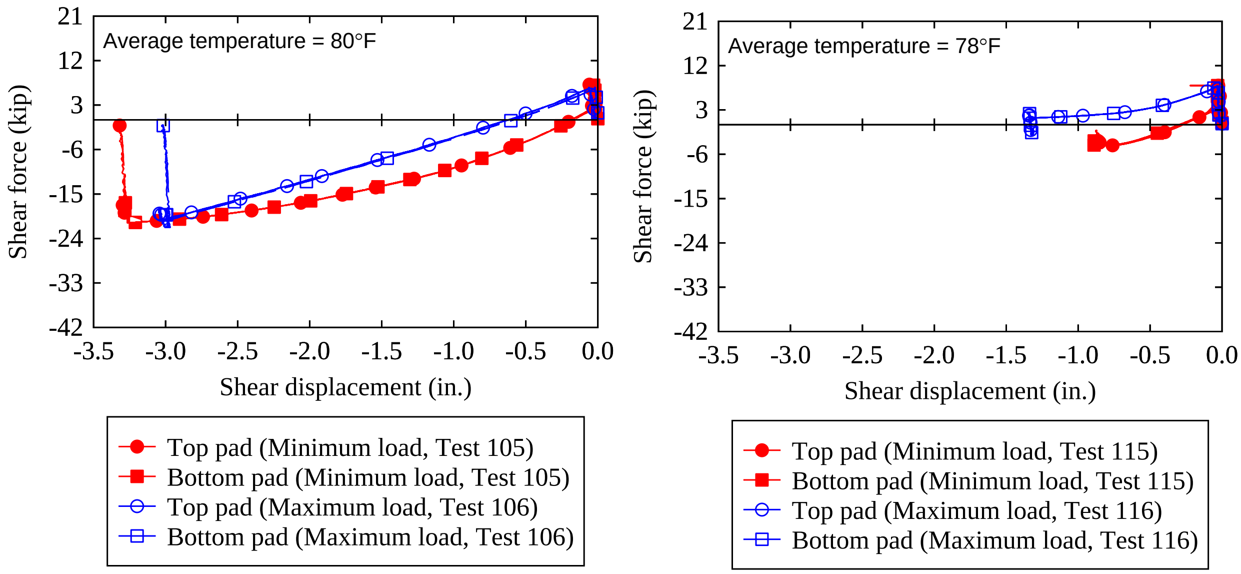

(a) (b)

Figure E-60 Slip test data of full-size F-2.5% pads: (a) Dry concrete surface (pair 1); (b) Wet steel surface (pair 2)

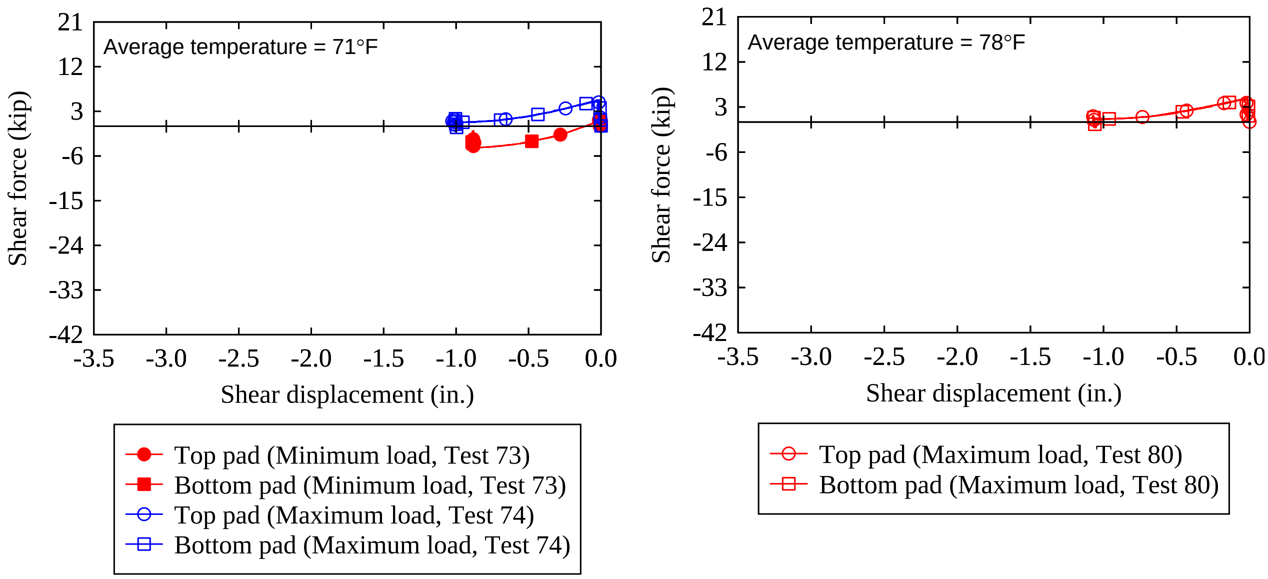

(a) (b)

Figure E-61 Dry steel surface slip test data of half-size E-5% pads: (a) pair 1; (b) pair 2

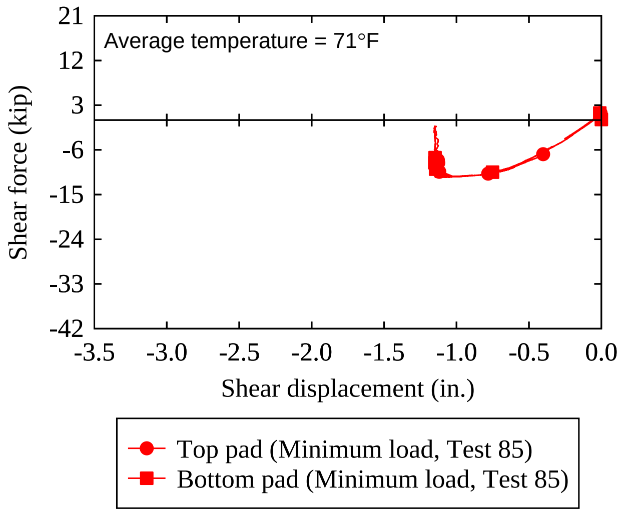

(a)

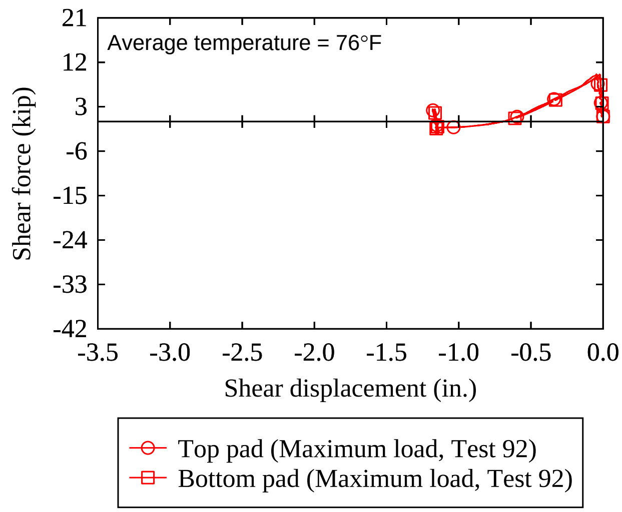

(b)

Figure E-62 Dry steel surface slip test data of full-size E-5% pads: (a) pair 1; (b) pair 2

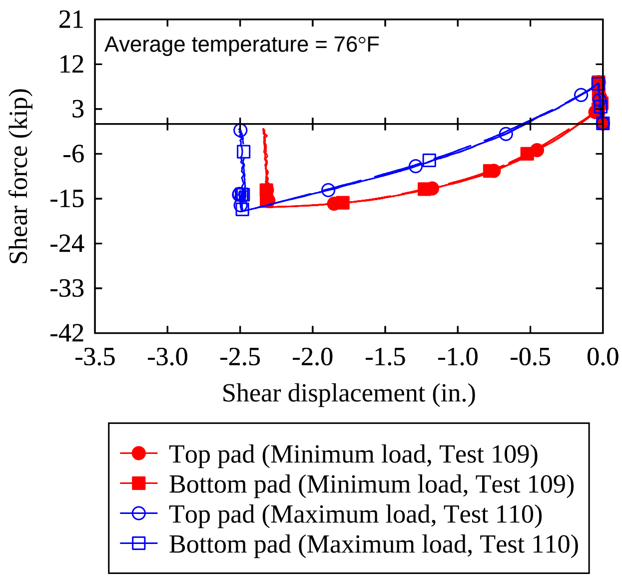

Figure E-63 Dry concrete surface slip test data of full-size E-5% pads (pair 1)

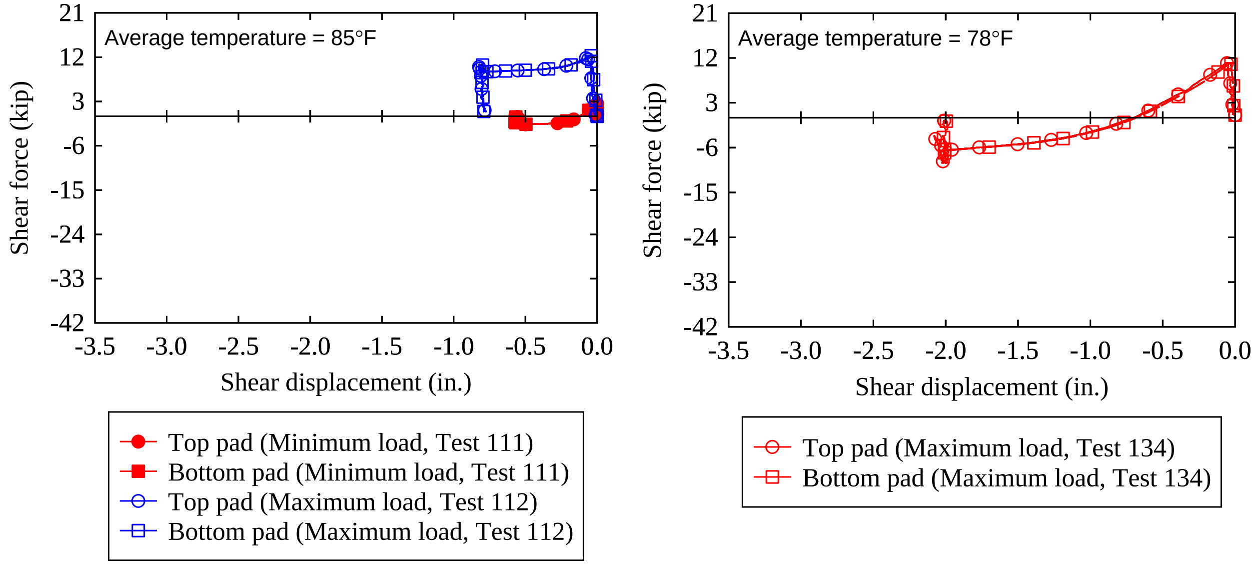

(a) (b)

Figure E-64 Slip test data of full-size E-5% pads (pair 2): (a) Wet steel surface; (b) Wet concrete surface

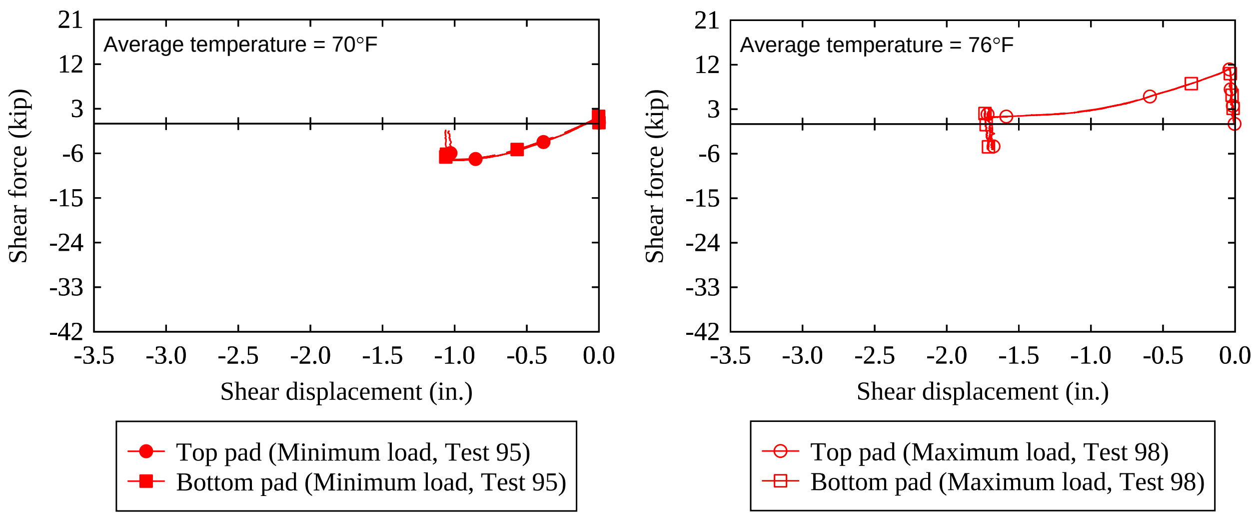

(a) (b)

Figure E-65 Dry steel surface slip test data of full-size F-5% pads: (a) pair 1; (b) pair 2

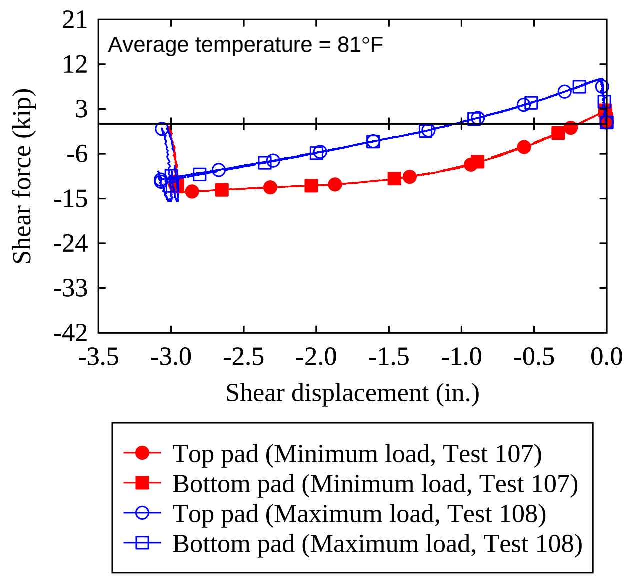

Figure E-66 Dry concrete surface slip test data of full-size F-5% pads (pair 1)

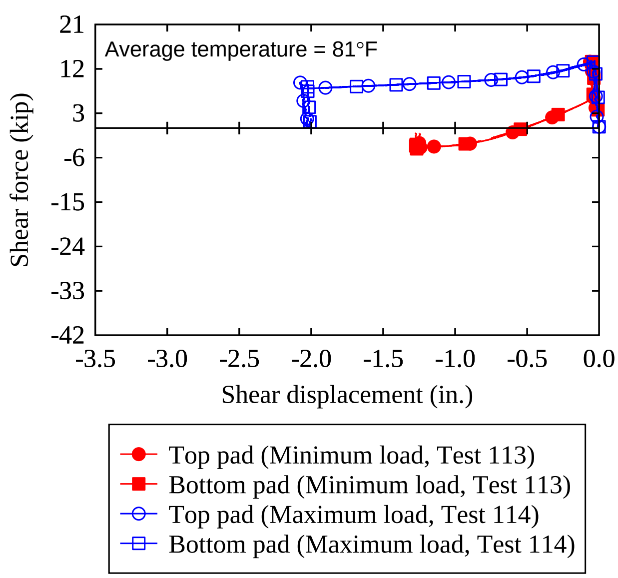

(a)

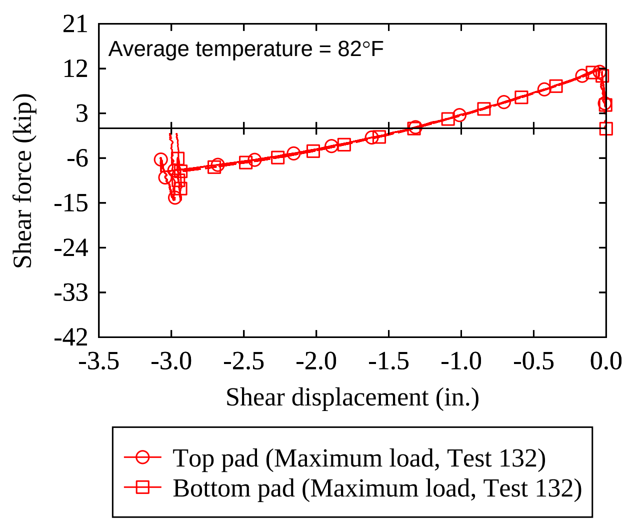

(b)

Figure E-67 Slip test data of full-size F-5% pads (pair 2): (a) Wet steel surface; (b) Wet concrete surface

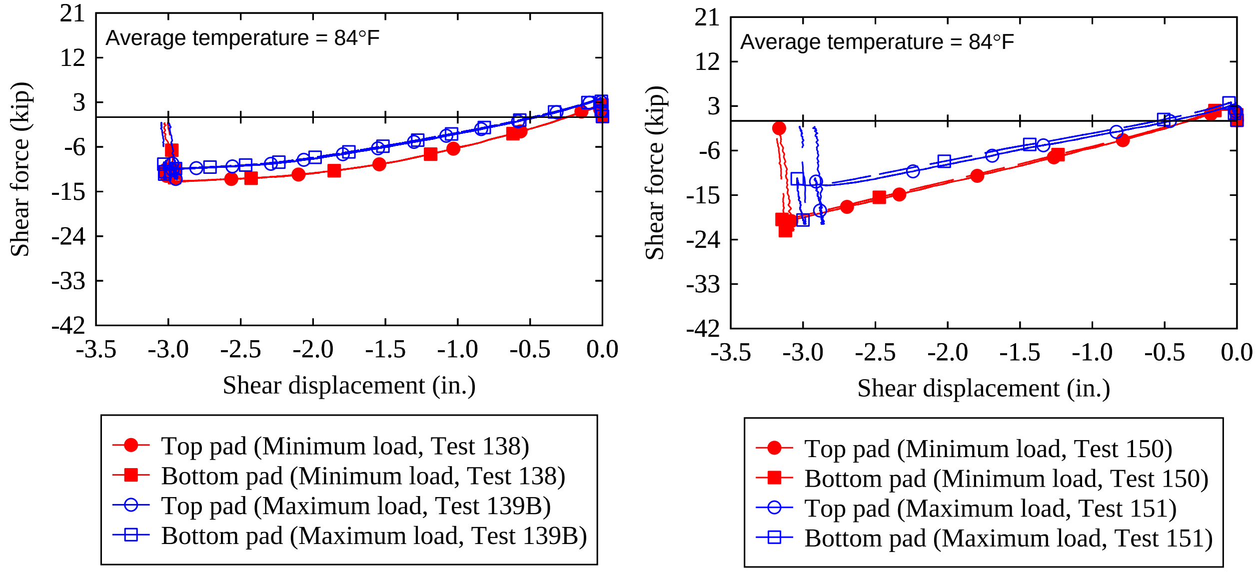

(a) (b)

Figure E-68 Slip test data of full-size K-0% pads (pair 2): (a) Dry steel surface; (b) Dry concrete surface

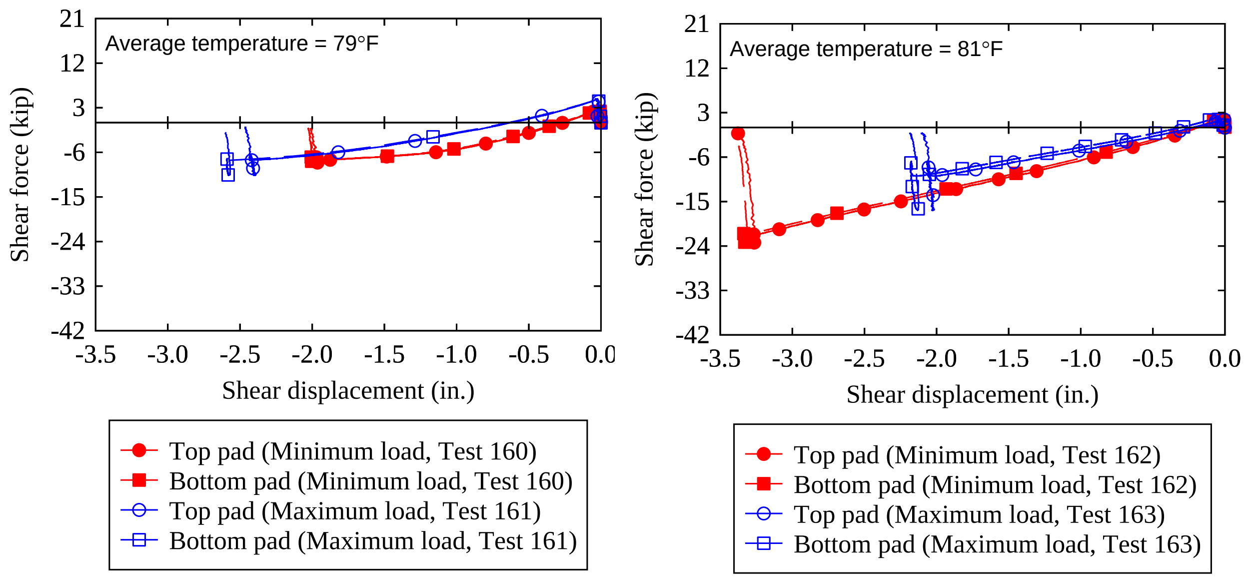

(a) (b)

Figure E-69 Slip test data of full-size K-0% pads (pair 2): (a) Wet steel surface; (b) Wet concrete surface

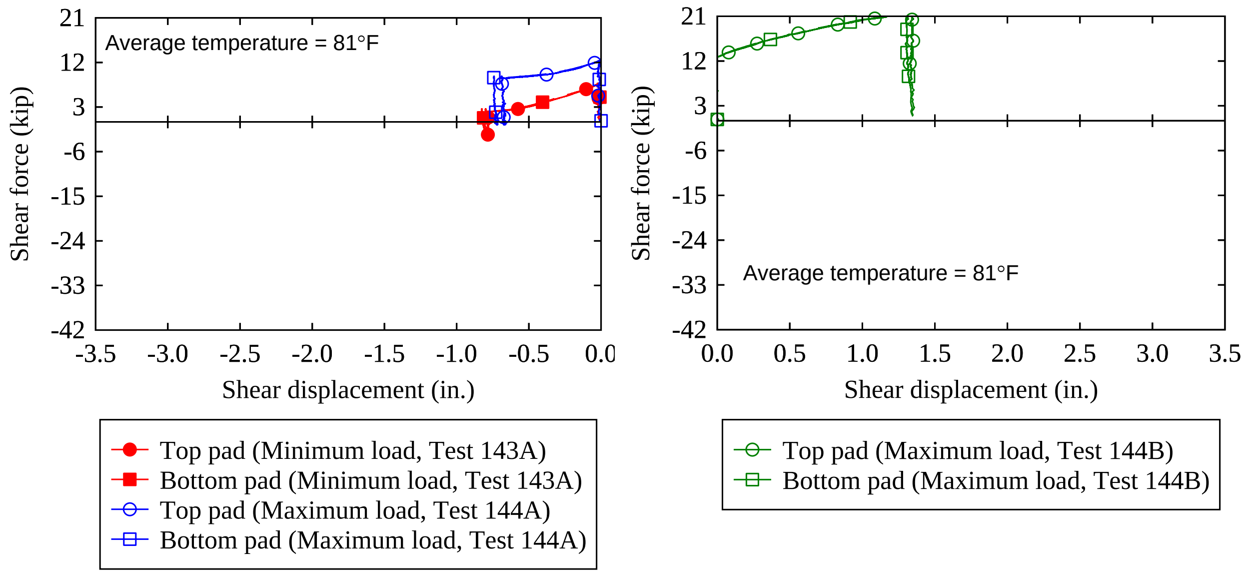

(a) (b)

Figure E-70 Dry steel surface slip test data of full-size K-2.1% pads: (a) negative strain; (b) positive strain

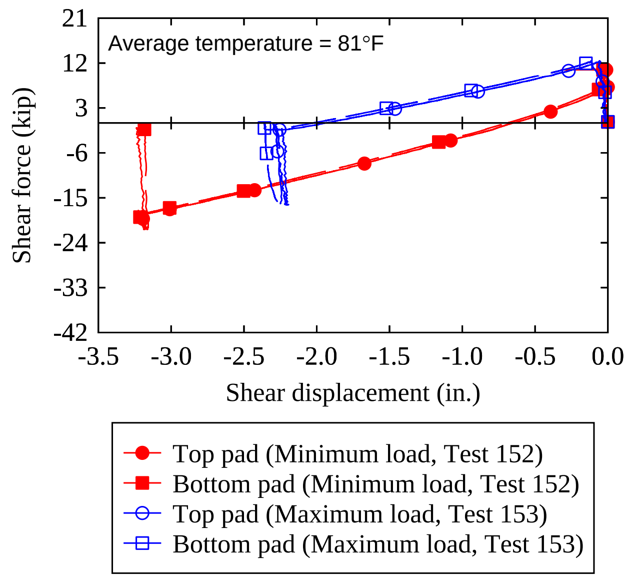

Figure E-71 Dry concrete surface slip test data of full-size K-2.1% pads

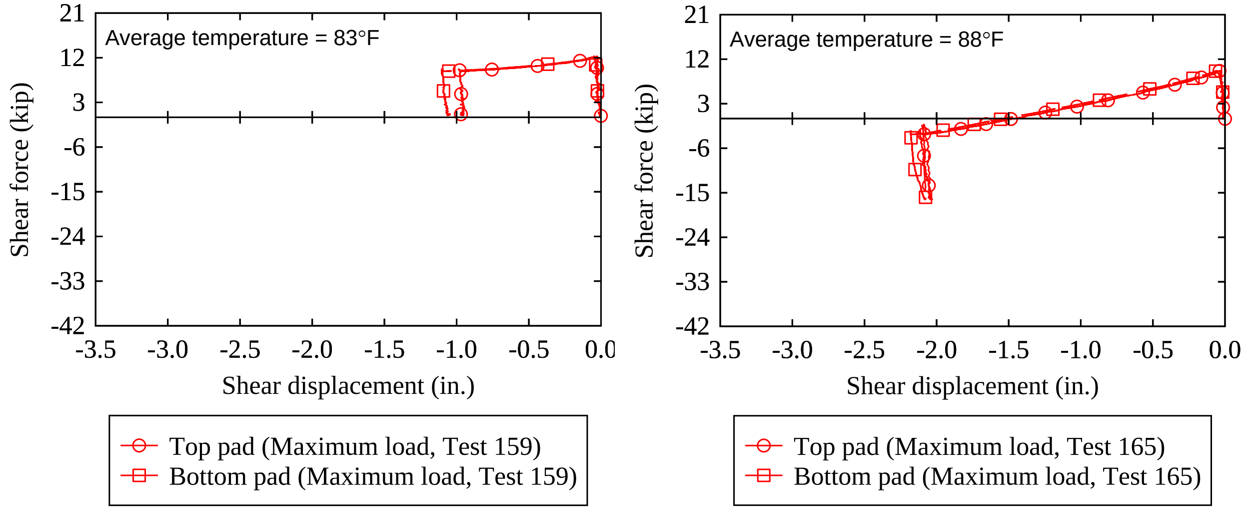

(a) (b)

Figure E-72 Slip test data of full-size K-2.1% pads: (a) Wet steel surface; (b) Wet concrete surface

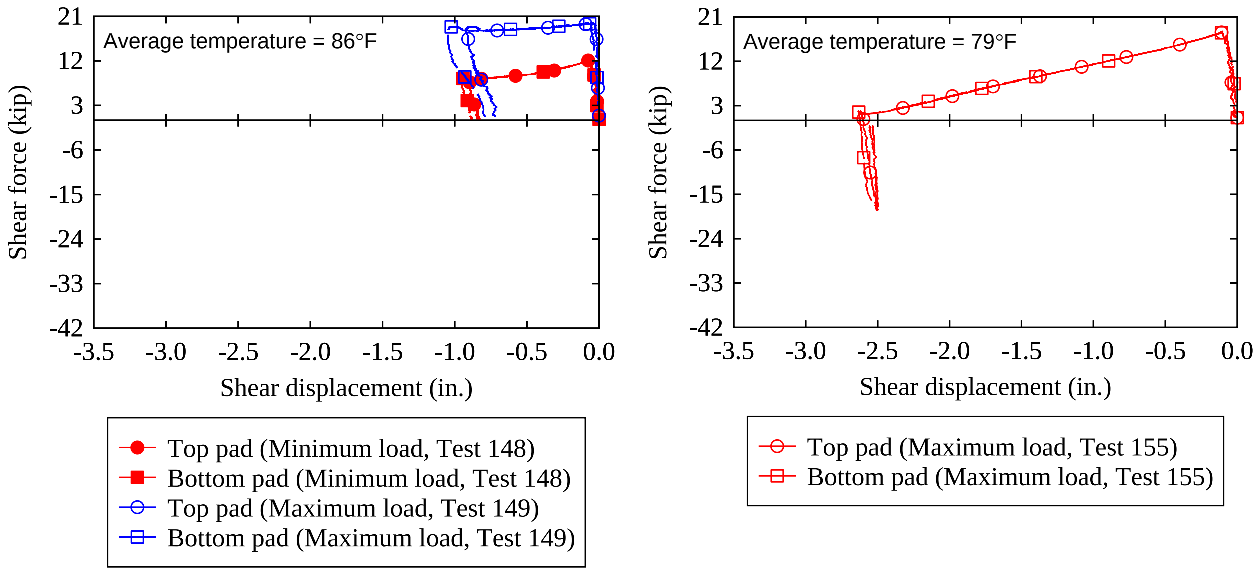

(a) (b)

Figure E-73 Slip test data of full-size K-4.2% pads: (a) Dry steel surface; (b) Dry concrete surface

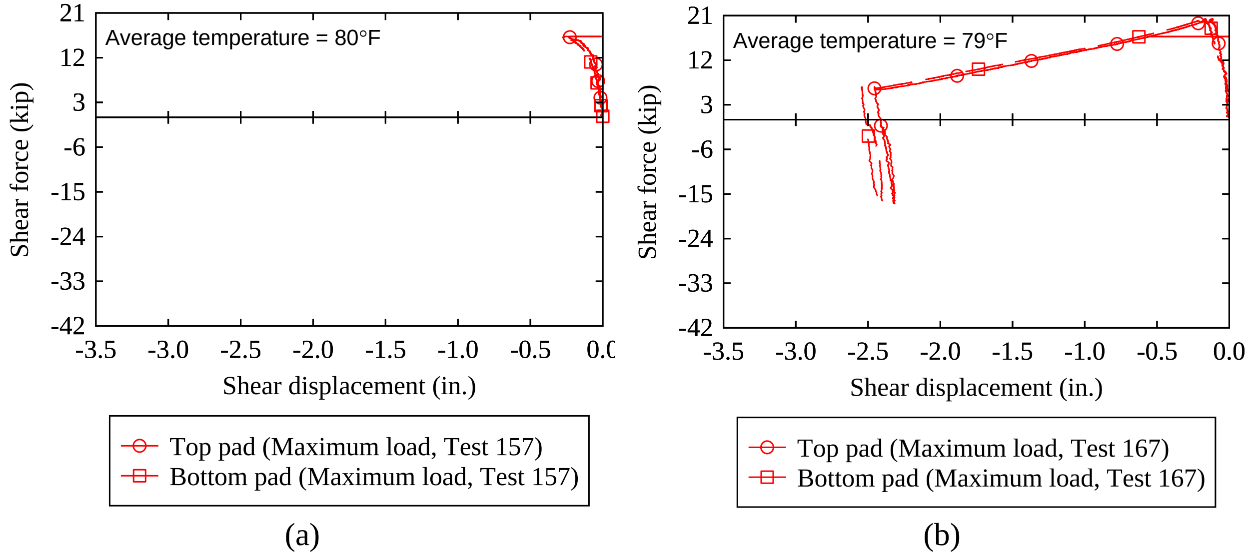

Figure E-74 Slip test data of full-size K-4.2% pads: (a) Wet steel surface (pads slipped before applying complete axial load); (b) Wet concrete surface